Short and Slender Concrete Columns Internally or Externally Reinforced with Longitudinal Fiber-Reinforced Polymer Composites

by

Koosha Khorramian

Submitted in partial fulfilment of the requirements
for the degree of Doctor of Philosophy

at

Dalhousie University
Halifax, Nova Scotia
July 2020

I dedicate this thesis to my Mother, Azadeh Baziar, who supported me in every stage of my life.

TABLE OF CONTENTS

LIST OF TABLES

LIST OF FIGURES

ABSTRACT

The goal of this thesis was to investigate the behavior of short and slender concrete columns internally and externally reinforced with longitudinal fiber-reinforced polymer (FRP) composites. The study was divided into two major parts. First part addressed the issues regarding the use of FRP as internal reinforcement for new constructions and the second part focused on external FRP reinforcement for strengthening of existing concrete columns. There is a lack of knowledge and experimental data on the use of longitudinal FRPs as external and internal reinforcement. The contribution of FRP bars in compression is ignored by many design guidelines and the use of longitudinally bonded FRPs in compression is not suggested by guidelines due to lack of experimental test data. There is also lack of knowledge regarding the effect of slenderness and associated parameters (e.g., critical slenderness ratio and flexural stiffness) for the columns. Also, the effectiveness of confinement for eccentrically loaded concrete columns is not well-known. Therefore, this thesis addressed the issues regarding the use of external and internal FRP reinforcement in concrete columns using experimental, analytical, numerical, and statistical approaches. To characterize the compressive behavior of FRP bars as internal reinforcement, three different experimental programs were conducted to include a total of 24 columns, including 10 large-scale and 14 small-scale tests, and 35 compressive FRP bar coupons, in part I of the study. In part II, the use of FRPs as external reinforcement were experimentally assessed by testing a total of 36 column in four different experimental programs, including 6 large-scale tests and 30 small-scale tests. For further investigation, a model was developed in MATLAB for second order analysis of concrete columns reinforced internally or externally with FRPs using one-dimensional finite difference method. The nonlinearity of material and geometry and the effect of eccentricity in confinement were also considered. After required verifications, the model was used to perform a parametric study for different parts of the study and to include 18432 different cases. The model was used for a preliminary reliability-based analysis including 800,000 second-order analysis to assess the reliability corresponding different critical slenderness ratios.

LIST OF SYMBOLS USED

A_f = the cross-sectional area of longitudinal FRP reinforcement;

A_{fc} = area of GFRP bars in compression side;

A_{ft} = area of GFRP bars in the tensile side;

AFRP = aramid fiber-reinforced polymer;

A_g = gross cross-sectional area of concrete;

A_{st} = the cross-sectional area of longitudinal steel reinforcement;

BFRP = basalt fiber-reinforced polymer;

COV = coefficient of variation;

CFRP = carbon fiber-reinforced polymer;

d_1 = the centroid distance of bars in the compression side;

d_2 = the centroid distance of bars in the tensile side;

d_C = the distance between the neutral axis and the resultant of the internal compressive forces of concrete;

d_{fc} = the distance between the neutral axis and the centroid of the compressive GFRP bars;

d_{ft} = the distance between the neutral axis and the centroid of the tensile GFRP bars;

e_0 = initial eccentricity;

E_c = modulus of elasticity of concrete;

E_f = modulus of elasticity of FRP bars;

E_{fc} = modulus of elasticity of GFRP bars in compression;

E_{ft} = modulus of elasticity of GFRP bars in tension;

E_s = modulus of elasticity of steel rebar;

EI = effective stiffness;

EI_D = experimental flexural stiffness corresponding to design strength (when the concrete reaches the design strain of 0.003 mm/mm per ACI 318-19);

EI_{GC} = experimental flexural stiffness corresponding to crushing of GFRP bars in compression;

EI_i = the calculated stiffness based on i^{th} equation provided in Table 5.6 (i =1 to 10);

EI_{peak} = experimental flexural stiffness corresponding to peak load;

EI_{SP} = experimental flexural stiffness corresponding to concrete spalling;

F_C = the resultant of internal forces of concrete in compression;

F_{fc} = the internal force of GFRP bars in compression;

F_{ft} = the internal force of GFRP bars in tension;

f'_c = compressive strength of concrete;

f'_{fcu} = ultimate crushing strength of GFRP bars in compression;

f'_{ftu} = ultimate rupture strength of GFRP bars in tension;

f'_y = yield strength of steel rebar;

$GFRP$ = Glass fiber reinforced polymer;

h = the width of column cross-section;

I_f = moment of inertia of all GFRP bars in the concrete column;

I_g = moment of inertia of gross cross-section of concrete (chamfers are excluded);

I_s = moment of inertia of all steel bars in the concrete column;

k = Effective length factor (unbraced length) of the concrete columns;

l = The length of the column;

M = Bending moment;

M_C = internal moment resistance due to compressive concrete;

M_{CC} = the bending moment corresponding to concrete crushing;

M_D = the experimental moment at design load;

M_{D_1st} = the experimental first-order moment calculated at design load;

M_{fc} = internal moment resistance due to compressive GFRP bars;

M_{ft} = internal moment resistance due to tensile GFRP bars;

M_{GC} = the bending moment corresponding to crushing of GFRP bar in compression;

M_u = the moment capacity of the specimens at their peak load;

M_{ult} = the ultimate factored moment;

M_{u_1st} = the experimental first-order moment calculated at peak load;

n = modular ratio (the ratio of modulus of elasticity of GFRP bars to concrete);

P = axial load;

P_{CC} = the axial load corresponding to concrete crushing;

P_{cr} = critical buckling load;

P_D = design load (when the concrete reaches the design strain of 0.003 mm/mm);

P_{GC} = the axial load corresponding to crushing of GFRP bar in compression;

P_o = nominal axial strength at zero eccentricity;

P_u = the axial capacity of the specimens at their peak load;

P_{ult} = the ultimate factored load;

r = the radius of gyration;

RC = reinforced concrete;

STD = standard deviation;

$\varepsilon_{CC,c}$ = the compressive strain of GFRP bar in compression side corresponding to crushing of concrete;

ε_{fcu} = the ultimate crushing strain of GFRP bars in compression;

ε_{fc} = the strain of GFRP bars in compression;

ε_{ftu} = the ultimate rupture strain of GFRP bars in tension;

ε_{ft} = the strain of GFRP bars in tension;

$\varepsilon_{GC,c}$ = the compressive strain of GFRP bar in compression side corresponding to crushing of GFRP bars in compression;

$\varepsilon_{peak,c}$ = the compressive strain of GFRP bar in compression side corresponding to peak;

ε_y = yield strain of steel rebar;

δ = moment magnification factor;

δ_{calc} = calculated moment magnification factor;

δ_{test} = experimental moment magnification factor;

Δ = lateral displacement at mid-span;

Δ_{axial} = the axial displacement of the specimens at their peak load;

Δ_{CC} = the lateral displacement corresponding to concrete crushing;

Δ_{GC} = the lateral displacement corresponding to crushing of GFRP bar in compression;

$\Delta_{lateral}$ = the lateral displacement of the specimens at their peak load;

λ = slenderness ratio;

ρ = reinforcement ratio;

ψ = the curvature of the column at the mid-section.

ACKNOWLEDGMENTS

I would like to thank my supervisor Dr. Pedram Sadeghian for his dedicated support, motivation, and encouragement during my journey in this PhD program. Also, I would like to thank Dr. Fadi Oudah for his support and assistance on chapter 6 of the thesis which is related to the reliability-based analysis. I wish to extend my appreciation to my committee members, Dr. Farid Taheri, and Dr. John Newhook, for their helpful comments on my thesis and constant support during my journey, as well as my external examiner, Dr. Berahim Benmokrane for his precious time and comments which improved the quality of the thesis. I would like to thank Dr. Fenton, Dr. Liu, and Dr. El Naggar for their helps during my PhD journey in Dalhousie University. For experimental studies, Jordan Maerz and Brian Kennedy were fantastic technicians who helped a lot during building and testing concrete specimens. Also, I would like to thank my colleagues (Dillon Betts, Raghad Kassab, Brandon Fillmore, Daina MacEachern, SeyedAli Hosseini, Abdelmoneim El Naggar, Aidan McCracken, Krishna Priyanka Garikapati, Kumari Bandarage, Ahmed Mahgoub, Mostafa Jafarian Abyaneh, Ali Iranikhah, and Ahmad Almallah), technical staff (Jesse Keane and Blair Nickerson), and civil office (June Ferguson and Shelley Parker) at the Department of Civil and Resource Engineering, for their support and help. Finally, I would like to thank my parents, Mohammad Khorramian and Azadeh Baziar for their motivation, support, and care throughout my educational journey, and especial thanks to my sister, Newsha Khorramian whose support was very effective. There are many other great friends of mine who helped me in this journey by their friendship. I would like to thank them all.

CHAPTER 1 INTRODUCTION

1.1 GENERAL

The fact that engineers have chosen concrete as one of the main materials for constructing structural members for a long time shows that there are many concrete structures old enough to be replaced or strengthened. In addition to aging issue, to comply with load demands for code revisions, to compensate flaws of construction, or to improve load-bearing capacity of existing structures, strengthening techniques can assist engineers. Among strengthening materials, CFRP laminates have outstanding physical characteristics, such as high tensile strength and modulus of elasticity, and light weight which make them appropriate for strengthening purposes. There have been two main different approaches for strengthening structures with FRP composites. One of them is wrapping concrete members with FRP sheets to provide confinement while the second approach is applying longitudinal FRP sheets to the surface of concrete either by bonding them directly to the concrete surface or by using near surface mounting (NSM) technique and embedding FRP strips inside the concrete at the surface. In the second approach, the FRP sheets or strips can be only used in the tensile side of the flexural members but not the compression side, due to the believes and guideline restrictions for using them in compression. Therefore, the assessment of compressive behavior of FRP sheets in compression required more studies. The same restrictions applied to the FRP bars in compression while their corrosion resistance characteristic along with their physical properties makes them suitable for harsh environmental conditions where the possibility of observing steel corrosion is high.

To clarify the subject of the current research, the thesis is divided into two major categories called “New Construction” and “Strengthening”. For concrete columns reinforced with GFRP bars, the term “New construction” is used, while for the existing steel reinforced concrete (RC) columns strengthened with FRPs, the term “Strengthening” is opted to separate them in two different topics of discussion. It should be mentioned that many different topics were covered in this thesis whose common point is the use of longitudinal elements. Therefore, for the first part of the thesis (i.e. new construction topic), the effect of longitudinal GFRP bars in concrete columns as internal reinforcement was considered while for the second part of the thesis (i.e. strengthening), the use of longitudinal FRPs as external reinforcement was considered.

1.1.1 New Construction

As an alternative to steel reinforcing bars in structural concrete members, GFRP bars have been used in construction industry mainly to improve the structural systems by avoiding corrosion. The corrosion resistance characteristic of GFRPs make them a suitable option for concrete structures prone to harsh environmental condition to help their functionality last longer which leads to less repair and maintenance costs in addition to save the valuable monumental structures. Moreover, GFRP bars are also lighter than conventional steel reinforcing bars, thus, leading to easier installation. Also, when electromagnetic transparency is demanded such as in buildings containing (magnetic resonance imaging) MRI units, GFRP bars could prevent the potential damage and unforeseen consequences. The strength of GFRP bars is higher than the conventional equivalent structural steel, however, there is no yielding characteristic for GFRP bars and their modulus of elasticity is considerably lower than steel which make the structures less stiff and allow more

displacements. Furthermore, GFRP bars cannot be bent and any curved shape must be considered at the time of manufacturing. Overall, GFRP bars have been recognized as a strong and accepted alternative material for usage in concrete slabs and beams, however, their usage in compressive members has not been widespread. Therefore, more research in this area is required to reveal the behavior of the GFRP bars for reinforcing concrete columns, especially for slender concrete columns which has not been investigated strongly. The demand for substitution of steel reinforcing bars in the corrosion prone regions from one side, and the lack of experimental assessment of the behavior of GFRP bars in concrete columns from the other side, were the motivation to design an experimental and analytical evaluation program to figure out the behavior of the concrete columns reinforced with GFRP bars.

1.1.2 Strengthening

The concrete structures have been widespread in the past decades because of their advantageous constructional features such as their strength and flexibility in design. Therefore, there are many concrete structures that are aged and required to be either replaced with another structure or rehabilitated to make sure that their functionality as well as strength criteria would be satisfied. The presence preservation of some of the old structures can be strongly demanded by the societies that own them for different reasons which might limit the mentioned options just to the renovation one instead of building a new structure. Moreover, financial comparison of theses two solutions might make the strengthening of structures more rational than the other ones. Furthermore, the need to comply with load demands dictated by new code revisions and improving the load carrying capacity of the structures can be fulfilled by repairing the current structures. To retrofit the

existing concrete structures, FRPs are one of the most reasonable options because of their outstanding physical characteristics which are comparable to steel while they are lighter and can be handled easier. In form of wraps, FRPs have been accepted as a great material to enhance the confinement of the wrapped member, especially for concrete columns. Moreover, the stiffness and strength of beams and slabs can be increased using FRP sheets or laminates attached on the tensile side of them using appropriate adhesives. However, their usage in compression is under question and is not accepted by the current design guidelines although there are researches that show their ability to improve the strength and stiffness characteristics of structural components in compression, especially for the case of slender concrete columns whose stiffness enhancement might be considerably affected by the longitudinal strengthening system. Therefore, in the current thesis, the effect of longitudinal CFRP strips and transverse FRP wrapping strengthening systems were investigated through experimental programs as well as modeling parts to figure out the characteristics of the strengthening system. It should be mentioned that in the experimental program, different length of wrapping (from strap to full wrapping) and different wrapping materials (carbon, basalt, and glass FRP wrapping was used as wrapping materials) was considered to show their effectiveness on providing the lateral support for longitudinal FRPs. For the sake of comparison specimens without any longitudinal FRP (i.e. only wrapped specimens) were tested in the experimental program. It should be highlighted that the performance of only wrapped specimens is better when wrapped with carbon, in comparison to glass. However, glass was considered in the program due to its lower cost.

1.2 THESIS STRUCTURE

The thesis is structured so that the first two chapters introduces the main concerns and objectives of the study briefly. It should be mentioned that the literature review is spread out in the introduction of chapter 3 to chapter 11. The first two chapters are introductory, chapters 3 to 6 explain the research on GFRP bars in concrete columns for new construction, chapters 7 to 11 show the studies performed on the use of FRPs in strengthening of the existing structures, and chapter 12 summarizes the findings and show a conclusion and recommendation for the study.

Chapter 3 to 6 form a part of study which presents experimental and numerical investigations on GFRP reinforced concrete columns and are related to the application of GFRP bars in new constructions. First, in chapter 3, the behavior of short concrete columns reinforced with GFRP bars were assessed through an experimental study. Also, an analytical-numerical model was developed and the compressive behavior of GFRP bars in compression was studied via a parametric study using the developed model. In chapter 4, the characterizations of GFRP bars in compression was addressed to give an understanding of material properties for GFRP bars using a new test method. After completion of this studies, chapter 5 shows the largescale experimental tests on slender concrete columns. A model was developed, and a parametric study was conducted to assess the behavior of slender GFRP reinforced concrete columns. As a conclusion of the part of study on the effect of GFRP reinforced concrete columns, chapter 6 presented an extensive case study using the model to find the effect of slenderness on the percentage drop of load in the concrete columns reinforced with GFRP bars and the change in the mode of failure by considering the difference between first order and second order analysis. As a conclusion

to the study of slenderness effects, a reliability-based approach and Monte Carlo simulation was used for the first time to assess the reliability index of the current proposed critical slenderness ratios.

Chapter 7 to 11 form a part of study which presents experimental and numerical investigations on longitudinal CFRP laminates for strengthening of existing reinforced concrete columns. In chapter 7, the near-surface-mounted (NSM) technique for strengthening of concrete columns was examined using a numerical-analytical model and experimental tests. The main issue with the NSM system of strengthening is the limited space for increasing the reinforcement ratio of FRP laminates due to space limitations for grooves. Thus, in the rest of the study, the FRP laminates were applied to the surface of columns, bonded without any grooves. Chapter 8 introduces an experimental study on the behavior of the rectangular concrete columns reinforced with longitudinal CFRP bonded laminates. The effect of different systems of transverse strips, and partial wrapping was examined for stabilizing the behavior of the longitudinal laminates and control their debonding and buckling. The results showed that partial wrapping and strips are not a good solution and does not prevent the laminates from buckling. Chapter 9 investigated the behavior of longitudinal CFRP laminates bonded on circular concrete columns with full wrapping. The experimental study was aimed to find a hybrid system of longitudinal CFRP laminates and transverse GFRP wrapping to control the buckling of the CFRP bars and change their mode of failure by assisting them reach their material level failure. It should be mentioned that, in general, the term “hybrid” is used when a combination of steel and FRP reinforcement is used in concrete member. The latter is attributed to the difference in the behavior of the material (i.e. ductile material with plastic deformations in steel versus

elastic material without permanent deformations). However, in this document the term "Hybrid" is used to show longitudinal CFRP stirps and GFRP or CFRP transverse wrapping system regardless of steel reinforcement in the concrete column. The study showed that by providing enough lateral support, the buckling of CFRP laminates can alter to the crushing of CFRP laminates. The experimental was aimed to validate the applicability of the system on small scale tests. It should be noted that the results showed that the wrapping system is more effective for strengthening of short columns. However, the hybrid system mainly was proposed for strengthening of slender concrete columns where the secondary effects are considerable and wrapping system is not as effective. Thus, Chapter 11 continues the study for the slender concrete columns by testing the large scale slender circular columns. Also, a model was developed to further investigate the behavior of the hybrid system. Inside the modeling a confinement model was used which was developed in chapter 10. The recommendations and conclusions are presented in chapter 12 as the conclusion of the study.

This thesis chapters are briefly summarized in the following:

- **Chapter 1** introduces the main core of the research and the thesis structures.
- **Chapter 2** defines the objectives of the research.
- **Chapter 3** presents the experimental and numerical investigation of the behavior of GFRP bars in short concrete columns. This chapter has been published: Khorramian, K., and Sadeghian, P. (2017). Experimental and analytical behavior of short concrete columns reinforced with GFRP bars under eccentric loading. *Engineering Structures*, 151, 761-773.

- **Chapter 4** presents a new test method to characterize compressive the material properties for GFRP bars. This chapter has been published: Khorramian, K., and Sadeghian, P. (2019). Material Characterization of GFRP Bars in Compression Using a New Test Method, *ASTM, Journal of Testing and Evaluation*, 49(2), DOI: 10.1520/JTE20180873.
- **Chapter 5** presents a study on the behavior of slender concrete columns reinforced with GFRP bars both experimentally and numerically. This chapter is under revised and under review: Khorramian, K., and Sadeghian, P. (2020). Experimental Investigation of Short and Slender Rectangular Concrete Columns Reinforced with GFRP Bars under Eccentric Axial Loads, *ASCE, Journal of composite for construction*.
- **Chapter 6** presents a study of secondary moment effects and assess the reliability index of the critical slenderness ratio for FRP reinforced concrete columns. This chapter has been accepted for a conference: Khorramian, K., and Sadeghian, P. (2020). A preliminary Reliability-Based Slenderness Limit of GFRP Reinforced Concrete Columns. *8th International Conference on Advanced Composite Materials in Bridges and Structures*, Sherbrooke, QC, Canada.
- **Chapter 7** presents a study on the behavior of NSM strengthening system for concrete columns. This chapter has been published: Khorramian, K., and Sadeghian, P. (2019). Performance of High-Modulus Near-Surface-Mounted FRP Laminates for Strengthening of Concrete Columns, *Composite Part B*, 164, 90-102.
- **Chapter 8** presents a study on the behavior of rectangular concrete columns strengthened with bonded longitudinal laminates and partial wrapping system. This

chapter has been published: Khorramian, K., and Sadeghian, P. (2018). Strengthening Short Concrete Columns Using Longitudinally Bonded CFRP Laminates, *ACI special publication-327*, 24.1-24.14.

- **Chapter 9** presents a study on validation of a hybrid strengthening system of longitudinal high modulus CFRP laminates and transverse GFRP wraps for short columns. This chapter is under review: Khorramian, K., and Sadeghian, P. (forthcoming). Hybrid System of Longitudinal CFRP Laminates and GFRP Wraps for Strengthening of Existing Concrete Columns, *under review*.
- **Chapter 10** presents the development of a new confinement model for FRP wrapped concrete columns to be used for modeling of the hybrid system. This chapter is submitted: Khorramian, K., and Sadeghian, P. (forthcoming). Plasticity-Based Ultimate Condition and Confined Stress-Strain Model for FRP Wrapped Circular Concrete Columns, *ready for submission*.
- **Chapter 11** presents the study on the behavior the hybrid system introduced in chapter 9 for slender columns using experimental tests and introduce the numerical modeling of the system using the model developed in chapter 10. This chapter is getting ready for submission.
- **Chapter 12** summarizes the results and presents recommendations for future research.

CHAPTER 2 PROBLEM/OBJECTIVES OF RESEARCH

2.1 PROBLEM DEFINITION

2.1.1 New Construction

There have been many investigations on the behavior of GFRP bars in concrete beams (Alsayed, 1998; Toutanji and Saafi, 2000; Thériault and Benmokrane, 1998; Ashour, 2006; Benmokrane and Masmoudi, 1996), slabs (Deitz et al., 1999; El-sayed et al., 2005; Michaluk et al., 1998; Newhook et al., 2002), bridge decks (Benmokrane et al., 2006; Berg et al., 2006; Mufti et al., 1993), and walls (Galati et al., 2006; Hamilton Iii and Dolan, 2001). As a result, the use of GFRP bars have become widespread in structural applications where bending capacity is needed. However, the application of GFRP bars in concrete columns has been limited, although multiple researchers performed different studies on GFRP bars in concrete columns (Afifi et al., 2013; Hadhood et al., 2017; Hadi and Youssef, 2016; Hales et al., 2016; Jiang and Teng, 2012; Zadeh and Nanni, 2013; Mirmiran et al., 2001). It is believed that GFRP bars are not effective in load bearing capacity of the concrete columns, and even in some guidelines such as ACI 440.1-15 (2015), the contribution of GFRP bars in compression is neglected. Other guidelines such as CAN/CSA S806-12 (2012) or fib Bulletin 40 (2007) mentioned the same restriction which requires the neglection of the GFRP bars in compression. According to the study performed by Choo et al. (2006) analytically and De Luca et al. (2010) experimentally the neglection of the compressive bars is conservative. However, Tobi et al. (2012) found that the contribution of GFRP bars and steel bars in concrete columns are very close to each other. Hales et al.

(2016) tested high strength slender concrete columns reinforced by GFRP bars and confined by GFRP spiral and found them an acceptable system. Furthermore, Mohamed et al. (2014) and Khorramian and Sadeghian (2017) observed the compressive strain levels for GFRP bars in compression which were higher than the defined crushing strain of the concrete in compression. These contrasts arise from lack of experimental data base for GFRP reinforced concrete columns in comparison to the steel RC columns. The database is even smaller for slender concrete columns reinforced with GFRP bars although their importance is not less than short columns.

As quickly mentioned, the literature indicates that there are unknowns and controversial opinions regarding the behavior of GFRP bars in concrete columns. There are doubts about modulus and strength of GFRP bars in compression and the possibility of their premature crushing and/or buckling in concrete columns. Lack of standard method for testing GFRP bars in compression has also caused a gap of data regarding the corresponding mechanical properties. Thus, more research is needed to evaluate if there is a safety issue regarding compressive behavior of GFRP bars in concrete. Moreover, as considering an accidental load eccentricity is mandatory in column design, the compressive behavior of GFRP bars in concrete columns under combined axial load and bending moment needs to be investigated more in-depth to address their effectiveness for more realistic cases. On the other hand, the slenderness limit for concrete columns reinforced with GFRP bars are less than steel RC columns. The slenderness limit or the critical slenderness ratio is a limit which determines the required type of analysis for columns. If the slenderness of the column (i.e. the ratio of the effective length over gyration radius) is lower than the slenderness limit, the column is categorized as short, if the slenderness ratio of column is higher than the

slenderness limit, the column is considered as a slender column. While ACI 318-14 (2014) established the critical slenderness ratio of 22 for steel RC columns, Mirmiran et al. (2001) proposed 17, Zadeh and Nanni (2013) proposed 14, and Abdelazim et al. (2020) proposed 18 for critical slenderness ratio. The latter result in having more GFRP RC columns in the category of slender columns where the second order effects or large deformations cannot be neglected in the design procedure which emphasizes the importance of studying slender GFRP RC columns. It should be mentioned that for the design of short columns, the secondary moment effects can be neglected and performing a first order analysis is sufficient for design purposes, while for slender columns, the secondary moment effects should be considered, and a second order analysis is required. The difference between the first-order and second-order analysis is that for second order analysis, the effect of the lateral displacement of the column on magnifying the bending moment in the columns is considered while for the first order analysis, only the initial eccentricities of the columns are considered in the analysis. From design perspective, the design of a concrete column can be affected by considering different critical slenderness ratios. For example, comparing slenderness limit of 18 versus 14, if columns of a building are designed based on slenderness ratio of 14, more columns would be considered as slender for the design which means the secondary moment should be considered in assessment of the capacity of more columns. In turn, lower capacities would be found which lead to bigger dimensions of the columns. Therefore, selection of a lower critical slenderness ratio, although is conservative, it has adverse effects on the economy of the building projects from structural design point of view.

The other issue for slender concrete columns reinforced with GFRP bars would be the adjustment of current design equations and methods such as the moment magnification method that is used for steel RC columns, which considers the second order effects, for slender GFRP reinforced concrete columns, especially defining the stiffness of the cracked concrete section.

All mentioned concerns lead to the idea of proposing an extensive experimental program to evaluate the behavior of slender concrete columns reinforced with GFRP bars. An analytical-numerical model, thereafter, can be developed and verified against the test data for further investigation performed via a parametric study. Finally, a design-oriented approach would be proper to study the slenderness ratio, and the required modifications in the moment magnification method to be adjusted for slender GFRP reinforced concrete columns.

2.1.2 Strengthening

Application of FRPs could be found in various forms such as applying them on the outer surface of concrete elements such as beams, slabs, and bridge decks in form of bonded laminates as well as near surface mounted (NSM) strips to increase their ultimate strength and stiffness, or in form of wraps to provide compressive structural members such as columns with confinement and increase their axial capacity. There have been many researches on the application of bonded laminates for strengthening of reinforced concrete beams (Triantafillou and Plevris, 1992; Sharif et al., 1994; Rahimi and Hutchinson, 2001; Buyukozturk and Hearing, 1998; Malek et al., 1998), slabs (Mosallam and Mosalam, 2003; Kim et al., 2008), bridge decks (Alkhrdaji et al., 1999; Tarek and Rizkalla, 2002; Atadero et al., 2005), and on the concrete columns wrapped with FRP (Shahawy et al., 2000;

Hussein et al., 2012; Mirmiran, et al., 1998; Bisby and Ranger, 2010; Hadi, 2007; Toutanji,1999; Sadeghian et al., 2010; Pham et al., 2016). However, limited researches have been conducted on the strengthening influences of FRPs on compressive members using longitudinal components build with FRPs (Gajdosova and Bilcik, 2013; Sadeghian and Fam, 2015; Khorramian and Sadeghian, 2017), mainly due to the fact that the contribution of FRP laminates in load carrying capacity of compressive structural elements have been neglected by the design guidelines (ACI 440.2R, 2008; CAN/CSA S806-12, 2012).

FRP wrapping have been known as a strong tool of strengthening for concrete columns, especially for concentrically loaded columns. For concentrically loaded wrapped concrete columns, the state of stress can be described as a major load in axial direction and two equal lateral minor compression stresses for any element selected from FRP-confined concrete. This state of stress explained would build a compression-compression Mohr circle, which means no tension in concrete would be experienced. In addition, due to presence of three-dimensional stresses, the concrete changes its nature and behave like a ductile material compared to unconfined concrete which is a brittle material. The latter is the reason why a secondary branch for stress-strain of confined concrete exists if enough confining pressure is provided by FRP wraps. In three-dimensional stress space, a plasticity flow rule can be involved for the confined concrete and stress state would flow on the compression meridian of a ductile failure surface. For eccentrically loaded columns, different states of stress can be seen in compression and tensile sides, which allow tensile stresses in concrete and decrease the efficiency of the concrete. Parvin and Wang (Parvin and Wang, 2001) recognized that short columns under eccentric compressive loading can successfully

increase the capacity. Hadi (2006) found out that usage of FRP wraps is effective for eccentrically loaded columns up to a certain margin. Bisby and Ranger (2010) showed that the effectiveness of FRP confinement for circular columns is reduced under combined axial and flexural loading. The other issue is the effect of cross-section on the effectiveness of wrapping system; wrapping for rectangular and square cross-sections is not as effective as for circular cross-sections due to the presence of sharp corners which transmit confining stresses to the concrete (Parvin and Brighton, 2014). Although FRP wraps are very effective for uniaxial loading, longitudinal reinforcement might be needed, especially for slender columns, for combined axial and flexural loading systems to increase the stiffness of the reinforced concrete columns.

Sadeghian and Fam (2015) investigated the effect of bonded longitudinal reinforcements analytically and found it more beneficial for eccentrically loaded slender columns than transverse wrapping, where large bending moments small axial loads exists. Shaat and Fam (2009) examined carbon FRP (CFRP) plates for strengthening of slender steel columns experimentally and analytically whose result showed the effectiveness of the CFRP system in increasing the axial strength of steel columns as slenderness increased. Chaallal and Shahawy (2000) figured out that the performance of bidirectional CFRP fabrics for strengthening of concrete beam-columns would improve their capacity, especially their flexural capacity. Sedeghian et al. (2010) performed experimental study on the behavior of concrete columns longitudinally and transversely strengthened with CFRP laminates and realized that the application of longitudinal layers improves the stiffness and moment capacity of the columns, however, their longitudinal bonded elements were made of fabrics. On the other hand, to achieve this desired stiffness enhancement, the CFRP laminates must

be survived from buckling phenomena to function properly. Khorramian et al. (2017) tested short rectangular concrete columns strengthened with longitudinal bonded CFRP laminates and observed bucking of longitudinal laminates at peak load with and abrupt drop in capacity after experiencing the ultimate load. In the same study, to support the columns partial Basalt wrapping of the concrete column strengthened with CFRP laminates showed to be effective to delay the buckling of laminates. This idea of buckling control allows the longitudinal laminates to last more and stiffen the system, which in turn, could influence the loading path of the slender columns and a gain in axial capacity. Moreover, the sudden break observed after buckling of longitudinal CFRP laminates can be concealed by the selection of a wrapping system that create confinement for the column, as well. Therefore, the combination of CFRP wrapping and longitudinal CFRP laminates for slender columns is a system that can take the advantage of both longitudinal stiffening elements and transverse elements with confinement and buckling support functions.

All mentioned concerns lead to the idea of proposing an extensive experimental program to investigate the behavior of slender steel RC columns strengthened with CFRP laminates. Then, a verified analytical model can be used to identify the effects of the proposed system on the behavior of the strengthened column. Eventually, the study can be extended to consider the effects of the longitudinal CFRP laminates in the equation used in the moment magnification method and propose some modifications for cases that would be strengthened by longitudinal CFRP strips.

2.2 OBJECTIVES

2.2.1 New Construction

- Characterizing the behavior of GFRP bars in compression when using as longitudinal reinforcement for concrete columns.
- Formulizing the behavior of slender GFRP RC columns to increase the available test data for this type of columns.
- Creating an analytical-numerical model to predict the behavior of GFRP RC columns and verifying the proposed model versus available test data.
- Investigating the effect of geometrical and material parameters on behavior of slender GFRP RC columns.
- Study the reliability of the critical slenderness ratio.

2.2.2 Strengthening

- Studying the effect of longitudinal CFRP laminates for strengthening of steel reinforced concrete columns and GFRP wrapping system, which is called hybrid system in this study.
- Creating an analytical-numerical model for concrete columns reinforced with longitudinal CFRP laminates and GFRP or CFRP wrapping.
- Verifying the proposed model versus the available test data.
- Performing a parametric study to understand the effects of different parameters on the behavior of the proposed hybrid system.

REFERENCES

Abdelazim, W., Mohamed, H. M., Afifi, M. Z., and Benmokrane, B. (2020). Proposed Slenderness Limit for Glass Fiber-Reinforced Polymer-Reinforced Concrete Columns Based on Experiments and Buckling Analysis. *ACI Structural Journal*, 117(1), 241–254.

ACI 318-14. (2014). Building Code Requirements for Structural Concrete. *American Concrete Institute.* Farmington Hills, MI.

ACI 440.1R. (2015). Guide for the Design and Construction of Structural Concrete Reinforced Fiber-Reinforced Polymer (FRP) Bars. *American Concrete Institute.* Farmington Hills, MI.

ACI 440.2R. (2008). Guide for the Design and Construction of Externally Bonded FRP Systems for Strengthening Concrete Structures. *American Concrete Institute.* Farmington Hills, MI.

Afifi, M. Z., Mohamed, H. M., and Benmokrane, B. (2013). Strength and Axial Behavior of Circular Concrete Columns Reinforced with CFRP Bars and Spirals. *Journal of Composites for Construction*, 18(2), 04013035.

Alkhrdaji, T., Nanni, A., Chen, G., and Barker, M. (1999). Upgrading the Transportation Infrastructure: Solid RC Decks Strengthened with FRP. *Concrete International: Design and Construction*, 21(10), 37-41.

Alsayed, S. H. (1998). Flexural Behaviour of Concrete Beams Reinforced with GFRP Bars. *Cement and Concrete Composites*, 20(1), 1-11.

Ashour, A. F. (2006). Flexural and Shear Capacities of Concrete Beams Reinforced with GFRP Bars. *Construction and Building Materials*, 20(10), 1005-1015.

Atadero, R., Lee, L., and Karbhari, V. M. (2005). Consideration of Material Variability in Reliability Analysis of FRP Strengthened Bridge Decks. *Composite Structures*, 70(4), 430-443.

Benmokrane, B., and Masmoudi, R. (1996). Flexural response of Concrete Beams Reinforced with FRP Reinforcing Bars. *ACI Structural Journal*, 93(1), 46-55.

Benmokrane, B., El-Salakawy, E., El-Ragaby, A., and Lackey, T. (2006). Designing and Testing of Concrete Bridge Decks Reinforced with Glass FRP Bars. *Journal of Bridge Engineering*, 11(2), 217-229.

Berg, A. C., Bank, L. C., Olivia, M. G., and Russell, J. S. (2006). Construction and Cost Analysis of An FRP Reinforced Concrete Bridge Deck. *Construction and Building Materials*, 20(8), 515-526.

Bisby, L., and Ranger, M. (2010). Axial–Flexural Interaction in Circular FRP-Confined Reinforced Concrete Columns. *Construction and Building Materials*, 24(9), 1672-1681.

Buyukozturk, O., and Hearing, B. (1998). Failure behavior of Precracked Concrete Beams Retrofitted with FRP. *Journal of composites for construction*, 138-144.

Chaallal, O., and Shahawy, M. (2000). Performance of Fiber-Reinforced Polymer-Wrapped Reinforced Concrete Column under Combined Axial-Flexural Loading. *ACI Structural Journal*, 97(4), 659-668.

Choo, C. C., Harik, I. E., and Gesund, H. (2006). Strength of Rectangular Concrete Columns Reinforced with Fiber-Reinforced Polymer Bars. *ACI Structural Journal*, 103(3), 452-459.

CSA S806-12. (2012). Design and construction of building Structures with Fiber-Reinforced Polymers. *Canadian Standards Association.*

De Luca, A., Matta, F., and Nanni, A. (2010). Behavior of Full-Scale Glass Fiber-Reinforced Polymer Reinforced Concrete Columns under Axial Load. *ACI Structural Journal*, 107(5), 589-596.

Deitz, D., Harik, I. E., and Gesund, H. (1999). One-Way Slabs Reinforced with Glass Fiber Reinforced Polymer Reinforcing Bars. *ACI Special Publication*, 188, 279-286.

El-sayed, A., El-Salakawy, E., and Benmokrane, B. (2005). Shear Strength of One-Way Concrete Slabs Reinforced with Fiber-Reinforced Polymer Composite Bars. *Journal of Composites for Construction*, 9(2), 147-157.

Fib Bulletin 40. (2007). FRP Reinforcement in RC Structures. *The International Federation for Structural Concrete*, Stuttgart.

Gajdosova, K., and Bilcik, J. (2013). Full-Scale Testing of CFRP-Strengthened Slender Reinforced Concrete Columns. *Journal of composites for construction*, 17, 239-248.

Galati, N., Tumialan, G., and Nanni, A. (2006). Strengthening with FRP Bars of URM Walls Subject to Out-of-Plane Loads. *Construction and Building Materials*, 20(1), 101-110.

Hadhood, A., Mohamed, H. M., and Benmokrane, B. (2016). Experimental Study of Circular High-Strength Concrete Columns Reinforced with GFRP Bars and Spirals under Concentric and Eccentric Loading. *Journal of Composites for Construction*, 21(2), 04016078.

Hadi, M. (2006). Behaviour of FRP Wrapped Normal Strength Concrete Columns under Eccentric Loading. *Composite Structures*, 72(4), 503-511.

Hadi, M. N. (2007). Behaviour of FRP Strengthened Concrete Columns under Eccentric Compression Loading. *Composite Structures*, 77(1), 92-96.

Hadi, M. N., and Youssef, J. (2016). Experimental Investigation of GFRP-Reinforced and GFRP-Encased Square Concrete Specimens under Axial and Eccentric Load, and Four-Point Bending Test. *Journal of Composites for Construction*, 20(5), 04016020.

Hales, T. A., Pantelides, C. P., and Reaveley, L. D. (2016). Experimental Evaluation of Slender High-Strength Concrete Columns with GFRP and Hybrid Reinforcement. *Journal of Composites for Construction*, 20(6), 04016050.

Hamilton Iii, H., and Dolan, C. (2001). Flexural Capacity of Glass FRP Strengthened Concrete Masonry Walls. *Journal of Composites for Construction*, 5(3), 170-178.

Hognestad, E. (1951). A Study of Combined Bending and Axial Load in Reinforced Concrete Members, *Bulletin Series No. 399*. Urbana: University of Illinois.

Hussein, M. E., Al-Salloum, Y. A., Alsayed, S. H., and Iqbal, R. A. (2012). Experimental and Numerical Investigation of Size Effects in FRP-wrapped Concrete Columns. *Construction and Building Materials*, 29, 56-72.

Jiang, T., and Teng, J. (2012). Theoretical Model for Slender FRP-Confined Circular RC Columns. *Construction and Building Materials*, 32, 66-76.

Khorramian, K., and Sadeghian, P. (2017a). Experimental and Analytical Behavior of Short Concrete Columns Reinforced with GFRP Bars under Eccentric Loading. *Engineering Structures*, 761–773.

Khorramian, K., and Sadeghian, P. (2017b). Short Concrete Columns Reinforced with GFRP Rebars Under Eccentric Loading. *CSCE Annual Conference. Vancouver, BC, Canada: Canadian Society of Civil Engineering.*

Khorramian, K., and Sadeghian, P. (2018). Strengthening Short Concrete Columns Using Longitudinally Bonded CFRP Laminates. *ACI Special Publication*, 327, 24-1:10.

Kim, Y. J., Longworth, J. M., and Wight, G. R. (2008). Flexure of Two-Way Slabs Strengthened with Prestressed or Non prestressed CFRP Sheets. *Journal of Composites for Construction*, 12(4), 366-374.

Malek, A. M., Saadatmanesh, H., and Ehsani, M. R. (1998). Prediction of Failure Load of R/C Beams Strengthened with FRP Plate due to Stress Concentration at The Plate End. *ACI structural Journal*, 95, 142-152.

Michaluk, C. R., Rizkalla, S. H., Tadros, G., and Benmokrane, B. (1998). Flexural Behavior of One-Way Concrete Slabs Reinforced by Fiber Reinforced Plastic Reinforcements. *ACI Structural Journal*, 95(3), 353-365.

Mirmiran, A., Shahawy, M., Samaan, M., El Echary, H., Mastrapa, J. C., and Pico, O. (1998). Effect of Column Parameters on FRP-Confined Concrete. *Journal of Composites for Construction*, 2(4), 175-185.

Mirmiran, A., Yuan, W., and Chen, X. (2001). Design for Slenderness in Concrete Columns Internally Reinforced with Fiber-Reinforced Polymer Bars. *Structural Journal*, 98(1), 116-125.

Mohamed, H. M., Afifi, M. Z., and Benmokrane, B. (2014). Performance Evaluation of Concrete Columns Reinforced Longitudinally with FRP Bars and Confined with FRP Hoops and Spirals under Axial Load. *Journal of Bridge Engineering*, 19(7), 04014020.

Mosallam, A. S., and Mosalam, K. M. (2003). Strengthening of Two-Way Concrete Slabs with FRP Composite Laminates. *Construction and Building Materials*, 17(1), 43-54.

Mufti, A. A., Jaeger, L. G., Bakht, B., and Wegner, L. D. (1993). Experimental Investigation of Fibre-Reinforced Concrete Deck Slabs without Internal Steel Reinforcement. *Canadian Journal of Civil Engineering*, 20(3), 398-406.

Newhook, J., Ghali, A., and Tadros, G. (2002). Concrete Flexural Members Reinforced with Fiber Reinforced Polymer: Design for Cracking and Deformability. *Canadian Journal of Civil Engineering*, 29(1), 125-134.

Parvin, A., and Brighton, D. (2014). FRP Composites Strengthening of Concrete Columns under Various Loading Conditions. *Polymers*, 6, 1040-1056.

Parvin, A., and Wang, W. (2001). Behaviour of FRP Jacketed Concrete Columns under Eccentric Loading. *Journal of Composites for Construction*, 5(3), 146-152.

Pham, T. M., and Hadi, M. N. S. (2013). Strain Estimation of CFRP-Confined Concrete Columns Using Energy Approach. *Journal of Composites for Construction*, 17(6), 1–11.

Rahimi, H., and Hutchinson, A. (2001). Concrete Beams Strengthened with Externally Bonded FRP Plates. *Journal of Composites for Construction*, 5(1), 44-56.

Sadeghian, P., and Fam, A. (2015). Strengthening Slender Reinforced Concrete Columns Using High-Modulus Bonded Longitudinal Reinforcement for Buckling Control. *Journal of structural Engineering*, 141, 04014127.

Sadeghian, P., Rahai, A. R., and Ehsani, M. R. (2010). Experimental Study of Rectangular RC Columns Strengthened with CFRP Composites under Eccentric Loading. *Journal of Composites for Construction*, 443-450.

Shaat, A., and Fam, A. Z. (2009). Slender Steel Columns Strengthened Using High-Modulus CFRP Plates for Buckling Control. *Journal of Composites for Construction*, 13(1), 2-12.

Shahawy, M., Mirmiran, A., and Beitelman, T. (2000). Tests and Modeling of Carbon-Wrapped Concrete Columns. *Composites Part B: Engineering*, 31(6), 471-480.

Sharif, A., Al-Sulaimani, G. J., Basunbul, I. A., Baluch, M. H., and Ghaleb, B. N. (1994). Strengthening of Initially Loaded Reinforced Concrete Beams Using FRP Plates. *ACI structural Journal*, 91(2), 160-168.

Tarek, H., and Rizkalla, S. (2002). Flexural Strengthening of Prestressed Bridge Slabs with FRP systems. *PCI Journal*, 47(1), 76-93.

Thériault, M., and Benmokrane, B. (1998). Effects of FRP Reinforcement Ratio and Concrete Strength on Flexural Behavior of Concrete Beams. *Journal of Composites for Construction*, 2(1), 7-16.

Tobbi, H., Farghaly, A. S., and Benmokrane, B. (2012). Concrete Columns Reinforced Longitudinally and Transversally with Glass Fiber-Reinforced Polymer Bars. *ACI Structural Journal*, 109(4), 551-558.

Toutanji, H. A. (1999). Stress-Strain Characteristics of Concrete Columns Externally Confined with Advanced Fiber Composite Sheets. *ACI materials journal*, 397-404.

Toutanji, H. A., and Saafi, M. (2000). Flexural Behavior of Concrete Beams Reinforced with Glass Fiber-Reinforced Polymer (GFRP) Bars. *ACI Structural Journal*, 97(5), 712-719.

Triantafillou, T. C., and Plevris, N. (1992). Strengthening of RC Beams with Epoxy-Bonded Fibre-Composite Materials. *Materials and Structures*, 25, 201-211.

Zadeh, H. J., and Nanni, A. (2013). Design of RC Columns Using Glass FRP Reinforcement. *Journal of Composites*, 17(3), 294–304.

CHAPTER 3 EXPERIMENTAL AND ANALYTICAL BEHAVIOR OF SHORT CONCRETE COLUMNS REINFORCED WITH GFRP BARS UNDER ECCENTRIC LOADING

ABSTRACT

This paper presents experimental and analytical studies on short concrete columns reinforced with glass fiber-reinforced polymer (GFRP) towards characterizing compressive behavior GFRP bars. The experimental program consisted of fourteen 500 mm-long specimens with a square cross-section (150x150 mm) including nine GFRP reinforced (6#5) and five plain concrete specimens. The specimens were tested under concentric and eccentric compressive load up to failure. Three eccentricity to width ratios of 0.1, 0.2, and 0.3 were considered, where the eccentricities applied symmetrically at both ends of simply supported columns. The experimental program showed no crushing of GFRP bars at peak load and the corresponding strain did not reach 50% of their crushing capacity obtained from material test. In addition, an analytical model was developed and verified against the experimental test data. The model considered both material nonlinearity and geometrical nonlinearity. Using the model, a parametric study was performed on the effect of eccentricity, reinforcement ratio, and concrete strength, which confirmed the capability of GFRP bars to sustain high strains without reaching the compressive strain capacity of the bars. The study showed that GFRP bars can be considered as load bearing longitudinal reinforcement of concrete columns and ignoring their effect is not necessary.

3.1 INTRODUCTION

Fiber-reinforced polymer (FRP) composite bars have been used in construction industry as an alternative to steel reinforcing bars (rebars) in concrete structures where high corrosion

resistance is needed (Mallick, 2008). Moreover, glass FRP (GFRP) have a unique electromagnetic transparency which makes them suitable for applications where electromagnetic fields are recognized as critical design criterion (De Luca et al. 2010). There have been many investigations on the behavior of GFRP bars in concrete beams (Alsayed, 1998; Toutanji and Saafi, 2000; Thériault and Benmokrane, 1998), slabs (Deitz et al., 1999; El-sayed et al., 2005; Michaluk et al., 1998), bridge decks (Benmokrane et al., 2006; Berg et al., 2006), and walls (Galati et al., 2006; Hamilton Iii and Dolan, 2001). As a result, the use of GFRP bars have become widespread in structural applications where bending capacity is needed. However, the application of GFRP bars in concrete columns has been limited, although multiple researchers performed different studies on GFRP bars in columns (Afifi et al., 2013; Hadhood et al., 2017; Hadi and Youssef, 2016; Hales et al., 2016; Jiang and Teng, 2012; Zadeh and Nanni, 2013; Mirmiran et al., 2001).

It is commonly believed that GFRP bars are not as effective as steel bars in load bearing capacity of concrete columns. For example, the ACI 440.1 (2015) design guide for GFRP bars neglects the contribution of the GFRP bars in compression and allows the replacement of them with concrete in calculations. Another example is CAN/CSA S806-12 (2012), Canadian standard for design and construction of building structures with GFRP, which allows the use of GFRP bars in concentrically loaded columns only if the designer neglects their contribution in strength. Furthermore, fib Bulletin 40 (2007) mentioned that since the contribution of the compressive GFRP rebars to the load carrying capacity of concrete column is less than the steel rebars, their contribution is ignored.

Choo et al. (2006) performed an analytical study on FRP reinforced concrete columns and mentioned that ignoring FRP rebars in the compression zone may be conservative,

however, they have not checked the compressive strain of FRPs in compression to see whether compressive failure of FRPs occur or not. Also, De Luca et al. (2010) tested large-scale concrete columns reinforced with GFRP bars under concentric compression and concluded that GFRP bars are more susceptible to instability since their compressive strength and stiffness in compression are less than in tension. On the other hand, Tobi et al. (2012) showed the compressive strength of GFRP bars at peak load of concrete columns is 35% of their capacity in tension. They also reported that the contribution of GFRP bars were 10% of column capacity, which is close to steel bars' contribution (12%) which proves that GFRP bars could be used in columns where adequate confinement is provided. Hales et al. (2016) conducted an experimental evaluation of slender high strength concrete columns reinforced with GFRP bars and found that GFRP spirals and longitudinal bars are a viable system of reinforcement for short and slender columns. Mohamed et al. (2014) studied the performance of concrete columns reinforced with longitudinal FRP bars and determined that carbon FRP (CFRP) and GFRP bars experienced the compressive strain of 0.004 and 0.007 mm/mm which confirm that the compressive FRP bars are effective in load-carrying capacity of columns. Also, Khorramian and Sadeghian (2017) and Fillmore and Sadeghian (2017) experienced similar results in experimental investigation of concrete columns and observed that GFRP bars can sustain a significant level of compressive strains in columns.

As shown, the literature indicates that there are unknowns and controversial opinions regarding the behavior of GFRP bars in concrete columns. There are doubts about modulus and strength of GFRP bars in compression and the possibility of their premature crushing and/or buckling in concrete columns. Lack of standard method for testing GFRP bars in

compression has also caused a gap of data regarding the corresponding mechanical properties. Thus, more research is needed to evaluate if there is a safety issue regarding compressive behavior of GFRP bars in concrete. Moreover, as considering an accidental load eccentricity is mandatory in column design, the compressive behavior of GFRP bars in concrete columns under combined axial load and bending moment needs to be investigated more in-depth to address their effectiveness for more realistic cases.

Since the contribution of FRP bars as longitudinal reinforcements of concrete columns has not been recognized by current design guidelines and their effects have been neglected, the industry and design engineers are skeptical of using FRP bars in compression, even ignoring their contribution. In addition, there is no standard test method for testing FRP bars in compression to establish a reliable data platform clarifying all unknown regarding compressive behavior of FRP bars. Manufacturers are also suffering from lack of a standard test method for evaluating the compressive behavior of their FRP products. Therefore, the motivation of this paper was to investigate the characteristics of FRP bars in compression where surrounded by concrete as well as proposing a simple coupon test method for testing FRP bars in compression. The results will help researchers, engineers, and manufacturers to understand better the behavior of FRP bars in compression.

This study focuses on the compressive behavior of GFRP bars in concrete columns under eccentric loading using both experimental and analytical methods for a selected square cross-section and GFRP rebar type which are explained in the following sections. In the experimental part, fourteen medium-scale GFRP reinforced concrete columns were tested under eccentric and concentric loads. In the analytical part, a model was developed and verified to mimic the behavior of the test columns and to perform a parametric study

providing more information about the compressive behavior of GFRP reinforced concrete columns.

3.2 EXPERIMENTAL PROGRAM

The experimental program consisted of testing of GFRP reinforced concrete columns as well as plain ones under concentric and eccentric loads. The major test parameter was load eccentricity. This section starts with details of test matrix and material properties, followed by explanation of fabrication and test set up, and concluded by results and discussion.

3.2.1 Test Matrix

A total of fourteen 500 mm long concrete columns with a square cross section (150×150 mm) were prepared and tested under concentric and eccentric compressive loadings. Nine of these specimens were reinforced with six GFRP bars #5 (16 mm diameter). Four specimens consisting two plain concrete and two specimens reinforced with GFRP bars were tested under concentric axial load and other specimens were tested under eccentric loads at 15, 30, and 45 mm, i.e. 10, 20, and 30 percent of width of the cross-section, respectively. The test matrix is provided in Table 3.1. To name the specimens, a label like "A-ex-y" was used where A, x, and y indicate the column type (P or R), the eccentricity (e0, e10, e20, or e30), and the specimen number (1, 2, or 3), respectively. The column type is identified by "P" for plain (i.e. no reinforcement), or "R" for GFRP reinforced concrete columns. For example, "R-e10-1" means that it is the first specimen reinforced with GFRP rebar and tested under 10 percent eccentricity.

Table 3. 1 Test Matrix

No.	Specimen ID	Eccentricity (mm)	Eccentricity ratio	Reinforcement
1	R-e0-1	0	0	GFRP
2	R-e0-2	0	0	GFRP
3	R-e10-1	15	0.1	GFRP
4	R-e10-2	15	0.1	GFRP
5	R-e10-3	15	0.1	GFRP
6	R-e20-1	30	0.2	GFRP
7	R-e20-2	30	0.2	GFRP
8	R-e30-1	45	0.3	GFRP
9	R-e30-2	45	0.3	GFRP
10	P-e0-1	0	0	Plain
11	P-e0-2	0	0	Plain
12	P-e10-1	15	0.1	Plain
13	P-e10-2	15	0.1	Plain
14	P-e10-3	15	0.1	Plain

3.2.2 Material Properties

A ready-mix concrete with maximum aggregate size of 12.5 mm was used for making the concrete specimens. The concrete strength at the time of testing was 37.0±0.8 MPa by testing three concrete cylinders (100×200 mm). It should be mentioned that the time between testing the beginning to the end of the testing program and the hydration of concrete would lead to higher concrete strength for different specimens during the testing program. For future tests, it is recommended to prepare and test more cylinders in different ages to build the relationship for concrete strength at different ages. To reinforce the concrete specimens, six #5 sand coated GFRP bars with a diameter of 16 mm and nominal cross-sectional area of 197.9 mm^2 were used (Bars were provided by V-Rod LM). The reinforcement ratio of bars is 5.28%. It should be highlighted that this reinforcement ratio is higher than 1% or 2% reinforcement ratio used in practical design which determines due to neglection of contribution of GFRP bars. To determine tensile characteristics of rebars,

five tensile specimens were prepared and tested per ASTM D7205M-06 (2011). The mean and standard deviation of the tensile strength, tensile modulus, and ultimate tensile strain of rebars were evaluated as 629±30 MPa, 38.7±1.5 GPa, and 0.0162±0.0011 mm/mm, respectively. Figure 3.1(a) shows the stress-strain curves.

The compression properties of rebars were also examined by applying pure compression load on five short rebar specimens with a free length twice the diameter of rebars as shown in Figure 3.1(b). In order to eliminate the stress concentration and premature failure at the ends of rebar specimens, two steel caps including a steel hollow cylindrical section with inner diameter of 32 mm and depth of 12.7 mm were used. The caps were filled with a high strength epoxy-based grout to fix the rebar specimens. For the compression test, a spherical platen was used at the bottom of the specimens to align them with the axis of loading minimizing accidental eccentricities. Mode of failure of rebars in compression test was crushing and no buckling observed during the test. The compression strength, compression modulus, and crushing strain of bars at peak were evaluated as 783±74 MPa, 41.2±1.2 GPa, and 0.0190±0.0017 mm/mm, respectively. It should be highlighted that there is no ASTM standard for the compression test.

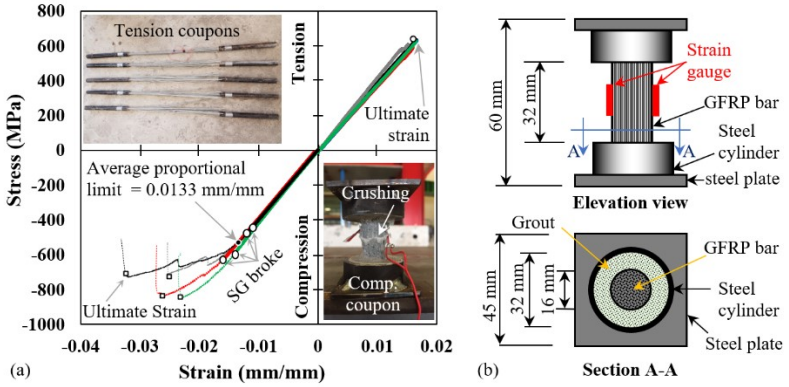

Figure 3. 1 Material test: (a) Stress-strain curves of GFRP bars in tension and compression, and (b) schematic drawing of GFRP bar coupon for compression test

Figure 3.1(a) also shows the stress-strain curve obtained from the compression and tension tests. Two strain gauges used at the center of the compression rebar specimens which were malfunctioned/broken before reaching the ultimate load. Therefore, in order to complete the stress-strain curves for compression specimens, the values of stroke divided by a proper gauge length, which gives the tangent slope of the point at which strain gauge broke, were used as shown in Figure 3.1. The average of compression strains at which the strain gauges were broken was 0.0133 mm/mm called "proportional limit" for compression strains, before which the stress-strain curves are linear. The average proportional limit is 70% of the average crushing strain of 0.0190 mm/mm. Moreover, the corresponding stress to the proportional limit was 534 MPa which was 68% of the average crushing stress (783 MPa). It was observed that the modulus of elasticity of GFRP rebar tested in compression and tension are close to each other. Thus, the assumption of having the same modulus of elasticity in tension and compression is rational and it can be used to model the behavior of GFRP bars. The other observation is the comparatively higher crushing strength of GFRP in compression than its rupture strength in tension. Thus, ignoring compressive strength of GFRP bars and considering their strength and modulus like concrete in compression per ACI 440.1R (2015) is too conservative. Since there is no standard method for testing FRP bars in compression, different values for the compressive strength have been reported. De Luca et al. (2010) reported reductions in the compressive strength and elastic modulus of GFRP bars by up to 45 and 20% with respect to the values in tension, respectively. On the other hand Khan et al. (2015) tested FRP bars both in compression and tension and the results showed considerably higher modulus and strength of tensile tests in comparison to compression tests while Mallick (2008) referred to the typical mechanical properties of

different laminas which shows lower, equal, or higher compressive strength than tensile ones depend on their type. Overall, the performance of GFRP bars in concrete could be different than coupon test. That is another reason for designing the experimental program.

3.2.3 Fabrication

Fresh concrete was casted in wooden molds which was prepared to hold the bars, and the movement of rebar was restricted by two wooden plates with holes, as shown in Figure 3.2(a), that were attached to the end of the mold as presented in Figure 3.2(b). The cover of GFRP rebar was selected as 25.4 mm in each direction which is consistent with available specifications for FRP rebar (2015). The center to center distance between two bars was 41.6 mm, and the distance from the edge of concrete to the center of rebar was 33.4 mm. There were two rows of rebar that each of them consisted of three rebar as is shown in Figure 3.2(a). The specimens were casted in one batch as shown in Figure 3.2(c) and were cured at room temperature by covering with plastic sheets to prevent losing the moisture as presented in Figure 3.2(d). In this experimental program, no tie was applied to the column specimens because of the scale of tests. Since the shear loads are very small because of the size of specimens and symmetric load eccentricities, and the confinement effect was not target of this study, the only possible function of ties could be providing GFRP bars with less unbraced length and prevent premature buckling before the specimens reach their ultimate capacity. In fact, the specimens were designed to allow any possible buckling of GFRP bars especially after the peak load to observe the post peak behavior of the specimens. Since the load concentration at bottom and top of the specimens, where the load applied, was expected to cause a premature failure, both ends of concrete columns were strengthened with two layers of 50 mm wide unidirectional basalt fabric and epoxy

resin. The surface of concrete was grinded at the location of basalt wraps before applying epoxy resin to provide roughness, and wet basalt fabrics stretched on the surface of concrete using hand to be fit to the edges and corners of specimens for end wrappings. The corners were not rounded. Then, the top and bottom surfaces were flattened using a grinder to provide a smooth surface at top and bottom of each specimen.

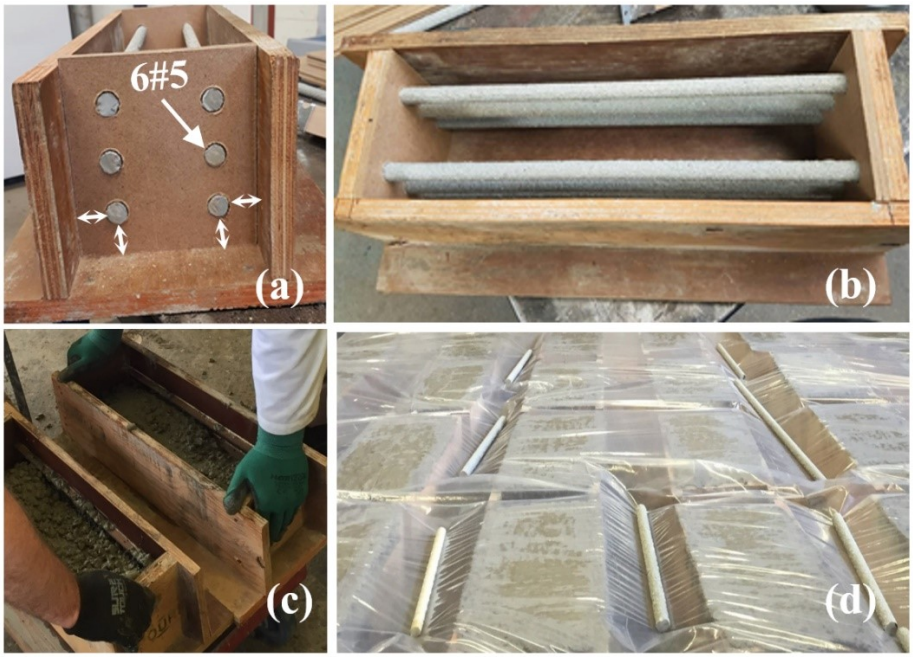

Figure 3. 2 Specimen fabrication: (a) cross section, (b) top view, (c) casting, and (d) curing

3.2.4 Test Set Up

In this study, the boundary condition was pin-pin, which allows rotation at end of column, and load applied with the same eccentricity at both ends of column. Thus, two symmetric steel caps were used at the end of columns to satisfy the boundary condition and loading condition, as shown in Figure 3.3. The steel cap consists of a notched, 30 mm thick steel plate welded on a rigid steel plate (250×250×10 mm). A steel cylinder with the same length of notch, lubricated with grease was put in contact with steel cap through notch which

permits the rotation of the specimen during testing. In addition, the location of steel caps on steel plate was adjusted based on different eccentricity demands using weld. Moreover, four adjustable angle profiles were attached to the steel cap to restrict the column's sway and cause consistent end rotation of steel cap and specimen. To make the steel cap more integrated with the testing specimens, two plastic bags were filled with fresh quick set cement based grout and placed between the interface of steel caps, including the interior surface of adjustable angles and the top steel plate, and the end of concrete specimens, both at top and bottom of column.

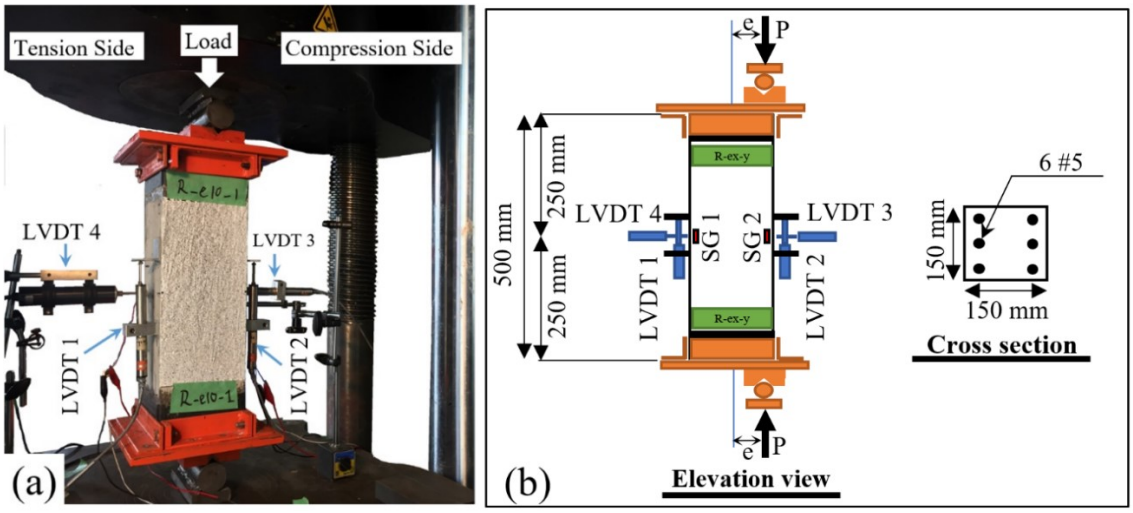

Figure 3. 3 Test set up and instrumentation: (a) testing machine and instrumentation, and (b) schematic testing specimen and reinforcement layout

To analyze the behavior of the specimens, the horizontal and vertical displacement of column as well as the strains at outer surface of bars were measured using a data acquisition system reading the data from strain gauges and linear variable differential transformers (LVDTs) at 0.1 sec. time steps, as shown in Figure 3.3. Vertical LVDTs (i.e. LVDT 1 and 2), with a gauge length of 100 mm, were applied to secure enough data in case of malfunctioned strain gauges. Furthermore, two horizontal LVDTs (i.e. LVDT 3 and 4)

were aligned with the center of concrete columns to measure the deflection of the mid-height of columns. The tests were performed by a 2 MN universal testing machine using a displacement control approach with a rate of 0.625 mm/min.

3.3 Results and Discussion

A summary of the test results is shown in Table 3.2, in terms of the peak load (P_u), the strain of extreme compressive rebar at P_u and its ratio to proportional strain (i.e. 0.0133 mm/mm) and crushing strain (i.e. 0.0190 mm/mm) of GFRP coupons in compression. The table also shows the strain of extreme compressive rebar at $0.85P_u$ (post peak) and its ratio to proportional strain and crushing strain plus failure modes. In this section, the failure modes of test specimens and the effect of eccentricity on the load- displacement and the strain of GFRP bars are discussed.

Table 3. 2 Summary of test results

Specimen group	Peak Load, P_u (kN)	Rebar strain at P_u (mm/mm)	Rebar strain at P_u to prop. limit	Rebar strain at P_u to crush. strain	Rebar strain at $0.85P_u$ (mm/mm)	Rebar strain at $0.85P_u$ to prop. limit	Rebar strain at $0.85P_u$ to crush. strain	Failure mode
P-e0	719.2	-	-	-	-	-	-	CS → CD
R-e0	774.9	0.00275	0.21	0.14	0.00459	0.35	0.24	CC → CS
P-e10	596.3	-	-	-	-	-	-	CS → CD
R-e10	692.8	0.00279	0.21	0.15	0.00416	0.31	0.22	CC → CS
R-e20	578.2	0.00289	0.22	0.15	0.00472	0.36	0.25	CC → CS
R-e30	354.1	0.00361	0.27	0.19	0.00588	0.45	0.31	CC → CS
Average	-	-	0.23	0.16	-	0.36	0.25	-

Note: The results are average of identical specimens. Rebar strain recorded by SG2 (see Figure 3) installed on the middle rebar at the extreme compressive layer; 0.85Pu is related to post peak; NA: not available; CC: concrete crushing; CS: concrete spalling; CD: concrete destruction; prop. limit = 0.0133 mm/mm; crush. strain = 0.0190 mm/mm.

3.3.1 Failure Mode

In this study, three modes of failure were detected including concrete crushing in compression (CC), concrete spalling in compression (CS), and concrete destruction (CD) as presented in Table 3.2. However, no buckling or crushing of GFRP bars were observed before the peak load. After peak load, some bars were locally buckled when the compressive concrete crushed and is not contributed to load bearing system. However, no crushing of GFRP bars were observed even after spalling of concrete and buckling of bars. The concrete crushing (CC) is defined as the state at which the strain at the extreme layer of compressive concrete reaches the strain of 0.003 mm/mm as is considered as the ultimate strain of concrete in compression by ACI 318-14 (2014). Most of time, crushing of concrete followed by the separation of concrete segments from the column which is defined as concrete spalling (CS). For nearly all eccentrically loaded specimens, the crushing and spalling of compressive concrete happened without crushing or buckling of bars as shown in Figure 3.4. For 10 percent eccentricity ratio, the plain concrete specimens (P-e10 group) immediately destructed after the spalling and split in half, which is called concrete destruction (CD) in this document. Overall, for GFRP reinforced specimens, no crushing of GFRP bars were observed after significant lateral deformations and tests were terminated for safety reason.

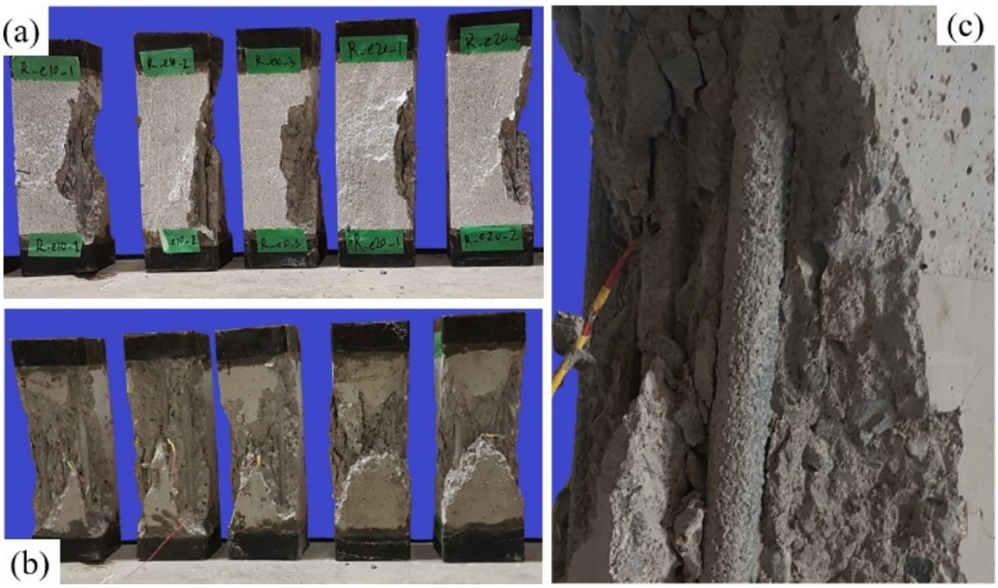

Figure 3. 4 Mode of failures: (a) side view, (b) compression side, and (c) crushed concrete and visually intact compressive rebar

3.3.2 Effect of GFRP Bars on Load-Displacement Behavior

Table 3.2 shows the average peak load of each group of specimens. It shows that the average load capacity of plain specimens under pure axial load was 719.2 kN and it increased to 774.9 kN for GFRP reinforced specimens (i.e. 7.74% increase). At the eccentricity ratio of 0.1, the load capacity of plain specimens was 596.3 kN and it increased to 692.8 kN for GFRP reinforced specimens (i.e. 16% increase). This indicates that GFRP bars contributed to the load bearing capacity of the specimens. Figure 3.5(a) shows the axial load vs. lateral displacement of the GFRP reinforced specimens under 0.1, 0.2, and 0.3 eccentricities. The curves of two identical specimens for each eccentricity are presented. It is observed that as the eccentricity increases, the peak load decreases and the lateral displacement at peak load increases. Overall, the post peak behavior of the GFRP reinforced specimens shows a gradual descending branch without sudden drops which is

compatible with the test observations indicated no crushing of GFRP bars. In the tested specimens with 0.1 and 0.2 eccentricity ratios, different post peak behaviors was observed which could be attributed to probability of having voids inside the concrete, there might be some issues regarding stain recording in compressive bars as compressive fiber micro buckling may influence the strain recordings. Also, in general, the post buckling behavior of columns is controlled by the lateral reinforcement, as they prevent bars from buckling and provide confinement for the concrete core.

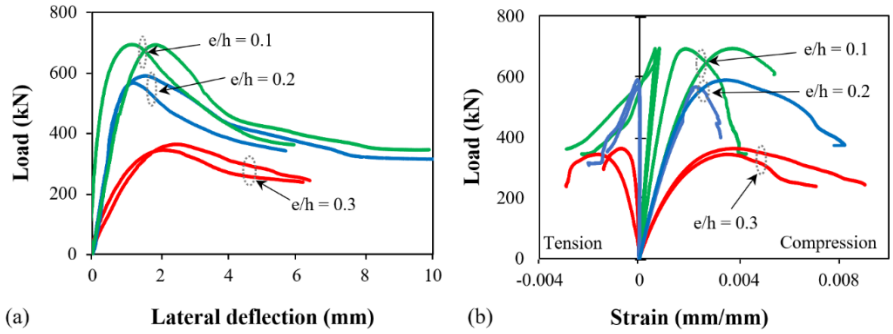

Figure 3. 5 Test results: (a) axial load vs. lateral displacement of specimens at mid-height; and (b) axial load vs. strain of compressive and tensile GFRP bars

3.3.3 Effect of Eccentricity on Strain of GFRP Rebars

Figure 3.5(b) shows the axial load vs. strain of GFRP bars under 0.1, 0.2, and 0.3 eccentricity ratios. The figure indicates, as the eccentricity ratio increased, the strain of GFRP bars at peak load increased. It also shows that GFRP bars sustained considerable level of strain at the compression side and the level of strains in GFRP bars were much less than their crushing strain obtained in coupon test, which means GFRP bars were stressed much less than their capacities in tension and compression. This is due to low modulus of GFRP bars. It should be noted that for one of specimens in group R-e20 shown in Figure 3.5(b), the strain in compressive rebar was not continued to the peak load while the strain

in tensile side was continued to the peak load, which could be due malfunction of the strain gauge in the compression side. In addition, it is observed that for specimens tested under eccentricity to width ratio, both strain gauges attached to GFRP bars experience compressive strain up to failure due to the comparatively low eccentricity. However, after the peak load the tests continued since the displacement control approach used for these experiments and as a result as the stroke displacement increases, the strain at compressive side increases and to satisfy the equilibrium of the section, the depth of neutral axis and compressive area contracted which leads to recording tensile strains after peak load on the tensile side. Table 3.2 shows that when the eccentricity ratio increased from 0 to 0.3, the strain of GFRP bars at peak load increased from 0.00275 to 0.00361 mm/mm. The ratio of recorded strains to proportional limit (i.e. 0.0133 mm/mm) and crushing strain (i.e. 0.0190 mm/mm) from coupon tests were calculated and presented in table 3.2. As shown, at peak load, the average ratios to proportional limit and crushing strain were 0.23 and 0.16, respectively. It means GFRP bars at peak load of specimens had a significant distance to their ultimate strain.

In order to have a better idea about post peak behavior of the specimens, an ultimate condition was defined for the specimen at which the axial load was dropped 15 percent according to a study on combined axial and flexural loads performed by Hognestad (1951). The importance of studying the post peak behavior reveals once the failure of GFRP bars did not observed at the peak load. Therefore, expectation of failure phenomenon such as crushing and buckling tracked up to a certain load after crushing which is 85% after peak load, ($0.85P_u$) in this study. Table 3.2 provides the average ratios of GFRP bar strains at 0.85 of peak load to the proportional limit and crushing strain of the GFRP bars. The results

reveal that, in average, the strain of GFRP bars in compression at 0.85 of peak load were 0.0048 mm/mm, about 0.36 and 0.25 of proportional limit and crushing strain of GFRP rebar, respectively. It means compressive GFRP bars did not reach their capacity in crushing. It is noted that no buckling at peak load were observed which leads to the conclusion that GFRP bars are reliable reinforcing bars in load carrying system at peak load. In addition, even after 15% drop of peak load, the average strain of compressive GFRP bars were just quarter of their crushing strain. It should be highlighted that the values of strain at 0.85 of peak load would be even less than 0.0048 mm/mm if lateral ties limited their susceptibility to local buckling. This also indicates that GFRP rebars should be considered different than steel rebars in design of concrete columns. The contribution of GFRP rebars is a function of their modulus and level of strain at the ultimate condition, rather than tensile/compressive strength of bar materials. In the next section, an analytical model is presented to consider the effect parameters such as reinforcement ratio and concrete strength which were not considered in the experimental program.

3.4 Analytical Studies

This section presents an analytical study to model the behavior of FRP reinforced concrete columns under eccentric loading. The model generates load-strain, moment-curvature, and load-displacement curves considering both material and geometrical nonlinearities using an iterative cross-sectional analysis in MATLAB software.

3.4.1 Model Description

The analytical model consists of a combination of cross-sectional analysis and second-order analysis which depends on column cross-section, rebar layout, material properties, length,

load eccentricity, and boundary condition. The cross-section of a rectangular column consisting of n layers of GFRP rebar is presented in Figure 3.6(a).

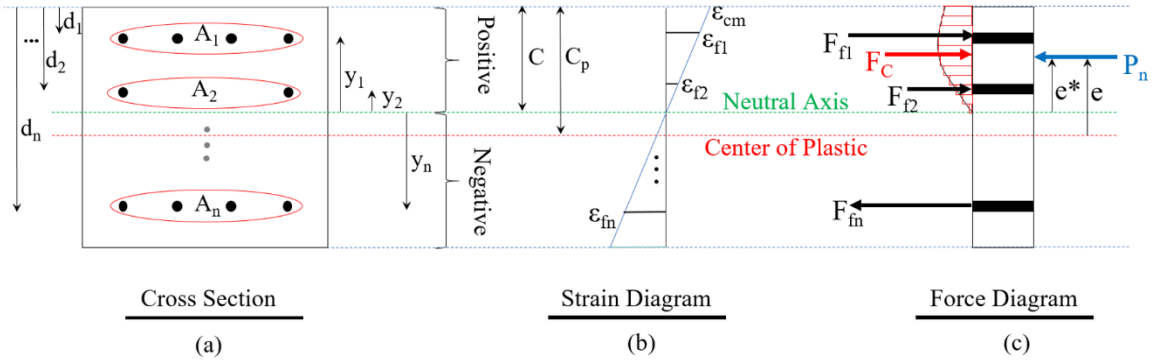

Figure 3. 6 Mechanism of cross-sectional analytical model: (a) section definitions; (b) strain diagram, and (c) force diagram

The cross-sectional area, the distance from the furthest compressive fiber, and the location of each rebar layer from the neutral axis are presented by "A", "d", and "y" in the figure, respectively. Moreover, the depth of neutral axis is shown by "C" and the plastic centroid is presented by "C_P". The sign convention is positive for compression zone and negative in tension zone. It is assumed that the perfect bond exists between the concrete and GFRP bars so that the stains profile is considered as a linear, continuous function through the section for both compressive and tensile sides as shown in Figure 3.6(b). In order to find lateral displacement of column, a moment-curvature relationship at each particular load is needed which is derived by assuming the strain at the furthest compressive fiber in the section, ε_{cm}, and the depth of neutral axis, C, as shown in Figure 3.6, discretizing the section to concrete fibers, finding strains, stresses, and controlling the satisfaction of equilibrium, which is explained in the following. The strain at the location of each rebar layer or at the center of every concrete fiber is calculated by:

$$\varepsilon_i = \left(\frac{\varepsilon_{cm}}{c}\right) y_i \tag{3.1}$$

where ε_i is strain of concrete or GFRP bar, and y_i is the location of GFRP layer, or concrete fiber as shown in Figure 3.6(a). Once the strains are determined, a proper stress-strain relationship for concrete and GFRP bars gives the stresses at each rebar layer or concrete fiber. This model considers the stress-strain relationship of concrete in compression proposed by Popovics (1973) as follows:

$$f_c = \frac{f'_c(\frac{\varepsilon_c}{\varepsilon'_c})r}{r - 1 + (\frac{\varepsilon_{ci}}{\varepsilon'_c})^r} \tag{3.2}$$

where ε_c is the strain of compressive concrete, and f_c is the corresponding stress of concrete, f'_c is the concrete compressive strength, and $E_c$is the compressive modulus of elasticity of concrete. In Equation 3.2, the other parameters are considered as $\varepsilon'_c = 1.7\frac{f'_c}{E_c}$, $E_c = 4700\sqrt{f'_c}$, $r = \frac{E_c}{E_c - E_{sec}}$, and $E_{sec} = \frac{f'_c}{\varepsilon'_c}$, where the values of concrete strength and modulus of elasticity of concrete are in MPa. Since the purpose of this model is to determine the behavior of concrete columns around the peak load, the tensile strength of concrete and tension stiffening effect are neglected to simplify the model. The stress-strain relationship of GFRP bars were considered as a linear, elastic curve up to the crushing in compression or rupture in tension with the same modulus of elasticity for both tension and compression sides as follows:

$$f_f = E_f \varepsilon_f \tag{3.3}$$

where f_f is the stress of GFRP bar, E_f is the modulus of elasticity of bars, and ε_f the strain corresponding to the stress. Although the modulus of elasticity assumed the same, the

strength in tension and compression are different. For each GFRP bar layer, the stress is evaluated using Equation 3.2, and the internal force corresponding to each GFRP layer is derived by multiplication of the cross-sectional area of all bars in that layer and the stress at the center of the layer. The concrete section is discretized to a number of fibers whose stress is evaluated at the center of each layer using Equation 3.1 and Equation 3.2. Then, the internal force of concrete derived by summation of forces in all fibers, which are obtained by multiplying the area of each fiber and its corresponding stress and considering the effects of bars in compression part, as follows:

$$F_c = \sum_{all\ \bar{y}_{c_i} \geq 0} \frac{1}{2}(f_{c_i} + f_{c_{i+1}}) b \delta_y - \sum_{all\ y_{fi} \geq 0} \frac{1}{2}(f_{c_i} + f_{c_{i+1}}) A_{fi} \tag{3.4}$$

where F_c is the concrete internal force, f_{c_i} and $f_{c_{i+1}}$ are concrete stresses at top and bottom of each concrete fiber, b is the width of section, δ_y is the height of each concrete fiber, $\bar{y}_{c_i}$ is the location of center of each concrete fiber from neutral axis, y_{f_i} is the location of compressive GFRP layer from neutral axis, and A_{fi} is the cross-sectional area of each GFRP layer. The number of layers in compressive zone was changed by changing the neutral axis location. In this study, the compressive zone always was divided into layers with 0.25 mm height. Afterwards, the sum of all internal loads gives the total internal force, P_n, which is calculated as follows:

$$P_n = F_c + \sum F_{fi} \tag{3.5}$$

where P_n is the sum of all internal forces, F_c is the internal force of concrete, and F_{fi} is the internal force of i^{th} layer of GFRP rebar. If the sum of internal forces is equal to the applied

load, the equilibrium is satisfied, otherwise, the whole process must be repeated by changing the depth of neutral axis until the satisfaction of equilibrium.

Once the equilibrium of forces is satisfied, the sum of all internal moments about the neutral axis is calculated for concrete and GFRP layers. For each GFRP layer the internal moment is calculated as the internal force times the corresponding distance from neutral axis while the internal moment of concrete fibers from neutral axis is calculated by:

$$M_c = \sum_{all\ \bar{y}_{c_i} \geq 0} \frac{1}{2}\left(f_{c_i} + f_{c_{i+1}}\right) b \delta_y \bar{y}_{c_i} - \sum_{all\ y_{fi} \geq 0} \frac{1}{2}\left(f_{c_i} + f_{c_{i+1}}\right) A_{fi} y_{f_i} \tag{3.6}$$

where, M_c is the concrete internal moment and other parameters are the same as Equation 3.4. Since the moment of internal forces is calculated about the neutral axis while the load eccentricity is measured from the center of plastic, the eccentricity is derived using Equation 3.7. The corresponding bending moment, M_n, for a determined curvature, which is defined as the furthest compressive concrete fiber divided by the depth of neutral axis, is then derived by Equation 3.8.

$$e^* = \frac{M_c + \sum F_{si} y_{si}}{P_n} \quad , \quad e = e^* - c + c_p \tag{3.7}$$

$$M_n = P_n e \tag{3.8}$$

In the equations, M_n is the total internal moment, P_n is the total internal force, e is the eccentricity of internal force from the center of plastic, e^* is the load eccentricity from the neutral axis, C is the depth of neutral axis, C_P is the depth of center of plastic, as shown in Figure 3.6(c), and other parameters are defined earlier. The mentioned process is repeated for a certain load and different values of furthest compressive concrete strain to find different curvatures and corresponding moments which leads to building the moment-

curvature diagram of a given load. In this study, the loading path is derived by assuming the curvature and, in turn, the deflected shape of the column as a sine function as follows:

$$\emptyset(x) = (\emptyset_m - \emptyset_0) sin\frac{\pi x}{L} + \emptyset_0 \quad (3.9)$$

where $\emptyset(x)$ is the curvature function of the column at the distance x from the bottom of the clumn, $\emptyset_m$ and $\emptyset_0$ are the curvatures at the middle and the bottom of the column, respectively, and L is the length of the column. White and Macgregor (2012) implemented a sine shape function for the deflected shape of slender steel-reinforced concrete columns and derivation of moment magnification factor. In addition, the assumption of deflected shape as a sine function was adopted from Broms and Viest (1961), Lloyd and Regan (1996), Claeson and Gylltoft (1998) for steel reinforced concrete columns which was later verified by Sadeghian et al. (2010) for FRP-wrapped concrete columns. Recently, the sine function was implemented for externally bonded concrete columns with longitudinal FRP laminates (Sadeghian and Fam, 2015). Although Mirmiran et al. (2001) used a half cosine function as the deflected shape of GFRP reinforced concrete columns, their model used only to predict the capacity of columns. The model presented in the current study predicts the load displacement, the loading path, strain of concrete and FRP rebars up to the peak load (ascending branch), and after peak load (descending branch) behavior of GFRP reinforced concrete columns, which includes post-buckling behavior of slender columns and the behavior of the columns after concrete crushing for short columns.

By applying the moment-area theorem and having the curvature function, the maximum deflection, δ_m, is derived in the form of Equation 3.10. By integration, Equation 3.10 is rewritten as Equation 3.11.

$$\delta_m = \int_0^{L/2} x\emptyset(x)dx = (\emptyset_m - \emptyset_0)\int_0^{L/2} xsin\frac{\pi x}{L}dx + \int_0^{L/2} x\emptyset_0\, dx \tag{3.10}$$

$$\delta_m = \frac{L^2}{\pi^2}\emptyset_m + \emptyset_0\left(\frac{L^2}{8} - \frac{L^2}{\pi^2}\right) \tag{3.11}$$

At a certain load, by building the moment-curvature and assuming the deflected shape of the column as a sine shape, an iterative process is used to find the deflection of column at its mid-height which is illustrated in Figure 3.7. In this process, three nodes are considered, one at the mid-height of column and two at the ends of column. An initial value of deflection at mid-height of column is assumed and based on that value and the initial eccentricity, the total load eccentricity and in turn, the corresponding moments are computed. Afterward, by using the moment-curvature diagram of that specific load, and reading the points corresponding to the initial and mid-height eccentricities, the values of curvature at the end of column, $\emptyset_0$, and at the middle of column, $\emptyset_m$, are determined.

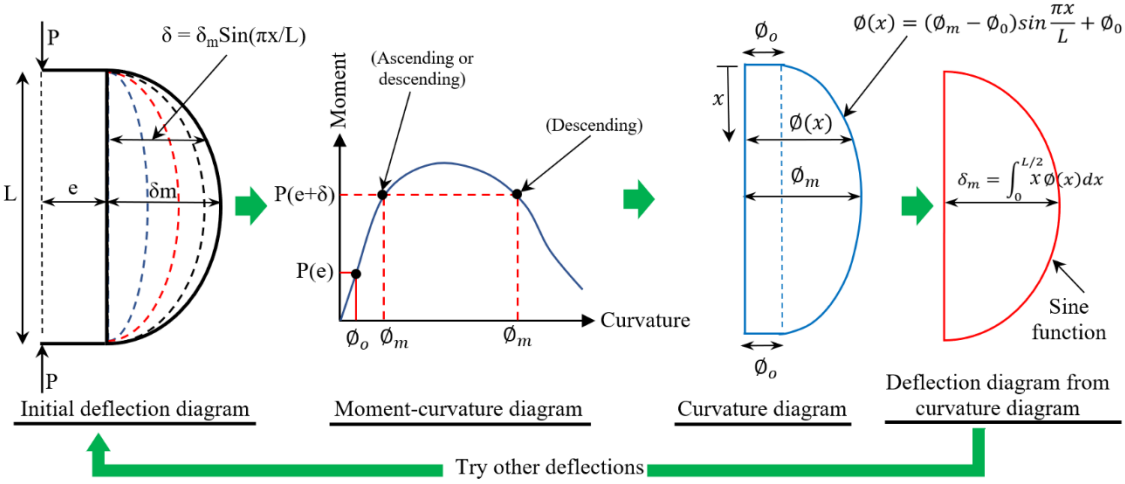

Figure 3. 7 Schematic iteration process for finding deflection at mid height of column

It is worth mentioning that for each step, by changing the axial load, the corresponding moment-curvature diagram was recalculated according to the mentioned process. By

substituting these values into Equation 3.11, the deflection of mid-height of column is computed. If the latter and the assumed deflection are the same, the answer is valid, otherwise, other values for deflection should be tried until a valid answer is found as shown in Figure 3.7. This process begins with an initial deflection at mid-height of column, followed by an increased increment in this deflection, which defines as the displacement step. The difference between the initial deflection and the deflection calculated based on the sine function assumption, which is defined as the control value, is tracked as the initial deflection increases. There is a certain deflection at which the sign of the control value changes, which means in the current step the answer is passed. Therefore, the process of finding a valid answer is started with a smaller displacement step repeatedly until the control value is less than 10^{-10} or approaches zero. In the latter case, if the control value decreased by changing the deflection at mid height of the column, the convergence would happen and a valid answer exists, otherwise, the code cannot find a valid answer. The explained process is the second-order analysis of the column which considers the effect of initial eccentricity and the deflection caused by axial force in finding the final deflected shape of the column. The latter is applied by considering $P(e+\delta)$ as the bending moment used to find the curvatures for the iterative process, as illustrated in Figure 3.7.

The applied load increases in some steps, and after finding a satisfaction of convergence achieved, the values of deflection at mid-height of column, strain of GFRP rebar in compression and tension, the bending moment, and curvature are captured for each load step. This process continues up to the point that the deflections are huge enough to demand moments higher than peak moment in the moment curvature diagram. It should be emphasized that no code limitation for the furthest strain of concrete in compression was

involved in the analysis and deriving the loading path. After the peak load, instead of increasing the load, the load will be decreased in each load step to build the descending branch using the same procedure. The critical control in this process is the record of curvature in each step, which means the curvature is not allowed to be less than the curvature in the past step. This condition helps to find the proper answer when there are two possible answers for a certain bending moment demand in moment curvature diagram for the descending branch as illustrated in Figure 3.7.

3.4.2 Verification

Using the experimental results which was presented in Section 3 of this paper, the proposed analytical model was verified. The analysis performed for three different GFRP reinforced concrete columns. The column used for verification is explained in the experimental section, however, the modulus of elasticity of GFRP bars were considered equal to 38.74 GPa for both tension and compressive bars. For the calculation of axial load-bending moment interaction diagram, the same process as finding the moment-curvature applied using Equation 3.1 through Equation 3.8, however, the strain at the furthest compressive fiber in concrete was taken 0.003 mm/mm as the point of crushing of concrete per ACI 318-14 (2014). Three eccentricity to width ratios of 0.1, 0.2, and 0.3 were used to analysis, and the results are shown in Figure 3.8. There were two sets of experimental data for each case which is reduced to one in Figure 3.8 by taking average of them.

In Figure 3.8(a), the strain of GFRP bars from strain gauges at the mid height of column in both tension and compression side are shown. The results show a good agreement between the strains predicted by the proposed model the average experimental strains. Figure 3.8(b) shows the moment- curvature of the column at mid-height derived from the model which

is in a good agreement with average experimental values calculated using the values of strain gauges. In Fig 3.8(c), the load versus the displacement of the column at its mid-height is shown, where the model predicts the slope and the peak load of the experimental curves very well, and predicts the descending branch up to the point that is numerically achievable. The loading path calculated by model, as shown in Figure 3.8(d), are exactly the same as the ones calculated from average experimental data.

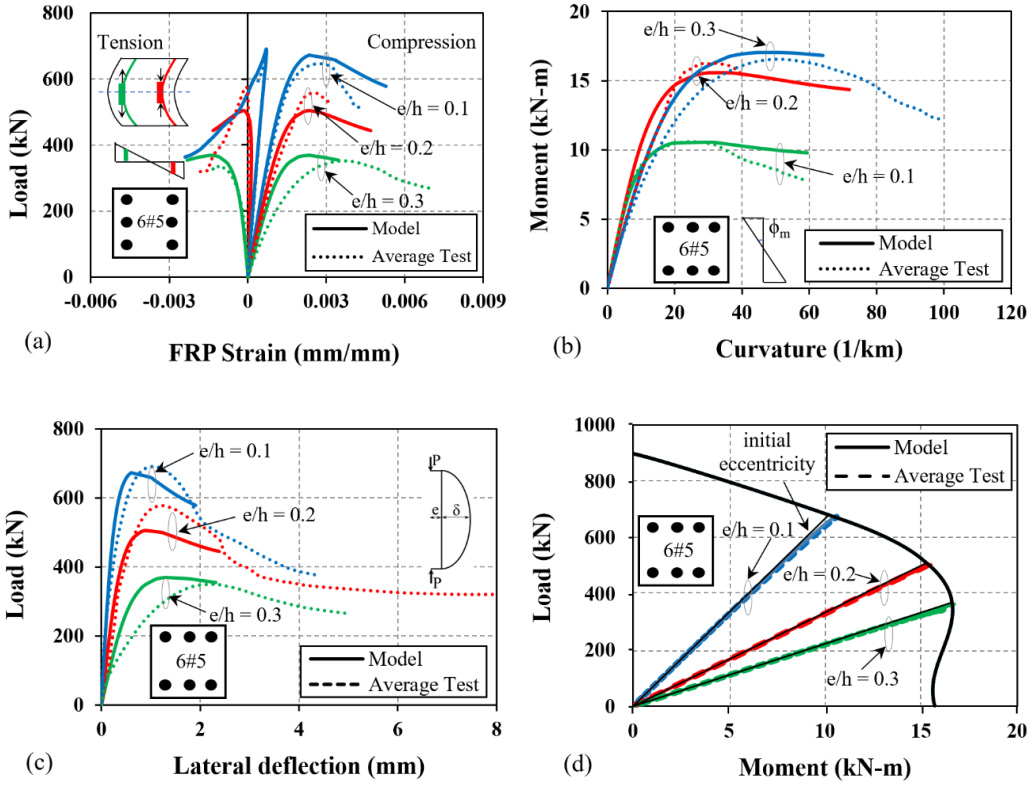

Figure 3. 8 Model verification: (a) axial load vs. strain of compressive and tensile GFRP bars at the mid height, (b) moment vs. curvature diagram at the mid-height, (c) axial load vs. lateral displacement of specimens at the mid-height, and (d) axial load vs. bending moment interaction diagram and loading path curves

The values of peak loads as well as the values of displacement, compressive and tensile strains, moment, and curvature at the peak load derived by analytical model as well as the average of test data are presented in Table 3.3. It is noticed that these average values are

different from average curves presented in Figure 3.8, since only the average of mentioned parameters were shown in Table 3.3. This means, if the peak loads of two specimens with the same eccentricity happens at different displacements, they are not summed in Figure 3.5 while the summation is presented in Table 3.3.

Table 3. 3 Comparison of model and experimental results

Characteristic	e/h (%)	Test	Model	Error (%)	Absolute Error (%)
Peak Load (kN)	10	692.8	667.7	3.62	6.73±6.20
	20	578.2	498.0	13.87	
	30	354.1	363.7	-2.7	
Lateral mid-height displacement at peak load (mm)	10	0.92	0.67	27.18	26.82±8.77
	20	1.11	0.91	17.87	
	30	2.03	1.31	35.4	
Compressive bar strain at peak load (mm/mm)	10	-0.00279	-0.00256	8.28	20.80±14.14
	20	-0.00289	-0.00237	17.98	
	30	-0.00360	-0.00230	36.14	
Tensile bar strain at peak load (mm/mm)	10	-0.00072	-0.00069	3.49	52.19±70.87
	20	0.00008	0.00019	-133.5	
	30	0.00117	0.00140	-19.58	
Moment at peak load (kN-m)	10	11.00	10.46	4.88	6.74±7.00
	20	18.00	15.39	14.48	
	30	16.70	16.84	-0.85	
Curvature at peak load (1/km)	10	20.85	22.19	-6.43	5.58±3.44
	20	29.91	30.44	-1.79	
	30	48.12	44.03	8.51	

Table 3.3 shows that model can predict the peak load and its corresponding bending moment with roughly 7% error. It is seen that as load eccentricity increases, the prediction

of the values of compressive strain of GFRP bars and deflection at the mid-height of the column specimens are less accurate. Moreover, another verification considered in which load displacement behavior and rebar strains of a circular column with a diameter of 305 mm and a length of 1500 mm (slenderness ratio of 20) reinforced with eight #5 GFRP rebars of 16 mm diameter in a study performed experimentally by Hadhood et al. (2017) is verified versus the model as shown in Figure 3.9. The cross-sectional area of each rebar was 199 mm2 and the cover was 25 mm. The modulus of elasticity and strength of GFRP were 54.9 GPa and 1289 MPa, respectively, while the concrete strength was 35 MPa. Four pin-pin columns called C2-P2, C3-P2, C4-P2, and C5-P2 with the load eccentricity of 25,50,100,200 mm, respectively, were verified against the analytical-numerical model. Overall, the results show a good agreement between the results of the proposed model and experimental data. In the next section, using the verified model, a parametric study on important parameters is presented. It should be mentioned that as the model worked for both medium scale tests performed in this study and the large-scale tests performed by Hadhood et al. (2017), the size effect would not be an issue for this testing program.

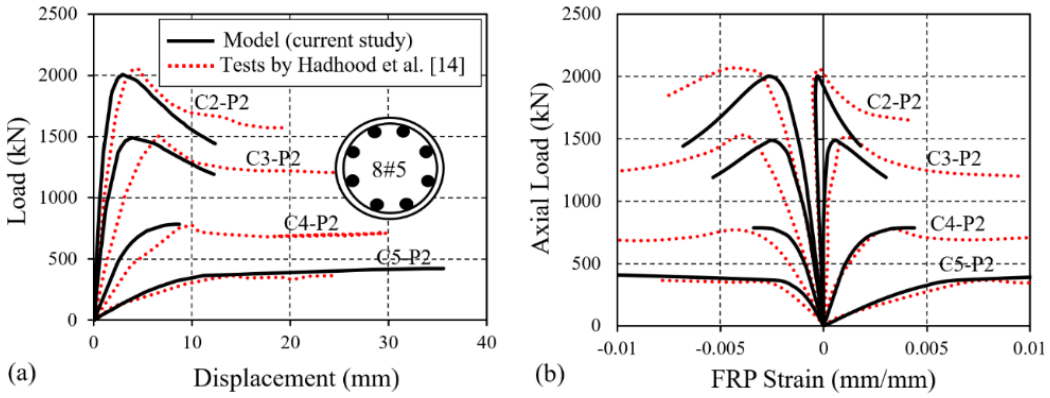

Figure 3. 9 Model verification with circular GFRP reinforced concrete column tested by Hadhood et al. (2017): (a) axial load vs. lateral displacement of specimens at mid-height, and (b) axial load vs. strain of compressive and tensile GFRP bars at the mid-height

3.4.3 Parametric Studies

In this section, the analytical model developed in this study used to perform a parametric study. As one of goals of this study was to find out the effectiveness of GFRP bars in compression, the first subsection is assigned to compressive GFRP bars. In addition, parameters such as the reinforcement ratio, and concrete strength are considered in the following sections.

3.4.3.1 Effect of ignoring compressive bars

In this subsection, the analytical model was used to investigate the effects of ignoring compressive GFRP bars in the behavior of short concrete columns as suggested by major design guides/codes. The parametric study considered the cross-section and material properties introduced in verification section, using different eccentricities. As it is presented in Figure 3.10, there is no significant difference in the load deflection behavior and loading path between considering GFRP bars in compression or neglecting them.

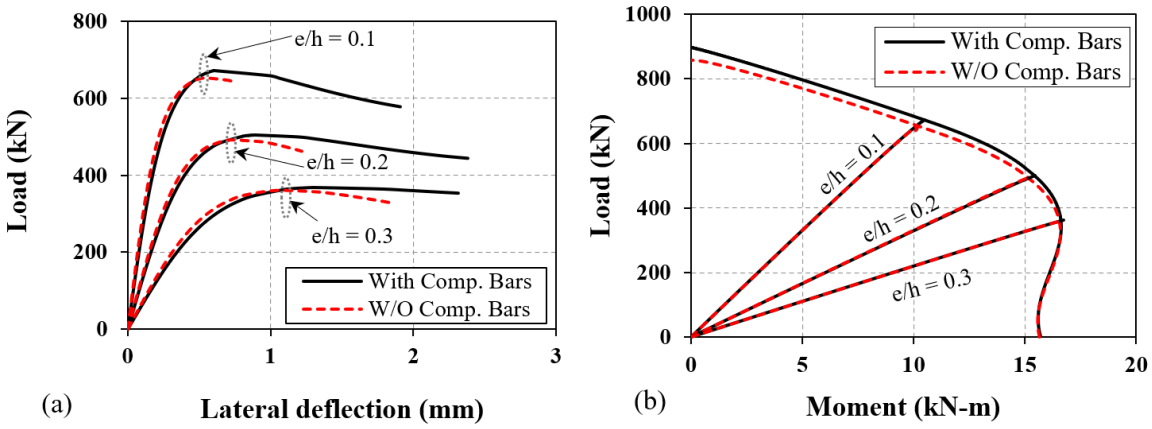

Figure 3. 10 Compressive rebar effect: (a) axial load vs. lateral displacement of specimens at mid-height, and (b) axial load vs. bending moment interaction diagram and loading path

Table 3. 4 Comparison of axial load and corresponding bending moment capacities with and without compressive bars based on parametric study

e/h (%)	@ compressive strain of 0.003						@ Peak load					
	Axial load (kN)			Bending moment (kN-m)			Axial load (kN)			Bending moment (kN-m)		
	with comp. rebar	W/O comp. rebar	Diff. (%)	with comp. rebar	W/O comp. rebar	Diff. (%)	with comp. rebar	W/O comp. rebar	Diff. (%)	with comp. rebar	W/O comp. rebar	Diff. (%)
0	898.9	856.9	4.67	-	-	-	908.7	870.6	4.19	-	-	-
5	762.4	744.4	2.35	6.09	5.87	3.70	762.5	744.4	2.37	6.10	5.87	3.84
10	664.8	645.9	2.85	10.37	10.04	3.23	667.7	645.9	3.27	10.46	10.04	4.07
15	579.4	565.2	2.46	13.44	13.07	2.71	581.8	565.2	2.87	13.54	13.07	3.41
20	495.1	486.3	1.76	15.25	14.95	2.00	498.0	486.3	2.34	15.39	14.95	2.92
25	420.4	415.7	1.11	16.15	15.95	1.22	424.5	415.7	2.07	16.37	15.95	2.56
30	357.0	355.1	0.51	16.44	16.34	0.62	363.7	355.8	2.17	16.84	16.39	2.71
35	306.1	305.5	0.19	16.43	16.38	0.30	315.9	307.6	2.64	17.08	16.53	3.23
40	266.1	266.1	-0.01	16.31	16.30	0.08	279.1	270.0	3.29	17.26	16.58	3.94
45	234.7	234.9	-0.10	16.17	16.17	-0.02	250.5	240.4	4.03	17.44	16.61	4.76
50	209.7	209.9	-0.07	16.04	16.04	0.00	227.8	216.9	4.78	17.64	16.65	5.63
60	172.8	173.0	-0.13	15.83	15.85	-0.08	195.3	181.8	6.90	18.24	16.73	8.27
80	128.3	128.3	0.03	15.63	15.62	0.06	151.9	138.1	9.06	18.79	16.90	10.09
100	102.2	102.1	0.07	15.53	15.52	0.09	124.2	111.8	9.96	19.12	17.07	10.75

Note: e/h is the load eccentricity to width ratio; “comp.”, “Diff.”, and “W/O” are used in the table instead of “compressive”, “Difference”, and “without”, respectively.

However, the interaction diagram shows higher axial capacities using the compressive layer of GFRP bars. Table 3.4 provides the results of the analysis, including the axial and the corresponding bending moment capacities of columns determined by the analytical model, once with considering GFRP bars in compression, and once by neglecting them. For all cases, the axial and bending moment capacities at peak load are higher when GFRP rebar is considered in the calculation which proves the effectiveness of compressive GFRP bars. In addition, the axial and bending moment capacities of the columns at strain of 0.003

mm/mm, which is used for design purpose suggested by ACI 318-14 (2014), approaches to the same values when compression rebar exists or not as the load eccentricity reaches higher values. As presented in Table 3.4. This means that the calculation of column capacity is not different by considering compressive GFRP bars in higher eccentricities.

3.4.3.2 Effect of reinforcement ratio

To investigate the effect of reinforcement ratio in the compressive strain of GFRP bars, a parametric study consisting of eight reinforcement ratios of 1.27, 1.90, 2.25, 3.38, 3.52, 5.07, 5.28, and 7.60% (4#3, 6#3, 4#4, 6#4, 4#5, 4#6, 6#5, and 6#6) were considered. In addition, the columns in three eccentricity to width ratios of 0.1, 0.2, and 0.3 were examined, and all other parameters were the same as the ones used for the model verification. The corresponding compressive strain at peak load are presented in Figure 3.11. The results show that as the reinforcement ratio increases, the strain in compressive rebar increases for all eccentricities, however, their values at peak load does not reach even half of the proportional limit which was introduced in Section 2.2 of this study. The results confirm the compressive strains sustained by the GFRP bars cannot lead to crushing of bars in compression.

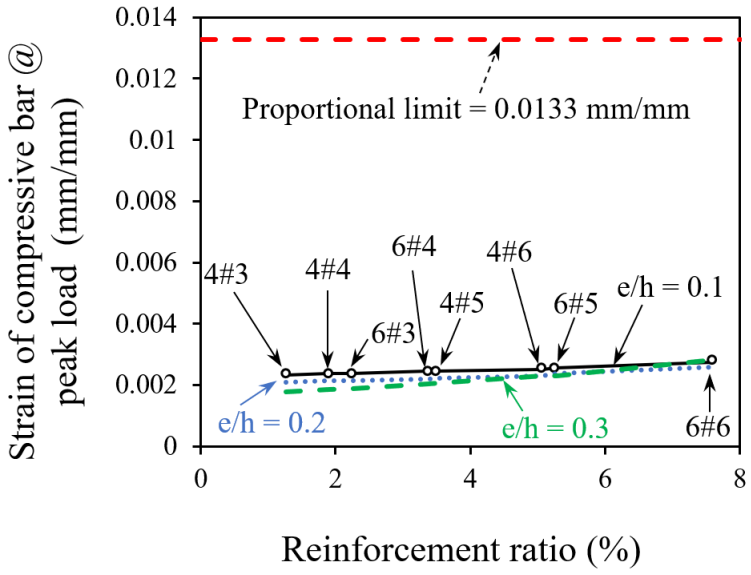

Figure 3. 11 Effect of reinforcement ratio on strain of compressive GFRP bars

3.4.3.3 Effect of concrete strength

In this subsection, a parametric study was performed to reveal the effect of concrete strength on the behavior of compressive GFRP bars. Thirteen concrete strength of 20, 25, 30, 35, 40, 45, 50, 55, 60, 65, 70, 75, and 80 MPa were examined with three eccentricity to width ratios of 0.1, 0.2, and 0.3 while all other parameters were kept unchanged and the same as verification section. The results including the compressive strain at peak load, and where available, the ones at 85 percent drop after peak load are presented in Figure 3.12. The results show that by increasing the concrete strength the compressive strain of GFRP increases in all eccentricities. Again, the results at peak load and 0.85 of peak load show that the compressive strains do not reach their critical value, and in turn, do not cause catastrophic damage in GFRP bars.

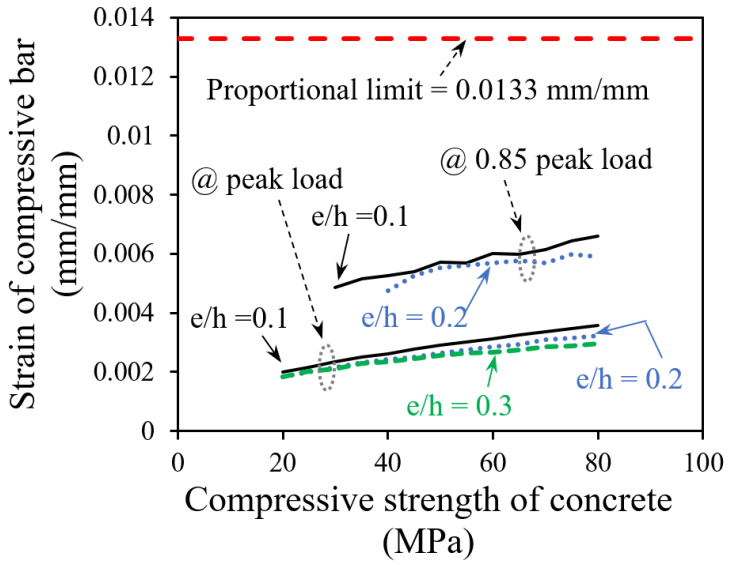

Figure 3. 12 Effect of compressive strength of concrete on strain of compressive GFRP bars

3.4.3.4 Effect of modulus of elasticity of GFRP bars

The effect of modulus of elasticity of GFRP bars on the behavior of compressive GFRP bars were also evaluated using eleven different values ranging from 30 to 80 GPa by analyzing the same model used in verification part and with three eccentricity to width ratios of 0.1, 0.2, and 0.3. The strain of GFRP bars in compression at peak load and 0.85 of peak load, which is recorded at mid-height of specimens, for various modulus of elasticities of GFRP bars and diverse load eccentricities are presented in Figure 3.13. For all eccentricity to width ratios, as modulus of elasticity of GFRP bars increases, the compressive strain of bars at peak load slightly decreases while this value at 85% of peak load is approximately constant, as shown in Figure 3.13. It is observed that the values of compressive strain of GFRP at peak load and 0.85 of peak load are getting closer as eccentricity increases. Similar to other subsections, no damage due to compressive failure

of GFRP is expected at peak load and 0.85 of peak load since the strain values are far below the crushing strength of GFRP bars.

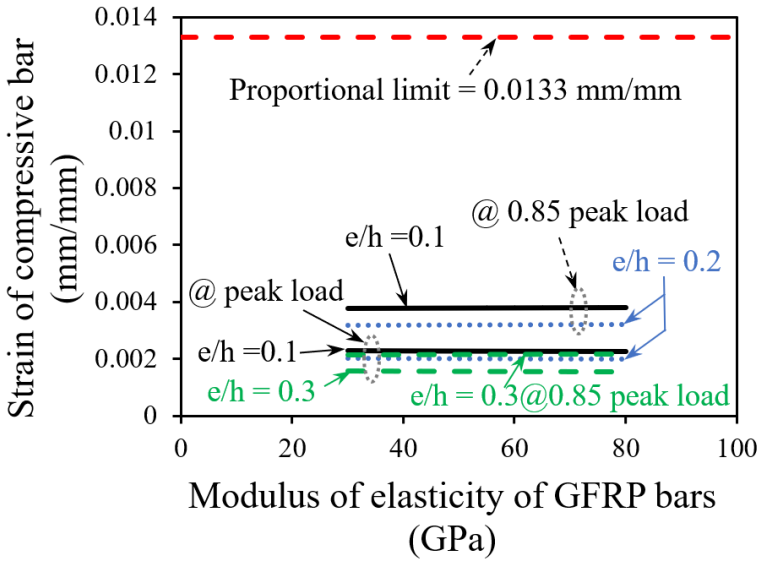

Figure 3. 13 Effect of modulus of elasticity of GFRP bars on strain of compressive bars

3.5 Conclusion

In this study, the performance of short concrete columns reinforced with GFRP bars were investigated experimentally and analytically. A total of fourteen column specimens including nine reinforced and five plain specimens were tested under four load eccentricity to width ratios of 0, 0.1, 0.2, and 0.3. Moreover, an analytical model was developed and verified with test results, and a parametric study was performed using the model. The following conclusions can be drawn:

- Based on coupon tests, the modulus of elasticity of GFRP bars used in this study were close in tension and compression, and the strength in compression was even higher than in tension.

- No buckling or crushing of GFRP bars in compression were observed during the test before the failure of specimens.
- The average of experimental compressive strain of GFRP bars, read from strain gauges after failure of specimens at peak load and 85% after the peak load, were 22% and 16% of the ultimate capacity of bars in compression, derived from coupon test, and were 36% and 25% of the proportional limit of 0.0133 mm/mm. In other words, even the 50% of capacity of compressive GFRP bars were not reached in the tests.
- The proposed analytical model showed very good agreement with the experimental results. The model predicted the peak load of the test specimens with an average error of less than 7%.
- The parametric study revealed that the capacity of column by considering GFRP bars in compression or neglecting them is similar up to the defined crushing strain of concrete 0.003 mm/mm, however there is a gain in capacity at the peak load which requires higher strains; even experimental results did not reach their peak load at 0.003 mm/mm which is compatible with the numerical model.
- Based on the results of the parametric study, it was observed that the values of compressive strain of GFRP bars in compression at peak load and even the compressive strain at 85% of peak load (after peak) did not reach 50% of crushing strain of GFRP bar. From design point of view, for the limited parameters considered in this study, this paper suggests considering GFRP bars in compression as linear elastic materials until concrete reached to its compressive strain limit of 0.003 mm/mm. However, more studies are required to give a design suggestion such as risk assessment study and more comprehensive experimental program considering more variability in parameters.

- Overall, for the selected set of tests and parametric study which has performed in this study, the contribution of GFRP bars in compression can be considered in the design of GFRP reinforced short concrete columns and its ignorance in design guidelines is conservatively recommended.

Acknowledgments

Authors would like to thank Blair Nickerson, Brian Kennedy, Jesse Keane, and Brian Liekens and for their assistance in the lab. The authors would also like to acknowledge and thank NSERC and Dalhousie University for their financial support.

References

ACI 318-14. (2014). Building Code Requirements for Structural Concrete. *American Concrete Institute.* Farmington Hills, MI.

ACI 440.1R. (2015). Guide for the Design and Construction of Structural Concrete Reinforced Fiber-Reinforced Polymer (FRP) Bars. *American Concrete Institute.* Farmington Hills, MI.

Afifi, M. Z., Mohamed, H. M., and Benmokrane, B. (2013). Strength and Axial Behavior of Circular Concrete Columns Reinforced with CFRP Bars and Spirals. *Journal of Composites for Construction*, 18(2), 04013035.

Alsayed, S. H. (1998). Flexural behaviour of concrete beams reinforced with GFRP bars. *Cement and Concrete Composites*, 20(1), 1-11.

ASTM D7205 / D7205M - 06. (2016). Standard Test Method for Tensile Properties of Fiber Reinforced Polymer Matrix Composite Bars. *American Society for Testing and Materials.* West Conshohocken, PA.

Benmokrane, B., El-Salakawy, E., El-Ragaby, A., and Lackey, T. (2006). Designing and Testing of Concrete Bridge Decks Reinforced with Glass FRP Bars. *Journal of Bridge Engineering*, 11(2), 217-229.

Berg, A. C., Bank, L. C., Olivia, M. G., and Russell, J. S. (2006). Construction and cost analysis of an FRP reinforced concrete bridge deck. *Construction and Building Materials*, 20(8), 515-526.

Broms, B., and Viest, I. M. (1961). Long Reinforced Concrete Columns: A symposium. *Transactions, ASCE,* 126(2), 308-400.

Choo, C. C., Harik, I. E., and Gesund, H. (2006). Strength of Rectangular Concrete Columns Reinforced with Fiber-Reinforced Polymer Bars. *ACI Structural Journal*, 103(3), 452-459.

Claeson, C., and Gylltoft, K. (1998). Slender High-Strength Concrete Columns Subjected to Eccentric Loading. *Journal of Structural Engineering*, 124(3), 233-240.

CSA A23.3-14. (2014). Design of concrete structures. *Canadian standard association.*

De Luca, A., Matta, F., and Nanni, A. (2010). Behavior of Full-Scale Glass Fiber-Reinforced Polymer Reinforced Concrete Columns under Axial Load. *ACI Structural Journal*, 107(5), 589-596.

Deitz, D., Harik, I. E., and Gesund, H. (1999). One-Way Slabs Reinforced with Glass Fiber Reinforced Polymer Reinforcing Bars. *ACI Special Publication*, 188, 279-286.

El-sayed, A., El-Salakawy, E., and Benmokrane, B. (2005). Shear Strength of One-Way Concrete Slabs Reinforced with Fiber-Reinforced Polymer Composite Bars. *Journal of Composites for Construction*, 9(2), 147-157.

Fib Bulletin 40. (2007). FRP Reinforcement in RC structures. *The International Federation for Structural Concrete*, Stuttgart.

Fillmore, B., and Sadeghian, P. (2017). Compressive Behavior of Concrete Cylinders Reinforced with Glass Fiber Reinforced Polymer Bars. *CSCE - Leadership in Sustainable Infrastructures.* Vancouver, Canada.

Galati, N., Tumialan, G., and Nanni, A. (2006). Strengthening with FRP bars of URM walls subject to out-of-plane loads. *Construction and Building Materials*, 20(1), 101-110.

Hadhood, A., Mohamed, H. M., and Benmokrane, B. (2016). Experimental study of circular high-strength concrete columns reinforced with GFRP bars and spirals under concentric and eccentric loading. *Journal of Composites for Construction*, 21(2), 04016078.

Hadi, M. N., and Youssef, J. (2016). Experimental Investigation of GFRP-Reinforced and GFRP-Encased Square Concrete Specimens under Axial and Eccentric Load, and Four-Point Bending Test. *Journal of Composites for Construction*, 20(5), 04016020.

Hales, T. A., Pantelides, C. P., and Reaveley, L. D. (2016). Experimental Evaluation of Slender High-Strength Concrete Columns with GFRP and Hybrid Reinforcement. *Journal of Composites for Construction*, 20(6), 04016050.

Hamilton Iii, H., and Dolan, C. (2001). Flexural capacity of glass FRP strengthened concrete masonry walls. *Journal of Composites for Construction*, 5(3), 170-178.

Hognestad, E. (1951). A Study of Combined Bending and Axial Load in Reinforced Concrete Members, *Bulletin Series No. 399*. Urbana: University of Illinois.

Jiang, T., and Teng, J. (2012). Theoretical model for slender FRP-confined circular RC columns. *Construction and Building Materials*, 32, 66-76.

Khan, Q. S., Sheikh, M., and Hadi, M. N. (2015). Tension and compression testing of fibre reinforced polymer (FRP) bars. *Joint Conference of the 12th International Symposium on Fiber Reinforced Polymers for Reinforced Concrete Structures (FRPRCS-12) and the 5th Asia-Pacific Conference on Fiber Reinforced Polymers in Structures (APFIS-2015).* Wollongong, New South Wales, Australia.

Khorramian, K., and Sadeghian, P. (2017). Short Concrete Columns Reinforced with GFRP Rebars Under Eccentric Loading. *CSCE Annual Conference. Vancouver, BC, Canada: Canadian Society of Civil Engineering.*

Lloyd, A. N., and Rangan, V. B. (1996). Studies on High-Strength Concrete Columns under Eccentric Compression. *ACI Structural Journal*, 93(6), 631-638.

Mallick, P. K. (2008). Fiber Reinforced Composites Materials, Manufacturing, and Design. Boca Raton, Florida: *CRC Press*.

Michaluk, C. R., Rizkalla, S. H., Tadros, G., and Benmokrane, B. (1998). Flexural Behavior of One-Way Concrete Slabs Reinforced by Fiber Reinforced Plastic Reinforcements. *ACI Structural Journal*, 95(3), 353-365.

Mirmiran, A., Yuan, W., and Chen, X. (2001). Design for slenderness in concrete columns internally reinforced with fiber-reinforced polymer bars. *Structural Journal*, 98(1), 116-125.

Mohamed, H. M., Afifi, M. Z., and Benmokrane, B. (2014). Performance Evaluation of Concrete Columns Reinforced Longitudinally with FRP Bars and Confined with FRP Hoops and Spirals under Axial Load. *Journal of Bridge Engineering*, 19(7), 04014020.

Popovics, S. (1973). A Numerical Approach to the Complete Stress-Strain Curve of Concrete. *Cements and Concrete Research*, 3(5), 583-599.

Sadeghian, P., and Fam, A. (2015). Improved design-oriented confinement models for FRP-wrapped concrete cylinders based on statistical analyses. *Engineering Structures*, 162–182.

Sadeghian, P., Rahai, A. R., and Ehsani, M. R. (2010). Experimental study of rectangular RC columns strengthened with CFRP composites under eccentric loading. *Journal of Composites for Construction*, 443-450.

Thériault, M., and Benmokrane, B. (1998). Effects of FRP Reinforcement Ratio and Concrete Strength on Flexural Behavior of Concrete Beams. *Journal of Composites for Construction*, 2(1), 7-16.

Tobbi, H., Farghaly, A. S., and Benmokrane, B. (2012). Concrete Columns Reinforced Longitudinally and Transversally with Glass Fiber-Reinforced Polymer Bars. *ACI Structural Journal*, 109(4), 551-558.

Toutanji, H. A., and Saafi, M. (2000). Flexural behavior of concrete beams reinforced with glass fiber-reinforced polymer (GFRP) bars. *ACI Structural Journal*, 97(5), 712-719.

Wight, J. K., and MacGregor, J. G. (2012). Reinforced Concrete Mechanics and Design. *Upper Saddle River*, NJ: Pearson Education Inc.

Zadeh, H. J., and Nanni, A. (2013). Design of RC Columns Using Glass FRP Reinforcement. *Journal of Composites*, 17(3), 294–304.

CHAPTER 4 MATERIAL CHARACTERIZATION OF GFRP BARS IN COMPRESSION USING A NEW TEST METHOD

ABSTRACT

This paper presents a new test method for determining the mechanical properties of glass fiber-reinforced polymer (GFRP) bars in compression including the compressive strength, the compressive modulus of elasticity, the ultimate crushing strain, and their compressive stress-strain curves. The contribution of GFRP bars in compression is currently neglected by major design guidelines related to GFRP-reinforced concrete columns. However, the demand for using GFRP bars is increasing since multiple researchers have shown the effectiveness of GFRP bars in concrete columns. Thus, the need for characterization of the mechanical properties of GFRP bars is increasing while there is no standardized test method to give the compressive properties of these bars. Therefore, in this paper, a new test method is proposed for evaluating the compressive characteristics of GFRP bars. The test method was examined through testing a total of 35 compressive specimens. It was observed that the test method was able to evaluate the compressive characteristics of the GFRP bars successfully. Three different modes of compressive failure were observed which were related to the crushing of GFRP bars in different locations in the bar, but no premature buckling was observed. Moreover, a comparison between tensile and compression characteristics of the GFRP bars showed that the tensile test results is not sufficient to estimate the compressive characteristics and performing compression test is necessary.

4.1 INTRODUCTION

The determination of compressive characteristics of glass fiber-reinforced polymer (GFRP) bars including the compressive strength, modulus of elasticity, and crushing strain, as well as obtaining their stress-strain relationship is the subject of the current paper. The knowledge of these characteristics assists the analysis and design of structural concrete members reinforced with GFRP bars which are under compression such as concrete columns reinforced with GFRP bars, compressive GFRP bars in flexural members (i.e. bridge decks, slabs, and beams), and GFRP reinforced walls (i.e. concrete or masonry walls). In addition, the deflection of the concrete members with GFRP bars in compression is influenced by the compressive modulus of elasticity of GFRP bars. Despite of numerus research on concrete members reinforced with GFRP bars, there is no standardized test method to determine the compressive characteristics of GFRP bars.

Due to the lack of the test method, there are some doubts and gaps in terms of the behavior of GFRP bars in compression which led to lack of study on their compressive characteristics. For example, the current American guideline for design of FRP bars in concrete structures (ACI 440.1R-15, 2015) neglects the contribution of GFRP bars in compression and allows the designer to replace them with the concrete for the design procedure. Moreover, the Canadian guideline for design and construction of building structures with FRP (CAN/CSA S806-12, 2012) allows the use of GFRP bars in concentrically loaded columns if their contribution in the strength of the column is neglected. However, recent studies have shown that neglecting the contribution of compressive GFRP bars in concrete columns is too conservative (Guérin et al., 2018; Fillmore and Sadeghian, 2018; Khorramian and Sadeghian, 2017; Hales et al., 2016;

Mohamed et al., 2014; Tobbi et al., 2012). Recent studies have already changed the trend of the very recent design guidelines. For example, in the draft of the Canadian highway bridge design code (CSA S6-14, 2014) which has been revised to be published in 2019, the longitudinal FRPs are allowed for members subjected to combined axial and flexural loads up to a strain level of 0.002 mm/mm. Therefore, the new trend is toward the acceptance of GFRP bars in compression that emphasizes the necessity of having a standardized test method for evaluating the compressive characteristics of GFRP bars.

It should be noted that recently there have been researches on the seismic behavior of the GFRP reinforced concrete columns (Sheikh and Kharal, 2018; Tavassoli et al., 2015). In terms of seismic applications, unlike the conventional design in which the neglection of GFRP bars in compression is conservative, the neglection of the compressive bars might cause lower expectations in the ultimate load levels and unconservative seismic designs. Thus, a knowledge of compressive characteristics is crucial which is not addressed in any standardizes guideline.

There have been multiple studies on the characterization of GFRP bars in compression. Kobayashi and Fujisaki (Kobayashi and Fujisaki, 1995) studied the compressive behavior of GFRP bars by conducting an experimental program in which the specimens were built so that GFRP bars were embedded in concrete prisms. The specimens were built to have a small space at the center (5 mm) and they were anchored to the testing machine using carbon fiber cones. They mentioned that the concrete prisms were fixed in the testing machine and the load applied only to the FRP bar at the center. They reported the compressive strength of GFRP bars as 30% of their tensile capacity. However, it should be noted that the small space between two concrete prisms was 5 mm which in comparison to

the tested bar diameters (varies from 6 to 10 mm), gives a ratio of free length to diameter of 0.5 to 0.83. It should be noted that this small ratio could cause stress concentration in the specimen plus increasing the chance of the specimen not to experience the unidirectional state of stress which leads to smaller ultimate loads.

Dietz et al. (2003) published a technical note on the properties of 45 GFRP bars with different slenderness ratio in compression. In their study, a single bar size #15 (15 mm diameter) from one manufacturer was tested using a length variation between 50 to 380 mm. Their observation showed three different modes of failure including crushing, buckling, and combined buckling and crushing. It should be noted that they used two threaded rods to install the specimen to the testing machine and inserted the bars inside the rod using a hole with a diameter of 17.5 mm which was slightly wider than the bar diameter and allows slight rotation at the ends of the bars. They reported a similar modulus of elasticity in tension and compression, however, their observation of compressive strength showed 50% less strength in compression in comparison to in tension. The length to diameter ratio for varied between 3.33 to 25.33 and concluded that the GFRP bars tested with free length to diameter ratio of 7.33 can be considered as non-slender bars. They also concluded that the modulus of elasticity of the bars in compression and tension is approximately equal while their compressive strength is about 50% of their tensile strength.

Khan et al. (2015) tested five GFRP and five carbon FRP (CFRP) bars. The GFRP bars were 80 mm long with a diameter of 15.9 mm and were tested by adopting ASTM D695-10 (2010), the standard test compression test method for rigid plastics. Their test included the use of two parallel steel plates at the ends of the GFRP bars and using a displacement control approach with a rate of 1.0 to 1.3 mm/min. It should be noted that the specimens

were directly located on the steel plates to simplify ASTM D695-10 (2010) by replacing the hardened end blocks with flat and high strength steel plates. The failure happened due to separation of fibers which might be due to failure of the resin as they reported in the paper (Khan et al., 2015). They observed that the modulus of elasticity and strength of GFRP bars in tension were 65% and 35% higher than their compressive counterparts, respectively.

Tavassoli et al. (2015) studied circular concrete columns reinforced with GFRP bars under simulated seismic loading for which they tested 15 GFRP bars from two different manufacturers. Their tests were on GFRP bars with a diameter of 25 mm and the free length was chosen based on the spiral pitch in the studied columns (spiral pitch varied between 50 to 275 mm), which gives the ratio of free length to diameter of 2 to 11. It should be noted that they have used steel rods with a hole which holds the GFRP bars in the machine which is similar to Dietz proposed method (Deitz et al., 2003). They observed that the compressive strength of GFRP bars were about 50% of their tensile strength while their modulus of elasticity in compression was similar to the tensile compartment.

Overall, there were various test fixtures for the characterization of GFRP bars in compression by researchers (Kobayashi and Fujisaki, 1995; Deitz et al., 2003; Khan et al., 2015; Tavassoli et al., 2015). However, there were different observations on the compressive strength and modulus of elasticity of these proposed test methods as mentioned earlier. The free length to diameter ratio was varied from test to test, and the modes of failure were either buckling of the bar or buckling of the fibers after separation of the resin, or end crushing. The latter may cause observations which shows less compressive strength for GFRP bars due to buckling (for high free length to diameter ratios)

or because of biaxial state of stress (for very small free length to diameter ratios). In addition, for some of the proposed test methods, there is a room for end rotation that enables the GFRP compressive coupon to experience a combined flexural and axial loading and, in turn, lower compressive capacity. The other issue would be crushing of the bar at the end of GFRP bars whose effect should be on the strength should be studied.

There is a clear gap in terms of capturing the material failure of GFRP bars or at least giving a better prediction of the crushing strength of GFRP bars which is distinct from their buckling. Therefore, the authors' research group started to design a new test method by considering the criteria for GFRP coupons to experience a uniform unidirectional state of stress, to avoid the buckling of GFRP bars or fibers due to separation of resin, and to avoid combined flexural and axial loading of GFRP compressive coupons. The idea of designing a steel cap filled with bonding agent and limitation of the ratio of the diameter to length ratio were motivation of the current paper. The authors' research group attempted testing GFRP bars in compression (Khorramian and Sadeghian, 2017; Fillmore and Sadeghian, 2018) and later presented a preliminary report (Khorramian and Sadeghian, 2018) on the test method. The current paper expands the research to a detailed test method and a comprehensive research program with a total of 35 test specimens with three different bar types from three different manufacturers. Moreover, more in-depth discussion and investigation of failure modes and their correlation to the compressive characteristics is discussed.

4.2 RESEARCH SIGNIFICANCE

Available test data and research on the compressive behavior of GFRP bars is very limited due to lack of a standardized and reliable test method and the neglection of their contribution in structural members when used in compression. However, the current trend of the engineering communities is toward the acceptance of their usage in compression in structural members because of recent studies on the behavior of GFRP reinforced concrete columns. On the other hands, various modulus of elasticity and strength have been reported for GFRP bars in compression by researchers using different methods. However, different modes of failures, such as buckling of GFRP bars or separation of resin and buckling of fibers, end crushing of GFRP bars, as well as different testing conditions, which may cause undesired eccentricity, caused an underestimation of the compressive strength of GFRP bars at the material level. Therefore, this study proposes a test method to characterize the compressive behavior of GFRP bars and presents an experimental study to examine the proposed test method that addresses the issues.

4.3 PROPOSED TEST METHOD

In this section, a new method is proposed for testing GFRP bars in compression. The proposed test method determines the mechanical properties of GFRP bars including the compressive strength, compressive modulus of elasticity, ultimate compressive strain, and their stress-strain curve in compression. As shown in Figure 4.1, the test coupon consists of a GFRP bar which is positioned in a mechanical testing machine and loaded with a certain displacement rate up to the failure while the values of axial load, strain, and displacement are recording.

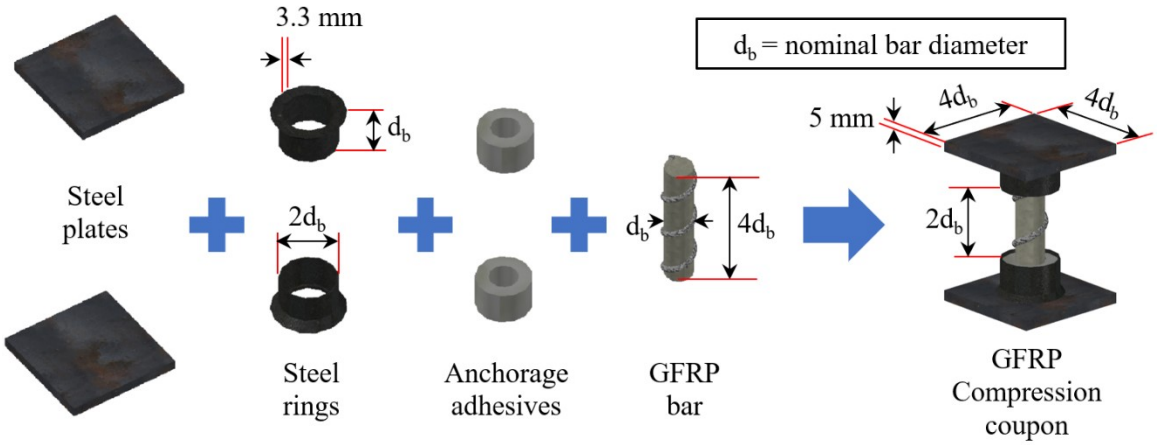

Figure 4. 1 Compressive GFRP coupon components and geometry

The compressive coupon consists of two steel plates, two steel rings, two anchoring adhesive agents, and a GFRP bar, as shown in Figure 4.1. The steel plates are square with a width of four times the diameter of the GFRP bar and a thickness of at least 5 mm. The steel rings are proposed to have a depth of equal to the diameter of the bar, a diameter twice as wide as the diameter of GFRP bar and a minimum thickness of 3.3 mm. The steel rings are welded to the center of the steel plates on top and bottom of the GFRP bar to form a solid unit, called steel cap in this text. The functions of steel cap are holding the GFRP bar, alignment, gripping action, and strengthening the ends of the specimens. It should be noted that the ease of alignment and gripping are the advantages of the use of the steel cap filled with a high strength, fast setting anchoring adhesive. The alignment of the GFRP bar and steel cap achieves when the GFRP bar inserts in the anchoring adhesive filled in the steel cap. It should be noted that the ends of the steel bars must be cut perpendicular to the longitudinal axis of bars, and the bars must be positioned at the center of the steel caps. Then, a level at the flat surface of GFRP bar can give the required alignment. Using a laser alignment tool can ensure the GFRP bar is centered and perpendicular to the steel cap.

Once the adhesive is set, the procedure should be repeated for the second steel cap. The coupons can be prepared quickly using a fast setting adhesive. After setting the adhesive, the steel caps provide a solid capping for the GFRP preventing any premature crushing at the ends. The lateral confinement provided for the end of the GFRP bar by the steel rings filled with adhesive also help further avoiding localized crushing of the GFRP bar at the ends. It is important to prepare the coupon accurately avoiding any eccentricity to give a uniform unidirectional compressive stress in the testing length of the GFRP bar.

The overall length of the GFRP bar is proposed to be four times the nominal diameter of the GFRP bar, which gives a free length to diameter ratio of 2, as shown in Figure 4.1. It should be noted that that the free length of GFRP bars tested in tension shall be 40 times greater than its diameter according to standard testing method for testing FRP bars in tension, ASTM D7205-16 (2016). However, in tension there is no concern about the buckling of GFRP bars or secondary bending moments due to additional displacement of the bar at the middle of the bar. Therefore, the standards for compressive testing of materials limited the free length to diameter or width ratio to avoid buckling to reach the material failure. For instant, the standard test method for testing polymer matrix composites using combined loading compression test fixture, ASTM D6641-16 (2016), suggests the compressive coupons using tabs for flat FRP laminates which gives a free length between tabs as short as the width of the specimen. Moreover, the standard test method for testing concrete cylinders in compression, ASTM C39-18 (2018), recommends the free length over diameter ratio of 2.

4.4 TEST METHOD IMPLEMENTATION

In this section, an experimental program consisting of testing of 35 compressive coupons built according to the proposed test method is explained. The section includes test matrix, fabrication process, and test set up and instrumentation.

4.4.1 Test Matrix

Table 4.1 presents the test matrix for the compressive GFRP coupons which were categorized in seven groups. Each group consists of five identical test specimens which were identified by an ID code as "Gx-y", where "G" stands for group, "x" represents the group number and "y" shows the specimen number in each group. The GFRP bar used in different groups are different from the other groups in terms of bar size, manufacturer, and the tensile characteristics.

Table 4. 1 Experimental Test Matrix

No.	Group	GFRP bar size	Nominal diameter (mm)	Nominal Area (mm^2)	E_t (GPa)	f_t (MPa)	Specimen IDs	M*
1	G1[a]	#4	13.0	126.7	46.0	758.0	G1-1, G1-2, G1-3, G1-4, G1-5	A
2	G2[b]	#5	16.0	197.9	42.5	940.0	G2-1, G2-2, G2-3, G2-4, G2-5	B
3	G3[c]	#6	19.0	285.0	46.0	690.0	G3-1, G3-2, G3-3, G3-4, G3-5	A
4	G4	#4	12.5	129.0	45.6	845.4	G4-1, G4-2, G4-3, G4-4, G4-5	C
5	G5	#4	13.9	129.0	61.1	1175.0	G5-1, G5-2, G5-3, G5-4, G5-5	C
6	G6	#6	19.2	284.0	51.0	884.3	G6-1, G6-2, G6-3, G6-4, G6-5	C
7	G7	#6	20.7	284.0	62.7	1150.0	G7-1, G7-2, G7-3, G7-4, G7-5	C

Note: E_t = tensile modulus of elasticity of GFRP bars; f_t = tensile strength of GFRP bars M*= Manufacturer.
[a] Adopted from Fillmore and Sadeghian (2018).
[b] Adopted from Khorramian and Sadeghian (2017).
[c] Adopted from Khorramian and Sadeghian (2018).

Overall, 35 GFRP coupons were tested from three different manufacturers, three different bar sizes, and seven different tensile characteristics. It should be noted that the tensile

strength and modulus of elasticity of GFRP bars that is presented in Table 4.1 were reported by the manufacturers. The bars tested in Group G1 and G3 were Aslan 100 product, Group G2 was provided by V-Rod LM, and Group G4 to G7 were provided by Tuf-Bar. In addition, the first three groups of specimens were adopted from the previous studies by the same research group as addressed in Table 4.1. However, all of the specimens were built using the proposed test method in this paper.

4.4.2 Specimen Fabrication

The preparation of the specimens directly relates to the quality of the test results, since the alignment and capping requirements must be satisfied in the preparation phase. Figure 4.2 presents the process of the of the preparation of the compressive GFRP coupon.

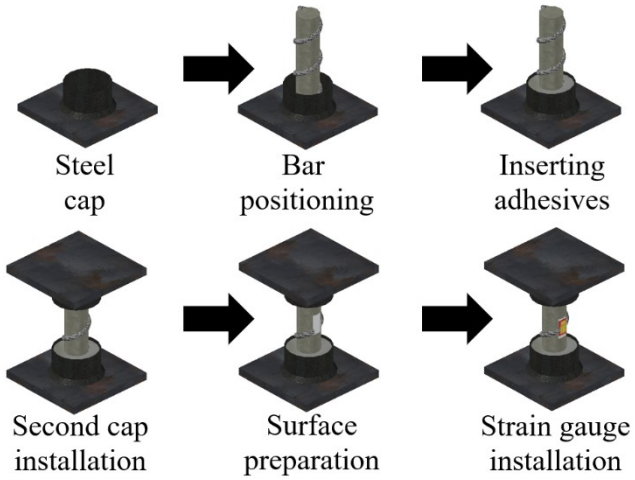

Figure 4. 2 Fabrication process

The steel cap, which consists of a steel plate welded to a steel ring, must be located at a horizontal and flat surface. Afterwards, the steel cap is filled with a quickset anchoring adhesive. Then, the GFRP bar, whose end surface is flat and perpendicular to the longitudinal axis, is positioned at the middle of the steel cap and inserted into the adhesive

until it touches the steel plate. The excessive adhesive should be removed to have the surface of the adhesive is flushed with the edge of steel ring. At this stage, a level should be placed at the top surface of the bar to make sure that the bar is not inclined. It should be noted that the location of the center of the capping should be marked and the GFRP bar must be inserted at the center of the capping. After the adhesive is set, the same procedure can be repeated for the other end of the bar to have both steel caps installed properly at the ends of the GFRP bar.

After the installation of the steel caps, the surface of the GFRP bar at the middle height must be machined shallowly for the installation of the strain gauges at two opposite sides of the bar. At the beginning stages of the research, the strain gauges were installed directly to the machined surface, however, there were observation of weird strain gauge records. The problem later fixed by additional surface preparation before the installation of the strain gauges. The latter achieved by adding high strength glue to the machined surface. Once the glue was set, a file was used to flatten the surface, and two different sandpapers (one course and one fine sandpapers) were used to polish the surface. Figure 4.3 shows the prepared GFRP coupons prepared according to the proposed test method in this study.

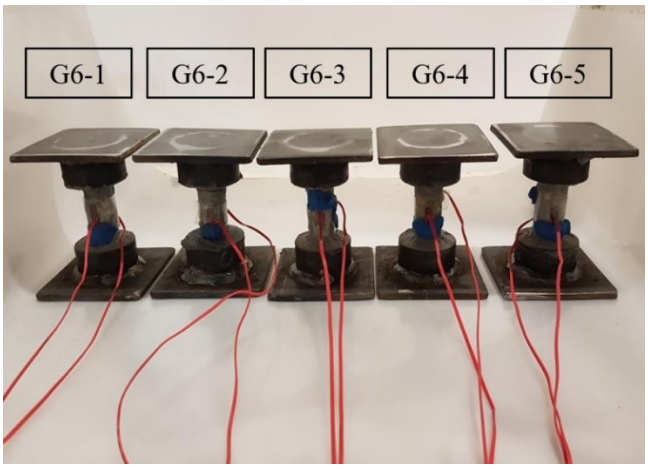

Figure 4. 3 Prepared specimens

4.4.3 Test Setup and Instrumentation

The schematic test set-up is presented in Figure 4.4, where the GFRP coupon is located in a mechanical testing machine. The test specimen must be located properly at the center of the testing machine to be aligned with the machine to produce pure compression loading. Moreover, to avoid accidental eccentricities, a spherical platen is placed beneath the compressive coupon which enables small rotations and the self-centering action. Furthermore, two thick steel plates were placed at the top and the bottom of the specimen (25 mm-thick plates were used in this study), as shown in Figure 4.4, to provide smooth surface at the ends of the specimen and to allow a uniform state of the stress. It should be noted that the weight of these plates was neglected since their corresponding load was very small in comparison to the applied load (i.e. almost 0.02% of the ultimate load).

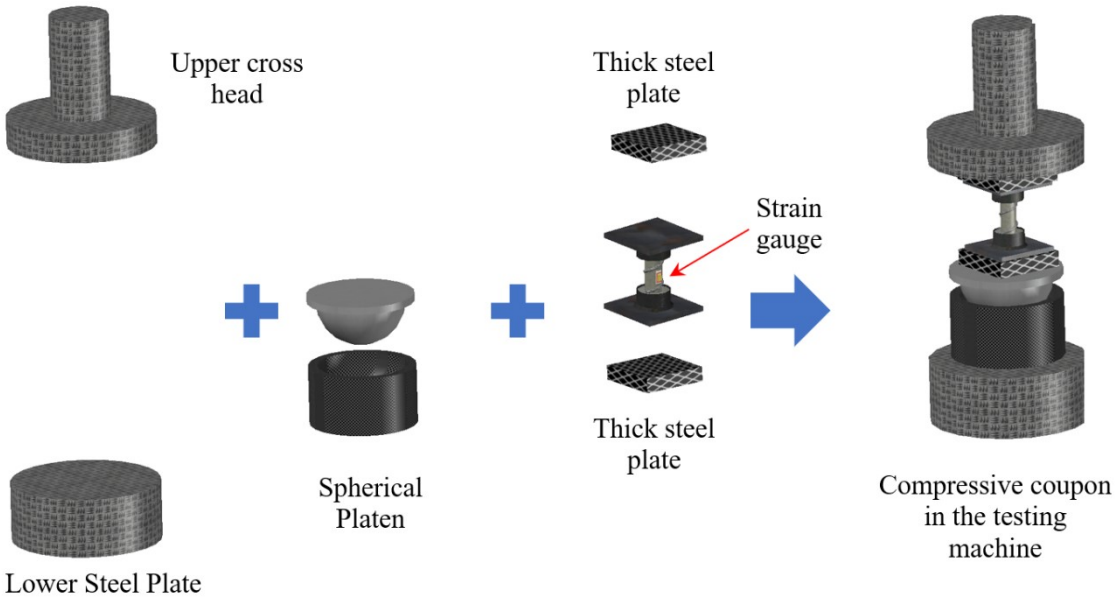

Figure 4. 4 Schematic test set-up

Figure 4.5 shows one of the specimens in the testing machine. To record the data, there are two strain gauges at the opposite sides and at the middle of the GFRP bar, whose average is considered as the strain value read for the calculation of modulus of elasticity. It should be noted that using two strain gauges and averaging the results was suggested by ASTM D7205 for testing FRP bars in tension (ASTM D7205-06, 2016), which is adopted here for testing GFRP bars in compression. The specimens were tested by a 2 MN loading machine with a displacement control approach using a testing rate of 0.5 mm/min. It should be noted that the tests were finished in about 5 minute which is compatible with the suggested rates for the tensile test of FRP bars (ASTM D7205-16, 2016). The sampling rate was 10 data per second which recorded the data including axial strain, axial load, and axial stroke displacement from the machine.

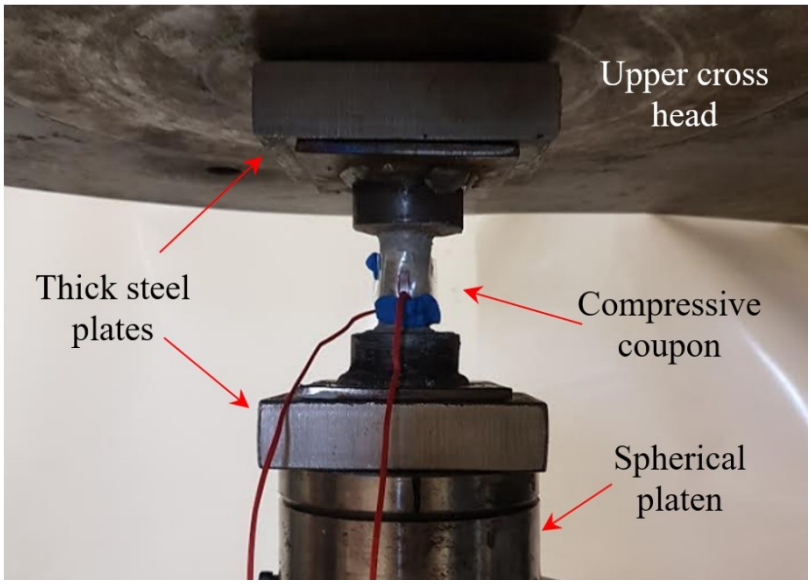

Figure 4. 5 G6-1 specimen in the testing machine

4.5 TEST RESULTS AND DISCUSSION

The results and findings from the experimental tests are presented in the following which includes a discussion in the observation of the modes of failure, the stress-strain curves, the obtained strength and modulus of elasticity of the GFRP coupons, and a comparison of compressive and tensile characteristics of the GFRP bars.

4.5.1 Failure Modes

In this study, three main modes of failure were observed including crushing of GFRP bar only in the free length, crushing of GFRP bars only inside the capping, and crushing both inside the capping and in the free length. It should be noted that no buckling of the GFRP bars were observed for the tested specimens. Figure 4.6 presents some specimens that were crushed in the free length [Figure 4.6(a)] as well as some GFRP coupons that reached the peak load without any visible sign in the free length [Figure 4.6(b)]. The crushing of GFRP bars happened to be at the middle or close to the ends of the bars, and some the failure line was eider horizontal or diagonal, as shown in Figure 4.6(a). It should be noted that crushing in the free length of the specimens observed in 56% of the tested specimens. For the rest of the specimens, there were no visible sign of the failure in the free length, as presented in Figure 4.6(b). However, the stress-strain graphs for both types of failure was similar to each other, and no difference in compressive strength or modulus of elasticity of these two groups were observed.

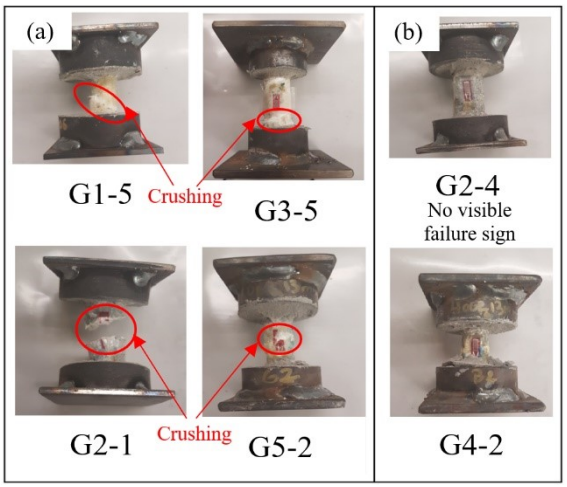

Figure 4. 6 Modes of failure: (a) crushing of GFRP bar, (b) failure inside capping

For further investigations, the specimens were cut in half longitudinally after testing. Three different types of observed failures are presented in Figure 4.7. The observations showed that for the specimens which experienced non-visible failure, the GFRP bars were crushed inside the capping area, while the capping agent and steel cap did not fail. Therefore, the modes of failure for the proposed test method can be categorized as crushing of GFRP bar only in the free length, crushing of the GFRP bar only inside the capping, and crushing of the GFRP bar both inside the capping and in the free length.

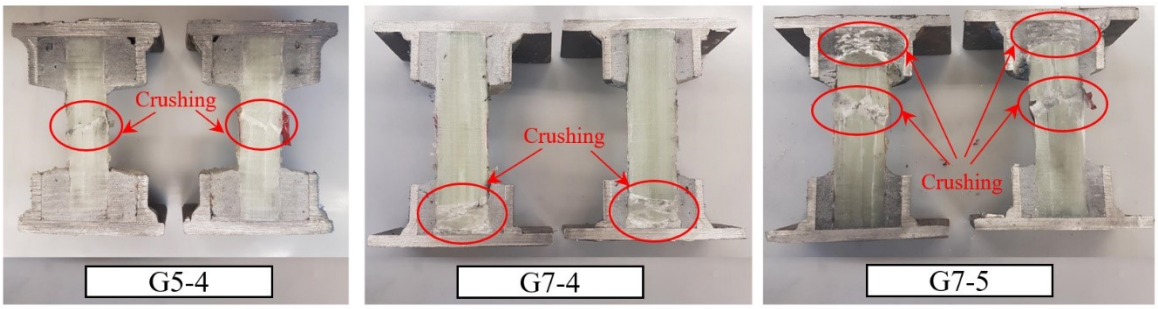

Figure 4. 7 Modes of failure: (a) crushing of GFRP bar in the free length, (b) crushing of GFRP bar inside the capping, (c) crushing of the GFRP bar both inside capping and in the free length

Figure 4.8 presents the failed compressive coupons from group G4 to G7. In terms of modes of failure, it should be noted that crushing of the GFRP bars inside the capping or in the free length were randomly distributed for the tested specimens, as shown in Figure 4.8. In terms the duration of the test, depends on the mode of failure, the test duration varied. For most of the specimens whose failure was only in the free length, failure happened with a sudden drop in the load carrying capacity and the tests were concluded [Figure 4.7(a)]. However, for specimen experiencing the GFRP bar failure only inside the capping or both inside the capping and in the free length, the tests last longer [Figure 4.7(b) and 4.7(c)]. For the latter case, it could be implied that the failure was progressive, started locally from some fibers, and propagated to reach the final crushing of the whole bar as well as dropping in the load capacity.

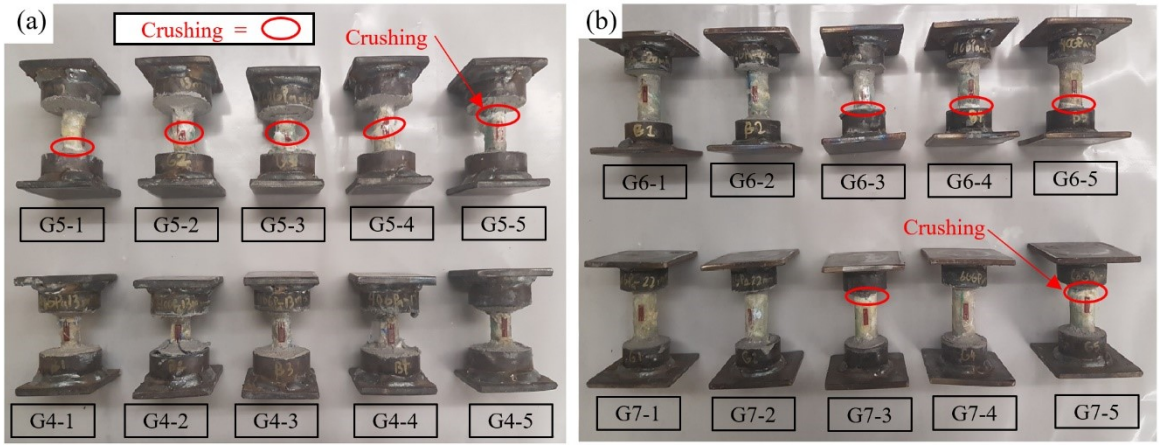

Figure 4. 8 Failed specimens: (a) G4 and G5 groups, (b) G6 and G7 groups

Overall, the tests predicted consistent results for the modulus of elasticity and compressive strength of the GFRP specimens regardless of the location of the failure in GFRP bars or the duration of the tests. However, the ultimate crushing strain cannot be determined based on the results of the strain gauges or the reading of the axial displacement directly. Since

the progressive nature of failure for the specimens which experienced failure inside the capping lead to successive gain and drop in the strain, the ultimate strain might be indistinguishable. Therefore, to calculate the crushing strain, reporting a nominal value is suggested when the proposed test method is used. The latter can be done by dividing the compressive strength by modulus of elasticity according to the hook's law; since the stress-strain behavior of the specimens shows a linearity as presented in the following section.

4.5.2 Stress-Strain Behavior

The stress-stain curves for all seven groups of tested compressive coupons (each including five specimens) is presented in Figure 4.9. It should be noted that the stress-strain curve for each compressive coupon was derived by averaging the strain values recorded from two strain gauges at the opposite side at the middle of the GFRP coupon like the procedure that was suggested by ASTM D7205-16 (2016) for testing GFRP bars in tension. For group G1, it was seen that the stress-strain curves were continued up to the crushing point and the load suddenly dropped after the failure. It should be noted that for all specimens in this group, the GFRP bar failure happened only in the free length of the specimens. It was observed that the stress-strain curves for different specimens in the same group were linear and tightly close to each other, which showed the consistency of the test results. Moreover, the average stress-strain line was very close to the single specimen curves and gives a god approximation of the compressive stress-strain behavior of the GFRP bars in compression. The average stress-strain lines were obtained using the average of strength and modulus of elasticity for every single specimen in a group, shown as the dashed line in Figure 4.9.

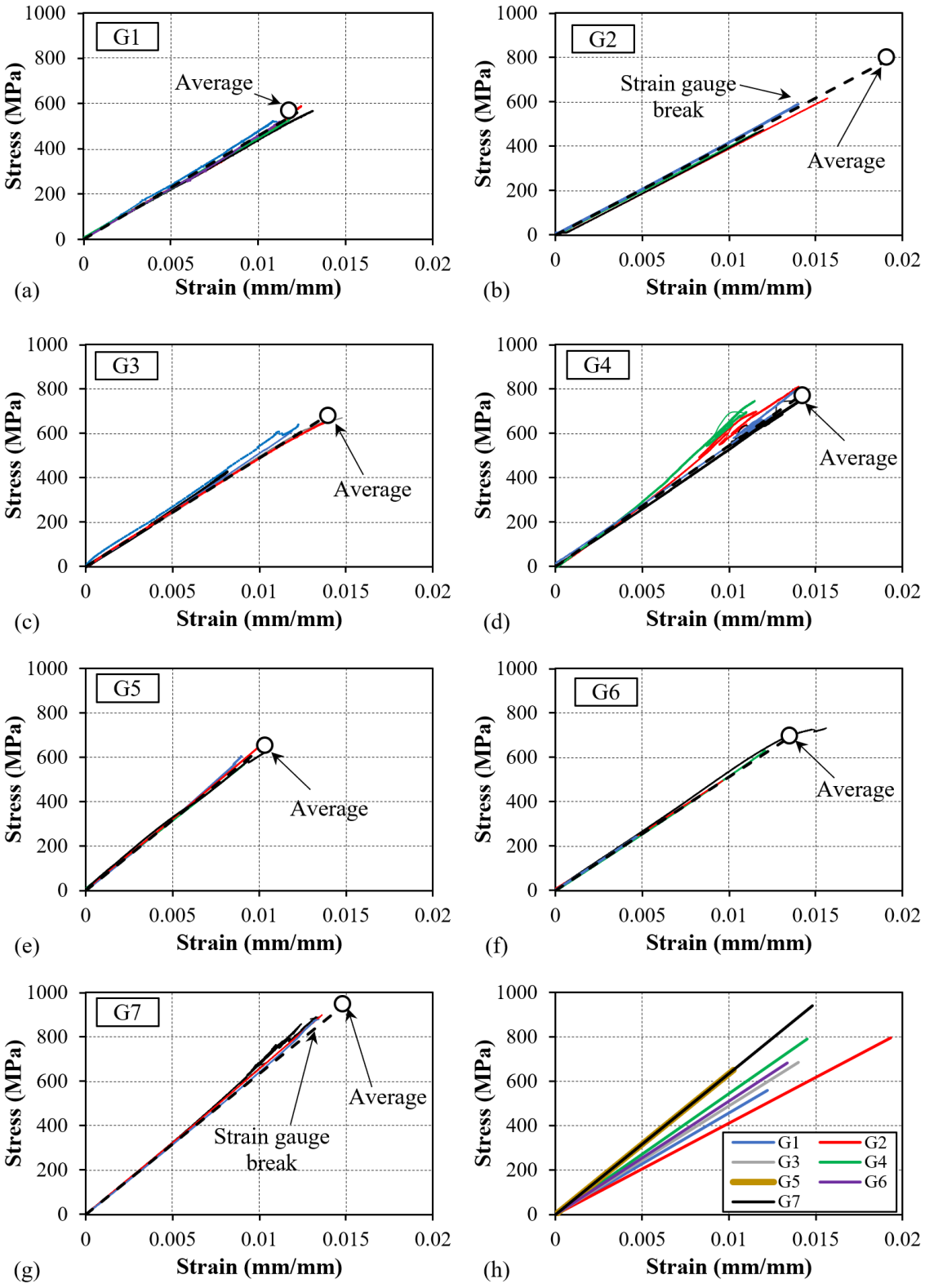

Figure 4. 9 Stress-strain curves: (a) G1, (b) G2, (c) G3, (d) G4, (e) G5, (f) G6, (g) G7, (h) Summary

The average compressive modulus of elasticity and compressive strength for all groups as well as their standard deviation and coefficient of variation is presented in Table 4.2. The results showed in the determination of the strength and modulus of elasticity due to small coefficient of variations. The average stress-strain lines for all groups is presented in Figure 4.9(h).

Table 4. 2 Comparison of compression and tensile properties

Group	f_t^* (MPa)	E_t^* (GPa)	$f_{c,ave}$ (MPa)	$E_{c,ave}$ (GPa)	σ_{fc} (MPa)	σ_{Ec} (GPa)	ε_c (mm/mm)	CoV_{fc} (%)	CoV_{Ec} (%)	R1	R2
G1	758.00	46.00	559.03	45.78	35.54	2.15	0.01221	6.36	0.05	0.74	1.00
G2	940.00	42.50	794.88	41.16	69.44	1.16	0.01931	8.74	2.81	0.85	0.97
G3	690.00	46.00	684.18	48.89	33.06	0.89	0.01400	4.83	1.83	0.99	1.06
G4	845.40	45.60	789.55	54.51	22.95	3.38	0.01449	2.91	6.19	0.93	1.20
G5	1175.00	61.10	651.73	63.46	38.04	1.98	0.01027	5.84	3.12	0.55	1.04
G6	884.30	51.00	683.45	51.19	75.21	0.77	0.01335	11.00	1.51	0.77	1.00
G7	1150.00	62.70	940.09	63.44	92.30	1.44	0.01482	9.82	2.27	0.82	1.01
Average								7.07	2.54	0.81	1.04

Note: E_t = tensile modulus of elasticity of GFRP bars; f_t = tensile strength of GFRP bars; E_c = average compressive modulus of elasticity of GFRP bars; f_c = average compressive strength of GFRP bars; ε_c = ultimate compressive strain of GFRP bars; σ_{Ec} = standard deviation of compressive modulus of elasticity of GFRP bars; σ_{fc} = standard deviation of compressive strength of GFRP bars; CoV_{Ec} = coefficient of variation of compressive modulus of elasticity of GFRP bars; CoV_{fc} = coefficient of variation of compressive strength of GFRP bars; R1 = the ratio of average compressive to tensile strength of GFRP bars; R2 = the ratio of average compressive to tensile modulus of elasticity of GFRP bars.
*The tensile properties used in this table were reported by the manufacturers.

For group G2, some of the strain gauges were broken after a certain load and the strain recording was not available after that point, as shown in Figure 4.9(b). It should be noted that the problem that caused the separation of the strain gauges from the GFRP bars was improved by enhancing the surface preparation of the strain gauges for the other groups as explained in the preparation section of this paper. It should be mentioned that in chapter 3, higher ratio of compressive to tensile strength was captured for G2 group since it was compared to the tensile coupon tests while in this chapter, it was compared to manufacturer reported values for tensile strength which lead to a different ratio.

For group G4, it was observed that the slope of the stress-strain curves deviated as the load increased, as shown in Figure 4.9(d). It should be noted that for all group G4, the progressive failure happened only inside the capping since the GFRP crushing happened only in the capping, as shown in Figure 7. Therefore, the drop and gain of the strain and the stress in the stress-strain curves were occurred as presented in Figure 4.9(d). However, for the specimens in group G5 which had the same diameter and produced by the same manufacturer as group G4, all the specimens experienced linear stress-strain curves without any drop and gain in the strain and the stress. It was observed that the mode of failure for specimens in group G5 was either crushing of the bar in the free length or GFRP bar crushing happening both inside capping and in the free length. Therefore, there should be a meaningful relation between the failure mode and the stress-strain curves. It was observed that for the specimens which experienced crushing only in the free length there was no drop and gain in the strain and the stress up to failure. In other words, the progressive failure inside the capping can be recognized from the shape of the stress-strain curves. Since the specimen in group G5 had higher modulus of elasticity, it might be implied that for GFRP bars with higher modulus of elasticity, the failure mode is dictated to be in the free length. However, observation of the results of group G6 and G7 which were produced by the same manufacturer and had the same diameter showed that higher modulus does not necessarily control the mode of failure. For example, specimens in group G7 has higher modulus of elasticity than the specimens in group G6, but the drop and gain in the strain and the stress in the stress-strain curves were mainly observed in group G7, as shown in Figure 4.9(f) and 9(g). The latter is in contrast with the results of the comparison made between group G4

and G5 as discussed earlier. Also, it was observed that for group G6 and G7, the failure modes were random, as shown in Fig 8.

4.5.3 Determination of Compressive Characteristics

It was observed that the proposed test method leads to three different modes of failure which causes a drop or gain in the stress and strain values for some specimens based on the mode of failure as discussed earlier. However, it should be noted that the drop and gain of the stress and the strain in the stress-strain curves started after a certain strain that was greater than 0.005 mm/mm for all specimens, as shown in Figure 4.9. Thus, for the calculation of compressive modulus of elasticity of GFRP bars, it is suggested by this paper to use the portion of the stress-strain curves which lies between the strain values of 0.001 and 0.003 mm/mm, which is compatible with ASTM D7205-16 (2016) suggestion for derivation of the tensile modulus of elasticity for the GFRP bars, as shown in Figure 4.10. Therefore, the mode of failure cannot have any effect on the calculation of the compressive modulus of elasticity based on the results of the experimental tests.

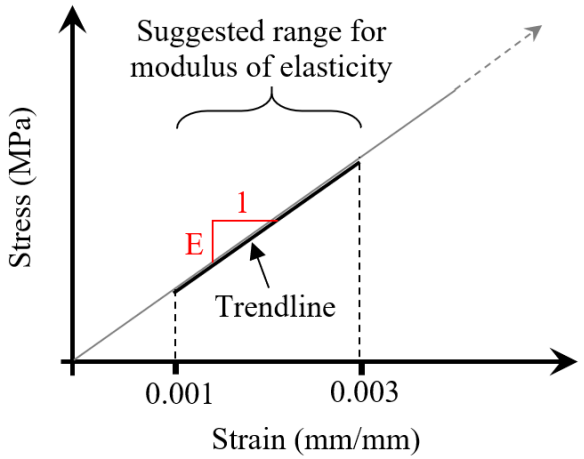

Figure 4. 10 Determination of modulus of elasticity

In this paper, the compressive modulus of elasticity was determined as the slope of the linear trendline that passes through the average of the five specimens in the mentioned rage of strain. The average of compressive modulus of elasticity and its standard deviation for all groups of tested specimens are presented in Table 4.2. The test results showed that the coefficient of variation for determination of compressive modulus of elasticity was 2.54% which showed that the proposed test method predicts the modulus of elasticity of the specimens very consistently.

The average and standard deviation for compressive strength of all groups is presented in Table 4.2. As mentioned earlier, there were three different modes of failure including crushing of GFRP only in the free length, only inside the capping, or both inside the capping and in the free length. The consequence of the crushing of the GFRP bar inside the capping was progressive failure and observing a drop and gain of the stress and strain in the stress-strain curves. The latter did not allow a unique crushing strain to be recognized by the proposed test method for all the specimens. Therefore, the ultimate crushing strains were derived by dividing the compressive strength by the compressive modulus of elasticity, as presented in Table 4.2. However, there was no difference between the specimens with different modes of failure in terms of determining their compressive strength and modulus of elasticity. The average coefficient of variation for determination of compressive strength for all tested specimens was 7.07% which shows an acceptable range of results and consistent values for the compressive strength of GFRP bars.

4.5.4 Comparison of Compressive and Tensile Properties

The average compressive modulus of elasticity and strength of each group of GFRP bars as well as the reported tensile properties of GFRP bars are presented in Table 4.2. It is seen

that the modulus of elasticity in compression and tension are quite close, and the strength is lower in compression. The compressive to tensile modulus of elasticity and strength ratios for the tested groups is presented in Figure 4.11 and Table 4.2.

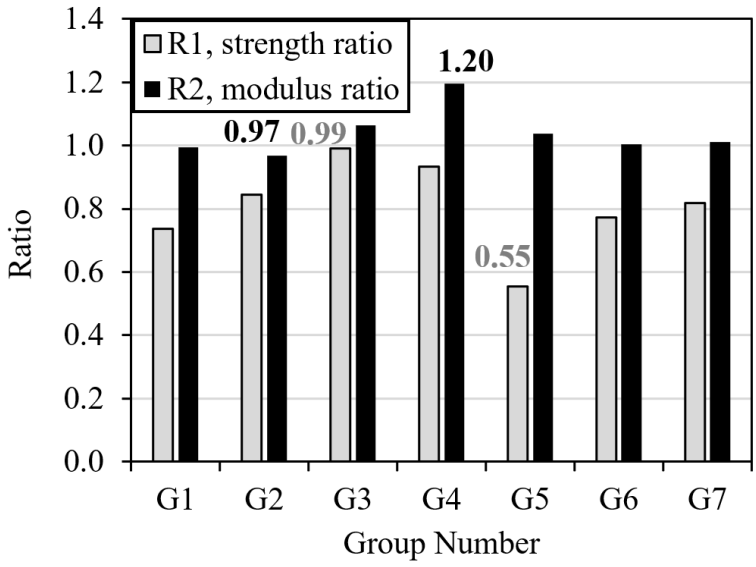

Figure 4. 11 Ratio of compressive to tensile modulus of elasticity and strength

It was observed that the modulus of elasticity in compression, in average, was between 97% to 120% of the modulus of elasticity in tension. Moreover, the average compressive strength was between 55% to 99% of the tensile strength. Overall, the average of the compressive to tensile modulus of elasticity and strength ratios were 0.81 and 1.04, respectively. The latter shows that the modulus of elasticity of GFRP bars in compression can be considered the same as in tension. However, for determining the compressive strength, the compressive test is necessary due to the wide variety of compressive to tensile strength ratios. In other words, the test of GFRP bars in tensile is not sufficient to estimate the compressive strength of the GFRP bars. It should be mentioned that in a later study, on

the subject of testing GFRP bars in compression, the test method was modified and used to consider the effect of different slenderness ratios of GFRP bars (AlAjarmeh et al., 2019).

4.6 CONCLUSIONS

This paper was dedicated to determination of the compressive strength, the modulus of elasticity, the crushing strain, and the compressive stress-strain curve of GFRP bars by proposing a new test method. A total of 35 GFRP bar compressive coupons were built and tested using the proposed test method which covered three different bar diameters, provided by three different manufacturers. The following conclusions can be drawn:

- The proposed test method was successfully implemented to obtain the compressive modulus of elasticity, compressive strength, ultimate crushing strain, and the compressive stress-strain curve of the GFRP bars.
- The results of the experimental study showed no buckling of GFRP bars as a mode of failure. Three different modes of failure were observed: i) crushing of GFRP bars only in the free length; ii) crushing of the GFRP bars only inside the capping; iii) crushing of GFRP bars both inside the capping and in the free length. It should be noted that the 56% of specimens experienced crushing of the GFRP bar in the free length while for the rest of the specimens there was no sign of crushing n the free length.
- It was observed that the compressive modulus of elasticity and compressive strength of GFRP bars which is assessed using the proposed test method is not affected by the difference in the modes of failure. However, the crushing strain cannot be evaluated directly from the test for the cases that experience GFRP crushing.

- It was observed that considering a linear behavior for the compressive stress-strain curves of GFRP bars is a good assumption. Therefore, the crushing strain is reported by dividing the compressive strength by the compressive modulus of elasticity.
- The average coefficient of variation for the calculation of compressive strength and modulus of elasticity for all tested groups were 7.07% and 2.54%, respectively, which shows that very consistent results can be obtained using the proposed method.
- The average of compressive to tensile modulus of elasticity and strength ratios varied from 0.97 to 1.20 and from 0.55 to 0.99, respectively, for different groups of the tested specimens. In average, the compressive to tensile strength and the modulus of elasticity ratios for all specimens were 1.04 and 0.81, respectively. The latter shows that the modulus of elasticity in compression and tension could be considered the same for GFRP bars. However, because of the wide range of variation in the ratio of the compressive to tensile strength, the tensile test of GFRP bars is not sufficient to estimate the compression strength. Therefore, performing a compression test is necessary for determination of the compressive strength of GFRP bars.

ACKNOWLEDGMENTS

Authors would like to thank Jordan Maerz, Jesse Keane, and Brian Kennedy for their assistance in the lab. The authors would also like to acknowledge and thank NSERC and Dalhousie University for their financial support. Aslan FRP, V-ROD Canada, and TUF-BAR companies are thanked for providing GFRP bars.

REFERENCES

ACI 318-14. (2014). Building Code Requirements for Structural Concrete. American Concrete Institute. Farmington Hills, MI.

ACI 440.1R. (2015). Guide for the Design and Construction of Structural Concrete Reinforced Fiber-Reinforced Polymer (FRP) Bars. *American Concrete Institute.* Farmington Hills, MI.

ACI 440.2R. (2008). Guide for the Design and Construction of Externally Bonded FRP Systems for Strengthening Concrete Structures. *American Concrete Institute.* Farmington Hills, MI.

Afifi, M. Z., Mohamed, H. M., and Benmokrane, B. (2013). Strength and Axial Behavior of Circular Concrete Columns Reinforced with CFRP Bars and Spirals. *Journal of Composites for Construction*, 18(2), 04013035.

AlAjarmeh, O. S., Manalo, A. C., Benmokrane, B., Vijay, P. V., Ferdous, W., and Mendis, P. (2019). Novel testing and characterization of GFRP bars in compression. *Construction and Building Materials*, 225, 1112-1126.

Alkhrdaji, T., Nanni, A., Chen, G., and Barker, M. (1999). Upgrading the Transportation Infrastructure: Solid RC Decks Strengthened with FRP. *Concrete International: Design and Construction*, 21(10), 37-41.

Alsayed, S. H. (1998). Flexural behaviour of concrete beams reinforced with GFRP bars. *Cement and Concrete Composites*, 20(1), 1-11.

ASTM C39/C39M − 18. (2018). Standard Test Method for Compressive Strength of Cylindrical Concrete Specimens. *American Society for Testing and Materials.* West Conshohocken, PA.

ASTM D3039/D3039M-14. (2014). Standard Test Method for Tensile Properties of Polymer Matrix Composite Materials. *American Society for Testing and Materials.* West Conshohocken, PA.

ASTM D6641/D6641M-16. (2016). Standard Test Method for Compressive Properties of Polymer Matrix Composite Materials Using a Combined Loading Compression (CLC) Test Fixture. *American Society for Testing and Materials.* West Conshohocken, PA.

ASTM D695-10. (2010). Standard Test Method for Compressive Properties of Rigid Plastics. *American Society for Testing and Materials.* West Conshohocken, PA.

ASTM D7205 / D7205M - 06. (2016). Standard Test Method for Tensile Properties of Fiber Reinforced Polymer Matrix Composite Bars. *American Society for Testing and Materials.* West Conshohocken, PA.

Atadero, R., Lee, L., and Karbhari, V. M. (2005). Consideration of material variability in reliability analysis of FRP strengthened bridge decks. *Composite Structures*, 70(4), 430-443.

Badawi, M., and Khaled, S. (2009). Flexural strengthening of RC beams with prestressed NSM CFRP rods – Experimental and analytical investigation. *Construction and Building Materials*, 23(10), 3292-3300.

Barros, J. A., Varma, R. K., Sena-Cruz, J. M., and Azevedo, A. F. (2008). Near surface mounted CFRP strips for the flexural strengthening of RC columns: Experimental and numerical research. *Engineering Structures*, 30(12), 3412-3425.

Benmokrane, B., El-Salakawy, E., El-Ragaby, A., and Lackey, T. (2006). Designing and Testing of Concrete Bridge Decks Reinforced with Glass FRP Bars. *Journal of Bridge Engineering*, 11(2), 217-229.

Berg, A. C., Bank, L. C., Olivia, M. G., and Russell, J. S. (2006). Construction and cost analysis of an FRP reinforced concrete bridge deck. *Construction and Building Materials*, 20(8), 515-526.

Bisby, L., and Ranger, M. (2010). Axial–flexural interaction in circular FRP-confined reinforced concrete columns. *Construction and Building Materials*, 24(9), 1672-1681.

Bournas, D. A., and Triantafillou, T. C. (2009). Flexural strengthening of reinforced concrete columns with near-surface-mounted FRP or stainless steel. *ACI Structural Journal*, 106(4), 495-505.

Broms, B., and Viest, I. M. (1961). Long Reinforced Concrete Columns: A symposium. *Transactions, ASCE,* 126(2), 308-400.

Ceroni, F. (2010). Experimental performances of RC beams strengthened with FRP materials. *Construction and Building Materials*, 24(9), 1547-1559.

Chaallal, O., and Shahawy, M. (2000). Performance of Fiber-Reinforced Polymer-Wrapped Reinforced Concrete Column under Combined Axial-Flexural Loading. *ACI Structural Journal*, 97(4), 659-668.

Choo, C. C., Harik, I. E., and Gesund, H. (2006). Strength of Rectangular Concrete Columns Reinforced with Fiber-Reinforced Polymer Bars. *ACI Structural Journal*, 103(3), 452-459.

Claeson, C., and Gylltoft, K. (1998). Slender High-Strength Concrete Columns Subjected to Eccentric Loading. *Journal of Structural Engineering*, 124(3), 233-240.

CSA A23.3-14. (2014). Design of concrete structures. *Canadian standard association.*

CSA S6-14. (2014). Canadian Highway Bridge Design Code. *Canadian Standards Association.*

CSA S806-12. (2012). Design and construction of building structures with fiber-reinforced polymers. *Canadian Standards Association.*

De Luca, A., Matta, F., and Nanni, A. (2010). Behavior of Full-Scale Glass Fiber-Reinforced Polymer Reinforced Concrete Columns under Axial Load. *ACI Structural Journal*, 107(5), 589-596.

Deitz, D. H., Harik, I. E., and Gesund, H. (2003). Physical Properties of Glass Fiber Reinforced Polymer Rebars in Compression. *Journal of Composites for Construction*, 7(4), 363-366.

Deitz, D., Harik, I. E., and Gesund, H. (1999). One-Way Slabs Reinforced with Glass Fiber Reinforced Polymer Reinforcing Bars. *ACI Special Publication*, 188, 279-286.

El-sayed, A., El-Salakawy, E., and Benmokrane, B. (2005). Shear Strength of One-Way Concrete Slabs Reinforced with Fiber-Reinforced Polymer Composite Bars. *Journal of Composites for Construction*, 9(2), 147-157.

Fib Bulletin 14. (2001). Externally bonded FRP reinforcement for RC structures. *The International Federation for Structural Concrete*, Stuttgart.

Fib Bulletin 40. (2007). FRP Reinforcement in RC structures. *The International Federation for Structural Concrete*, Stuttgart.

Fillmore, B., and Sadeghian, P. (2017). Compressive Behavior of Concrete Cylinders Reinforced with Glass Fiber Reinforced Polymer Bars. *CSCE - Leadership in Sustainable Infrastructures.* Vancouver, Canada.

Fillmore, B., and Sadeghian, P. (2018). Contribution of longitudinal glass fiber-reinforced polymer bars in concrete cylinders under axial compression. *Canadian Journal of Civil Engineers*, 45, 458-468.

Foret, G., and Limam, O. (2008). Experimental and numerical analysis of RC two-way slabs strengthened with NSM CFRP rods. *Construction and Building Materials*, 22(10), 2025-2030.

Gajdosova, K., and Bilcik, J. (2013). Full-scale testing of CFRP-strengthened slender reinforced concrete columns. *Journal of composites for construction*, 17, 239-248.

Galati, N., Tumialan, G., and Nanni, A. (2006). Strengthening with FRP bars of URM walls subject to out-of-plane loads. *Construction and Building Materials*, 20(1), 101-110.

Guérin, M., Mohamed, H. M., Benmokrane, B., Nanni, A., and Shield, C. K. (2018a). Eccentric Behavior of Full-Scale Reinforced Concrete Columns with Glass Fiber-Reinforced Polymer Bars and Ties. *ACI Structural Journal*, 115(2), 489-499.

Hadhood, A., Mohamed, H. M., Ghrib, F., and Benmokrane, B. (2017). Efficiency of glass-fiber reinforced-polymer (GFRP) discrete hoops and bars in concrete columns under combined axial and flexural loads. *Composites Part B*, 114, 223-236.

Hadi, M. (2006). Behaviour of FRP wrapped normal strength concrete columns under eccentric loading. *Composite Structures*, 72(4), 503-511.

Hadi, M. N., and Youssef, J. (2016). Experimental Investigation of GFRP-Reinforced and GFRP-Encased Square Concrete Specimens under Axial and Eccentric Load, and Four-Point Bending Test. *Journal of Composites for Construction*, 20(5), 04016020.

Hales, T. A., Pantelides, C. P., and Reaveley, L. D. (2016). Experimental Evaluation of Slender High-Strength Concrete Columns with GFRP and Hybrid Reinforcement. *Journal of Composites for Construction*, 20(6), 04016050.

Hamilton Iii, H., and Dolan, C. (2001). Flexural capacity of glass FRP strengthened concrete masonry walls. *Journal of Composites for Construction*, 5(3), 170-178.

Hognestad, E. (1951). A Study of Combined Bending and Axial Load in Reinforced Concrete Members, *Bulletin Series No. 399*. Urbana: University of Illinois.

Hussein, M. E., Al-Salloum, Y. A., Alsayed, S. H., and Iqbal, R. A. (2012). Experimental and numerical investigation of size effects in FRP-wrapped concrete columns. *Construction and Building Materials*, 29, 56-72.

Jiang, T., and Teng, J. (2012). Theoretical model for slender FRP-confined circular RC columns. *Construction and Building Materials*, 32, 66-76.

Khan, Q. S., Sheikh, M., and Hadi, M. N. (2015). Tension and compression testing of fibre reinforced polymer (FRP) bars. *Joint Conference of the 12th International Symposium on Fiber Reinforced Polymers for Reinforced Concrete Structures (FRPRCS-12) and the 5th Asia-Pacific Conference on Fiber Reinforced Polymers in Structures (APFIS-2015).* Wollongong, New South Wales, Australia.

Khorramian, K., and Sadeghian, P. (2017a). Experimental and analytical behavior of short concrete columns reinforced with GFRP bars under eccentric loading. *Engineering Structures*, 761–773.

Khorramian, K., and Sadeghian, P. (2017b). Short Concrete Columns Reinforced with GFRP Rebars Under Eccentric Loading. *CSCE Annual Conference. Vancouver, BC, Canada: Canadian Society of Civil Engineering.*

Khorramian, K., and Sadeghian, P. (2017c). Strengthening Concrete Columns Using Near Surface Mounted (NSM) Carbon Fiber Reinforced Polymer (CFRP) Laminates. *Sixth Asia-Pacific Conference on FRP in Structures. Singapore, Singapore.*

Khorramian, K., and Sadeghian, P. (2018). New Testing Method of GFRP Bars in Compression. *CSCE Annual Conference. Fredericton, NB, Canada: Canadian Society of Civil Engineering.*

Kim, Y. J., Longworth, J. M., and Wight, G. R. (2008). Flexure of Two-Way Slabs Strengthened with Prestressed or Non prestressed CFRP Sheets. *Journal of Composites for Construction*, 12(4), 366-374.

Kobayashi, K., and Fujisaki, T. (1995). Compressive behaviour of FRP reinforcement in non prestressed concrete members. *Non metallic (FRP) reinforcement for concrete structures, Proceedings of the second international RILEM Symposium (FRPRCS-2).* London, UK.

Lloyd, A. N., and Rangan, V. B. (1996). Studies on High-Strength Concrete Columns under Eccentric Compression. *ACI Structural Journal*, 93(6), 631-638.

Mallick, P. K. (2008). Fiber Reinforced Composites Materials, Manufacturing, and Design. Boca Raton, Florida: *CRC Press*.

Michaluk, C. R., Rizkalla, S. H., Tadros, G., and Benmokrane, B. (1998). Flexural Behavior of One-Way Concrete Slabs Reinforced by Fiber Reinforced Plastic Reinforcements. *ACI Structural Journal*, 95(3), 353-365.

Mirmiran, A., Shahawy, M., Samaan, M., El Echary, H., Mastrapa, J. C., and Pico, O. (1998). Effect of Column Parameters on FRP-Confined Concrete. *Journal of Composites for Construction*, 2(4), 175-185.

Mirmiran, A., Yuan, W., and Chen, X. (2001). Design for slenderness in concrete columns internally reinforced with fiber-reinforced polymer bars. *Structural Journal*, 98(1), 116-125.

Mohamed, H. M., Afifi, M. Z., and Benmokrane, B. (2014). Performance Evaluation of Concrete Columns Reinforced Longitudinally with FRP Bars and Confined with FRP Hoops and Spirals under Axial Load. *Journal of Bridge Engineering*, 19(7), 04014020.

Mosallam, A. S., and Mosalam, K. M. (2003). Strengthening of two-way concrete slabs with FRP composite laminates. *Construction and Building Materials*, 17(1), 43-54.

Nordin, H., and Täljsten, B. (2006). Concrete Beams Strengthened with Prestressed Near Surface Mounted CFRP. *Journal of Composites for Construction*, 10(1), 60-68.

Parvin, A., and Brighton, D. (2014). FRP Composites Strengthening of Concrete Columns under. *Polymers*, 6, 1040-1056.

Parvin, A., and Wang, W. (2001). Behaviour of FRP jacketed concrete columns under eccentric loading. *Journal of Composites for Construction*, 5(3), 146-152.

Pham, T. M., and Hadi, M. N. S. (2013). Strain estimation of CFRP-confined concrete columns using energy approach. *Journal of Composites for Construction*, 17(6), 1–11.

Popovics, S. (1973). A Numerical Approach to the Complete Stress-Strain Curve of Concrete. *Cements and Concrete Research*, 3(5), 583-599.

Rahimi, H., and Hutchinson, A. (2001). Concrete Beams Strengthened with Externally Bonded FRP Plates. *Journal of Composites for Construction*, 5(1), 44-56.

Sadeghian, P., and Fam, A. (2015). Strengthening slender reinforced concrete columns using high-modulus bonded longitudinal reinforcement for buckling control. *Journal of structural Engineering*, 141, 04014127.

Sadeghian, P., and Fillmore, B. (2018). Strain distribution of basalt FRP-wrapped concrete cylinders. *Case Studies in Construction Materials*, 9, e00171.

Sadeghian, P., Rahai, A. R., and Ehsani, M. R. (2010). Experimental study of rectangular RC columns strengthened with CFRP composites under eccentric loading. *Journal of Composites for Construction*, 443-450.

Shaat, A., and Fam, A. Z. (2009). Slender Steel Columns Strengthened Using High-Modulus CFRP Plates for Buckling Control. *Journal of Composites for Construction*, 13(1), 2-12.

Shahawy, M., Mirmiran, A., and Beitelman, T. (2000). Tests and modeling of carbon-wrapped concrete columns. *Composites Part B: Engineering*, 31(6), 471-480.

Sharif, A., Al-Sulaimani, G. J., Basunbul, I. A., Baluch, M. H., and Ghaleb, B. N. (1994). Strengthening of Initially Loaded Reinforced Concrete Beams Using FRP Plates. *ACI structural Journal*, 91(2), 160-168.

Sheikh, S. A., and Kharal, Z. (2018). GFRP-Reinforced Concrete Columns Subjected to Seismic Loads. *ACI Special Publication*, 326, 56-1:10.

Tarek, H., and Rizkalla, S. (2002). Flexural Strengthening of Prestressed Bridge Slabs with FRP systems. *PCI Journal*, 47(1), 76-93.

Tavassoli, A., Liu, J., and Sheikh, S. (2015). Glass Fiber-Reinforced Polymer-Reinforced Circular Columns under Simulated Seismic Loads. *ACI Structural Journal*, 103-114.

Teng, J., Lorenzis, L., Wang, B., Li, R., Wong, T., and Lam, L. (2006). Debonding Failures of RC Beams Strengthened with Near Surface Mounted CFRP Strips. *Journal of composites for construction*, 92(105), 92-105.

Thériault, M., and Benmokrane, B. (1998). Effects of FRP Reinforcement Ratio and Concrete Strength on Flexural Behavior of Concrete Beams. *Journal of Composites for Construction*, 2(1), 7-16.

Tobbi, H., Farghaly, A. S., and Benmokrane, B. (2012). Concrete Columns Reinforced Longitudinally and Transversally with Glass Fiber-Reinforced Polymer Bars. *ACI Structural Journal*, 109(4), 551-558.

Todeschini, C. E., Bianchini, A. C., and Kesler, C. E. (1964). Behavior of Concrete Columns Reinforced with High Strength Steels. *ACI Journal*, 61(6), 701-716.

Toutanji, H. A., and Saafi, M. (2000). Flexural behavior of concrete beams reinforced with glass fiber-reinforced polymer (GFRP) bars. *ACI Structural Journal*, 97(5), 712-719.

Triantafillou, T. C., and Plevris, N. (1992). Strengthening of RC beams with epoxy-bonded fibre-composite materials. *Materials and Structures*, 25, 201-211.

Wight, J. K., and MacGregor, J. G. (2012). Reinforced Concrete Mechanics and Design. *Upper Saddle River*, NJ: Pearson Education Inc.

Zadeh, H. J., and Nanni, A. (2013). Design of RC Columns Using Glass FRP Reinforcement. *Journal of Composites*, 17(3), 294–304.

CHAPTER 5 EXPERIMENTAL INVESTIGATION OF SLENDER RECTANGULAR CONCRETE COLUMNS REINFORCED WITH GFRP BARS UNDER ECCENTRIC AXIAL LOADS

ABSTRACT

In this paper, the experimental behavior of short and slender concrete columns reinforced with glass fiber-reinforced polymer (GFRP) bars under eccentric loading condition is presented. A total of ten large-scale concrete specimens with a rectangular cross-section (205 × 306 mm) loaded under single curvature condition with equal load eccentricities at both ends of the column were tested. Four slenderness ratios of 16.6, 21.5, 39.7, and 59.5, two eccentricity-to-column width of 23% and 21%, and two reinforcement ratios of 2.78% and 4.80% were considered. The results showed that no crushing of GFRP bars occurred prior to concrete spalling. The columns were able to sustain load, moment, and deformation after concrete spalling of concrete up to the crushing of GFRP bars in compression. The latter was attributed to the contribution of GFRP bars in compression. Also, the flexural stiffness and magnified moment factor obtained from the experimental program were compared to those calculated using equations from the literature. The results showed that the majority of the equations underestimated the flexural stiffness and the magnified moment.

5.1 INTRODUCTION

The interest in using fiber-reinforced polymer (FRP) bars as an alternative to steel reinforcing bars in concrete structures has been increasing due to the superior characteristics of FRPs such as high corrosion resistance, high tensile strength, and their electromagnetic transparency. Among structural members, GFRP reinforced concrete (RC)

columns have been treated with extra caution. Currently, ACI 440.1R-15 (2015) guideline does not consider compressive FRP bars for reinforcing concrete columns due to a lack of research data. However, the guideline is in the process of being converted into an accompanied code to ACI 318-19 (2019) for GFRP-RC members and inclusion of both short and slender GFRP-RC concrete columns in under consideration. For GFRP RC columns, a critical slenderness ratio of 17 is under consideration form a numerical study performed by Mirmiran et al. (2001) which is lower than the limit of 22 defined for steel-RC columns (ACI 318-19, 2019). The latter shows that FRP-RC columns are more susceptible to be categorized as slender columns in comparison with steel-RC columns and the lack of experimental data on the behavior of slender FRP-RC columns leads to conservative decision making. There have been many studies on the behavior of short concrete columns reinforced with glass FRP (GFRP) bars (Pantelides et al., 2013; Afifi et al., 2014; Mohamed et al., 2014; Guérin et al., 2018a and 2018b; Hadhood et al., 2019). Different concrete types (Elchalakani et al., 2018; Salah-Eldin et al., 2019), different loading conditions (Maranan et al., 2016; Hadhood et al., 2016; Hadi et al., 2016; Sun et al., 2017), and different cross-sections (Alajarmeh et al., 2019a and 2019b) were considered. However, the studies on the behavior of slender GFRP-RC columns have been very limited (Tikka et al., 2010; Hales et al., 2016; Maranan et al., 2016; Elchalakani and Ma, 2017; Xue et al., 2018; Khorramian and Sadeghian, 2019a).

Tikka et al. (2010) conducted experimental tests on eight square GFRP-RC columns with a width of 150 mm, slenderness ratio of 41.6, reinforcement ratios of 2.3 and 3.4% and eccentricity-to-column width ratios of 0.2, 0.4, 0.6, and 0.8. The study showed that specimens tolerated considerable displacement before failure. Hales et al. (2016) studied

the behavior of high strength circular concrete columns reinforced with GFRP bars, in which six slender columns with a slenderness ratio of 49 were tested with two different eccentricities. They observed that for 8.3% and 33% eccentricity to diameter ratios, the failure was governed by material failure and global buckling, respectively. It was reported that the system of GFRP bars and GFRP spirals is a viable system for slender columns. Maranan et al. (2016) tested two slender circular GFRP reinforced geopolymer concrete columns with a slenderness ratio of 32, a diameter of 250 mm, and a reinforcement ratio of 2.43%. They observed that the slender columns were failed at a load of 66% and 82% of the strength of their short-column counterparts. Elchalakani and Ma (2017) tested seven rectangular GFRP RC columns (160x260 mm) with a slenderness ratio of 26, eccentricities of 0, 25, 35, and 45 mm and with a reinforcement ratio of 1.83%. They observed that the average increase in the capacity of GFRP-RC specimens was 3.2%. Xue et al. (2018) tested fifteen slender rectangular concrete columns reinforced with GFRP bars. The cross-section was square with a width of 300 mm. The slenderness ratios of 20.8, 27.7, 34.6, and 41.6 with eccentricity-to-column width ratios of 0, 0.2, 0.5, and 1 and reinforcement ratios of 0.9, 1.34, and 2.55% were tested. They observed only concrete crushing as the mode of failure. However, no rupture of FRPs was observed. Also, very little post-peak deformation was observed by Xue et al. (2018). Khorramian and Sadeghian (2019a) developed an analytical-numerical method verified by test data and conducted a preliminary study on the behavior of slender concrete columns, but no experimental test on slender columns was added. Overall, there are a few experimental tests conducted on slender GFRP RC columns in comparison to short columns. In a recent study, Elmessalami et al. (2019) listed FRP-RC columns tested and available in the literature: 129 short FRP-RC columns tested under

concentric loading; 100 short FRP-RC columns tested under eccentric loading; 22 slender FRP-RC columns. The statistics show that there is a lack of test data on the behavior of the slender FRP-RC columns and more experimental tests are required which was the motivation of the current study.

The other motivation of the current study was the evaluation of the behavior of GFRP bars in compression (advancements in the industry) and their ability to work in the system after concrete spalling. Many of the experimental tests were stopped once the concrete spalling happened during the tests (Khorramian and Sadeghian, 2017b; Afifi et al., 2014; Tobbi et al., 2014; De Luca et al., 2010), which does not consider the potential of the FRP-RC columns to bear loads after concrete spalling. If compressive bars are effective in the system, due to their high strength and linearity of stress-strain curves, as the deformation increases and in turn strain of concrete, the column could still sustain loads even after concrete spalled. However, to examine this idea experimental evidence is required. This issue comes from neglection of the effect of the compressive bars. And the belief that they are not effective in compression. It should be noted that the contribution of GFRP bars in compression is neglected by ACI 440.1R-15 (2015) and other design codes such as CAN/CSA S806-12 (2017), CAN/CSA S6-14 (2014), and FIB Bulletin 40-07 (2007). The assumption not only underestimates the capacity of short GFRP-RC columns (Tobbi et al., 2012, Khorramian and Sadeghian, 2017a) but also underestimates the flexural stiffness of slender ones. For example, Zadeh and Nani (2017) conducted a study on the flexural stiffness of FRP RC columns in concrete frames and proposed an equation for flexural stiffness used in the moment magnification method for considering second-order effects in which the compression bars were neglected in the derivation of their suggested equations.

Therefore, in this research, the experimental tests were not stopped after the spalling of concrete to understand the behavior of the GFRP-RC columns after concrete spalling, and the unloading behavior of the columns was captured. In addition, the performance of available equations for estimating the flexural stiffness was examined using the test results. Also, moment magnification factors from calculation and experimental study were reported.

5.2 EXPERIMENTAL PROGRAM

5.2.1 Test Matrix

A total of ten concrete reinforced concrete columns with a rectangular cross-section of 205 × 306 mm were designed to be tested under combined axial and flexural loads. It should be mentioned that the capacity of the testing device governed the size of the specimens. The test matrix is presented in Table 5.1.

Table 5. 1 Test Matrix

No.	Specimen ID	λ	e/h	ρ (%)	Class
1	G17-e23-r4-N1	16.6	0.23	4.80	GFRP
2	G17-e23-r4-N2	16.6	0.23	4.80	GFRP
3	G22-e23-r4-N1	21.5	0.23	4.80	GFRP
4	G22-e21-r4-N2	21.5	0.21	4.80	GFRP
5	S22-e23-r2-N3	21.5	0.23	1.00	Steel
7	G40-e23-r2-N1	39.7	0.23	2.87	GFRP
9	G40-e23-r4-N2	39.7	0.23	4.80	GFRP
6	G40-e21-r2-N3	39.7	0.21	2.87	GFRP
8	G40-e21-r4-N4	39.7	0.21	4.80	GFRP
10	G60-e23-r4-N1	59.5	0.23	4.80	GFRP

Note: Class = reinforcement type.

The dimensions of the cross-section initially were selected so that the actuator can reach the capacity of the columns. Nine of the concrete columns were reinforced with #6 GFRP bars with a cross-sectional area of 285 mm^2. One specimen was reinforced with six 10M steel rebars, with a nominal cross-sectional area of 100 mm^2, as the control specimen. For lateral reinforcement, four U-shapes #3 GFRP bars, with a cross-sectional area of 71 mm^2, were tied inside each other to form two closed rectangular ties with an outer radius of 63.5 mm. For lateral reinforcement, #3 was selected its diameter (10mm) was a match with the minimum bar tie size for steel per ACI 318-19 (2019). The concrete cover provided for specimens was 25.4 mm that measured from the outer surface of the GFRP ties to the edge of the specimens. Moreover, the corners of the specimens were chamfered with a straight leg of 40 mm to prevent sharp corners.

The experimental variables were slenderness ratio, reinforcement ratio, and the load eccentricity. Four different specimen lengths of 1020, 1320, 2440, and 3660 mm were prepared, corresponding to slenderness ratios ($\lambda=kl/r$) of 16.6, 21.5, 39.7, and 59.5, respectively. Slenderness ratio of 17 was proposed by Mirmiran et al. (2001) as the critical slenderness ratio for GFRP-RC concrete columns while ACI 318-19 (2019) suggested a critical slenderness ratio of 22 for unbraced steel RC columns. A range of 25 to 33 for slenderness limit is a very common slenderness ratio for residential buildings. For non-residential buildings, commercial buildings, columns in a gym, bridge piers, and etc., there higher slenderness ratios are applicable. Therefore, the slenderness ratio of 39.7 was the core of the study and to further observe the effect of slenderness, the slenderness ratio of 59.5 was selected. Three reinforcement ratios were considered as 4.80, 2.87, and 1.00 % which were corresponding to 10 GFRP bars, 6 GFRP bars, and 6 steel bars, respectively. It

should be noted that 1% is the minimum reinforcement ratio for steel RC columns per ACI 318-19 (2019). For the sake of comparison, for longitudinal reinforcement, 10#6 GFRP bars were considered which provides similar axial stiffness as 6-10M. Also, to compare the effect of reinforcement ratio, 6#6 GFRP bars were considered as the second reinforcement ratio as almost half of the first one.

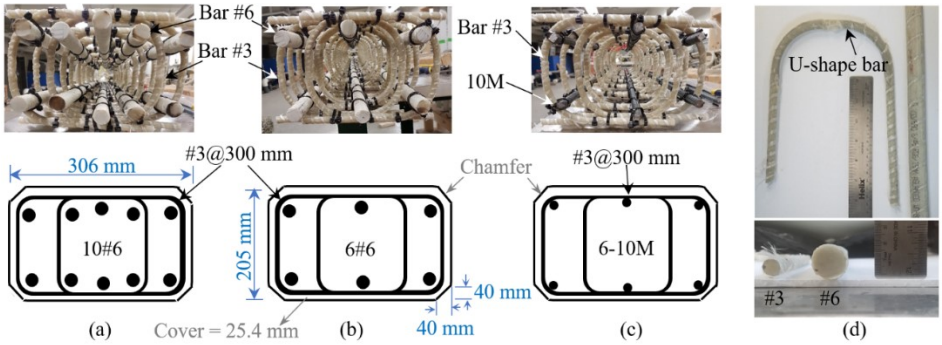

Figure 5. 1 Rebar layout: (a) GFRP-RC column with 4.80 % reinforcement ratio, (b) GFRP-RC column with 2.87% reinforcement ratio, (c) steel RC column with 1.00% reinforcement ratio, (d) U-shape bar and cross-sections

The bar layout for specimens reinforced with 10 GFRP bars, 6 GFRP bars, and 6 steel rebar are presented in Figure 5.1(a), (b), and (c), respectively, and Figure 5.1(d) shows a photograph of the bars used in the research, including a ruler. Moreover, two different load eccentricities of 42.5 and 47.5 mm were selected which were corresponding to 21 and 23 % of the width of column cross-section (205 mm). The eccentricity is applied on the width of the column cross-section (205 mm) because it provides a lower lever arm for bars and the testing machine can reach the column capacity. The center to center spacing of GFRP ties was 150 mm throughout the column. The minimum spacing of the transverse reinforcement was determined by the least of three according to Nanni et al. (2014): least dimension of the column (205 mm); Twelve times longitudinal bar diameter (228 mm); Twenty-four times tie bar diameter (240 mm). It was determined by Paultre and Légeron

(2008) and confirmed later for GFRP ties by Maranan et al. (2016) that the effect of confining reinforcement in restraining concrete is zero when the ties are spaced more than half of the minimum core cross-section. Moreover, Guérin et al. (2018a) studied eccentric behavior of GFRP-RC columns using bars and ties which confirmed the findings regarding confinement for eccentric loading. As the current study was not designed to account for the confinement effect, 150 mm was selected for spacing in order to minimize the confining effect, which is lower than the minimum (205 mm) and higher than half of the core cross-section, and to prevent bars from buckling, especially after concrete spalling. To prevent the premature failure at the ends of columns at a distance twice the depth of column the spacing of ties reduced to 75 mm. To provide the same confinement level for all specimens, even the steel RC column was reinforced with transverse GFRP ties. Previously, Hales et al. (2016) used longitudinal steel reinforcement and GFRP spirals to maximize the confined core area by reducing the cover made possible by a non-corrosion characteristic of GFRPs. It should be mentioned that the design philosophy for minimum required amount of spiral or ties for steel material is based on their confinement of the core. The behavior of steel ties showed a second peak load while for FRPs, the confinement did not lead to a second peak load. The latter can be attributed to the low modulus of GFRP in comparison to steel. Plus, the U-shape tie is not the best confining device. However, it should be mentioned that steel, as confining material is ductile and yields at a strain of 0.002 mm/mm and after that the modulus of elasticity became zero while for GFRP, the mentioned strain is at the beginning of the elasticity part and higher strains can be reached.

Both ends of all specimens were strengthened by applying three layers of GFRP wrapping in a total length of 200 mm, to prevent premature failure at the ends of the specimens. As

presented in Table 5.1, the general form of specimen ID is like "(A)(a)-e(b)-r(c)-N(d)", where the first letter (A) introduces the type of reinforcing bar, G for GFRP and S for steel, letters (a), (b), (c), and (d) represent the slenderness ratio, eccentricity-to-column width, reinforcement ratio, and the test number in a certain slenderness ratio, respectively. For example, a specimen ID like "G40-e21-r2-N3" represents a GFRP-RC column with a slenderness ratio of 39.7, eccentricity-to-column width of 0.21, reinforcement ratio of 2.87 %, and it shows that it was the third test in that eccentricity ratio.

5.2.2 Material Properties

The summary of the material properties is presented in Table 5.2. To determine the tensile characteristics of longitudinal GFRP bars, with a nominal diameter of 19 mm and a nominal area of 285 mm^2 (Aslan 100 products), five tensile GFRP coupons were built and tested per ASTM D7205M-06 (2016). It should be noted that for calculation of the tensile strength and modulus of the GFRP bars, the nominal cross-section of the bars was used. However, according to the immersion test performed on 5 coupons for #6 and #3, the cross-sections were determined as 314 mm2 and 86 mm2, respectively (with an error of ±9 mm^2).

Table 5. 2 Summary of material properties

Test Type	Material	Strength / Yielding		Modulus of elasticity		Ultimate / Yield strain	
		Symbol	(MPa)	Symbol	(GPa)	Symbol	(mm/mm)
Compression	Concrete	f'_c	56.8 ± 1.9	E_c	35.0 ± 1.2		-
	#6 GFRP bar	f'_{fcu}	684.2 ± 33.1	E_{fc}	48.9 ± 0.9	ε_{fcu}	0.0140
Tension	#3 GFRP bar	$*f'_{ftu}$	827	$*E_{ft}$	46	$*\varepsilon_{ftu}$	0.0179
	#6 GFRP bar	f'_{ftu}	963.0 ± 62.1	E_{ft}	43.4 ± 0.9	ε_{ftu}	0.0222
	Steel rebar	f'_y	442.6 ± 4.7	E_s	209.4 ± 5.6	ε_y	0.0021

Note: * = guaranteed values reported by manufacturer tested per ASTM D7205 (2016). It should be mentioned that guaranteed means the average for modulus of elasticity and an average minus three times the standard deviation for tensile strength per ACI 440.1R-15 (2015).

The compressive properties of GFRP bars were determined by testing five compressive coupons based on the test method proposed by Khorramian and Sadeghian (Khorramian and Sadeghian, 2019b and 2018). The ties were built using #3 GFRP bars with a nominal diameter and cross-sectional area of 10 mm and 71.26 mm2, respectively. The concrete was ready-mix with a maximum aggregate size of 12 mm and a slump of 200 mm. The 28-day concrete strength was determined as 48.4 ± 0.7 MPa by testing three 100×200 mm concrete cylinders per ASTM C39M-18 (ASTM 2018), and at the time of testing five concrete cylinders (150×300 mm) were tested whose results are presented in Table 5.2. It should be mentioned that all columns were cast from the same concrete batch. Moreover, five tensile coupons of the steel rebars were prepared and tested per ASTM A370M-18 (2018). It should be noted that in order to calculate the tensile strength and modulus of elasticity of steel bars, the nominal cross-section minus two machined areas for strain gauging (100-2× (6×1) = 88 mm^2), was used.

5.2.3 Specimen Fabrication and Preparation

Figure 5.2 presents the manufacturing process of the GFRP-RC column specimens. FRP bar cages with different slenderness ratios are shown in Figure 5.2(a). The center to center spacing of GFRP ties were 150 mm throughout the column. To prevent the premature failure at the ends of columns at a distance twice the depth of column the spacing of ties reduced to 75 mm. The molds were built by plywood and two-by-four lumber as shown in Figure 5.2(b). Four right-angle wooden sticks with a leg of 40 mm were installed at four corners of the specimens to give chamfers. Figure 5.2(c) shows the molds for all the specimens before pouring concrete. The molds were lubricated using oil for the plywood

surfaces and grease for chamfer surfaces. A ready-mix concrete was poured as shown in Figure 5.2(d) where the slump was kept at 200 mm using superplasticizer. The concrete specimens were cured for seven days by having them covered with wet burlap and plastic sheets as shown in Figure 5.2(f). The concrete specimens after demolding are presented in Figure 5.2(g). Both ends of all specimens were strengthened by applying three layers of GFRP wrapping in a total length of 200 mm, to prevent premature failure at the ends of the specimens.

Figure 5. 2 Fabrication: (a) GFRP cages, (b) G40 wooden mold and GFRP cage, (c) prepared columns before casting concrete, (d) fresh concrete inside molds, (e)curing, and (f) prepared columns

5.2.4 Test Setup and Instrumentation

The concrete columns were tested under axial loading using the test setup presented in Figure 5.3. The test fixture includes two concrete end blocks, a swivel, a 2MN actuator, a spherical platen, a load cell, a tunnel, a shaft, two sets of steel caps, two sets of steel belt, three sets of steel rollers. The V-notched welded plate was put at the center of the steel roller installed on the shaft and end block which provides the simply supported boundary condition for each end of the columns, as shown in Figure 5.3. The distance between the

center of the V-notched plate and the center of the specimen gave the desired load eccentricity. To increase the integrity of the column and steel cap setting, two grout bags were put between steel cap and concrete columns at both ends. Since the tests were performed horizontally, three sets of steel rollers were installed at the bottom of the concrete specimens as shown in Figure 5.3.

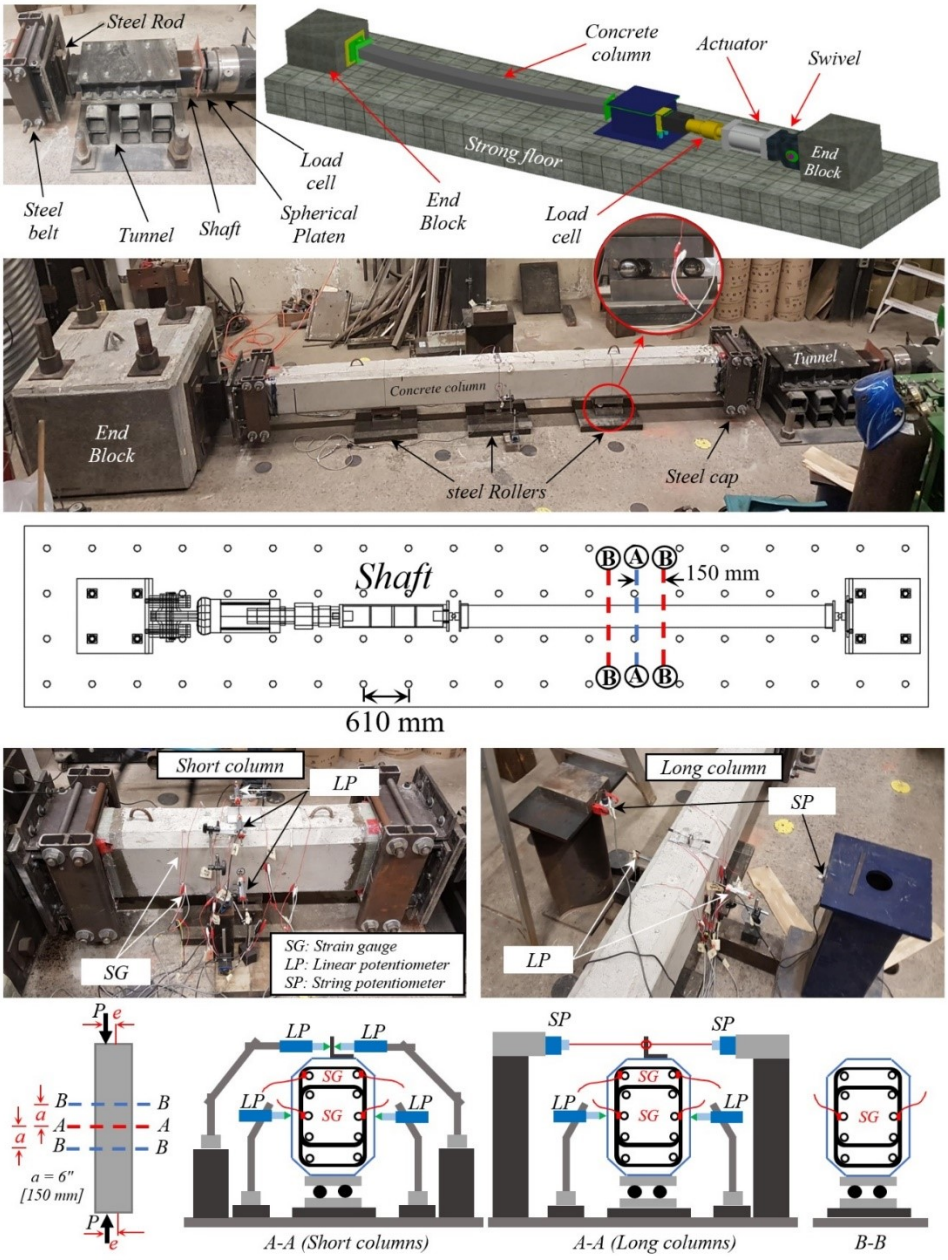

Figure 5. 3 Test set up and instrumentation

The data acquisition system included linear potentiometers (LPs), string pods (SPs), strain gauges (SGs) as presented in Figure 5.3. It should be noted that the load and stroke position was recorded both by the controller and the data acquisition system. The lateral displacement of the concrete columns was recorded at the middle height of the columns using four LPs. Two of the LPs were installed at the midsection in compression and tension sides as shown in Figure 5.3. On top of the specimen and at the centerline of the specimens, an angle-shaped aluminum profile with a length of 50 mm was bonded to the specimen using adhesives. For short columns, two more LPs were installed to capture the lateral displacement from to aluminum angle. However, for slender columns, due to the existence of larger lateral displacements, two SPs were used to track the lateral displacement of the column at the center of the aluminum angle as shown in Figure 5.3. To record the strain of the GFRP bars, eight strain gauges were used. The stains were recorded at three different sections through the length of the column; at midsection (section A-A) and at two sections that were 150 mm away from the mid-height of the columns (section B-B). The strains of the middle bars in tension and compression were recorded in all mentioned sections as shown in Figure 5.3. In addition, the tensile and compression strain of the corner bars were recorded in the middle section. The tests were performed by using a displacement control approach with a displacement rate of 2 mm/min. Moreover, the data was recorded with a rate of 10 data per second.

5.3 EXPERIMENTAL RESULTS AND DISCUSSION

The axial capacity of the tested specimens at their peak load (P_u) as well as their axial displacement (Δ_{axial}), lateral displacement ($\Delta_{lateral}$), and bending moment (M_u) corresponding to their peak loads are presented in Table 5.3. It should be noted that

specimen G17-e23-r4-N1 was tested three times and had experienced premature failure at the end of the specimen twice. The latter happened because the steel cap was not tight enough to make the specimen rotate at the ends. Each time, the end of the specimen was strengthened with grout and wrapped with GFRP wrapping before retesting. This was at the early stages of the testing, and later the issue was fixed by using steel belts to tighten the steel caps at the ends as discussed in the previous section. Therefore, this specimen will not be considered in the rest of the study.

Table 5. 3 Summary of test results

Group	No.	Specimen ID	P_u (kN)	Δ_{axial} (mm)	$\Delta_{lateral}$ (mm)	M_u (kN-m)	d_1 (mm)	d_2 (mm)
Short Columns	1	G17-e23-r4-N1	1401	21.1	11.0	80.8	58.2	150.2
	2	G17-e23-r4-N2	1480	17.5	6.6	80.1	54.3	149.1
	3	G22-e23-r4-N1	1550	17.1	7.8	84.7	54.3	150.6
	4	G22-e21-r4-N2	1410	17.6	9.3	73.4	53.1	148.4
	5	S22-e23-r2-N3	1564	17.4	9.0	87.4	47.1	150.1
Slender Columns	6	G40-e23-r2-N1	1210	22.2	21.8	83.8	55.7	150.0
	7	G40-e23-r4-N2	1116	15.6	23.1	78.8	52.2	154.4
	8	G40-e21-r2-N3	1204	16.9	23.9	78.4	53.1	153.9
	9	G40-e21-r4-N4	1315	17.2	23.7	87.1	54.6	144.3
	10	G60-e23-r4-N1	844	17.3	34.6	69.6	57.6	149.7

By comparing the results in Table 5.3, it is observed that some of the results were not as expected (i.e. G40-e23-r4-N2 and G22-e23-r4-N1). For example, a column with a higher slenderness ratio (i.e. G22-e23-r4-N1) sustained more load than the specimen with a lower slenderness ratio (i.e. G17-e23-r4-N2), which was not expected. Therefore, further investigation showed that the location of the bars was not the same for all specimens, as presented in Table 5.3. After testing, the specimens were cut perpendicular to their longitudinal axis to find out a more accurate location of the longitudinal bars in the cross-

section. It was observed that the bars were moved, and they were not in the same line since the location of the bars was dictated by the corner of U-shape stirrups along the bar. The GFRP stirrups are not flexible like steel ones, therefore, the difference in the bar locations is unavoidable, and the situation is a representative of real practice. After the section was cut, the location of the center of each bar was measured from the furthest compression fiber. The centroid of GFRP bars in the compression side (d_1) and in the tension side (d_2) were measured from the furthest compression fiber in concrete and presented in Table 5.3. Other sources of error were the inaccuracy in the eccentricity that varied as much as ±3 mm (due to the existence of the grout bags between concrete and steel caps), and the variability in the size of chamfers (±2 mm for the legs of chamfers), and variability in the dimension of the columns (±1 mm for width of columns). Also, the manufacturing process and the quality of stirrups could be another source of error. The behavior and results are discussed in more detail in the following sections.

5.3.1 Failure Modes

In the current study, a total of three modes of failure were observed including concrete spalling/ crushing (CC), global buckling (GB), and crushing of GFRP bars (GC), as presented in Figure 5.4. It should be highlighted that no GFRP crushing was observed prior to concrete failure. No rupture of tensile GFRP bars occurred during the tests. Figure 5.5(a) and Figure 5.5(b) present axial load-axial displacement curves of the slender concrete columns. It is seen that the unloading part was captured for slender columns.

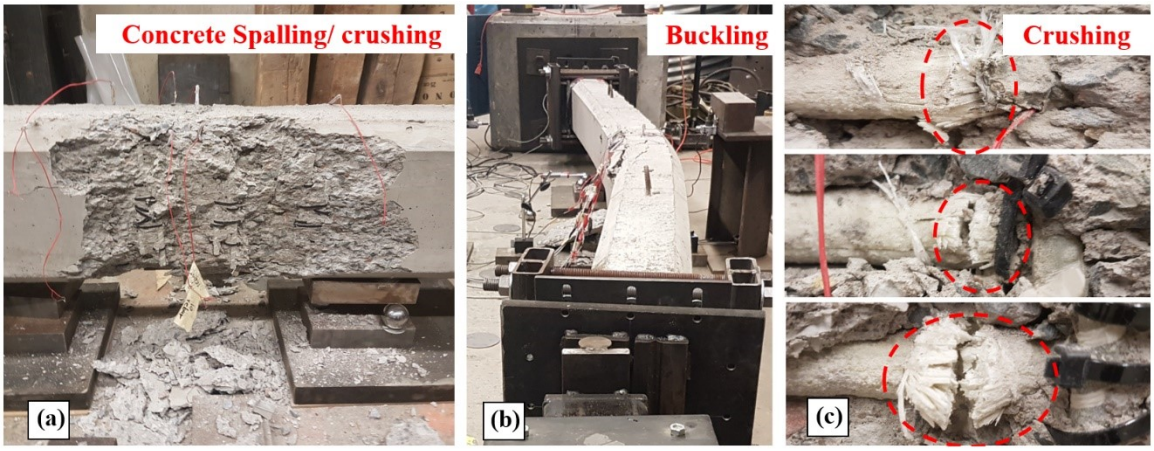

Figure 5. 4 Failure modes: (a) concrete crushing/ spalling (CC), (b) global buckling (GB), and (c) GFRP crushing (GC)

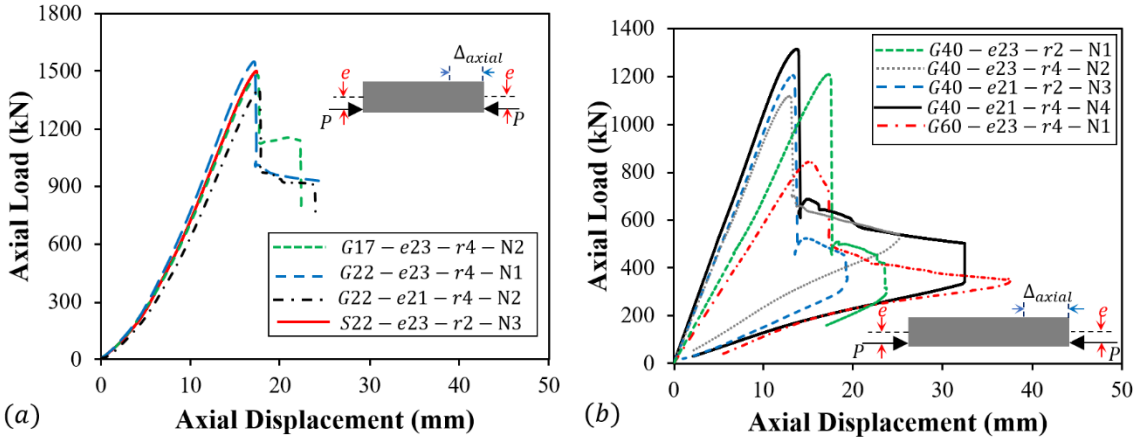

Figure 5. 5 Axial load-axial displacement curves: (a) short columns; and (b) slender columns

The loading stages are shown in Figure 5.6. For short columns, the specimens did not experience buckling and the peak load was almost corresponding to the spalling/crushing of the concrete. A very slight drop after peak load was observed. For slender columns, the columns buckled first, and concrete crushing happened afterward as shown in Figure 5.6. After concrete spalling/ crushing, the behavior of both slender and short GFRP-RC columns

was the same. A sudden drop in axial capacity was observed after concrete crushed as shown in Figure 5.6.

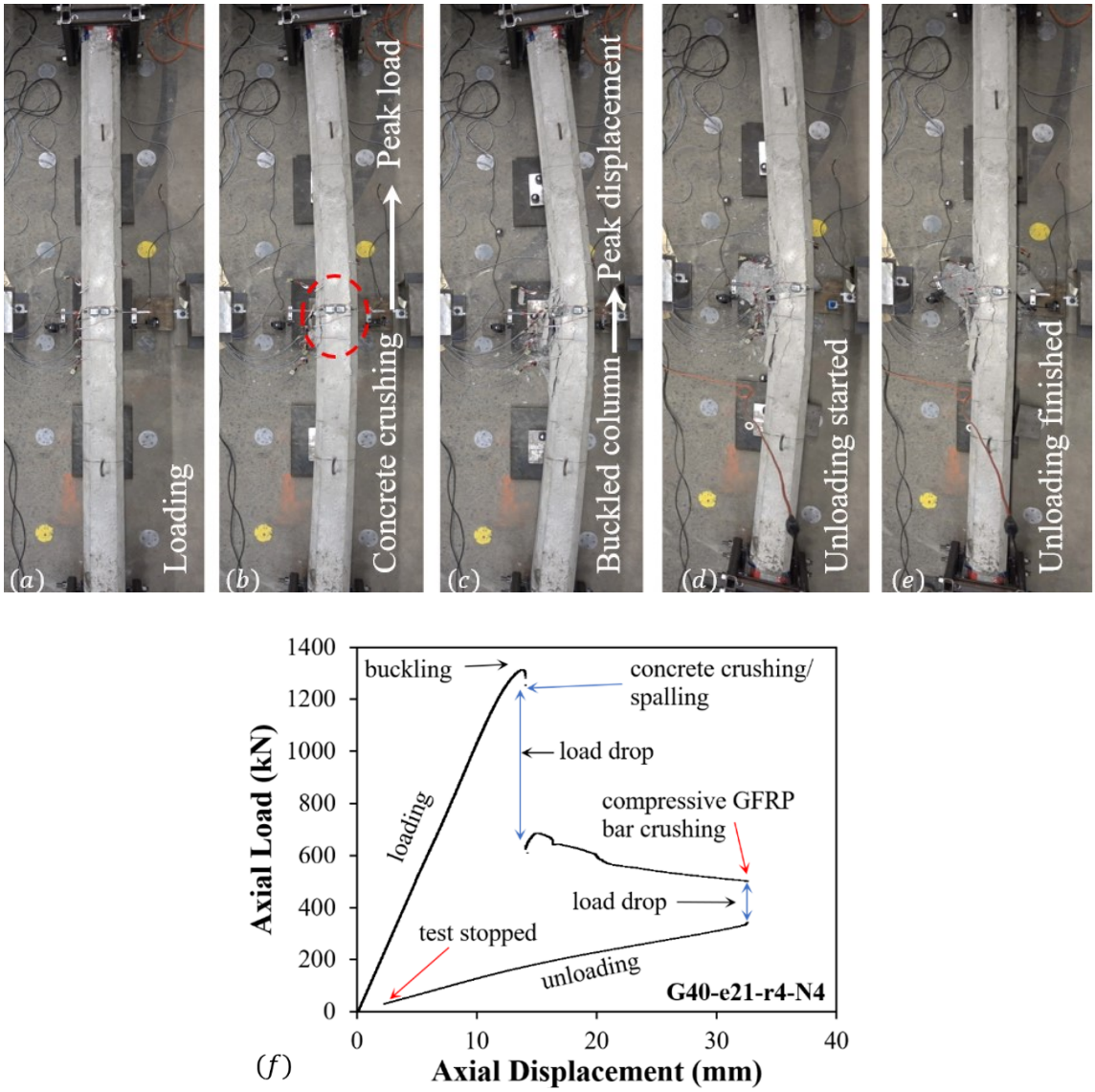

Figure 5. 6 Test observations: (a) loading, (b) concrete spalling/crushing, (c) buckled column, (d) column during unloading, (e) unloaded specimen, (f) Loading stages of slender GFRP RC columns

As the test was performed with a displacement control approach, testing was continued after load dropped. At this stage, the capacities of the specimens were dropped as the axial displacement increased, with a very slight slope to reach the crushing of GFRP bars in

compression, as presented in Figure 5.6. After GFRP bar crushing, a sudden drop happened as the displacement increased. Therefore, the tests were stopped, and the unloading procedure started with a displacement rate of 4 mm/min to capture the unloading part as presented in Figure 5.6. It was observed that as the displacement decreases in the unloading part, the specimens became straight and the axial load-axial displacement curves tend to come back to the origin, as shown in Figure 5.5 and Figure 5.6.

The additional ability to sustain loads after concrete spalling/ crushing can be attributed to GFRP compressive bars. Such behavior was not observed in the steel-reinforced concrete specimen. Instead, after concrete crushed, the deformation was not reversible like GFRP bars. It should be noted that there was not enough steel reinforcement to see ductile behavior (i.e. for S22-e23-r2-N3 a minimum reinforcement ratio of 1% was considered). However, even if steel was sufficient, at large deformations, many layers of reinforcements would be yielded and then the column would experience a permanent displacement, due to permanent plastic deformations after steel yielded, which is different than observations for GFRP-RC columns (since once stress is removed, there is no permanent deformation for GFRP bars). The axial stiffness of steel RC column and GFRP-RC column at slenderness ratio of 22 (which is known as the critical slenderness ratio for the steel-RC columns in unbraced frames) was kept the same which lead to almost the same axial capacity of the column. It was observed that before failure steel-RC column experienced more lateral deformation and hence more moment capacity in comparison to the GFRP-RC column. However, there was no additional capacity after concrete crushed in the steel RC column.

5.3.2 Load-Displacement Behavior

The axial load-lateral displacement curves for short and slender columns are presented in Figure 5.7(a) and Figure 5.7(b), respectively. It is seen that for all GFRP reinforced specimens, there was a sudden jump in the lateral displacement after concrete crushed at the midspan. However, the specimens continued to experience more lateral displacement up to the crushing of GFRP bars in compression. It should be noted that the slenderest column did not experience GFRP bar crushing since the test was stopped due to safety concerns in the lab. For G60-e23-r4-N1, a considerable lateral displacement at the midspan was observed (i.e. 193.7 mm) and the rotational capacity of the test fixture at the ends of the columns was very considerable before the test stopped. It was observed that specimens with higher slenderness ratio experiences more lateral deformation. Table 5.4 presents the displacement values corresponding to concrete spalling/crushing and crushing of GFRP bars or termination of the test. On average, specimens experienced 61.2 mm additional displacement after concrete crushing which is almost three times more than the displacement at the crushing point.

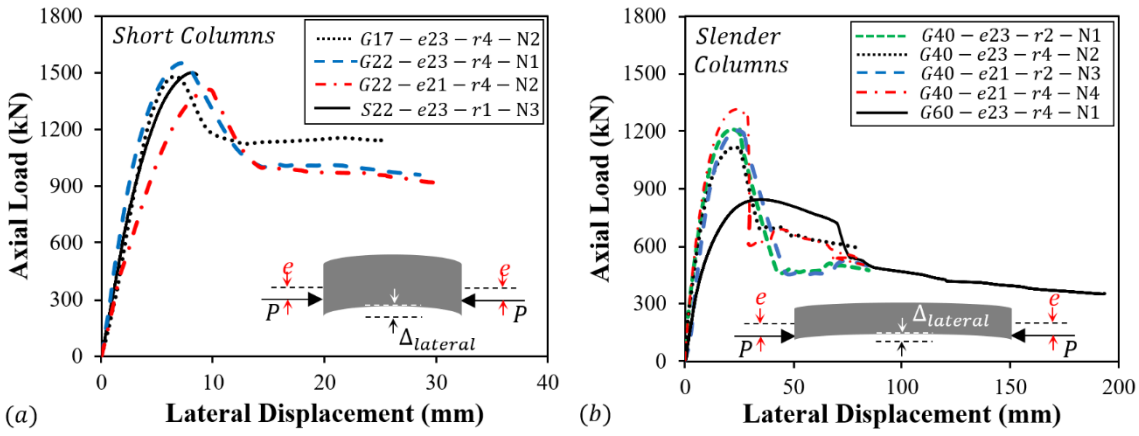

Figure 5. 7 Axial load- lateral displacement curves for: (a) short columns; and (b) slender columns

By multiplying the axial load (P) by the sum of lateral displacement (Δ) and initial eccentricity (e_0), at each loading step, the corresponding bending moment ($M = P\times(e_0+\Delta)$) can be calculated. The loading path for short and slender specimens is presented in Figure 5.8(a) and Figure 5.8(b), respectively.

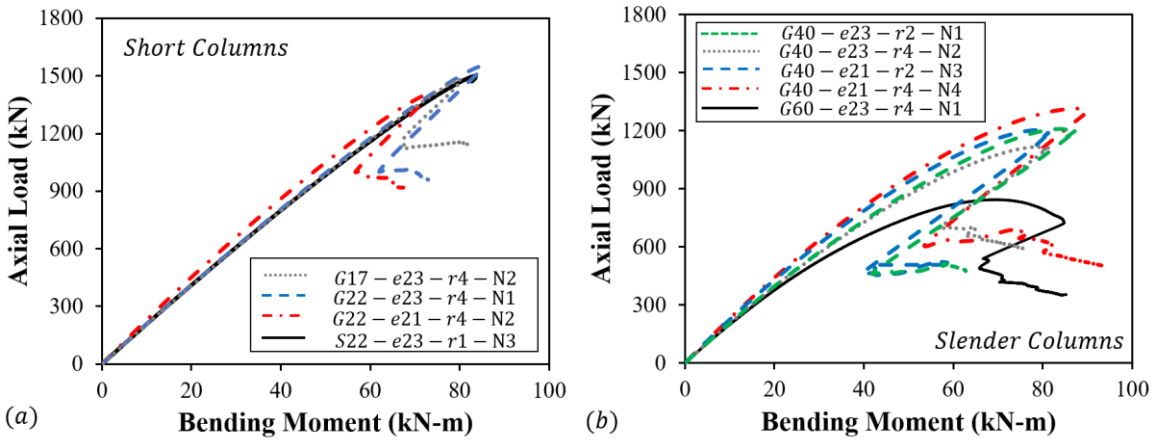

Figure 5. 8 Axial load- bending moment curves for: (a)short columns; and (b)slender columns

After concrete crushed and a sudden drop in load happened, there was an additional moment resistance in the specimens. Table 5.4 shows that on average, the moment capacity is dropped only 9% after concrete crushed up to the crushing of GFRP bars in compression. Therefore, the ability of the column to sustain more lateral displacement leads to similar moment capacities at concrete spalling/crushing and after that up to GFRP bar crushing.

By using the data presented in Table 5.3 for the values of peak load, and Table 5.4 for the values of the load when concrete crushed, the drop of the load before crushing can be determined. The average drop in load from peak load to the crushing point was 0.62% for short specimens, 1.00% for specimens with a slenderness ratio of 39.7, 15.60% for the specimen with a slenderness ratio of 59.5, and 4.79% for the steel-reinforced column. The

tests showed that, for the slenderness ratio of 22, the average drop of load after peak load up to concrete spalling for GFRP-RC columns (0.46%) was more than ten times smaller than the drop for the steel-reinforced specimen (4.79%). The latter shows that the slenderness effect was less for GFRP-RC columns than for steel RC columns. The average load drop from concrete spalling/crushing to crushing of GFRP bars in compression was 48.5% as presented in Table 5.4.

Table 5. 4 Axial load, bending moment, and lateral displacement capacities of columns after concrete crushing up to failure

No.	Specimen ID	P_{CC} (kN)	P_{GC} (kN)	Load drop (%)	M_{CC} (kN-m)	M_{GC} (kN-m)	Moment drop (%)	Δ_{CC} (mm)	Δ_{GC} (mm)	Δ_{CC} - Δ_{GC} (mm)
1	G17-e23-r4-N2	1466	1140	-22.2	80.0	82.7	3.3	7.1	25.0	18.0
2	G22-e23-r4-N1	1544	930	-39.8	85.1	73.0	-14.2	7.6	28.5	20.9
3	G22-e21-r4-N2	1403	900	-35.9	73.5	67.2	-8.7	9.9	30.6	20.7
4	S22-e23-r2-N3	1489	NA	NA	83.5	NA	NA	8.6	NA	NA
6	G40-e23-r2-N1	1205	421	-65.1	87.7	62.8	-28.4	25.2	84.6	59.4
8	G40-e23-r4-N2	1108	536	-51.6	80.5	76.3	-5.2	25.1	81.7	56.6
5	G40-e21-r2-N3	1201	449	-62.6	82.0	59.1	-27.9	25.8	74.0	48.2
7	G40-e21-r4-N4	1281	504	-60.7	89.1	93.3	4.7	27.1	142.8	115.7
9*	G60-e23-r4-N1	712	353	-50.4	84.0	85.3	1.4	43.8	193.7	149.9
Average				-48.5			-9.4			61.2
STD				14.0			12.4			45.0
COV				-28.8			-132.2			73.5

Note: * = test stopped before crushing of GFRP bar due to excessive deformation.

In terms of strain records, since the location of the bars was different in the section as shown in Table 5.3, the strain of GFRP bars even in the same section was different. It is seen that short specimens reached higher compressive strain when concrete crushed. On average, GFRP bars in compression experienced 63% and 36% more strain in comparison to slender specimens. The latter justifies that slender columns were able to sustain more than four times extra lateral displacement in comparison to short columns. Thus, slender GFRP

columns show more deformability and are able to reach higher strains at much larger lateral displacements.

Table 5.5 presents the compressive strain of the GFRP bars at the midsection. It should be noted that in some cases, the strains at the final stage (GC) were not available. Therefore, for those cases, the maximum strain recorded was selected which is less than the actual strain at the end of the loading stage.

Table 5. 5 The compressive strain of GFRP/steel bars at different loading stages

No.	Specimen ID	SG2 (mm/mm)				SG4 (mm/mm)			
		$\varepsilon_{peak,c}$	$\varepsilon_{CC,c}$	$\varepsilon_{GC,c}$	$\varepsilon_{GC,c}$ - $\varepsilon_{CC,c}$	$\varepsilon_{peak,c}$	$\varepsilon_{CC,c}$	$\varepsilon_{GC,c}$	$\varepsilon_{GC,c}$ - $\varepsilon_{CC,c}$
1	G17-e23-r4-N2	-0.0041	-0.0049	-0.0150	-0.0101	-0.0023	-0.0024	NA	NA
2	G22-e23-r4-N1	-0.0023	-0.0025	NA	NA	-0.0030	-0.0033	NA	NA
3	G22-e21-r4-N2	-0.0022	-0.0023	-0.0103	-0.0080	-0.0028	-0.0030	NA	NA
4	S22-e23-r2-N3	-0.0039	-0.0039	NA	NA	-0.0018	-0.0018	NA	NA
5	G40-e23-r2-N1	-0.0020	-0.0025	-0.0103	-0.0078	-0.0024	-0.0029	-0.0100	-0.0071
6	G40-e23-r4-N2	-0.0022	-0.0023	-0.0052	-0.0029	-0.0030	-0.0034	-0.0140	-0.0107
7	G40-e21-r2-N3	-0.0020	-0.0037	NA	NA	-0.0028	-0.0041	NA	NA
8	G40-e21-r4-N4	-0.0016	-0.0018	-0.0068	-0.0050	-0.0029	-0.0072	NA	NA
9*	G60-e23-r4-N1	-0.0010	-0.0016	NA	NA	-0.0011	-0.0018	-0.0055	-0.0037
Average					-0.0068				-0.0072
STD					0.0025				0.0028
COV					-37.6				-39.4

Note: * = test stopped before crushing of GFRP bar due to excessive deformation.

It was observed that on average, the additional stains that GFRP bars experienced after concrete crushed were 0.0070 mm/mm and 0.0099 mm/mm for the compression side and tensile sides, respectively. This justifies the extra moment capacity of the specimens after concrete crushed and explains the mechanism of failure (presented later in the contribution of the GFRP bars section). The failure of concrete led to a decrease in the resultant concrete compressive force in section, which suddenly led to a drop in axial and moment capacity. However, due to the presence of the compressive GFRP bars, after a drop, equilibrium was satisfied in the section. As the loading continued after the concrete spalling/crushing stage,

the strain in both compressive and tensile sides increased and the compressive force in GFRP bars increased and contributed more in bending capacity of the columns up to the crushing of GFRP bars in compression. The GFRP bars were started to buckle once the concrete spalled which lowered down the capacity of longitudinal bars and caused failure before GFRP bars reached their compressive crushing strain obtained from material tests. The average compressive strain of GFRP bars at the ultimate stage (GC) was 0.0102 mm/mm which was 73% of the average crushing strain found by material testing (0.01399 mm/mm). Since the slenderest specimen did not experience crushing of bars, it was excluded from this average. Therefore, overall, the compressive GFRP bars are very effective especially in creating deformability and keep the section in equilibrium after concrete spalling/crushing.

5.3.3 Moment-Curvature Behavior

The moment-curvature curves of the specimens at mid-height are presented in Figure 5.9. The moments and curvatures were determined from strain profiles at each load step.

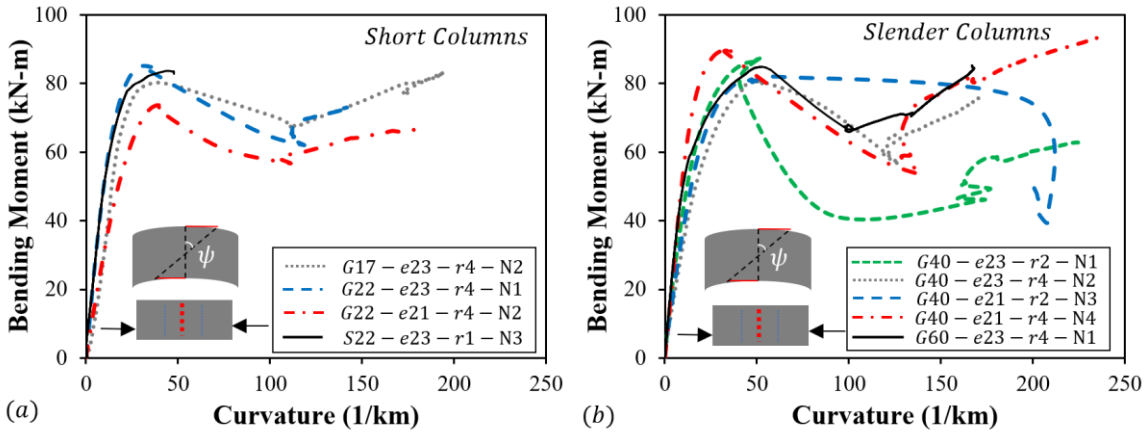

Figure 5. 9 Moment-curvature curves for: (a) short columns, and (b) slender columns

The strain profile was derived by fitting a straight line to the values of strain gauge records at the mid-height section. The strains at each section for each strain gauge can be found in Figure 5.10.

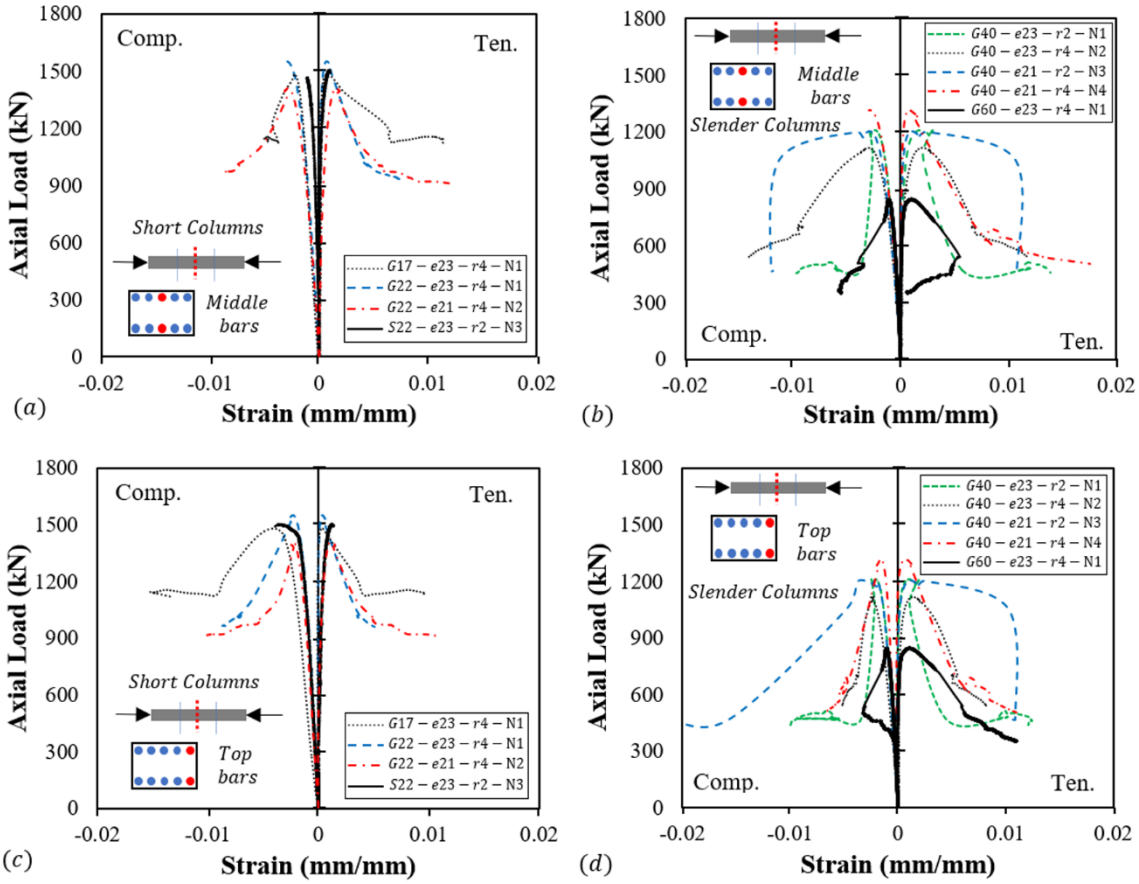

Figure 5. 10 The axial load-axial strain of GFRP bars for: (a)short columns at middle bars, (b) slender columns at middle bars, (c) short columns at top bars, and (d) slender columns at top bars

As shown in Figure 5.9, it is observed that for all GFRP reinforced concrete specimens, the moment-curvatures curves showed a secondary hardening part after failure. In other words, it was observed that after GFRP-RC specimens reached their capacity, the equilibrium was satisfied, and the specimens were able to sustain loads to gain extra moment capacity after the drop in the peak load. The latter can be attributed to the effect of GFRP bars in

compression. After concrete spalling/ crushing, the equilibrium is disturbed and while the lateral deformation increases, the moment decreases due to a sudden drop in the axial load capacity. Meanwhile, the curvature of the crushed column increases which causes an increase in the strains of compressive GFRP bars. Thus, although concrete is able to sustain less compressive loads, compressive GFRP bars start to contribute more considerably in the compressive side.

As the contribution of GFRP bars in compression increases due to an increase in the curvature, the bending moment increases up to the moment that GFRP reaches its crushing in compression or buckles. This mechanism is attributed to the linear stress-strain relationship of FRPs which makes them gain strength even after concrete failure. It should be mentioned that in a recent study on the moment-curvature behavior of GFRP-RC columns, Hasan et al. (2019) observed similar moment-curvature behavior using analytical-numerical methods.

5.3.4 Flexural Stiffness

To further investigate the behavior of the tested specimens, their flexural stiffness was evaluated from the moment-curvature curves. Figure 5.11 shows four different points on the moment-curvature curves that represent different flexural stiffnesses corresponding to peak load (EI_{Peak}), concrete spalling (EI_{SP}), design strain or a strain level of 0.003 mm/mm (EI_{D}), and corresponding to GFRP crushing (EI_{GC}). These calculated stiffnesses from experimental test data can be compared to the available formulas for the estimation of the flexural stiffness used in the literature.

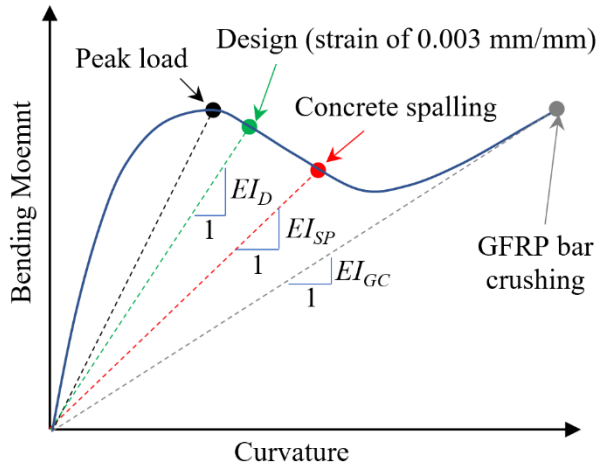

Figure 5. 11 Moment-curvature curves for: (a) short columns, and (b) slender columns

Table 5.6 presents the available formulas for the prediction of the flexural stiffness of the concrete columns used in the moment magnification method to account for the slenderness effects. It should be mentioned that a high presumed eccentricity is embedded in Equation 5.1, Equation 5.2, Equation 5.7, and Equation 5.9, since they meant to be used for design purposes where the eccentricity values are not known in advance.

For consistency in the calculations, all formulas were normalized to have the same stiffness reduction factor of 0.75. It should be noted that for the calculation of the stiffness, the effect of chamfers was deducted from the concrete section, and the values of d_1 and d_2 (see Table 5.3) were used to calculate the effect of reinforcing bars in the calculations. Moreover, the modulus of elasticity of concrete was calculated based on the proposed equation (i.e. $E_c = 4700\sqrt{f_c'}$) by ACI 318-19 (2019). Also, the nominal cross-sectional area of bars was considered, and the modulus of elasticity of steel and FRP were considered as 200 GPa and 43.4 GPa, respectively, as reported by the manufacturer.

Table 5. 6 Equations in the literature for calculating flexural stiffness of RC columns

No.	Flexural stiffness equation		Reference
1	$EI_1 = 0.4E_cI_g$	(5.1)	(ACI 318-19, 2019) (6.6.4.4.4a)
2	$EI_2 = 0.2E_cI_g + E_sI_s$	(5.2)	(ACI 318-19, 2019) (6.6.4.4.4b)
3	$EI_3 = E_cI;\ 0.35I_g \le I = \left(0.80 + 25\frac{A_{st}}{A_g}\right)\left(1 - \frac{M_{ult}}{P_{ult}h} - 0.5\frac{P_{ult}}{P_o}\right)I_g \le 0.875I_g$	(5.3)	(ACI 318-19, 2019) (6.6.4.4.4a) and (Table 6.6.3.1.1b)
4	$EI_4 = \frac{0.7}{0.75} \times [(0.27 + 0.003\,l/h - 0.3\,e/h)E_cI_g + E_sI_s]$	(5.4)	(Mirza, 1990)
5	$EI_5 = \frac{0.7}{0.75} \times [(0.3 - 0.3\,e/h)E_cI_g + E_sI_s]$	(5.5)	(Mirza, 1990)
6	$EI_6 = \frac{(0.36 + 0.05n - 0.3e/h)}{0.75} \times (0.2E_cI_g + E_fI_f)$	(5.6)	(Mirmiran et al., 2001)
7	$EI_7 = \frac{(0.2 + 0.06n)}{0.75} \times (0.2E_cI_g + E_fI_f)$	(5.7)	(Mirmiran et al., 2001)
8	$EI_8 = E_cI;\ I = \left(0.80 + 25\frac{A_f}{A_g}\frac{E_f}{E_s}\right)\left(1 - \frac{M_{ult}}{P_{ult}h} - 0.5\frac{P_{ult}}{P_o}\right)I_g \le 0.875I_g$	(5.8)	(Zadeh and Nanni, 2013)
9	$EI_9 = 0.2E_cI_g + 0.75E_fI_f$	(5.9)	(Zadeh and Nanni, 2017)
10	$EI_{10} = \frac{0.7}{0.75} \times \left(\left[0.45 - \left(1 + 0.01\frac{l}{h}\right)\left(\frac{e}{h}\right) + 0.008\frac{l}{h}\right]E_cI_g + E_fI_f\right)$	(5.10)	(Xue et al., 2018)

Note: All formulas have been normalized to 0.75 to have the same stiffness reduction factor per ACI 318-19 (2019).

To calculate P_{ult} and M_{ult}, which are the ultimate factored loads, $0.65P_D$ and $0.65M_D$ were considered, in order to consider a reduction factor of 0.65 per ACI 440.1R-15 (2015) for calculation of ultimate factored loads. It should be noted that the values of P_D and M_D are presented in Table 5.8. The value of P_o was calculated based on Equation 5.11 (ACI 318-19 2019) in which f_y was replaced by the modulus of elasticity of GFRP bars times the design strain of 0003 mm/mm, and A_{st} was replaced by A_f for GFRP RC columns.

$$P_o = 0.85f'_c\left(A_g - A_{st}\right) + f_yA_{st} \tag{5.11}$$

The results for the flexural stiffness calculated with different formulas presented in Table 5.6 are presented in Table 5.7 along with the ones calculated based on the experimental test data. Moreover, Figure 5.12 presents a comparison of the EI equations from literature with the design flexural stiffness calculated based on the experimental tests at the strain of 0.003 mm/mm.

Table 5. 7 The flexural stiffness of test specimens at different loading stages in comparison with values obtained from the literature

No.	Specimen ID	Flexural stiffness, EI (kN-m^2)													
		At loading stages of Fig. 13				From the literature (See Table 6)									
		EI_{peak}	EI_D	EI_{SP}	EI_{GC}	EI_1	EI_2	EI_3	EI_4	EI_5	EI_6	EI_7	EI_8	EI_9	EI_{10}
1	G17-e23-r4-N2	2232	1864	1864	429	2748	1652	6012	1644	1741	776	602	6012	1583	1852
2	G22-e23-r4-N1	2960	2497	2633	288	2748	1661	6012	1680	1749	780	606	6012	1589	1914
3	G22-e21-r4-N2	1968	2086	1853	225	2748	1655	6012	1714	1782	791	604	6012	1585	2045
4	S22-e23-r2-N3	1543	NA	1788	NA	2748	1694	6012	1711	1780	1295	1217	6012	1614	1945
6	G40-e23-r2-N1	2247	2433	1675	186	2748	1539	6012	1672	1635	723	561	5690	1498	2000
8	G40-e23-r4-N2	1870	2096	1675	188	2748	1697	6012	1819	1783	797	619	6012	1616	2147
5	G40-e21-r2-N3	2241	2110	1355	463	2748	1563	6012	1732	1696	746	570	5691	1516	2165
7	G40-e21-r4-N4	3465	2744	2729	397	2748	1624	6012	1790	1753	776	592	6012	1561	2222
9*	G60-e23-r4-N1	3135	2583	1468	511	2748	1637	6012	1877	1726	769	597	6012	1571	2308
Average		2407	2302	1893	336	2748	1636	6012	1738	1738	828	663	5940	1570	2066
STD		603	285	450	121	0	51	0	72	45	166	197	133	38	145
COV (%)		25	12	24	36	0	3	0	4	3	20	30	2	2	7

Note: * = test stopped before crushing of GFRP bar due to excessive deformation.

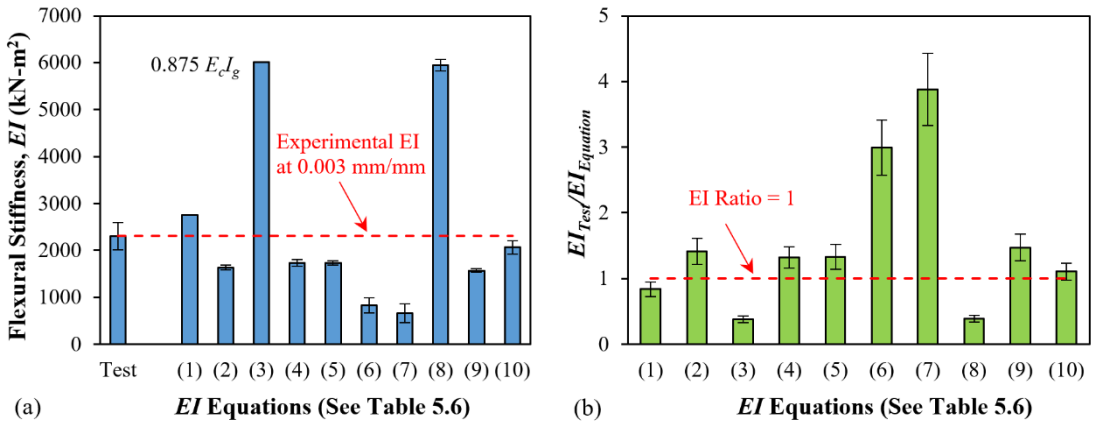

Figure 5. 12 Comparison of flexural stiffness obtained from the current experimental program and major equations from the literature: (a) EI values; and (b) EI ratios

The results showed that most of the current equations underestimated the flexural stiffness. Equation 5.10 gives the closest value to the experimental design flexural stiffness corresponding to the strain of 0.003 mm/mm. Equation 5.4 and Equation 5.5 are giving the best estimation of the flexural stiffness at concrete spalling. It was observed that Equation 5.1, Equation 5.3, and Equation 5.8 overestimates the flexural stiffness, and for most cases, the upper limit of $0.875E_cI_g$ was controlling Equation 5.3 and Equation 5.8. Also, the results showed that flexural stiffnesses which were calculated by Equation 5.6 and Equation 5.7 are considerably underestimating the experimental values. Therefore, by neglecting these equations, Equation 5.2 and Equation 5.9 are the most conservative equations for estimation of the flexural stiffness. Since Equation 5.9 was derived based on neglecting GFRP bars in compression from Equation 5.2, it gave lower stiffness values than Equation 5.2. However, stiffness values calculated by Equation 5.2 are closer than Equation 5.9 to experimental stiffness at the design level, which shows the equation which considered the contribution of GFRP bars was more realistic and accurate. It should be noted that this conclusion is valid for the range of tested eccentricity.

5.3.5 Moment Magnification Factor

The equations for moment magnification factor (δ) per ACI 318-19 (ACI 2019) are presented in the following:

$$P_{cr} = \frac{\pi^2 EI}{(kl)^2} \tag{5.12}$$

$$\delta = \frac{C_m}{1 - \frac{P_{ult}}{0.75P_{cr}}} \tag{5.13}$$

Table 5.8 presents experimental and calculated moment magnification factors at design loads and at peak loads. For calculation, C_m was considered as 1 since the columns were tested under pin-pin boundary condition. To calculate P_{ult}, which is the ultimate factored load, $0.65P_D$ and 0.65Pu were considered to calculate moment magnification factors corresponding to EI_D and EI_u, respectively. It should be noted that to reflect the effect of the factored loads, a reduction factor of 0.65 was considered for columns per ACI 440.1R-15 (2015) and ACI 318-19 (2019). For calculation of the experimental ratios, the moments at design and peak loads to their corresponding first-order moments (initial eccentricity times load), were considered as the experimental moment magnification factors. The results showed that the ratio of the calculated to experimental moment magnification factors at design loads and peak load are 0.95 and 0.94, respectively.

Table 5. 8 Moment magnification factor at the design load level and at the peak load

No.	Specimen ID	At the design strain of 0.003 mm/mm						At the peak load			
		P_D (kN)	M_D (kN-m)	M_{D_1st} (kN-m)	δ_{calc}	δ_{test}	$\delta_{calc}/\delta_{test}$	M_{u_1st} (kN-m)	δ_{calc}	δ_{test}	$\delta_{calc}/\delta_{test}$
1	G17-e23-r4-N2	1472	80.0	69.2	1.10	1.16	0.95	69.6	1.09	1.15	0.94
2	G22-e23-r4-N1	1546	84.0	72.6	1.13	1.16	0.98	72.9	1.11	1.16	0.95
3	G22-e21-r4-N2	1403	72.5	60.3	1.15	1.20	0.95	60.6	1.16	1.21	0.95
4	S22-e23-r2-N3	NA	NA	NA	NA	NA	NA	73.5	1.24	1.19	1.04
6	G40-e23-r2-N1	1206	81.8	56.7	1.41	1.44	0.98	56.9	1.46	1.47	0.99
8	G40-e23-r4-N2	1101	74.0	51.8	1.45	1.43	1.01	52.5	1.54	1.50	1.03
5	G40-e21-r2-N3	1203	79.6	51.7	1.50	1.54	0.98	51.8	1.46	1.51	0.96
7	G40-e21-r4-N4	1302	89.5	56.0	1.39	1.60	0.87	56.6	1.29	1.54	0.84
9	G60-e23-r4-N1	830	75.6	39.0	1.69	1.94	0.87	39.7	1.52	1.76	0.87
Average*		1258	79.6	57.2	1.35	1.43	0.95	79.6	1.33	1.41	0.94
STD*		228	5.6	10.6	0.21	0.27	0.05	5.6	0.19	0.22	0.06
COV (%) *		18	7	19	15	19	5	7	14	15	7

Note: * = The steel RC column is excluded in the calculation of average, standard deviation, and coefficient of variation; The loads and moments corresponding to peak load were presented in Table 3.

The observation showed that for the range of tested specimens, the calculated moment magnification factor is less than experimental values which is not conservative. Thus,

further investigations are required to validate the performance of equations for calculation of the moment magnification factors for GFRP RC columns.

5.3.6 Contribution of GFRP Bars

The procedure followed to determine the contribution of GFRP bars in axial and moment capacities is illustrated in Figure 5.13(a).

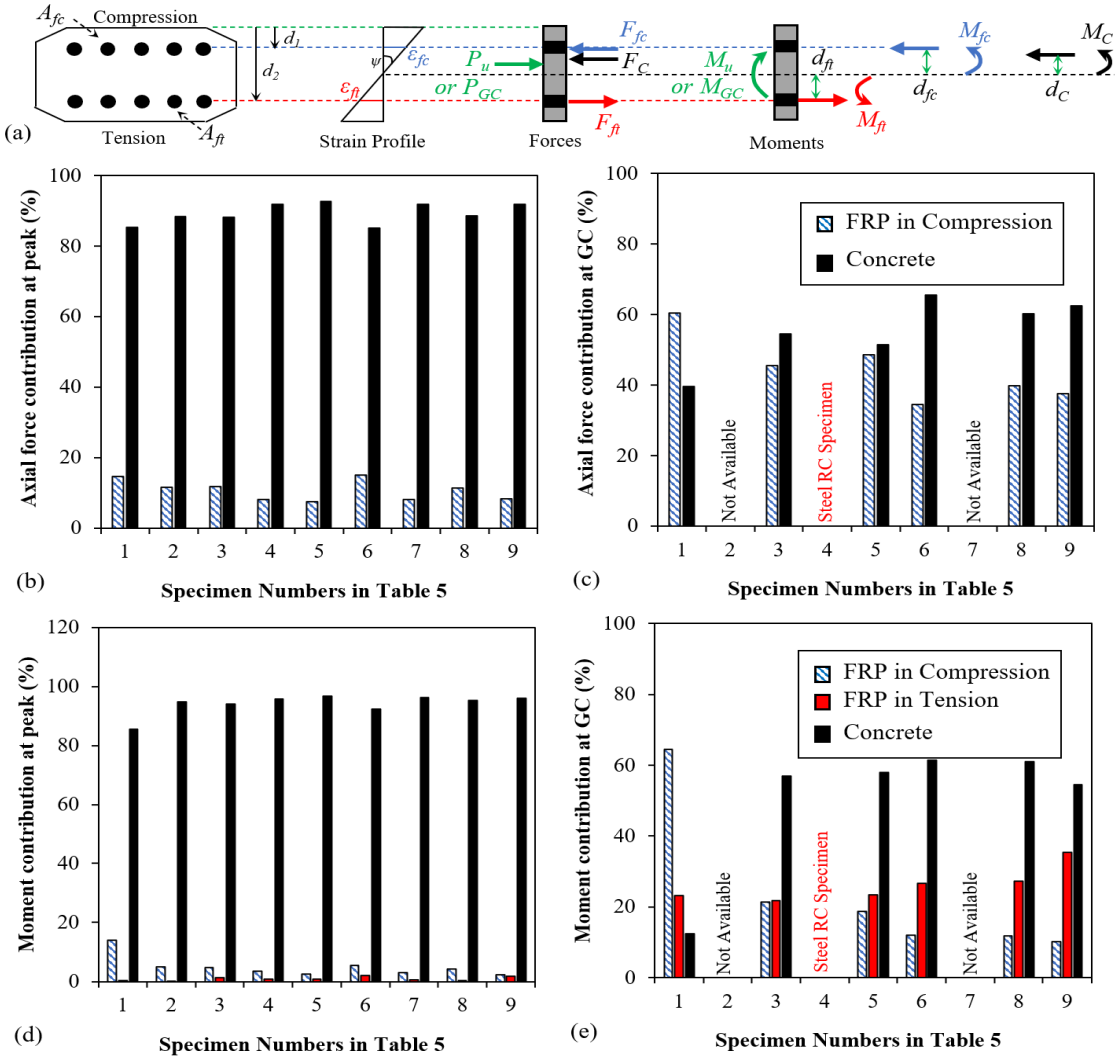

Figure 5. 13 Contribution of GFRP bars: (a) illustration of calculations, (b) axial force contribution at peak load, (c) axial force contribution at compressive GFRP bar crushing, (d) bending moment contribution at peak load, and (e) bending moment contribution at compressive GFRP bar crushing

In order not to overestimate the effect of bars, the minimum recorded strain at compression and tensile sides were used to assess the internal forces of the GFRP bars at peak load and crushing of GFRP bars using Equation 5.14.

$$F_{fc} = E_{fc}\varepsilon_{fc}A_{fc};\ F_{ft} = E_{ft}\varepsilon_{ft}A_{ft};\ F_C = (P_u\ or\ P_{GC}) - F_{fc} - F_{ft} \quad (5.14)$$

To calculate the internal moment corresponding to GFRP bars and concrete, the curvature of the section was determined using the compressive and tensile strains of GFRP bars using Equation 5.15, and from the curvature the lever arms for the internal forces in GFRP bars were found. Afterward, the moment resistance due to GFRP bars in compression, GFRP bars in tension, and concrete in compression at peak load and crushing of compressive bars were calculated using Equation 5.16.

$$\psi = \frac{\varepsilon_{ft} - \varepsilon_{fc}}{d_2 - d_1} \quad (5.15)$$

$$M_{fc} = F_{fc}d_{fc};\ M_{ft} = F_{ft}d_{ft};\ M_C = (M_u\ or\ M_{GC}) - M_{fc} - M_{ft} \quad (5.16)$$

Table 5. 9 Calculated internal forces and moments at peak load and at GFRP bar crushing

No.	Specimen ID	Contribution at peak load					Contribution at GC (GFRP bar crushing)				
		F_{fc} (kN)	F_C (kN)	M_{fc} (kN-m)	M_{ft} (kN-m)	M_C (kN-m)	F_{fc} (kN)	F_C (kN)	M_{fc} (kN-m)	M_{ft} (kN-m)	M_C (kN-m)
1	G17-e23-r4-N2	222	1293	17.9	0.5	61.7	1044	685	60.5	21.7	0.5
2	G22-e23-r4-N1	183	1399	14.7	0.5	69.5	NA	NA	NA	NA	NA
3	G22-e21-r4-N2	176	1318	10.9	2.8	59.7	719	865	33.1	33.7	0.4
4	S22-e23-r2-N3	133	1505	9.6	2.2	75.5	NA	NA	NA	NA	NA
5	G40-e21-r2-N1	93	1170	5.3	2.0	76.5	420	445	18.1	22.8	22.0
6	G40-e23-r4-N2	182	1041	11.2	4.4	63.2	359	681	14.2	31.5	30.5
7	G40-e21-r2-N3	101	1141	7.1	1.2	70.1	NA	NA	NA	NA	NA
8	G40-e21-r4-N4	154	1207	10.4	1.0	75.7	472	712	16.1	37.7	39.4
9	G60-e23-r4-N1	75	834	3.5	2.9	63.2	384	642	11.9	41.2	32.2

Note: NA = not available.

The Calculated values for compressive forces and all moments are available in Table 5.9.

Figure 5.13(b) and Figure 5.13(c) show the contribution of concrete and GFRP bars in compression to resisting the sum of external compressive load and internal tensile force at peak load and at crushing of GFRP bars in compression. On average, the contribution of GFRP bars in compression and concrete in load resistance at peak load were 11% and 89%, respectively, while at crushing of GFRP bars were 44% and 56%, respectively. The results showed that the contribution of GFRP bars in compression increases after concrete spalling and reaches 80% of concrete contribution at crushing of GFRP bars, which means GFRP bars in compression significantly contributed to carrying capacity after concrete spalled. The contribution of steel bars at peak load was 8% which is less than the contribution of GFRP bars in compression (11%) while the axial stiffness was kept the same. The latter showed that GFRP bars in compression are as effective as steel in compression up to peak load.

Figure 5.13(d) and Figure 5.13(e) show the contribution of concrete, GFRP bars in compression, and GFRP bars in tension at peak load and at crushing of GFRP bars in compression. On average, the contribution of concrete, GFRP bars in compression, and GFRP bars in tension to moment resistance at peak load were 94%, 5%, and 1%, respectively, while at crushing of GFRP bars in compression were 51%, 23%, and 26%, respectively. At peak load, the contribution of concrete was superior, and for tensile GFRP bars, it was almost negligible (1%). However, after concrete spalled, the contribution of GFRP bars in compression and tension increased drastically. For short columns, the concrete contribution in moment resistance was 35% in comparison to 43% contribution of GFRP bars in compression. As slenderness increases, the contribution of GFRP bars in

compression in the moment resistance declined while the contribution of concrete and tensile GFRP bars increased. It should be highlighted that the effect of confinement is embedded in the contribution of the concrete and does not affect the values presented for the contribution of GFRP bars, as their contribution have been directly calculated using recorded strain values at each loading stage. Overall, it was observed that GFRP bars in compression were as effective as steel bars in providing the axial flexural capacities.

5.4 NUMERICAL MODELING

This section presents an analytical approach to model the behavior of the slender concrete columns reinforced with GFRP bars as described in the previous section. It should be mentioned that one-dimensional finite difference was involved in solving the differential equation of the column numerically. The model considers second order effects as well as the material nonlinearity and is verified against an independent test result.

5.4.1 Model Description

To study the behavior of concrete columns reinforced with GFRP, the columns were divided into thirty points. The characteristics of the columns such as displacement at middle of the column and the corresponding bending moment as well as the compressive and tensile strain of the GFRP bars were determined at different load levels. Using an iterative method for each load step, as illustrated in Figure 5.14, the displacement of at the middle section of the column was determined. The main differential equation used for column analysis is the central expansion of the curvature formula as the second derivative of the deflection of the column, as presented in Equation 5.17. Since the column is divided into a

number of nodes, the displacement of each node can be related to the displacement of the two previous nodes and the curvature of the previous node, as presented in Equation 5.18.

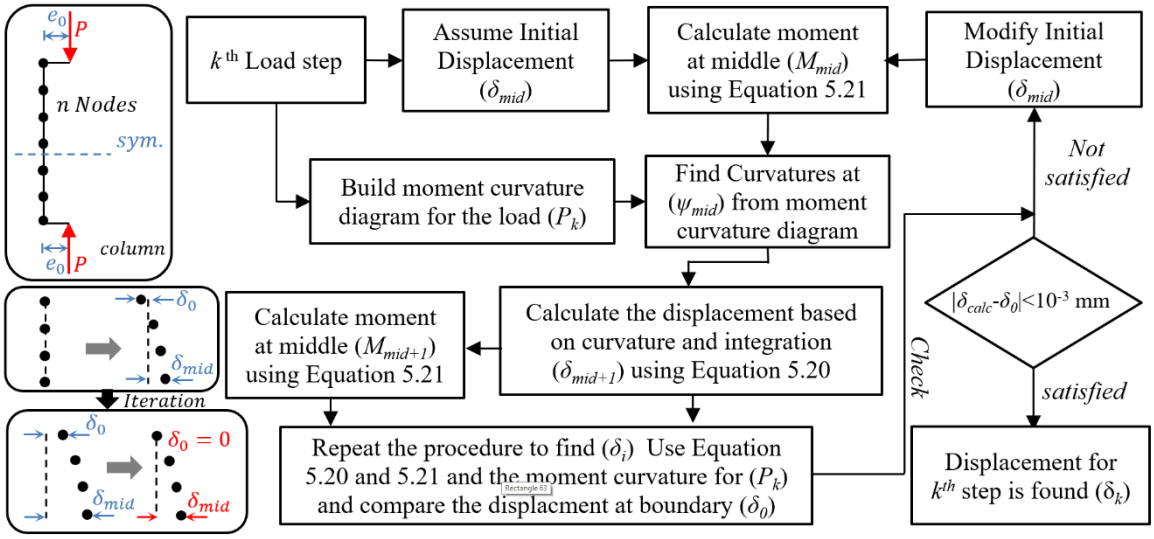

Figure 5. 14 Illustration of the numerical procedure for a certain load step

Due to the symmetry in the column, loading condition, and the boundary condition, the displacement at the node before and after the node at the middle of the column (i.e. δ_{mid-1} and δ_{mid+1}) are the same as presented in Equation 5.19. Therefore, by satisfying symmetry condition, Equation 5.20 shows the displacement at node after the node at the middle of the column which only relates to the middle node.

$$\varphi = -\frac{d^2y}{dx^2} = -\lim_{\Delta x \to 0} \frac{\frac{y(x+\Delta x)-y(x)}{\Delta x} - \frac{y(x)-y(x-\Delta x)}{\Delta x}}{\Delta x} \tag{5.17}$$

$$\delta_{i+1} = 2\delta_i - \delta_{i-1} - \varphi_i \Delta x^2 \tag{5.18}$$

$$\delta_{mid+1} = \delta_{mid-1} \rightarrow \delta_{mid+1} = 2\delta_{mid} - \delta_{mid-1} - \varphi_{mid}\Delta x^2 \tag{5.19}$$

$$\delta_{mid+1} = \delta_{mid} - \frac{\varphi_{mid}}{2}\Delta x^2 \tag{5.20}$$

To find the displacement at each load step, the moment curvature diagram at that load step required to be built. Then, by assuming a displacement at the middle of the column (δ_{mid}), the moment corresponding to that displacement can be calculated by multiplying the axal load by the sum of initial eccentricity and the displacement, as presented in Equation 5.21.

$$M_i = P_k(e_0 + \delta_i) \tag{5.21}$$

Having known the bending moment corresponding to the assumed displacement at the middle, the curvature of the middle node can be found. Then, using Equation 5.20, the displacement of the node after the middle node can be found. By determining two displacement, the procedure can be repeated for each node, using equation 5.18, to find all displacements. Afterward, the displacement at the end of the column is checked, and if its tolerance is less than 0.001 mm, the displacement of the column for that certain load step is found. Otherwise, the displacement at the middle of the columns would be changed so that the boundary condition at the end of the column is satisfied using an iterative procedure as illustrated in Figure 5.14. For implementation of the procedure, the determination of the moment-curvature diagram of the column at a certain load level is required.

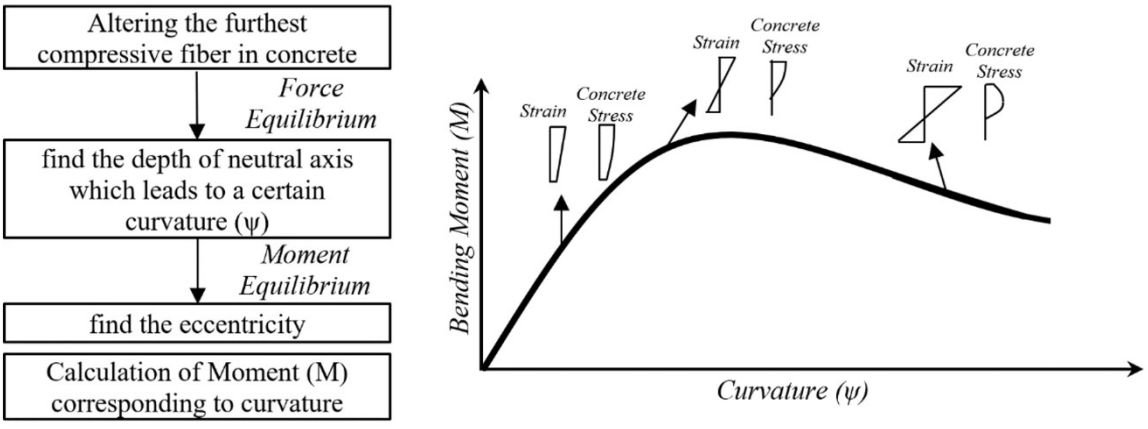

Figure 5. 15 Moment curvature diagram for a certain load step

To find the moment-curvature of column at each load step, each concrete section was discretized into rectangular fibers with a height of 0.25 mm in order to calculate the stress at the center of each fiber. The strain variation in the section was assumed linear, and the stress train relationship of GFRP bars was considered linear up to failure, while for concrete the nonlinear Popovics (1973) stress strain curve was considered. It should be noted that the stress of concrete in tension was neglected. At a certain load, the curvature of the section varied by alteration of the values of the furthest compressive concrete fiber and calculating the depth of neutral axis from satisfying the force equilibrium to find the moment corresponding to the curvature, as illustrated in Figure 5.15.

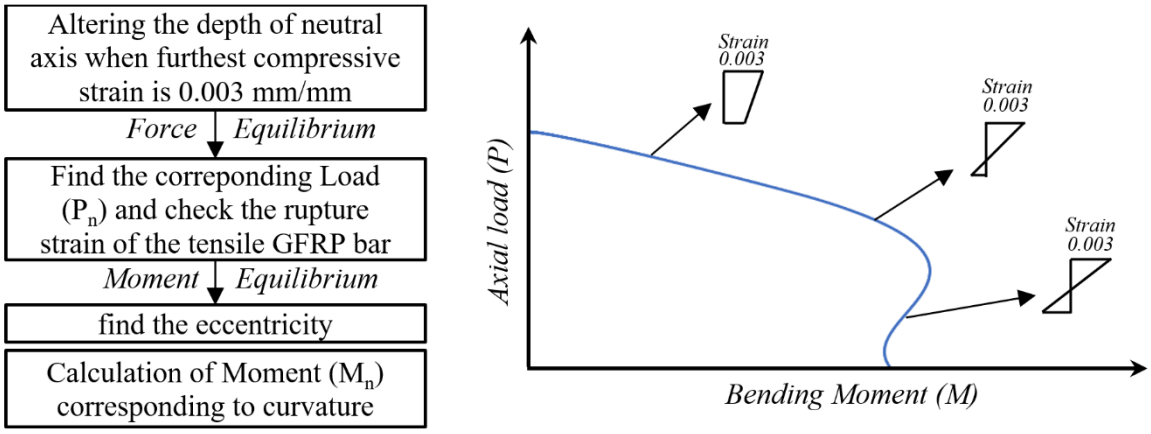

Figure 5. 16 Bending moment-axial load interaction diagram

It is noticed that the bending moment-axial load interaction diagram was derived using a similar procedure for finding the moment-curvature with the difference that the ultimate compressive fiber was considered as a constant value of 0.003 mm/mm according to ACI 318-14 (2014). Then by changing the depth of neutral axis and satisfying equilibrium equations in the section, the corresponding load and bending moment, or load eccentricity, was determined for as many points as needed to drive the diagram, as shown in Figure 11.

Moreover, the tensile strain of bars was checked versus the tensile rupture strain of GFRP material at each step. For the steps at which the tensile strain of the GFRP bars reached the maximum value, instead of having the furthest compressive strain as 0.003 mm/mm, this value is allowed to change while the tensile strain of GFRP bars were constant and set to the rupture strain. It is noticed that for the current research, all points in the interaction diagrams were derived by setting the furthest strain as 0.003 mm/mm since the tensile strains of the GFRP bars did not reach their rupture values.

5.4.2 Model Verification

Figure 5.17 shows the verification of the explained model versus experimental tests results presented in this study for both load-displacement curves and load-strain curves. The comparison shows a very good agreement between the test results and the model. It should be noted that for slenderness ration of 60, the model is underpredicting the test results.

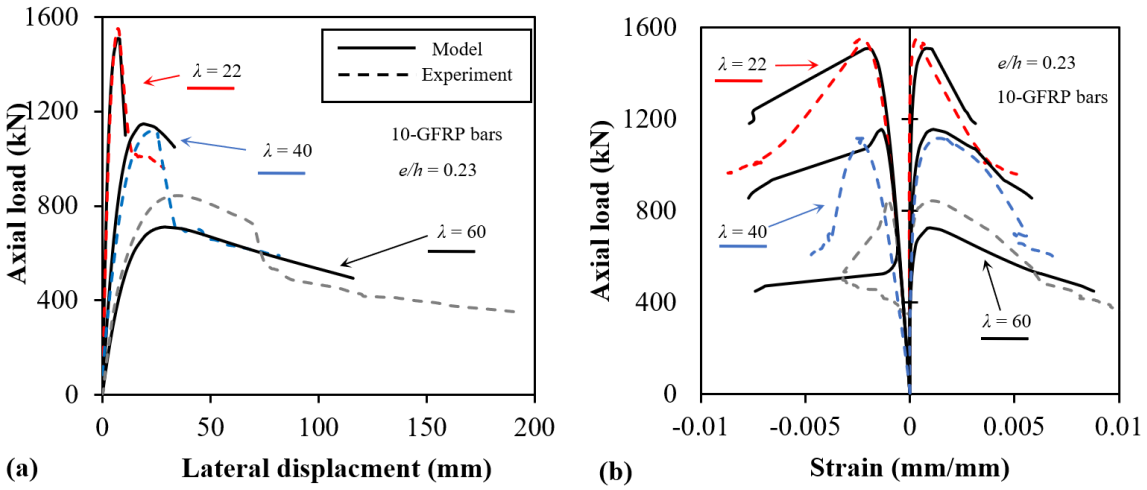

Figure 5. 17 Model verification: (a) load-deflection, (b) load-strain, (c) loading path, (d) moment-curvature

Also, the model was verified versus an experimental study performed by Hadhood et. al (2017) in which four circular concrete columns reinforced with eight #5 GFRP bars with slenderness ratios of 20, length of 1500 mm, and diameter of 305 mm were considered. Column labels C2-P2, C3-P2, C4-P2, and C5-P2 presents 25, 50 100, and 200 mm eccentricities, respectively. The results showed a good agreement between the experimental and model as presented in Figure 5.18.

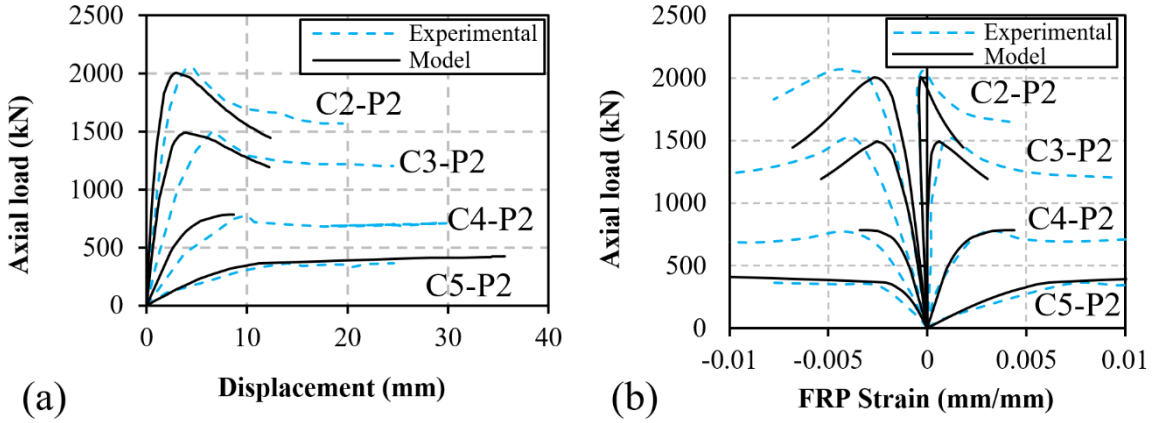

Figure 5. 18 Verification against Hadhood et al. (2017): (a) load-deflection, (b) load-strain

5.4.3 Parametric Study

Due to the limited test results presented in this study, further studies on the behavior of the columns was done using the developed model. In the following, a parametric study on the effect of slenderness ratio, load eccentricity, reinforcement ratio, concrete strength, and the modulus of elasticity of the reinforcing bars are presented. It should be mentioned that for the parametric study, the section and material properties introduced in the section related to the experimental tests was used. Also, the main section with 10#6 GFRP bars, slenderness ratio of 40, eccentricity-to-column width of 0.25 was the base of the study, and in each subsection, one parameter changed at a time.

5.4.3.1 Effect of Slenderness Ratio

Six slenderness ratios of 17, 22 30, 40, 50, and 60 were considered for the parametric study on the effect of slenderness ratio. Figure 5. 19 shows the load-displacement curves and loading path. It was observed that as slenderness ratio increases, the capacity of the column decreases while the displacement at the peak load increases and the mode of failure change from concrete crushing to global buckling of the concrete column. However, no crushing of GFRP bars in compression or tensile rupture of the bars were observed which is compatible with the results of the experimental study.

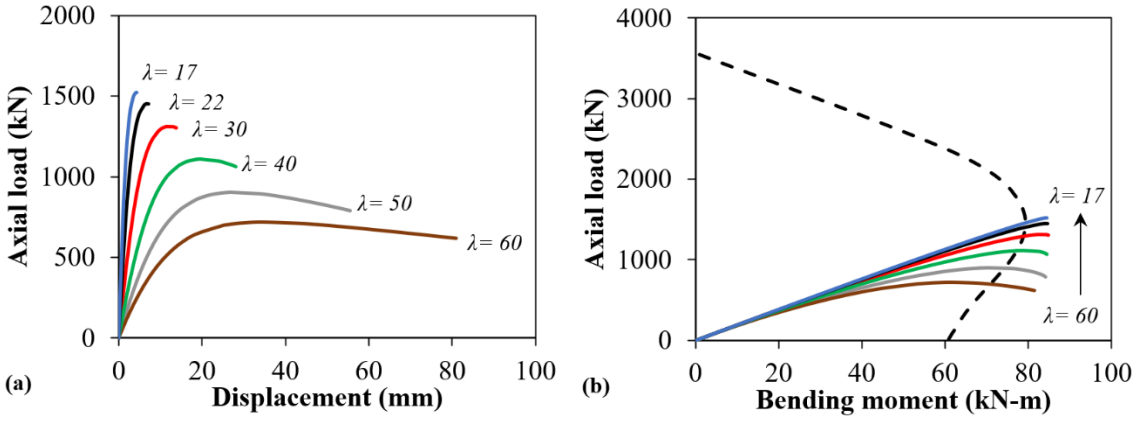

Figure 5. 19 Effect of slenderness ratio: (a) axial load-displacement behavior; (b) axial load-bending moment behavior

5.4.3.2 Effect of Eccentricity

Since the experimental tests covered only two eccentricities of 0.21 and 0.23, in this part, four more eccentricity- to-columns width ratios of 0.05, 0.1, 0.2, 0.3, and 0.5 were considered. Figure 5.20 shows the effect of eccentricity on the load-displacement curves and loading path. It was observed that as the eccentricity increases, the axial load capacity

decreases, and the displacement at the peak load increases. The mode of failure is crushing of concrete in compression and no crushing of GFRP bars in compression was observed up to the peak load.

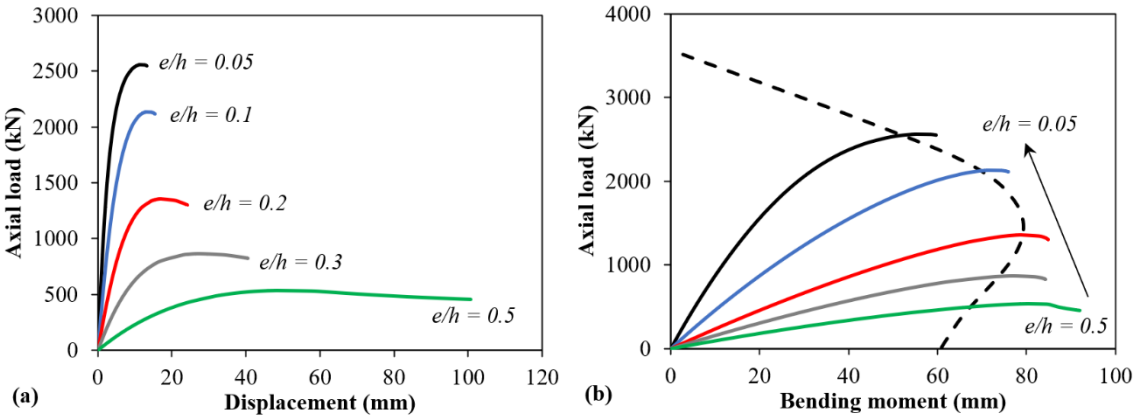

Figure 5. 20 Effect of eccentricity: (a) axial load-displacement behavior; (b) axial load-bending moment behavior

5.4.3.3 Effect of Reinforcement Ratio

Figure 5.21 presents the load-displacement curves and loading path for GFRP-RC column with different reinforcement ratios of 0.84%, 1.68%, 3.3.6%, 5.04%, 6.72%, and 8.40%. It was observed that as the reinforcement ratio increases, the axial and flexural capacity of the column increases. Also, from the interaction diagram shown in Figure 5.21, it was seen that as the reinforcement ratio increase, the increase in the flexural capacity of the columns are higher for columns with lower level of axial capacity. From the results of the parametric study, as the slenderness ratio and the load eccentricity increase, the axial load decreases. Therefore, the increase in the reinforcement ratio is more effective in improvement of flexural capacity of the GFRP-RC columns with high slenderness ratios and loaded with high eccentricities. However, the short columns and columns loaded concentrically or

under low eccentricities, the flexural and axial capacities would not improve significantly if the reinforcement ratio increases.

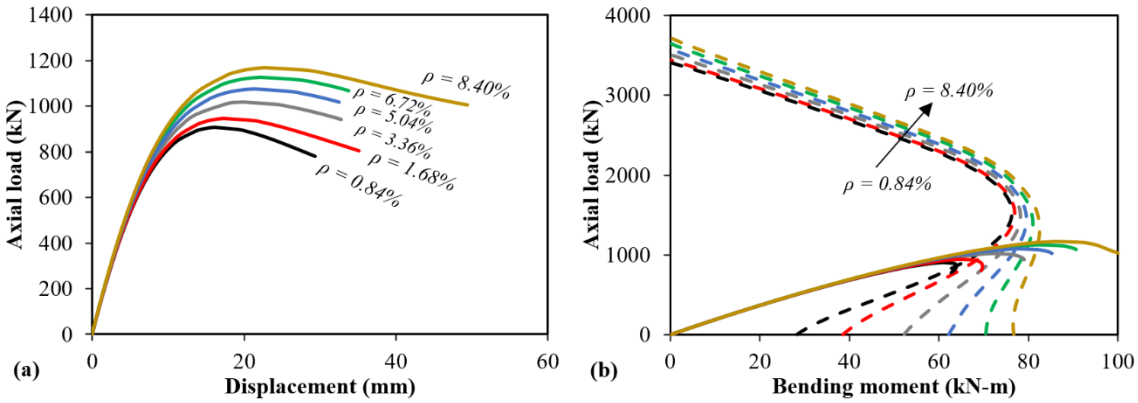

Figure 5. 21 Effect of reinforcement ratio: (a) axial load-displacement behavior; (b) axial load-bending moment behavior

Figure 5.21(b) shows the interaction diagram of the columns. It was observed that as the reinforcement ratio increases, the flexural capacity of the beam with no axial load would be higher than the flexural capacity of a beam with very small level of axial load, if the reinforcement ratio increases. The latter may cause unconservative designs for GFRP-RC beams, as they may experience slight axial loads while their effect was not considered in the design. Thus, it is recommended to perform experimental studies on the behavior of the GFRP-RC beam with low levels of axial loading to further investigate this subject which lead to design recommendations. The latter requires a complete study and is out of scope of the current study.

5.4.3.4 Effect of Modulus of Elasticity of FRP bars

To study the effect of modulus of elasticity of FRP bars on the behavior of the FRP-RC columns, four different modulus of elasticities of 40, 60, 80, and 100 GPa were considered for the FRP bars. It was observed that as the modulus of elasticity of the FRP bars increases, the slope of load-displacement curves increases which means the flexural stiffness of the columns increases. Also, as the modulus of elasticity increases both axial and flexural capacities of the FR-RC columns increases due to additional flexural stiffness provided by stiffer FRP bars.

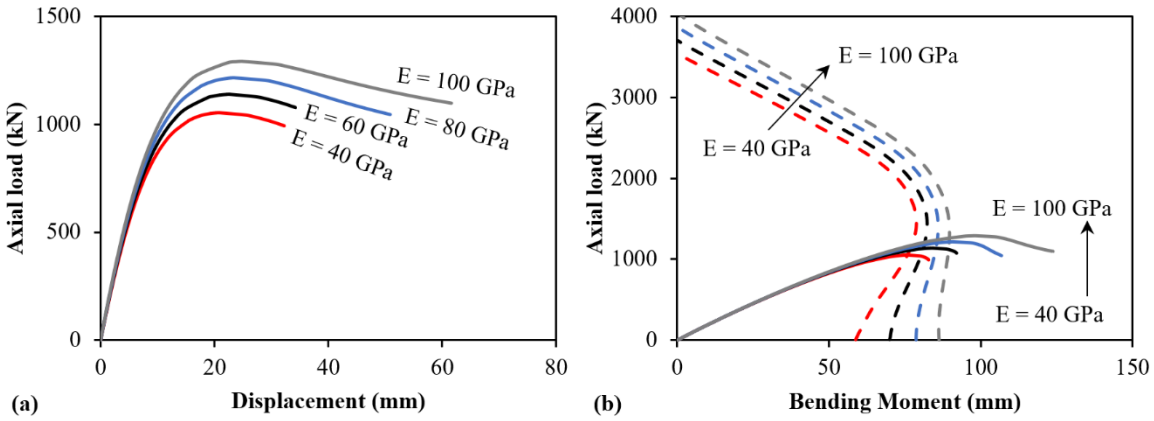

Figure 5. 22 Effect of modulus of elasticity of FRP bars: (a) axial load-displacement behavior; (b) axial load-bending moment behavior

5.4.3.5 Effect of Concrete Strength

To study the effect of concrete strength, six different concrete strength of 30, 40, 50, 60, 70, and 80 MPa were considered. Figure 5. 23 shows the effect of the concrete strength. It was observed that as the concrete strength increases, the axial and flexural capacities of the columns increase. However, the mode of failure is the crushing of concrete in compression.

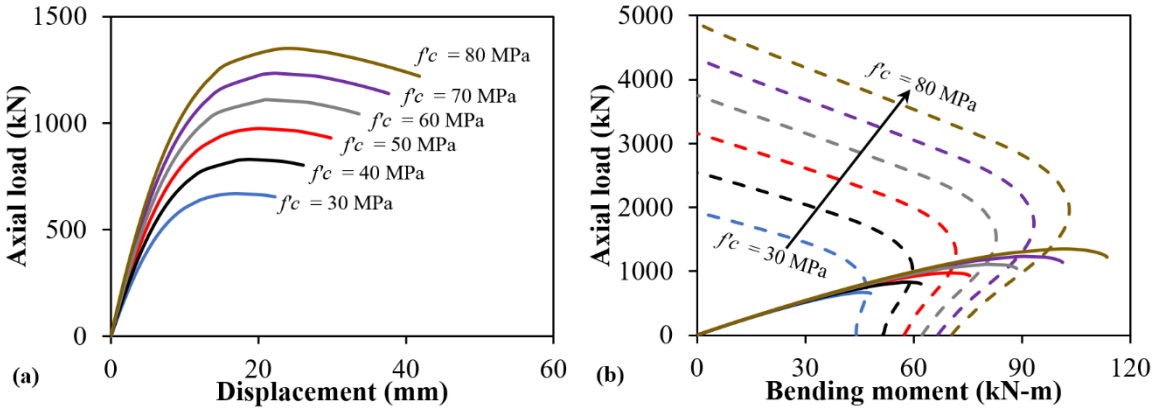

Figure 5. 23 Effect of concrete strength: (a) axial load-displacement behavior; (b) axial load-bending moment behavior

5.5 FUTURE STUDIES

The behavior of GFRP-RC columns after concrete spalling requires more investigations to define a proper ductility or deformability index. The tests showed that the behavior of the columns with slenderness ratios of 17 and 22 was not different and there were very slight secondary moment effects. Therefore, more studies are required to give a more realistic critical slenderness ratio, since the critical slenderness ratio defines the borders between short and slender columns. More investigations are required for proposing a flexural stiffness which predicts the experimental results more accurately. Moreover, a reliability-based analysis is needed to find a proper stiffness reduction factor. Also more studies are required on the behavior of beams with slight axial loads as they present less flexural capacity as the reinforcement ratio increases.

5.6 CONCLUSION

In this paper, the behavior of the slender GFRP-RC columns was investigated experimentally. Ten large-scale specimens with two different eccentricity-to-column width

ratios of 0.21 and 0.23, two different GFRP reinforcement ratios of 4.8% and 2.78%, and four different slenderness ratios of 16.6, 21.5, 39.7, and 59.5 were tested up to their ultimate failure. The following conclusions can be drawn:

- A total of three modes of failure were observed including concrete spalling/crushing (CC), global buckling (GB), and crushing of GFRP bars (GC). For short specimens, the specimens did not experience GB, (i.e. specimens with a slenderness ratio of less than or equal 22). For slender specimens, first, the global buckling happened which followed by the spalling/ crushing of concrete. No GFRP crushing occurred prior to the spalling/crushing of concrete columns. No rupture of GFRP bars in tension observed in the tests.
- The loading continued after concrete failure. It was observed that the GFRP-RC columns were able to sustain almost a constant load after spalling/crushing of concrete up to the crushing of the GFRP bars in compression. The specimens were able to tolerate lateral displacement at a certain load level which led to an increase in the moment capacity of the crushed specimens. This moment capacity is attributed to the compressive GFRP bars which were contributed to the axial and bending capacity especially after concrete spalling/crushing. Linear stress-strain behavior of GFRP bars and constant increase in curvature, and in turn strains, make the contribution of GFRP bars in compression more effective.
- The average compressive strain of GFRP bars in compression was 0.0102 mm/mm at the ultimate loading stage (GC) which was 73% of the average crushing strain found by material compressive testing. The buckling of GFRP bars after spalling/crushing of concrete was the reason for not reaching the ultimate crushing strain for GFRP bars in

compression. Crushing of GFRP bars in compression was corresponding to a total drop in the load capacity for the tested specimens which led to stop the tests.

- The unloading stage after failure showed that the bent specimens became straight and their load -axial displacement curve approaches the origin.
- The flexural stiffness of the specimens calculated from the experimental study and the ones calculated from the available formulas of the literature were compared. Many of the formulas were overestimating or underestimating the flexural stiffness.
- Overall, the contribution of GFRP bars after failure is considerable. Moreover, GFRP bars in compression were as effective as steel bars in providing the axial force and moment resistance at peak load. Also, by considering them in the calculations of flexural stiffness, more accurate results can be obtained. Therefore, it is suggested not to neglect the effect of GFRP bars in compression.
- A numerical modeling developed which account for secondary moment effects and nonlinearity in material and geometry. The model was verified against the experimental tests and showed a good agreement with the test results.
- A parametric study performed on the behavior of the columns reinforced with FRP bars using the verified analytical numerical model. Concrete strength, eccentricity, slenderness ratio, reinforcement ratio, and the modulus of elasticity of bars were considered. It was observed that as the eccentricity and slenderness ratio increase, the axial and flexural capacity decreases, and as the modulus of elasticity of FRP bars, concrete strength, and reinforcement ratios increases, the axial and flexural strengths increase.

- The results of parametric study showed that an increase in the reinforcement ratio is a good solution for enhancing the capacity of slender columns while for short columns, the reinforcement ratio does not significantly affect the capacity.

Acknowledgments

Authors would like to thank Jordan Maerz, Blair Nickerson, Brian Kennedy, Jesse Keane, and Brian Liekens and for their assistance in the lab. The authors would also like to acknowledge and thank NSERC and Dalhousie University for their financial support as well as Aslan FRP for providing GFRP bars.

References

ACI 318-19. (2019). Building Code Requirements for Structural Concrete. *American Concrete Institute.* Farmington Hills, MI.

ACI 440.1R. (2015). Guide for the Design and Construction of Structural Concrete Reinforced Fiber-Reinforced Polymer (FRP) Bars. *American Concrete Institute.* Farmington Hills, MI.

Afifi, M. Z., Mohamed, H. M., and Benmokrane, B. (2014a). Axial Capacity of Circular Concrete Columns Reinforced with GFRP Bars and Spirals. *Journal of Composites for Construction*, ASCE, 18(1), 04013017.

Afifi, M. Z., Mohamed, H. M., and Benmokrane, B. (2014b). Strength and axial behavior of circular concrete columns reinforced with CFRP bars and spirals. *Journal of Composites for Construction*, 18(2), 04013035.

AlAjarmeh, O. S., Manalo, A. C., Benmokrane, B., Karunasena, W., and Mendis, P. (2019a). Axial performance of hollow concrete columns reinforced with GFRP composite bars with different reinforcement ratios. *Composite Structures*, 213, 153-164.

AlAjarmeh, O. S., Manalo, A. C., Benmokrane, B., Karunasena, W., Mendis, P., and Nguyen, K. T. (2019b). Compressive behavior of axially loaded circular hollow concrete columns reinforced with GFRP bars and spirals. *Construction and Building Materials*, 194, 12-23.

ASTM A370/A370M-18 (2018). "Standard Test Methods and Definitions for Mechanical Testing of Steel Products. *American Society for Testing and Materials.* West Conshohocken, PA.

ASTM C39/C39M − 18. (2018). Standard Test Method for Compressive Strength of Cylindrical Concrete Specimens. *American Society for Testing and Materials.* West Conshohocken, PA.

ASTM D7205 / D7205M - 06. (2016). Standard Test Method for Tensile Properties of Fiber Reinforced Polymer Matrix Composite Bars. *American Society for Testing and Materials.* West Conshohocken, PA.

CSA S6-14. (2014). Canadian Highway Bridge Design Code. *Canadian Standards Association.*

CSA S806-12. (2012). Design and construction of building structures with fiber-reinforced polymers. *Canadian Standards Association.*

De Luca, A., Matta, F., and Nanni, A. (2010). Behavior of Full-Scale Glass Fiber-Reinforced Polymer Reinforced Concrete Columns under Axial Load. *ACI Structural Journal*, 107(5), 589-596.

Elchalakani, M., Karrech, A., Dong, M., Alib, M., and Yang, B. (2018). Experiments and Finite Element Analysis of GFRP Reinforced Geopolymer Concrete Rectangular Columns Subjected to Concentric and Eccentric Axial Loading. *Structures*, 14, 273-289.

Elmessalami, N., El Refai, A., and Abed, F. (2019). Fiber-reinforced polymers bars for compression reinforcement: a promising alternative to steel bars. *Construction and Building Materials*, 209, 725-737.

Fib Bulletin 40. (2007). FRP Reinforcement in RC structures. *The International Federation for Structural Concrete*, Stuttgart.

Guérin, M., Mohamed, H. M., Benmokrane, B., Nanni, A., and Shield, C. K. (2018a). Eccentric Behavior of Full-Scale Reinforced Concrete Columns with Glass Fiber-Reinforced Polymer Bars and Ties. *ACI Structural Journal*, 115(2), 489-499.

Guérin, M., Mohamed, H. M., Benmokrane, B., Shield, C. K., and Nanni, A. (2018b). Effect of glass fiber-reinforced polymer reinforcement ratio on axial-flexural strength of reinforced concrete columns. *ACI Structural Journa*l, 155(4), 1049-3.

Hadhood, A., Mohamed, H. M., and Benmokrane, B. (2016). Experimental study of circular high-strength concrete columns reinforced with GFRP bars and spirals under concentric and eccentric loading. *Journal of Composites for Construction*, 21(2), 04016078.

Hadhood, A., Mohamed, H. M., and Benmokrane, B. (2017). Experimental study of circular high-strength concrete columns reinforced with GFRP bars and spirals under concentric and eccentric loading. *Journal of Composites for Construction*, 21(2), 04016078.

Hadhood, A., Mohamed, H. M., Benmokrane, B., Nanni, A., and Shield, C. K. (2019). "Assessment of Design Guidelines of Concrete Columns Reinforced with Glass Fiber-Reinforced Polymer Bars." *ACI Structural Journal*, 116(4), 193-207.

Hales, T. A., Pantelides, C. P., and Reaveley, L. D. (2016). Experimental Evaluation of Slender High-Strength Concrete Columns with GFRP and Hybrid Reinforcement. *Journal of Composites for Construction*, 20(6), 04016050.

Hasan, H. A., Karim, H., Sheikh, M. N., and Hadi, M. N. (2019). Moment-Curvature Behavior of Glass Fiber-Reinforced Polymer Bar-Reinforced Normal-Strength Concrete and High-Strength Concrete Columns. *ACI Structural Journal*, 116(4), 65-76.

Khorramian, K., and Sadeghian, P. (2017a). Experimental and analytical behavior of short concrete columns reinforced with GFRP bars under eccentric loading. *Engineering Structures*, 761–773.

Khorramian, K., and Sadeghian, P. (2017b). Short Concrete Columns Reinforced with GFRP Rebars Under Eccentric Loading. *CSCE Annual Conference. Vancouver, BC, Canada: Canadian Society of Civil Engineering.*

Khorramian, K., and Sadeghian, P. (2018a). New Testing Method of GFRP Bars in Compression. *CSCE Annual Conference. Fredericton, NB, Canada: Canadian Society of Civil Engineering.*

Khorramian, K., and Sadeghian, P. (2019a). Behavior of Slender GFRP Reinforced Concrete Columns. *ASCE-SEI Structures Congress, American Society of Civil Engineers.* St. Louis, Missouri, USA.

Khorramian, K., and Sadeghian, P. (2019b). Material Characterization of GFRP Bars in Compression using a New Test Method. *Journal of Testing and Evaluation (ASTM)*, 49, 2.

Maranan, G. B., Manalo, A. C., Benmokrane, B., Karunasena, W., and Mendis, P. (2016). Behavior of concentrically loaded geopolymer-concrete circular columns reinforced longitudinally and transversely with GFRP bars. *Engineering Structures*, 117, 422-436.

Mirmiran, A., Yuan, W., and Chen, X. (2001). Design for slenderness in concrete columns internally reinforced with fiber-reinforced polymer bars. *Structural Journal*, 98(1), 116-125.

Mirza, S. A. (1990). Flexural Stiffness of Rectangular Reinforced Concrete Columns. *ACI Structural Journal*, 87(4), 425-435.

Mohamed, H. M., Afifi, M. Z., and Benmokrane, B. (2014). Performance Evaluation of Concrete Columns Reinforced Longitudinally with FRP Bars and Confined with FRP Hoops and Spirals under Axial Load. *Journal of Bridge Engineering*, 19(7), 04014020.

Nanni, A., De Luca, A., and Zadeh, H. J. (2014). Reinforced Concrete with FRP Bars: Mechanics and Design. *CRC Press*.

Pantelides, C. P., Gibbons, M. E., and Reaveley, L. D. (2013). Axial load behavior of concrete columns confined with GFRP spirals. *Journal of Composites for Construction*, 17(3), 305-313.

Paultre, P., and Légeron, F. (2008). Confinement reinforcement design for reinforced concrete columns. *Journal of structural engineering*, 134(5), 738-749.

Salah-Eldin, A., Mohamed, H. M., and Benmokrane, B. (2019). Structural performance of high-strength-concrete columns reinforced with GFRP bars and ties subjected to eccentric loads. *Engineering Structures*, 185, 286-300.

Sun, L., Wei, M., and Zhang, N. (2017). Experimental study on the behavior of GFRP reinforced concrete columns under eccentric axial load. *Construction and Building Materials*, 152, 214-225.

Tikka, T., Francis, M., and Teng, B. (2010). "Strength of Concrete Beam-Columns Reinforced with GFRP Bars." *2nd International structures specialty conference*, Winnipeg, Manitoba, 46.1-46.10.

Tobbi, H., Farghaly, A. S., and Benmokrane, B. (2012). Concrete Columns Reinforced Longitudinally and Transversally with Glass Fiber-Reinforced Polymer Bars. *ACI Structural Journal*, 109(4), 551-558.

Tobbi, H., Farghaly, A. S., and Benmokrane, B. (2014). Behavior of Concentrically Loaded Fiber-Reinforced Polymer Reinforced Concrete Columns with Varying Reinforcement Types and Ratios. *ACI Structural Journal*, 111(2), 375-385.

Xue, W., Peng, F., and Fang, Z. (2018). Behavior and Design of Slender Rectangular Concrete Columns Longitudinally Reinforced with Fiber-Reinforced Polymer Bars. *ACI Structural Journal*, 115(2), 311-322.

Zadeh, H. J., and Nanni, A. (2013). Design of RC Columns Using Glass FRP Reinforcement. *Journal of Composites*, 17(3), 294–304.

Zadeh, H. J., and Nanni, A. (2017). Flexural Stiffness and Second-Order Effects in Fiber-Reinforced Polymer-Reinforced Concrete Frames. *ACI Structural Journal*, 114(2), 533–544.

CHAPTER 6 A PRELIMINARY RELIABILITY-BASED ANALYSIS FOR SLENDERNESS LIMIT OF FRP REINFORCED CONCRETE COLUMNS

ABSTRACT

The critical slenderness ratio of concrete columns reinforced with fiber-reinforced polymer (FRP) bars in ACI 440.1R is based on a deterministic approach and a failure criterion of 5% drop in axial capacity. There is an urging need to quantify the safety associated with the recommended slenderness ratio for the purpose of optimizing the design of FRP reinforced columns. A research programme developed by the authors is currently underway to develop a novel reliability-based approach to recommend slenderness ratios for possible inclusion in ACI 440.1R. In the proposed approach, recommended slenderness ratios are formulated based on achieving a predefined target reliability index as opposed to the deterministic approach of setting a failure criterion of 5% drop in axial capacity. The approach is aligned with the general philosophy of limit state design adopted by North American codes and standards in which failure limit states are established based on reliability principles and not deterministically. In this paper, some aspects of the proposed approach are described while limited preliminary analysis results are included. The preliminary results showed a range of 3.59 to 3.95 reliability indices for slenderness ratios between 17 to 22 based on the limited parameters considered in this study. Considerable future research is needed to complete the proposed approach and bring it to a level suitable for application in calibrating code slenderness ratio limits.

6.1 INTRODUCTION

The critical slenderness ratio of a column is a limit that determines whether the second-order analysis should be considered or not. Columns with slenderness ratio greater than the critical slenderness ratio require second-order analysis and they are called slender columns. For non-slender columns, the slenderness effect is neglected by ACI 318-19 (2019) code and only first-order analysis is recognized to be sufficient. For steel reinforced concrete (RC) columns, a slenderness limit of 22 is considered for unbraced columns as per ACI 318-19 (2019). This limit corresponds to the slenderness ratio at which the difference between the first order and the second-order analysis (or the drop in the capacity) is 5% (MacGregor et al. 1970).

For concrete columns reinforced with fiber-reinforced polymer (FRP) bars, the same concept was adopted by Mirmiran et al. (2001). They developed and analytical-numerical model based on modeling the columns using the overall deformed shape as a sine function. Then, the critical slenderness ratio corresponding to 5% of the axial capacity of the columns was established using a database including 4608 cases. By eliminating ineffective parameters, a reduced database was formed. The slenderness limit corresponding to 1 percentile of reduced population was chosen as the critical slenderness ratio. Mirmiran et al. (2001) proposed a critical slenderness ratio of 17 for GFRP-RC columns. Zadeh and Nanni (2017) proposed a critical slenderness ratio of 14 for GFRP-RC columns and 19 for CFRP-RC columns based on considering a 5% drop in the axial capacity and using the moment magnification formulation. Abdelazim et al. (2020) proposed a critical slenderness ratio of 18 based on experimental databases and Euler-Johnson's stability envelope with a criterion of 5% drop in the capacity.

The common consideration in all mentioned studies was the criteria of a 5% drop in the axial capacity. However, the crucial question is that what would be the probability of failure of a column if it was considered as a short column and was designed using the first-order analysis while the second order-analysis indicates the failure of the column. In other words, the probability of failure of a column designed based on a 5% drop criterion is not yet established and the effect of neglecting secondary moment effects for short columns is not quantified from a safety perspective. Therefore, in this study, for the first time, a rationale-based reliability method is employed to define the strength limit criteria of columns instead of the commonly used 5% drop approach. The paper is structured to briefly explain the analysis method followed by presenting a sensitivity analysis and concludes with an MC simulation.

6.2 Analysis Method

In this study, a verified model developed by in chapter 5 was used to predict the response of slender columns. The model accounts for material and geometric nonlinearities and can predict three modes of failures: crushing of concrete in compression, crushing of FRP bars in compression, and rupture of FRP bars in tension. If the secondary moment effect due to displacements at each load step is not considered into the calculation, the predicted values correspond to first-order analysis which shows a linear response in load-moment space. Figure 6.1(a) shows a schematic plot of the first order and second order loading path of an FRP-RC column whose mode of failure is concrete crushing, the strain equals 0.003 mm/mm as per ACI 318-19 (2019). Figure 6.1(b) shows the change in the second-order analysis results while the first-order result is constant, which causes a greater percentage drop as the slenderness ratio increases. In this study, for each case, the percentage drop in

axial load is the difference between the second-order and first-order analysis as shown in Figure 6.1(a) for the failure mode that occurs prior to the others.

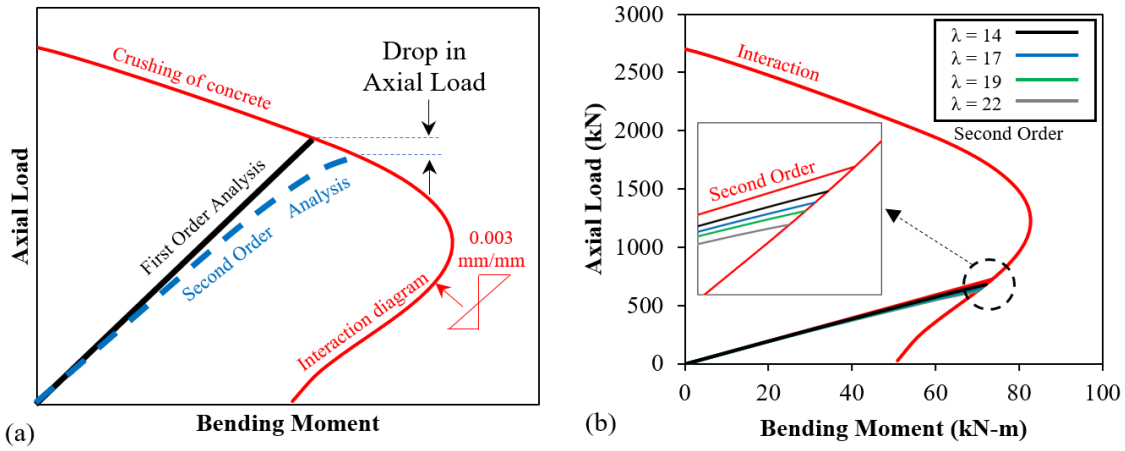

Figure 6. 1 Analysis Procedure: (a) schematic, (b) analysis for different slenderness ratios

6.3 SENSITIVITY ANALYSIS

In this study, the column cross-section (254x254 mm^2) and analysis cases that were studied by Mirmiran et al. (2001) were considered as presented in Table 6.1.

Table 6. 1 Matrix of Sensitivity Analysis Cases

Parameter	Value	No. of cases	Worst Case
concrete strength (f'_c)	27.6 and 41.4 MPa	2	41.4 MPa
Reinforcement depth ratio (γ)	0.6 and 0.8	2	0.6
Strength ratio (f_{ftu}/f'_c)	15, 25, and 35	3	35
Compressive/tensile strength ratio (f_{fcu}/f_{ftu})	0.1, 0.2, 0.5, and 1.0	4	0.1
Reinforcement ratio (ρ)	1, 2, 3, and 4%	4	1%
Modular ratio ($n= E_f/E_c$)	2, 4, 6, and 8	4	2
Eccentricity ratio (e/h)	0.05, 0.2, 0.4, 0.5, 0.75, and 1.0	6	0.4
Slenderness ratio (λ)	14, 17, 19, and 22	4	14, 17, 19, and 22
Total cases		18432	-

It should be mentioned that Mirmiran et al. (2001) calculated the slenderness ratio corresponding to a 5% capacity drop. However, in this study, four different slenderness ratios of 14, 17, 19, and 22 were selected and the percentage drop of each case was calculated (with a total of 18,432 cases). In addition, the modes of failure for each case are tracked and the sensitivity to modes of failure and percentage drop was assessed by changing the introduced parameters. Moreover, the case susceptible to the highest percentage drop was recognized for each slenderness ratio – referred to as the worst case as presented in Table 6.1.

Table 6. 2 Effect of concrete strength

Concrete Strength (MPa)	Slenderness Ratio	Percentage Drop (%)			Failure mode (%)		
		Min	Average	Max	Concrete crushing	FRP crushing	FRP rupture
f'c = 27.6	λ = 14	0	1.55	5.42	44.75	52.17	3.08
	λ = 17	0	2.27	7.82	44.92	51.95	3.13
	λ = 19	0	2.82	9.63	45.01	51.86	3.13
	λ = 22	0	3.73	12.62	45.05	51.82	3.13
f'c = 41.4	λ = 14	0	1.75	6.03	52.73	45.32	1.95
	λ = 17	0	2.55	8.73	52.78	45.27	1.95
	λ = 19	0	3.16	10.77	52.86	45.19	1.95
	λ = 22	0	4.20	14.15	52.99	45.06	1.95

Table 6.2 shows the effect of concrete strength. It was observed that as the concrete strength increases, the percentage drop increases in all slenderness ratios. Also, the mode of failure is mostly concrete crushing and FRP crushing in compression, while few columns failed under tensile rupture. As the concrete strength increased, the concrete crushing mode of failure became the more dominant mode of failure. It should be mentioned that only two concrete strengths of 27.6 and 41.4 MPa were considered in this study and in the study

conducted by Mirmiran et al. (2001). However, the results showed that an increase in concrete strength leads to a more severe percentage drop. Figure 6.2 considered two more concrete strengths for the worst-case defined in Table 6.1. Since the first-order analysis is a straight line in the load-moment space, the loading path intersect the interaction diagram at a higher load which makes the first-order analysis overpredict the analysis as the concrete strength increases, shown in Figure 6.2(a). The percentage drop in the capacity for the worst-case reached 17.5% as the concrete strength increased to 68.9 MPa.

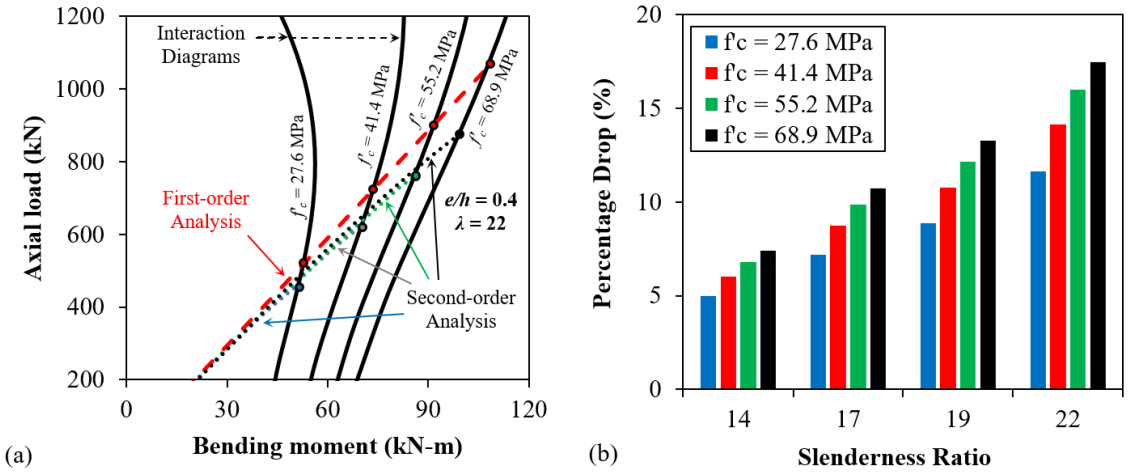

Figure 6. 2 Effect of concrete strength: (a) analysis results, and (b) percentage drop

As confirmed in this study, the higher the concrete strength, the more severe the percentage drop in the capacity. Therefore, considering higher concrete strength for assessing the critical slenderness ratio is crucial. Also, an additional critical slenderness ratio can be introduced for high strength concrete columns (i.e. strength of more than 80 MPa). However, in this study, the scope is limited to the range defined in Table 6.1.

Table 6.3 presents the reinforcement depth ratio at the ratio of the center to the center of compressive and tensile FRP bars to the width of the cross-section. As expected, as reinforcement depth decreases, since the lever arm of compressive and tensile forces decreases, the percentage drop increases, and the dominant mode of failure changes from crushing of FRP in compression to concrete crushing.

Table 6. 3 Effect of reinforcement depth ratio

Reinforcement depth ratio	Slenderness Ratio	Percentage Drop (%)			Failure mode (%)		
		Min	Average	Max	Concrete crushing	FRP crushing	FRP rupture
γ =0.6	λ = 14	0	1.84	6.03	53.73	43.41	2.86
	λ = 17	0	2.69	8.73	53.86	43.23	2.91
	λ = 19	0	3.33	10.77	53.91	43.18	2.91
	λ = 22	0	4.41	14.15	54.04	43.05	2.91
γ =0.8	λ = 14	0	1.46	5.08	43.75	54.08	2.17
	λ = 17	0	2.13	7.38	43.84	53.99	2.17
	λ = 19	0	2.65	9.13	43.97	53.86	2.17
	λ = 22	0	3.52	12.04	44.01	53.82	2.17

Table 6.4 presents the effect of the reinforcement strength ratio defined as the ratio of tensile rupture strength of FRP bars (f_{ftu}) to the compressive strength of concrete (f'_c). The analysis showed that the percentage drop or secondary moments was not influenced by the strength ratio. However, the mode of failure was affected so that as the reinforcement strength ratio decreases, the possibility of failure due to FRP rupture in tension increases.

Table 6. 4 Effect of reinforcement strength ratio

Strength ratio	Slenderness Ratio	Percentage Drop (%)			Failure mode (%)		
		Min	Average	Max	Concrete crushing	FRP crushing	FRP rupture
$f_{ftu}/f'_c = 15$	λ = 14	0	1.44	6.03	31.64	61.78	6.58
	λ = 17	0	2.10	8.73	31.77	61.59	6.64
	λ = 19	0	2.61	10.77	31.84	61.52	6.64
	λ = 22	0	3.45	14.14	31.97	61.39	6.64
$f_{ftu}/f'_c = 25$	λ = 14	0	1.68	6.03	52.28	46.74	0.98
	λ = 17	0	2.45	8.73	52.34	46.68	0.98
	λ = 19	0	3.05	10.77	52.41	46.61	0.98
	λ = 22	0	4.04	14.14	52.47	46.55	0.98
$f_{ftu}/f'_c = 35$	λ = 14	0	1.83	6.03	62.30	37.70	0
	λ = 17	0	2.67	8.73	62.43	37.57	0
	λ = 19	0	3.32	10.77	62.57	37.43	0
	λ = 22	0	4.40	14.15	62.63	37.37	0

In Table 6.4, it was observed that for lower reinforcement strength ratios, the crushing of FRP bars became the dominant mode of failure. The latter is attributed to the way cases are defined in Table 6.1 since the compressive strength of FRP bars are considered to be a percentage of its tensile strength. Table 6.5 presents the compressive (f_{fcu}) to the tensile (f_{ftu}) strength ratio of FRP bars. As this ratio increases from 0.1 up to 1, the dominant mode of failure changed from FRP crushing to concrete crushing. However, the ratios of 0.1 and 0.2 are not realistic and were originally selected due to a lack of experimental evidence. Recently, Khorramian and Sadeghian (2018, 2019b) reported that the compressive to tensile strength ratio ranges from 0.55 to 0.99, and AlAjarmeh et al. (2019) reported a range of 0.65 to 0.75. Moreover, the tests of concrete columns reinforced with GFRP bars showed concrete crushing prior to GFRP crushing in compression (Khorramian and Sadeghian 2017b, Hadhood et al. 2017).

Table 6.5 showed that as the compressive to tensile strength ratio increases, the average percentage drop increases while the maximum drop remains unchanged. Also, it was observed that for ratios of 0.1 and 0.2, the minimum percentage drop was zero due to the dominant failure mode of FRP crushing in compression, which caused the premature failure and led to the same first-order and second-order analysis results.

Table 6. 5 Effect of compressive/tensile strength ratio

Compressive /tensile strength ratio	Slenderness Ratio	Percentage Drop (%)			Failure mode (%)		
		Min	Average	Max	Concrete crushing	FRP crushing	FRP rupture
f_{fcu}/f_{ftu} = 0.1	λ = 14	0	0.92	6.03	7.90	91.84	0.26
	λ = 17	0	1.34	8.73	8.07	91.67	0.26
	λ = 19	0	1.66	10.77	8.16	91.58	0.26
	λ = 22	0	2.20	14.15	8.25	91.49	0.26
f_{fcu}/f_{ftu} = 0.2	λ = 14	0	1.45	6.02	26.13	73.00	0.87
	λ = 17	0	2.12	8.73	26.13	73.00	0.87
	λ = 19	0	2.63	10.77	26.30	72.83	0.87
	λ = 22	0	3.50	14.14	26.56	72.57	0.87
f_{fcu}/f_{ftu} = 0.5	λ = 14	0.02	2.04	6.03	69.53	27.08	3.39
	λ = 17	0.25	2.98	8.73	69.62	26.91	3.47
	λ = 19	0.25	3.70	10.77	69.70	26.83	3.47
	λ = 22	0.46	4.90	14.14	69.70	26.83	3.47
f_{fcu}/f_{ftu} = 1.0	λ = 14	0.66	2.19	6.03	91.41	3.03	5.56
	λ = 17	1.01	3.20	8.73	91.58	2.86	5.56
	λ = 19	1.26	3.97	10.77	91.58	2.86	5.56
	λ = 22	1.72	5.26	14.14	91.58	2.86	5.56

Table 6.6 presents the effect of the reinforcement ratio (ρ). As the reinforcement ratio decreases, the percentage drop increases, and the chance of FRP rupture increases, although the dominant mode of failure does not change.

Table 6. 6 Effect of reinforcement ratio

Reinforcement ratio	Slenderness Ratio	Percentage Drop (%)			Failure mode (%)		
		Min	Average	Max	Concrete crushing	FRP crushing	FRP rupture
ρ = 1%	λ = 14	0	2.15	6.03	47.83	44.70	7.47
	λ = 17	0	3.14	8.73	48.09	44.36	7.55
	λ = 19	0	3.89	10.77	48.35	44.10	7.55
	λ = 22	0	5.14	14.15	48.44	44.01	7.55
ρ = 2%	λ = 14	0	1.65	4.45	49.48	48.70	1.82
	λ = 17	0	2.42	6.46	49.48	48.70	1.82
	λ = 19	0	3.00	7.98	49.48	48.70	1.82
	λ = 22	0	3.99	10.50	49.48	48.70	1.82
ρ = 3%	λ = 14	0	1.45	3.76	48.96	50.43	0.61
	λ = 17	0	2.13	5.47	48.96	50.43	0.61
	λ = 19	0	2.65	6.76	49.05	50.34	0.61
	λ = 22	0	3.51	8.91	49.31	50.08	0.61
ρ = 4%	λ = 14	0	1.33	3.36	48.70	51.13	0.17
	λ = 17	0	1.95	4.89	48.87	50.96	0.17
	λ = 19	0	2.42	6.05	48.87	50.96	0.17
	λ = 22	0	3.22	7.98	48.87	50.96	0.17

Table 6.6 shows the effect of modular ratio (n), which defines as the ratio of modulus of elasticity of FRP (E_f) to the modulus of elasticity of concrete (E_c). As the modular ratio decreases, the percentage drop increases, and the concrete crushing becomes the dominant mode of failure. It should be noted that different modular ratios can be considered for different materials, and the modular ratio of 2 is almost representative of GFRP bars if the concrete strength is kept as low as 27.6 MPa. However, for higher concrete strength, the modular ratio of 2 cannot be a representative of GFRP bars. Therefore, it is recommended that for future studies, it is recommended that instead of changing the modular ratio, a certain range of modulus of elasticity is selected for FRP bars with a certain material type.

Table 6. 7 Effect of modular ratio

Modular ratio	Slenderness Ratio	Percentage Drop (%)			Failure mode (%)		
		Min	Average	Max	Concrete crushing	FRP crushing	FRP rupture
n = 2	λ = 14	0	2.55	6.03	76.65	22.74	0.61
	λ = 17	0	3.72	8.73	76.74	22.65	0.61
	λ = 19	0	4.61	10.77	76.91	22.48	0.61
	λ = 22	0	6.09	14.15	77.08	22.31	0.61
n = 4	λ = 14	0	1.69	4.65	51.22	46.7	2.08
	λ = 17	0	2.48	6.53	51.3	46.62	2.08
	λ = 19	0	3.09	8.06	51.39	46.53	2.08
	λ = 22	0	4.09	10.59	51.48	46.44	2.08
n = 6	λ = 14	0	1.29	4.43	39.41	57.55	3.04
	λ = 17	0	1.89	6.36	39.5	57.37	3.13
	λ = 19	0	2.34	7.81	39.5	57.37	3.13
	λ = 22	0	3.12	10.21	39.58	57.29	3.13
n = 8	λ = 14	0	1.06	4.78	27.69	67.97	4.34
	λ = 17	0	1.55	6.91	27.86	67.8	4.34
	λ = 19	0	1.93	8.51	27.95	67.71	4.34
	λ = 22	0	2.56	10.95	27.95	67.71	4.34

Table 6.8 presents the effect of the eccentricity ratio. The highest percentage drop is reached for an eccentricity ratio of 0.4, and concrete crushing becomes the dominant failure mode as the ratio increases. The latter shows that for further investigations, a range of eccentricity ratio between 0.4 to 0.5 gives the worst-case scenario and high eccentricities are not as critical. In simplified equations used for initial estimation of effective flexural stiffness, which is used in assessment of the moment magnification factor, usually the mentioned range of eccentricity is replaced in a general formula provided for variable eccentricities that is compatible with the analysis results provided in Table 6.8.

Table 6. 8 Effect of eccentricity ratio

Eccentricity ratio	Slenderness Ratio	Percentage Drop (%)			Failure mode (%)		
		Min	Average	Max	Concrete crushing	FRP crushing	FRP rupture
e/h = 0.05	λ = 14	0	0.85	1.48	42.45	57.55	0
	λ = 17	0	1.25	2.19	42.71	57.29	0
	λ = 19	0	1.55	2.74	42.71	57.29	0
	λ = 22	0	2.07	3.68	42.71	57.29	0
e/h = 0.2	λ = 14	0	1.49	2.7	44.79	55.21	0
	λ = 17	0	2.17	3.96	44.79	55.21	0
	λ = 19	0	2.7	4.92	44.79	55.21	0
	λ = 22	0	3.61	6.57	44.79	55.21	0
e/h = 0.4	λ = 14	0	2.17	6.03	50.26	49.74	0
	λ = 17	0	3.17	8.73	50.52	49.48	0
	λ = 19	0	3.93	10.77	50.78	49.22	0
	λ = 22	0	5.2	14.15	50.91	49.09	0
e/h = 0.5	λ = 14	0	2.11	5.88	51.82	47.4	0.78
	λ = 17	0	3.08	8.48	51.82	47.27	0.91
	λ = 19	0	3.81	10.42	51.95	47.14	0.91
	λ = 22	0	5.03	13.61	51.95	47.14	0.91
e/h = 0.75	λ = 14	0	1.79	4.65	52.21	42.97	4.82
	λ = 17	0	2.6	6.53	52.34	42.84	4.82
	λ = 19	0	3.23	8.06	52.34	42.84	4.82
	λ = 22	0	4.27	10.49	52.6	42.58	4.82
e/h = 1.0	λ = 14	0	1.49	3.8	50.91	39.58	9.51
	λ = 17	0	2.19	5.55	50.91	39.58	9.51
	λ = 19	0	2.72	6.96	51.04	39.45	9.51
	λ = 22	0	3.61	9.28	51.17	39.32	9.51

Table 6.9 shows the effect of slenderness ratio on the modes of failure. It was observed that an increase in the slenderness ratio does not change the overall mode of failure. However, in cases that experienced more than a 5% drop in the axial capacity, the dominant mode of failure is concrete crushing. Also, it was observed that as the slenderness ratio increases,

the percentage of cases that failed in FRP crushing or rupture increases. Changing slenderness ratio from 14 to 17 showed huge difference in the modes of failure. For slenderness ratio of 14, there was no sign of FRP crushing of rupture and the only mode of failure was concrete crushing for specimens which experienced more than 5% drop. However, there is a big shift by moving to slenderness ratio of 17; almost ten percent less concrete crushing and increase in FRP rupture and crushing. Moreover, the results showed that as slenderness ratio increases from 17 toward 22, the number of columns failed due to concrete crushing and FRP rupture decreases while the number of cases which failed due to FRP crushing in compression increases. However, concrete crushing is still the dominant mode of failure by increasing the slenderness ratio as presented in Table 6.9.

Table 6. 9 Effect of eccentricity ratio

Slenderness Ratio	All database (%)			Data with more than 5% drop (%)		
	Concrete crushing	FRP crushing	FRP rupture	Concrete crushing	FRP crushing	FRP rupture
$\lambda = 14$	48.74	48.74	2.52	100	0	0
$\lambda = 17$	48.85	48.61	2.54	90.31	2.5	7.19
$\lambda = 19$	48.94	48.52	2.54	89.74	4.4	5.86
$\lambda = 22$	49.02	48.44	2.54	87.79	7.44	4.77

6.4 MONTE CARLO (MC) SIMULATION

6.4.1 Methodology

In this section, the worst-case scenarios introduced in Table 6.1, corresponding to the highest percentage drop in the axial capacity for four slenderness ratios of 14, 17, 19, and 22 were considered. It should be noted that for all of the slenderness ratios, the worst-case

is the same and the mode of failure is concrete crushing. The base design equation is presented in Equation 6.1.

$$\emptyset K_R P_n = \gamma_D K_D P_D + \gamma_L K_L P_L \quad (6.1)$$

A resistance reduction factor (ϕ) of 0.65, a dead load factor (γ_D) of 1.2, and a live load factor (γ_L) of 1.6 were considered as per ACI 318-19 (2019). The bias ratio, defined as the ratio of measured over predicted, of dead load (K_D) and live load (K_L) were found from the literature, and the bias ratio of resistance (K_R) was considered as 1. A first-order analysis was performed using the input parameters defined for the worst-case presented in Table 6.1 and the value of nominal strength (P_n) was determined. Then, using the design equation (Equation 6.1), and a dead-to-live load ratio of 4, the predicted values of the dead load (P_D) and live load (P_L) were determined. By multiplying the design values for the worst-case introduced in Table 6.1 and the predicted dead and live loads by their corresponding bias ratios, the mean of input parameters for analysis and the mean of the dead and live load were determined. The distribution of analysis inputs and loads were found from the literature. Then using a Monte Carlo simulation, sets of inputs parameters and loads were randomly generated. The randomly generated input sets were used for the second-order analysis which represents the actual capacity of the columns. It should be emphasized that no code limitation for the furthest strain of concrete in compression was involved in the finding the resistance of the columns. Finally, the unfactored loads were deducted from the axial capacity derived using second-order analysis. The process was repeated for 200,000 trials for each slenderness ratio (i.e. a total of 800,000 trials). Then, the number of failed trials were counted to give the probability of failure of the column with a certain slenderness ratio and certain design values. Then the distribution corresponding to the difference

between the resistance and loads was built and the reliability index for each slenderness ratio was determined.

6.4.2 Distributions

In this section, the distribution of required variables for performing a second-order analysis to find the capacity of the columns is presented. Concrete strength (f'_c), tensile strength of FRP bars (f_{ftu}), compressive strength of FRP bars (f_{fcu}), modulus of elasticity of FRP bars (E_f), the depth of compressive FRP bars (d_{fc}), the depth of tensile FRP bars (d_{ft}), width of the column cross-section (b), height of the column cross-section (h), dead load (DL), and Live load (LL) were considered as random variables, and other parameters were considered as certain.

6.4.2.1 Distribution of bar locations

The real location of the FRP bars in the column cross-section plays a key role in the determination of the capacity of the columns, as it controls the lever arm of the resultant compressive and tensile forces in the cross-section. Figure 6.3 presents ten concrete columns from which nine specimens were reinforced with GFRP bars, from a study conducted by Khorramian and Sadeghian (2020).

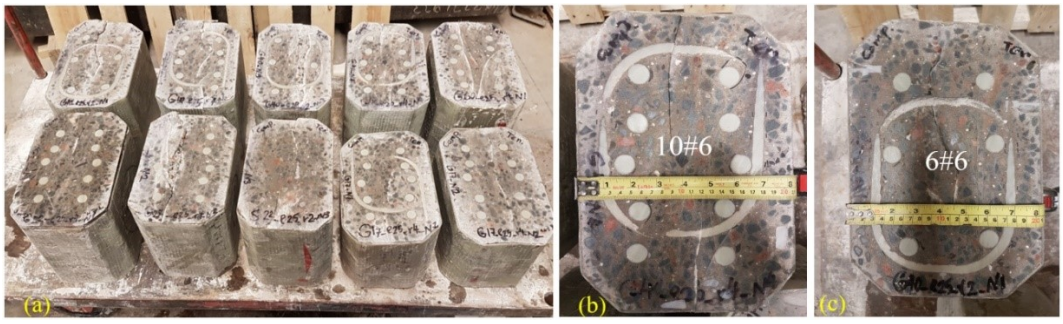

Figure 6. 3 Section cuts for rectangular GFRP-RC columns: (a) all specimen, (b) G40-N4, (c) G40-N1

After testing the specimens, the concrete sections were cut to find out the location of the bars. As observed in Figure 6.3, the bars are not in the same row due to construction issues. While for steel RC columns, the ties can be bent, for FRPs, the ties are premanufactured and do not have the flexibility to be bent for after manufacturing is done. Moreover, the longitudinal bars were located at the corner of ties, while all ties were not the same. Therefore, there is variability in the location of the bars. Table 6.10 presents the location of each bar measured from the edge of the concrete in the compressive side or tensile side for compressive and tensile bars, respectively, as shown in Figure 6.4 (a).

Table 6. 10 Location of bars from the edge of the concrete

No.	Specimen ID	Location of compressive bars (mm)					Location of tensile bars (mm)				
		Bar#1	Bar#2	Bar#3	Bar#4	Bar#5	Bar#6	Bar#7	Bar#8	Bar#9	Bar#10
1	G17 -N1	58.11	63.23	47.82	59.18	62.56	61.15	54.72	45.08	56.04	57.04
2	G17-N2	57.22	58.03	44.91	58.29	52.99	58.49	54.24	47.79	60.31	58.49
3	G22-N1	56.63	55.92	44.77	55.82	58.16	57.72	57.40	45.63	55.90	55.24
4	G22- N2	53.96	55.51	43.98	53.69	58.22	59.67	62.10	47.32	56.75	57.24
5	S22-N3*	51.48	38.36	51.37	-	-	56.22	42.22	66.33	-	-
6	G40-N1	58.47	46.07	62.60	-	-	59.66	48.48	57.00	-	-
7	G40- N2	54.48	50.44	45.08	53.52	57.71	58.93	42.83	45.10	51.89	54.22
8	G40-N3	56.10	44.53	58.54	-	-	53.17	45.26	55.01	-	-
9	G40-N4	59.30	57.10	44.14	57.80	54.53	60.05	60.80	49.44	66.58	66.72
10	G60-N1	60.12	63.56	45.79	57.28	61.19	53.89	58.82	46.03	56.84	60.73

Note: * = The recorded values for the steel bar is not considered into calculations.

The bar locations presented in Table 6.10 for FRP bars were used to generate the histogram of the bar location as presented in Figure 6.4(b). A total number of 82 values were considered which resulted in a coefficient of variation of 0.107 for the bar location distribution.

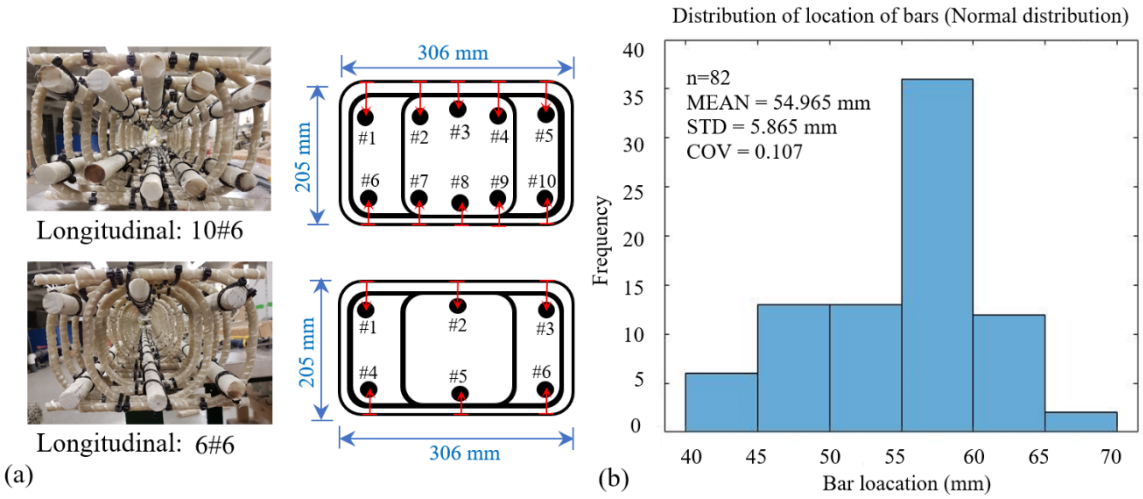

Figure 6. 4 Location of bars: (a) manufacturing and schematic, and (b) distribution of the location of bars

6.4.2.2 Load and Resistance Distributions

The distributions of all random variables required for Monte Carlo analysis are presented in Table 6.11, including the distribution types, bias factor, and statistical characteristics.

Table 6. 11 Statistical characteristics of the random variables for MC simulation

No.	Item	Type	Bias factor	COV	Distribution Type	Reference
1	f_c'	Random	Equation 6.2	0.10	Normal	Nowak and Szerszen (2003)
2	f_{fcu}	Random	1.20	0.08	Lognormal	Gulbrandsen (2005)
3	f_{ftu}	Random	1.20	0.08	Lognormal	Gulbrandsen (2005)
4	E_f	Random	1.04	0.08	Lognormal	Gulbrandsen (2005)
5	d_{fc}	Random	1	0.11	Normal	Current Study
6	d_{ft}	Random	1	0.11	Normal	Current Study
7	b	Random	1.01	0.04	Normal	Nowak and Szerszen (2003)
8	h	Random	1.01	0.04	Normal	Nowak and Szerszen (2003)
9	DL	Random	1.05	0.10	Lognormal	Oudah et al. (2019)
10	LL	Random	0.90	0.17	Lognormal	Oudah et al. (2019)

$$\lambda_{f'_c} = -0.0081\, {f'_c}^3 + 0.1509 {f'_c}^2 - 0.9338 f'_c + 3.0649\,, \left(f'_c\ in\ ksi\right) \qquad (6.2)$$

The mean of each random variable was set to the bias factor times the predicted values, which are design values (presented in Table 6.1) for inputs of second-order analysis and the predicted loads found by Equation 6.1 as explained in the methodology section. Then the inverse of each cumulative probability distribution (CDF) and random number generator of MATLAB software was used to generate different random sets of loads and resistance. For each slenderness ratio, a different set of randomly generated data was used. As a sample of generated data, for slenderness ratio of 22, randomly generated dead load, live load, and resistance distributions are presented in Figure 6.5 and the randomly generated input data used for analysis is presented in Figure 6.6.

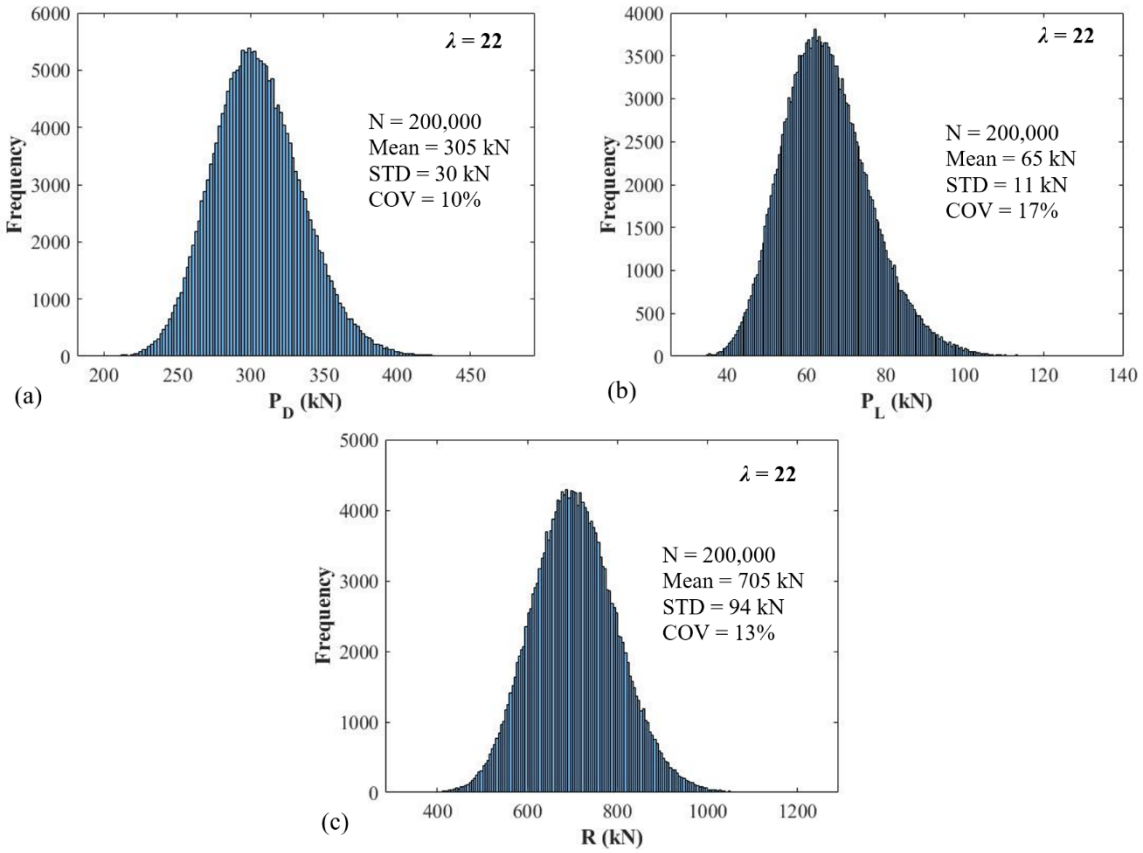

Figure 6. 5 Randomly generated load and resistance for slenderness ratio of 22: (a) the distribution of dead load, (b) the distribution of live load, (c) the distribution of resistance

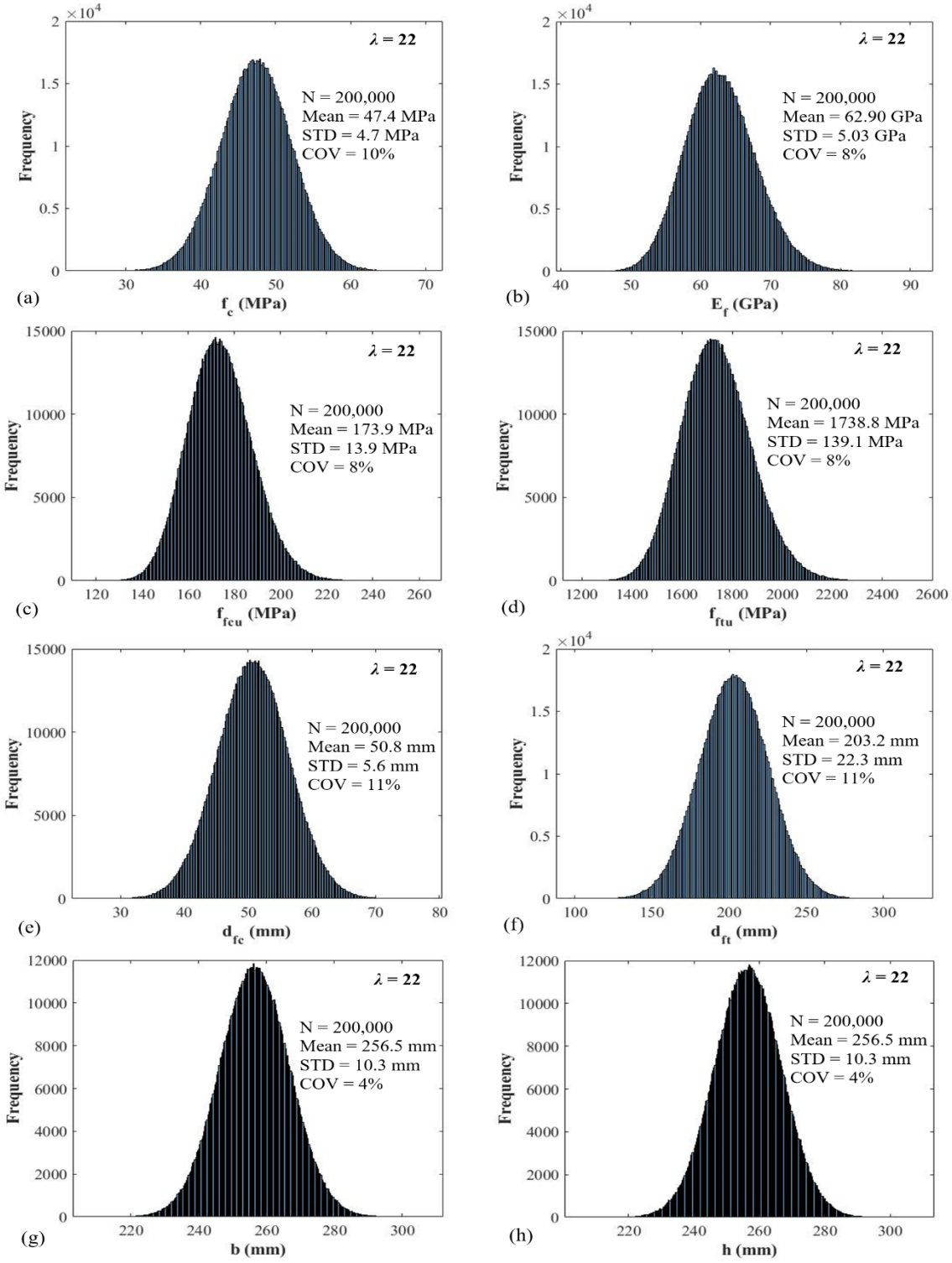

Figure 6. 6 Randomly generated inputs for slenderness ratio of 22: (a) concrete strength, (b) modulus of elasticity of FRP bars, (c) compressive strength of FRP bars, (d) tensile strength of FRP bars , (e) the depth of compressive FRP bars , (f) the depth of tensile FRP bars , (g) width of the column cross-section , (h) height of the column cross-section (note: bias factors were considered for all distributions)

6.5 Results and Discussion

The Monte Carlo simulation was performed for four slenderness ratios of 14, 17, 19, and 22 for the worst-cases recognized in Table 6.1. The results of the Monte Carlo simulation led to the determination of the distribution of the so-called "extra resistance" variable (Y) defined as resistance (R) minus dead load (P_D) and live load (P_L) for four slenderness ratios of 14, 17, 19, and 22 as presented in Figure 6.7(a), 6.7(b), 6.7(c), and 6.7(d), respectively. It was concluded that this distribution corresponds to a normal distribution.

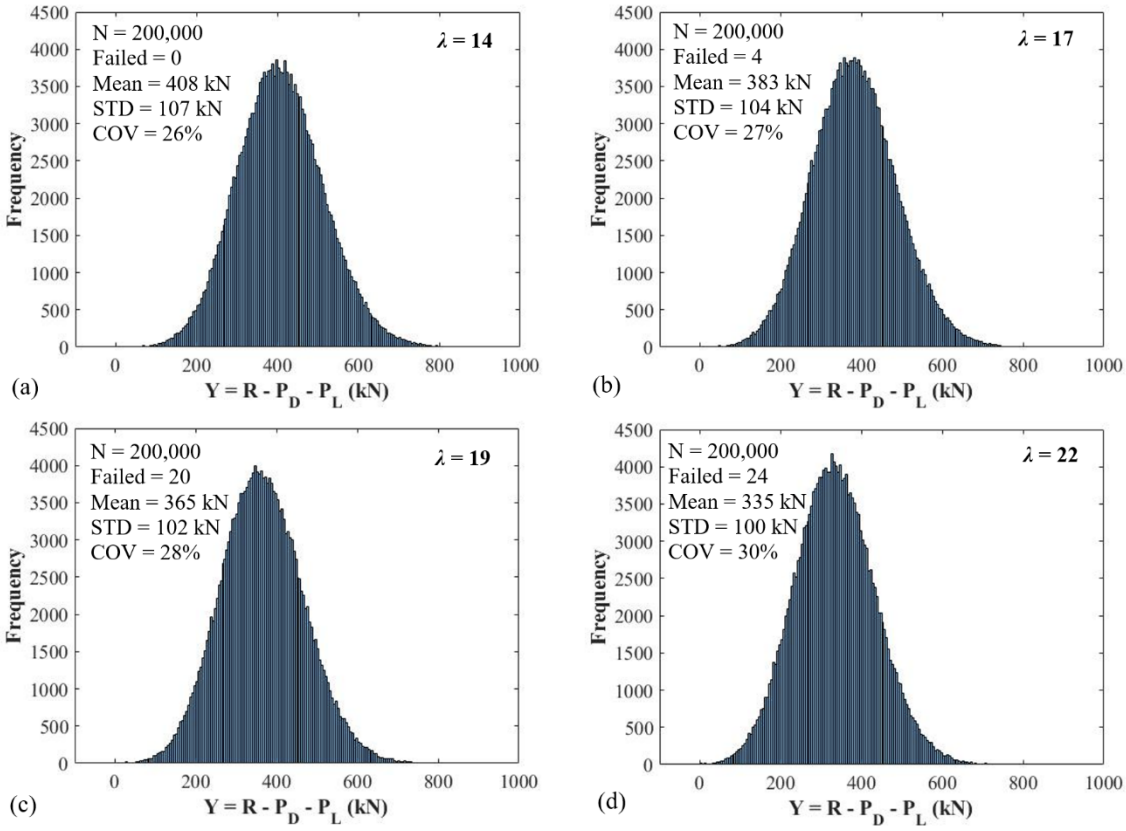

Figure 6. 7 Distribution of Y for slenderness ratios of: (a) 14, (b) 17, (c) 19, and (d) 22.

Once a set of random load and resistance were generated for each slenderness ratio, failure was defined as the state when the load exceeds resistance (i.e. Y<0), as presented in Equation 6.3. And, the probability of failure was calculated using Equation 6.4, and its corresponding reliability index was calculated using Equation 6.5 and Equation 6.6.

$$Y = R - P_D - P_L \quad , \quad Failure \equiv Y < 0 \tag{6.3}$$

$$P_f = \frac{n}{N} \tag{6.4}$$

$$P_f = P[Y < 0] = P[Y < 0] = P\left[\frac{Y-\mu_Y}{\sigma_Y} < \frac{0-\mu_Y}{\sigma_Y}\right] = P[Z < -\beta] \quad , \quad \beta = \frac{\mu_Y}{\sigma_Y} \tag{6.5}$$

$$\beta = \Phi^{-1}(1 - P_f) \tag{6.6}$$

Where Y is distribution of goal which defines failure if it gives negative values, R is randomly generated resistance distribution, P_D is randomly generated dead load distribution, P_L is randomly generated live load distribution, n is number of trials that resistance was less than loads (number of failed trials), N is total number of trials, p_f is probability of failure, Z is standard normal distribution of the Y distribution, Φ^{-1} is a function that returns inverse of standard normal distribution, β is reliability index, μ_Y is mean of Y distribution, and σ_Y is standard deviation of Y distribution. It was observed that as slenderness ratio increases, the number of failed cases increases which, in turn, causes an increase in the probability of failure and a decline in its corresponding reliability index. The second-order analysis performed for MC simulation was time-consuming, as it considered the nonlinearity in material and geometry and followed an iterative procedure (Khorramian and Sadeghian, 2017a and 2019a). Therefore, a limited number of cases (200,000) was selected for each slenderness ratio to form a total of 800,000 cases.

Sources of inaccuracy in the predicted reliability index for the introduced procedure can be related to the MC analysis accuracy, the input data accuracy, and factors that were not considered in the analysis. To account for the accuracy of the results, the confidence intervals of the probability of failure was calculated according to the method given by Griffiths and Fenton (2008) using Equation 6.7 and Equation 6.8.

$$[L, U]_{1-\alpha} = P_f \pm z_{\alpha/2}\sqrt{\frac{P_f(1-P_f)}{N}} \tag{6.7}$$

$$z_{\alpha/2} = \Phi^{-1}\left(1-\alpha/2\right) \qquad or \qquad P\left[Z < \alpha/2\right] = z_{\alpha/2} \tag{6.8}$$

Where L is lower bound of the confidence interval, U is upper bound of the confidence interval, P_f is probability of failure, $z_{\alpha/2}$ is a point in standard normal distribution whose cumulative distribution function (CDF) is $\alpha/2$, Φ^{-1} is a function that returns inverse of standard normal distribution, $1-\alpha$ is confidence of a two-sided confidence interval, and N is the total number of trials. In this study, a 95% confidence interval was considered and its corresponding probability of failure and reliability indices were calculated for all studied slenderness ratios, as presented in Table 6.12 and Figure 6.8.

Table 6. 12 Simulation results

Slenderness Ratio	**Failed trials**	**P_f**	**β**	**(95% confidence interval)**		
				Tolerance	**Upper P_f**	**Lower β**
λ = 14	0	Less than 0.000005	More than 4.4172	-	-	-
λ = 17	4	0.0000200	4.11	0.0000196	0.0000396	3.95
λ = 19	20	0.0001000	3.72	0.0000438	0.0001438	3.63
λ = 22	24	0.0001200	3.67	0.0000480	0.0001680	3.59

The results showed that the lower bound for the reliability index of the column with a slenderness ratio of 22, with 95% confidence, was 3.59 is more than the lower bound of 3.5 defined for the target reliability index range of 3.5 to 4 for GFRP RC structures given by ACI 440.1R-15 (2015). Recently, a value of 17 is considered as the critical slenderness ratio for the draft ACI 440 code accompanied to ACI 318-19 (2109). The results showed that higher critical slenderness ratios can be selected for GFRP-RC columns. However, conclusive remarks cannot be established based on this limited study. The authors are planning for a future research programme to cover a wider spectrum of influential variables.

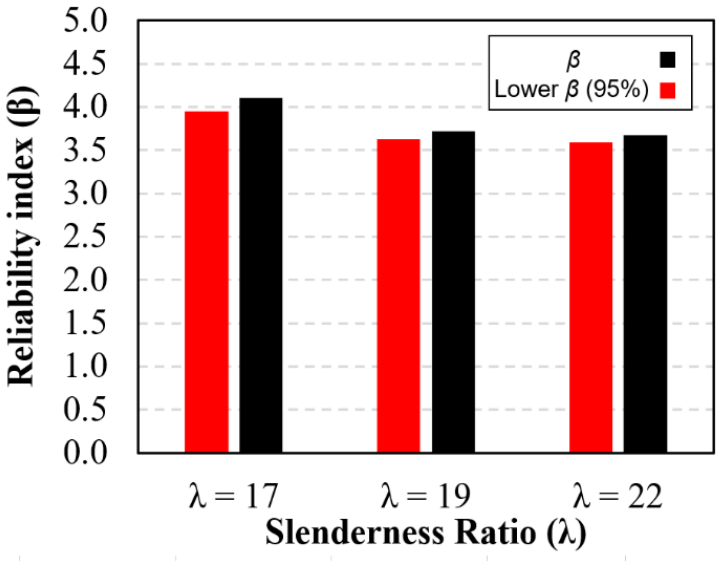

Figure 6. 8 Slenderness ratio versus reliability index

6.6 Conclusion and Future Studies

In this paper, the reliability index associated with the critical slenderness ratios of 14, 17, 19, and 22 for GFRP reinforced concrete columns was studied for the first time. The results showed that as the critical slenderness ratio decreases from 22 to 17, the reliability index increases from 3.59 to 3.95. However, it must be mentioned that the current study was only

a preliminary study and a more comprehensive study must be performed to cover a wider spectrum of realistic cases. The concrete strength of 41.4 MPa was the limit for this study, however, the results showed that as concrete strength increases, the difference between first-order and second-order analysis increases as well as the percentage drop in the capacity. Thus, higher concrete strength should be considered. In addition, a minimum modular ratio of 2 was considered in this study. However, lower modular ratios can be representative of GFRPs, especially as the concrete strength and modulus of elasticity increases. The strength of FRP bars in compression considered to be less than 50% of its tensile strength which should be modified to be compatible with the most recent findings. Also, only the crushing of concrete was considered. Cases that represent the rupture or crushing of FRP bars should be also considered. Different eccentricities for both ends can be considered, and their randomness can be considered in the analysis which leads to single and double curvature bending. Furthermore, a database of existing experimental studies can be used to find the bias of the second-order model and involve the database inside the simulation. Moreover, circular concrete columns, different dead to live load ratios, and different reinforcement layouts should be studied, which will be considered in future studies to give more accurate reliability indices.

ACKNOWLEDGMENTS

Authors would like to thank Dr. Fadi Oudah for his contribution in the supervision of this chapter. Also, the authors would also like to acknowledge and thank NSERC and Dalhousie University for their financial support.

REFERENCES

Abdelazim, W., Mohamed, H. M., Afifi, M. Z., and Benmokrane, B. (2020). Proposed Slenderness Limit for Glass Fiber-Reinforced Polymer-Reinforced Concrete Columns Based on Experiments and Buckling Analysis. *ACI Structural Journal*, 117(1), 241–254.

ACI 318-19. (2019). Building Code Requirements for Structural Concrete. *American Concrete Institute.* Farmington Hills, MI.

ACI 440.1R. (2015). Guide for the Design and Construction of Structural Concrete Reinforced Fiber-Reinforced Polymer (FRP) Bars. *American Concrete Institute.* Farmington Hills, MI.

AlAjarmeh, O. S., Manalo, A. C., Benmokrane, B., Vijay, P. V., Ferdous, W., and Mendis, P. (2019). Novel testing and characterization of GFRP bars in compression. *Construction and Building Materials*, 225, 1112-1126.

Griffiths, D. V., and Fenton, G. A. (2008). Risk assessment in geotechnical engineering. *John Wiley and Sons Inc*, 381-400.

Gulbrandsen, P. W. (2005). Reliability Analysis of the Flexural Capacity of Fibre Reinforced Polymer Bars in Concrete Beams, *Doctoral dissertation*, University of Minnesota.

Hadhood, A., Mohamed, H. M., and Benmokrane, B. (2017). Experimental study of circular high-strength concrete columns reinforced with GFRP bars and spirals under concentric and eccentric loading. *Journal of Composites for Construction*, 21(2), 04016078.

Khorramian, K., and Sadeghian, P. (2017a). Experimental and analytical behavior of short concrete columns reinforced with GFRP bars under eccentric loading. *Engineering Structures*, 761–773.

Khorramian, K., and Sadeghian, P. (2017b). Short Concrete Columns Reinforced with GFRP Rebars Under Eccentric Loading. *CSCE Annual Conference. Vancouver, BC, Canada: Canadian Society of Civil Engineering.*

Khorramian, K., and Sadeghian, P. (2018). New Testing Method of GFRP Bars in Compression. *CSCE Annual Conference. Fredericton, NB, Canada: Canadian Society of Civil Engineering.*

Khorramian, K., and Sadeghian, P. (2019a). Behavior of Slender GFRP Reinforced Concrete Columns. *ASCE-SEI Structures Congress, American Society of Civil Engineers.* St. Louis, Missouri, USA.

Khorramian, K., and Sadeghian, P. (2019b). Material Characterization of GFRP Bars in Compression using a New Test Method. *Journal of Testing and Evaluation (ASTM)*, 49, 2.

MacGregor, J. G., and Breen, J. E. (1970). Design of slender concrete columns. *In Journal Proceedings* 67(1), 6-28.

Mirmiran, A., Yuan, W., and Chen, X. (2001). Design for slenderness in concrete columns internally reinforced with fiber-reinforced polymer bars. *Structural Journal*, 98(1), 116-125.

Nowak, A. S., and Szerszen, M. M. (2003). Calibration of design code for buildings (ACI 318): Part 1-Statistical models for resistance. *ACI Structural Journal*, 100(3), 377-382.

Oudah, F., El Naggar, M. H., and Norlander, G. (2019). Unified system reliability approach for single and group pile foundations–Theory and resistance factor calibration. *Computers and Geotechnics*, 108, 173-182.

Zadeh, H. J., and Nanni, A. (2017). Flexural Stiffness and Second-Order Effects in Fiber-Reinforced Polymer-Reinforced Concrete Frames. *ACI Structural Journal*, 114(2), 533–544.

CHAPTER 7 PERFORMANCE OF HIGH-MODULUS NEAR-SURFACE-MOUNTED FRP LAMINATES FOR STRENGTHENING OF CONCRETE COLUMNS

ABSTRACT

This study investigates the performance of high-modulus near-surface-mounted (NSM) fiber-reinforced polymer (FRP) laminates in strengthening of existing concrete columns. The focus of this study is on the compressive and buckling characteristics of carbon FRP (CFRP) laminates installed on short columns for strengthening to validate their sufficiency for further studies on slender columns. In this paper, an experimental study was designed to consider the effect of eccentric loading on short concrete columns (500×150×150 mm) strengthened with four longitudinal NSM CFRP laminates (1.2×10 mm). All specimens were tested symmetrically under the eccentricity to width ratios of 0, 10, 20, and 30% to give a single curvature bending combined with axial load. The experimental results showed no buckling/debonding failure of CFRP laminates, while some of the CFRP laminates reached to crushing points long after the peak load. Moreover, material coupon tests showed that the strength and elastic modulus of the CFRPs in compression were 34% and 86% of those in tension, respectively. The average compressive strain of NSM CFRP laminates for all column specimens under eccentric loading at peak load and after 15% drop from the peak load was 41% and 84% of their ultimate compressive strain obtained from compression coupon tests, respectively. Furthermore, a robust analytical model was developed considering the material and geometrical nonlinearities and it was verified against experimental results. Overall, the results indicated that strengthening short concrete columns with NSM CFRP laminates improved the capacity of the columns without any

premature buckling, debonding, or crushing of CFRP laminates. The results will open new avenues in the FRP strengthening of concrete columns, especially slender columns, where the high-modulus NSM system can also enhance the lateral stiffness of the columns for buckling control.

7.1 INTRODUCTION

In the past decades, researchers have studied the effectiveness of near-surface-mounted (NSM) fiber-reinforced polymer (FRP) laminates for strengthening of existing reinforced concrete (RC) beams. The NSM technique, like externally bonded FRP (EBF) technique, has been implemented to the tension side of concrete beams. In contrast to EBF sheets, NSM FRPs are inserted into grooves created in the concrete cover of concrete beam using an adhesive. Moreover, NSM technique provides more surfaces of concrete in interaction with adhesives which makes debonding less conceivable in comparison to the EBF technique. There have been considerable researches on the behavior of NSM FRP reinforcements for strengthening concrete beams (Badawi and Khaled, 2009; Ceroni, 2010; Nordin and Täljsten, 2006; Teng, et al., 2006) and concrete slabs (Khorramian and Sadeghian, 2017; Foret and Limam, 2008). However, a few researches have been conducted on NSM FRP applications on columns (Bournas and Triantafillo, 2009; Gajdosova and Bilcik, 2013; Barros et al., 2008).

NSM FRP laminates has not been used for strengthening concrete columns because it is believed that they are not efficient in compression. For example, Fib Bulletin 14 (2001) mentioned that the modulus of elasticity of FRP in compression is lower than its modulus in tension. ACI 440.2R (2008) emphasized that the usage of FRP systems as compressive reinforcement is not recommended. CAN/CSA S806-12 (2012) clarified that FRP

reinforcing elements in concrete compression zone shall be deemed to have zero compression strength and stiffness for design purposes. The use of FRPs in compression is not recommended by ACI 440.2R (2008) because of possible premature failures such as micro buckling of fibers, buckling of unsupported or poorly supported laminates, and improperly anchorage of substrate and FRP surface as well as unreliability in the compressive strength of laminates. Micro buckling could arise from performing weak quality control of the FRP production which is attributed to the presence of voids in the resin by ACI 440.2R (2008), although commitment in quality control can fix this problem. On the other hand, Barros et al. (2008) performed a numerical and experimental investigation to evaluate the effectiveness of NSM carbon FRP (CFRP) strips on the flexural strengthening of RC columns whose result showed a significant increase of load carrying capacity of columns failing in bending. In another study, Gajdosova and Bilcik (2013) studied slender RC columns strengthened with NSM CFRPs experimentally and found that resistance enhancement is achieved for both short and slender concrete columns. Sadeghian and Fam (2015) investigated the application of high-modulus externally bonded longitudinal FRPs on slender RC columns which showed that by applying longitudinal FRP laminates, the loading path of slender columns is improved to gain higher axial capacity due to the additional gain in stiffness of columns. Regarding the neglection of FRP laminates in compression on one hand and their effectiveness in compressive behavior on the other hand, the compressive behavior of NSM FRPs in compression needs to be investigated in depth. There are insufficient researches on the adequacy of longitudinal compressive NSM FRP laminates in both flexural and axially loaded concrete columns in terms of their strength and stiffness which requires a better knowledge of behavior of FRPs

in compression. Moreover, the possibility of premature crushing, debonding, buckling failures of NSM FRP-strengthened concrete columns indicates the necessity of more studies in this field. Addressing these issues requires compression tests with high degree of accuracy. Therefore, the current research tries to address some of these vague prospective problems.

This research was designed to evaluate the behavior of NSM CFRP strips used for strengthening of short concrete columns under eccentric and concentric loadings using experimental and analytical methods. The experimental program consists of fourteen medium-scale concrete columns strengthened with NSM CFRP strips and tested under single curvature bending and compressive axial loads. The analytical part includes a verified model which considers the nonlinearity of both geometry and material and predicts the behavior of these columns. Furthermore, a parametric study performed to provided supporting information about the compressive behavior of NSM CFRP strengthened short concrete columns. This study is a part of a comprehensive project on application of longitudinal FRPs in concrete columns, especially slender columns. The authors believe that high-modulus NSM FRPs can be effective for strengthening of slender RC columns through enhancing the lateral stiffness of the columns. The results of this study will establish a data platform on compressive behavior of NSM FRPs for more in-depth studies on strengthening of slender RC columns.

7.2 EXPERIMENTAL PROGRAM

In this section, the experimental program consisting of fourteen medium-scale short concrete columns tested under concentric and eccentric loads is explained, where nine of these specimens were reinforced with NSM CFRP laminates. In the following, the test

matrix, material properties, fabrication, and test set up for both plain and reinforced concrete column specimens are explained.

7.2.1 Test Matrix

A total of fourteen 500 mm long concrete columns with a square cross-section (150×150 mm) were prepared and tested under pure axial and combined flexural and axial loadings. Nine of these specimens were strengthened with NSM CFRP laminates. Four specimens consisting two plain concrete and two specimens strengthened with NSM CFRP laminates were tested under concentric axial load and other specimens were tested under eccentric loads at 15, 30, and 45 mm, i.e. 10, 20, and 30 percent of width of the cross-section, respectively, as presented in Table 7.1.

Table 7. 1 Test specimen properties

No.	Specimen ID	Eccentricity ratio, e/h (%)	Eccentricity, e (mm)	Reinforcement
1	N-e0-1	0	0	CFRP
2	N-e0-2	0	0	CFRP
3	N-e10-1	10	15	CFRP
4	N-e10-2	10	15	CFRP
5	N-e10-3	10	15	CFRP
6	N-e20-1	20	30	CFRP
7	N-e20-2	20	30	CFRP
8	N-e30-1	30	45	CFRP
9	N-e30-2	30	45	CFRP
10	P-e0-1	0	0	None
11	P-e0-2	0	0	None
12	P-e10-1	10	15	None
13	P-e10-2	10	15	None
14	P-e10-3	10	15	None

It should be noted that for the sake of simplicity and focusing on the modes of failure of NSM reinforcement, the plain concrete specimens were considered to be reinforced only with NSM FRPs. Moreover, studying only plain concrete and FRPs highlights the effect of NSM FRPs even for strengthening cases in which the longitudinal steel reinforcement would not be effective structurally anymore due to corrosion. To name the specimens, a label like "A-ex-y" was used where A, x, and y indicate the column type, the eccentricity, and the specimen number, respectively. The column type is identified by "P" for plain or "N" for NSM CFRP strengthened concrete columns.

7.2.2 Material Properties

The concrete was ready-mixed, and the maximum aggregate size was 12.5 mm. The compressive strength of concrete at the time of testing of columns measured as 37.0±0.8 MPa using three concrete cylinders (100 mm diameter and 200 mm height). To strengthen concrete specimens, pre-manufactured unidirectional CFRP strips with a thickness and width of 1.2 and 10 mm, respectively, were used. The NSM CFRP strips were inserted in grooves using a compatible adhesive for bonding purpose. The tensile strength, compressive modulus of elasticity, tensile rupture strain, and bond strength of adhesive were reported by manufacturer as 27.06 MPa, 3.06 GPa, 0.01 mm/mm, and 13.8 MPa, respectively.

The tensile characteristics of CFRP strips were also evaluated by testing five tensile coupons prepared per ASTM D3039/D3039M (2014). The average ± standard deviation of ultimate tensile strength, tensile modulus of elasticity, and rupture strain of tested specimens were 3006±288 MPa, 180.5±8.3 GPa, and 0.01668±0.00176 mm/mm,

respectively. The stress-strain behavior of CFRP laminates in tension was linear as shown in Figure 7.1(a).

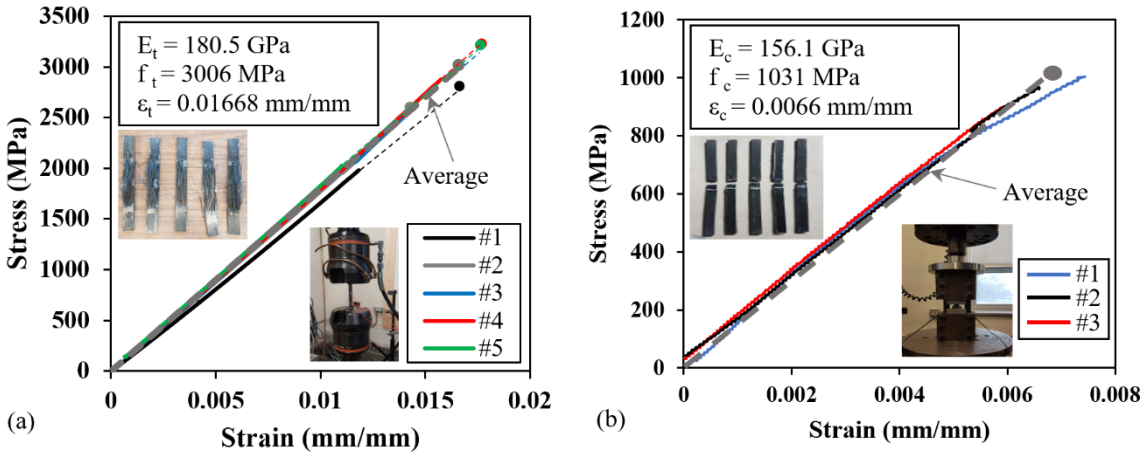

Figure 7. 1 Experimental stress-strain curves of CFRP laminates in (a) tension and (b) compression

To assess the compressive characteristics of the CFRP laminates, five compressive coupons were prepared and tested under pure compressive load using a test fixture that was prepared per ASTM D6641/D6641M-16 (2016). Width and thickness of each compressive coupon was 1.2 and 12.2 mm, respectively, while the length of each coupon was 216 mm which was tabbed with two 102 mm long CFRP strips at each end so that the free length of the specimen was 12 mm as shown in Figure 7.2(a). The test fixture consists of two thick steel cubes which can move using two alignment rods, two thick steel plates that holds the specimen in place during testing, and four patterned steel tabs to decrease the chance of premature failure, as shown in Figure 7.2(b). It should be noted that the tests were performed using displacement control approach with a rate of 0.5 mm/min. All the specimens were crushed in the gauge length as presented in Figure 7.2(c). No buckling was observed during the test, and all specimens failed with a crushing failure mode in the gauge length. This failure is described by ASTM D6641/D6641M-16 (2016) as the transverse

shear or through thickness failure modes at grip/tab on top (TAT or HAT) as shown in Figure 7.2(d).

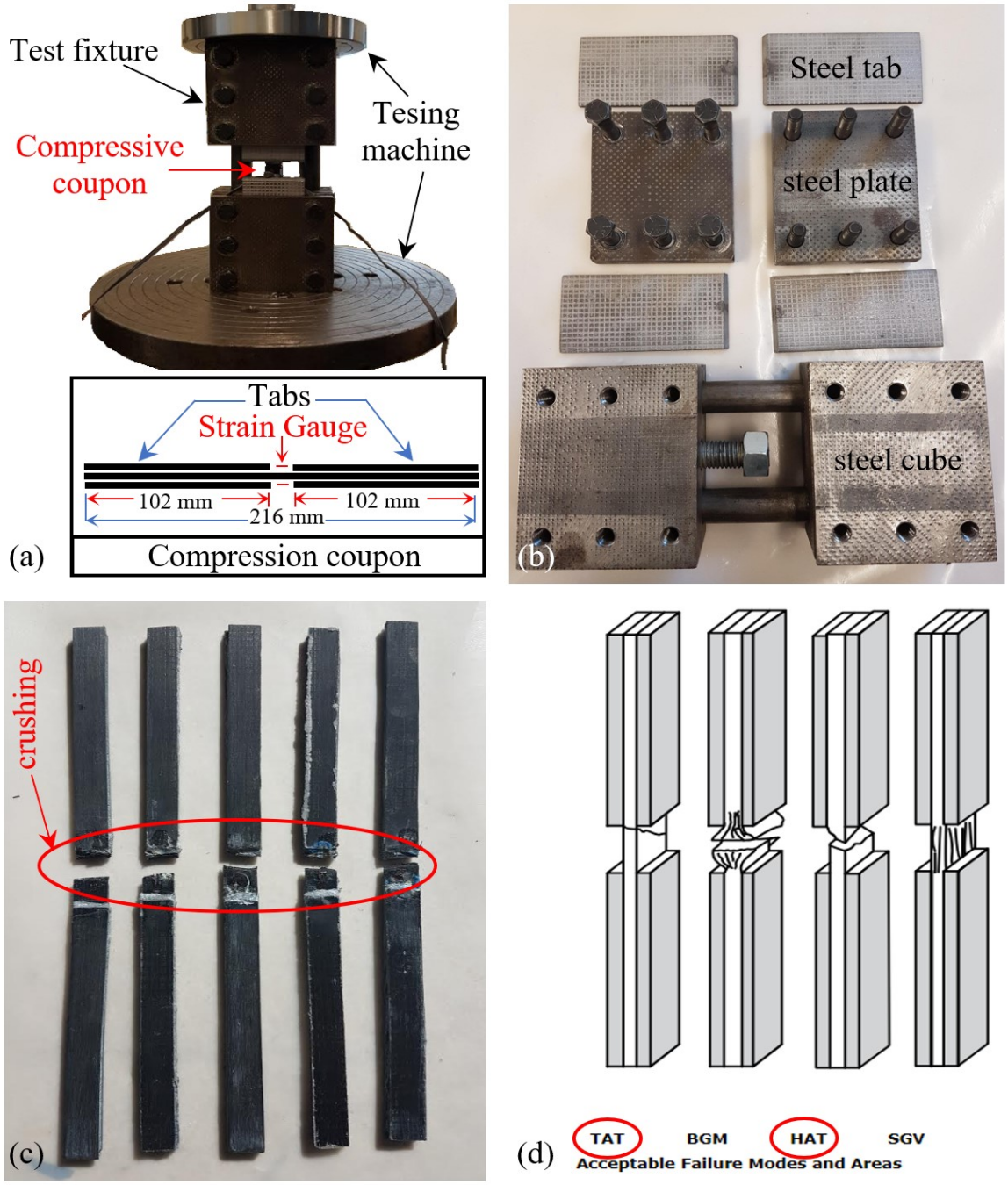

Figure 7. 2 Compression coupon test: (a) compressive coupon and test set-up, (b) Test fixture components, (c) broken specimen, and (d) accepted failure modes by ASTM D6641-16 (2016)

The average ± standard deviation of ultimate compressive strength, compressive modulus of elasticity, and crushing strain of tested specimens were 1031±47 MPa, 156.1±5 GPa, and 0.0066 mm/mm, respectively. The crushing strain was derived by division of average compressive strength to modulus of elasticity of the compressive coupons. For capturing strains, two strain gauges were installed on the gauge length of the coupons, and the average strain for each coupon represented the stress-strain curves. The stress-strain behavior of CFRP laminates in compression was linear as shown in Figure 7.1(b).

The average strength of the tested CFRP coupons in compression was 34% of the average strength of the coupons in tension. The average compressive strength was considerably lower than the tensile strength of CFRP laminate, however, it should be considered that the strength is still considerably high (1031 MPa) which is more than two times higher than conventional steel rebar. It was observed that the average modulus of elasticity of the CFRP coupons in compression was only 86% of the average modulus of elasticity of the coupons in tension. Although the average crushing strain of the CFRP coupons was 0.0066 mm/mm (60% of the average rupture strain in tension), it is still almost two times higher than the design crushing strains of concrete, i.e. 0.003 and 0.0035 mm/mm defined by ACI 318-14 (2014) and CSA A23.3-14 (2014), respectively. Therefore, material tests showed proper characteristics for CFRP laminates in compression for structural usage purposes.

7.2.3 Fabrication

To provide the concrete specimens with proper grooves for NSM strips, four wooden strips with width and thickness of 15 mm and 5 mm, respectively, were attached to each wooden mold. The method of creating the grooves in fresh concrete was selected for the laboratory safety reason instead of cutting the grooves in hard concrete using concrete saw. The

wooden strips were hold in place using both adhesive in the longitudinal direction and four holes at the ends of molds as shown in Figure 7.3(a). The clear distance between wooden strips was 30 mm and their distance from the edges of molds was 55 mm. All concrete specimens were casted with a ready-mix concrete as shown in Figure 7.3(b). The specimens cured at the room temperature and saved their moisture using plastic covers shown in Figure 7.3(c). In fourteen days after pouring concrete, the wooden molds were removed from the specimens [Figure 7.3(d)], and grooves were prepared for mounting of CFRP strips by cleaning and grinding the interior surface of grooves which gave a better friction between bonding agent and concrete surface as well as removing dust and wood particles from grooves, as presented in Figure 7.3(e).

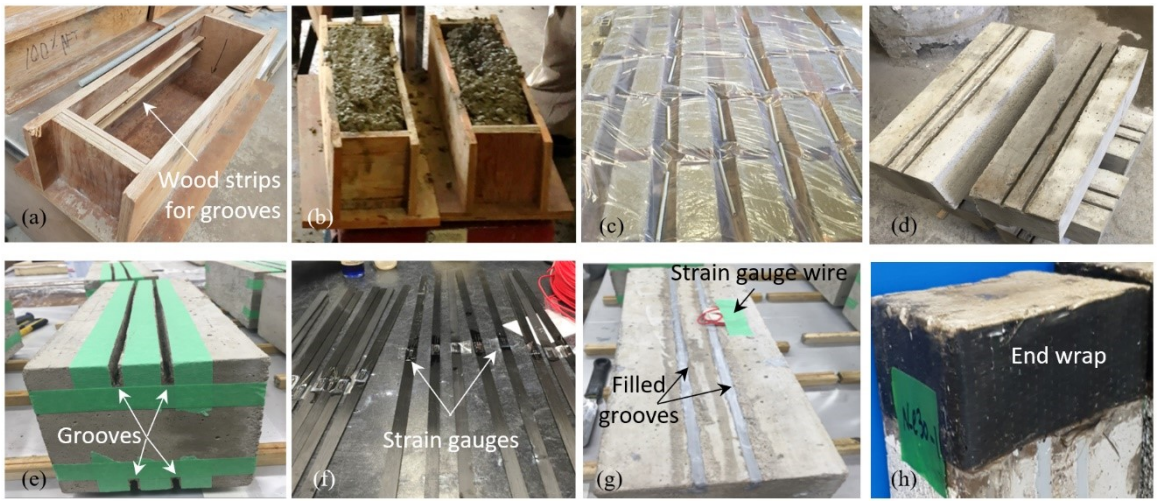

Figure 7. 3 Specimen fabrication: (a) mold; (b) fresh concrete; (c) curing; (d) concrete specimens; (e) prepared grooves; (f) CFRP strips; (g) filled groves; and (h) end wrap

For each side of every specimen, a strain gauge installed on the surface of NSM CFRP strip [Figure 7.3(f)] which was coated with nitrile rubber coating agent and covered by aluminum tape. The CFRP strips were embedded in the groves of concrete specimens using a compatible adhesive as bonding material as is shown in Figure 7.3(g). To avoid prospective

premature failure caused by load concentration at the ends of specimens which are close to the load application point, both ends of the specimens were wrapped with two layers of unidirectional basalt fabrics and epoxy resin as shown in Figure 7.3(h). The top and bottom of each specimen then grinded to give a flat column end surface.

7.2.4 Test Set Up

The test set up and instrumentation of specimens used in this study are presented in Figure 7.4(a). Two steel caps were installed on top and bottom of each specimen provided both load eccentricity and simply supported condition for the specimens tested under combined flexural and axial loads. As shown in Figure 7.4(b), each steel cap was created by welding a 30-mm thick steel plate, with a V-shape notch, on top of a square steel plate with width and thickness of 250 mm and 10 mm, respectively. For testing specimens under different load eccentricities, the location of notched plate altered to meet new eccentricity demand by removing welds and rewelding them in the new location. Two steel cylinders attached to the testing machine upon which the notched steel caps stands and provide the rotation at the ends of specimens so that pin-pin testing condition satisfied, as shown in Figure 7.4(b). The symmetricity of steel cylinders and notches at the ends of the specimens made columns experience single curvature bending. To ensure that steel caps and specimens rotating together without sliding on each other, four steel angle profiles surrounded the specimen circumference at both ends and attached to the steel cap using bolt fasteners, as presented in Figure 7.4(b). To increase the degree of integration between steel cap and specimens, before fastening the adjustable steel angles to the steel cap, a plastic bag filled with quick set fresh grout placed on top of specimen so that it covers the interface of concrete column, steel cap, and angles.

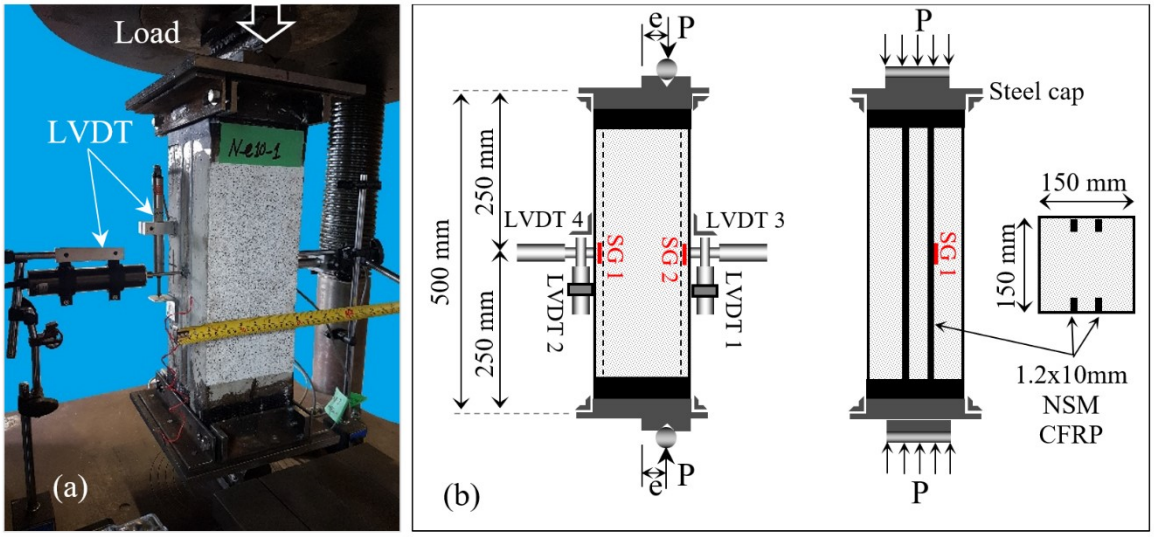

Figure 7. 4 Test set up and instrumentation: (a) testing machine and instrumentation, and (b) schematic testing specimen and reinforcement layout

The final position of the specimen with steel cap after putting inside the 2 MN universal testing machine is shown in Figure 7.3(a). The instrumentation designed to capture longitudinal strain of CFRP strips at both compressive and tensile sides using strain gauges one strain gauge at each side on the surface of CFRP strip (i.e. SG 1 and SG 2) as well as recording the lateral displacement of specimens at the mid height of columns using two horizontal linear variable differential transformers (LVDTs) on compressive (i.e. LVDT 3) and tensile side (i.e. LVDT 4), as shown in Figure 7.4(b). To secure the data recorded by strain gauges, two vertical LVDTs (i.e. LVDT 1 and LVDT 2) were installed at the mid height of specimens on the concrete surface by an aluminum plate holding each strain gauge and adhered to concrete surface. On top of these LVDTs, two aluminum angles were glued to the concrete surface to provide a gauge length of 100 mm as shown in Figure 7.4(a) and 4(b). All tests were conducted using displacement control approach with a loading rate of 0.625 mm/min and data acquisition rate of 10 data point per second.

7.3 EXPERIMENTAL RESULTS AND DISCUSSION

The experimental result of the tests conducted in this study, consisting of fourteen short specimen columns are discussed in this section starting from failure modes description, passing to the behavior of NSM CFRP laminates in compression, and concluding with their effect on the load bearing capacity of the tested columns. A summary of test results is shown in Table 7.2.

Table 7. 2 Summary of test results

No.	Specimen ID	Peak Load, P_u (kN)	SG1 at peak load (mm/mm)	SG1 at peak load to rupture strain ratio	SG2 at peak load (mm/mm)	SG2 at peak load to crushing strain ratio	SG1 at 0.85 P_u (mm/mm)	SG1 at 0.85 P_u to rupture strain ratio	SG2 at 0.85 P_u (mm/mm)	SG2 at 0.85 P_u to crushing strain ratio
1	N-e0	774.5	-0.00197	-0.12	-0.00156	0.24	-	-	-	-
2	N-e10	661.2	-0.00004	0.00	-0.00280	0.42	0.00059	0.04	-0.00568	0.86
3	N-e20	545.0	0.00058	0.03	-0.00329	0.50	0.00111	0.07	-0.00508	0.77
4	N-e30	398.9	0.00239	0.14	-0.00327	0.50	0.00480	0.29	-0.00591	0.90
5	P-e0	719.2	-	-	-	-	-	-	-	-
6	P-e10	596.3	-	-	-	-	-	-	-	-

Note: CFRP strains were recorded by SG1 (tension side) and SG2 (compression side), as shown in Figure 3; the sign convention is positive for tensile strains and negative compressive strains; rupture strain = 0.01668 mm/mm; crushing strain =0.0066 mm/mm.

7.3.1 Failure Mode

Overall, four modes of failure were observed in reinforced specimens consisting of concrete spalling (CS), concrete crushing (CC), compressive FRP crushing (CFC), tensile FRP rupture (TFR), however, no buckling or debonding of NSM FRP strips observed during the tests. Concrete spalling (CS) happened about the peak load or at peak load where the compressive stresses in concrete were critical and cracks caused the separation of a concrete segment in compressive side of the specimens, as is shown in Figure 7.5(a).

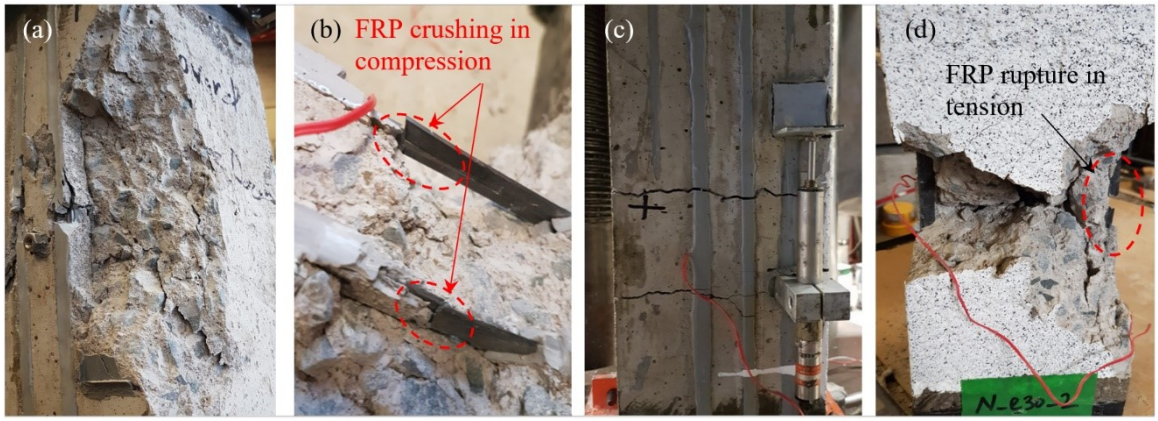

Figure 7. 5 Modes of failure: (a) concrete spalling (CS), (b) compressive FRP crushing (CFC), (c) tensile cracks, and (d) tensile FRP rupture (TFR)

It was observed that the average compressive strain of CFRP at peak load for 0, 10, 20, and 30 percent eccentricity to width ratios, were 0.00156, 0.00270, 0.00329, and 0.00327 mm/mm, respectively, which result in 0.0027 mm/mm as the average of compressive strain of CFRP in compression. Therefore, at peak load, the compressive strain of concrete was close to 0.003 mm/mm or 0.0035 mm/mm that justifies the observation of concrete spalling about the peak load. Concrete crushing (CC) defined where the strain of furthest compressive fiber in concrete reached 0.003 mm/mm or 0.0035 mm/mm, which were the ultimate design strain of concrete introduced by ACI 318-14 (2014) or CSA A23.3-14 (2014), respectively. The compressive FRP crushing (CFC), which is presented in Figure 7.5(b), happened long after the peak load with a noise and sudden appearance of crack on the surface of adhesive. The tensile cracks shown in Figure 7.5(c) happened prior to tensile FRP rupture (TFR) which was sudden and with noise, as shown in Figure 7.5(d).

For both plain concrete and strengthened specimens tested under pure compression, the mode of failure was concrete spalling (CS). For NSM specimens tested with 10 percent eccentricity to width ratio [Figure 7.6(a)], first concrete spalling (CS) happened followed

by crushing of at both CFRP strips in compressive zone (CFC). Because the concrete spalling and crushing of CFRP strips for all strengthened specimens happened nearly at the mid-height of column except N-e10-2, it was recognized as premature failed specimen and its results were removed from the rest of this study. As shown in Figure 7.6(b), both strengthened specimens tested under 20 percent eccentricity to width ratio, crushing of one of CFRP strips under compression (CFC) observed followed by concrete spalling (CS). As shown in Figure 7.6(c), N-e30-1 specimen experienced spalling (CS) and crushing of concrete (CC) before crushing of one of the compressive strips (CFC) while for N-e30-2, the tensile CFRP rupture (TFR) happened followed by concrete spalling (CS) and crushing of one compressive CFRP strip (CFC). It should be noted that this failure modes were observed after the peak load, however, up to the peak load, no rupture, crushing, debonding, or buckling of CFRP strips were observed.

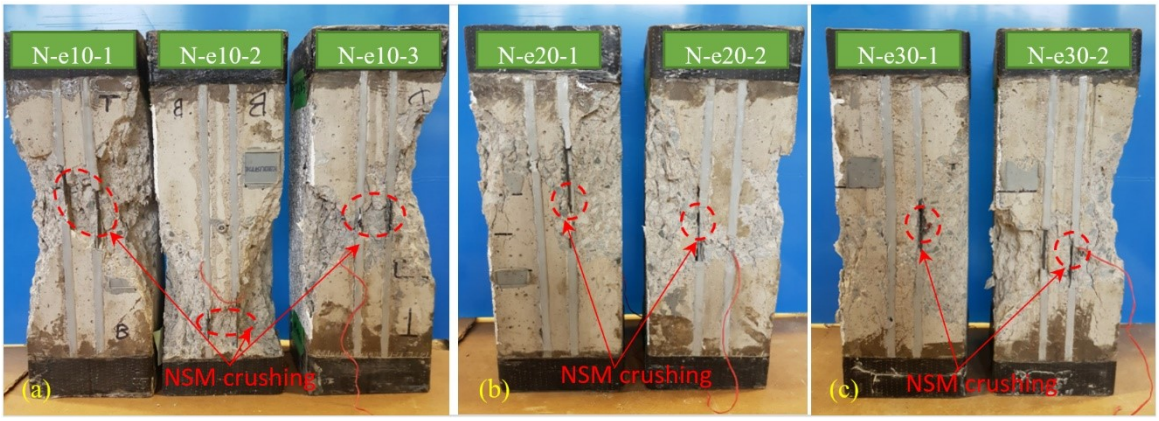

Figure 7. 6 Compressive side of tested specimens: (a) e10 group; (b) e20 group; and (c) e30 group

7.3.2 Compressive Behavior of NSM CFRPs

Overall, all NSM CFRP strips of the specimens tested under eccentric loading, experienced considerable compressive strains without debonding and/or buckling. The strain of CFRP

strips recorded by strain gauges for eccentrically loaded specimens is drawn in Figure 7.7(a). It was observed that as the load eccentricity increases, the peak load decreases. Moreover, Figure 7.7(a) shows that compressive CFRP strips experienced higher levels of strain in comparison to tensile strips. The average of strain of CFRP strips at tension side (SG1) as well as compression side (SG2) at peak load and a defined ultimate level are presented in Table 7.2.

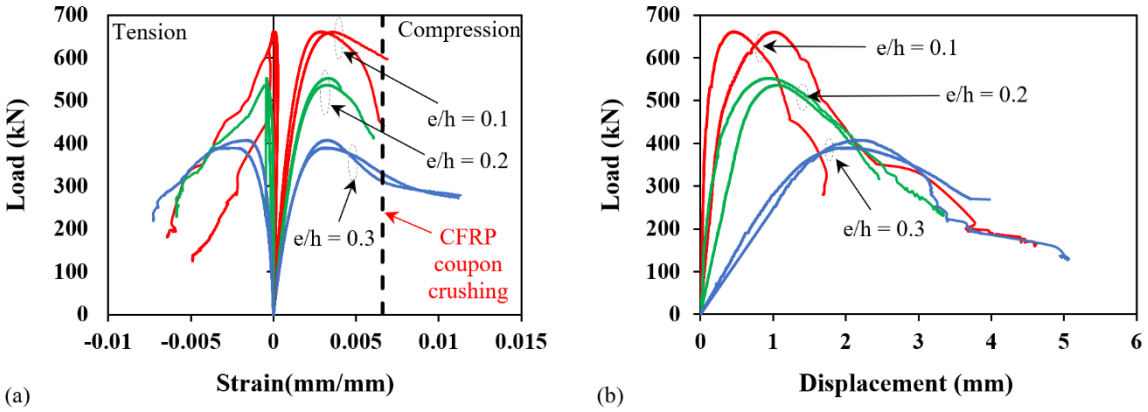

Figure 7. 7 Test results: (a) axial load vs. strain of compressive and tensile CFRP strips; and (b) axial load vs. lateral displacement of specimens at mid-height

To define a criterion for the ultimate strain of CFRP strips, the strain values at loads corresponding to 15 percent drop after peak load were considered as the ultimate values which is similar to the one used in a study performed by Hognestad for concrete (Hognestad, 1951). Table 7.2 shows that the tensile strain of the CFRP strips did not reach 14% of the rupture strain, while for compression strips the compartment strain was 50% of the crushing strain obtained from material test. This infers that the behavior of the CFRP strips are more critical when used in compression than when used in tension, however, up to peak load the CFRP strips worked effectively. Moreover, in average the CFRP strips in tension reached 4%, 7%, and 29% of their rupture strain for specimens tested under 0.1,

0.2, and 0.3 eccentricity-to-width ratios, respectively, while the strips in compression reached 86%, 77%, and 90% of their crushing strain, respectively, for the mentioned eccentricities. Overall, the average compressive strain of CFRP strips for all tested specimens was 41% and 84% of their crushing strain at peak load and after 15% drop from the peak load, respectively. Moreover, for CFRP strips in compression, the results showed no evidence of buckling or debonding of CFRP strips before compressive crushing. The latter shows the NSM technique limit the behavior of CFRP strips so that the ultimate material capacity, or crushing, controls the failure mode. Therefore, CFRP strips in compression were able to sustain strains up to their crushing capacity using the NSM technique without any buckling for both eccentric and concentric loadings which shows their effectiveness and capability in strengthening of compressive members.

7.3.3 Effect of NSM CFRPs on Load Bearing Capacity of Columns

As it is shown in Table 7.2, the load carrying capacity of plain concrete specimens enhanced by installing NSM CFRP strips in both pure compression and combined axial and compressive loading cases. The load capacity of NSM-strengthened specimens tested under concentric and 10 percent eccentricity were 7.7 and 10.9% higher than their corresponding plain specimens. Also, for NSM-strengthened specimens, as the load eccentricity increases to 10, 20, and 30%; the load capacity decreases 14.6, 29.6, and 48.5% with respect to the specimens under concentric loading, respectively. Figure 7.7(b) presents the load-displacement diagrams of eccentrically loaded specimens using the average values of LVDT 3 and LVDT 4 as the lateral displacement at the mid-height of the columns. It is seen that in higher eccentricities, the stiffness of strengthened specimens, which is defined as the slope of load-deflection curves, decreases as well as the axial capacity of columns.

7.4 ANALYTICAL STUDIES

In order to analyze the results of experimental program, an analytical model was developed which considers the nonlinear behavior of material as well as geometry, using MATLAB software. The model predicts the compressive and tensile strains of the NSM FRP strips, deflection at the mid-height of columns, and second-order moments. This section begins with a description of the model and major assumptions in developing it, followed by verification of the model and eventually concluded by a parametric study.

7.4.1 Model Description

The program progress by changing the values of compressive load in some steps up to failure and find the corresponding lateral displacement and strains by satisfying equilibrium equation for both internal and external forces. The model considers pin-pin boundary condition as well as the same load (P) and initial eccentricity (e_0) at both ends of column which gives the symmetry of load and boundary condition. The model divides the column length into three nodes, one at the mid-height of column and two at the ends of column.

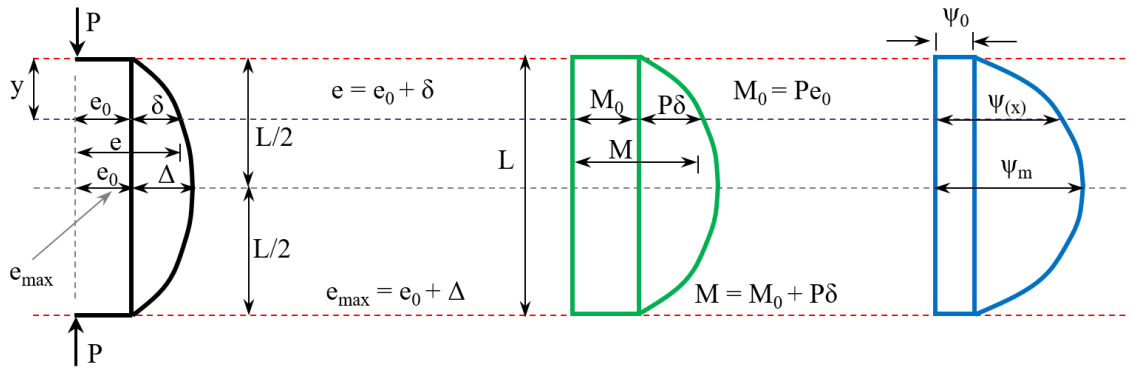

(a) Deflected shape (b) Moment diagram (c) Curvature diagram

Figure 7. 8 Schematic illustration of iteration process: (a) deflected shape of column; (b) moment diagram; and (c) curvature diagram

Figure 7.8 provides the schematic illustration of the process through which the displacement at mid-height of column is determined. At each load step, an arbitrary displacement assumed as the displacement of the middle node of column, as shown by Δ in Figure 7.8(a). Having known displacement, the total eccentricity of middle node is the summation of the displacement and the initial eccentricity ($e = e_0 + \Delta$), and the corresponding bending moment is the product of the total eccentricity and the given load ($M = Pe_0 + P\delta$) as illustrated in Figure 7.8(b). The curvature of end nodes (ψ_0) and middle node (ψ_m), whose diagram is depicted in Figure 7.8(c), is calculated using the moment-curvature diagram of the cross section at each certain load from the moment at end nodes (M_0) and at middle node of column (M), respectively. In this model, the shape of curvature diagram is assumed as a sine function [Equation 7.1-a] from which by applying the moment-area theorem [Equation 7.1-b], the deflection at the mid-height of the column is determined.

$$\psi(y) = (\psi_m - \psi_0) sin\frac{\pi y}{L} + \psi_0 \tag{7.1-a}$$

$$\delta_m = \int_0^{L/2} y\psi(y)dx = (\psi_m - \psi_0)\int_0^{L/2} ysin\frac{\pi y}{L}dx + \int_0^{L/2} y\psi_0\, dy \tag{7.1-b}$$

The symbols used in Equation 7.1 are y, ψ_0, ψ_m, $\psi(x)$, and δ_m which present the distance from the top of column, the curvature at the end of column, the curvature at the middle of column, curvature at x from the top of column, and the displacement of column at its mid-height, respectively, as shown in Figure 7.8. The assumed shape of curvature function and, in turn, displacement diagram, was adopted from Broms and Viest (1961), Lloyd and Regan (1996), Claeson and Gyltoft (1998) for steel reinforced concrete columns, as well as from Sadeghian and Fam (2015), and Mirmiran et al. (2001) for externally FRP-bonded RC

columns and GFRP-reinforced concrete columns, respectively. However, the mentioned models focused on the column capacity while the developed model in this study predicts the strains of compressive and tensile FRP reinforcements, lateral deflection at mid-height of column as well as the loading path and moment-curvature of the NSM FRP columns.

At the stage that the deflection of the middle node is calculated, the calculated value is compared to the initial assumed deflection. An iterative process through which displacement alters until the initial value and the calculated value based are the same implements to find the corresponding displacement of the column including second order effects. The explained process requires the knowledge moment-curvature diagram of the cross-section which is just a characteristic of loading and cross-section but not the length and displacement of the column.

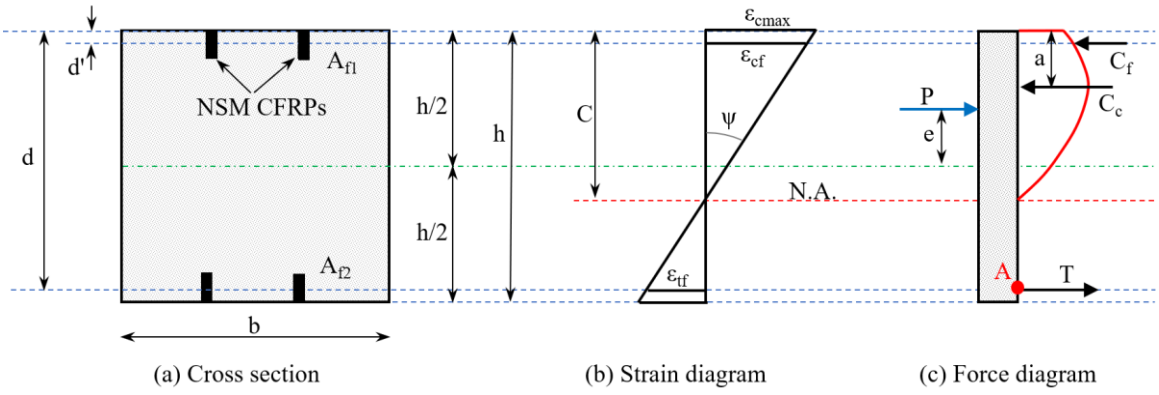

Figure 7. 9 Mechanism of cross-sectional analytical model: (a) section definitions; (b) strain diagram; and (c) force diagram

The moment-curvature diagram for a given load (P) and cross-section is essentially calculated based on the equilibrium of internal forces. In this study, a square concrete cross-section and four NSM CFRP reinforcement were used as shown in Figure 7.9(a). The width and height of cross-section are called b and h, respectively, while the distance between the

furthest compression fiber (the top edge of concrete) to the top and bottom center of NSM CFRP layers are d and d', respectively, as shown in Figure 7.9(a). The strain profile assumed to be linear in the section which is compatible with the major assumption that transverse plane sections remain plane after bending. The strain of concrete at the furthest compressive fiber, the strain of compressive NSM CFRP (at top), and the strain of tensile NSM CFRP layer (at bottom), at their centers, are presented by ε_{cmax}, ε_{cf}, and ε_{tf}, respectively [Figure 7.9(b)]. The depth of neutral axis (N.A.) and the curvature are presented as C and ψ, respectively [Figure 7.8(a)], which related to each other by Equation 7.2.

$$\psi = \frac{\varepsilon_{cmax}}{C} \tag{7.2}$$

To derive the curvature for a given load (P) and eccentricity (e), which is measured from the center of the section [Figure 7.9(c)], an iterative process is involved, where ε_{cmax} is assumed and the depth of neutral axis (C) is determined by satisfying force and moment equilibrium for internal forces as well as the external load (P) presented in Equation 7.3. If the equilibrium equations are not satisfied by changing the depth of neutral axis, the iterative process continues by assigning new values to ε_{cmax} and a new try for finding the depth of neutral axis until equilibrium equations [Equation 7.3] is satisfied, which is presented in the following:

$$\sum F = 0 \quad \rightarrow \quad P = C_f + C_c - T \tag{7.3-a}$$

$$\sum M_A = 0 \quad \rightarrow \quad P \times \left(d - \frac{h}{2} + e\right) = C_f \times (d - d') + C_c \times (d - a) \tag{7.3-b}$$

where C_c, C_f, T, and a are the resultant of compressive stresses of concrete, the internal compressive force in NSM CFRP (top layer), the tension force in NSM CFRP (bottom layer), and the center of application of internal compressive stresses of concrete. It is noticed that the value of T, considered positive (in Equation 7.3) if the bottom NSM CFRP layer is in tension and negative if the mentioned layer is in compression. The tensile stresses are concrete are very small values, therefore, their contribution in the equilibrium equations are negligible in comparison to the tension stresses sustained by NSM CFRP, and as a result the stress of concrete fibers in tension considered as zero.

The forces of NSM CFRP layers (i.e. C_f and T) are calculated as the production of total area and the stress of the CFRP layer [Equation 7.4]. For concrete, the compression zone, from neutral axis to the edge of cross section, is divided into rectangular layers with a height of 0.25 mm and the same width as the section. The compressive Force of concrete (i.e. C_c), then, is calculated as the sum of forces from each layer as presented in Equation 7.5-a, and the center of application of concrete compressive force (i.e. a), determined by Equation 7.5-b, in which the stress of compressive NSM CFRP layers are subtracted in both formulas.

$$C_s = f_{f1}A_{f1} \quad , \quad T = f_{f2}A_{f2} \tag{7.4}$$

$$C_c = \sum \frac{1}{2}\left(f_{c_i} + f_{c_{i+1}}\right) b\delta_y - \sum \frac{1}{2}\left(f_{c_i} + f_{c_{i+1}}\right) A_{fi} \tag{7.5-a}$$

$$a = \frac{1}{C_c}\left[\sum \frac{1}{2}\left(f_{c_i} + f_{c_{i+1}}\right) b\delta_y \bar{y}_{c_i} - \sum \frac{1}{2}\left(f_{c_i} + f_{c_{i+1}}\right) A_{fi} y_{f_i}\right] \tag{7.5-b}$$

In Equations 8.4 and 8.5, the stress and the corresponding sectional areas of each NSM CFRP layer is presented as f_{fi} and A_{fi}, where index i can take value of 1 or 2 for top or bottom layers. Moreover, the stress at bottom and top, width, height of each concrete layer,

and the distance between the center of each concrete layer to the neutral axis are named f_{c_i} and $f_{c_{i+1}}$, b, δ_y, and $\bar{y}_{c_i}$, respectively. The stresses introduced in Equation 7.4 and 7.5 are calculated from the stress strain relationship for CFRP and concrete material.

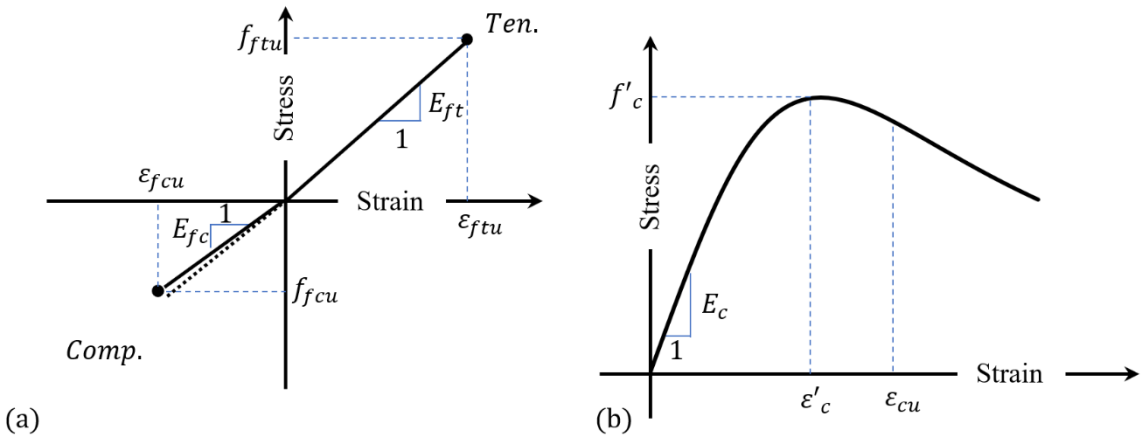

Figure 7. 10 Material properties for model: (a) stress-strain curve of CFRP laminate in tension and compression, and (b) stress-strain curve of concrete in compression

The stress-strain relationship of CFRP and concrete material used in this analysis is shown in Figure 7.10. The CFRP material considered to have the different modulus of elasticity and strength in tension (E_{ft}, f_{ftu}) and compression (E_{fc}, f_{fcu}). The CFRP stress-strain material property was considered linear from zero up to rupture strain (ε_{ftu}) in tension or crushing (ε_{fcu}) in compression. For concrete, the tensile stresses considered as zero for the sake of simplicity while the Popovics (1973) stress-strain relationship was considered for the compressive part. The following equations shows Popovics curve:

$$f_c = \frac{f'_c \left(\varepsilon_c / \varepsilon'_c\right) r}{r - 1 + \left(\varepsilon_c / \varepsilon'_c\right)^r} \qquad (7.6\text{-a})$$

$$r = \frac{E_c}{(E_c - E_{sec})} \tag{7.6-b}$$

$$E_{sec} = f_c'/\varepsilon_c' \tag{7.6-c}$$

where f_c' is concrete strength and ε_c' is its corresponding strain. Moreover, f_c, ε_c, and E_c are defined as the concrete stress, strain, and modulus of elasticity, respectively. To calculate the modulus of elasticity of concrete Equation 7.7(a) (ACI 318-14, 2014), and to calculate the strain corresponding to the concrete strength, Equation 7.7(b) (Todeschini et al., 1964) were considered.

$$E_c = 4700\sqrt{f_c'} \tag{7.7-a}$$

$$\varepsilon_c' = 1.7\,\frac{f_c'}{E_c} \tag{7.7-b}$$

Once the calculation of mid-height displacement is concluded for one load step, the load step increases, and the same procedure would be repeated for different load steps up to the peak load. The criterion which determine the peak load is defined when the required moment at the mid-height of the column (i.e. $M = Pe_0 + P\delta$) exceeds the capacity of the moment-curvature diagram built for that certain load (P). Once the latter happens, the procedure to finding the load step refines by decreasing the load step and repeating the procedure from the last valid found load and displacement set. Eventually, when the peak load is determined, the same procedure will be proceeds to find the nodes for the descending branch by using descending load steps. It should be noted that for the descending branch, the repetition of the iterative procedure would result in finding the nodes on the ascending branch if proper restrictions are not defined. The restrictions for descending branch are the

curvature and displacement at the mid-height which must be found to be greater than the previous load step.

In addition, the axial load-bending moment interaction diagram can be built using the section analysis explained earlier by the difference that the criteria are crushing of the concrete in compression, crushing of the FRP in compression, or rupture of FRP in tension. Firstly, the ultimate concrete fiber in compression is set to be 0.003 mm/mm (or 0.0035 mm/mm) as the crushing strain of concrete for design purposes defined by ACI 318-14 (2014) or CSA A23.3-14 (2014)). Then the depth of neutral axis could vary to give different sets of axial loads and bending moments by satisfying load and moment equilibrium for each different depth of neutral axis. Secondly, the crushing of FRP must be considered to see if in any case the strain in the compressive FRP layer exceeds the crushing strain or not. It should be noted that since in general the crushing strain of FRPs are higher than 0.003 mm/mm or (0.0035 mm/mm), there would be no crushing criterion for FRPs in practice and for design purposes up to ultimate design load. The third criterion is the rupture of the FRP layers in tension which can be achieved by determining the balance point. The balance point in this case is the point in the axial load-bending moment interaction diagram at which the crushing of ultimate compressive fiber in concrete and the rupture in the ultimate tensile FRP layer happens simultaneously. Above the balance point, the crushing of concrete is the controlling criterion and below that the rupture of FRP is controlling criterion. For determining the points below the balance point, the strain at the ultimate tensile FRP layer is set to the tensile rupture strain of FRP, which is determined from material test, and the depth of neutral axis alters which gives the remaining sets of axial loads and bending moments to complete the interaction diagram.

7.4.2 Model Verification

The described numerical-analytical model was verified by the experimental test results presented in this paper as well as another experimental result (Gajdosova and Bilcik, 2013) for a study performed on slender concrete columns reinforced with NSM CFRP strips. For verification of the model, two different modulus of elasticity and strength for CFRP strips in compression and tension were considered as explained in section 3. It should be noted that to obtain axial load-bending moment interaction diagram, the crushing strain of concrete in compression was considered as 0.003 mm/mm.

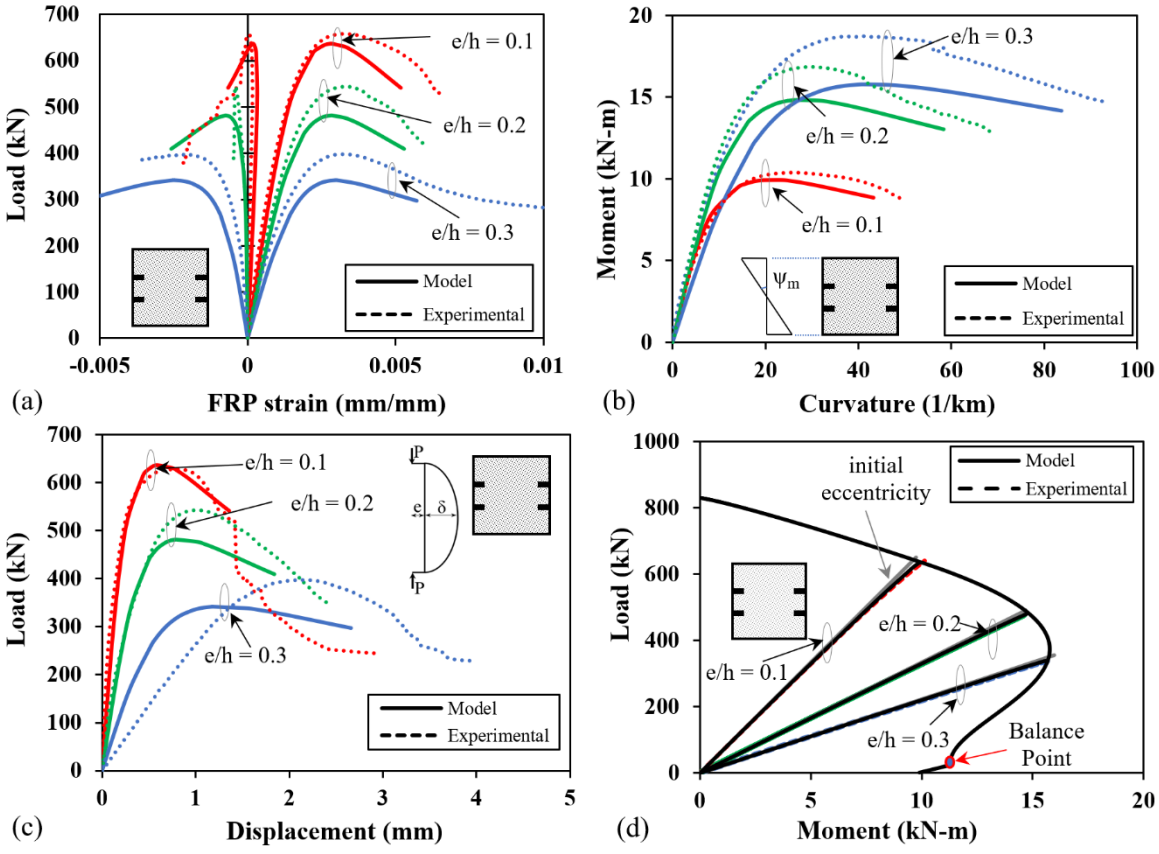

Figure 7. 11 Model verification: (a) axial load vs. strain of compressive and tensile CFRP strips, (b) moment vs. curvature diagram at the mid-height, (c) axial load vs. lateral displacement of specimens at mid-height, and (d) axial load vs. bending moment interaction diagram and loading path curves

Overall, the results of the analysis of the strengthened columns using the describe model, versus the average of experimental test data, are presented in Figure 7.11. The graphs for the average of experimental test data was obtained using the test results from Figure 7.7. It should be noted that because there were two or three graphs for averaging and they did not finish at the same value on the horizontal axis, once one of the graphs was concluded, the average shows the average of the remaining curves. The test results show a good agreement between the model and experimental test data. It should be noted that the slope of load-displacement curve for eccentricity-to-width ratio of 0.3 is different because of possible inaccuracies in the experimental measurement for the lateral displacement [Figure 7.1(c)], the same issue appears in the moment-curvature [Figure 7.1(d)].

Table 7.3 shows the values of peak loads for different eccentricities as well as the corresponding displacement, bending moment, compressive and tensile strain, and the curvature of the columns. It should be noted that this time instead of averaging a graph, the peak loads and their corresponding values for displacement and etc. were considered for averaging. The results show and average of 9% error at the peak load. Moreover, as shown in both Table 7.3 and Figure 7.11, the model is in a better agreement when is used to predict the behavior of the specimens with lower load-eccentricities. However, as shown in Figure 7.11(d), the loading path is predicted accurately for all specimens up to the axial load-bending moment interaction diagram.

Table 7. 3 Comparison of model and experimental results

Characteristic	e/h (%)	Test	Model	Test to model ratio	Test to model ratio (AVG±SD)
Peak Load (kN)	10	628.4	636.7	0.98	1.15±0.02
	20	542.7	481.7	1.13	
	30	397.4	341.7	1.16	
Lateral mid-height displacement at peak load (mm)	10	0.76	0.59	1.29	1.49±0.32
	20	1.04	0.79	1.32	
	30	2.20	1.19	1.85	
Compressive strip strain at peak load (mm/mm)	10	-0.00280	-0.00284	0.99	1.11±0.10
	20	-0.00329	-0.00285	1.14	
	30	-0.00327	-0.00301	1.19	
Moment at peak load (kN-m)	10	9.9	9.9	1.00	1.11±0.10
	20	16.8	14.8	1.14	
	30	18.8	15.8	1.19	
Curvature at peak load (1/km)	10	16.3	19.7	0.83	0.97±0.12
	20	28.4	26.6	1.07	
	30	40.8	41.0	1.00	

Note: e/h is the load eccentricity to width ratio; AVG=average; and SD=standard deviation.

Furthermore, the loading path of the model was verified versus an experimental test result from a study performed on slender concrete columns strengthened with NSM CFRP strips by Gajdosova (2013). There were two similar specimens named “C3” and “C4” which rectangular columns (210 mm × 150 mm) tested under the same load eccentricities of 40 mm at both ends. There were two layers of steel reinforcement (4 Φ10) located at 31 mm from the edge of concrete symmetrically. There were three grooves (3 mm × 15 mm) on each side of the concrete columns containing three CFRP strips (1.4 mm × 15 mm). The modulus of elasticity and strength of steel rebar were reported as 560 MPa and 208 GPa,

respectively, while these values were 2500 MPa and 168 GPa for CFRP. It should be noted that the modulus of elasticity was considered the same in tension and compression, however, the compressive strength of the CFRP material was considered to be equal to one third of its tensile strength to be compatible with the observations of this study in the experimental part. The results of the analysis using the model described in this paper and the mentioned test data is presented in Figure 7.12. The results for the loading path show a good agreement between the test data and the model. Therefore, the introduced model was used to perform a parametric study to further investigations presented in the following sections.

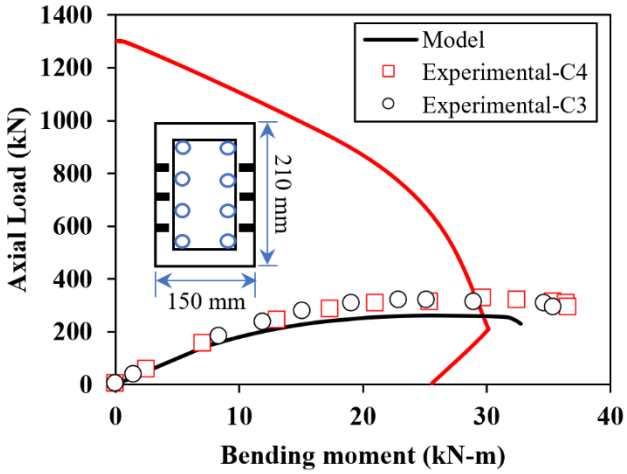

Figure 7. 12 Model verification versus test results by Gajdosova and Bilcik (2013)

7.4.3 Parametric Studies

In this section further investigations were done for CFRP NSM strengthening system on the behavior of concrete columns by altering the reinforcement ratio and the concrete strength. It should be noted that in the parametric study section all the parameters are the

same as the ones introduced in section 3 for the experimental test, however, the eccentricity-to load ratio is kept as 0.2 as the reference.

7.4.3.1 Effect of Reinforcement Ratio

In this section, the thickness of the CFRP strips used for strengthening was double and tripled without changing the height and their position in the experimental concrete specimens. Therefore, three reinforcement ratios of 0.21% (4×1.2 mm×10 mm), 0.43% (4 ×2.4 mm×10 mm), and 0.64% (4×3.6 mm×10 mm) were considered in the parametric study. The model was implemented for the cases and the results are shown in Figure 7.13.

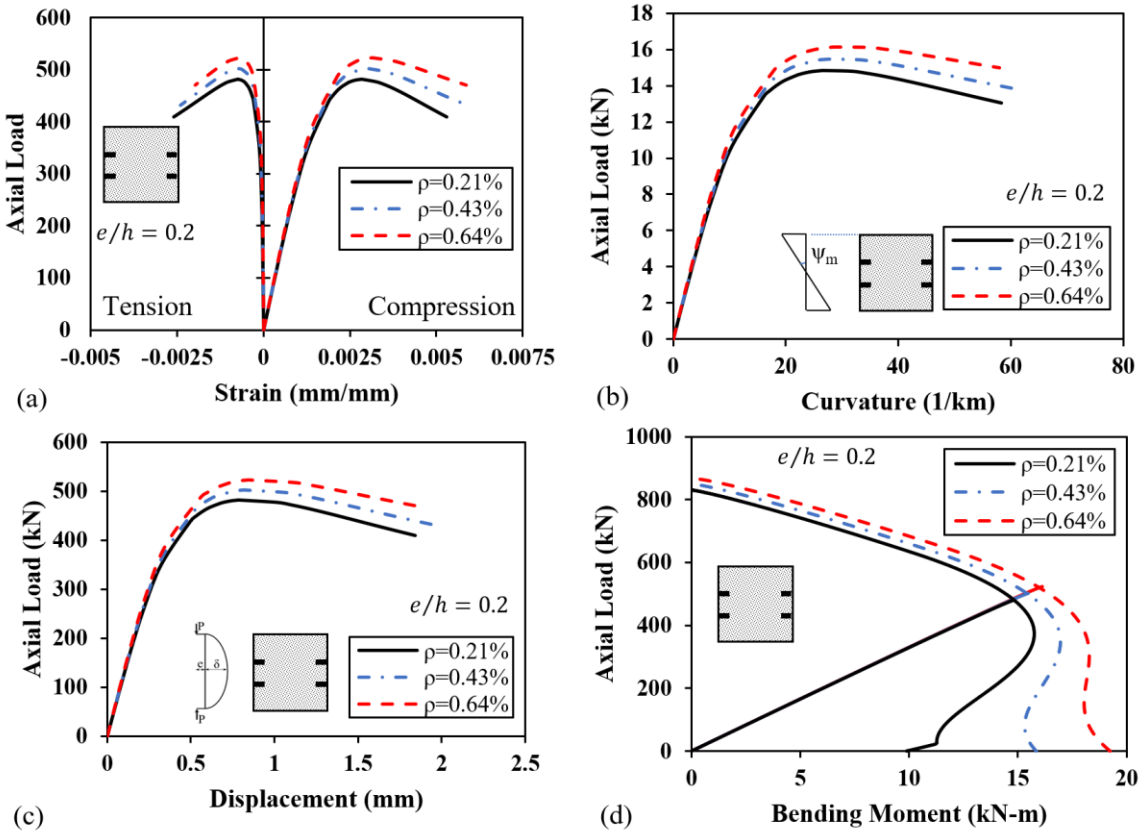

Figure 7. 13 Effect of the reinforcement ratio: (a) axial load vs. strain of compressive and tensile CFRP strips, (b) moment vs. curvature diagram at the mid-height, (c) axial load vs. lateral displacement of specimens at mid-height, and (d) axial load vs. bending moment interaction diagram and loading path curves

The results showed 4.32% and 8.61% gain in the capacity of the specimens as the reinforcement ratio increased from 0.21% to 0.43% and 0.64%, respectively. It should be noted that the interaction diagram enlarges in tension control region as the reinforcement increases as is presented in Figure 7.13(d). Moreover, there would be no rupture of CFRP strips in the tension control side of the interaction diagram by increasing the reinforcement ratio [Figure 7.13(d)], since there is a balance point for reinforcement ratio of 0.21% while for the other reinforcement ratios there is no observation of balance point. Furthermore, the compressive strain of the CFRP strips at peak load was less than 50% of the expected crushing strain of the CFRPs (i.e. 43%, 46%, and 48% of the crushing strain of CFRP for 0.21%, 0.42%, and 0.64% reinforcement ratios, respectively) which is in an agreement with the observations from the experimental test results [Figure 7.13(b)].

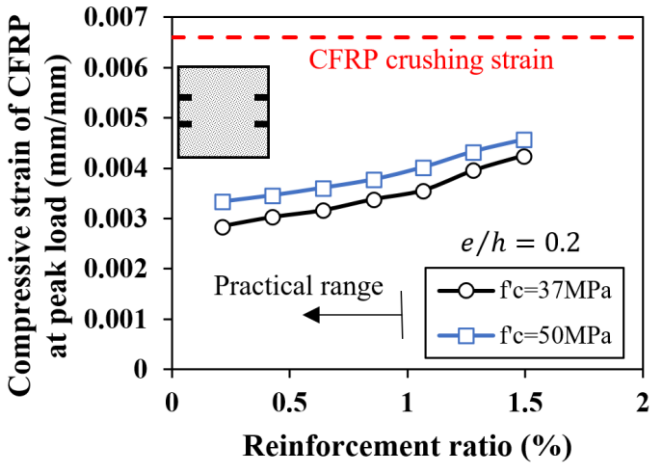

Figure 7. 14 Reinforcement ratio vs. compressive strain of CFRP strip at peak load

For further studies on a higher level of compressive strain that might be experienced, the reinforcement ratio varied from 0.21% (the same as experimental study) up to 1.5% as presented in Figure 7.14. To observe further effects, in addition to the concrete strength of 37 MPa (the same as experimental study), a higher concrete strength of 50 MPa was

examined. The results show that as the reinforcement ratio increases, the compressive strain of CFRP strips at peak load increases. However, after a certain reinforcement ratio, which is 1.7% for 37 MPa concrete strength and 2.5% for 50 MPa concrete strength, respectively, the compressive strain at peak load does not increase as the reinforcement ratio increases. It was observed that the ratio of CFRP compressive strain at the peak load to the crushing strain varies from 43% to 64% and from 50% to 69% for 37 MPa and 50 MPa concrete strength, respectively. It should be noted that if the reinforcement ratio increases, in theory, the compressive CFRP strain equal to the crushing strain will achieve. However, practically the range of reinforcement ratio that might be used for strengthening may not exceed 1% which is corresponding to strain levels that were equal to 54% and 61% of the ultimate compressive strain of CFRP strips for 37 MPa and 50 MPa concrete strength, respectively. Therefore, crushing would not happen at the peak load.

7.4.3.2 Effect of Concrete Strength

To find out the effect of concrete strength, three different concrete strength of 25 MPa, 35 MPa, and 45 MPa for two different reinforcement ratios of 0.21% and 0.64% were considered, as shown in Figure 7.15 and Figure 7.16. The compressive strain of the CFRP strips in compression at peak load were 36%, 42%, and 48% of the ultimate compressive strain of CFRP for 25 MPa, 35 MPa, and 45 MPa concrete strength for reinforcement ratio of 0.21%, respectively, and 42%, 47%, and 52% for reinforcement ratio of 0.64%. The latter shows that compressive CFRP strips experience more strains as concrete strength increases, however, their peak load strain is still less than 50% of their compressive crushing strain. For all the specimens, as concrete strength increases, the strength of specimen increases, however, for 0.21% reinforcement ratio the gain is axial capacity was

more than the gain for 0.64% reinforcement ratio for specimens with respect to the specimen with 25 MPa concrete strength.

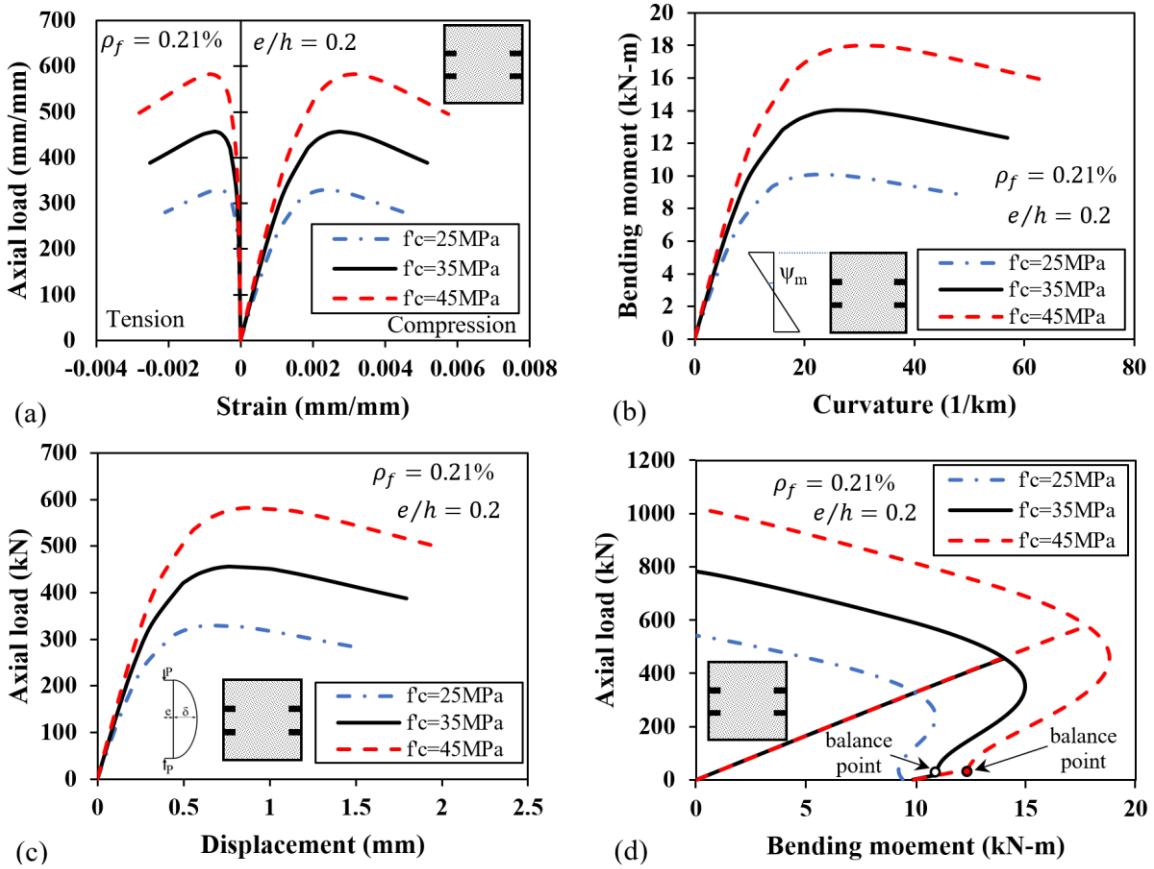

Figure 7. 15 Effect of the concrete strength (reinforcement ratio of 0.21%): (a) axial load vs. strain of compressive and tensile CFRP strips, (b) moment vs. curvature diagram at the mid-height, (c) axial load vs. lateral displacement of specimens at mid-height, and (d) axial load vs. bending moment interaction diagram and loading path curves

It should be noted that there is a difference in the axial load- bending moment interaction diagram of the specimens with 0.21% [Figure 7.15(d)] and 0.64% [Figure 7.16(d)] reinforcement ratios. In Figure 7.15(d), as the concrete strength increases, the balance point (the point at which the extreme compressive fiber in concrete reaches the strain level of 0.003 mm/mm, as the defined crushing strain, and the tensile CFRP reaches its rupture strain) occurs at higher load levels which cause tension rupture of CFRP. This controls the

lower part of the interaction diagram shown as a line below the balance point for specimens with 35 and 45 MPa concrete strength [Figure 7.15(d)]. However, by increasing the reinforcement ratio from 0.21% to 0.64%, there is no observation for the same range of concrete strength [Figure 7.16(d)]. Therefore, an increase in concrete strength might result in the appearance of the rupture of tensile CFRPs in the interaction diagram which can be avoided by increasing the reinforcement ratio.

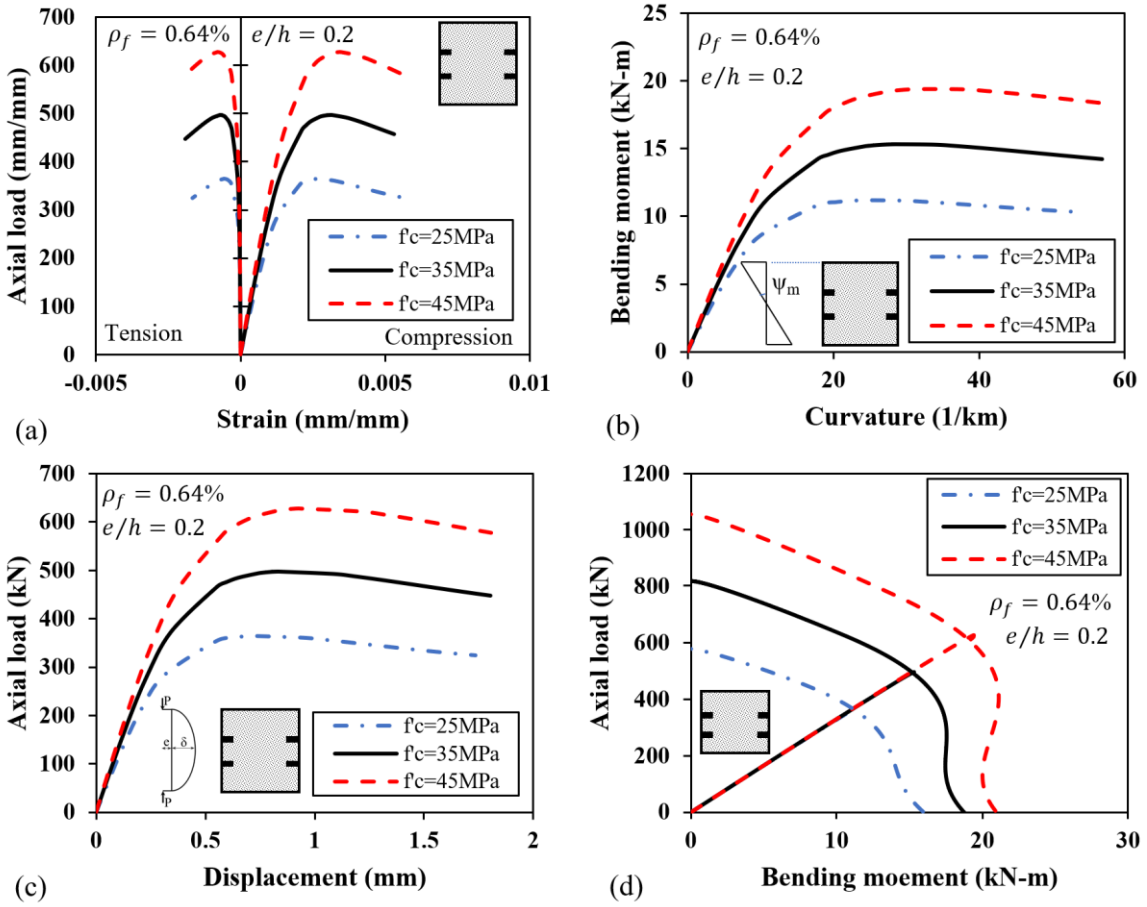

Figure 7. 16 Effect of the concrete strength (reinforcement ratio of 0.64%): (a) axial load vs. strain of compressive and tensile CFRP strips; (b) moment vs. curvature diagram at the mid-height; (c) axial load vs. lateral displacement of specimens at mid-height; and (d) axial load vs. bending moment interaction diagram and loading path curves

To justify the observation, consider the internal forces created in the concrete and FRP strips to satisfy the force and moment equilibrium in the section. If the concrete strength increases the depth of the neutral axis tends to decrease since the required internal compressive force in concrete to satisfy force equilibrium demands less concrete area in compression. Then, the shallower depth of neutral axis causes higher tensile strains in tensile CFRP strips, which makes it susceptible to experience rupture. Thus, an increase in concrete strength may lead to tensile rupture of CFRP strips. However, if the reinforcement ratio increases, the internal tensile force created by tensile CFRP strips increases which demands more area of concrete to be stressed in compression for satisfying force equilibrium in the section which leads to deeper depth of neutral axis. Therefore, the CFRP strips in tension side experience lower strains which might avoid the occurrence of their tensile rupture in the interaction diagram. To examine the above explanation, a range of 0.21% to 3.2% reinforcement ratios were considered for four different concrete strength of 25, 35, 45, and 55 MPa to see how the balance point can be affected for a wider range of reinforcement ratio and concrete strength, as shown in Figure 7.17. The results showed that as reinforcement ratio increases, the balance load decreases and tends to be at tensile side of the interaction diagram. This observation showed that the balance load is negative for higher reinforcement ratios and higher concrete strength. Therefore, the rupture of CFRP strips in tension side can be eliminated from interaction diagram if higher reinforcement ratios are used. It should be mentioned that one of the limitations of using NSM system is the space limitations and limitations on the groove spacing which lead to using lower reinforcement ratios for strengthening.

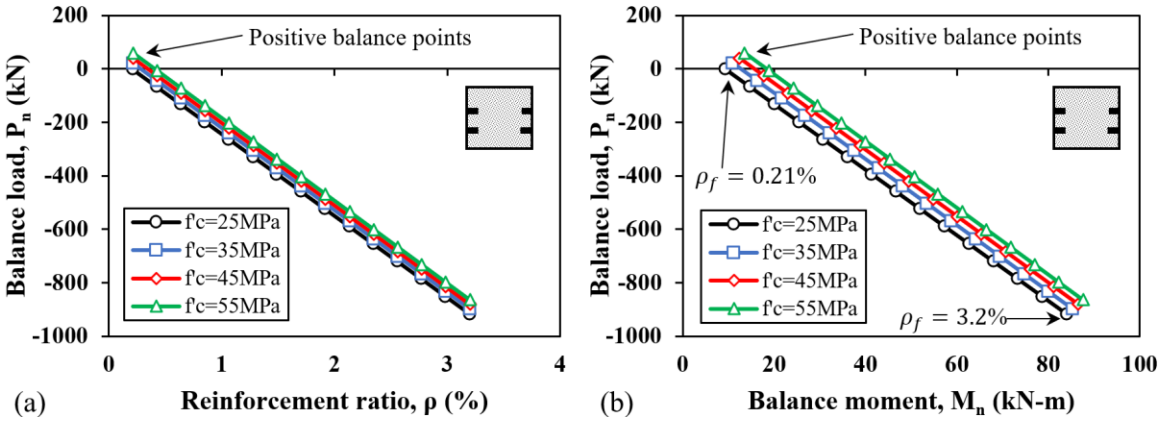

Figure 7. 17 Balance points for interaction diagram: (a) balance load vs. reinforcement ratio and (b) balance load vs. balance moment

7.5 CONCLUSIONS

In this study, the behavior of the short concrete columns reinforced with longitudinal NSM CFRP laminates were investigated using experimental and analytical methods. A total of fourteen reinforced concrete specimens were prepared and tested under four different load eccentricities of 0, 10%, 20%, and 30% of the width of the specimen. Furthermore, an analytical model was developed and verified against the available experimental test data which led to a parametric study. The following conclusions can be drawn:

- The results of the material coupon tests on the CFRP laminates used in this study showed that both compressive and tensile stress-strain curves are linear for this material up to ultimate strain of CFRP in compression or in tension. The compressive to tensile strength, modulus of elasticity, and ultimate strain ratios for the tested coupons were 34%, 86%, and 40%, respectively. It should be noted that even ratio of 0.34 for compressive to tensile strength of CFRP still gives a compressive strength twice greater than conventional structural steel.

- Four modes of failure were observed in reinforced specimens consisting of concrete spalling (CS), concrete crushing (CC), compressive FRP crushing (CFC), tensile FRP rupture (TFR), however, no buckling or debonding of NSM FRP strips observed during the tests. It should be noted that no crushing or rupture of CFRP strips were observed until long after the peak load.
- The average compressive strain of CFRP strips for all concrete specimens under eccentric loading was only 41% and 84% of the ultimate compressive strain of CFRP at peak load and after 15% drop from the peak load, respectively. This indicates that crushing of the CFRP strips is not a concern for the specimens considered in this study.
- For experimental test data with CFRP reinforcement ratio of 0.21%, the load capacities of the strengthened specimens were improved by 7.7% and 10.9% of the capacity of the plain concrete tested under pure compression and under eccentricity-to-width ratio of 10%, respectively.
- The results of parametric study showed that as the reinforcement ratio increases, the compressive strain of CFRP laminates in compression increases. However, in a practical range of reinforcement ratio (considering less than 1% reinforcement ratio), the CFRP strain level at peak load does not reach the crushing value. It was observed that the stain levels in compressive CFRP strips were equal to 54% and 61% of their crushing strain of CFRP strips for 37 MPa and 50 MPa concrete strength, respectively, for the eccentricity-to-width ratio of 20%.
- It was observed by the parametric study that as the concrete strength increases from 25 MPa to 45 MPa, the CFRP compressive strain at the peak load increases.

However, the strain of compressive CFRP strips did not pass 50% of their crushing strain per coupon tests.

- Overall, this study showed that for short concrete columns strengthen with NSM CFRP laminates, crushing, buckling, or debonding failures of CFRP laminates in compression did not affect the load capacity of the columns and crushing of CFRP strips happened long after peak loads. The results showed that the strengthening of concrete columns using longitudinal NSM FRPs is a viable approach. Further studies are needed to implement the system enhancing the performance of slender columns through increasing their lateral stiffness.

ACKNOWLEDGMENTS

The authors would like to thank Blair Nickerson, Brian Kennedy, Jesse Keane, and Brian Liekens of Dalhousie University for their assistance in the lab. The authors would also like to acknowledge and thank NSERC and Dalhousie University for their financial support. Randy Nason of Pinnacle Agencies Ltd (Dartmouth, NS, Canada) is thanked for providing the BASF adhesive. Finally, authors specially thank Dr. Farid Taheri for his precious technical guidance in material testing and Dr. John Newhook for providing Sika CFRP laminates and his support for the tests.

REFERENCES

ACI 318-14. (2014). Building Code Requirements for Structural Concrete. *American Concrete Institute.* Farmington Hills, MI.

ACI 440.1R. (2015). Guide for the Design and Construction of Structural Concrete Reinforced Fiber-Reinforced Polymer (FRP) Bars. *American Concrete Institute.* Farmington Hills, MI.

ACI 440.2R. (2008). Guide for the Design and Construction of Externally Bonded FRP Systems for Strengthening Concrete Structures. *American Concrete Institute.* Farmington Hills, MI.

Afifi, M. Z., Mohamed, H. M., and Benmokrane, B. (2013). Strength and Axial Behavior of Circular Concrete Columns Reinforced with CFRP Bars and Spirals. *Journal of Composites for Construction*, 18(2), 04013035.

Alkhrdaji, T., Nanni, A., Chen, G., and Barker, M. (1999). Upgrading the Transportation Infrastructure: Solid RC Decks Strengthened with FRP. *Concrete International: Design and Construction*, 21(10), 37-41.

Alsayed, S. H. (1998). Flexural behaviour of concrete beams reinforced with GFRP bars. *Cement and Concrete Composites*, 20(1), 1-11.

ASTM C39/C39M − 18. (2018). Standard Test Method for Compressive Strength of Cylindrical Concrete Specimens. *American Society for Testing and Materials.* West Conshohocken, PA.

ASTM D3039/D3039M-14. (2014). Standard Test Method for Tensile Properties of Polymer Matrix Composite Materials. *American Society for Testing and Materials.* West Conshohocken, PA.

ASTM D6641/D6641M-16. (2016). Standard Test Method for Compressive Properties of Polymer Matrix Composite Materials Using a Combined Loading Compression (CLC) Test Fixture. *American Society for Testing and Materials.* West Conshohocken, PA.

ASTM D695-10. (2010). Standard Test Method for Compressive Properties of Rigid Plastics. *American Society for Testing and Materials.* West Conshohocken, PA.

ASTM D7205 / D7205M - 06. (2016). Standard Test Method for Tensile Properties of Fiber Reinforced Polymer Matrix Composite Bars. *American Society for Testing and Materials.* West Conshohocken, PA.

Atadero, R., Lee, L., and Karbhari, V. M. (2005). Consideration of material variability in reliability analysis of FRP strengthened bridge decks. *Composite Structures*, 70(4), 430-443.

Badawi, M., and Khaled, S. (2009). Flexural strengthening of RC beams with prestressed NSM CFRP rods – Experimental and analytical investigation. *Construction and Building Materials*, 23(10), 3292-3300.

Barros, J. A., Varma, R. K., Sena-Cruz, J. M., and Azevedo, A. F. (2008). Near surface mounted CFRP strips for the flexural strengthening of RC columns: Experimental and numerical research. *Engineering Structures*, 30(12), 3412-3425.

Benmokrane, B., El-Salakawy, E., El-Ragaby, A., and Lackey, T. (2006). Designing and Testing of Concrete Bridge Decks Reinforced with Glass FRP Bars. *Journal of Bridge Engineering*, 11(2), 217-229.

Berg, A. C., Bank, L. C., Olivia, M. G., and Russell, J. S. (2006). Construction and cost analysis of an FRP reinforced concrete bridge deck. *Construction and Building Materials*, 20(8), 515-526.

Bisby, L., and Ranger, M. (2010). Axial–flexural interaction in circular FRP-confined reinforced concrete columns. *Construction and Building Materials*, 24(9), 1672-1681.

Bournas, D. A., and Triantafillou, T. C. (2009). Flexural strengthening of reinforced concrete columns with near-surface-mounted FRP or stainless steel. *ACI Structural Journal*, 106(4), 495-505.

Broms, B., and Viest, I. M. (1961). Long Reinforced Concrete Columns: A symposium. *Transactions, ASCE,* 126(2), 308-400.

Ceroni, F. (2010). Experimental performances of RC beams strengthened with FRP materials. *Construction and Building Materials*, 24(9), 1547-1559.

Chaallal, O., and Shahawy, M. (2000). Performance of Fiber-Reinforced Polymer-Wrapped Reinforced Concrete Column under Combined Axial-Flexural Loading. *ACI Structural Journal*, 97(4), 659-668.

Choo, C. C., Harik, I. E., and Gesund, H. (2006). Strength of Rectangular Concrete Columns Reinforced with Fiber-Reinforced Polymer Bars. *ACI Structural Journal*, 103(3), 452-459.

Claeson, C., and Gylltoft, K. (1998). Slender High-Strength Concrete Columns Subjected to Eccentric Loading. *Journal of Structural Engineering*, 124(3), 233-240.

CSA S6-14. (2014). Canadian Highway Bridge Design Code. *Canadian Standards Association.*

CSA S806-12. (2012). Design and construction of building structures with fiber-reinforced polymers. *Canadian Standards Association.*

De Luca, A., Matta, F., and Nanni, A. (2010). Behavior of Full-Scale Glass Fiber-Reinforced Polymer Reinforced Concrete Columns under Axial Load. *ACI Structural Journal*, 107(5), 589-596.

Deitz, D. H., Harik, I. E., and Gesund, H. (2003). Physical Properties of Glass Fiber Reinforced Polymer Rebars in Compression. *Journal of Composites for Construction*, 7(4), 363-366.

Deitz, D., Harik, I. E., and Gesund, H. (1999). One-Way Slabs Reinforced with Glass Fiber Reinforced Polymer Reinforcing Bars. *ACI Special Publication*, 188, 279-286.

El-sayed, A., El-Salakawy, E., and Benmokrane, B. (2005). Shear Strength of One-Way Concrete Slabs Reinforced with Fiber-Reinforced Polymer Composite Bars. *Journal of Composites for Construction*, 9(2), 147-157.

Fib Bulletin 14. (2001). Externally bonded FRP reinforcement for RC structures. *The International Federation for Structural Concrete*, Stuttgart.

Fib Bulletin 40. (2007). FRP Reinforcement in RC structures. *The International Federation for Structural Concrete*, Stuttgart.

Fillmore, B., and Sadeghian, P. (2017). Compressive Behavior of Concrete Cylinders Reinforced with Glass Fiber Reinforced Polymer Bars. *CSCE - Leadership in Sustainable Infrastructures.* Vancouver, Canada.

Fillmore, B., and Sadeghian, P. (2018). Contribution of longitudinal glass fiber-reinforced polymer bars in concrete cylinders under axial compression. *Canadian Journal of Civil Engineers*, 45, 458-468.

Foret, G., and Limam, O. (2008). Experimental and numerical analysis of RC two-way slabs strengthened with NSM CFRP rods. *Construction and Building Materials*, 22(10), 2025-2030.

Gajdosova, K., and Bilcik, J. (2013). Full-scale testing of CFRP-strengthened slender reinforced concrete columns. *Journal of composites for construction*, 17, 239-248.

Galati, N., Tumialan, G., and Nanni, A. (2006). Strengthening with FRP bars of URM walls subject to out-of-plane loads. *Construction and Building Materials*, 20(1), 101-110.

Guérin, M., Mohamed, H. M., Benmokrane, B., Nanni, A., and Shield, C. K. (2018). Eccentric Behavior of Full-Scale Reinforced Concrete Columns with Glass Fiber-Reinforced Polymer Bars and Ties. *ACI Structural Journal*, 115(2), 489-499.

Hadhood, A., Mohamed, H. M., and Benmokrane, B. (2017). Experimental study of circular high-strength concrete columns reinforced with GFRP bars and spirals under concentric and eccentric loading. *Journal of Composites for Construction*, 21(2), 04016078.

Hadi, M. N., and Youssef, J. (2016). Experimental Investigation of GFRP-Reinforced and GFRP-Encased Square Concrete Specimens under Axial and Eccentric Load, and Four-Point Bending Test. *Journal of Composites for Construction*, 20(5), 04016020.

Hales, T. A., Pantelides, C. P., and Reaveley, L. D. (2016). Experimental Evaluation of Slender High-Strength Concrete Columns with GFRP and Hybrid Reinforcement. *Journal of Composites for Construction*, 20(6), 04016050.

Hamilton Iii, H., and Dolan, C. (2001). Flexural capacity of glass FRP strengthened concrete masonry walls. *Journal of Composites for Construction*, 5(3), 170-178.

Hognestad, E. (1951). A Study of Combined Bending and Axial Load in Reinforced Concrete Members, *Bulletin Series No. 399*. Urbana: University of Illinois.

Hussein, M. E., Al-Salloum, Y. A., Alsayed, S. H., and Iqbal, R. A. (2012). Experimental and numerical investigation of size effects in FRP-wrapped concrete columns. *Construction and Building Materials*, 29, 56-72.

Jiang, T., and Teng, J. (2012). Theoretical model for slender FRP-confined circular RC columns. *Construction and Building Materials*, 32, 66-76.

Khan, Q. S., Sheikh, M., and Hadi, M. N. (2015). Tension and compression testing of fibre reinforced polymer (FRP) bars. *Joint Conference of the 12th International Symposium on Fiber Reinforced Polymers for Reinforced Concrete Structures (FRPRCS-12) and the 5th Asia-Pacific Conference on Fiber Reinforced Polymers in Structures (APFIS-2015).* Wollongong, New South Wales, Australia.

Khorramian, K., and Sadeghian, P. (2017a). Experimental and analytical behavior of short concrete columns reinforced with GFRP bars under eccentric loading. *Engineering Structures*, 761–773.

Khorramian, K., and Sadeghian, P. (2017b). Short Concrete Columns Reinforced with GFRP Rebars Under Eccentric Loading. *CSCE Annual Conference. Vancouver, BC, Canada: Canadian Society of Civil Engineering.*

Khorramian, K., and Sadeghian, P. (2017c). Strengthening Concrete Columns Using Near Surface Mounted (NSM) Carbon Fiber Reinforced Polymer (CFRP) Laminates. *Sixth Asia-Pacific Conference on FRP in Structures. Singapore, Singapore.*

Khorramian, K., and Sadeghian, P. (2018a). New Testing Method of GFRP Bars in Compression. *CSCE Annual Conference. Fredericton, NB, Canada: Canadian Society of Civil Engineering.*

Kim, Y. J., Longworth, J. M., and Wight, G. R. (2008). Flexure of Two-Way Slabs Strengthened with Prestressed or Non prestressed CFRP Sheets. *Journal of Composites for Construction*, 12(4), 366-374.

Kobayashi, K., and Fujisaki, T. (1995). Compressive behaviour of FRP reinforcement in non prestressed concrete members. *Non metallic (FRP) reinforcement for concrete structures, Proceedings of the second international RILEM Symposium (FRPRCS-2).* London, UK.

Lloyd, A. N., and Rangan, V. B. (1996). Studies on High-Strength Concrete Columns under Eccentric Compression. *ACI Structural Journal*, 93(6), 631-638.

Mallick, P. K. (2008). Fiber Reinforced Composites Materials, Manufacturing, and Design. Boca Raton, Florida: *CRC Press*.

Michaluk, C. R., Rizkalla, S. H., Tadros, G., and Benmokrane, B. (1998). Flexural Behavior of One-Way Concrete Slabs Reinforced by Fiber Reinforced Plastic Reinforcements. *ACI Structural Journal*, 95(3), 353-365.

Mirmiran, A., Shahawy, M., Samaan, M., El Echary, H., Mastrapa, J. C., and Pico, O. (1998). Effect of Column Parameters on FRP-Confined Concrete. *Journal of Composites for Construction*, 2(4), 175-185.

Mirmiran, A., Yuan, W., and Chen, X. (2001). Design for slenderness in concrete columns internally reinforced with fiber-reinforced polymer bars. *Structural Journal*, 98(1), 116-125.

Mohamed, H. M., Afifi, M. Z., and Benmokrane, B. (2014). Performance Evaluation of Concrete Columns Reinforced Longitudinally with FRP Bars and Confined with FRP Hoops and Spirals under Axial Load. *Journal of Bridge Engineering*, 19(7), 04014020.

Mosallam, A. S., and Mosalam, K. M. (2003). Strengthening of two-way concrete slabs with FRP composite laminates. *Construction and Building Materials*, 17(1), 43-54.

Nordin, H., and Täljsten, B. (2006). Concrete Beams Strengthened with Prestressed Near Surface Mounted CFRP. *Journal of Composites for Construction*, 10(1), 60-68.

Parvin, A., and Brighton, D. (2014). FRP Composites Strengthening of Concrete Columns under. *Polymers*, 6, 1040-1056.

Parvin, A., and Wang, W. (2001). Behaviour of FRP jacketed concrete columns under eccentric loading. *Journal of Composites for Construction*, 5(3), 146-152.

Pham, T. M., and Hadi, M. N. S. (2013). Strain estimation of CFRP-confined concrete columns using energy approach. *Journal of Composites for Construction*, 17(6), 1–11.

Popovics, S. (1973). A Numerical Approach to the Complete Stress-Strain Curve of Concrete. *Cements and Concrete Research*, 3(5), 583-599.

Rahimi, H., and Hutchinson, A. (2001). Concrete Beams Strengthened with Externally Bonded FRP Plates. *Journal of Composites for Construction*, 5(1), 44-56.

Sadeghian, P., and Fam, A. (2015). Strengthening slender reinforced concrete columns using high-modulus bonded longitudinal reinforcement for buckling control. *Journal of structural Engineering*, 141, 04014127.

Sadeghian, P., and Fillmore, B. (2018). Strain distribution of basalt FRP-wrapped concrete cylinders. *Case Studies in Construction Materials*, 9, e00171.

Sadeghian, P., Rahai, A. R., and Ehsani, M. R. (2010). Experimental study of rectangular RC columns strengthened with CFRP composites under eccentric loading. *Journal of Composites for Construction*, 443-450.

Shaat, A., and Fam, A. Z. (2009). Slender Steel Columns Strengthened Using High-Modulus CFRP Plates for Buckling Control. *Journal of Composites for Construction*, 13(1), 2-12.

Shahawy, M., Mirmiran, A., and Beitelman, T. (2000). Tests and modeling of carbon-wrapped concrete columns. *Composites Part B: Engineering*, 31(6), 471-480.

Sharif, A., Al-Sulaimani, G. J., Basunbul, I. A., Baluch, M. H., and Ghaleb, B. N. (1994). Strengthening of Initially Loaded Reinforced Concrete Beams Using FRP Plates. *ACI structural Journal*, 91(2), 160-168.

Sheikh, S. A., and Kharal, Z. (2018). GFRP-Reinforced Concrete Columns Subjected to Seismic Loads. *ACI Special Publication*, 326, 56-1:10.

Tarek, H., and Rizkalla, S. (2002). Flexural Strengthening of Prestressed Bridge Slabs with FRP systems. *PCI Journal*, 47(1), 76-93.

Tavassoli, A., Liu, J., and Sheikh, S. (2015). Glass Fiber-Reinforced Polymer-Reinforced Circular Columns under Simulated Seismic Loads. *ACI Structural Journal*, 103-114.

Teng, J., Lorenzis, L., Wang, B., Li, R., Wong, T., and Lam, L. (2006). Debonding Failures of RC Beams Strengthened with Near Surface Mounted CFRP Strips. *Journal of composites for construction*, 92(105), 92-105.

Thériault, M., and Benmokrane, B. (1998). Effects of FRP Reinforcement Ratio and Concrete Strength on Flexural Behavior of Concrete Beams. *Journal of Composites for Construction*, 2(1), 7-16.

Tobbi, H., Farghaly, A. S., and Benmokrane, B. (2012). Concrete Columns Reinforced Longitudinally and Transversally with Glass Fiber-Reinforced Polymer Bars. *ACI Structural Journal*, 109(4), 551-558.

Todeschini, C. E., Bianchini, A. C., and Kesler, C. E. (1964). Behavior of Concrete Columns Reinforced with High Strength Steels. *ACI Journal*, 61(6), 701-716.

Toutanji, H. A., and Saafi, M. (2000). Flexural behavior of concrete beams reinforced with glass fiber-reinforced polymer (GFRP) bars. *ACI Structural Journal*, 97(5), 712-719.

Triantafillou, T. C., and Plevris, N. (1992). Strengthening of RC beams with epoxy-bonded fibre-composite materials. *Materials and Structures*, 25, 201-211.

Wight, J. K., and MacGregor, J. G. (2012). Reinforced Concrete Mechanics and Design. *Upper Saddle River*, *NJ: Pearson Education Inc*.

Zadeh, H. J., and Nanni, A. (2013). Design of RC Columns Using Glass FRP Reinforcement. *Journal of Composites*, 17(3), 294–304.

CHAPTER 8 STRENGTHENING SHORT CONCRETE COLUMNS USING LONGITUDINALLY BONDED CFRP LAMINATES

ABSTRACT

This paper investigates the behavior of short concrete columns strengthened with externally bonded longitudinal carbon fiber-reinforced polymer (CFRP) laminates combined with transverse basalt fiber-reinforced polymer (BFRP) wraps. A total of eighteen 500 mm-long [19.69 in-long] concrete column specimens with a square cross section (150 mm [5.91 in] width) were tested with different longitudinal and transverse reinforcement combinations under concentric and eccentric axial loadings. For eccentric loading, three end eccentricity to width ratios of 0.1, 0.2, and 0.3 were applied symmetrically at both ends of each simply supported column specimen to provide single curvature condition. The compressive longitudinal CFRP strips, in average, experienced 38% of their tensile rupture strain. The experimental results showed debonding of longitudinal CFRP laminates from concrete surface and buckling of bonded specimens as the dominant mode of failure and revealed that transverse wrapping system is efficient in postponing the buckling/debonding failure.

8.1 INTRODUCTION

The strengthening of reinforced concrete structures using fiber-reinforced polymer (FRP) composites have become popular due to their outstanding physical and mechanical characteristics including high-strength, low-weight, and high-corrosion resistance. Application of FRPs could be found in various forms such as applying them on the outer surface of concrete elements such as beams, slabs, and bridge decks in form of bonded laminates as well as near surface mounted (NSM) strips to increase their ultimate strength

and stiffness, or in form of wraps to provide compressive structural members such as columns with confinement and increase their axial capacity. There have been many researches on the application of bonded laminates for strengthening of reinforced concrete beams (Triantafillou and Plevris, 1992; Sharif et al., 1994; Rahimi and Hutchinson, 2001), slabs (Mosallam and Mosalam, 2003; Kim et al., 2008), bridge decks (Alkhrdaji et al., 1999; Tarek and Rizkalla, 2002; Atadero et al., 2005), and on the concrete columns wrapped with FRP (Shahawy et al., 2000; Hussein et al., 2012; Mirmiran et al., 1998). In addition, some researchers have investigated columns strengthened with NSM technique using FRP composites (Bournas and Triantafillou, 2009; Gajdosova and Bilcik, 2013), however, very few researches have done on the application of concrete columns strengthened with longitudinally bonded FRP strips.

FRP wrapping have been known as a strong tool of strengthening for concrete columns, especially for concentrically loaded columns. Parvin and Wang (Parvin and Wang, 2001) recognized that short columns under eccentric compressive loading can successfully increase the capacity. Hadi (2006) found out that usage of FRP wraps is effective for eccentrically loaded columns up to a certain margin. Bisby and Ranger (2010) showed that the effectiveness of FRP confinement for circular columns is reduced under combined axial and flexural loading. The other issue is the effect of cross-section on the effectiveness of wrapping system; wrapping for rectangular and square cross-sections is not as effective as for circular cross-sections due to the presence of sharp corners which transmit confining stresses to the concrete (Parvin and Brighton, 2014). Although FRP wraps are very effective for uniaxial loading, longitudinal reinforcement might be needed, especially for slender

columns, for combined axial and flexural loading systems to increase the stiffness of the reinforced concrete columns.

Sadeghian and Fam (2015) investigated the effect of bonded longitudinal reinforcements analytically and found it more beneficial for eccentrically loaded slender columns than transverse wrapping, where large bending moments small axial loads exists. Shaat and Fam (2009) examined carbon FRP (CFRP) plates for strengthening of slender steel columns experimentally and analytically whose result showed the effectiveness of the CFRP system in increasing the axial strength of steel columns as slenderness increased. Chaallal and Shahawy (2000) figured out that the performance of bidirectional CFRP fabrics for strengthening of concrete beam-columns would improve their capacity, especially their flexural capacity. Sadeghian et al. (2010) performed experimental study on the behavior of concrete columns longitudinally and transversely strengthened with CFRP laminates and realized that the application of longitudinal layers improves the bending stiffness and moment capacity of the columns, however, their longitudinal bonded elements were made of fabrics. In addition, Pham et al. (2016) experimentally studied different wrapping arrangements on the confinement mechanism of circular column tested under axial loading and found the partial wrapping as an effective method to improve the axial capacity of the columns.

Due to lack of experimental data, the behavior of longitudinal unidirectional FRP laminates for strengthening concrete columns is not well-known, and there are some doubts about their performance under compression loads. The deboning of longitudinally bonded FRP strips to concrete columns as well as their buckling under compressive loads need an in depth understanding of the systems. Since an experimental program is needed to study the

effect of bonded FRP strips on slender concrete columns, this research was designed to address the doubts and identify potential issues related to the application of CFRP bonded short concrete columns as a preparation phase for testing large scale slender columns. In this paper, CFRP and basalt FRP (BFRP) reinforcements opted as longitudinal and transverse reinforcing systems, respectively, to be attached externally on the surface of short concrete columns. The tests were conducted on pin-pin column specimens under different load eccentricities as well as combinations of transverse and longitudinal FRP reinforcements.

8.2 Research Significance

This paper experimentally investigates the behavior of longitudinally bonded CFRP strips to short concrete column surfaces under eccentric loading, with and without transverse BFRP wrapping systems. Longitudinal CFRP strip reinforcement could be used as a strengthening method for slender columns with large eccentricity for which the knowledge of buckling of FRP strip is required as well as their debonding from concrete surface. Transverse FRP wraps as a modifier of buckling behavior by providing lateral support and limiting the length of buckling whose performance on longitudinal FRP strips attached to concrete columns is to be investigated in this study.

8.3 Experimental Program

A total of eighteen medium-scale plain concrete specimens with square cross-section were prepared and tested under concentric and eccentric loading up to failure. Thirteen of specimens were externally bonded with two CFRP laminates. Four of these specimens were partially and fully wrapped with unidirectional BFRP to decrease the buckling length of the

longitudinal CFRP laminates. It should be mentioned that the terms fully wrapped and partially wrapped, used in this chapter, refers to the use of 60% wrap at the middle and a single strap, respectively. In this section, experimental test matrix, material properties, fabrication, and the test set up for CFRP strengthened concrete specimens as well as plain ones is explained.

8.3.1 Test matrix

A total of eighteen 500 mm [19.69 in] long concrete column specimens with a square cross-section (150×150 mm) [5.9×5.9 in] were tested under pure axial and combined axial and flexural loading. Five specimens were made of plain concrete, nine specimens were externally bonded with two symmetrically attached longitudinal CFRP strips (500×50×1.2 mm) [19.68×1.97×0.05 in] and epoxy adhesive. Four of the CFRP-bonded specimens were wrapped laterally with two layers of unidirectional basalt fabric and epoxy resin (BFRP); two of them with a narrow strip of 51 mm [2 in] wide BFRP, which is called partial wrap (WP) in this paper, and two of them with strips of 305 mm [12 in] width, which is called full wrap (WF), as presented in Table 8.1 and Figure 8.1. Four specimens were tested under pure axial load, including two plain concrete columns and two bonded specimens, while other specimens were tested under combined axial and flexural loads with eccentricities of 15, 30, and 45 mm [0.59, 1.18, and 1.77 in], which are 10, 20, and 30 percent of width of the specimens. The specimen ID that is presented in Table 8.1 is like “A-ex-y” for specimen without lateral reinforcement and “A-Wz-ex-y”; where A, x, y, and z are representatives of column type (“P” for plain or “B” for bonded), the eccentricity to width ratio (0, 10, 20, or 30), the specimen number (1, 2, or 3), and the type of lateral reinforcement (“P” for partial or “F” for full), respectively. For example, B-WF-e30-2 represents the second bonded

specimen which is fully wrapped and was tested under eccentricity to width ratio of 30 percent.

Table 8. 1 Test specimen properties

No.	Specimen ID	Eccentricity, e (mm) [in]	Eccentricity to width ratio, e/h	Longitudinal Reinforcement	Lateral Reinforcement
1	B-e0-1	0 [0]	0	2 CFRP strip	None
2	B-e0-2	0 [0]	0	2 CFRP strip	None
3	B-e10-1	15 [0.59]	0.1	2 CFRP strip	None
4	B-e10-2	15 [0.59]	0.1	2 CFRP strip	None
5	B-e10-3	15 [0.59]	0.1	2 CFRP strip	None
6	B-e20-1	30 [1.18]	0.2	2 CFRP strip	None
7	B-e20-2	30 [1.18]	0.2	2 CFRP strip	None
8	B-e30-1	45 [1.77]	0.3	2 CFRP strip	None
9	B-e30-2	45 [1.77]	0.3	2 CFRP strip	None
10	B-WP-e30-1	45 [1.77]	0.3	2 CFRP strip	2” BFRP wrap
11	B-WP-e30-2	45 [1.77]	0.3	2 CFRP strip	2” BFRP wrap
12	B-WF-e30-1	45 [1.77]	0.3	2 CFRP strip	12” BFRP wrap
13	B-WF-e30-2	45 [1.77]	0.3	2 CFRP strip	12” BFRP wrap
14	P-e0-1	0 [0]	0	Plain	None
15	P-e0-2	0 [0]	0	Plain	None
16	P-e10-1	15 [0.59]	0.1	Plain	None
17	P-e10-2	15 [0.59]	0.1	Plain	None
18	P-e10-3	15 [0.59]	0.1	Plain	None

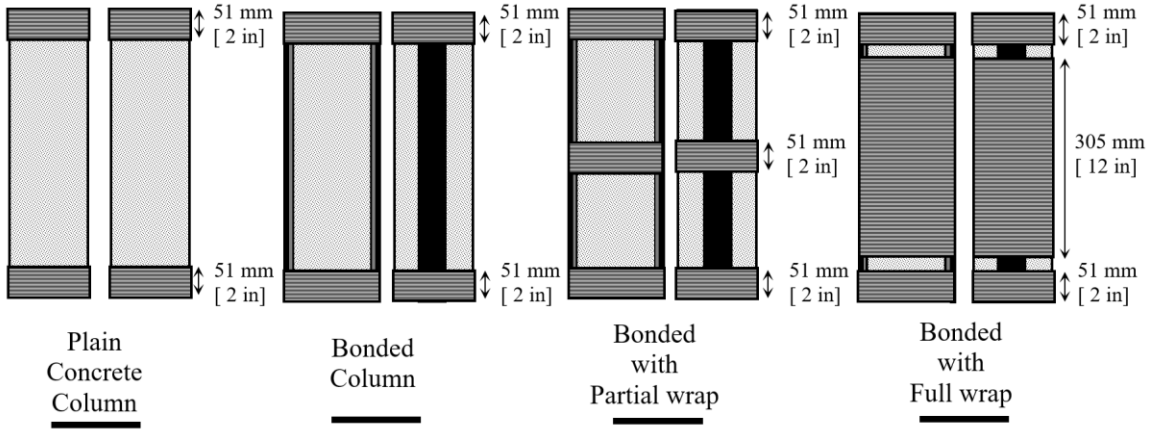

Figure 8. 1 Test specimen types and strengthening schemes

8.3.2 Material properties

In this study, unidirectional CFRP laminate was used as the reinforcing material. The laminate was available in the form of 50 mm [1.97 in] wide and 1.2 mm [0.05] thick strips. The CFRP laminate was an old version of the commercial product. Per ASTM D3039/3039M-14 (2014), five tensile CFRP coupons were tested to determine the tensile characteristic of longitudinal CFRP strips. All coupons showed a linear behavior up to a sudden rupture at their maximum tensile capacity. The average tensile modulus of elasticity, ultimate tensile strength, and ultimate tensile strain of the CFRP laminates derived from the tests were 180 GPa [26107 ksi], 3006 MPa [436 ksi], and 0.01668 mm/mm [0.01668 in/in], respectively. Furthermore, a compatible adhesive was used as the bonding material to attach the strips to the surface of the concrete specimens with a thickness of 1.5 mm [0.059 in]. The tensile strength, compressive modulus of elasticity, ultimate tensile strain, and the bond strength were 27.6 MPa [4003 psi], 3.06 GPa [444 ksi], 0.01 mm/mm [0.01 in/in], and 13.8 MPa [2002 psi], respectively, as reported by manufacturer. For wrapping, a unidirectional basalt fabric and epoxy resin were used. For resin, a mixture of epoxy resin and slow hardener was opted, which reported by manufacturer to have the tensile strength, tensile modulus, and maximum elongation of 50 MPa [7252 psi], 2.8 GPa [406 ksi], and 0.045 mm/mm [0.045 in/in], respectively. The epoxy resin was reinforced by a unidirectional basalt fabric with the areal weight of 300 g/m2 [12.66 oz/ya^2] and nominal thickness of 0.115 mm [0.0045 in]. The tensile strength, tensile modulus, and ultimate tensile strain of basalt fibers were 2100 MPa [305 ksi], 105 GPa [15229 ksi], and 0.026 mm/mm [0.026 in/in], respectively, per manufacturer. Furthermore, the average

rupture stress, rupture strain, and tensile modulus of elasticity of basalt fabric was reported by Fillmore and Sadeghian (2017) as 624.1 MPa [90.5 ksi], 0.0279 mm/mm [0.0279 in/in], and 24.62 GPa [3570.8 ksi], respectively. Moreover, a ready-mix concrete with maximum aggregate size of 12.5 mm [0.5 in] was used. For concrete material, three cylinders (100 × 200 mm) [4 × 6 in] were tested at the time of testing, where the average compressive strength of 37 MPa were observed for the concrete material.

8.3.3 Fabrication

All concrete specimens were casted in one batch where the fresh concrete [Figure 8.2(b)] poured in wooden formworks [Figure 8.2(a)], and the specimens were cured in room temperature using plastic covers [Figure 8.2(c)] to keep their moisture. Four column specimen types were fabricated in this experimental program whose schematic layout of longitudinal and transverse reinforcements are presented in Figure 8.1. Due to the expectation of stress concentration and in turn occurrence of premature failure, the top and bottom of the specimens were transversely reinforced using two layers of 51 mm [2 in] wide unidirectional BFRP wraps [Figure 8.2(d)], as shown in Figure 8.1. After removing the formworks, the concrete side surfaces were polished to provide specimens with a better friction and bonding. Then a layer of 1.5 mm [0.059 in] tick adhesive was applied to both sides and two 500×50×1.2 mm [19.68×1.97×0.05 in] unidirectional CFRP strips were attached at the center of opposite concrete surfaces of column specimens to build the strengthening system [Figure 8.1]. In addition, for partially and fully wrapped bonded specimens, two layers of epoxy reinforced with 50 mm [1.97 in] and 305 mm [12 in] wide unidirectional BFRP were applied transversely to the center of the bonded columns, respectively. At the end, the top and bottom surfaces of specimens were smoothened using

grinder to vanish the imperfections of the surfaces, and two plastic bags filled with fresh quick set cement based grout were applied on the top and the bottom surfaces of the specimens to integrate the column specimen and the steel caps, which were used for applying eccentric loading [Figure 8.3].

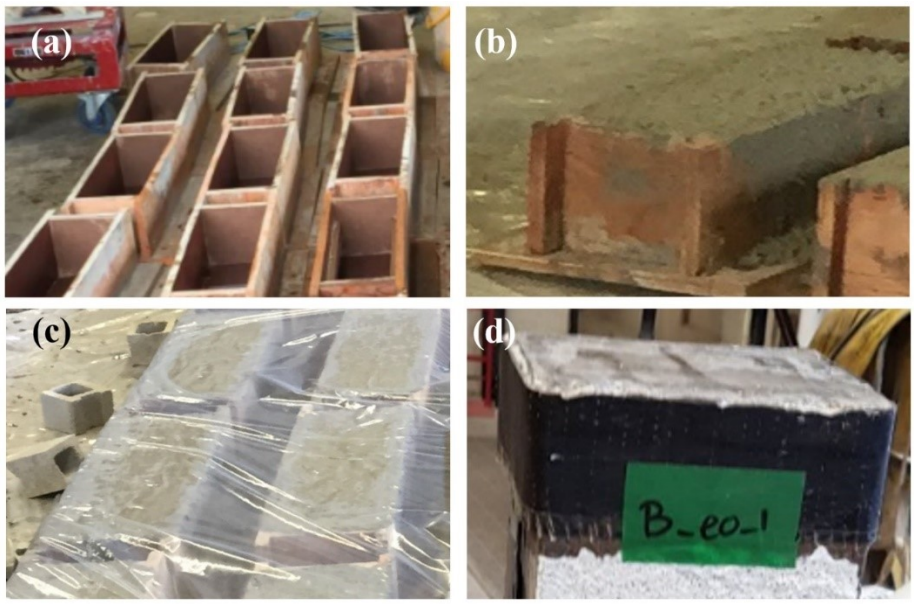

Figure 8. 2 Specimen preparation: (a) molds, (b) fresh concrete, (c) curing, (d) end wrap

8.3.4 Test set-up and instrumentation

Two symmetric steel caps [Figure 8.3], consisting of four adjustable angle steel profiles bolted to a wide steel plate on top of which a tick notched steel plate is welded, were tightened to the top and bottom of column specimens. Two steel rollers laid on the notch surface whose rotation ability provide the specimens with the simply supported boundary condition. The symmetricity of the steel caps and rollers, upon which load was applied, creates a single curvature deformation shape and a combined axial and flexural loading condition, as shown in Figure 8.3. Load eccentricity and axial compressive loads at the top and the bottom of specimens are shown as “e” and “P”, respectively, in Figure 8.3. It is

noticed that because of difficulties in providing loading condition in lab so that the column would be under double curvature and the fact that double curvature bending is sum of two single curvature but with different length, the test performed in single curvature as is usual in testing columns. To measure the strains of longitudinally bonded CFRP strips and lateral displacement, a data acquisition system including four linear variable differential transformers (LVDTs) and two strain gauges obtained the data at a frequency of 10 Hz as shown in Figure 8.3. Strain gauges where installed at the center of the CFRP strips on the outer surface as well as two vertical LVDTs (i.e. LVDT 1 and LVDT 2), with a gauge length of 100 mm [4 in], to measure the axial strain of the CFRP strips. Moreover, for measuring the lateral displacement of the specimens, two lateral LVDTs (i.e. LVDT 3 and LVDT 4) were pointed at the center of the tested specimens [Figure 8.3]. All tests were performed using a displacement control approach with a displacement rate of 0.625 mm/min [0.025 in/min] by a 2 MN [450 kips] universal testing machine.

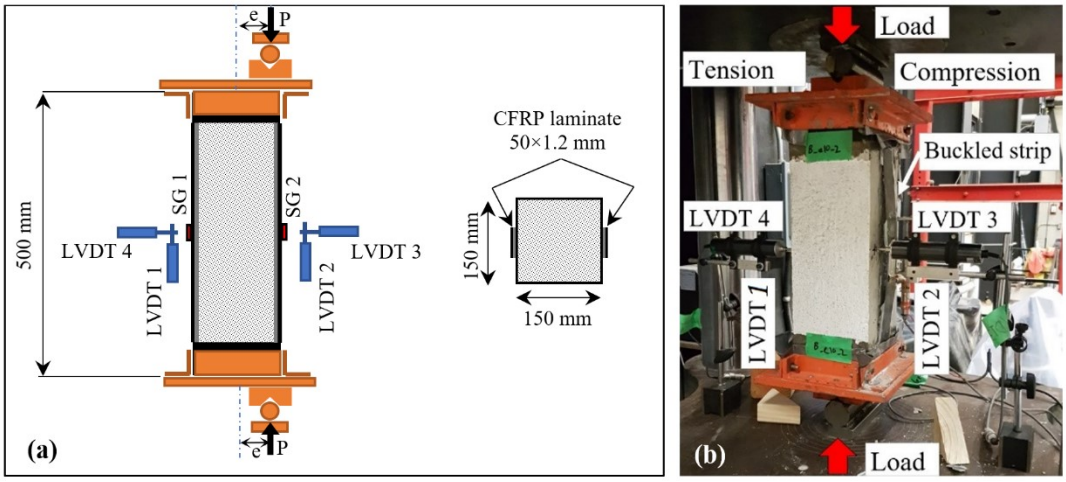

Figure 8. 3 Test set up and instrumentation: (a) schematic testing specimen and reinforcing layout, and (b) testing machine and instrumentation

8.4 RESULTS AND DISCUSSION

In this section, the modes of failure discussed for plain and bonded specimens with or without transverse wrap. Then the effect of CFRP strips is discussed in terms of their influence in the load carrying capacity of the system and their impact in changing the mode of failure. The section eventually concluded with considering the effects of the load eccentricity on the behavior of the tested specimens.

8.4.1 Modes of failure

Overall, five modes of failure including concrete crushing (CC), concrete spalling (CS), concrete destruction (CD), debonding of CFRP stirps in compression side (DS), and buckling of CFRP strips in compression (BS) were observed during testing the column specimens, as mentioned in Table 8.2. The concrete crushing (CC) was considered as the mode of failure for a specimen when the extreme compressive strain reached 0.003 mm/mm [0.003 in/in] which was defined as the ultimate concrete strain in compression by ACI 318-14 (2014). The concrete spalling (CS) happened when a concrete segment in compression part separated from the column which had happened after concrete crushing occurred. All specimens built with plain concrete and tested under 10 percent eccentricity to width ratio (P-e10 group) were suddenly failed and split in half from, approximately, the mid-height of the columns which named as concrete destruction (CD). For all bonded specimen, whether with or without wrap, the debonding of CFRP strips in compression (DS) happened which immediately followed by the buckling of them (BS). For all bonded specimens, the buckling of strips in compression was simultaneously occurred at the peak load the bonded columns experienced.

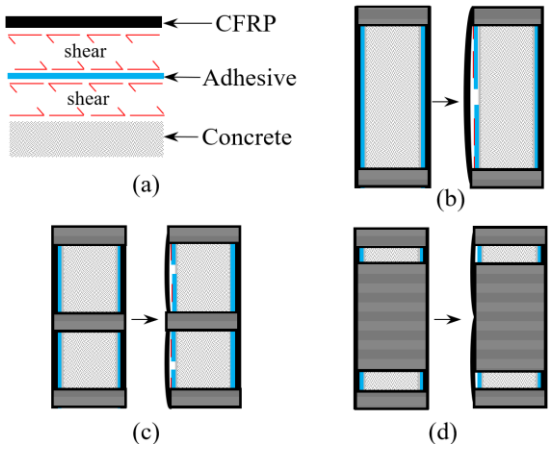

Figure 8. 4 Schematic failure modes: (a) shear flow in the interface of adhesive with CFRP and concrete; (b) buckling and debonding of bonded specimen; (c) buckling and debonding of partially wrapped specimens; (d) buckling and debonding of fully wrapped specimens

The schematics of Figure 8.4 illustrate the failure mode of failure for the bonded specimens. It should be mentioned that in the figure, there are interruptions in the adhesives which represents the debonding failure of longitudinal CFRP strips schematically. The shear stresses [Figure 8.4(a)] created in the interface of the concrete and adhesive as well as the interface of adhesive and CFRP strips was increased as the load increased to a certain extend at which a debonding between one of these surfaces started and propagated through the length of the strip. As these debonding cracks spread along the compression strips, the strips functioned separately and tend to buckle due to the tendency of concrete column to bend and the compressive forces that they tolerated. The buckling of bonded columns without wrap happened with full unbraced length [Figure 8.4(b) and Figure 8.5(a)], or with a fraction of the unbraced length [Figure 8.5(b)]. Moreover, the debonding happened between concrete and adhesive interface [Figure 8.5(a)], between CFRP strip and adhesive [Figure 8.5(b)], or both at the same time [Figure 8.5(c)]. For some specimens, the occurrence of the buckling followed by crushing in compression concrete [Figure 8.5(d)],

however, for some of them the test stopped before observation of the crushing since the load dropped after buckling of CFRP strip in compression. For partially wrapped bonded specimens, the length of buckling was controlled with the transverse BFRP wrap at the middle of the column [Figure 8. 4(c)] which delayed the buckling and in turn gave a higher capacity in comparison to the bonded specimens without wrap. For these specimens, the buckling happened mostly in one side and followed by the crushing of the concrete [Figure 8.5(e)]. The fully wrapped bonded specimens experienced buckling [Figure 8.4(d)] although the unbraced length was very limited; the unbraced length was about 46.5 mm [1.83 in] in each side. However, the buckling for these specimens did not happen in that limited length and spread even inside the wrapped area [Figure 8.5(f)]. Albeit the buckling spread inside the wrapped area, the capacity of these specimens was still more than the bonded ones due to stronger control of the buckling for these specimens provided by extended transverse BFRP wrap.

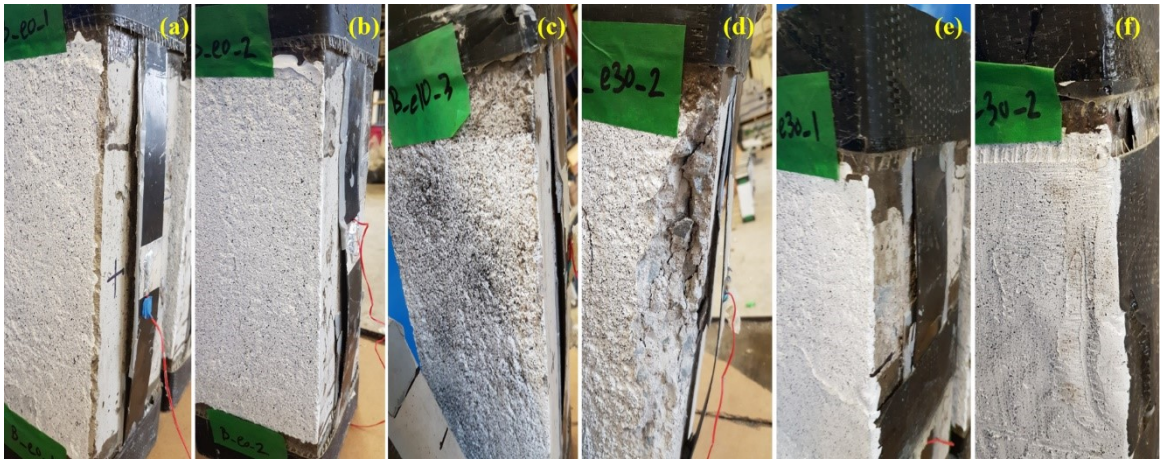

Figure 8. 5 Failure modes of reinforced specimens: (a) concrete and adhesive interface failure and buckling; (b) CFRP and adhesive interface failure and partial buckling; (c) combined adhesive and concrete plus adhesive and CFRP interface failure and buckling; (d) Concrete crushing and CFRP buckling; (e) buckling of partially wrapped CFRP strip; (f) buckling of fully wrapped CFRP strip

8.4.2 Effect of eccentricity

It is seen that as the load eccentricity increases, the bonded specimens experience more curvature since the displacement of these columns at the mid-height of specimen, corresponding to the peak load, tends to be increased as shown in Figure 8.6(a). Moreover, it is observed that the slope of load-displacement curves, which is corresponding to the stiffness of the columns, as well as their peak loads decrease as the load eccentricity increases [Figure 8.6(a)]. Furthermore, for bonded test specimens the ultimate displacement experienced is closer to the displacement corresponding to peak load for columns tested under higher eccentricity [Figure 8.6(a)], which shows that a lower axial load and bending moment sustainability for specimens tested in higher eccentricities is achieved.

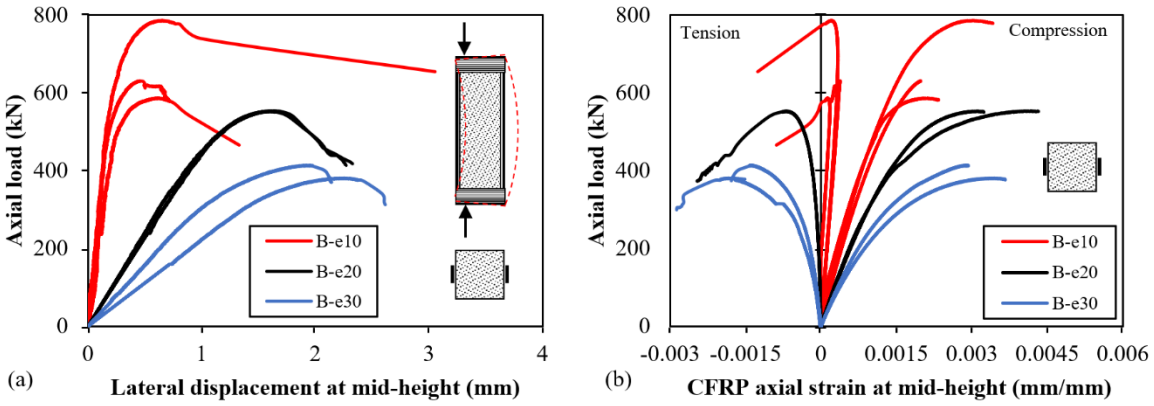

Figure 8. 6 Test results of the bonded specimens: (a) axial load vs. lateral displacement of bonded specimens, and (b) axial load vs. strain of compressive and tensile CFRP strips for bonded specimens

It is observed that as the load eccentricity increases, the strain corresponding to the peak load increases [Figure 8.6(b)]. In addition, the strain experienced in compression side is higher than the ones experienced in the tensile side as presented in Table 8.2 for bonded specimens.

Table 8. 2 Summary of test results

No.	Specimen ID	Peak Load, P_u (kN)	Comp. strain of laminate at P_u (mm/mm)	R1	Tensile strain of laminate at P_u (mm/mm)	R2	Maximum comp. strain of laminate (mm/mm)	R3	Maximum tensile strain of laminate (mm/mm)	R4	Mode of Failure
1	B-e0	835.0	-0.0035	0.21	-0.0017	0.10	-0.0054	0.32	-0.0022	0.13	SD → SB
2	B-e10	667.9	-0.0024	0.14	-0.0002	0.01	-0.0026	0.16	-0.0003	0.02	SD → SB
3	B-e20	553.4	-0.0036	0.22	0.0007	0.04	-0.0038	0.23	0.0025	0.015	SD → SB → CC
4	B-e30	397.4	-0.0032	0.19	0.0016	0.10	-0.0033	0.20	0.0030	0.18	SD → SB
5	B-WP-e30	444.8	-0.0036	0.22	0.0017	0.10	-0.0039	0.23	0.0026	0.16	SD → SB
6	B-WF-e30	416.5	-0.0043	0.26	0.0015	0.09	-0.0051	0.31	0.0016	0.10	SD → SB
7	P-e0	719.2	-	-	-	-	-	-	-	-	CS
8	P-e10	596.3	-	-	-	-	-	-	-	-	CS → CD
Average		-	-	0.21	-	0.04	-	0.24	-	0.07	

Note: CFRP strip strain recorded by SG2 (see Figure 8.1) installed on the middle the strips at the extreme compressive layer; R1: the ratio of compressive strain of laminate at Pu to tensile rupture strain; R2: the ratio of tensile strain of laminate at Pu to tensile rupture strain; R3: the ratio of maximum compressive strain of laminate to tensile rupture strain; R4: the ratio of the maximum tensile strain of laminate to tensile rupture strain; CC: concrete crushing; CS: concrete spalling; CD: concrete destruction; SB: strip buckling; SD: strip debonding; the tensile rupture strain = 0.01668 mm/mm; Tensile strains are positive and compression ones are negative. [1 mm = 0.0394 in; 1 kN = 224.8201 lb]

Table 8.2 also provides the ratios of tensile and compressive strains at peak load to the ultimate tensile strain, or tensile rupture strain, derived from the material test. The average ratios of compressive and tensile strain of CFRP strips in compression to the rupture strain for all specimens at the peak load were 21% and 4%, respectively, while these values at the ultimate read strains were 24% and 7%, respectively [Table 8.2]. It is noticed that the values of strain at peak load are the corresponding strain at which buckling of CFRP compressive strips occurred. Moreover, Table 8.2 presents the axial load carrying capacity of specimens

which reveals that for all bonded specimens, the capacity of bonded specimens was higher than plain specimens. In addition, the capacity even was more affected when the wrapping system used which is discussed in the following subsection.

8.4.3 Effect of wrapping

It was observed that all bonded specimens were capable of sustaining higher axial loads both in concentrically and eccentrically loaded specimens, as is shown in Table 8.2. In addition, the wrapping system which was used to control the unbraced length of compressive CFRP strips was quite effective and caused gain in the capacity of partially and fully wrapped specimens rather than bonded ones without lateral wraps. It is seen that the average axial capacity of specimens with partial wrap was even higher than the ones with full wrap whose reason could be explained as the degree of control over the unbraced length for the buckling of CFRP strip in compression. For partially wrapped specimens, the buckling length was exactly the complete length between the middle wrap and the end wrap while for the full wrapped case it was not determined. For B-WF-e30-2 specimen, the length of buckled CFRP strip in compression was 110 mm [4.33 in] and its axial capacity was 348.9 kN [87.4 kips] while for B-WF-e30-1, the same values were 190 mm [7.48 in] and 484.0 kN [108.8 kips], and for average of partially wrapped specimens these values are 173 mm [6.81 in] and 444.8 kN [100.0 kips], as shown in Figure 8.7. It is noted that for two similar fully wrapped specimens, the length of buckling is different and the specimen with the lower length of buckling experienced lower loads. The justification for the latter is that buckling happened after the debonding, and for the specimen with longer buckling length more energy consumed to create a continuous debonding. Furthermore, the experimental program shows a more consistent axial capacity of partially wrapped

specimens. Therefore, since the unbraced length is properly controlled using transverse wraps, the length of buckling can be reduced more appropriately using more strips instead of wrapping the full length of the column. Another result of the latter observation is that the longitudinal strips have more impact in the load capacity of the bonded specimens than the lateral wrapping since after buckling of CFRP strips in fully wrapped specimens the wrap still worked however a drop in the applied load observed.

Figure 8. 7 Buckling length: (a) fully wrapped bonded column with 110 mm [4.33 in] buckling length and 348.9 kN [87.4 kips] axial capacity; (b) fully wrapped bonded column with 190 mm [7.48 in] buckling length and 484.0 kN [108.8 kips] axial capacity; (c) partially wrapped bonded column with 173 mm [6.81 in] buckling length and 444.8 kN [100.0 kips] axial capacity. Note: the full wraps were cut to show the buckling length

It is seen that as the wrapping system added to the bonded specimens, the displacement of wrapped columns at the mid-height of specimen, corresponding to the peak load, increased as shown in Figure 8.8(a). It is noted that in Figure 8.8(b), the values of all strains were the ones recorded by strain gauges, but the ones for fully wrapped specimens are calculated based on the longitudinal LVDTs that had attached to specimens [Figure 8.3] due to the loss of strain gauge data.

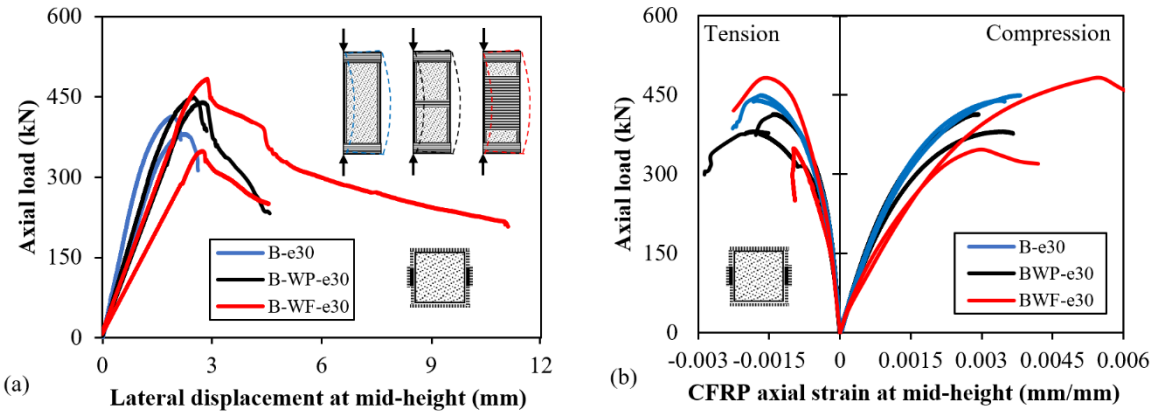

Figure 8. 8 Test results of the wrapped bonded specimens: (a) axial load vs. lateral displacement of bonded and wrapped specimens, and (b) axial load vs. strain of compressive and tensile CFRP strips for bonded and wrapped specimens

It is observed that the slope of load-displacement curves decreases when the transverse wraps added to bonded specimens [Figure 8.8(a)]. Moreover, by adding transverse wrapped specimens experienced higher values of ultimate displacement in comparison to bonded ones [Figure 8.8(a)], particularly for fully wrapped columns. Moreover, for nearly all specimens, it is seen that the strain of CFRP strips at peak load for bonded specimens with and without wraps are similar in tension and compression, as presented in Figure 8.8(b). In addition, the strain experienced in compression side was higher than the ones experienced in the tensile side for both discussed types of specimens. For specimens tested under 30 percent eccentricity to width ratio, the average ratios of compressive and tensile strain of CFRP strips for bonded specimens without wraps, partially wrapped, and fully wrapped specimens in compression to the rupture strain for all specimens at the peak load were 19%, 22%, and 26%, respectively, while these values at the ultimate read strains were 20%, 23% and 31%, respectively [Table 8.2].

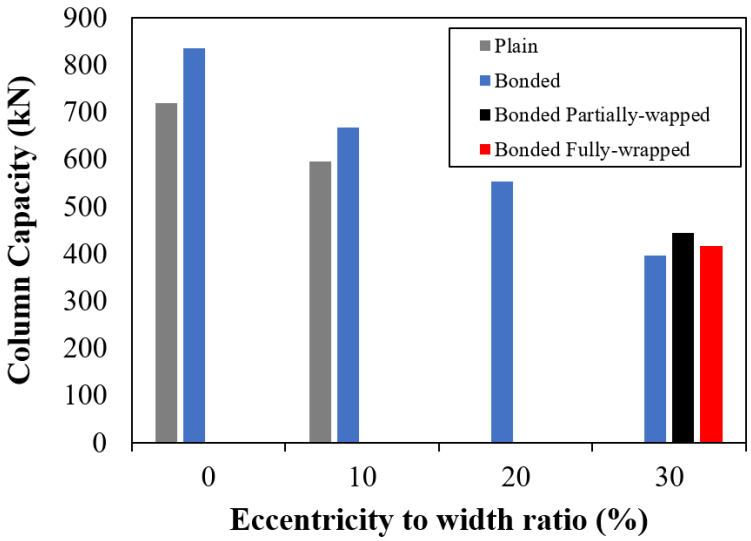

Figure 8. 9 Summary of test results

The summary of test results is presented in Figure 8.9. Overall, plain specimens gained improvement in their load carrying capacity by adding the longitudinal CFRP strips. In addition, the combined application of longitudinal bonded CFRP and lateral wrapping was more efficient method than using just longitudinal CFRP strips, as shown in Figure 8.9. Therefore, for strengthening purposes the combined lateral and longitudinal system is suggested. It is noticed that lateral BFRP wraps were not initially considered in the test matrix and the specimens with wrapping added to the test matrix after observation of the results of bonded specimens to prevent the buckling of CFRP strips or limit the unbraced length of this strips. However, the plain specimens with just confinement were not examined due to limitation of specimen numbers. Thus, the contribution of longitudinal CFRP strips and lateral BFRP strips in strengthening of the specimens cannot be separated and another study is required to address this issue. On the other hand, since the cross section is square, the effect of confinement is limited due to the existence of the sharp corners. Also, it is observed that by using narrow BFRP strips, the capacity improved better than

wider strips which implies that the gain in laterally reinforced specimens were mainly because of the lateral support that these wraps provided for longitudinal strips and to a lesser extend duo to their confinement effect. Regarding the difference between two specimens in B-WF-e30 group, shown in Fig. 8.8, the lack of statistical evidence exists as there is only two replicant specimens tested in that group. The quality of wrapping for rectangular sections due to the presence of sharp corners would be a source of this difference and inconsistency in the results. Therefore, more experimental evidence and tests are required to present a more solid conclusion.

The aim of this study was recognizing the behavior of short concrete columns strengthened using longitudinal CFRP strips, especially the compressive behavior of CFRP strips in compression where buckling of these strips is critical. However, the main beneficial application of this system is in slender columns in which the gain of stiffness provided by longitudinal CFRP strips alter the loading path of the column so that it intersects the axial load – bending moment interaction diagram of column in a higher axial load and cause gain in strength as numerically approved by Sadeghian and Fam (2015). Therefore, although the concrete crushing in compression would happen about 0.0035 mm/mm and the longitudinal strips cannot reach their ultimate crushing capacity, they are still advantageous in increasing the stiffness of column and in turn the capacity of the column.

8.5 CONCLUSION

In this study, the behavior of short concrete columns strengthened with longitudinal CFRP strips and transversely with BFRP wraps were examined experimentally. A total of eighteen simply supported column specimens consisting of five plain concrete, nine longitudinally CFRP bonded, and four longitudinally bonded and transversely wrapped specimens were

tested under four load eccentricity to width ratios of 0, 0.1, 0.2, and 0.3. The following conclusions can be drawn from this study:

- Five modes of failure including concrete crushing, concrete spalling, concrete destruction, debonding of CFRP stirps in compression side, and buckling of CFRP strips in compression were observed. However, no crushing of CFRP strips in compression were observed. The ultimate capacity of each specimen occurred at the peak load for all specimen strengthened with CFRP strips which started by debonding and followed by compressive strip buckling of CFRP strip in compression.
- The average experimental compressive strain of CFRP strips in compression at the time of strip buckling, or peak load, was 21% of tensile rupture strain while the average of the ultimate recorded compressive strain was 24%.
- Test results showed that the performance of the longitudinally bonded specimens was improve by adding wrapping system. However, the debonding and buckling of compressive CFRP strips was not avoided even by wrapping nearly the whole length of the specimens. The experimental results showed that by using narrow transverse wraps, the unbraced length of longitudinal strips is determined and certain while wide wraps do not provide that preciseness and unbraced length could vary even in two specimens tested under the same condition.
- The effect of narrow transverse BFRP wraps in limiting the length of buckling of longitudinal CFRP bonded strips is similar to the effect of stirrups in restricting the unbraced length for rebars in concrete columns. Therefore, further studies on

the behavior of lateral wraps in concrete columns strengthened with longitudinal bonded specimens is suggested.

- It should be noted that the tested specimens were limited, and more specimens for each group is required to reach a more solid statistical conclusion. Therefore, more further tests are recommended.

ACKNOWLEDGMENTS

Authors would like to thank Blair Nickerson, Brian Kennedy, Jesse Keane, and Brian Liekens and for their assistance in the lab. The authors would also like to acknowledge and thank NSERC and Dalhousie University for their financial support.

REFERENCES

ACI 318-14. (2014). Building Code Requirements for Structural Concrete. *American Concrete Institute.* Farmington Hills, MI.

Alkhrdaji, T., Nanni, A., Chen, G., and Barker, M. (1999). Upgrading the Transportation Infrastructure: Solid RC Decks Strengthened with FRP. *Concrete International: Design and Construction*, 21(10), 37-41.

ASTM D3039/D3039M-14. (2014). Standard Test Method for Tensile Properties of Polymer Matrix Composite Materials. *American Society for Testing and Materials.* West Conshohocken, PA.

Atadero, R., Lee, L., and Karbhari, V. M. (2005). Consideration of material variability in reliability analysis of FRP strengthened bridge decks. *Composite Structures*, 70(4), 430-443.

Bisby, L., and Ranger, M. (2010). Axial–flexural interaction in circular FRP-confined reinforced concrete columns. *Construction and Building Materials*, 24(9), 1672-1681.

Bournas, D. A., and Triantafillou, T. C. (2009). Flexural strengthening of reinforced concrete columns with near-surface-mounted FRP or stainless steel. *ACI Structural Journal*, 106(4), 495-505.

Chaallal, O., and Shahawy, M. (2000). Performance of Fiber-Reinforced Polymer-Wrapped Reinforced Concrete Column under Combined Axial-Flexural Loading. *ACI Structural Journal*, 97(4), 659-668.

Gajdosova, K., and Bilcik, J. (2013). Full-scale testing of CFRP-strengthened slender reinforced concrete columns. *Journal of composites for construction*, 17, 239-248.

Hadi, M. (2006). Behaviour of FRP wrapped normal strength concrete columns under eccentric loading. *Composite Structures*, 72(4), 503-511.

Hussein, M. E., Al-Salloum, Y. A., Alsayed, S. H., and Iqbal, R. A. (2012). Experimental and numerical investigation of size effects in FRP-wrapped concrete columns. *Construction and Building Materials*, 29, 56-72.

Kim, Y. J., Longworth, J. M., and Wight, G. R. (2008). Flexure of Two-Way Slabs Strengthened with Prestressed or Non prestressed CFRP Sheets. *Journal of Composites for Construction*, 12(4), 366-374.

Mirmiran, A., Shahawy, M., Samaan, M., El Echary, H., Mastrapa, J. C., and Pico, O. (1998). Effect of Column Parameters on FRP-Confined Concrete. *Journal of Composites for Construction*, 2(4), 175-185.

Mirmiran, A., Yuan, W., and Chen, X. (2001). Design for slenderness in concrete columns internally reinforced with fiber-reinforced polymer bars. *Structural Journal*, 98(1), 116-125.

Mosallam, A. S., and Mosalam, K. M. (2003). Strengthening of two-way concrete slabs with FRP composite laminates. *Construction and Building Materials*, 17(1), 43-54.

Parvin, A., and Brighton, D. (2014). FRP Composites Strengthening of Concrete Columns under. *Polymers*, 6, 1040-1056.

Parvin, A., and Wang, W. (2001). Behaviour of FRP jacketed concrete columns under eccentric loading. *Journal of Composites for Construction*, 5(3), 146-152.

Pham, T. M., and Hadi, M. N. S. (2013). Strain estimation of CFRP-confined concrete columns using energy approach. *Journal of Composites for Construction*, 17(6), 1–11.

Rahimi, H., and Hutchinson, A. (2001). Concrete Beams Strengthened with Externally Bonded FRP Plates. *Journal of Composites for Construction*, 5(1), 44-56.

Sadeghian, P., and Fam, A. (2015). Strengthening slender reinforced concrete columns using high-modulus bonded longitudinal reinforcement for buckling control. *Journal of structural Engineering*, 141, 04014127.

Sadeghian, P., and Fillmore, B. (2018). Strain distribution of basalt FRP-wrapped concrete cylinders. *Case Studies in Construction Materials*, 9, e00171.

Sadeghian, P., Rahai, A. R., and Ehsani, M. R. (2010). Experimental study of rectangular RC columns strengthened with CFRP composites under eccentric loading. *Journal of Composites for Construction*, 443-450.

Shaat, A., and Fam, A. Z. (2009). Slender Steel Columns Strengthened Using High-Modulus CFRP Plates for Buckling Control. *Journal of Composites for Construction*, 13(1), 2-12.

Shahawy, M., Mirmiran, A., and Beitelman, T. (2000). Tests and modeling of carbon-wrapped concrete columns. *Composites Part B: Engineering*, 31(6), 471-480.

Sharif, A., Al-Sulaimani, G. J., Basunbul, I. A., Baluch, M. H., and Ghaleb, B. N. (1994). Strengthening of Initially Loaded Reinforced Concrete Beams Using FRP Plates. *ACI structural Journal*, 91(2), 160-168.

Tarek, H., and Rizkalla, S. (2002). Flexural Strengthening of Prestressed Bridge Slabs with FRP systems. *PCI Journal*, 47(1), 76-93.

Triantafillou, T. C., and Plevris, N. (1992). Strengthening of RC beams with epoxy-bonded fibre-composite materials. *Materials and Structures*, 25, 201-211.

CHAPTER 9 HYBRID SYSTEM OF LONGITUDINAL CFRP LAMINATES AND GFRP WRAPS FOR STRENGTHENING EXISTING OF CONCRETE COLUMNS

ABSTRACT

This paper presents an investigation on the behavior of a hybrid strengthening system of longitudinal premanufactured carbon fiber-reinforced polymer (CFRP) laminates and transverse Glass FRP (GFRP) wrapping for strengthening concrete columns. The idea behind using the longitudinal CFRP strips was to enhance the system by increasing the flexural stiffness of the column which is effective for the strengthening of slender columns and eccentrically loaded columns where additional flexural stiffness is required for buckling control. However, the effectiveness and mechanism of the system should be validated via experimental tests. Thus, a total of eighteen specimens were prepared and tested to characterize the hybrid system. It was observed that by applying GFRP wraps, the failure mode of CFRP laminates changed from buckling/debonding to crushing to achieve the full capacity of the system. However, test results showed that the usage of wrapping without longitudinal CFRP laminates was more effective than the proposed hybrid system for the strengthening of short concrete columns subjected to pure axial loading. For slender columns in presented in chapter 11, the hybrid system enhanced the axial capacity, flexural capacity, and lateral displacement of the wrapping system, by altering the second-order load-deflection path of the slender columns to a higher performance level.

9.1 INTRODUCTION

During the past decades, fiber-reinforced polymer (FRP) composites have become widespread for the rehabilitation of existing concrete structures. One of the major

applications of FRPs for construction has been known as the wrapping of concrete columns with FRPs to provide confinement for the concrete core. Wrapping of concrete columns enhances their axial load capacity and ductility (Nanni and Bradford, 1995; Toutanji, 1999; Hadi, 2006; Sadeghian et al., 2010; Bisby and Ranger, 2010; Yu et al., 2018). Therefore, FRP wrapping has been known very effective especially for concentrically loaded columns (Pessiki et al., 2001; Ozbakkaloglu, 2013; Xiao and Wu, 2000; Cui and Sheikh, 2010; Smith et al., 2010). However, for eccentrically loaded columns and slender columns, wrapping is not as effective as concentrically loaded columns. Parvin and Wang (2001) recognized that wrapping of short concrete columns under eccentric compressive loading can successfully increase their capacity. However, Hadi (2006) found out that the FRP wraps are effective for eccentrically loaded columns up to a certain margin. Bisby and Ranger (2010) reported a reduction in the effectiveness of FRP wrapping for circular concrete columns loaded under combined axial and flexural loading. Al-Nimry and Soman (2018) studied the slenderness effect of eccentrically loaded circular concrete columns confined with FRP wraps and observed that the efficiency of the wraps in confining concrete columns decreases as the slenderness ratio increases. Also, ACI-440.2R-17 (2017) limits the effective rupture strain of FRP wraps to 0.004 mm/mm where the load eccentricities are more than 10% of the diameter of the column. Moreover, ACI-440.2R-17 (2017) is silent regarding slender columns. Since wrapping design tends to improve the columns providing confinement, the fiber orientation is set to give the strong modulus of elasticity in the hoop direction. Thus, in many cases wrapping is used just unidirectionally in the hoop direction. Therefore, to increase the flexural stiffness, additional longitudinal reinforcement would be

required for strengthening of eccentrically loaded columns or slender columns to overcome the limitation of the wrapping system.

The idea of a hybrid system using high modulus longitudinal laminates such as CFRP premanufactured laminates is to address the mentioned issue and provide the required additional flexural stiffness to strengthen slender concrete columns where wrapping is not as effective due to the nature of loading and secondary moment effects. Many researchers have evaluated the performance of CFRP laminates for concrete beams (Triantafillou and Plevris, 1992; Sharif et al., 1994; Shahawy et al., 1996; Buyukozturk and Hearing, 1998; Malek et al., 1998; Rahimi and Hutchinson, 2001; Ashour et al., 2004), concrete slabs (Mosallam and Mosalam, 2003; Kim et al., 2008), and bridge decks (Alkhrdaji et al., 1999; Tarek and Rizkalla, 2002; Atadero et al., 2005). However, the application of longitudinal CFRP laminates in compression for the strengthening of columns is limited by ACI 440.2R-17 (2017) and CSA S806-12 (2012) due to lack of experimental test data and its unknown behavior in structural applications for strengthening. On the other hand, recent studies on concrete columns strengthened with longitudinal FRPs (Gajdosova and Bilcik, 2013; Sadeghian and Fam, 2015; Khorramian and Sadeghian, 2017a, 2018a, b, and c, 2019a; Abdallah et al., 2018; Chellapandian et al., 2018; Al-Salloum et al., 2018) as well as the columns which were built with FRP bars (Tobbi et al., 2012; Mohamed et al., 2014; Khorramian and Sadeghian, , 2017b and c, 2018d, 2019b; Fillmore and Sadeghian, 2018; Guérin et al., 2018; Elchalakani et al., 2018; Xue et al., 2018) have shown the effectiveness of longitudinal FRPs in compression. Researchers found out that longitudinal layers of FRP improve the stiffness and moment capacity of the strengthened columns (Chaallal and

Shahawy, 2000; Shaat and Fam, 2009; Sadeghian et al., 2010; Siddiqui et al., 2014; Sadeghian and Fam, 2015).

Application of near-surface mounted (NSM) CFRP strips for strengthening of columns was studied for short (Khorramian and Sadeghian, 2019a) and slender (Gajdosova and Bilcik, 2013) columns showed an improvement of the column capacity. However, the limitation of spacing between the groove imposed by ACI 440.2R-17 (2017) affects the number of strips that can be installed on the surface of calm and limit the reinforcement ratio. The other solution is using FRPs bonded to the surface of the column to provide more reinforcement. However, in compressive members, there buckling and debonding of the bonded FRP laminates is expected which limits the effectiveness of the strengthening system. Therefore, providing lateral support for longitudinal FRPs can be considered as a solution that can be provided by wrapping. However, studies showed that providing lateral support was not enough to control the debonding or buckling of FRP laminates in the bonded system of strengthening. Khorramian and Sadeghian tested short rectangular (2018a) and circular (2018b) concrete columns strengthened with longitudinal bonded CFRP laminates and laterally supported with wraps or straps. The results showed an improvement in the column capacity. However, the occurrence of debonding of longitudinal CFRP laminates led to a sudden drop of the load and was not controlled, and the premature debonding of FRP strips governed the system capacity before component level capacities were not reached (i.e. crushing of longitudinal CFRP laminates or rupture of straps or wrapping in hoop direction or concrete crushing). Thus, there is room to improve the system to control the premature failure and reach the component level capacity which leads to higher reliability of the system and optimizing the material used for

strengthening. In the previous research, the GFRP either straps or partial wraps were used as the lateral support for the longitudinal CFRP laminates. It was observed that even the existence of small gaps in the wrapping system (i.e. only 10 mm) caused the debonding of CFPR laminates. Therefore, for the current study, the columns were fully wrapped, and the focus of the study was on preventing debonding of longitudinal CFRP laminates by examining a different number of layers for wrapping. The effect of confinement was separated from the effect of longitudinal laminates by performing separate tests on columns that were only wrapped.

Khorramian and Sadeghian (2018c) developed an analytical-numerical model and showed that eccentrically loaded slender concrete columns strengthened with the hybrid system of longitudinal CFRP laminates and transverse GFRP wrapping can be more effective than using conventional wrapping system if premature failure is prevented. Therefore, the objective of this research is to validate the effectiveness of the hybrid system of longitudinal CFRP laminates and transverse GRP wraps for slender concrete columns. Thus, two phases of experimental studies were designed. The validation of the system, mechanism of the hybrid system, and the requirements for reaching component level efficiency (i.e. finding the situation in which longitudinal CFRPs does not buckle) was investigated in this study. Eighteen tests of concrete columns strengthened with different combinations of longitudinal laminates and transverse wrapping performed.

9.2 EXPERIMENTAL PROGRAM

9.2.1 Test Matrix

A total of eighteen short circular concrete columns (150 mm ×300 mm) strengthened with longitudinal CFRP strips, transverse GFRP wrapping, or a combination of both were prepared and tested under pure compression, as presented in Table 9.1. The specimens were divided into six groups, each consists of three identical specimens. The difference between testing groups was the variation in longitudinal and transverse strengthening systems as shown in Figure 9.1.

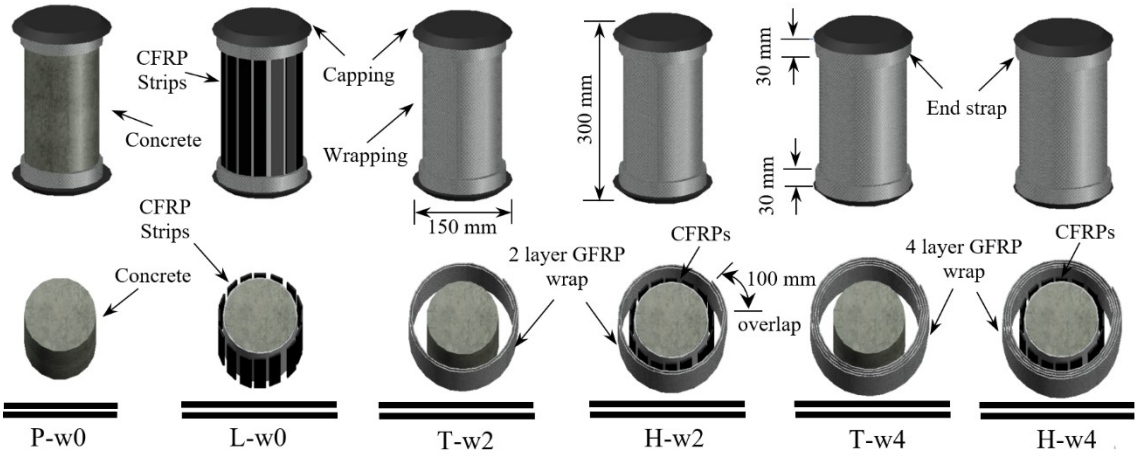

Figure 9. 1 Groups of specimens

The specimen IDs were presented in the format of "x-wy-z", where "x" represents specimen type (i.e. "P" for plain concrete, "L" for longitudinally reinforced only, "T" for transversely reinforced only, and "H" for hybrid or combined reinforcement), "y" shows the number of wrapping layers, "w" showed wrapping and is a fixed letter as a contraction for wrapping, and "z" shows the specimen number within the group as presented in Table 9.1.

Table 9. 1 Test matrix

No.	Specimen ID	Longitudinal Reinforcement	Transverse Reinforcement	Reinforcement Code
1	P-w0-1	-	-	Plain Concrete
2	P-w0-2	-	-	
3	P-w0-3	-	-	
4	L-w0-1	16 CFRP strips	-	Longitudinal reinforcement only
5	L-w0-2	16 CFRP strips	-	
6	L-w0-3	16 CFRP strips	-	
7	T-w2-1	-	2 layer GFRP wraps	Transverse with 2 layer wrapping
8	T-w2-2	-	2 layer GFRP wraps	
9	T-w2-3	-	2 layer GFRP wraps	
10	H-w2-1	16 CFRP strips	2 layer GFRP wraps	Hybrid with 2 layer wrapping
11	H-w2-2	16 CFRP strips	2 layer GFRP wraps	
12	H-w2-3	16 CFRP strips	2 layer GFRP wraps	
13	T-w4-1	-	4 layer GFRP wraps	Transverse with 4 layer wrapping
14	T-w4-2	-	4 layer GFRP wraps	
15	T-w4-3	-	4 layer GFRP wraps	
16	H-w4-1	16 CFRP strips	4 layer GFRP wraps	Hybrid with 4 layer wrapping
17	H-w4-1	16 CFRP strips	4 layer GFRP wraps	
18	H-w4-3	16 CFRP strips	4 layer GFRP wraps	

9.2.2 Specimen Fabrication

Figure 9.2 presents the process of specimen fabrication for typical specimens. For each longitudinally reinforced specimen, sixteen CFRP laminates with a rectangular cross-section (25 mm ×1.2 mm) were cut in strips with a length of 295 mm. The length of the longitudinal strips was considered less than the full length of the concrete specimens because of the prevention of strips from damaging the capping at the end of the specimens. The strips were considered slightly shorter than the length of the concrete cylinders to provide more room for adjustment as well as avoiding direct contact of CFRP strips with

the loading system. To install CFRP strips, a compatible adhesive was applied to the surface of concrete and strips were positioned in a symmetric fashion using predefined guidelines on the surface. Afterward, two strain gauges were installed on CFRP strips which were on the opposite sides of the specimen. The surface of strain gauges was coated with a proper coating material and covered with an aluminum tape to be protected against resin for hybrid specimens.

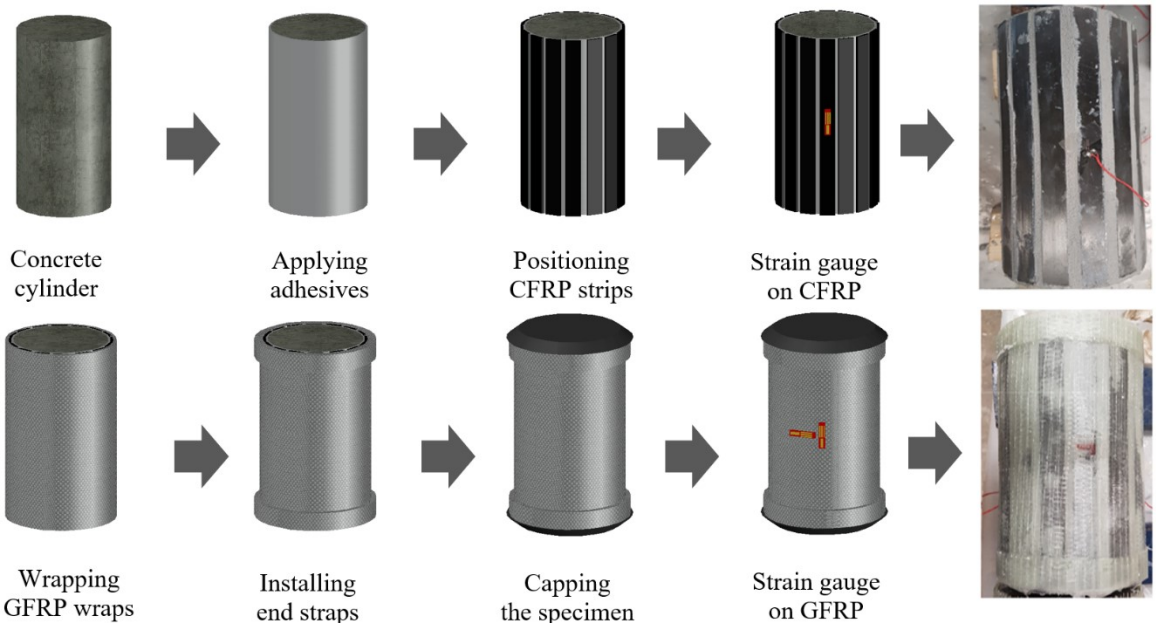

Figure 9. 2 Fabrication process

For all wrapped specimens, the width of the GFRP fabric was the same as the height of concrete cylinders to provide full wrapping. Both two- and four-layer wrappings were continued to give 100 mm overlap at the end. To avoid premature failure at the ends of the specimens, the ends were strengthened using four layers of GFRP straps with a width of 30 mm. Finally, the surface of GFRP wraps was prepared and four more strain gauges were installed on the surface of the GFRP wraps (two in hoop direction and two in the axial direction).

9.2.3 Material Properties

For CFRP and GFRP materials, five tensile coupon tests were performed per ASTM D3039M-14 (2014). Table 9.2 presents a summary of the material properties for different elements used to build the specimens including ultimate tensile strength f_t, modulus of elasticity E, and ultimate tensile strain ε_t. The average ± standard deviation of ultimate tensile strength, the tensile modulus of elasticity, and rupture strain of the tested specimens were 3267±348 MPa, 177.8±0.8 GPa, and 0.0179±0.0002 mm/mm, respectively, for CFRP strips while the mentioned values were 391±5 MPa, 25.7±2.4 GPa, and 0.0152±0.0011 mm/mm, respectively, for GFRP coupons based on the nominal ply thickness of 0.54 mm. Five compression coupon tests were also conducted on an older batch of the CFRP laminates per ASTM D6641M-16 (2016) whose results were presented in an earlier study (Khorramian and Sadeghian, 2019a). It should be noted that these two products were from the same manufacturer and model. The results showed that the average modulus of elasticity of CFRP laminates in compression was only fourteen percent lower than that in tension. Moreover, the compressive strength of CFRP laminates was about one-third of their tensile strength. Thus, the compressive strength of CFRP strips was considered as 1089 MPa which is one-third of the tensile strength, the compressive modulus of elasticity considered as 152.9 GPa which is fourteen percent lower than the tensile modulus, and the ultimate crushing strain of CFRPs in compression was considered as 0.0071 mm/mm which is derived by dividing the compressive strength by compressive modulus of elasticity. The material characteristics for bonding adhesive which was used to install CFRP strips on concrete, and the properties of resin in wrapping are presented in Table 9.2, that reported by the manufacturer.

Table 9. 2 Material properties

No.	Material Type	f_t (MPa)	E (GPa)	ε_t (mm/mm)	F_b (MPa)
1	CFRP laminate in tension	3267	177.8	0.0179	-
2	CFRP laminate in tension	1086	152.9	0.0071	-
3	GFRP wrap	391	25.7	0.0152	-
4	Bonding adhesive	25	4.4	0.0100	21.3
5	Epoxy resin	50	2.8	0.0450	-

Note: *= propertiesin compressionare reported; f_t = ultimate tensile strength; E = modulus of elasticity; ε_t = ultimate tensile strain; F_b = bond strength.

9.2.4 Test Set-up and Instrumentation

Figure 9.3 presents the schematic test set-up used for testing the hybrid system. The test set-up components are spherical platen, steel rings, and thick steel plate. It should be noted that all the tests were done using a 2MN universal testing machine via a displacement control approach with a loading rate of 0.5 mm/min. For specimens in the longitudinal group (specimens with just CFRP strips), there were only two strain gauges installed axially at the center of two opposite CFRP strips. For all wrapped specimens, there were two strain gauges installed axially on two opposite sides on the GFRP wrap as well as two strain gauges in the hoop direction.

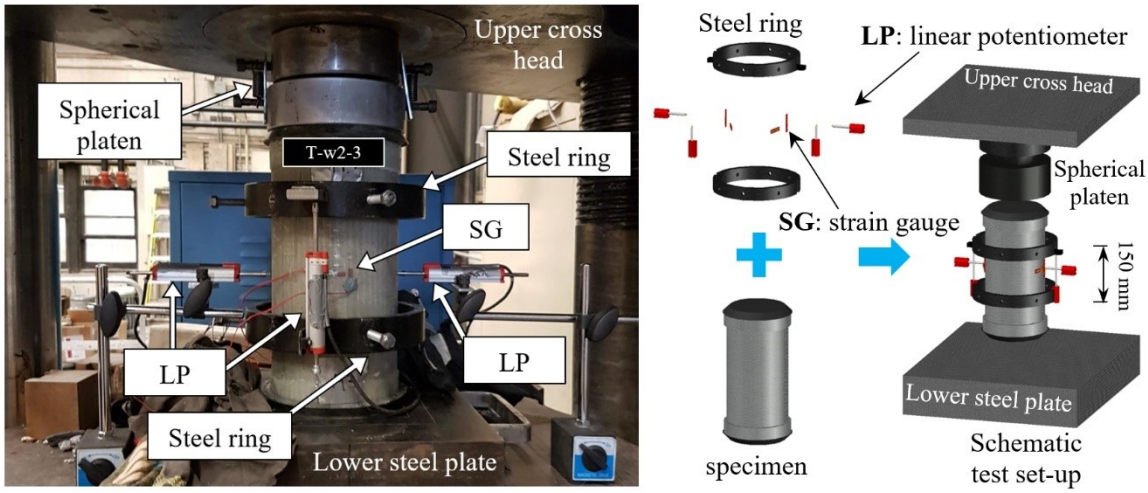

Figure 9. 3 Test set-up and instrumentation

In addition to strain gauges, four linear potentiometers (LPs) were installed for all groups of specimens. There were two steel rings in Figure 9.3, which were installed on the specimens to make vertical LPs measure the relative axial displacement. The center of steel rings was the same as the center of the specimen, and they were bolted to the specimens to make a gauge length of 150 mm as shown in Figure 9.3. It should be noted that LPs were necessary for capturing lateral strain of specimen built with only with plain concrete or the ones with only longitudinal CFRP strips. However, the LPs were used during the testing as a controlling tool for strain gauges. A data acquisition system with a frequency of 10 Hz recorded the strain, load and displacement values.

9.3 Experimental Results and Discussion

A summary of test results including peak loads and an average of the hoop and axial strains is presented in Table 9.3. The average peak load for the hybrid system and wrapped only system are 1274.7 kN and 1246.5 kN for two layers of wrapping., respectively.

Table 9. 3 Summary of test results

Group	Specimen ID	Strength (kN)	SG on CFRP	SG on GFRP		LP	
			$\varepsilon_{Axial\text{-}SG\text{-}C}$	$\varepsilon_{Axial\text{-}SG\text{-}G}$	$\varepsilon_{Lateral\text{-}SG}$	$\varepsilon_{Axial\text{-}LP}$	$\varepsilon_{Lateral\text{-}LP}$
Plain	P1	965.0	-	-	-	0.00300	0.00268
	P2	1046.9	-	-	-	0.00281	0.00275
	P3	1001.1	-	-	-	0.00295	0.00116
Longitudinal	L1	1099.8	0.00240	-	-	0.00094	0.00231
	L2	1183.0	0.00256	-	-	0.00158	0.00207
	L3	1199.7	0.00244	-	-	0.00191	0.00207
Transverse 2 layer wrap	T1-2w	1188.3	-	0.00374	0.01422	0.00788	0.01530
	T2-2w	1226.7	-	0.00678	0.01329	0.00895	0.01365
	T3-2w	1324.3	-	0.00932	0.01480	0.01193	0.01623
Hybrid 2 layer wrap	H1-2w	1280.3	0.00140	-	-	0.00292	0.00311
	H2-2w	1215.8	-	-	-	0.00297	0.01271
	H3-2w	1328.1	-	0.00320	0.00204	0.00302	0.00208
Transverse 4 layer wrap	T1-4w	1733.2	-	0.00985	0.01864	0.01285	0.01657
	T2-4w	1731.2	-	0.01405	0.01607	0.01309	0.01874
	T3-4w	1819.8	-	0.01751	0.01678	0.01477	0.02049
Hybrid 4 layer wrap	H1-4w	1712.5	-	-	0.01061	0.00865	0.00459
	H2-4w	1605.4	-	0.00477	0.01186	0.01011	0.00816
	H3-4w	1783.4	-	0.00635	0.01408	0.00629	0.01202

Note: $\varepsilon_{Axial\text{-}SG\text{-}C}$ = average axial strain gauge recording on CFRP strips; $\varepsilon_{Axial\text{-}SG\text{-}G}$ = average axial strain gauge recording on GFRP wrapping; $\varepsilon_{Lateral\text{-}SG}$ = average lateral strain gauge recording on GFRP wrapping; $\varepsilon_{Axial\text{-}LP}$ = average axial strain calculated from the recording of longitudinal LPs; $\varepsilon_{Lateral\text{-}LP}$ = equivalent lateral strain calculated from the recording of lateral LPs.

The results showed that the hybrid system with two layers of wrapping enhanced the capacity of the column by 2.8% with respect to the wrapped system and by 11.3% with respect to the longitudinal only system in which only longitudinal CFRP strips were used. However, for four layers of wrapping, the results. However, the average peak load for the hybrid system and wrapped only system were 1700.4 kN and 1761.4 kN for four layers of wrapping., respectively, which shows that the hybrid system gain was 6.1% less than only

wrapped system while 53.7% increase in capacity was observed with respect to the longitudinal only system. Therefore, it was observed that adding wrapping to longitudinal CFRP strips drastically increased the capacity of the columns while the only wrapped system is more effective in increasing the capacity of the columns without longitudinal CFRP strips.

Table 9. 4 Average test results at peak load

Group	P_u (kN)	Gain in Capacity (%)	ε_{long} (mm/mm)	$\Delta\varepsilon_{long}$ (mm/mm)	ε_{lat} (mm/mm)	$\Delta\varepsilon_{lat}$ (mm/mm)
Plain	1004.3	-	0.00292	-	0.00219	-
Longitudinal	1160.8	15.6	0.00197	-0.00095	0.00215	-0.00004
Transverse 2 layer wrap	1246.5	24.1	0.00810	0.00518	0.01458	0.01239
Hybrid 2 layer wrap	1274.7	26.9	0.00270	-0.00022	0.00499	0.00279
Transverse 4 layer wrap	1761.4	75.4	0.01369	0.01077	0.01788	0.01569
Hybrid 4 layer wrap	1700.4	69.3	0.00723	0.00431	0.01022	0.00803

Note: P_u = average of peak loads; ε_{long} = average longitudinal strain; ε_{lat} = average lateral strain; $\Delta\varepsilon_{long}$ = the additional longitudinal strain with respect to the plain group; $\Delta\varepsilon_{lat}$ = the additional lateral strain with respect to plain group.

The average capacities, the gain in the capacity, the average longitudinal strains, and the average lateral strains are presented in Table 9.4. The results showed that wrapped only group reached the peak load with 0.00540 mm/mm and 0.00959 mm/mm more longitudinal and lateral strains with respect to the hybrid system with two layers of wrapping, respectively, and 0.00646 mm/mm and 0.00766 for four layers of wrapping. Thus, the average strain recording at peak load showed that the hybrid system experienced much less longitudinal and lateral strains than the wrapped system at the peak load. Also, the results showed that the longitudinal only system and hybrid system with two layers of wrapping

experienced less longitudinal strain than the plain group. However, the wrapping caused an increase in lateral and longitudinal strains of the hybrid system with respect to only longitudinal system once the number of wrapping layers increased. Therefore, the gain in the capacity and increase in lateral and longitudinal strain with increasing the number of wrapping layers improved the overall behavior of the hybrid system. This improvement changed the modes of failure, as well, which is discussed in the following section.

9.3.1 Failure Modes

Figure 9.4 presents four different types of failure corresponding to different reinforcement systems. As shown in Figure 9.4(a), the longitudinal specimens (i.e. specimens that were only reinforced with longitudinal wrapping) were experienced debonding of the CFRP strips from the concrete specimens at the peak load which followed by a sudden drop in load-bearing capacity and buckling of CFRP strips. The capacity and stiffness of the specimens in the longitudinal group were enhanced in comparison to the plain specimens, although they were limited due to lack of lateral support for longitudinal CFRP strips and debonding. By strengthening longitudinal CFRP strips with 2 layers of GFRP wrapping, their axial capacity improved. However, there were observations that showed CFRP strips did not reach their crushing capacity and instead debonding cause separation between CFRP strips and concrete. Figure 9.4(c) shows the rupture of GFRP wrap for the hybrid system with two layers of wrapping, which was localized over one of the CFRP strips. It was possible that the debonding of CFRP laminate caused the buckling of one of the strips and formed a longitudinal pattern of rupture in GFRP wrapping.

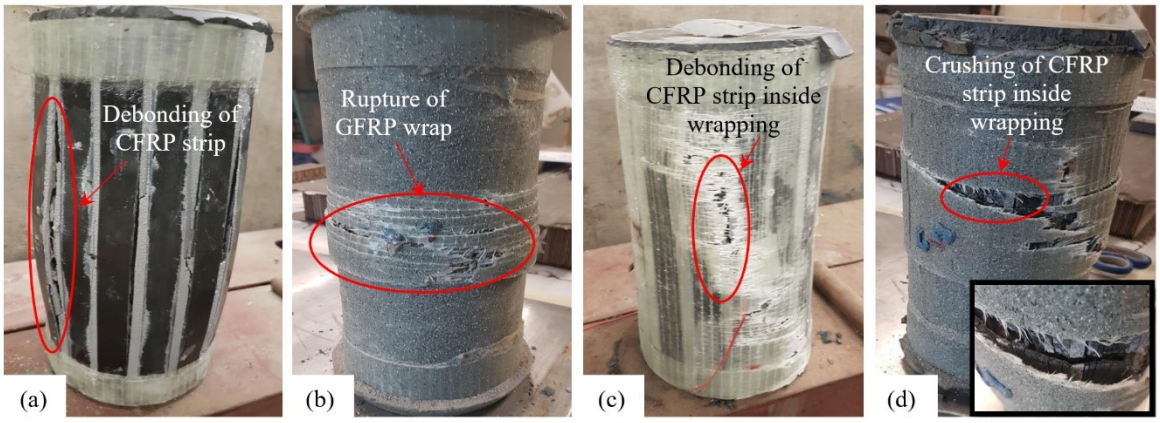

Figure 9. 4 Typical failure modes of phase I: (a) L-w0-1, (b) T-w4-1, (c) H-w2-1, and (d) H-w4-1

On the other hand, the specimens which were reinforced with only wrapping in hoop direction (both two and four layers of wrapping) show rupture of GFRP wrapping at the middle height of the specimen, and propagation of cracks in GFRP wrapping was along the hoop direction as shown in Figure 9.4(b). Therefore, the localized longitudinal rupture pattern of GFRP wrapping in hybrid specimens with two layers of GFRP wrapping can be attributed to the debonding of longitudinal CFRP strips and their buckling afterward. On the contrary, for hybrid specimens wrapped with four layers of GFRP, there was no observation of a longitudinal rupture pattern of GFRP wrapping. Instead, a rupture pattern similar to wrapped only specimens was observed as shown in Figure 9.4(d). Moreover, more evidence confirmed that idea after observing the specimen after failure; crushing of longitudinal CFRP strips was observed inside the GFRP wrapping. Also, the capacity of these specimens was significantly improved in comparison to the longitudinal or hybrid specimens with two layers of GFRP wrapping. Thus, providing specimens with more lateral support (i.e. using four layers wrapping instead of two layers) alternated the mode of failure from CFRP debonding and buckling to CFRP crushing. It can be concluded that minimum

lateral support by GFRP wraps was needed to ensure CFRP strips reach to crushing rather than their debonding and buckling (which cause a premature rupture for the GFRP wrap). Later in this paper, the mechanism of the failure is explained and verified.

9.3.2 Load-Strain Behavior

Figure 9.5 presents the load-strain curves of all specimens. The average load-strain curves and the capacity of each group of specimens are presented in Figure 9.6. Test results showed that the slope of load-strain curves for all specimens reinforced with longitudinal CFRP strips (i.e. L-w0, H-w2, and H-w4 groups) was higher than other specimens. In other words, it was observed that L-w0, H-w2, and H-w4 groups experienced the same loading history up to failure, as shown in Figure 9.6(a). As the strain in the specimens increased, due to the dilation of the concrete, the tendency for debonding of CFRP strips increased. Thus, the specimens which were not supported laterally (i.e. L-w0 group) experienced debonding of CFRP laminates following by their buckling before reaching the CFRP crushing strain. By adding 2 layers of GFRP wrapping, the lateral support for specimens in the H-w2 group was improved in comparison to the L-w0 group and they were able to sustain more load before failure and they failed at a higher strain level. Considering even two more layers of wrapping (i.e. four layers of GFRP wrapping) showed that even higher strain levels can be reached. The additional GFRP layers cause a decrease in concrete dilation and provide lateral support for the CFRP strips which, in turn, enable CFRP strips to sustain loads up to their crushing strain without experiencing any debonding or buckling. Therefore, the hybrid system was able to reach the maximum component level capacity (i.e. crushing of CFRP laminates).

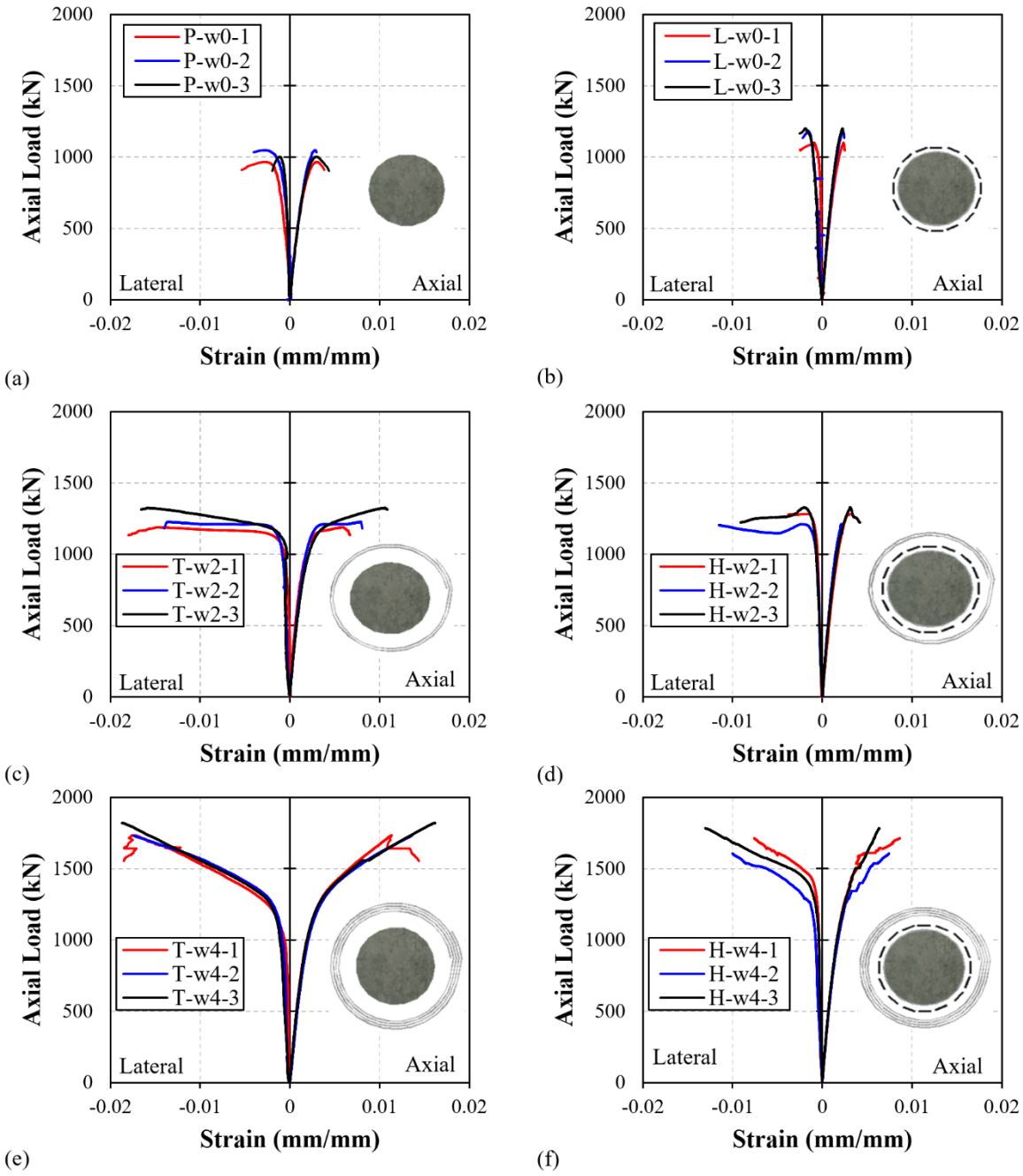

Figure 9. 5 Load-strain curves: (a) P-w0; (b) L-w0; (c) T-w2; (d) H-w2; (e) T-w4; and (f) H-w4

The load-strain curves in Figure 9.5 show that there is strain hardening behavior for only wrapped specimens (i.e. T-w2 and T-w4) as well as hybrid specimens wrapped with four layers of GFRP (i.e. H-4w). It should be noted that the presence of the GFRP wraps, in

addition to providing lateral support for the CFRP strips, provides confinement for the hybrid specimens with four layers of GFRP wrapping. However, for the hybrid specimens with two layers of wrapping, the load-strain curves showed a drop after the peak load which was considered with debonding and buckling of CFRP strips. Thus, load-strain curves showed two different behavior for the hybrid system which depends on layers of GFRP wrapping.

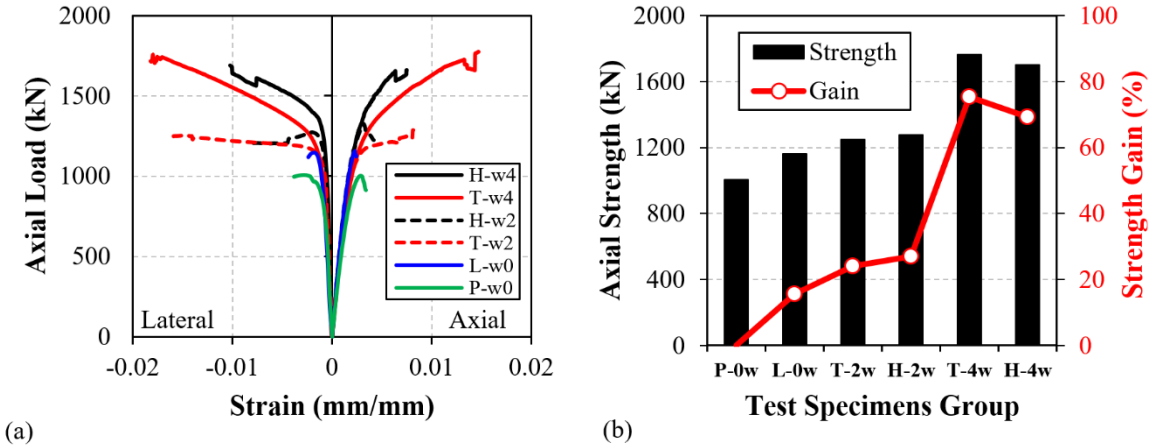

Figure 9. 6 Summary of test results: (a) average load-strain curves, and (b) average compressive strength

The average gain in the capacity of each group of the tested specimens is presented in Figure 9.6(b). The capacity of the hybrid specimens did not reach the capacity of the wrapped specimens with similar GFRP wrapping although the hybrid system with four layers of wrapping was successfully able to survive up to the crushing capacity of CFRP strips. The reason behind this difference in capacity is the difference between the modes of failure. While, for the wrapped specimens, the rupture of GFRP wrapping was corresponding to the peak load, for the hybrid specimens either debonding or crushing of CFRP strips caused failure initiation at peak load at lower levels of strain. Therefore, for the hybrid system, the controlling part is longitudinal CFRP strips and GFRP wrapping are

supporting elements whose presence is more important for the prevention of debonding and buckling of CFRP laminates. Thus, more layers of GFRP wrapping would not be economically proper for this system, since way before reaching the rupture of GFRP wrapping, CFRP laminate would be crushed. At the same time, fewer layers of GFRP wrapping would lead to debonding and buckling of CFRP laminates. Determination of this limit requires a solid experimental database that is out of the scope of the current study. However, this study showed that this limit exists, and that the system can be optimized to reach the component level capacity.

9.3.3 Confinement Effect

To study the effect of confinement in the hybrid system, the confining pressure of the tested specimens wrapped with GFRP were calculated using three different values as effective strain: a) the ultimate tensile strain found from the tensile test of coupons ($\varepsilon_{fe} = \varepsilon_{frp}$); b) the suggested effective strain suggested by ACI 440.2R -17 (2017) as 55 percent of the ultimate tensile strain ($\varepsilon_{fe} = 0.55\ \varepsilon_{frp}$); c) the hoop rupture strain of GFRP wraps at the time of failure or peak load ($\varepsilon_{fe} = \varepsilon_{h,rup}$). The confining pressure (f'_l) was calculated based on Equation 9.1 per ACI 440.2R-17 (2017).

$$f'_l = \frac{2E_f t_f \varepsilon_{fe}}{D} \tag{9.1}$$

Where D is the diameter of the concrete column (150 mm), E_f is the modulus of elasticity of GFRP wrap (25.7 GPa), t_f is the total thickness of GFRP wrapping (0.54 mm per layer), and ε_{fe} is the effective strain of GFRP wrapping. The calculated values for the confining pressure are presented in Table 9.5. Per ACI 440.2R-17 (2017), there is a limit of 0.08 for confining pressure (f'_l) over the unconfined concrete strength (f'_{co}) after which the

confinement is considered as effective. If the confinement ratio (f'_l / f'_{co}) is greater than 0.08, the stress-strain curve of confined concrete with FRP wrapping may have a descending branch. For two layers of wrapping, wrapped only specimens reached higher confinement limit than 0.08 in the tests and their stress-strain curves did not experience a descending branch and reached higher capacity than unconfined concrete strength while for the hybrid system the confinement ratio calculated from hoop rupture strain dd not pass the limit of 0.08. Therefore, the confinement was considered enough to be effective for wrapped specimens, but not for the hybrid specimen with two layers of wrapping. Once four layers of wrapping used, both groups showed confinement ratios higher than 0.08 as expected. Therefore, in this study, the confinement was considered as "activated" for four layers of wrapping and as "not activated" for two layers of wrapping for the hybrid system.

Table 9. 5 Confinement Effect

No.	Specimen ID	t_f (mm)	f'_{cc} (MPa)	f_{cc}/f'_{co}	$\varepsilon_{h,rup}$ (%)	$\varepsilon_{h,rup}$ /ε_{frp}	f_l (MPa)	$f_{l,0.55}$ (MPa)	$f_{l,hr}$ (MPa)	f_l/f'_{co}	$f_{l,0.55}$ /f'_{co}	$f_{l,hr}$ /f'_{co}
1	T-w2-1	1.08	67.2	1.18	1.80	1.19	5.63	3.09	6.67	0.10	0.05	0.12
2	T-w2-2	1.08	69.4	1.22	1.40	0.92	5.63	3.09	5.17	0.10	0.05	0.09
3	T-w2-3	1.08	74.9	1.32	1.66	1.09	5.63	3.09	6.14	0.10	0.05	0.11
4	H-w2-1	1.08	63.6	1.12	0.38	0.25	5.63	3.09	1.40	0.10	0.05	0.02
5	H-w2-2	1.08	56.6	1.00	1.15	0.76	5.63	3.09	4.26	0.10	0.05	0.08
6	H-w2-3	1.08	62.4	1.10	0.91	0.60	5.63	3.09	3.37	0.10	0.05	0.06
7	T-w4-1	2.16	98.1	1.73	1.85	1.22	11.25	6.19	13.70	0.20	0.11	0.24
8	T-w4-2	2.16	98.0	1.72	1.74	1.15	11.25	6.19	12.89	0.20	0.11	0.23
9	T-w4-3	2.16	103.0	1.81	1.87	1.23	11.25	6.19	13.86	0.20	0.11	0.24
10	H-w4-1	2.16	61.4	1.08	0.76	0.50	11.25	6.19	5.63	0.20	0.11	0.10
11	H-w4-2	2.16	60.3	1.06	1.00	0.66	11.25	6.19	7.41	0.20	0.11	0.13
12	H-w4-3	2.16	75.0	1.32	1.31	0.86	11.25	6.19	9.66	0.20	0.11	0.17

Note: $\varepsilon_{h,rup}$ = hoop rupture strain of GFRP wrapping read from column test; ε_{frp} = the ultimate tensile strain of GFRP wrap from tensile coupon tests; $f_{l,hr}$ = confining pressure calculated using $\varepsilon_{h,rup}$; $f_{l,0.55}$ = confining pressure calculated using 0.55 ε_{frp}; f_l = confining pressure calculated using ε_{frp}.

Also, the confined concrete strength (f'_{cc}) is presented in Table 9.5. For only wrapped specimens, the confined concrete strength was calculated simply by dividing the axial capacity recorded at the peak load by the cross-sectional area of the columns. However, for hybrid specimens, the effect of CFRP strips was deducted from the peak load to separate the confining effect and the effect of the longitudinal CFRP strips. The material tests showed that the stress-strain curve for FRPs is linear. Thus, the contribution of the CFRP strips (P_{CFRP}) was calculated by multiplying the cross-sectional area of all CFRP strips (A_{CFRP}), the modulus of elasticity of CFRP strips (E_{CFRP}), and the average value of strain recorded at the peak load (ε_{CFRP}), presented in Equation 9.2. The contribution of CFRP strips was deducted from the peak load (P_u) to give the load corresponding to the confined concrete ultimate load (P_{cc}), which in turn gives the confined concrete strength (f'_{cc}) by being divided by the cross-sectional area of the concrete column (A_c), presented in Equation 9.3 and Equation 9.4.

$$P_{CFRP} = A_{CFRP} \times E_{CFRP} \times \varepsilon_{CFRP} \tag{9.2}$$

$$P_{cc} = P_u - P_{CFRP} \tag{9.3}$$

$$f'_{cc} = \frac{P_{cc}}{A_c} \tag{9.4}$$

The results showed that the average confined concrete strength for only wrapped specimens and hybrid specimens were 70.5 MPa and 60.9 MPa for two layers of wrapping, respectively, and 99.7 MPa and 65.6 MPa for four layers of wrapping. By deducting the concrete strength for unconfined concrete (56.8 MPa), the gain in strength due to the presence of confining pressure for wrapped only specimens was determined as 13.7 MPa and 42.9 MPa, for two and four layers of wrapping, respectively. It should be highlighted

that for the hybrid system, these values are only 4.1 MPa and 8.8 MPa for two and four layers of wrapping, respectively. In other words, it was observed that the additional gain in strength due to wrapping for the hybrid system was reduced to 29.6% and 20.4% of the only wrapped system for two and four layers of wrapping, respectively. On the other hand, although the gain due to GFRP wrapping is reduced as wrapping layers increases, the wrapping served as the lateral support for the CFRP strips and assisted CFRP strips to sustain higher strains before peak load and to reach their ultimate compressive capacity by changing the mode of failure from debonding/ buckling of strips to crushing of them. Since the capacity of the hybrid system was more than only wrapped system for two layers of wrapping and was almost comparable to that for four layers of wrapping, the longitudinal CFRPs were effective and considerably contributed to the strength gain for the hybrid system. The latter is studied more in the following section by showing the mechanism of the hybrid system.

9.4 Failure Mechanism

In this section, an analytical approach is presented to determine the mechanism of the hybrid system through a cross-section analysis isolating the contribution of longitudinal CFRP strips and concrete core confined with transverse GFRP wraps. Figure 9.7 shows the typical load-strain curves of longitudinal CFRP strips, unconfined concrete, and confined concrete. To derive the load-strain curves, the loads at each strain can be derived by considering that a perfect bond is between CFRP laminate and concrete. Thus, at a certain axial strain, the stress of each component (i.e. concrete or CFRP laminates) can be found from the stress-stress curve of each component, and then by multiplying the area of each component by their corresponding stress the corresponding loads can be calculated. The

stress-strain relationship of the CFRP laminates was considered linear elastic. For unconfined concrete, the stress-strain curve proposed by Popovics (1973) was adopted while for confined concrete, the model proposed by ACI 440.2R (2017) was used.

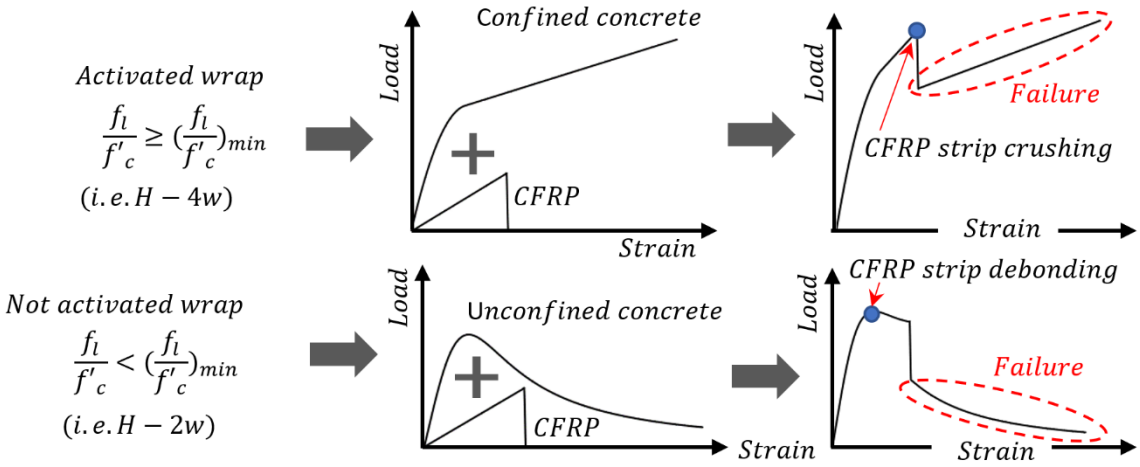

Figure 9. 7 Mechanics of the hybrid system

Two different scenarios can be introduced regarding the contribution of GFRP wrapping in the hybrid system depends on whether the wrap is activated or not activated, as shown in Figure 9.7. As it was observed in Figure 9.6(a), for the specimens with four layers of GFRP wrapping, there is a secondary slope in the load-strain curves which shows the confinement effect was contributed to the capacity (this case is named as an activated wrap in this study). However, for two layers of wrapping, there was no observation of the secondary slope in load-strain curves and no confinement effect was observed (this case is named as a not activated wrap in this study). The slope of load-strain curves was higher for all specimens with longitudinal CFRP strips while for the wrapped specimens the slope was the same as plain concrete specimens. The latter implies that in all hybrid specimens, CFRP was contributing to the load-carrying capacity. However, the system experienced failure once CFRP strips were deboned/ buckled or crushed. It was observed that for the specimens with

two layers of GFRP wrapping, the concrete was controlling the failure instead of CFRP strips. At the strain corresponding to the peak load of unconfined concrete, the debonding of CFRPs happened. For deriving the load-strain curve, if the load of unconfined concrete and CFRP strip were added at each strain level to give the total load of the hybrid system (without wrap activation), the debonding would happen at a strain corresponding to the peak load of unconfined concrete, as shown in Figure 9.7. In this case, the unconfined concrete wants to expand as the strain increases and after peak load the rate of expansion increases which causes the elimination of the bond between CFRP and concrete as well as the failure of the system. Moreover, the lateral support provided by two layers of wrapping is not sufficient to prevent the expansion of concrete. However, this lateral support causes a delay in the debonding of CFRP strips for two layers of GFRP wrapping in comparison to specimens without any lateral support. Figure 9.6(a) shows that the concrete specimens wrapped with longitudinal CFRPs with or without wrapping followed the same path in the load-strain curves, but the ones without any lateral support experience debonding of CFRPs earlier. In contrast, when there is enough lateral support, CFRPs continue to sustain loads after the peak load of unconfined concrete and even showed a secondary branch in their load-strain curves. The latter shows that both wrapping and CFRP laminates were effective in the load-carrying capacity of the system for this case. Therefore, to derive the load-strain curve of this case CFRP laminate load can be added to the confined concrete load to give the total load for the hybrid system (with wrap activation). The failure of the system governs by crushing of longitudinal CFRP laminates.

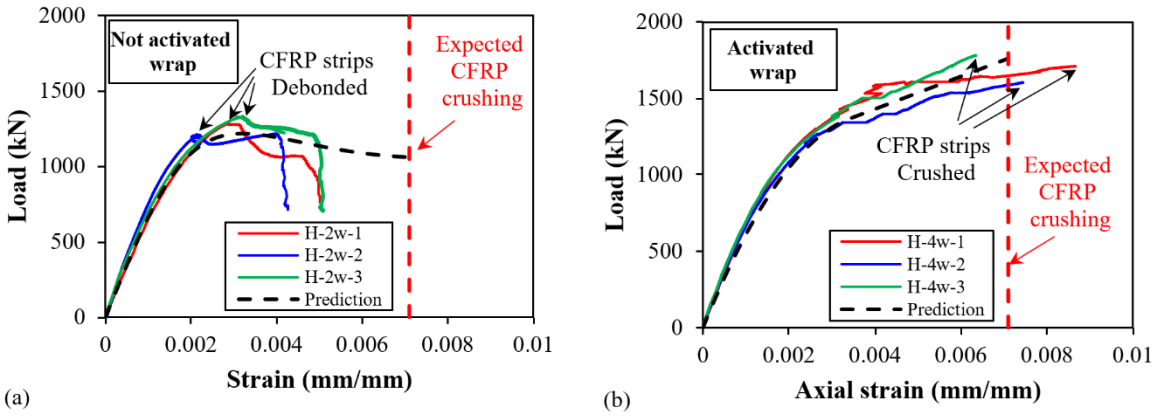

Figure 9. 8 Verification of the predictions based on the hybrid system mechanism: (a) Specimen H-2w without activated wrap, and (b) Specimen H-4w with activated wrap

The verification of the explained mechanism is presented in Figure 9.8, where the experimental load-strain test results and the prediction of the results based on the hybrid mechanism are in a very good agreement. As shown in Figure 9.8(a), for four layers of GFRP wrapping, the load at each strain can be calculated by combining the confined concrete and longitudinal CFRP strip loads up to crushing. In this case, the GFRP wrapping not only provides enough support for longitudinal CFRP to last up to its crushing but also provides confinement effect. Therefore, the dilation of concrete can be controlled by the confinement effect which prevents the debonding of CFRPs in turn. However, as shown in Figure 9.8(b), two layers of GFRP wraps were not able to provide enough lateral support for the concrete core and longitudinal CFRP strips, and the debonding of the strips at the peak load controlled the capacity of the specimens according to both experimental and analytical results.

Overall, the hybrid system is validated for concrete columns loaded axially, and it was observed that enough layers of wrapping (which is correlated to the amount of confining pressure provided by confining device) make it possible for CFRP strips to reach the

crushing strength in compression without buckling. Also, the system gains from both wrapping and longitudinal strips, but up to the crushing of the CFRP strips. Therefore, for pure compression, only wrapped system is more effective since there would be no interruption for GFRP wraps to reach higher strains and to give higher capacities. However, for slender columns or eccentrically loaded columns, where wrapping was not recognized as effective as in pure compressive loading, the hybrid system is expected to increase the capacity of the system due to providing additional flexural stiffness for the concrete column while longitudinal strips can reach their capacities due to presence of wrapping.

9.5 Future Research

It should be noted that in this study, only two different levels of confinement (i.e. 2 and 4 layers of GFRP wrapping) were considered. However, a confinement limit is required to determine if the hybrid mechanism should be considered with or without an activated wrapping effect. Moreover, this limit would be very economically effective since extra layers of wrapping would not lead to considerable change in the capacity of the system because the system is controlled by CFRP crushing if lateral support is enough. It should be also noted that for wrapped concrete columns, there is a limit of 0.08 for confinement pressure over unconfined concrete strength that was defined by ACI 440.2R (2017). The formula was derived based on experimental observations as well as using a mathematically derived formula for the collected database for confined concrete columns. Their major criterion was to find the confinement levels that make the corresponding strength to the FRP hoop rupture strain equal to or greater than the unconfined concrete strength (Spoelstra and Monti, 1999; Lam and Teng, 2003). However, the presence of CFRP strips between concrete and GFRP wrapping in the hybrid system, make the situation more complicated

since there might be no corresponding point to the rupture of GFRP wrapping since longitudinal CFRP failure, due to crushing or debonding, is before wrapping failure. Therefore, to establish the limit that dictates wrap activation, further studies and experimental evidence are required, and more experimental data assist in building a database and find the limit. It should be highlighted again that the experimental program was intended to characterize only the behavior of the hybrid system in the component level and check the validity of its performance for short columns and extend it to slender columns. However, the main application of the hybrid system is to enhance the performance of slender columns and to improve eccentrically loaded columns that require flexural stiffness. The latter requires further experimental studies and verification. Also, a numerical-analytical study would help to perform further analysis and doing a parametric study.

9.6 CONCLUSION

In this study, a total of eighteen short concrete columns were tested under pure axial loading up to failure to validate the effectiveness and performance of a hybrid strengthening system of longitudinal premanufactured bonded CFRP laminates laterally supported with GFRP wrapping. The following conclusions can be drawn:

- The experimental results validated the effectiveness of the hybrid strengthening system of longitudinal CFRP laminates and transverse GFRP wraps.
- The hybrid system is not efficient in axially loaded concrete columns since the capacity is controlled by the crushing of CFRP laminates and does not allow the system to reach the full capacity of the GFRP wrapping for short concrete columns and the hybrid system does not have an advantage over the wrapping system.

- For axially loaded short concrete columns, two major modes of failure for the hybrid system were observed: i) debonding of CFRP laminates following by rupture of GFRP wraps, and ii) crushing of CFRP laminates followed by rupture of GFRP wraps. The mode of failure changed as the number of GFRP wrapping increased and caused the mode of failure change from buckling/ debonding of CFRP strips to crushing of CFRPs in compression followed by the rupture of GFRP wrapping.
- The mechanism of the hybrid system was determined for the short concrete columns. For two layers of GFRP wrapping, the total load capacity of the hybrid system can be calculated by adding the load capacity of unconfined concrete core and the load capacity of CFRP strips at a strain corresponding to the peak load of unconfined concrete (wrapping is not activated). For four layers of GFRP wrapping, the total load capacity of the hybrid system can be calculated by adding the load capacity of the confined concrete core at a strain corresponding to the crushing strain of CFRP strips and the full load capacity of CFRP strips (wrapping is activated). The system followed the same path on the load-strain curves and fails based on the level of the lateral support. For the hybrid system with two layers of GFRP wrapping, the debonding of longitudinal CFRPs happened at the peak load of unconfined concrete. For the hybrid system with four layers of wrapping, the crushing of CFRP laminates controlled the system failure.
- This study is the experimental validation of the performance of the system and more evidence is required to evaluate the hybrid system. Thus, further studies are required to assess the activation limit of the hybrid system and its application for the strengthening of slender concrete columns by conducting more experimental tests.

A verified numerical model for the system should be developed to perform a parametric study and suggestion for the design. Also, safety and reliability-based analysis is required to assess the safety of the studied hybrid system.

Acknowledgments

The authors would like to thank Jordan Maerz, Brian Kennedy, and Jesse Keane for their assistance in the lab, and Raghad Kassab for providing test results of tensile GFRP coupons. The authors would also like to acknowledge and thank NSERC and Dalhousie University for their financial support as well as Sika Canada for providing CFRP laminates and adhesive material.

References

Abdallah, M. H., Mohamed, H. M., and Masmoudi, R. (2018). Experimental assessment and theoretical evaluation of axial behavior of short and slender CFFT columns reinforced with steel and CFRP bars. *Construction and Building Materials*, 181, 535–550.

ACI 318-19. (2019). Building Code Requirements for Structural Concrete. *American Concrete Institute.* Farmington Hills, MI.

ACI 440.2R. (2008). Guide for the Design and Construction of Externally Bonded FRP Systems for Strengthening Concrete Structures. *American Concrete Institute.* Farmington Hills, MI.

Alkhrdaji, T., Nanni, A., Chen, G., and Barker, M. (1999). Upgrading the Transportation Infrastructure: Solid RC Decks Strengthened with FRP. *Concrete International: Design and Construction*, 21(10), 37-41.

Al-Nimry, H., and Soman, A. (2018). On the slenderness and FRP confinement of eccentrically-loaded circular RC columns. *Engineering Structures*, 164, 92-108.

Al-Salloum, Y. A., Al-Amri, G. S., Siddiqui, N. A., Almusallam, T. H., and Abbas, H. (2018). Effectiveness of CFRP Strengthening in Improving Cyclic Compression Response of Slender RC Columns. *Journal of Composites for Construction*, 22(3), 04018009.

Ashour, A., El-Refaie, S., and Garrity, S. (2004). Flexural strengthening of RC continuous beams using CFRP laminates. *Cement and concrete composites*, 26(7), 765-775.

ASTM D3039/D3039M-14. (2014). Standard Test Method for Tensile Properties of Polymer Matrix Composite Materials. *American Society for Testing and Materials.* West Conshohocken, PA.

ASTM D6641/D6641M-16. (2016). Standard Test Method for Compressive Properties of Polymer Matrix Composite Materials Using a Combined Loading Compression (CLC) Test Fixture. *American Society for Testing and Materials.* West Conshohocken, PA.

Atadero, R., Lee, L., and Karbhari, V. M. (2005). Consideration of material variability in reliability analysis of FRP strengthened bridge decks. *Composite Structures*, 70(4), 430-443.

Bisby, L., and Ranger, M. (2010). Axial–flexural interaction in circular FRP-confined reinforced concrete columns. *Construction and Building Materials*, 24(9), 1672-1681.

Buyukozturk, O., and Hearing, B. (1998). Failure behavior of precracked concrete beams retrofitted with FRP. *Journal of composites for construction*, 138-144.

Chaallal, O., and Shahawy, M. (2000). Performance of Fiber-Reinforced Polymer-Wrapped Reinforced Concrete Column under Combined Axial-Flexural Loading. *ACI Structural Journal*, 97(4), 659-668.

Chellapandian, M., Suriya Prakash , S., and Raj, A. (2018). Analytical and finite element studies on hybrid FRP strengthened RC column elements under axial and eccentric compression. *Composite Structures*, 184, 234-248.

CSA S806-12. (2012). Design and construction of building structures with fiber-reinforced polymers. *Canadian Standards Association.*

Cui, C., and Sheikh, S. A. (2010). Cui, C., and S. A. Sheikh. Experimental study of normal- and high-strength concrete confined with fiber-reinforced polymers. *Journal of Composites for Construction*, 14(5), 553-561.

Elchalakani, M., Karrech, A., Dong, M., Alib, M., and Yang, B. (2018). Experiments and Finite Element Analysis of GFRP Reinforced Geopolymer Concrete Rectangular Columns Subjected to Concentric and Eccentric Axial Loading. *Structures*, 14, 273-289.

Fillmore, B., and Sadeghian, P. (2018). Contribution of longitudinal glass fiber-reinforced polymer bars in concrete cylinders under axial compression. *Canadian Journal of Civil Engineers*, 45, 458-468.

Gajdosova, K., and Bilcik, J. (2013). Full-scale testing of CFRP-strengthened slender reinforced concrete columns. *Journal of composites for construction*, 17, 239-248.

Guérin, M., Mohamed, H. M., Benmokrane, B., Nanni, A., and Shield, C. K. (2018a). Eccentric Behavior of Full-Scale Reinforced Concrete Columns with Glass Fiber-Reinforced Polymer Bars and Ties. *ACI Structural Journal*, 115(2), 489-499.

Hadi, M. (2006). Behaviour of FRP wrapped normal strength concrete columns under eccentric loading. *Composite Structures*, 72(4), 503-511.

Khorramian, K., and Sadeghian, P. (2017a). Experimental and analytical behavior of short concrete columns reinforced with GFRP bars under eccentric loading. *Engineering Structures*, 761–773.

Khorramian, K., and Sadeghian, P. (2017b). Short Concrete Columns Reinforced with GFRP Rebars Under Eccentric Loading. *CSCE Annual Conference. Vancouver, BC, Canada: Canadian Society of Civil Engineering.*

Khorramian, K., and Sadeghian, P. (2017c). Strengthening Concrete Columns Using Near Surface Mounted (NSM) Carbon Fiber Reinforced Polymer (CFRP) Laminates. *Sixth Asia-Pacific Conference on FRP in Structures. Singapore, Singapore.*

Khorramian, K., and Sadeghian, P. (2018a). New Testing Method of GFRP Bars in Compression. *CSCE Annual Conference. Fredericton, NB, Canada: Canadian Society of Civil Engineering.*

Khorramian, K., and Sadeghian, P. (2018b). Strengthening of Slender Circular Concrete Columns with Longitudinal CFRP Laminates and Transverse GFRP wraps. *CSCE Annual Conference. Fredericton, NB, Canada: Canadian Society of Civil Engineering.*

Khorramian, K., and Sadeghian, P. (2018c). Strengthening Short Concrete Columns Using Longitudinally Bonded CFRP Laminates. *ACI Special Publication*, 327, 24-1:10.

Khorramian, K., and Sadeghian, P. (2019a). Behavior of Slender GFRP Reinforced Concrete Columns. *ASCE-SEI Structures Congress, American Society of Civil Engineers.* St. Louis, Missouri, USA.

Khorramian, K., and Sadeghian, P. (2019b). Material Characterization of GFRP Bars in Compression using a New Test Method. *Journal of Testing and Evaluation (ASTM)*, 49, 2.

Khorramian, K., and Sadeghian, P. (2019c). Performance of high-modulus near-surface-mounted FRP laminates for strengthening of concrete columns. *Composites Part B*, 164, 90-102.

Khorramian, K., and Sadeghian, P. (2020). Experimental Investigation of Short and Slender Rectangular Concrete Columns Reinforced with GFRP Bars under Eccentric Axial Loads. *Journal of Composites for Construction, under review.*

Kim, Y. J., Longworth, J. M., and Wight, G. R. (2008). Flexure of Two-Way Slabs Strengthened with Prestressed or Non prestressed CFRP Sheets. *Journal of Composites for Construction*, 12(4), 366-374.

Lam, L., and Teng, J. (2003). Design-oriented stress–strain model for FRP-confined concrete. *Construction and building materials*, 2003(6-7), 471-489.

Lin, G., and Teng, J. G. (2019). Stress-strain model for FRP-confined concrete in eccentrically loaded circular columns. *Journal of Composites for Construction*, 23(3), 04019017.

Malek, A. M., Saadatmanesh, H., and Ehsani, M. R. (1998). Prediction of failure load of R/C beams strengthened with FRP plate due to stress concentration at the plate end. *ACI structural Journal*, 142-152.

Mohamed, H. M., Afifi, M. Z., and Benmokrane, B. (2014). Performance Evaluation of Concrete Columns Reinforced Longitudinally with FRP Bars and Confined with FRP Hoops and Spirals under Axial Load. *Journal of Bridge Engineering*, 19(7), 04014020.

Mosallam, A. S., and Mosalam, K. M. (2003). Strengthening of two-way concrete slabs with FRP composite laminates. *Construction and Building Materials*, 17(1), 43-54.

Nanni, A., and Bradford, N. (1995). FRP jacketed concrete under uniaxial compression. *Construction and Building Materials*, 9(2), 115-124.

Ozbakkaloglu, T. (2013). Compressive behavior of concrete-filled FRP tube columns: Assessment of critical column parameters. *Engineering Structures*, 51, 188-199.

Parvin, A., and Wang, W. (2001). Behaviour of FRP jacketed concrete columns under eccentric loading. *Journal of Composites for Construction*, 5(3), 146-152.

Pessiki, S., Harries, K. A., Kestner, J. T., Sause, R., and Ricles, J. M. (2001). Axial Behavior of Reinforced Concrete Columns Confined with FRP Jackets. *Journal of Composites for Construction*, 5(4), 237-245.

Popovics, S. (1973). A Numerical Approach to the Complete Stress-Strain Curve of Concrete. *Cements and Concrete Research*, 3(5), 583-599.

Rahimi, H., and Hutchinson, A. (2001). Concrete Beams Strengthened with Externally Bonded FRP Plates. *Journal of Composites for Construction*, 5(1), 44-56.

Sadeghian, P., and Fam, A. (2015). Strengthening slender reinforced concrete columns using high-modulus bonded longitudinal reinforcement for buckling control. *Journal of structural Engineering*, 141, 04014127.

Sadeghian, P., Rahai, A. R., and Ehsani, M. R. (2010). Experimental study of rectangular RC columns strengthened with CFRP composites under eccentric loading. *Journal of Composites for Construction*, 443-450.

Shaat, A., and Fam, A. Z. (2009). Slender Steel Columns Strengthened Using High-Modulus CFRP Plates for Buckling Control. *Journal of Composites for Construction*, 13(1), 2-12.

Shahawy, M., Arockiasamy, M., Beitelman, T., and Sowrirajan, R. (1996). Reinforced concrete rectangular beams strengthened with CFRP laminates. *Composites Part B: Engineering*, 27(3-4), 225-233.

Sharif, A., Al-Sulaimani, G. J., Basunbul, I. A., Baluch, M. H., and Ghaleb, B. N. (1994). Strengthening of Initially Loaded Reinforced Concrete Beams Using FRP Plates. *ACI structural Journal*, 91(2), 160-168.

Siddiqui, N. A., Alsayed, S. H., Al-Salloum, Y. A., Iqbal, R. A., and Abbas, H. (2014). Experimental investigation of slender circular RC columns strengthened with FRP composites. *Construction and Building Materials*, 69, 323–334.

Smith, S. T., Kim, S. J., and Zhang, H. (2010). Behavior and Effectiveness of FRP Wrap in the Confinement of Large Concrete Cylinders. *Journal of Composites for Construction*, 14(5), 573-582.

Spoelstra, M. R., and Monti, G. (1999). FRP-Confined Concrete Model. *Journal of Composites for Construction*, 3(3), 143-150.

Tarek, H., and Rizkalla, S. (2002). Flexural Strengthening of Prestressed Bridge Slabs with FRP systems. *PCI Journal*, 47(1), 76-93.

Tobbi, H., Farghaly, A. S., and Benmokrane, B. (2012). Concrete Columns Reinforced Longitudinally and Transversally with Glass Fiber-Reinforced Polymer Bars. *ACI Structural Journal*, 109(4), 551-558.

Toutanji, H. A. (1999). Stress-strain characteristics of concrete columns externally confined with advanced fiber composite sheets. *ACI materials journal*, 397-404.

Triantafillou, T. C., and Plevris, N. (1992). Strengthening of RC beams with epoxy-bonded fibre-composite materials. *Materials and Structures*, 25, 201-211.

Xiao, Y., and Wu, H. (2000). Compressive Behavior of Concrete Confined by Carbon Fiber Composite Jackets. *Journal of Materials in Civil Engineering*,12(2), 139–146.

Xue, W., Peng, F., and Fang, Z. (2018). Behavior and Design of Slender Rectangular Concrete Columns Longitudinally Reinforced with Fiber-Reinforced Polymer Bars. *ACI Structural Journal*, 115(2), 311-322.

Yu, F., Xu, G., Niu, D., Cheng, A., Wua, P., and Kong, Z. (2018). Experimental study on PVC-CFRP confined concrete columns under low cyclic loading. *Construction and Building Materials*, 177, 287–302.

CHAPTER 10 PLASTICITY-BASED ULTIMATE CONDITION AND CONFINED STRESS-STRAIN MODEL FOR FRP WRAPPED CIRCULAR CONCRETE COLUMNS

ABSTRACT

The analysis and design of FRP-confined concrete columns required the knowledge of axial stress-strain behavior and the ultimate condition of the system. While many sophisticated analysis-oriented models have been developed during the past decades, the design guidelines and practice engineers use the design-oriented models for their simplicity and accuracy. However, most of the available design-oriented models were empirically developed using a variety of regression techniques to estimate the ultimate condition of FRP-confined concrete. Moreover, most of the studies derived the stress-strain curves using a large database that incorporated the ultimate condition, instead of the full experimental stress-strain curves. Therefore, there is a gap for improvement of the design-oriented models using a mechanics-based approach. Thus, in this study, a five parameter William-Warnke plasticity model was utilized to find a new design-oriented equation for the ultimate condition with an updated database of 788 FRP-wrapped concrete specimens. Also, a new stress-strain curve model was proposed using 200 full stress-strain experimental curves extracted from sixteen different independent studies. A comparison of the experimental ultimate condition and stress-strain curves with the proposed model and the available models in the literature revealed very good accuracy for the proposed model and improvement of the available design-oriented models.

10.1 INTRODUCTION

It has been almost four decades that FRP-confined concrete columns are being continuously investigated by researchers and various predictions of the stress-strain curves and the ultimate condition is being updated. Recent studies showed that the finite element modelling (FEM) of the FRP-confined concrete is in a very agreement with the experimental tests (Ferrotto et al., 2018; Jawdhari et al., 2020; Piscesa et al., 2018; Yu et al., 2010). The requirement for accurate FEM modelling is precise plasticity-based failure criteria and damage models. Thus, many researchers focused on the development of characteristics of failure surfaces of FRP-confined concrete columns using Mohr-Coulomb criterion (Moran et al., 2019; Moran and Pantelides, 2012) and Drucker-Prager failure criterion (Jiang and Wu, 2016; Mohammadi et al., 2019) as well as developing damage models (Mohammadi and Wu, 2019; Ozbakkaloglu et al., 2016; Saberi et al., 2020). The latter shows the importance of the plasticity-based modeling which can be incorporated into the prediction of ultimate confined strength of FRP-confined concrete column. The literature showed that only a few studies considered a plasticity-based approach to develop estimation for the ultimate confined strength (Afifi et al., 2015; Bing et al., 2001; Hales et al., 2017; Mander et al., 1988; Wu and Zhou, 2010; Yan et al., 2006) while most of the available models were empirically developed using a variety of regression techniques (Bisby et al., 2005; Fallah Pour et al., 2018; Karbhari and Gao, 1997; Lam and Teng, 2003; Richart et al., 1928; Saafi et al., 1999; Sadeghian and Fam, 2015; Samaan et al., 1998; Teng et al., 2009; Toutanji, 1999). Mander et al. (1988) developed a model to predict the strength of the concrete confined by steel reinforcement using a five-parameter Willam-Warnke model (Willam and Warnke, 1975) which was later improved by Bing et al. (2001)

transverse steel. Later, Afifi et al. (2015) and Hales et al. (2017) for FRP ties and spirals. Yan and Pantelides (2006), calibrated the model for FRP-wrapped concrete columns. However, the test data used for the calibration was limited (i.e. less than 20 data points). Recently, an updated database of 788 FRP-confined concrete columns is available in the literature (Sadeghian and Fam, 2015) and Table 10.1. Therefore, there is a gap in the assessment of the ultimate confined strength using a mechanics-based model which engages the most recent FRP-confined column database.

Table 10. 1 Experimental Database containing 260 Cylindrical specimens confined with unidirectional FRP wraps in the hoop direction

No.	Source of data	Fiber type	D (mm)	t_f (mm)	E_f (GPa)	f'_{co} (MPa)	f'_{cc} (MPa)	f'_{cc} / f'_{co}	ε_{co} (%)	ε_{cc} (%)	ε_{cc} / ε_{co}	$\varepsilon_{h,rup}$ (%)
1	Rousakis (2001)	C	150	0.17	377	25.2	41.6	1.65	0.21	1.44	6.84	0.70
2	Rousakis (2001)	C	150	0.17	377	25.2	38.8	1.54	0.21	1.21	5.74	0.58
3	Rousakis (2001)	C	150	0.34	377	25.2	60.1	2.38	0.21	1.88	8.96	0.64
4	Rousakis (2001)	C	150	0.34	377	25.2	55.9	2.22	0.21	2.10	9.99	0.55
5	Rousakis (2001)	C	150	0.51	377	25.2	67.0	2.66	0.21	2.45	11.68	0.45
6	Rousakis (2001)	C	150	0.51	377	25.2	67.3	2.67	0.21	2.43	11.58	0.37
7	Rousakis (2001)	C	150	0.17	377	47.4	72.3	1.53	0.25	1.09	4.41	0.77
8	Rousakis (2001)	C	150	0.17	377	47.4	64.4	1.36	0.25	0.87	3.52	0.51
9	Rousakis (2001)	C	150	0.34	377	47.4	82.4	1.74	0.25	1.40	5.69	0.66
10	Rousakis (2001)	C	150	0.34	377	47.4	82.4	1.74	0.25	1.35	5.49	0.54
11	Rousakis (2001)	C	150	0.51	377	47.4	96.3	2.03	0.25	1.59	6.45	0.44
12	Rousakis (2001)	C	150	0.51	377	47.4	95.2	2.01	0.25	1.69	6.86	0.58
13	Rousakis (2001)	C	150	0.17	377	51.8	78.7	1.52	0.25	0.75	2.98	0.54
14	Rousakis (2001)	C	150	0.17	377	51.8	72.8	1.41	0.25	0.66	2.64	0.40
15	Rousakis (2001)	C	150	0.34	377	51.8	95.4	1.84	0.25	1.05	4.17	0.55
16	Rousakis (2001)	C	150	0.34	377	51.8	90.7	1.75	0.25	1.00	3.98	0.36
17	Rousakis (2001)	C	150	0.51	377	51.8	110.5	2.13	0.25	1.29	5.14	0.44
18	Rousakis (2001)	C	150	0.51	377	51.8	103.6	2.00	0.25	1.20	4.79	0.31
19	Rousakis (2001)	C	150	0.85	377	51.8	112.7	2.18	0.25	1.59	6.34	0.29
20	Rousakis (2001)	C	150	0.85	377	51.8	126.7	2.45	0.25	1.61	6.41	0.36
21	Dai et al. (2011)	A	152	0.17	115	39.2	61.4	1.57	0.23	2.33	9.94	3.16
22	Dai et al. (2011)	A	152	0.17	115	39.2	62.7	1.60	0.23	2.33	9.94	3.13
23	Dai et al. (2011)	A	152	0.17	115	39.2	55.8	1.42	0.23	2.07	8.83	3.21
24	Dai et al. (2011)	A	152	0.34	115	39.2	90.1	2.30	0.23	3.80	16.21	2.89
25	Dai et al. (2011)	A	152	0.34	115	39.2	88.3	2.25	0.23	3.45	14.71	3.05
26	Dai et al. (2011)	A	152	0.34	115	39.2	83.3	2.13	0.23	3.68	15.70	2.96
27	Dai et al. (2011)	A	152	0.51	115	39.2	113.2	2.89	0.23	4.39	18.72	2.74
28	Dai et al. (2011)	A	152	0.51	115	39.2	116.3	2.97	0.23	4.60	19.62	2.46
29	Dai et al. (2011)	A	152	0.51	115	39.2	118.0	3.01	0.23	4.78	20.39	2.97
30	Liang et al. (2012)	C	100	0.17	242	25.9	64.3	2.48	0.21	2.31	10.93	1.48
31	Liang et al. (2012)	C	100	0.17	242	25.9	63.0	2.43	0.21	1.93	9.13	1.07
32	Liang et al. (2012)	C	100	0.17	242	25.9	66.4	2.56	0.21	2.16	10.22	1.39
33	Liang et al. (2012)	C	100	0.17	242	25.9	64.8	2.50	0.21	2.16	10.22	1.22
34	Liang et al. (2012)	C	200	0.33	242	22.7	64.3	2.83	0.20	2.29	11.20	1.09
35	Liang et al. (2012)	C	200	0.33	242	22.7	69.1	3.04	0.20	2.37	11.59	1.12
36	Liang et al. (2012)	C	200	0.33	242	22.7	60.1	2.65	0.20	2.00	9.78	0.89
37	Liang et al. (2012)	C	200	0.33	242	22.7	66.3	2.92	0.20	2.48	12.13	1.16
38	Liang et al. (2012)	C	300	0.50	242	24.5	58.8	2.40	0.21	1.84	8.83	0.98

Table 10.1 Continued

No.	Source of data	Fiber type	D (mm)	t_f (mm)	E_f (GPa)	f'_{co} (MPa)	f'_{cc} (MPa)	f'_{cc} / f'_{co}	ε_{co} (%)	ε_{cc} (%)	ε_{cc} / ε_{co}	$\varepsilon_{h,rup}$ (%)
39	Liang et al. (2012)	C	300	0.50	242	24.5	59.4	2.42	0.21	1.71	8.20	1.33
40	Liang et al. (2012)	C	300	0.50	242	24.5	63.0	2.57	0.21	2.27	10.89	1.70
41	Liang et al. (2012)	C	300	0.50	242	24.5	60.6	2.47	0.21	2.09	10.03	1.22
42	Vincent and Ozbakkaloglu (2013)	C	152	0.12	240	35.5	44.0	1.24	0.23	0.77	3.37	1.20
43	Vincent and Ozbakkaloglu (2013)	C	152	0.12	240	35.5	43.9	1.24	0.23	0.82	3.59	1.10
44	Vincent and Ozbakkaloglu (2013)	C	152	0.12	240	35.5	43.1	1.21	0.23	0.82	3.59	1.10
45	Vincent and Ozbakkaloglu (2013)	C	152	0.23	240	38.0	63.5	1.67	0.23	1.51	6.49	1.17
46	Vincent and Ozbakkaloglu (2013)	C	152	0.23	240	38.0	66.1	1.74	0.23	1.65	7.09	1.17
47	Vincent and Ozbakkaloglu (2013)	C	152	0.23	240	36.1	58.6	1.62	0.23	1.27	5.53	1.11
48	Vincent and Ozbakkaloglu (2013)	A	152	0.60	120	49.4	109.0	2.21	0.25	3.73	15.02	2.54
49	Vincent and Ozbakkaloglu (2013)	A	152	0.60	120	49.4	103.4	2.09	0.25	3.40	13.69	2.10
50	Vincent and Ozbakkaloglu (2013)	A	152	0.60	120	49.4	105.3	2.13	0.25	3.37	13.57	2.08
51	Vincent and Ozbakkaloglu (2013)	A	152	0.60	120	49.4	107.7	2.18	0.25	3.41	13.73	2.18
52	Vincent and Ozbakkaloglu (2013)	A	152	0.60	120	49.4	104.0	2.11	0.25	3.22	12.96	2.12
53	Vincent and Ozbakkaloglu (2013)	A	152	0.60	120	49.4	110.1	2.23	0.25	3.48	14.01	2.22
54	Song et al. (2013)	C	100	0.13	237	22.4	56.2	2.51	0.20	0.90	4.43	0.87
55	Song et al. (2013)	C	100	0.26	237	22.4	78.2	3.49	0.20	1.76	8.64	0.94
56	Song et al. (2013)	C	100	0.39	237	22.4	118.7	5.30	0.20	3.31	16.25	1.07
57	Song et al. (2013)	C	150	0.13	237	22.4	45.7	2.04	0.20	1.22	5.97	1.12
58	Song et al. (2013)	C	150	0.26	237	22.4	65.4	2.92	0.20	2.00	9.81	1.18
59	Song et al. (2013)	C	150	0.39	237	22.4	85.0	3.79	0.20	2.56	12.58	1.21
60	Song et al. (2013)	C	100	0.13	237	40.9	71.1	1.74	0.24	1.98	8.37	0.92
61	Song et al. (2013)	C	100	0.26	237	40.9	97.6	2.39	0.24	1.65	6.95	1.04
62	Song et al. (2013)	C	100	0.39	237	40.9	125.0	3.06	0.24	2.18	9.20	1.03
63	Song et al. (2013)	C	150	0.13	237	40.9	57.1	1.40	0.24	0.87	3.66	1.24
64	Song et al. (2013)	C	150	0.26	237	40.9	78.4	1.92	0.24	1.42	5.97	1.07
65	Song et al. (2013)	C	150	0.39	237	40.9	100.4	2.45	0.24	1.89	7.99	1.16
66	Lim and Ozbakkaloglu (2014a)	A	150	0.20	129	29.6	52.5	1.77	0.22	2.12	9.70	2.13
67	Lim and Ozbakkaloglu (2014a)	A	150	0.20	129	29.6	50.3	1.70	0.22	1.95	8.92	1.88
68	Lim and Ozbakkaloglu (2014a)	A	150	0.20	129	29.6	50.5	1.71	0.22	2.01	9.20	1.84
69	Lim and Ozbakkaloglu (2014a)	C	150	0.17	236	29.6	57.3	1.94	0.22	1.84	8.42	1.52
70	Lim and Ozbakkaloglu (2014a)	C	150	0.17	236	29.6	60.4	2.04	0.22	2.03	9.29	1.52
71	Lim and Ozbakkaloglu (2014a)	C	150	0.17	236	29.6	61.2	2.07	0.22	2.23	10.20	1.50
72	Lim and Ozbakkaloglu (2014a)	G	150	0.20	95	29.6	50.8	1.72	0.22	1.82	8.33	2.00
73	Lim and Ozbakkaloglu (2014a)	G	150	0.20	95	29.6	46.6	1.57	0.22	1.51	6.91	1.89
74	Lim and Ozbakkaloglu (2014a)	G	150	0.20	95	29.6	49.4	1.67	0.22	2.02	9.24	2.00
75	Lim and Ozbakkaloglu (2014a)	A	150	0.40	129	49.6	83.1	1.68	0.25	2.60	10.46	1.80
76	Lim and Ozbakkaloglu (2014a)	A	150	0.40	129	49.6	87.2	1.76	0.25	2.32	9.33	1.80
77	Lim and Ozbakkaloglu (2014a)	A	150	0.40	129	49.6	84.0	1.69	0.25	2.75	11.06	1.77
78	Lim and Ozbakkaloglu (2014a)	C	150	0.33	236	49.6	98.0	1.98	0.25	2.48	9.97	1.22
79	Lim and Ozbakkaloglu (2014a)	C	150	0.33	236	49.6	95.3	1.92	0.25	2.17	8.73	1.33
80	Lim and Ozbakkaloglu (2014a)	C	150	0.33	236	49.6	100.3	2.02	0.25	2.07	8.32	1.36
81	Lim and Ozbakkaloglu (2014a)	G	150	0.40	95	49.6	78.3	1.58	0.25	1.82	7.32	1.59
82	Lim and Ozbakkaloglu (2014a)	G	150	0.40	95	49.6	75.6	1.52	0.25	1.85	7.44	1.69
83	Lim and Ozbakkaloglu (2014a)	G	150	0.40	95	49.6	71.4	1.44	0.25	1.42	5.71	1.23
84	Lim and Ozbakkaloglu (2014a)	A	150	0.60	129	74.1	123.5	1.67	0.27	2.28	8.29	1.69
85	Lim and Ozbakkaloglu (2014a)	A	150	0.60	129	74.1	126.4	1.71	0.27	2.51	9.13	1.80
86	Lim and Ozbakkaloglu (2014a)	A	150	0.60	129	74.1	108.8	1.47	0.27	2.09	7.60	1.35
87	Lim and Ozbakkaloglu (2014a)	C	150	0.50	236	74.1	141.7	1.91	0.27	1.49	5.42	1.17
88	Lim and Ozbakkaloglu (2014a)	C	150	0.50	236	74.1	146.1	1.97	0.27	1.47	5.35	1.03
89	Lim and Ozbakkaloglu (2014a)	C	150	0.50	236	74.1	147.6	1.99	0.27	1.71	6.22	1.29
90	Lim and Ozbakkaloglu (2014a)	G	150	0.60	95	74.1	90.8	1.23	0.27	0.54	1.96	0.43
91	Lim and Ozbakkaloglu (2014a)	G	150	0.60	95	74.1	91.8	1.24	0.27	1.22	4.44	0.84
92	Lim and Ozbakkaloglu (2014a)	G	150	0.60	95	74.1	93.0	1.26	0.27	1.21	4.40	0.93
93	Lim and Ozbakkaloglu (2014a)	A	150	0.80	129	98.0	125.8	1.28	0.29	2.06	6.99	1.19
94	Lim and Ozbakkaloglu (2014a)	A	150	0.80	129	98.0	130.9	1.34	0.29	1.73	5.87	1.17
95	Lim and Ozbakkaloglu (2014a)	A	150	0.80	129	98.0	132.8	1.36	0.29	2.39	8.11	1.47
96	Lim and Ozbakkaloglu (2014a)	C	150	0.66	236	98.0	173.1	1.77	0.29	2.16	7.33	1.20
97	Lim and Ozbakkaloglu (2014a)	C	150	0.66	236	98.0	180.3	1.84	0.29	2.03	6.89	1.48

Table 10.1 Continued

No.	Source of data	Fiber type	D (mm)	t_f (mm)	E_f (GPa)	f'_{co} (MPa)	f'_{cc} (MPa)	f'_{cc} / f'_{co}	ε_{co} (%)	ε_{cc} (%)	ε_{cc} / ε_{co}	$\varepsilon_{h,rup}$ (%)
98	Lim and Ozbakkaloglu (2014a)	C	150	0.66	236	98.0	174.4	1.78	0.29	2.20	7.46	1.34
99	Lim and Ozbakkaloglu (2014a)	G	150	0.80	95	98.0	135.2	1.38	0.29	2.29	7.77	1.64
100	Lim and Ozbakkaloglu (2014a)	G	150	0.80	95	98.0	140.3	1.43	0.29	2.80	9.50	1.74
101	Lim and Ozbakkaloglu (2014a)	G	150	0.80	95	98.0	133.9	1.37	0.29	2.40	8.14	1.54
102	Lim and Ozbakkaloglu (2014b)	A	150	1.20	129	85.7	166.2	1.94	0.29	2.02	7.09	1.50
103	Lim and Ozbakkaloglu (2014b)	A	150	1.20	129	85.7	168.0	1.96	0.29	2.18	7.65	1.48
104	Lim and Ozbakkaloglu (2014b)	A	150	1.20	129	85.6	165.2	1.93	0.29	2.09	7.33	1.45
105	Lim and Ozbakkaloglu (2014b)	A	150	1.20	129	112.6	165.5	1.47	0.31	1.97	6.45	1.37
106	Lim and Ozbakkaloglu (2014b)	A	150	1.20	129	112.3	168.4	1.50	0.31	1.74	5.70	1.48
107	Lim and Ozbakkaloglu (2014b)	A	150	1.20	129	112.5	163.1	1.45	0.31	1.87	6.13	1.47
108	Lim and Ozbakkaloglu (2014b)	A	150	1.20	129	121.1	167.1	1.38	0.31	1.77	5.69	1.14
109	Lim and Ozbakkaloglu (2014b)	A	150	1.20	129	121.2	172.1	1.42	0.31	1.76	5.66	1.39
110	Lim and Ozbakkaloglu (2014b)	A	150	1.20	129	121.2	168.4	1.39	0.31	1.78	5.73	1.33
111	Lim and Ozbakkaloglu (2014b)	A	150	1.20	129	113.7	186.5	1.64	0.31	2.04	6.67	1.50
112	Lim and Ozbakkaloglu (2014b)	A	150	1.20	129	113.8	170.7	1.50	0.31	1.75	5.72	1.19
113	Lim and Ozbakkaloglu (2014b)	A	150	1.20	129	113.7	178.5	1.57	0.31	1.94	6.34	1.45
114	Lim and Ozbakkaloglu (2014b)	G	150	1.20	95	84.8	184.1	2.17	0.28	2.91	10.23	2.24
115	Lim and Ozbakkaloglu (2014b)	G	150	1.20	95	84.7	182.0	2.15	0.28	2.71	9.54	1.99
116	Lim and Ozbakkaloglu (2014b)	G	150	1.20	95	84.5	178.4	2.11	0.28	2.90	10.21	2.18
117	Lim and Ozbakkaloglu (2014b)	G	150	1.20	95	84.6	187.9	2.22	0.28	2.83	9.96	1.96
118	Lim and Ozbakkaloglu (2014b)	G	150	1.20	95	84.7	180.4	2.13	0.28	2.78	9.78	2.46
119	Lim and Ozbakkaloglu (2014b)	G	150	1.20	95	84.8	176.3	2.08	0.28	2.65	9.32	1.94
120	Lim and Ozbakkaloglu (2014b)	G	150	1.20	95	84.6	188.6	2.23	0.28	3.61	12.70	2.38
121	Lim and Ozbakkaloglu (2014b)	G	150	1.20	95	84.5	181.7	2.15	0.28	3.26	11.47	2.35
122	Lim and Ozbakkaloglu (2014b)	G	150	1.20	95	84.7	164.3	1.94	0.28	2.74	9.64	1.99
123	Lim and Ozbakkaloglu (2014b)	G	150	0.80	95	57.4	125.7	2.19	0.26	3.54	13.73	2.48
124	Lim and Ozbakkaloglu (2014b)	G	150	0.80	95	57.3	127.2	2.22	0.26	3.61	14.00	2.67
125	Lim and Ozbakkaloglu (2014b)	G	150	0.80	95	57.3	131.2	2.29	0.26	3.80	14.74	2.50
126	Lim and Ozbakkaloglu (2014b)	G	150	0.80	95	52.1	119.4	2.29	0.25	2.81	11.16	2.56
127	Lim and Ozbakkaloglu (2014b)	G	150	0.80	95	52.2	126.8	2.43	0.25	3.48	13.82	2.60
128	Lim and Ozbakkaloglu (2014b)	G	150	0.80	95	52.2	125.3	2.40	0.25	3.36	13.34	2.58
129	Lim and Ozbakkaloglu (2014b)	G	150	0.80	95	54.3	109.2	2.01	0.25	3.44	13.52	2.30
130	Lim and Ozbakkaloglu (2014b)	G	150	0.80	95	54.4	123.5	2.27	0.25	4.28	16.82	2.39
131	Lim and Ozbakkaloglu (2014b)	G	150	0.80	95	54.3	126.5	2.33	0.25	4.54	17.85	2.57
132	Ozbakkaloglu and Vincent (2014)	C	74	0.12	240	43.0	67.4	1.57	0.24	1.35	5.63	1.07
133	Ozbakkaloglu and Vincent (2014)	C	74	0.12	240	43.0	71.0	1.65	0.24	1.44	6.00	1.32
134	Ozbakkaloglu and Vincent (2014)	C	74	0.12	240	43.0	61.1	1.42	0.24	0.92	3.83	0.91
135	Ozbakkaloglu and Vincent (2014)	C	74	0.12	240	47.8	60.9	1.27	0.25	0.84	3.41	0.83
136	Ozbakkaloglu and Vincent (2014)	C	74	0.12	240	55.0	56.5	1.03	0.26	0.80	3.14	0.72
137	Ozbakkaloglu and Vincent (2014)	C	74	0.23	240	55.0	96.0	1.75	0.26	1.43	5.60	1.13
138	Ozbakkaloglu and Vincent (2014)	C	74	0.23	240	50.3	98.1	1.95	0.25	1.71	6.85	0.95
139	Ozbakkaloglu and Vincent (2014)	C	74	0.23	240	52.0	105.7	2.03	0.25	2.41	9.58	1.07
140	Ozbakkaloglu and Vincent (2014)	C	152	0.12	240	37.3	42.0	1.13	0.23	0.79	3.41	1.20
141	Ozbakkaloglu and Vincent (2014)	C	152	0.12	240	34.6	41.6	1.20	0.23	0.66	2.90	0.77
142	Ozbakkaloglu and Vincent (2014)	C	152	0.23	240	35.5	59.1	1.66	0.23	1.43	6.25	1.32
143	Ozbakkaloglu and Vincent (2014)	C	152	0.23	240	36.3	60.9	1.68	0.23	1.53	6.65	1.36
144	Ozbakkaloglu and Vincent (2014)	C	152	0.23	240	37.3	61.7	1.65	0.23	1.45	6.26	1.23
145	Ozbakkaloglu and Vincent (2014)	C	302	0.23	240	36.3	38.6	1.06	0.23	0.80	3.48	1.08
146	Ozbakkaloglu and Vincent (2014)	C	302	0.47	240	36.3	57.0	1.57	0.23	1.52	6.61	1.17
147	Ozbakkaloglu and Vincent (2014)	A	100	0.20	120	37.0	70.6	1.91	0.23	2.06	8.91	2.22
148	Ozbakkaloglu and Vincent (2014)	A	100	0.20	120	35.5	65.5	1.85	0.23	1.75	7.65	2.08
149	Ozbakkaloglu and Vincent (2014)	A	100	0.20	120	34.0	62.8	1.85	0.23	1.88	8.31	2.25
150	Ozbakkaloglu and Vincent (2014)	A	100	0.30	99	37.2	89.1	2.40	0.23	3.10	13.40	2.11
151	Ozbakkaloglu and Vincent (2014)	A	100	0.30	99	37.2	91.9	2.47	0.23	3.31	14.30	2.39
152	Ozbakkaloglu and Vincent (2014)	A	100	0.30	99	35.4	86.7	2.45	0.23	3.04	13.30	2.21
153	Ozbakkaloglu and Vincent (2014)	C	152	0.19	640	36.3	46.4	1.28	0.23	0.28	1.22	0.12
154	Ozbakkaloglu and Vincent (2014)	C	152	0.19	640	36.3	46.0	1.27	0.23	0.30	1.30	0.11
155	Ozbakkaloglu and Vincent (2014)	C	152	0.19	640	36.3	43.3	1.19	0.23	0.25	1.09	0.18

Table 10.1 Continued

No.	Source of data	Fiber type	D (mm)	t_f (mm)	E_f (GPa)	f'_{co} (MPa)	f'_{cc} (MPa)	f'_{cc} / f'_{co}	ε_{co} (%)	ε_{cc} (%)	ε_{cc} / ε_{co}	$\varepsilon_{h,rup}$ (%)
156	Abbasnia and Ziaadiny (2015)	C	150	0.35	241	32.0	66.5	2.08	0.22	2.29	10.25	0.99
157	Abbasnia and Ziaadiny (2015)	C	150	0.35	241	47.0	82.2	1.75	0.25	1.90	7.75	0.95
158	Hany et al. (2015)	C	200	0.13	230	16.6	24.1	1.45	0.19	1.76	9.30	0.90
159	Lim (2015)	A	150	0.80	129	74.8	130.1	1.74	0.28	1.88	6.82	1.65
160	Lim (2015)	A	150	0.80	129	75.0	130.5	1.74	0.28	1.69	6.13	1.67
161	Lim (2015)	A	150	0.80	129	74.9	139.3	1.86	0.28	2.14	7.76	2.02
162	Lim (2015)	G	150	0.80	95	73.9	136.0	1.84	0.27	2.69	9.79	2.45
163	Lim (2015)	G	150	0.80	95	74.2	138.7	1.87	0.27	2.74	9.96	2.46
164	Lim (2015)	G	150	0.80	95	74.1	136.3	1.84	0.27	2.61	9.49	2.23
165	Lim (2015)	G	150	0.40	95	34.8	78.1	2.25	0.23	3.39	14.90	2.45
166	Lim (2015)	G	150	0.40	95	34.7	76.3	2.20	0.23	3.63	15.96	2.48
167	Lim (2015)	G	150	0.40	95	34.8	75.1	2.16	0.23	3.23	14.20	2.49
168	Albitar et al. (2015)	A	150	0.60	129	42.5	95.8	2.25	0.24	3.67	15.34	1.60
169	Albitar et al. (2015)	A	150	0.60	129	42.5	101.0	2.38	0.24	4.01	16.76	1.54
170	Albitar et al. (2015)	A	150	0.60	129	42.5	102.8	2.42	0.24	3.99	16.68	1.36
171	Albitar et al. (2015)	A	150	0.60	129	42.5	100.0	2.35	0.24	3.80	15.88	1.33
172	Albitar et al. (2015)	A	150	0.60	129	42.5	100.0	2.35	0.24	4.17	17.43	1.48
173	Albitar et al. (2015)	A	150	0.60	129	42.5	102.2	2.40	0.24	3.96	16.55	1.25
174	Albitar et al. (2015)	A	150	1.20	129	82.4	171.8	2.08	0.28	2.85	10.10	0.96
175	Albitar et al. (2015)	A	150	1.20	129	82.4	174.6	2.12	0.28	3.05	10.80	0.97
176	Albitar et al. (2015)	A	150	1.20	129	82.4	147.9	1.79	0.28	2.96	10.49	0.60
177	Albitar et al. (2015)	A	150	1.20	129	82.4	154.5	1.88	0.28	2.93	10.38	0.94
178	Albitar et al. (2015)	A	150	1.20	129	82.4	161.6	1.96	0.28	3.68	13.04	0.89
179	Albitar et al. (2015)	A	150	1.20	129	82.4	157.2	1.91	0.28	3.46	12.26	0.69
180	Albitar et al. (2015)	G	150	1.20	95	82.4	165.7	2.01	0.28	3.58	12.68	1.11
181	Albitar et al. (2015)	G	150	1.20	95	82.4	168.2	2.04	0.28	3.50	12.40	1.28
182	Albitar et al. (2015)	G	150	1.20	95	82.4	166.5	2.02	0.28	4.50	15.94	1.66
183	Albitar et al. (2015)	G	150	1.20	95	82.4	152.1	1.85	0.28	3.48	12.33	1.54
184	Albitar et al. (2015)	G	150	1.20	95	82.4	170.8	2.07	0.28	4.55	16.12	1.34
185	Albitar et al. (2015)	G	150	1.20	95	82.4	151.4	1.84	0.28	3.78	13.39	1.01
186	Albitar et al. (2015)	A	150	0.60	129	42.5	99.1	2.33	0.24	3.70	15.47	1.64
187	Albitar et al. (2015)	A	150	0.60	129	42.5	91.2	2.15	0.24	3.35	14.00	1.48
188	Albitar et al. (2015)	A	150	1.20	129	82.4	185.5	2.25	0.28	2.58	9.14	1.38
189	Albitar et al. (2015)	A	150	1.20	129	82.4	192.1	2.33	0.28	3.00	10.63	1.51
190	Albitar et al. (2015)	A	150	1.20	129	82.4	191.4	2.32	0.28	3.29	11.65	1.65
191	Albitar et al. (2015)	A	150	1.20	129	82.4	199.1	2.42	0.28	3.40	12.04	1.49
192	Albitar et al. (2015)	A	150	1.20	129	82.4	196.9	2.39	0.28	3.23	11.44	1.03
193	Albitar et al. (2015)	A	150	1.20	129	82.4	201.8	2.45	0.28	3.15	11.16	1.20
194	Albitar et al. (2015)	A	150	1.80	129	82.4	233.0	2.83	0.28	3.99	14.13	1.29
195	Albitar et al. (2015)	A	150	1.80	129	82.4	226.2	2.75	0.28	3.54	12.54	1.30
196	Albitar et al. (2015)	G	150	1.20	95	82.4	176.3	2.14	0.28	3.10	10.98	1.68
197	Albitar et al. (2015)	G	150	1.20	95	82.4	165.1	2.00	0.28	2.81	9.95	1.62
198	Xie and Ozbakkaloglu (2015)	C	150	1.20	129	123.5	174.0	1.41	0.31	2.07	6.63	0.96
199	Xie and Ozbakkaloglu (2015)	C	150	1.20	129	127.0	160.6	1.26	0.31	1.68	5.34	0.91
200	Xie and Ozbakkaloglu (2015)	C	150	1.20	129	125.7	180.6	1.44	0.31	2.16	6.88	1.07
201	Xie and Ozbakkaloglu (2015)	C	150	1.20	129	131.6	179.8	1.37	0.32	1.91	6.02	1.23
202	Xie and Ozbakkaloglu (2015)	C	150	1.20	129	124.6	171.3	1.37	0.31	1.78	5.69	1.19
203	Xie and Ozbakkaloglu (2015)	C	150	1.20	129	132.7	169.7	1.28	0.32	1.68	5.28	1.14
204	Xie and Ozbakkaloglu (2015)	C	150	1.20	129	123.9	191.6	1.55	0.31	2.00	6.40	1.37
205	Xie and Ozbakkaloglu (2015)	C	150	1.20	129	131.4	204.7	1.56	0.32	2.50	7.88	1.68
206	Xie and Ozbakkaloglu (2015)	C	150	1.20	129	124.2	191.2	1.54	0.31	1.95	6.23	1.11
207	Xie and Ozbakkaloglu (2015)	C	150	1.20	129	124.0	191.8	1.55	0.31	2.05	6.56	1.40
208	Xie and Ozbakkaloglu (2015)	C	150	1.20	129	127.1	188.1	1.48	0.31	1.82	5.78	1.42
209	Xie and Ozbakkaloglu (2015)	C	150	1.20	129	126.4	185.2	1.47	0.31	1.95	6.21	1.20
210	Xie and Ozbakkaloglu (2015)	C	150	1.20	129	122.5	199.9	1.63	0.31	2.65	8.50	1.75
211	Xie and Ozbakkaloglu (2015)	C	150	1.20	129	126.4	195.3	1.55	0.31	2.16	6.88	1.49
212	Xie and Ozbakkaloglu (2015)	C	150	1.20	129	124.8	204.1	1.64	0.31	2.31	7.38	1.86

Table 10.1 Continued

No.	Source of data	Fiber type	D (mm)	t_f (mm)	E_f (GPa)	f'_{co} (MPa)	f'_{cc} (MPa)	f'_{cc} / f'_{co}	ε_{co} (%)	ε_{cc} (%)	ε_{cc} / ε_{co}	$\varepsilon_{h,rup}$ (%)
213	Xie and Ozbakkaloglu (2015)	C	150	1.20	129	116.1	171.1	1.47	0.31	1.77	5.75	1.11
214	Xie and Ozbakkaloglu (2015)	C	150	1.20	129	115.7	175.0	1.51	0.31	1.90	6.18	1.16
215	Xie and Ozbakkaloglu (2015)	C	150	1.20	129	118.6	162.8	1.37	0.31	1.64	5.30	1.00
216	Xie and Ozbakkaloglu (2015)	C	150	1.20	129	127.1	201.9	1.59	0.31	2.43	7.72	1.47
217	Xie and Ozbakkaloglu (2015)	C	150	1.20	129	125.9	168.8	1.34	0.31	1.75	5.58	1.01
218	Xie and Ozbakkaloglu (2015)	C	150	1.20	129	122.8	165.0	1.34	0.31	1.68	5.39	1.28
219	Xie and Ozbakkaloglu (2015)	C	150	1.20	129	110.1	144.7	1.31	0.30	2.32	7.64	1.22
220	Xie and Ozbakkaloglu (2015)	C	150	1.20	129	112.6	139.3	1.24	0.31	2.31	7.57	1.13
221	Xie and Ozbakkaloglu (2015)	C	150	1.20	129	93.3	159.6	1.71	0.29	2.67	9.17	1.35
222	Xie and Ozbakkaloglu (2015)	C	150	1.20	129	119.4	195.3	1.64	0.31	2.58	8.33	1.17
223	Xie and Ozbakkaloglu (2015)	C	150	1.20	129	114.0	185.1	1.62	0.31	2.55	8.33	1.42
224	Xie and Ozbakkaloglu (2015)	C	150	1.20	129	116.6	196.3	1.68	0.31	2.34	7.60	1.40
225	Deng and Qu (2015)	A	100	0.53	24	83.1	130.4	1.57	0.28	1.28	4.51	0.90
226	Deng and Qu (2015)	A	100	1.06	24	82.8	168.0	2.03	0.28	1.81	6.39	1.47
227	Deng and Qu (2015)	A	100	1.60	24	82.9	208.1	2.51	0.28	1.97	6.96	1.51
228	Deng and Qu (2015)	G	100	0.78	18	83.0	122.8	1.48	0.28	1.11	3.92	0.78
229	Deng and Qu (2015)	G	100	1.55	18	82.6	165.2	2.00	0.28	1.67	5.91	1.06
230	Deng and Qu (2015)	G	100	2.33	18	83.0	204.1	2.46	0.28	1.89	6.69	1.19
231	Deng and Qu (2015)	C	100	0.51	44	82.6	110.7	1.34	0.28	0.87	3.08	0.53
232	Deng and Qu (2015)	C	100	1.01	44	82.9	162.4	1.96	0.28	1.04	3.69	0.69
233	Deng and Qu (2015)	C	100	1.52	44	83.0	213.2	2.57	0.28	1.29	4.54	0.90
234	Deng and Qu (2015)	C	100	0.60	40	82.8	154.0	1.86	0.28	1.01	3.58	0.72
235	Deng and Qu (2015)	C	100	1.21	40	82.8	192.2	2.32	0.28	1.47	5.18	1.08
236	Deng and Qu (2015)	C	100	1.81	40	82.9	260.2	3.14	0.28	1.89	6.70	1.25
237	Deng and Qu (2015)	C	100	0.96	31	83.0	128.6	1.55	0.28	1.03	3.65	0.69
238	Deng and Qu (2015)	C	100	1.59	34	82.7	201.7	2.44	0.28	1.61	5.69	1.12
239	Deng and Qu (2015)	C	100	1.11	28	83.0	139.5	1.68	0.28	1.05	3.69	0.63
240	Deng and Qu (2015)	C	100	1.88	30	82.8	195.3	2.36	0.28	1.50	5.29	1.07
241	Vincent and Ozbakkaloglu (2016)	C	152	0.11	230	52.0	96.4	1.85	0.25	2.31	9.18	1.61
242	Vincent and Ozbakkaloglu (2016)	C	152	0.11	230	52.0	94.0	1.81	0.25	2.22	8.82	1.55
243	Vincent and Ozbakkaloglu (2016)	C	152	0.11	230	52.0	92.1	1.77	0.25	2.14	8.50	1.35
244	Vincent and Ozbakkaloglu (2016)	C	152	0.22	230	52.0	103.6	1.99	0.25	2.48	9.86	1.60
245	Vincent and Ozbakkaloglu (2016)	C	152	0.22	230	52.0	95.4	1.83	0.25	2.25	8.94	1.60
246	Vincent and Ozbakkaloglu (2016)	C	152	0.22	230	52.0	96.1	1.85	0.25	2.19	8.70	1.69
247	Vincent and Ozbakkaloglu (2016)	C	152	0.33	230	52.0	100.6	1.93	0.25	2.20	8.74	1.57
248	Vincent and Ozbakkaloglu (2016)	C	152	0.33	230	52.0	96.6	1.86	0.25	2.12	8.43	1.69
249	Vincent and Ozbakkaloglu (2016)	C	152	0.11	230	84.7	160.1	1.89	0.28	1.66	5.84	1.23
250	Vincent and Ozbakkaloglu (2016)	C	152	0.11	230	84.7	172.5	2.04	0.28	1.80	6.33	1.49
251	Vincent and Ozbakkaloglu (2016)	C	152	0.11	230	84.7	179.6	2.12	0.28	1.95	6.86	1.34
252	Fillmore and Sadeghian (2018)	B	150	0.90	25	40.0	55.9	1.40	0.24	0.84	3.58	1.59
253	Fillmore and Sadeghian (2018)	B	150	0.90	25	40.0	56.1	1.40	0.29	0.79	2.71	1.93
254	Fillmore and Sadeghian (2018)	B	150	0.90	25	40.0	56.8	1.42	0.29	0.76	2.63	1.81
255	Fillmore and Sadeghian (2018)	B	150	1.80	25	40.0	76.3	1.90	0.29	1.95	6.74	1.84
256	Fillmore and Sadeghian (2018)	B	150	1.80	25	40.0	76.4	1.91	0.29	2.07	7.14	2.19
257	Fillmore and Sadeghian (2018)	B	150	1.80	25	40.0	78.2	1.95	0.29	1.99	6.85	1.94
258	Fillmore and Sadeghian (2018)	B	150	2.70	25	40.0	95.4	2.38	0.29	2.32	8.00	1.79
259	Fillmore and Sadeghian (2018)	B	150	2.70	25	40.0	99.0	2.47	0.29	2.79	9.62	1.76
260	Fillmore and Sadeghian (2018)	B	150	2.70	25	40.0	89.3	2.23	0.29	2.02	6.98	1.55

Note: A = aramid; B = basalt; C = carbon; G = glass; N =number of specimens.

Recently, more sophisticated methods such as using artificial intelligence (Jiang et al., 2020; Naderpour and Mirrashid, 2020) and extensive numerical models (Ceccato et al., 2020; Li et al., 2019) were engaged to predict the ultimate condition. However, for design

and analysis purposes, simplified design-oriented models are the most practical because of their simplicity, accuracy, and ease of use. The same concept applies to the stress-strain curves, since many analysis-oriented models predict the FRP-confined concrete strength (Binici, 2005; Fam and Rizkalla, 2001; Ferrotto et al., 2018; Jiang and Teng, 2007; Moran and Pantelides, 2002; Pan et al., 2017; Spoelstra and Monti, 1999; Xiao et al., 2010; Yang et al., 2020) while the design guidelines (ACI 440.2R, 2017; CSA S806, 2012), and in turn practice engineers, use the design-oriented models for analysis and design purposes.

Fardis and Khalili (1982) proposed a design-oriented model to predict the axial stress-strain curve of FRP-confined concrete columns. The model was adopted for actively confined concrete columns or the ones confined with steel tubes which expressed in form of a single parabolic curve, whose accuracy was later improved by other researchers (Ahmad et al. 1991; Li et al. 2003; Saadatmanesh et al., 1994). The problem with a single parabolic stress-strain model, which mainly is based on the model proposed by Popovics (1973), is that these curves do not accurately predict the bilinear form of the stress-strain curves for FRP-confined concrete columns as observed in the experimental tests. Thus, many researchers used the bilinear stress-strain curves to distinguish the FRP-confined concrete behavior from steel confined concrete columns (Binici, 2008; Demersan Neale, 1994; Karbhari and Gao, 1997; Saiid Saiidi et al., 2005; Xiao and Wu, 2000). These curves consisted of two lines defined by three points including the origin, a transition point close to the location of the unconfined concrete strength, and the point corresponding to the ultimate condition. However, the problem is that the unconfined concrete and confined concrete showed similar behavior in the initial ascending branch of the stress-strain curves for low levels of concrete dilation where the confinement is not activated.

Therefore, in the recent studies, an improved version of the stress-strain curve for FRP-confined columns was developed which show an initial parabolic curve followed by a linear part. Some researchers have adopted the parabolic part proposed by Hognestad (1951) as the initial part followed by a secondary linear portion that connects the transition point to the point corresponding to the ultimate condition (Lillistone et al., 2000; Miyauchi et al., 1997 and 1999), while Lam and Teng developed a new prediction for the initial portion (Lam and Teng, 2003) which was adopted by other researchers (Bai et al. 2019; Fahmy and Wu 2010; Jiang and Teng 2006; Teng et al. 2009; Yu and Teng 2011). In form of a single equation, a model was proposed by Toutanji (Toutanji, 1999) based on a general expression developed by Sargin (Sargin, 1971) and improved by Ahmad and Shah (Shuaib H. Ahmad and Surendra P. Shah 1982) for steel tubes, which was adopted by researchers (Berthet et al., 2006; Saafi et al., 1999). The other popular format of the confined concrete stress-strain curve with one single power equation is the general expression proposed by Richard and Abbott (1975) which required four parameters (i.e. the slope of the initial ascending branch, the secondary slope, the intercept of secondary slope and the stress axis, and a polynomial constant which determine the smoothness of transition), which was adopted by many researchers (Djafar-Henni and Kassoul, 2018; Jesus et al., 2018; Samaan et al., 1998a; Lobo et al., 2018; Wu and Wang, 2010; Wu et al., 2009; Xiao and Wu, 2003).

Most of the mentioned models relate the secondary slope of the stress-strain curve to the ultimate condition and the intercept of the secondary line with the stress axis. However, the ultimate condition is related to the rupture strain of FRP wraps which showed a high variability (Chen et al., 2013; Sadeghian et al., 2018; Sadeghian and Fam, 2014). Chen et al. (Chen et al., 2013) studied the factors affecting the variability in the ultimate condition

based on an extensive literature survey and found that rupture of FRP may occur near the outer part, inner part, or outside of the overlap if FRP rupture controls the failure, and mixed debonding and rupture of FRPs may be the cause of the failure which may start at the middle of the column or near the ends of the columns. It was also found that seventeen factors may affect the FRP rupture (Chen et al., 2013) that directly related to the ultimate confined strength and strain. The latter showed that the secondary slope of the stress-strain of the FRP-confined concrete may experience errors by involving the ultimate condition. However, only a few stress-strain curves are available in the literature which consider the secondary slope to the FRP wrap properties and unconfined concrete strength instead of the ultimate condition (Bai et al., 2019; Fahmy and Wu, 2010; Samaan et al., 1998; Xiao and Wu, 2003). Fahmy et al. (Fahmy and Wu 2010) adopted the model developed by Lam and Teng (2003) and improved the model by relating the secondary slope. However, the intercept stress was kept constant as the unconfined concrete. Samman et al. (1998) used only 30 specimens for calibration of the model. Xiao and Wu (2003) incorporate an analysis-oriented approach and verified their model versus an experimental database. Bai et al. (2019) proposed a model for large rupture strain FRP-confined concrete.

Therefore, in the current study, a stress-strain curve was proposed by adopting a four-parameter Richard and Abbot (1975) general expression, which is a single equation, using 200 full stress-strain curves from sixteen independent studies included 130 carbon, 22 aramid, 42 glass, and 6 basalt FRP-wrapped concrete columns. The curve parameters were determined independent of the ultimate condition and the intercept stress was considered as a variable. Also, the accuracy of the curves was evaluated using a total of 3272 data points from the experimental curves comparing to fifteen other studies. In the end, based

on the stress-stain curve and the proposed plasticity-based confined strength equation, a prediction of ultimate confined strain was given.

10.2 CALIBRATION OF WILLAM-WARNKE MODEL FOR ULTIMATE STRENGTH

To obtain a relationship for predicting the ultimate strength of concrete columns confined with FRP wraps, the five parameter Willam-Warnke plasticity model was used (Willam and Warnke, 1975). This plasticity model describes the failure surface in principal stress space (σ_1, σ_2, σ_3). The failure surface can be expressed in terms of octahedral normal stress (σ_{oct}) and octahedral shear stress (τ_{oct}) as presented in Equation 10.1 and 10.2.

$$\sigma_{oct} = \frac{1}{3}(\sigma_1 + \sigma_2 + \sigma_3) \tag{10.1}$$

$$\tau_{oct} = \frac{1}{3}\sqrt{[(\sigma_1 - \sigma_2)^2 + (\sigma_1 - \sigma_3)^2 + (\sigma_2 - \sigma_3)^2]} \tag{10.2}$$

Figure 10.1(a) shows the schematic interpretation of the five parameter Willam-Warnke failure surface in ξ-r- θ coordinate system; where ξ is the norm of projection of stress state on the hydrostatic axis ($\sigma_1 = \sigma_2 = \sigma_3$); r is the norm of projection of stress state on a deviatoric plane which is a plane perpendicular to the hydrostatic axis ($\sigma_1 + \sigma_2 + \sigma_3$ = constant); θ is the angle of similarity which is the angle between stress state point (σ_1, σ_2, σ_3) and the projection of σ_1 axis in its deviatoric plane, as presented in Figure 10.1(b). The octahedral normal and shear stresses are directly proportional to ξ and r, respectively, as shown in Figure 10.1(a). The angle of similarity is defined in Equation 10.3 where S_1 is the deviatoric principal stress corresponding to σ_1, J_2 is the second invariant of the deviatoric stress tensor, and σ_1, σ_2, σ_3 are the principal stresses (Chen, 1982).

$$\theta = \frac{\sqrt{3}}{2}\frac{S_1}{\sqrt{J_2}} = \frac{2\sigma_1 - \sigma_2 - \sigma_3}{2\sqrt{3}\sqrt{\frac{1}{6}[(\sigma_1 - \sigma_2)^2 + (\sigma_1 - \sigma_3)^2 + (\sigma_2 - \sigma_3)^2]}} \tag{10.3}$$

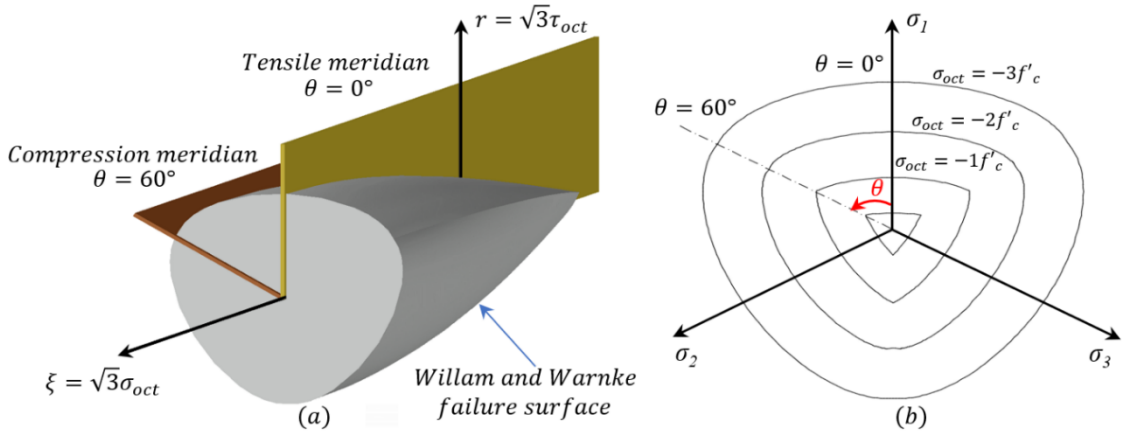

Figure 10. 1 Five-parameter plasticity model of Willam and Warnke (1975): (a) Three-dimensional scheme and(b) Schematic deviatoric sections

When two of the principal stresses are the same, the compression meridian ($\sigma_3 < \sigma_1 = \sigma_2$) and tensile meridian ($\sigma_2 = \sigma_3 < \sigma_1$) can be derived. Meridians are the intersection of the failure surface and the meridian plane which contains the hydrostatic axis with a constant angle of similarity (θ). It should be noted that the sign convention was defined so that tensile stresses are positive and compressive stresses are negative. By substituting the mentioned condition in Equation 10.3, angles of similarity of 60 and 0 degrees are derived for compression meridian and tensile meridians, respectively, as shown in Figure 10.1(a).

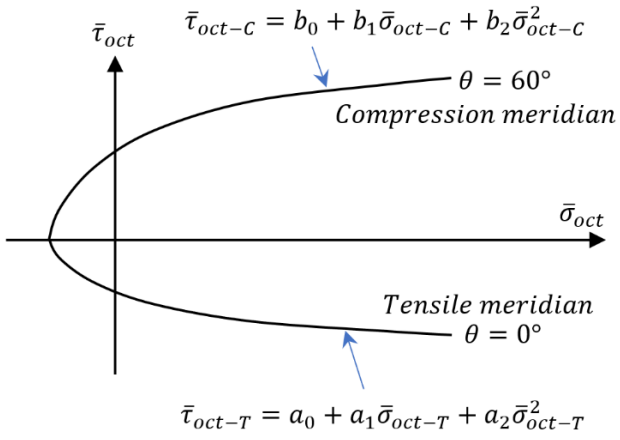

Figure 10. 2 Compression and tensile meridians

In Willam-Warnke five parameter model, the tensile and compression meridians are in parabolic form as shown in Figure 10.2 and expressed in Equation 10.4 and 10.5, respectively (Willam and Warnke, 1975).

$$\bar{\tau}_{oct-T} = \ a_0 + a_1\bar{\sigma}_{oct-T} + a_2\bar{\sigma}^2_{oct-T} \quad (10.4)$$

$$\bar{\tau}_{oct-C} = \ b_0 + b_1\bar{\sigma}_{oct-C} + b_2\bar{\sigma}^2_{oct-C} \quad (10.5)$$

Equation 10.4 and 10.5 are expressed in terms of octahedral stresses normalized with the unconfined concrete strength (f'_{co}) and parameters a_0, a_1, a_2, b_0, b_1, b_2 are constants. The index T appears for tensile meridian, the index C appears for compression meridian, $\bar{\sigma}_{oct}$ is the normalized octahedral stress, and $\bar{\tau}_{oct}$ is the normalized octahedral shear stress which are presented in Equation 10.6.

$$\bar{\sigma}_{oct} = \frac{\sigma_{oct}}{f'_{co}} \ ; \ \bar{\tau}_{oct} = \frac{\tau_{oct}}{f'_{co}} \quad (10.6)$$

In this study, a database including concrete specimens wrapped with FRP and tested under pure compression was used to find the strength model. The database includes 778 tests of confined concrete columns collected by Sadeghian and Fam (2015) and expanded by Table 10.1. The summary of the database is presented in Table 10.2.

Table 10. 2 Summary of the experimental database for FRP-wrapped concrete specimens

Material	No.	Parameter	Unit	Mean	STD	COV (%)	Min.	Max.
Concrete	1	D_c	mm	154.00	47.13	31	51.00	406.00
	2	f'_{co}	MPa	52.1	29.4	57	16.6	188.2
FRP Wrap	3	t_f	mm	0.83	0.91	111	0.09	7.26
	4	E_f	GPa	178.53	117.66	66	10.50	662.50
	5	f_f	MPa	2710.1	1337.8	49	220.0	4441.0
	6	ε_f	mm/mm	0.01785	0.00698	39	0.00255	0.04690

Note: STD = standard deviation; COV = coefficient of variation; Min. = minimum; Max. = maximum; D_c = diameter of concrete specimen; f'_{co} = unconfined concrete strength; t_f = thickness of FRP wrap; E_f = modulus of elasticity of FRP wrap; and f_f = tensile strength of FRP wrap.

For all points in the database, the ultimate confining pressure (f_l) was calculated based on Equation 10.7 in which D is the diameter of concrete columns, E_f and t_f are the modulus of elasticity and the thickness of FRP wraps, respectively, and ε_{hr} is the actual hoop rupture strain of the wraps in the compression test of columns.

$$f_l = \frac{2E_f t_f \varepsilon_{hr}}{D} \tag{10.7}$$

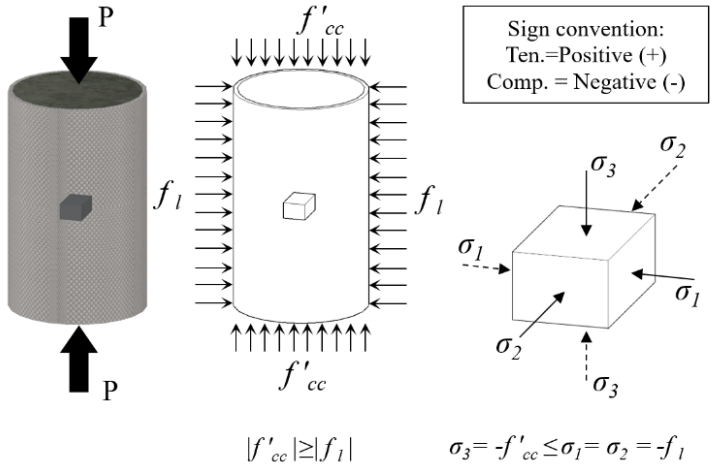

Figure 10. 3 Principal stresses in FRP-wrapped concrete column under pure compression

Figure 10.3 shows the state of stress for the compressive tests in which the ultimate confining pressure (f'_{cc}) is greater than axisymmetric confining pressure (f_l). Therefore, the state of stress for tests of and their relationship with principal stresses can be explained in Equation 10.8.

$$\sigma_3 = -f'_{cc} \; ; \; \sigma_1 = \sigma_2 = -f_l \; ; \; |f'_{cc}| \geq |f_l| \; ; \; \sigma_3 \leq \sigma_1 = \sigma_2 \tag{10.8}$$

The state of stress for the confined concrete tests is the same as the compressive meridian explained earlier, and each experimental test represents a point on the compression meridian in the octahedral space. Each set of (f'_{cc}, f_l) was transformed into an octahedral set of ($\bar{\sigma}_{oct}$, $\bar{\tau}_{oct}$) by substituting the stress state from Equation 10.8 into Equation 10.1, 10.2, and 10.6 which leads to Equation 10.9 and 10.10.

$$\bar{\sigma}_{oct} = \frac{-(f'_{cc} + 2f_l)}{3f'_{co}} \tag{10.9}$$

$$\bar{\tau}_{oct} = \frac{\sqrt{2}(f'_{cc} - f_l)}{3f'_{co}} \tag{10.10}$$

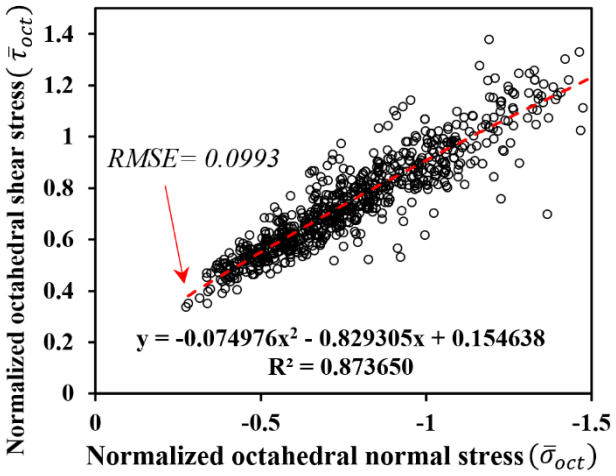

Figure 10. 4 Derivation of the best-fitted curve in octahedral space for compression meridian

Figure 10.4 shows the database in the normalized octahedral stress space to which a parabolic equation was fitted. The root mean squared error (RMSE) for the fitted equation is 0.0993 and the coefficient of determination (R^2) is not very close to one (i.e. 0.87) which is quite reasonable and shows a very good degree of accuracy. By comparing Equation 10.5 with the fitted equation in the figure, three constants of compression meridian can be found (b_0 = 0.1546, b_1 = 0.8293, and b_2 = -0.0750), and the results leads to Equation 10.11 that presents the compression meridian of confined concrete.

$$\bar{\tau}_{oct-C} = +0.1546 - 0.8293\bar{\sigma}_{oct-C} - 0.0750\bar{\sigma}^2_{oct-C} \tag{10.11}$$

To predict the ultimate confined concrete strength (f'_{cc}) from the ultimate confining pressure (f_l) and unconfined concrete strength (f'_{co}), Equation 10.9 and 10.10 were substituted in Equation 10.5 that led to Equation 10.12, and it was simplified and rearranged in the form of Equation 10.13.

$$\frac{\sqrt{2}(f'_{cc}-f_l)}{3f'_{co}} = b_0 - b_1\frac{(f'_{cc}+2f_l)}{3f'_{co}} + b_2\left(\frac{(f'_{cc}+2f_l)}{3f'_{co}}\right)^2 \quad (10.12)$$

$$\frac{f'_{cc}}{f'_{co}} = \frac{3(b_1+\sqrt{2})}{2b_2} + \sqrt{\left[\frac{3(b_1+\sqrt{2})}{2b_2}\right]^2 - \frac{9b_0}{b_2} - \frac{9\sqrt{2}}{b_2}\frac{f_l}{f'_{co}}} - 2\frac{f_l}{f'_{co}} \quad (10.13)$$

By substituting the constants of the compressive meridian parabola from Equation 10.11 into Equation 10.13, the strength ratio of confined concrete can be presented in the form of Equation 10.14.

$$\frac{f'_{cc}}{f'_{co}} = -11.702 + 12.470\sqrt{1+1.092\frac{f_l}{f'_{co}}} - 2\frac{f_l}{f'_{co}} \quad (10.14)$$

It should be noted that for analysis purposes, it is conventional to satisfy the boundary condition which shows equal confined and unconfined strength in the absence of the confining pressure. Thus, Equation 10.15 was adjusted by keeping the format of Equation 10.14 and minimizing the RMSE error for the experimental database to satisfy the boundary condition which required the same confined and unconfined strength in absence of confinement.

$$\frac{f'_{cc}}{f'_{co}} = -11.702 + 12.702\sqrt{1+0.935\frac{f_l}{f'_{co}}} - 2\frac{f_l}{f'_{co}} \quad (10.15)$$

10.3 Performance of The New Ultimate Confined Strength Model

In order to evaluate the performance of the new ultimate confined strength model, a group well-known plasticity-based and empirical models were selected from the literature and their performance was compared with the performance of the new model. The relationship between the ultimate confined concrete strength and the confining pressure can be written down in the form of Equation 10.16 and 10.17.

$$\frac{f'_{cc}}{f'_{co}} = A + \sqrt{A^2 - B - C\frac{f_l}{f'_{co}}} - 2\frac{f_l}{f'_{co}} \quad \rightarrow \quad \frac{f'_{cc}}{f'_{co}} = A + \lambda\sqrt{1 + \gamma\frac{f_l}{f'_{co}}} - 2\frac{f_l}{f'_{co}} \tag{10.16}$$

$$C = -\gamma\lambda^2 \; ; \; B = A^2 - \lambda^2 \tag{10.17}$$

By setting Equation 10.16 equal to Equation 10.13 and simplifying, the constants required for the deriving the compression meridian (Equation 10.5) can be found as presented in Equation 10.18.

$$b_0 = \frac{b_2 B}{9} \; ; \; b_1 = \frac{2Ab_2}{3} - \sqrt{2}; \; b_2 = \frac{9\sqrt{2}}{C} \tag{10.18}$$

A comparison in the octahedral space was performed using five different formulas derived based on the Willam-Warnke failure surface as presented in Table 10.3. Mander et al. (1988) developed a model for confined concrete columns confined by steel spirals and hoops using experimental test data and the explained procedure. Bing et al. (2001) proposed an equation for high strength concrete columns reinforced with transverse steel. Afifi et al. (2015) and Hales et al. (2017) for columns reinforced transversely with FRP spirals and hoops. For FRP wrapped columns, the only formula available in the literature which derived the ultimate confined strength based on the Willam-Warnke failure surface is a study performed by Yan and Pantelides (2006), which was derived based on limited test data (less than 20 data points). For comparing the available equations, the root mean square error (RMSE) and average absolute error (AAE) were calculated using Equation 10.19 and Equation 10.20, respectively, where Exp_i is the i^{th} experimental test data, $Calc_i$ is the i^{th} calculated value from a predicting equation, and N is the total number of data points.

$$RMSE = \sqrt{\frac{\sum(Exp._i - Calc._i)^2}{N}} \tag{10.19}$$

$$AAE = \frac{\sum\left|\frac{Calc._i - Exp._i}{Exp._i}\right|}{N} \tag{10.20}$$

Table 10. 3 Comparison of some of the plasticity-based formulas in octahedral space

Model	Compressive meridian equation	RMSE	AAE
Current study (Equation 10.11)	$\bar{\tau}_{oct} = 0.1546 - 0.8293\bar{\sigma}_{oct} - 0.0750\bar{\sigma}_{oct}^2$	0.0993	0.0785
Yan and Pantelides (2006) *	$\bar{\tau}_{oct} = 0.0546 - 1.0218\bar{\sigma}_{oct} - 0.1362\bar{\sigma}_{oct}^2$	0.1402	0.0991
Mander et al. (1988)	$\bar{\tau}_{oct} = 0.1230 - 1.1505\bar{\sigma}_{oct} - 0.3155\bar{\sigma}_{oct}^2$	0.1949	0.1301
Hales et al. (2017) *	$\bar{\tau}_{oct} = 0.2684 - 0.7129\bar{\sigma}_{oct} - 0.3119\bar{\sigma}_{oct}^2$	0.3956	0.2029
Bing et al. (2001)	$\bar{\tau}_{oct} = 0.113 - 1.26\bar{\sigma}_{oct} - 0.559\bar{\sigma}_{oct}^2$	0.4363	0.1587
Afifi et al. (2015)	$\bar{\tau}_{oct} = -0.1229 - 2.541\bar{\sigma}_{oct} - 1.98\bar{\sigma}_{oct}^2$	1.6977	0.5024

Note: * the presented coefficients are derived based on Equation 10.16 to Equation 10.18.

Table 10.3 shows that Equation 10.11 gives the best estimation for the database in the octahedral space between the equations developed using the Willam-Warnke model.

Table 10. 4 Comparison of plasticity-based models

Model	Formula	RMSE	AAE
Current study (Equation 10.15)	$\frac{f'_{cc}}{f'_{co}} = -11.702 + 12.702\sqrt{1 + 0.935\frac{f_l}{f'_{co}}} - 2\frac{f_l}{f'_{co}}$	0.3647	0.1335
Current study (Equation 10.14)	$\frac{f'_{cc}}{f'_{co}} = -11.702 + 12.470\sqrt{1 + 1.092\frac{f_l}{f'_{co}}} - 2\frac{f_l}{f'_{co}}$	0.3791	0.1324
Yan and Pantelides (2006)	$\frac{f'_{cc}}{f'_{co}} = -4.322 + 4.721\sqrt{1 + 4.193\frac{f_l}{f'_{co}}} - 2\frac{f_l}{f'_{co}}$	0.4269	0.1662
Mander et al. (1988)	$\frac{f'_{cc}}{f'_{co}} = -1.254 + 2.254\sqrt{1 + 7.940\frac{f_l}{f'_{co}}} - 2\frac{f_l}{f'_{co}}$	0.4710	0.1971
Wu and Zhou (2010)	$\frac{f'_{cc}}{f'_{co}} = \sqrt{1 + (\frac{16.7}{f'^{0.42}_{co}} - \frac{f'^{0.42}_{co}}{16.7})\frac{f_l}{f'_{co}}} + \frac{f_l}{f'_{co}}$	0.5077	0.1585
Bing et al. (2001)	$\frac{f'_{cc}}{f'_{co}} = -0.413 + 1.413\sqrt{1 + 11.4\frac{f_l}{f'_{co}}} - 2\frac{f_l}{f'_{co}}$	0.5848	0.1576
Hales et al. (2017)	$\frac{f'_{cc}}{f'_{co}} = -3.373 + 4.373\sqrt{1 + 2.134\frac{f_l}{f'_{co}}} - 2\frac{f_l}{f'_{co}}$	0.6943	0.1881
Afifi et al. (2015)	$\frac{f'_{cc}}{f'_{co}} = 0.850 + \sqrt{0.17 + 6.43\frac{f_l}{f'_{co}}} - 2\frac{f_l}{f'_{co}}$	0.9057	0.2255

Table 10.4 shows the format of the equations which predicts the ultimate confined strength. The results of the comparison showed the lowest error for Equation 10.14 and Equation 10.15 developed in the current study. To compare the proposed formula with empirical (non-plasticity-based) formulas for prediction of ultimate confined strength, different formats of design-oriented equations were presented in Table 10.5 and their error was calculated for the database.

Table 10. 5 Comparison of non-plasticity-based models

Model	Formula	RMSE	AAE
Sadeghian and Fam (2015)	$\frac{f'_{cc}}{f'_{co}} = 1 + (2.77\rho_K^{0.77} - 0.07)\rho_\varepsilon^{0.91}$	0.3603	0.1246
Lam and Teng (2003)	$\frac{f'_{cc}}{f'_{co}} = 1 + 3.3\frac{f_l}{f'_{co}}$	0.3882	0.1244
Teng et al. (2009)	$\frac{f'_{cc}}{f'_{co}} = 1 + 3.5(\rho_K - 0.01)\rho_\varepsilon$	0.4203	0.1264
Toutanji (1999)	$\frac{f'_{cc}}{f'_{co}} = 1 + 3.5\left(\frac{f_l}{f'_{co}}\right)^{0.85}$	0.4339	0.1799
Fallah Pour et al. (2018)	$\frac{f'_{cc}}{f'_{co}} = 1 + (2.5 - 0.01f'_{co})\frac{f_l}{f'_{co}}$	0.5528	0.1854
Rousakis et al. (2012)	$\frac{f'_{cc}}{f'_{co}} = 1 + (\rho_f E_f / f'_{co})(\alpha E_f 10^{-6}/E_{\mu f} + \beta)$	0.6601	0.1770
Mirmiran and Shahawy (1997)	$\frac{f'_{cc}}{f'_{co}} = 1 + 4.269\frac{f_l^{0.587}}{f'_{co}}$	0.8106	0.2437

Note: $\boldsymbol{\rho_K = \frac{2E_f t}{(f'_{co}/\varepsilon_{co})D}}$; $\boldsymbol{\rho_\varepsilon = \frac{\varepsilon_{hr}}{\varepsilon_{co}}}$; $\boldsymbol{\rho_f = \frac{4t}{D}}$; $\boldsymbol{\varepsilon_{co} = 9.37 \times 10^{-4}\sqrt[4]{f'_{co}}}$; t = thickness of FRP wrap; E_f = modulus of elasticity of FRP wrap; ε_{hr} = hoop rupture strain of FRP wrap; D = dimeter of concrete column; and ε_{co} = strain of unconfined concrete corresponding to f'_{co}; α = -0.336 and β = 0.0223 for FRP wraps; $E_{f\mu}$ = 10 MPa which is given for units' compliance.

The results showed that the formulas developed by Sadeghian and Fam (2015) and Lam and Teng (2003) presented the lowest error to predict the ultimate confined strength whose error is comparable to Equation 10.14 and Equation 10.15. Figure 10.5 shows the experimental versus model for the models developed in the current study and some of the models available in the literature. The results showed that the new models improved the current plasticity-based predictions and they are very close to non-plasticity-based models.

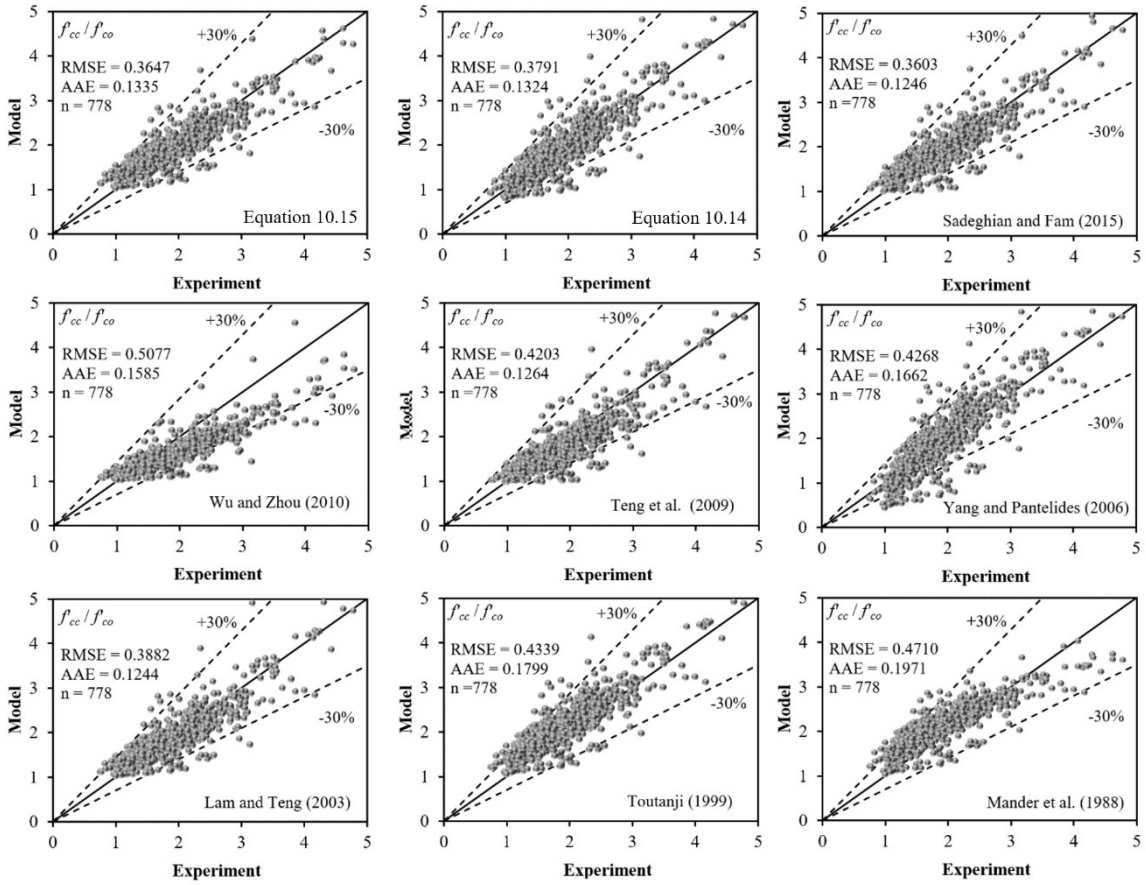

Figure 10. 5 Comparison of the predicted values and the experimental tests for strength

Figure 10.6 presents a comparison of the database and different confinement models by showing the normalized confined concrete strength (f'_{cc}/f'_{co}) versus the normalized confining pressure (f_l/f'_{co}). Figure 10.6(a) showed as the normalized confining pressure increases, some of the models underpredict the confined concrete strength, while the developed models are in good alignment with the trend of the database. Also, Figure 10.6(a) showed that the data points are concentrated up to a range of 0.6 for the formalized confining pressure (f_l/f'_{co}). Thus, in Figure 10.6(b), the selected range of normalized confining pressure is presented, and the data points are removed for the comparison. The proposed model by Mander et al. (1988) overpredicts the confining strength while the one

proposed by Yan and Pantelides (2006) underpredicts and then overpredicts the confined concrete strength. Other models showed almost similar behavior up to a normalized confining pressure of 1. However, for normalized confining pressures between 1 to 2, the proposed equations proposed by Lam and Teng (2003) and Teng et al. (2009) overpredicts the confinement effect.

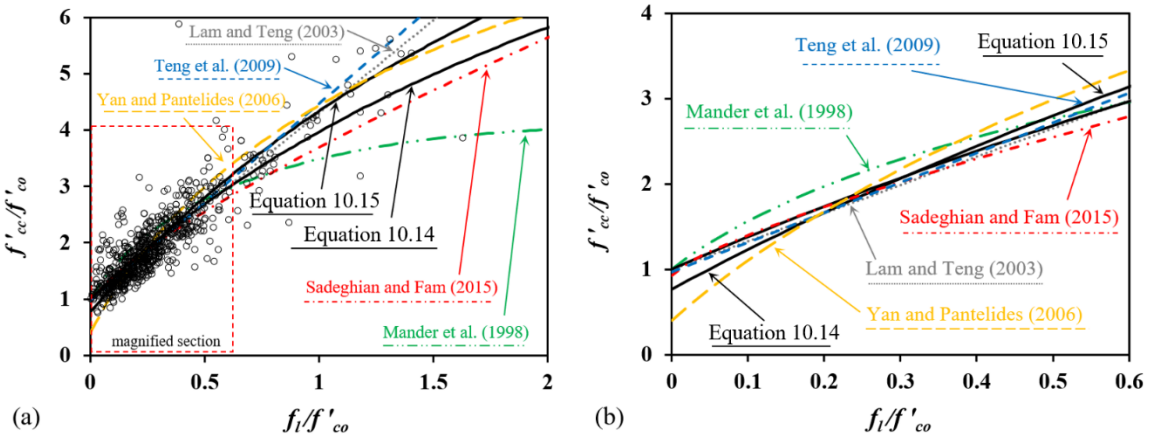

Figure 10. 6 Comparison of confined concrete equations: (a) database and (b) selected range

Equation 10.14, which is developed which is the best fit for the failure surface in the octahedral space, showed that a minimum confining pressure is required so that the confined and unconfined concrete strength become equal which is called the confinement limit. To find the confinement limit Equation 10.16 and 10.17 which show the general form of the ultimate confined strength is rewritten in the form of Equation 10.21 and 10.22 to show the equation for the confining pressure given the ultimate confined strength.

$$\frac{f_l}{f'_{co}} = L - M\sqrt{1 + N\frac{f'_{cc}}{f'_{co}}} - \frac{1}{2}\frac{f'_{cc}}{f'_{co}} \tag{10.21}$$

$$L = \frac{A}{2} + \frac{1}{8}\lambda^2\gamma \;;\; M = \sqrt{\frac{1}{8}\lambda^2\gamma A + \frac{1}{4}\left[\left(\frac{1}{4}\lambda^2\gamma\right)^2 + \lambda^2\right]} \;;\; N = -\frac{\frac{1}{8}\lambda^2\gamma}{M^2} \tag{10.22}$$

By substituting the values from Equation 10.14 into Equation 10.21 and 10.22, the confining pressure can be presented in the form presented in Equation 10.23.

$$\frac{f_l}{f'_{co}} = 15.369 - 15.519\sqrt{1 - 0.0881\frac{f'_{cc}}{f'_{co}}} - \frac{1}{2}\frac{f'_{cc}}{f'_{co}} \tag{10.23}$$

The relationship between the normalized confining pressure and normalized confined strength found in Equation 10.23, can be used to determine the confinement limit, which is considered as the minimum confinement required to activate the unconfined concrete. To find the confinement limit, the value of normalized confined strength was set to one in Equation 10.23 which gave a confinement limit of 0.05. It should be noted that ACI 440.2R (2017) which adopted the proposed model by Lam and Teng (2003), proposed a confinement limit of 0.08. for a better presentation of the limit and the database, Figure 10.7(a) shows a reduced database including 200 data points used for further studies in the next section.

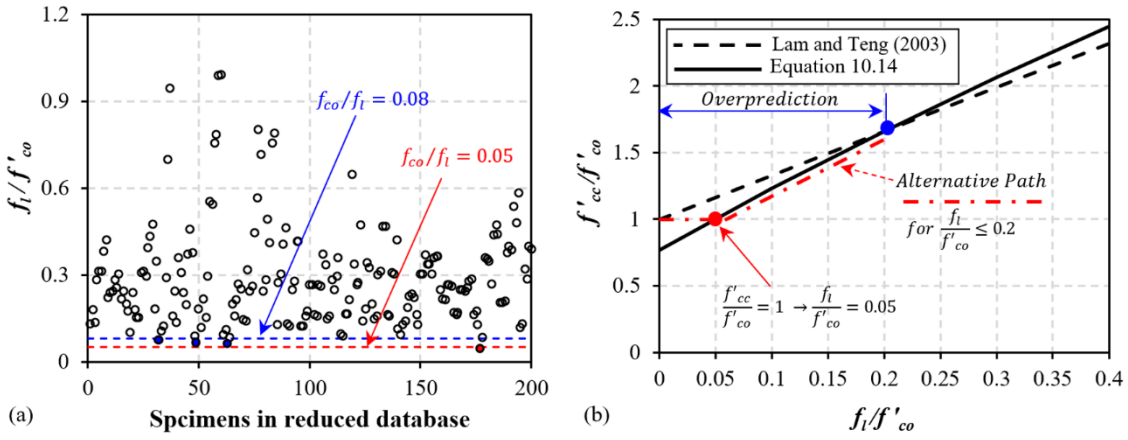

Figure 10. 7 Minimum required confinement limit: (a) reduced database and (b) comparison

It should be mentioned that only one data point was below the normalized confining limit of 0.05 while four of them were below 0.08 limit in the reduced database. For all data points, 33 and 65 specimens experienced a normalized confining pressure less than 0.05

and 0.08, respectively. Therefore, the limit of 0.08 is more conservative although 0.05 represents the limit more accurately. Figure 10.7(b) compares Equation 10.14 and Lam and Teng (2003) which revealed that the Lam and Teng model overpredicts the ultimate confined pressure up to a normalized confining pressure limit of 0.2. The statistics from the database showed that 38% of the tested specimen (i.e. 302 out of 778) had a normalized confining pressure of less than 0.2. Thus, the overprediction leads to unconservative designs per ACI 440.2R (2017) for a confining range up to 0.2. An alternative path is suggested by this study to cover the mentioned issues, shown as a dashed red line in Figure 10.7(b). The suggestion is to neglect the effect of confinement on the strength up to normalized confining pressures below 0.05 (i.e. $f'_{cc}/f'_{co} = 1$ if $f_l/f'_{co} < 0.05$). Also, Equation 10.14 can be used for the normalized confining pressures greater than 0.08. It should be mentioned that Figure 10.6(a) showed that for the normalized confining pressures greater than 1, Lam and Teng (2003) and in turn ACI 440.2R (2017) are not conservative as many data points have lower confined concrete strength than their predicted values. Thus, for the mentioned range, the use of Equation 10.14 is suggested in this study.

10.4 Stress-Strain Model

This study presents a design-oriented stress-strain curve for FRP-confined concrete columns with only the ascending branch. Design-oriented models are popular for design engineers because of their simplicity and accuracy at the same time. Many of previous studies related the stress-strain curve to the ultimate condition of FRP-confined concrete (Fardis and Khalili 1982, Lam and Teng 2003, Samaan et al. 1998, Teng et al. 2009, Wu et al. 2009). The ultimate condition of FRP-confined concrete is composed of the ultimate confined concrete strength (f'_{cc}) and ultimate confined concrete strain (ε_{cc}). Since many of

the studies performed separate statistical regression to find the ultimate concrete strain and strength, there is a possibility that the ultimate strain and stress do not yield on the stress-strain curve of the confined concrete. Thus, the stress-strain curves that are built based on the ultimate condition may predict a different secondary slope which is related to the confinement. In addition, in the prediction of the confined concrete strength and strain, the confining pressure (f_l) is involved as defined in Equation 10.24 per ACI 440-2R (2017).

$$f_l = \frac{2E_f t_f \varepsilon_{fe}}{D};\ \varepsilon_{fe} = k_e \varepsilon_{fu} \tag{10.24}$$

where E_f and t_f are the modulus of elasticity and the thickness of the FRP wrap, respectively, D is the diameter of the concrete member, ε_{fe} is the effective rupture strain, ε_{fu} is the ultimate tensile strain of FRP found from the coupon tests, and k_e is the strain efficiency factor. The strain efficiency factor is considered as 0.55 per ACI 440.2R (2017), and as a constant in most of the studies. However, multiple studies are proposing a variable strain efficiency factor (Chen et al., 2013; El-Hacha and Abdelrahman, 2013; Sadeghian et al., 2018; Sadeghian and Fam, 2014; Smith et al., 2010; Wu and Jiang, 2013). In the current study, the strain efficiency factor was found as 0.7 which is the average of 788 data points. The performance of the strain efficiency factor of 0.7 has also been verified by Sadeghian and Fillmore (2018). The point of using effective rupture stain and its variability inserts lots of uncertainties in the prediction of the confining pressure at the ultimate condition and in turn the prediction of the ultimate condition. Therefore, the use of the confining pressure in the stress-strain curves through the ultimate condition is one of the sources of inaccuracy. The elimination of the rupture strain from the predicting equations for the stress-strain relationships leads to the confinement modulus (E_L) which only relates to the properties of the FRP wrap and the column diameter as shown in Equation 10.25.

$$E_L = \frac{2E_f t_f}{D} \; ; \quad f_l = E_L \, \varepsilon_{fe} \tag{10.25}$$

To find the stress-strain curve for the FRP-confined concrete columns, a four-parameter Richard and Abbott model (1975) was adopted. The model is presented in the format of a power equation which consists of an initial ascending portion followed by a secondary linear portion up to the ultimate condition, as presented in Figure 10.8.

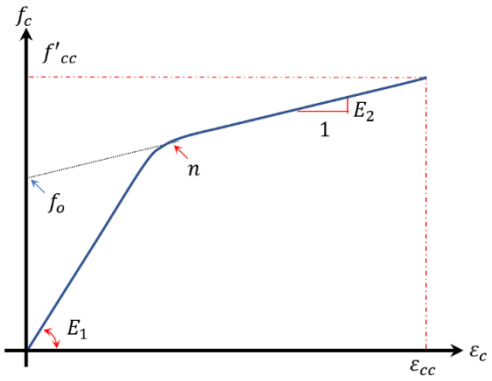

Figure 10. 8 Schematic Stress-Strain Curve Models

The four parameters of the curve are the initial modulus of elasticity (E_1), the secondary modulus of elasticity (E_2), a polynomial constant (n) which to fit a smooth transition between the two portions, and f_o which is the intercept stress defined as the intersection of the secondary portion and the vertical stress axis. Equation 10.26 presents the curve equation which relates the stress (f_c) to the strain (ε_c) for the confined concrete.

$$f_c = \frac{(E_1 - E_2)\varepsilon_c}{\left[1 + \left(\frac{(E_1 - E_2)\varepsilon_c}{f_o}\right)^n\right]^{1/n}} + E_2\varepsilon_c \tag{10.26}$$

The model was first adjusted by Samaan et al. (1998) to predict the stress-strain curve of concrete-filled FRP tubes (CFFTs) and later it was validated for CFRP-wrapped concrete specimens (Shahawy et al., 2000). Since the FRP wraps are mainly activated at a level of lateral expansion in the vicinity of the unconfined concrete strength, the initial slope (E_1)

was adopted from ACI 318 (2019) equation and the rest of the parameters were calibrated based on 30 tests of confined concrete presented in the study performed by Samaan et al. (1998). The secondary modulus was considered as a function of the stiffness of the confining tubes in the hoop direction, and the unconfined strength of the concrete. Also, the intercept stress was considered as a function of unconfined concrete strength and the confining pressure, and the polynomial constant was chosen as 1.5. Later, Xiao and Wu (2003) improved the estimation of the parameters based on an updated database and a new approach. The secondary slope was found when the stress of confined concrete reaches the yield surface which involves the axial and confining pressure relationship and the initial slope of axial-lateral strain curves. The intercept stress was derived as the coefficient of reference plastic strength using regression analysis, and the constant n was selected as 2. In another study, Wu et al. (2009) proposed a modification to the proposed parameters by Samaan et al. (1998) for high strength concrete columns confined by Aramid FRP (AFRP) and set the constant n equal to 2.5. It should be mentioned that for the secondary slope, instead of the confining stiffness, the ultimate condition for AFRPs was used. Djafar-Henni and Kassoul (2018) used a database of 81 AFRP-confined concrete columns and proposed a new estimation of the parameters presented in Equation 10.26 for AFRP confined concrete with a constant n equal to 2.25. Lobo et al. (2019) developed a model for AFRPs using 29 specimens, proposed new equations for the curve parameters, and found the constant n as $\sqrt{2}$. Also, Jesus et al. (1988) proposed a model for GFRPs using 60 specimens. It should be mentioned that for the last four introduced studies, the secondary slope was a function of the ultimate condition. Later, Bai et al. (2001) found the curve parameters for large rupture strain FRP-confined concrete using a database of 62 specimens.

In the current study, a reduced database including 200 full stress-strain curves from sixteen independent studies was extracted from the literature as presented in Table 10.6. The selected curves included 130 carbon, 22 aramid, 42 glass, and 6 basalt FRP-wrapped concrete columns. This is the broadest database of full stress-strain curves (not the ultimate condition) that have been collected for the calibration of the four parameters of Richard and Abbott model (Richard and Abbott, 1975).

Table 10. 6 Database of parameters compiled out of 200 experimental full stress-strain curves from the literature

No.	Source of data	FRP wrap	D (mm)	t_f (mm)	E_f (GPa)	f'_{co} (MPa)	f'_{cc} (MPa)	f'_{cc} / f'_{co}	E_L^* (GPa)	E_1^* (GPa)	E_2^* (GPa)	f_o^* (MPa)	f_o / f'_{co}	E_2 / E_1 (%)
1	Xiao and Wu (2000)	CFRP	152	0.38	105	33.7	47.9	1.42	0.53	27.04	1.27	32.6	0.97	4.70
2	Xiao and Wu (2000)	CFRP	152	0.38	105	33.7	49.7	1.47	0.53	27.44	1.31	33.6	1.00	4.77
3	Xiao and Wu (2000)	CFRP	152	0.38	105	33.7	49.4	1.47	0.53	26.93	1.21	33.7	1.00	4.49
4	Xiao and Wu (2000)	CFRP	152	0.76	105	33.7	64.6	1.92	1.05	23.13	1.76	35.5	1.05	7.61
5	Xiao and Wu (2000)	CFRP	152	0.76	105	33.7	75.2	2.23	1.05	19.82	1.59	39.1	1.16	8.02
6	Xiao and Wu (2000)	CFRP	152	0.76	105	33.7	71.8	2.13	1.05	22.08	1.57	38.2	1.13	7.11
7	Xiao and Wu (2000)	CFRP	152	1.14	105	33.7	82.9	2.46	1.58	19.56	1.74	40.1	1.19	8.90
8	Xiao and Wu (2000)	CFRP	152	1.14	105	33.7	95.4	2.83	1.58	21.14	1.77	41.8	1.24	8.37
9	Xiao and Wu (2000)	CFRP	152	0.76	105	43.8	84.0	1.92	1.05	28.72	2.23	49.7	1.13	7.76
10	Xiao and Wu (2000)	CFRP	152	0.76	105	43.8	79.2	1.81	1.05	28.50	2.14	49.8	1.14	7.51
11	Xiao and Wu (2000)	CFRP	152	0.76	105	43.8	85.0	1.94	1.05	26.16	2.03	52.5	1.20	7.76
12	Xiao and Wu (2000)	CFRP	152	1.14	105	43.8	96.5	2.20	1.58	22.75	2.55	52.9	1.21	11.21
13	Xiao and Wu (2000)	CFRP	152	1.14	105	43.8	92.6	2.11	1.58	24.88	2.47	51.8	1.18	9.93
14	Xiao and Wu (2000)	CFRP	152	1.14	105	43.8	94.0	2.15	1.58	24.85	2.51	52.0	1.19	10.10
15	Xiao and Wu (2000)	CFRP	152	1.14	105	55.2	106.5	1.93	1.58	33.55	3.28	64.0	1.16	9.78
16	Xiao and Wu (2000)	CFRP	152	1.14	105	55.2	108.0	1.96	1.58	28.76	3.00	66.9	1.21	10.43
17	Xiao and Wu (2000)	CFRP	152	1.14	105	55.2	103.3	1.87	1.58	31.28	4.09	57.5	1.04	13.08
18	Lam and Teng (2004)	CFRP	152	0.17	258.8	35.9	50.4	1.40	0.56	30.47	1.36	33.9	0.94	4.46
19	Lam and Teng (2004)	CFRP	152	0.17	258.8	35.9	47.2	1.31	0.56	26.51	1.20	34.1	0.95	4.53
20	Lam and Teng (2004)	CFRP	152	0.17	258.8	35.9	53.2	1.48	0.56	24.92	1.46	34.6	0.96	5.86
21	Lam and Teng (2004)	CFRP	152	0.33	258.8	35.9	68.7	1.91	1.12	27.50	1.91	37.2	1.04	6.95
22	Lam and Teng (2004)	CFRP	152	0.33	258.8	35.9	69.9	1.95	1.12	24.58	1.66	37.8	1.05	6.75

Table 10. 6 Continued

No.	Source of data	FRP wrap	D (mm)	t_f (mm)	E_f (GPa)	f'_{co} (MPa)	f'_{cc} (MPa)	f'_{cc} / f'_{co}	E_L^* (GPa)	E_1^* (GPa)	E_2^* (GPa)	f_o^* (MPa)	f_o / f'_{co}	E_2 / E_1 (%)
23	Lam and Teng (2004)	CFRP	152	0.33	258.8	35.9	71.6	1.99	1.12	21.91	2.00	37.2	1.04	9.13
24	Lam and Teng (2004)	CFRP	152	0.50	258.8	34.3	82.6	2.41	1.69	22.55	2.34	35.6	1.04	10.38
25	Lam and Teng (2004)	CFRP	152	0.50	258.8	34.3	90.4	2.64	1.69	21.57	2.18	36.6	1.07	10.11
26	Lam and Teng (2004)	CFRP	152	0.50	258.8	34.3	97.3	2.84	1.69	25.73	2.41	36.4	1.06	9.37
27	Lam and Teng (2004)	GFRP	152	1.27	22.46	38.5	51.9	1.35	0.38	31.73	1.08	38.1	0.99	3.40
28	Lam and Teng (2004)	GFRP	152	1.27	22.46	38.5	58.3	1.51	0.38	25.92	1.01	43.7	1.14	3.90
29	Lam and Teng (2004)	GFRP	152	2.54	22.46	38.5	75.7	1.97	0.75	18.28	1.38	42.9	1.11	7.55
30	Lam and Teng (2004)	GFRP	152	2.54	22.46	38.5	77.3	2.01	0.75	24.27	1.53	44.2	1.15	6.30
31	Rousakis and Tepfers (2004)	CFRP	150	0.17	377	25.2	41.6	1.65	0.85	10.93	1.39	22.3	0.88	12.72
32	Rousakis and Tepfers (2004)	CFRP	150	0.17	377	25.2	38.8	1.54	0.85	13.43	1.72	20.0	0.79	12.81
33	Rousakis and Tepfers (2004)	CFRP	150	0.34	377	25.2	55.9	2.22	1.71	11.06	1.65	21.8	0.87	14.92
34	Rousakis and Tepfers (2004)	CFRP	150	0.51	377	25.2	67.0	2.66	2.56	10.95	1.78	24.0	0.95	16.26
35	Rousakis and Tepfers (2004)	CFRP	150	0.51	377	25.2	67.3	2.67	2.56	9.64	1.94	21.2	0.84	20.12
36	Rousakis and Tepfers (2004)	CFRP	150	0.17	377	51.8	78.7	1.52	0.85	26.99	3.43	53.3	1.03	12.71
37	Rousakis and Tepfers (2004)	CFRP	150	0.17	377	51.8	72.8	1.41	0.85	27.46	3.85	48.5	0.94	14.02
38	Rousakis and Tepfers (2004)	CFRP	150	0.34	377	51.8	95.4	1.84	1.71	26.25	4.57	47.9	0.92	17.41
39	Rousakis and Tepfers (2004)	CFRP	150	0.34	377	51.8	90.7	1.75	1.71	25.36	3.36	57.4	1.11	13.25
40	Rousakis and Tepfers (2004)	CFRP	150	0.51	377	51.8	110.5	2.13	2.56	25.85	4.29	55.8	1.08	16.60
41	Rousakis and Tepfers (2004)	CFRP	150	0.51	377	51.8	103.6	2.00	2.56	23.00	3.94	57.0	1.10	17.13
42	Rousakis and Tepfers (2004)	CFRP	150	0.85	377	51.8	126.7	2.45	4.27	28.35	4.51	59.6	1.15	15.91
43	Berthet et al. (2005)	CFRP	160	0.17	230	25.0	42.8	1.71	0.47	25.79	1.21	26.3	1.05	4.69
44	Berthet et al. (2005)	CFRP	160	0.33	230	25.0	55.2	2.21	0.95	19.87	1.48	32.2	1.29	7.45
45	Berthet et al. (2005)	CFRP	160	0.11	230	40.1	50.8	1.27	0.32	33.48	1.03	43.9	1.09	3.08
46	Berthet et al. (2005)	CFRP	160	0.17	230	40.1	53.7	1.34	0.47	36.83	1.40	45.3	1.13	3.80
47	Berthet et al. (2005)	CFRP	160	0.22	230	40.1	59.7	1.49	0.63	31.97	1.72	47.6	1.19	5.38
48	Berthet et al. (2005)	CFRP	160	0.44	230	40.1	91.6	2.28	1.27	31.70	2.73	53.9	1.34	8.61
49	Berthet et al. (2005)	CFRP	160	0.99	230	40.1	142.4	3.55	2.85	25.31	3.16	65.7	1.64	12.49
50	Berthet et al. (2005)	CFRP	160	1.32	230	40.1	166.3	4.15	3.80	31.24	3.81	66.0	1.65	12.20
51	Berthet et al. (2005)	CFRP	160	0.33	230	52.0	82.8	1.59	0.95	54.70	2.53	65.7	1.26	4.63
52	Berthet et al. (2005)	CFRP	160	0.66	230	52.0	108.1	2.08	1.90	48.61	3.31	72.0	1.38	6.81
53	Berthet et al. (2005)	CFRP	70	0.33	230	112.6	141.1	1.25	2.17	58.50	4.09	120.8	1.07	6.99

Table 10. 6 Continued

No.	Source of data	FRP wrap	D (mm)	t_f (mm)	E_f (GPa)	f'_{co} (MPa)	f'_{cc} (MPa)	f'_{cc} / f'_{co}	E_L^* (GPa)	E_1^* (GPa)	E_2^* (GPa)	f_o^* (MPa)	f_o / f'_{co}	E_2 / E_1 (%)
54	Berthet et al. (2005)	CFRP	70	0.82	230	112.6	189.5	1.68	5.39	66.25	5.55	142.5	1.27	8.38
55	Berthet et al. (2005)	CFRP	70	0.99	230	169.7	296.4	1.75	6.51	60.05	13.56	158.3	0.93	22.58
56	Berthet et al. (2005)	GFRP	160	0.33	74	25.0	42.8	1.71	0.31	25.42	0.92	27.6	1.10	3.62
57	Lam et al. (2006)	CFRP	152	0.17	250	41.1	57.0	1.39	0.54	26.68	1.51	39.0	0.95	5.66
58	Lam et al. (2006)	CFRP	152	0.17	250	41.1	55.4	1.35	0.54	30.83	1.54	38.5	0.94	5.00
59	Lam et al. (2006)	CFRP	152	0.33	250	38.9	79.1	2.03	1.09	28.87	2.00	38.6	0.99	6.93
60	Almusallam (2007)	GFRP	150	3.90	27	47.7	100.1	2.10	1.40	24.61	1.90	48.8	1.02	7.72
61	Almusallam (2007)	GFRP	150	3.90	27	50.8	90.8	1.79	1.40	28.90	2.00	51.7	1.02	6.92
62	Almusallam (2007)	GFRP	150	3.90	27	60.0	99.6	1.66	1.40	31.36	2.42	61.4	1.02	7.72
63	Almusallam (2007)	GFRP	150	3.90	27	90.3	110.0	1.22	1.40	48.56	1.81	94.4	1.05	3.73
64	Jiang and Teng (2007)	GFRP	152	0.17	80.1	33.1	42.4	1.28	0.18	18.62	0.46	36.7	1.11	2.47
65	Jiang and Teng (2007)	GFRP	152	0.17	80.1	33.1	41.6	1.26	0.18	21.44	0.54	35.1	1.06	2.52
66	Jiang and Teng (2007)	GFRP	152	0.34	80.1	45.9	52.8	1.15	0.36	33.29	0.47	47.0	1.02	1.41
67	Jiang and Teng (2007)	GFRP	152	0.34	80.1	45.9	55.2	1.20	0.36	34.11	0.59	47.5	1.03	1.73
68	Jiang and Teng (2007)	GFRP	152	0.51	80.1	45.9	64.6	1.41	0.54	23.06	1.03	49.3	1.07	4.47
69	Jiang and Teng (2007)	GFRP	152	0.51	80.1	45.9	65.9	1.44	0.54	17.63	0.79	50.9	1.11	4.48
70	Jiang and Teng (2007)	CFRP	152	0.68	240.7	38.0	110.1	2.90	2.15	17.48	2.22	55.9	1.47	12.70
71	Jiang and Teng (2007)	CFRP	152	0.68	240.7	38.0	107.4	2.83	2.15	20.09	2.36	48.7	1.28	11.75
72	Jiang and Teng (2007)	CFRP	152	1.02	240.7	38.0	129.0	3.39	3.23	21.66	2.70	56.1	1.48	12.47
73	Jiang and Teng (2007)	CFRP	152	1.02	240.7	38.0	135.7	3.57	3.23	16.83	2.63	55.0	1.45	15.63
74	Jiang and Teng (2007)	CFRP	152	1.36	240.7	38.0	161.3	4.24	4.31	19.53	2.79	59.7	1.57	14.29
75	Jiang and Teng (2007)	CFRP	152	1.36	240.7	38.0	158.5	4.17	4.31	14.69	2.77	61.1	1.61	18.86
76	Jiang and Teng (2007)	CFRP	152	0.11	260	37.7	48.5	1.29	0.38	27.59	1.09	38.9	1.03	3.95
77	Jiang and Teng (2007)	CFRP	152	0.11	260	37.7	50.3	1.33	0.38	27.39	1.32	38.3	1.02	4.82
78	Jiang and Teng (2007)	CFRP	152	0.11	260	44.2	48.1	1.09	0.38	27.64	1.15	40.2	0.91	4.16
79	Jiang and Teng (2007)	CFRP	152	0.11	260	44.2	51.1	1.16	0.38	30.25	0.91	43.1	0.98	3.01
80	Jiang and Teng (2007)	CFRP	152	0.22	260	44.2	65.7	1.49	0.75	30.07	1.87	43.9	0.99	6.22
81	Jiang and Teng (2007)	CFRP	152	0.22	260	44.2	62.9	1.42	0.75	27.00	2.12	41.0	0.93	7.85
82	Jiang and Teng (2007)	CFRP	152	0.33	260	47.6	82.7	1.74	1.13	31.99	2.52	50.2	1.05	7.88
83	Jiang and Teng (2007)	CFRP	152	0.33	260	47.6	85.5	1.80	1.13	31.83	2.13	51.5	1.08	6.69

Table 10. 6 Continued

No.	Source of data	FRP wrap	D (mm)	t_f (mm)	E_f (GPa)	f'_{co} (MPa)	f'_{cc} (MPa)	f'_{cc} / f'_{co}	E_L^* (GPa)	E_1^* (GPa)	E_2^* (GPa)	f_o^* (MPa)	f_o / f'_{co}	E_2 / E_1 (%)
84	Jiang and Teng (2007)	CFRP	152	0.33	260	47.6	85.5	1.80	1.13	28.92	2.09	49.4	1.04	7.23
85	Wang and Wu (2008)	CFRP	150	0.17	219	30.9	55.8	1.81	0.48	29.05	1.31	32.3	1.05	4.51
86	Wang and Wu (2008)	CFRP	150	0.17	219	52.1	67.9	1.30	0.48	34.96	1.57	49.6	0.95	4.49
87	Wang and Wu (2008)	CFRP	150	0.33	197	52.1	99.3	1.91	0.87	34.49	2.35	53.6	1.03	6.81
88	Benzaid et al. (2010)	CFRP	160	1.00	34	25.9	39.6	1.53	0.43	24.77	0.84	28.7	1.11	3.39
89	Benzaid et al. (2010)	CFRP	160	3.00	34	25.9	66.1	2.55	1.28	45.54	2.10	34.4	1.33	4.61
90	Benzaid et al. (2010)	CFRP	160	3.00	34	49.5	82.9	1.68	1.28	39.45	3.48	58.2	1.18	8.82
91	Benzaid et al. (2010)	CFRP	160	3.00	34	61.8	93.2	1.51	1.28	25.48	2.11	71.5	1.16	8.28
92	Cui and Sheikh (2010)	CFRP	152	1.00	84.6	48.1	80.9	1.68	1.11	31.95	2.40	47.2	0.98	7.51
93	Cui and Sheikh (2010)	CFRP	152	1.00	84.6	48.1	86.6	1.80	1.11	29.28	2.55	49.3	1.02	8.71
94	Cui and Sheikh (2010)	CFRP	152	2.00	84.6	48.1	109.4	2.27	2.23	28.26	2.99	50.2	1.04	10.58
95	Cui and Sheikh (2010)	CFRP	152	2.00	84.6	48.1	126.7	2.63	2.23	24.25	2.71	55.8	1.16	11.18
96	Cui and Sheikh (2010)	CFRP	152	3.00	84.6	48.1	162.7	3.38	3.34	29.15	3.42	58.7	1.22	11.73
97	Cui and Sheikh (2010)	CFRP	152	3.00	84.6	48.1	153.6	3.19	3.34	29.34	3.45	57.1	1.19	11.76
98	Cui and Sheikh (2010)	CFRP	152	1.00	84.6	48.1	84.2	1.75	1.11	32.48	2.26	50.6	1.05	6.96
99	Cui and Sheikh (2010)	CFRP	152	1.00	84.6	48.1	87.9	1.83	1.11	32.74	2.30	50.3	1.05	7.03
100	Cui and Sheikh (2010)	CFRP	152	2.00	84.6	48.1	123.3	2.56	2.23	29.07	2.92	55.1	1.15	10.04
101	Cui and Sheikh (2010)	CFRP	152	2.00	84.6	48.1	108.2	2.25	2.23	31.04	3.11	52.6	1.09	10.02
102	Cui and Sheikh (2010)	CFRP	152	3.00	84.6	48.1	156.5	3.25	3.34	30.10	3.30	55.8	1.16	10.96
103	Cui and Sheikh (2010)	CFRP	152	3.00	84.6	48.1	157.0	3.26	3.34	31.62	3.59	56.6	1.18	11.35
104	Cui and Sheikh (2010)	CFRP	152	1.00	84.6	79.9	105.3	1.32	1.11	53.05	2.59	86.3	1.08	4.88
105	Cui and Sheikh (2010)	CFRP	152	2.00	84.6	79.9	142.1	1.78	2.23	48.96	4.58	88.8	1.11	9.35
106	Cui and Sheikh (2010)	CFRP	152	2.00	84.6	79.9	140.8	1.76	2.23	44.66	4.92	89.6	1.12	11.02
107	Cui and Sheikh (2010)	CFRP	152	3.00	84.6	79.9	172.9	2.16	3.34	54.30	5.69	88.4	1.11	10.48
108	Cui and Sheikh (2010)	CFRP	152	3.00	84.6	79.9	181.8	2.28	3.34	51.54	5.80	94.8	1.19	11.25
109	Cui and Sheikh (2010)	CFRP	152	0.11	241.3	45.6	57.7	1.27	0.35	31.30	0.86	47.5	1.04	2.75
110	Cui and Sheikh (2010)	CFRP	152	0.11	241.3	45.6	55.4	1.21	0.35	36.41	0.86	44.1	0.97	2.36
111	Cui and Sheikh (2010)	CFRP	152	0.22	241.3	45.6	78.0	1.71	0.70	26.92	1.68	46.0	1.01	6.24
112	Cui and Sheikh (2010)	CFRP	152	0.22	241.3	45.6	86.8	1.90	0.70	28.08	1.79	48.8	1.07	6.37
113	Cui and Sheikh (2010)	CFRP	152	0.33	241.3	45.6	106.5	2.34	1.06	31.18	2.14	45.9	1.01	6.86

Table 10. 6 Continued

No.	Source of data	FRP wrap	D (mm)	t_f (mm)	E_f (GPa)	f'_{co} (MPa)	f'_{cc} (MPa)	f'_{cc} / f'_{co}	E_L^* (GPa)	E_1^* (GPa)	E_2^* (GPa)	f_o^* (MPa)	f_o / f'_{co}	E_2 / E_1 (%)
114	Cui and Sheikh (2010)	CFRP	152	0.33	241.3	45.6	106.0	2.32	1.06	32.22	2.20	48.2	1.06	6.83
115	Cui and Sheikh (2010)	CFRP	152	0.11	241.3	45.6	56.3	1.23	0.35	38.63	1.01	43.5	0.95	2.61
116	Cui and Sheikh (2010)	CFRP	152	0.11	241.3	45.6	58.8	1.29	0.35	38.72	1.31	44.2	0.97	3.38
117	Cui and Sheikh (2010)	CFRP	152	0.22	241.3	45.6	81.9	1.80	0.70	31.08	1.89	46.9	1.03	6.08
118	Cui and Sheikh (2010)	CFRP	152	0.22	241.3	45.6	82.8	1.82	0.70	38.69	1.66	46.7	1.02	4.29
119	Cui and Sheikh (2010)	CFRP	152	0.33	241.3	45.6	107.3	2.35	1.06	32.44	2.16	47.3	1.04	6.66
120	Cui and Sheikh (2010)	CFRP	152	0.33	241.3	45.6	108.6	2.38	1.06	32.96	2.21	48.3	1.06	6.71
121	Cui and Sheikh (2010)	CFRP	152	0.16	437.5	45.7	67.5	1.48	0.94	39.02	2.40	41.8	0.91	6.15
122	Cui and Sheikh (2010)	CFRP	152	0.16	437.5	45.7	64.1	1.40	0.94	42.57	2.47	39.2	0.86	5.80
123	Cui and Sheikh (2010)	CFRP	152	0.33	437.5	45.7	84.2	1.84	1.88	33.43	3.32	40.6	0.89	9.93
124	Cui and Sheikh (2010)	CFRP	152	0.33	437.5	45.7	83.1	1.82	1.88	32.97	3.33	43.1	0.94	10.10
125	Cui and Sheikh (2010)	CFRP	152	0.49	437.5	45.7	99.7	2.18	2.81	32.23	3.53	45.1	0.99	10.95
126	Cui and Sheikh (2010)	CFRP	152	0.49	437.5	45.7	94.9	2.08	2.81	36.01	3.67	42.8	0.94	10.19
127	Cui and Sheikh (2010)	CFRP	152	0.16	437.5	45.7	65.8	1.44	0.94	36.59	2.49	42.1	0.92	6.81
128	Cui and Sheikh (2010)	CFRP	152	0.16	437.5	45.7	65.9	1.44	0.94	35.49	2.41	41.7	0.91	6.79
129	Cui and Sheikh (2010)	CFRP	152	0.33	437.5	45.7	88.1	1.93	1.88	38.43	3.30	41.2	0.90	8.59
130	Cui and Sheikh (2010)	CFRP	152	0.33	437.5	45.7	82.0	1.79	1.88	33.51	3.33	42.2	0.92	9.94
131	Cui and Sheikh (2010)	CFRP	152	0.65	437.5	45.7	103.2	2.26	3.75	33.70	3.94	43.7	0.96	11.69
132	Cui and Sheikh (2010)	CFRP	152	0.65	437.5	45.7	105.6	2.31	3.75	35.01	3.31	45.0	0.98	9.45
133	Cui and Sheikh (2010)	CFRP	152	0.33	437.5	85.7	117.7	1.37	1.88	45.57	3.70	90.4	1.05	8.12
134	Cui and Sheikh (2010)	CFRP	152	0.33	437.5	85.7	117.5	1.37	1.88	42.86	4.45	89.9	1.05	10.38
135	Cui and Sheikh (2010)	CFRP	152	0.65	437.5	85.7	161.6	1.89	3.75	44.32	7.53	86.4	1.01	16.99
136	Cui and Sheikh (2010)	CFRP	152	0.65	437.5	85.7	162.6	1.90	3.75	46.49	7.16	94.8	1.11	15.40
137	Cui and Sheikh (2010)	GFRP	152	1.25	21.47	47.7	59.1	1.24	0.35	59.65	1.30	42.8	0.90	2.18
138	Cui and Sheikh (2010)	GFRP	152	1.25	21.47	47.7	59.8	1.25	0.35	51.96	1.49	43.0	0.90	2.87
139	Cui and Sheikh (2010)	GFRP	152	2.50	21.47	47.7	88.9	1.86	0.71	42.60	1.99	47.3	0.99	4.67
140	Cui and Sheikh (2010)	GFRP	152	2.50	21.47	47.7	88.0	1.84	0.71	36.34	1.92	47.2	0.99	5.28
141	Cui and Sheikh (2010)	GFRP	152	3.75	21.47	47.7	113.2	2.37	1.06	31.03	2.24	52.3	1.10	7.22
142	Cui and Sheikh (2010)	GFRP	152	3.75	21.47	47.7	112.5	2.36	1.06	27.13	2.20	52.0	1.09	8.11
143	Cui and Sheikh (2010)	GFRP	152	1.25	21.47	47.7	63.4	1.33	0.35	36.99	1.10	47.0	0.99	2.97

Table 10. 6 Continued

No.	Source of data	FRP wrap	D (mm)	t_f (mm)	E_f (GPa)	f'_{co} (MPa)	f'_{cc} (MPa)	f'_{cc} / f'_{co}	E_L^* (GPa)	E_1^* (GPa)	E_2^* (GPa)	f_o^* (MPa)	f_o / f'_{co}	E_2 / E_1 (%)
144	Cui and Sheikh (2010)	GFRP	152	1.25	21.47	47.7	62.4	1.31	0.35	49.53	1.14	47.7	1.00	2.30
145	Cui and Sheikh (2010)	GFRP	152	2.50	21.47	47.7	89.7	1.88	0.71	40.00	1.98	47.9	1.00	4.95
146	Cui and Sheikh (2010)	GFRP	152	2.50	21.47	47.7	88.3	1.85	0.71	34.73	2.01	48.8	1.02	5.79
147	Cui and Sheikh (2010)	GFRP	152	3.75	21.47	47.7	108.0	2.26	1.06	32.03	2.20	52.5	1.10	6.87
148	Dai et al. (2011)	AFRP	152	0.17	115.2	39.2	61.4	1.57	0.26	16.70	0.85	41.8	1.07	5.09
149	Dai et al. (2011)	AFRP	152	0.17	115.2	39.2	62.7	1.60	0.26	13.54	0.83	43.8	1.12	6.13
150	Dai et al. (2011)	AFRP	152	0.17	115.2	39.2	55.8	1.42	0.26	14.87	1.00	35.3	0.90	6.72
151	Dai et al. (2011)	AFRP	152	0.34	115.2	39.2	90.1	2.30	0.51	16.26	1.22	47.3	1.21	7.50
152	Dai et al. (2011)	AFRP	152	0.34	115.2	39.2	88.3	2.25	0.51	19.04	1.35	43.0	1.10	7.09
153	Dai et al. (2011)	AFRP	152	0.34	115.2	39.2	83.3	2.13	0.51	11.70	1.19	40.6	1.04	10.17
154	Dai et al. (2011)	AFRP	152	0.51	115.2	39.2	113.2	2.89	0.77	15.30	1.51	52.6	1.34	9.87
155	Dai et al. (2011)	AFRP	152	0.51	115.2	39.2	116.3	2.97	0.77	11.68	1.42	53.8	1.37	12.16
156	Dai et al. (2011)	AFRP	152	0.51	115.2	39.2	118	3.01	0.77	12.28	1.38	53.4	1.36	11.24
157	Wang et al. (2012)	CFRP	204	0.17	244	24.5	46.1	1.88	0.40	13.22	0.77	27.8	1.13	5.82
158	Wang et al. (2012)	CFRP	204	0.33	244	24.5	65.2	2.66	0.80	13.59	1.03	29.2	1.19	7.58
159	Lim and Ozbakkaloglu (2014a)	AFRP	150	0.20	128.5	29.6	52.5	1.77	0.34	29.30	1.03	31.4	1.06	3.52
160	Lim and Ozbakkaloglu (2014a)	AFRP	150	0.20	128.5	29.6	50.3	1.70	0.34	25.00	1.02	30.6	1.03	4.08
161	Lim and Ozbakkaloglu (2014a)	AFRP	150	0.20	128.5	29.6	50.5	1.71	0.34	28.87	0.93	32.2	1.09	3.22
162	Lim and Ozbakkaloglu (2014a)	CFRP	150	0.17	236	29.6	57.3	1.94	0.52	32.13	1.18	36.1	1.22	3.67
163	Lim and Ozbakkaloglu (2014a)	CFRP	150	0.17	236	29.6	60.4	2.04	0.52	27.86	1.25	35.9	1.21	4.49
164	Lim and Ozbakkaloglu (2014a)	CFRP	150	0.17	236	29.6	61.2	2.07	0.52	31.65	1.18	35.2	1.19	3.73
165	Lim and Ozbakkaloglu (2014a)	GFRP	150	0.20	95.3	29.6	50.8	1.72	0.25	30.38	0.87	35.8	1.21	2.86
166	Lim and Ozbakkaloglu (2014a)	GFRP	150	0.20	95.3	29.6	46.6	1.57	0.25	26.08	0.87	33.8	1.14	3.34
167	Lim and Ozbakkaloglu (2014a)	GFRP	150	0.20	95.3	29.6	49.4	1.67	0.25	24.38	0.76	34.9	1.18	3.12
168	Lim and Ozbakkaloglu (2014a)	AFRP	150	0.40	128.5	49.6	83.1	1.68	0.69	33.90	1.34	49.6	1.00	3.95

Table 10. 6 Continued

No.	Source of data	FRP wrap	D (mm)	t_f (mm)	E_f (GPa)	f'_{co} (MPa)	f'_{cc} (MPa)	f'_{cc} / f'_{co}	E_L^* (GPa)	E_1^* (GPa)	E_2^* (GPa)	f_o^* (MPa)	f_o / f'_{co}	E_2 / E_1 (%)
169	Lim and Ozbakkaloglu (2014a)	AFRP	150	0.40	128.5	49.6	87.2	1.76	0.69	24.50	1.55	53.0	1.07	6.33
170	Lim and Ozbakkaloglu (2014a)	AFRP	150	0.40	128.5	49.6	84	1.69	0.69	35.15	1.26	51.1	1.03	3.58
171	Lim and Ozbakkaloglu (2014a)	CFRP	150	0.33	236	49.6	98	1.98	1.04	37.96	1.92	52.5	1.06	5.06
172	Lim and Ozbakkaloglu (2014a)	CFRP	150	0.33	236	49.6	95.3	1.92	1.04	43.99	2.01	54.0	1.09	4.57
173	Lim and Ozbakkaloglu (2014a)	CFRP	150	0.33	236	49.6	100.3	2.02	1.04	38.93	2.11	58.2	1.17	5.42
174	Lim and Ozbakkaloglu (2014a)	GFRP	150	0.40	95.3	49.6	78.3	1.58	0.51	44.20	1.33	55.3	1.11	3.01
175	Lim and Ozbakkaloglu (2014a)	GFRP	150	0.40	95.3	49.6	75.6	1.52	0.51	34.78	1.15	55.6	1.12	3.31
176	Lim and Ozbakkaloglu (2014a)	GFRP	150	0.40	95.3	49.6	71.4	1.44	0.51	43.93	1.20	55.5	1.12	2.73
177	Lim and Ozbakkaloglu (2014a)	GFRP	150	0.60	95.3	74.1	90.8	1.23	0.76	51.91	1.66	81.8	1.10	3.20
178	Lim and Ozbakkaloglu (2014a)	GFRP	150	0.60	95.3	74.1	91.8	1.24	0.76	41.65	1.53	74.0	1.00	3.67
179	Lim and Ozbakkaloglu (2014b)	AFRP	150	1.20	128.5	85.7	166.2	1.94	2.06	36.49	2.89	107.0	1.25	7.92
180	Lim and Ozbakkaloglu (2014b)	AFRP	150	1.20	128.5	85.7	168	1.96	2.06	51.10	2.95	101.3	1.18	5.77
181	Lim and Ozbakkaloglu (2014b)	AFRP	150	1.20	128.5	85.6	165.2	1.93	2.06	45.65	2.80	102.9	1.20	6.13
182	Lim and Ozbakkaloglu (2014b)	AFRP	150	1.20	128.5	112.3	168.4	1.50	2.06	54.73	3.49	107.5	0.96	6.38
183	Lim and Ozbakkaloglu (2014b)	GFRP	150	0.80	95.3	57.4	125.7	2.19	1.02	49.45	1.74	67.5	1.18	3.52
184	Lim and Ozbakkaloglu (2014b)	GFRP	150	0.80	95.3	57.3	127.2	2.22	1.02	41.29	1.58	71.4	1.25	3.83
185	Lim and Ozbakkaloglu (2014b)	GFRP	150	0.80	95.3	57.3	131.2	2.29	1.02	26.10	1.60	72.8	1.27	6.13
186	Lim (2015)	AFRP	150	0.80	128.5	74.8	130.1	1.74	1.37	42.94	2.33	89.9	1.20	5.43
187	Lim (2015)	AFRP	150	0.80	128.5	75.0	130.5	1.74	1.37	48.23	1.92	91.4	1.22	3.98
188	Lim (2015)	AFRP	150	0.80	128.5	74.9	139.3	1.86	1.37	42.50	2.19	91.8	1.23	5.15
189	Lim (2015)	GFRP	150	0.80	95.3	73.9	136.0	1.84	1.02	44.02	1.76	90.4	1.22	4.00
190	Lim (2015)	GFRP	150	0.80	95.3	74.2	138.7	1.87	1.02	38.41	1.76	90.5	1.22	4.58
191	Lim (2015)	GFRP	150	0.80	95.3	74.1	136.3	1.84	1.02	48.89	1.82	87.1	1.18	3.72

Table 10. 6 Continued

No.	Source of data	FRP wrap	D (mm)	t_f (mm)	E_f (GPa)	f'_{co} (MPa)	f'_{cc} (MPa)	f'_{cc} / f'_{co}	E_L^* (GPa)	E_1^* (GPa)	E_2^* (GPa)	f_o^* (MPa)	f_o / f'_{co}	E_2 / E_1 (%)
192	Lim (2015)	GFRP	150	0.40	95.3	34.8	78.1	2.25	0.51	30.16	1.19	40.3	1.16	3.95
193	Lim (2015)	GFRP	150	0.40	95.3	34.7	76.3	2.20	0.51	27.67	1.10	39.4	1.14	3.98
194	Lim (2015)	GFRP	150	0.40	95.3	34.8	75.1	2.16	0.51	30.71	1.13	40.8	1.17	3.68
195	Fillmore and Sadeghian (2018)	BFRP	150	0.90	24.62	40.0	55.9	1.40	0.30	38.46	1.32	45.0	1.13	3.43
196	Fillmore and Sadeghian (2018)	BFRP	150	0.90	24.62	40.0	56.8	1.42	0.30	34.86	1.44	45.6	1.14	4.13
197	Fillmore and Sadeghian (2018)	BFRP	150	1.80	24.62	40.0	76.4	1.91	0.59	30.67	1.42	49.4	1.24	4.63
198	Fillmore and Sadeghian (2018)	BFRP	150	1.80	24.62	40.0	78.2	1.95	0.59	44.75	1.55	49.7	1.24	3.46
199	Fillmore and Sadeghian (2018)	BFRP	150	2.70	24.62	40.0	95.4	2.38	0.89	32.39	2.14	50.5	1.26	6.61
200	Fillmore and Sadeghian (2018)	BFRP	150	2.70	24.62	40.0	99.0	2.47	0.89	41.14	1.71	54.5	1.36	4.16
Mean			151	0.89	178.2	47.8	90.5	1.94	1.29	31.56	2.21	52.43	1.10	7.36
STD			11.6	0.9	122.5	18.4	36.7	0.6	1.05	10.7	1.4	20.6	0.14	3.9
COV(%)			8	105	69	38	41	30	82	34	64	40	13	53

Note: * The values are found in the current study; STD = standard deviation; COV = coefficient of variation.

To calibrate the parameters, a parabola was fitted to the first portions of the curves and the initial slope of the parabola was considered as the initial modulus of elasticity (E_1). Also, a straight line was fitted to all secondary portions of the curve and the slope of the curves was found as the slope of the fitted line (E_2) and the intercept stress was evaluated as the line intercepts the stress axis (f_o). For each curve, the values of the initial slope, secondary slope, the intercept stress, and the confining stiffness are presented in Table 10.6. Also, the ratio of the secondary slope to the initial slope (E_2/E_1) and the ratio of the intercept stress to the unconfined concrete strength (f_o/f_{co}) were presented in Table 10.6. To show the range of the data used in the database, the mean, standard deviation (STD), and the coefficient of variation (COV) of each column is presented at the end of Table 10.6.

To drive equations for the parameters of the stress-strain curve, a regression analysis was performed by considering the confining stiffness (E_L) and unconfined concrete strength (f'_{co}) as the effective parameters. For initial slope for the first region, the regression showed the best-fitted equation as $E_1 = 4691\sqrt{f'_{co}}$ with $(R^2 = 0.4818)$ which is quite close to the prediction of unconfined concrete modulus proposed by ACI 318 (2019). Thus, Equation 10.27 from ACI 318 (2019) was adopted instead of the one found from the regression. Equation 10.27 through Equation 10.29 show the results of the regression analysis (Figure 10.9), in which all the units are in MPa.

$$E_1 = 4700\sqrt{f'_{co}} \qquad (R^2 = 0.4817) \tag{10.27}$$

$$E_2 = 9.6\sqrt{E_l}\ \sqrt{f'_{co}} \qquad (R^2 = 0.8251) \tag{10.28}$$

$$f_o = (1 + 0.15\frac{\sqrt{E_l}}{f'_{co}})f'_{co} \qquad (R^2 = 0.9083) \tag{10.29}$$

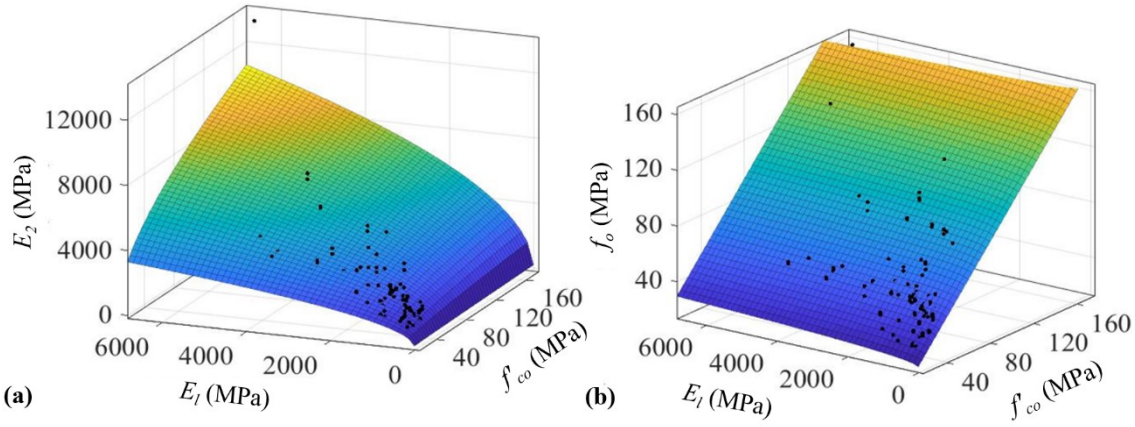

Figure 10. 9 Regression results for deriving equations for: (a) E_2 and (b) f_o

Equation 10.28 predicts the slope of the secondary portion of the stress-strain curves. The equation showed that an increase in confining stiffness and unconfined concrete strength directly increase the secondary modulus of the curve. However, the comparison between the initial slope and the secondary slope shows that the constant coefficient for Equation

10.28 is much lower than the one for Equation 10.27. The latter is compatible with the results of experimental stress-strain curves presented in Table 10.6, as the average ratio of secondary to the initial slope of the curve is 7.36 %. The coefficient of determination (R^2) for Equation 10.28 is 0.8251 which shows a very good agreement between the experimental results and the prediction as presented in Figure 10.9(a).

Equation 10.29 predicts the intercept stress as the sum of unconfined concrete strength and a percentage of confining stiffness which is compatible with the results of experimental tests as presented in Table 10.6. The average ratio of intercept stress to unconfined concrete strength is 1.10 showed in Table 10.6, which shows an average upward shift of 10% in the intercept stress with respect to the unconfined concrete strength. The additional shift is attributed to the confining stiffness in Equation 10.29 which showed a very good agreement with the tests results ($R^2 = 0.9083$), as presented in Figure 10.9(b). Also, the coefficient of variation of the data is 13% which shows the variability of the intercept stress, while it was considered as a constant in many of the models. Thus, it is recommended to consider the intercept stress as a variable parameter instead of a constant.

To find the polynomial constant n, all points in 200 curves, which sums to a total of 3272 points (without the origin points), were evaluated by the Equation 10.26 with parameters introduced in Equation 10.27 to Equation 10.29 and the polynomial constant n was found to minimize the RMSE error of all points. The results of the analysis showed that a polynomial constant of 2.5 minimizes the error (n = 2.5). By substituting curve parameters (Equation 10.27 to Equation 10.29 and a polynomial constant of 2.5) into the Equation 10.26, the stress-strain of the FRP-confined concrete can be shown as a single equation (Equation 10.30).

$$f_c = 9.6\sqrt{\frac{2E_f t_f f'_{co}}{D}}\left\{1+\left(489.6\sqrt{\frac{D}{2E_f t_f}}-1\right)\left[1+\left(\frac{4700-9.6\sqrt{\frac{2E_f t_f}{D}}}{\sqrt{f'_{co}}+0.15\sqrt{\frac{2E_f t_f}{Df'_{co}}}}\varepsilon_c\right)^{2.5}\right]^{-1/2.5}\right\}\varepsilon_c \quad (10.30)$$

To evaluate the performance of the proposed model, fourteen design-oriented stress-strain curves for FRP-confined concrete columns were compared with the experimental curves, as presented in Table 10.7. In addition to RMSE and AAE (Equation 10.19 and 10.20), two more measures of error were considered (Equation 10.31 and 10.32) for mean square error (MSE) and standard deviation (SD).

$$MSE = \frac{\sum\left(\frac{Calc._i - Exp._i}{Exp._i}\right)^2}{N} \quad (10.31)$$

$$SD = \sqrt{\frac{\sum\left(\frac{Calc._i}{Exp._i} - \frac{Calc._{ave}}{Exp._{ave}}\right)^2}{N-1}} \quad (10.32)$$

Table 10. 7 Performance comparison of the proposed axial stress-strain model against the models from the literature (sorted based on the lowest RMSE)

No.	Resource	RMSE	AAE	MSE	SD
1	Current study	6.17	0.0930	0.0185	0.1361
2	Fahmy and Wu (2010)	7.20	0.1021	0.0196	0.1320
3	Teng et al. (2009)	7.53	0.1036	0.0202	0.1282
4	Lam and Teng (2003)	8.13	0.1054	0.0209	0.1377
5	Yu and Teng (2011)	8.19	0.1192	0.0238	0.1287
6	Xiao and Wu (2003)	8.97	0.1132	0.0245	0.1466
7	Samaan et al. (1998)	13.48	0.1872	0.0483	0.1394
8	Saadatmanesh et al. (1994)*	16.55	0.2105	0.0688	0.2320
9	Youssef et al. (2007)	18.71	0.2166	0.0632	0.1490
10	Djafar-Henni and Kassoul (2018)	19.24	0.1928	0.0842	0.2894
11	Yan and Pantelides (2007)	32.60	0.4394	0.2287	0.2489
12	Wu et al. (2009)	44.98	0.3987	0.2784	0.4413
13	Xiao and Wu (2000)	45.24	0.5768	1.0240	0.8686
14	Wu and Wang (2010)	48.94	0.4289	0.3251	0.4733
15	Fardis and Khalili (1982)	49.83	0.6904	0.5020	0.1648

Table 10.7 shows that the proposed stress-strain curve improved the available design-oriented confined stress-strain curves. The distribution of the error measures for the current study and the curve proposed by Lam and Teng (2003), which is the base for the ACI 440.2R (2017), is presented in Figure 10.10. The comparison of the error distribution showed that the model improved the error of every curve considerably, in addition to the overall error presented in Table 10.7.

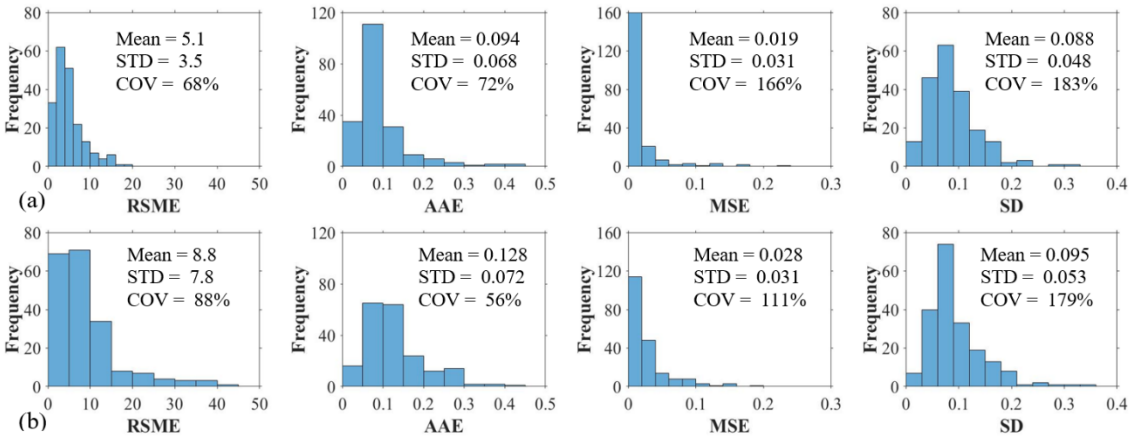

Figure 10. 10 Error distribution for axial stress-strain: (a) Current study and (b) Lam and Teng (2003)

Some samples of the fitted curves are presented in Figure 10.11 which compares the experimental curves from different studies with the five of the best estimations of the stress-strain curves according to Table 10.7. The results showed the proposed stress-strain curves are in a very good agreement with the experimental test results. It should be mentioned that in the formulas showed in Figure 10.11, rather than the proposed equation in this study, the intercept stress was considered constant. Also, for equations proposed by Lam and Teng (2003) and Teng et al. (2009), the secondary is related to the ultimate condition. The results showed that for some cases, using these equations for the prediction leads to a very good fit [as shown in Figure 10.11(f), (h), (i), (j) and (k)]. However, for some cases, the slope

would not be matched with the experimental results [as shown in Figure 10.11(b), (c), (e), and (g)], and for some cases, although the slope is matched, the constant stress intercept leads to lowering down the curves [as shown in Figure 10.11(a), (d), and (l)].

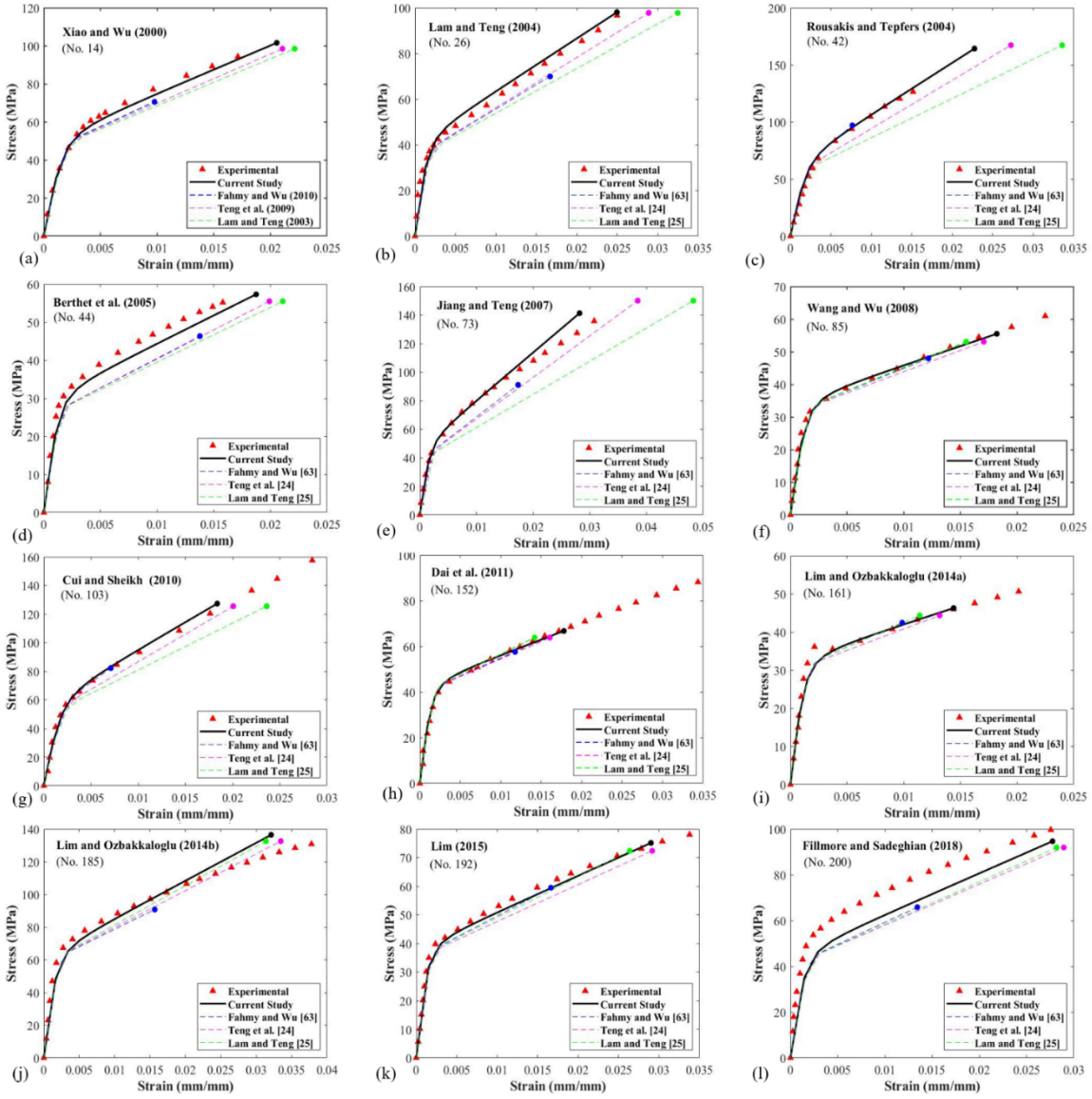

Figure 10. 11 Sample of axial stress-strain curves: (a) Xiao and Wu (2000); (b) Lam and Teng (2004); (c) Rousakis and Tepfers (2004); (d) Berthet et al. (2005); (e) Jiang and Teng (2007); (f) Wang and Wu (2008); (g) Cui and Sheikh (2010); (h) Lim (2015); (i) Dai et al. (2011); (j) Lim and Ozbakkaloglu (2014a); (k) Lim and Ozbakkaloglu (2014b); (l) Fillmore and Sadeghian (2018)

For the proposed model in this study, the intercept stress is a variable which shifts the secondary part up and down, and the ultimate condition is only a point on the curve that cuts the curve and does not affect the secondary slope. Also, the curve predictions by Fahmy and Wu (2010) showed better predictions in comparison to proposed curves by Lam and Teng (2003) and Teng et al. (2009), since the secondary slope was selected independent of the ultimate condition although the main equation format kept the same as Lam and Teng (2003). Thus, it can be concluded that excluding the ultimate condition from the adjustment of stress-strain curves of confined concrete lead to more accurate predictions. Then, the ultimate condition can be used as a cut-off point for the stress-strain curves instead of involving in predicting the curve parameters. It should be mentioned that a safety strain limit of 0.01 mm/mm is considered by ACI 440.2R (2017) which is the cutting point of the stress-strain curves for most of the situations. In the main database including 788 tests, the minimum axial strain at the time of FRP rupture was 0.019 mm/mm. The latter shows that the ultimate condition does not enter the analysis which leads to the designs, as a cutting point of 0.01 mm/mm occur prior to the ultimate confined strain for the majority of cases and govern the designs, although the ultimate confined strain is very effective for analysis purposes which tends to assess the most accurate behavior of the structures without design limitations.

10.5 Comparison of The Ultimate Strain Equations

In this study, the ultimate confined strain is defined as the axial strain corresponding to the ultimate confined concrete strength on the stress-strain curve as presented in Equation 10.33.

$$\varepsilon_{cc} = \frac{f'_{cc} - f_o}{E_2} \tag{10.33}$$

Since Equation 10.33 is not directly found from the regression analysis on the ultimate strains available in the database, the ultimate strain and stress kept their correlation. It should be highlighted that the rupture strain affects directly the prediction of ultimate stress and strain through the confining pressure. This study suggests the use of a strain efficiency of 0.7 which is the average ratio of the rupture strain of FRP wrap in the hoop direction to the ultimate tensile strength of FRP coupons available in the database.

To examine the fineness of the proposed ultimate strain equation, the predictions from four selected studies were compared (Lim and Ozbakkaloglu, 2015; Pham and Hadi, 2013; Teng et al., 2009; Wu and Cao, 2017). Teng et al. (2009) refined the design-oriented stress-strain model for FRP-confined concrete proposed by Lam and Teng (2003) based on experimental tests and an accurate analysis-oriented stress-strain model and regression. Table 10.8 presents the proposed estimation for the ultimate confined strain defined by Teng et al. (2009).

Pham and Hadi (2013) estimated the ultimate for CFRP-confined concrete columns using an energy approach. The concept was introduced by Mander et al. (1988) which stated that the additional energy absorption in the concrete core is the same as the total work done by the FRP wrap. However, it was realized by Pham and Hadi (2013) that the volumetric strain energy of FRP was proportional to the volumetric strain energy of the confined concrete by a factor k. The ultimate confined strain and the proportional factor k were found for a database including 98 circular columns and 69 square specimens via regression analysis, as presented in Table 10.8. Later.

Table 10. 8 Comparison of the ultimate confined strain

Selected rupture strain	No.	Resource	Formula	RMSE for $\frac{\varepsilon_{cc}}{\varepsilon_{co}}$	AAE for $\frac{\varepsilon_{cc}}{\varepsilon_{co}}$
Hoop rupture strain (ε_{hr}) used for the ultimate condition	**1**	**Current study (Equation 10.33)**	$\varepsilon_{cc} = \frac{f'_{cc} - f_o}{E_2}$	2.675	0.316
	2	**Teng et al. (2009)**	$\frac{\varepsilon_{cc}}{\varepsilon_{co}} = 1.75 + 12\rho_K \rho_\varepsilon^{1.45}$ $\rho_K = \frac{2E_f t_f}{(f'_{co}/\varepsilon_{co})D}$; $\rho_\varepsilon = \frac{\varepsilon_{hr}}{\varepsilon_{co}}$	3.46	0.361
	3	**Pham and Hadi (2013)**	$\varepsilon_{cc} = \varepsilon_{co} + \frac{4kt_f f_{fe}\varepsilon_{fe}}{D(f'_{co} + f'_{cc})}$ $\varepsilon_{co} = \left(-0.067 f'^{2}_{co} + 29.9 f'_{co} + 1053\right) \times 10^{-6}$ $f_{fe} = E_f \varepsilon_{fe}$; $k = 7.6$	4.83	0.416
Effective rupture strain ($\varepsilon_{fe} = k_e \times \varepsilon_{fu}$) was used for the ultimate condition	**4**	**Current study (Equation 10.33)**	$\varepsilon_{cc} = \frac{f'_{cc} - f_o}{E_2}$	3.208	0.452
	5	**Wu and Cao (2017)**	$\frac{\varepsilon_{cc}}{\varepsilon_{co}} = 1.75 + 27.34\left(\frac{f_{30}}{f_{co}}\right)^{0.354}\left(\frac{E_L}{f_{co}}\right)^{-0.165}\frac{E_1}{E_{sec} + 1.75E_2}\left(\frac{\varepsilon_{fu}}{\varepsilon_{co}}\right)^{1.16}$ $E_2 = n_2(245.6 f_{co}^{n1} + 0.6728E_L)$ $f_{30} = 30MPa$; $E_{sec} = f_{co}/\varepsilon_{co}$ $n_1 = 0.5$, $n_2 = 0.83$ $for\ f'_{co} \le 40MPa$ $n_1 = 0.2$, $n_2 = 1.73$ $for\ f'_{co} > 40MPa$	4.048	0.488
	6	**Lim and Ozbakkaloglu (2015)**	$\varepsilon_{cc} = \frac{\varepsilon_{hr}}{v_i\left[1 + \left(\frac{\varepsilon_{hr}}{v_i\varepsilon_{co}}\right)^n\right]^{1/n}} + 0.04\varepsilon_{hr}^{0.7}\left[1 + 21\left(\frac{f_l}{f'_{co}}\right)^{0.8}\right]$ $v_i = 8 \times 10^{-6} f'^{2}_{co} + 0.0002 f'_{co} + 0.138$ $\varepsilon_{co} = (-0.067 f'^{2}_{co} + 29.9 f'_{co} + 1053) \times 10^{-6}$ $n = 1 + f'_{co}$ $\varepsilon_{hr} = k_e \varepsilon_{fu}$; $k_e = 0.9 - 2.3 f'_{co} \times 10^{-3} - 0.75 E_f \times 10^{-6}$	4.14	0.422

Note: For comparison of errors, all predicted values of ultimate confined strain (ε_{cc}) were normalized by the strain corresponding to the unconfined concrete strength ($\boldsymbol{\varepsilon_{co} = 9.37 \times 10^{-4}\sqrt[4]{f'_{co}}}$).

Lim and Ozbakkaloglu (2015) proposed a model that predicts the dilation characteristic of the FRP-confined concrete for passively and actively confined concrete based on regression analysis on a large database. It should be noted that the strain efficiency factor (k_e) was found as a function of the unconfined concrete strength and the modulus of elasticity of the

FRP wrap in the hoop direction. Table 10.8 presented the ultimate confined strain from the axial-lateral relationship evaluated at the rupture strain, provided by Lim and Ozbakkaloglu (2015).

Wu and Cao (2017) improved the strain model using the energy balance method and regression analysis. Inside the model, a strain efficiency factor of 0.9 ($k_e = 0.9$) was used. While Hadi and Pham (2013) defined a constant value for the proportional factor k (introduced earlier), Wu and Cao (2017) proposed a parametric equation for this factor as presented in Table 10.8.

Using Equation 10.30 and 10.33, the ultimate confined strain for all the data points was evaluated as the proposed prediction, as presented in Table 10.8. Also, Table 10.8 shows the fineness of the model by comparing the prediction versus experimental values for the models adjusted in the current study and some of the models available in the literature by RMSE and AAE error measures. The model was evaluated using the actual hoop rupture strain to compare to the models developed by Teng et al. (2009) and Pham and Hadi (2013). However, the model was evaluated using a strain efficiency factor of 0.7 to be compared with the models developed by Lim and Ozbakkaloglu (2015) and Wu and Cao (2017) as they developed their models based on different strain efficiency factors. The results showed that the proposed model is rational and improved the compared models for ultimate confined strain by comparing RMSE error for the database. It should be mentioned that the model proposed by Lim and Ozbakkaloglu (2015) showed a better AAE error, which proposed a variable strain efficiency factor, in comparison with the model adjusted in this study, in which a constant strain efficiency factor of 0.7 was used. Overall, the prediction

of the ultimate confined strain using the proposed model showed a very good agreement with the experimental results.

10.6 Conclusion

In this paper, a design-oriented model for the stress-strain curve of FRP-wrapped concrete columns was calibrated using 200 full stress-strain curves from sixteen different sets of experimental tests which extracted an overall 3272 different points form the literature by adopting a general expression of Richard and Abbot. The initial slope, secondary slope, and intercept stress for all the curves were found and reported in the paper. Also, a database including 788 FRP-wrapped concrete specimens collected by the research group was utilized to find the ultimate strength of the confined concrete. The proposed ultimate confined strain was found as the strain corresponding to the confined concrete strength on the confined stress-stress curve which did not involve direct regression of the ultimate confined strain from the database. The following conclusions were drawn:

- The stress-strain model parameters were related only to the FRP wrap stiffness and the unconfined concrete strength instead of the ultimate condition or the confining pressure. Also, the intercept stress was considered as a variable. Thus, the slope and location of the secondary portion were improved in this study.
- It was concluded that excluding the ultimate condition from the adjustment of stress-strain curves of confined concrete leads to more accurate predictions, as it eliminates the effect of rupture strain which impose a large variability in the predictions. The study showed that the stress-strain curve is a function of unconfined concrete strength, modulus of elasticity and thickness of FRP wrap, and

the diameter of the column. The ultimate condition was recognized only as the cut-off point for the stress-strain curve.

- The proposed design-oriented stress-strain curve for the FRP-confined concrete columns was in a very good agreement with the experimental test results and the prediction improved the available predictions in the literature by showing the least error in comparison to fourteen different studies.
- The study of 200 stress-strain curves of FRP-confined columns revealed an average and standard deviation of 1.10 and 13 % for the ratio of the intercept stress to the unconfined concrete strength, respectively. The latter shows the variability of the intercept stress while it was considered as a constant value in many of the available models. Therefore, considering the intercept stress as a variable is suggested instead of a constant value.
- A five parameter Willam-Warnke failure criterion was used to develop an equation for ultimate confined strength using 788 datapoints. The model improved the available plasticity-based models and showed a very good agreement with the experimental tests.
- The ultimate confined strain was derived using the stress-strain curve and the ultimate confined strength which kept the correlation of the ultimate confined strength, ultimate confined strain, and the confining pressure by making them interrelated. A comparison of the ultimate confined strain prediction showed that the predicted values are in a very good agreement with the experimental tests.
- A normalized confining pressure of 0.05 was introduced as the confining limit after which the FRP-confined concrete can be activated.

- A comparison of the developed model for the ultimate strength in this study and the model proposed by ACI 440.2R showed that the model is not conservative for normalized confining pressure to unconfined concrete strength ratio of less than 0.2 or more than 1. However, more data are required to assess the need to be more conservative for confining pressures of more than 1. Also, an alternative confining model was proposed.

ACKNOWLEDGMENTS

The authors would also like to acknowledge and thank NSERC and Dalhousie University for their financial support.

REFERENCES

Abbasnia, R., and Ziaadiny, H. (2015). Experimental investigation and strength modeling of CFRP-confined concrete rectangular prisms under axial monotonic compression. *Materials and Structures*, 48(1-2), 485-500.

ACI 318-19. (2019). Building Code Requirements for Structural Concrete. *American Concrete Institute.* Farmington Hills, MI.

ACI 440.2R. (2017). Guide for the Design and Construction of Externally Bonded FRP Systems for Strengthening Concrete Structures. *American Concrete Institute.* Farmington Hills, MI.

Afifi, M. Z., Mohamed, H. M., and Benmokrane, B. (2015). Theoretical stress-strain model for circular concrete columns confined by GFRP spirals and hoops. *Engineering Structures*, 102, 202–213.

Ahmad, S. H., and Shah, S. P. (1982). Complete triaxial stress-strain curves for concrete. *ASCE J STRUCT DIV*, 108(ST4), 728-742.

Ahmad, S. H., Khaloo, A. R., and Irshaid, A. (1991). Behaviour of concrete spirally confined by fibreglass filaments. *Magazine of Concrete Research*, 43(156), 143–148.

Albitar, M., Ozbakkaloglu, T., and Fanggi, B. L. (2015). Behavior of FRP-HSC-Steel double-skin tubular columns under cyclic axial compression. *Journal of Composites for Construction*, 19(2), 04014041.

Bai, Y. L., Dai, J. G., Mohammadi, M., Lin, G., and Mei, S. J. (2019). Stiffness-based design-oriented compressive stress-strain model for large-rupture-strain (LRS) FRP-confined concrete. *Composite Structures*, 223, 110953.

Berthet, J. F., Ferrier, E., and Hamelin, P. (2006). Compressive behavior of concrete externally confined by composite jackets: Part B: Modeling. *Construction and Building Materials*, 20(5), 338–347.

Bing, L., Park, R., and Tanaka, H. (2001). Stress-strain behavior of high-strength concrete confined by ultra-high- and normal-strength transverse reinforcements. *ACI Structural Journal*, 98(3), 395–406.

Binici, B. (2005). An analytical model for stress-strain behavior of confined concrete. *Engineering Structures*, 27(7), 1040–1051.

Binici, B. (2008). Design of FRPs in circular bridge column retrofits for ductility enhancement. *Engineering Structures*, 30(3), 766-776.

Bisby, L. A., Dent, A. J. S., and Green, M. F. (2005). Comparison of confinement models for fiber-reinforced polymer-wrapped concrete. *ACI Structural Journal*, 102(1), 62–72.

Ceccato, C., Teng, J. G., and Cusatis, G. (2020). Numerical prediction of the ultimate condition of circular concrete columns confined with a fiber reinforced polymer jacket. *Composite Structures*, 24, 112103.

Chen, J. F., Li, S. Q., and Bisby, L. A. (2013). Factors Affecting the Ultimate Condition of FRP-Wrapped Concrete Columns. *Journal of Composites for Construction*, 17(1), 67–78.

Chen, W.-F. (1982). Plasticity in reinforced concrete. *McGraw-Hill*.

CSA S806-12. (2012). Design and construction of building structures with fiber-reinforced polymers. *Canadian Standards Association.*

Demers, M., and Neale K. W. (1994). Strengthening of concrete columns with unidirectional composite sheets. *Developments in short and medium span bridge engineering*, 895–905.

Deng, Z. C., and Qu, J. L. (2015). The experimental studies on behavior of ultrahigh-performance concrete confined by hybrid fiber-reinforced polymer tubes. *Advances in Materials Science and Engineering*, Vol 2015, 1–18.

Djafar-Henni, I., and Kassoul, A. (2018). Stress–strain model of confined concrete with Aramid FRP wraps. *Construction and Building Materials*, 186, 1016–1030.

El-Hacha, R., and Abdelrahman, K. (2013). Slenderness effect of circular concrete specimens confined with SFRP sheets. *Composites Part B: Engineering*, 44(1), 152–166.

Fahmy, M. F. M., and Wu, Z. (2010). Evaluating and proposing models of circular concrete columns confined with different FRP composites. *Composites Part B: Engineering*, 41(3), 199–213.

Fallah Pour, A., Ozbakkaloglu, T., and Vincent, T. (2018). Simplified design-oriented axial stress-strain model for FRP-confined normal- and high-strength concrete. *Engineering Structures*, 175, 501–516.

Fam, A. Z., and Rizkalla, S. H. (2001). Confinement model for axially loaded concrete confined by circular fiber-reinforced polymer tubes. *ACI Structural Journal*, 98(4), 451–461.

Fardis, M. N., and Khalili, H. H. (1982). FRP-encased concrete as a structural material. *Magazine of Concrete Research*, 34(121), 191–202.

Ferrotto, M. F., Fischer, O., and Cavaleri, L. (2018a). A strategy for the finite element modeling of FRP-confined concrete columns subjected to preload. *Engineering Structures*, 173, 1054–1067.

Ferrotto, M. F., Fischer, O., and Cavaleri, L. (2018b). Analysis-oriented stress–strain model of CRFP-confined circular concrete columns with applied preload. *Materials and Structures/Materiaux et Constructions*, 51(2), 1–16.

Hales, T. A., Pantelides, C. P., Sankholkar, P., and Reaveley, L. D. (2017). Analysis-oriented stress-strain model for concrete confined with fiber-reinforced polymer spirals. *ACI Structural Journal*, 114(5), 1263–1272.

Hany, N. F., Hantouche, E. G., and Harajli, M. H., (2015). Axial stress-strain model of CFRP-confined concrete under monotonic and cyclic loading. *Journal of Composites for Construction*, 19(6), 04015004.

Hoek, E., and Brown, E. T., (1980). Empirical strength criterion for rock masses. *Journal of Geotechnical and Geoenvironmental Engineering*, 106, 1013-1035.

Hognestad, E. (1951). A Study of Combined Bending and Axial Load in Reinforced Concrete Members, *Bulletin Series No. 399*. Urbana: University of Illinois.

Jawdhari, A., Adheem, A. H., and Kadhim, M. M. A. (2020). Parametric 3D finite element analysis of FRCM-confined RC columns under eccentric loading. *Engineering Structures*, 212, 110504.

Jesus, M., Silva Lobo, P., and Faustino, P. (2018). Design models for circular and square RC columns confined with GFRP sheets under axial compression. *Composites Part B: Engineering*, 141, 60–69.

Jiang, J. F., and Wu, Y. F. (2014). Characterization of Yield Surfaces for FRP-Confined Concrete. *Journal of Engineering Mechanics*, 140(12).

Jiang, J. F., and Wu, Y. F. (2016). Plasticity-based criterion for confinement design of FRP jacketed concrete columns. *Materials and Structures/Materiaux et Constructions*, 49(6), 2035–2051.

Jiang, K., Han, Q., Bai, Y., and Du, X. (2020). Data-driven ultimate conditions prediction and stress-strain model for FRP-confined concrete. *Composite Structures*, 242, 112094.

Jiang, T., and Teng, J. G. (2007). Analysis-oriented stress-strain models for FRP-confined concrete. *Engineering Structures*, 29(11), 2968–2986.

Karbhari, V. M., and Gao, Y. (1997). Composite Jacketed Concrete under Uniaxial Compression—Verification of Simple Design Equations. *Journal of Materials in Civil Engineering*, 9(4), 185–193.

Lam, L., and Teng, J. (2003). Design-oriented stress–strain model for FRP-confined concrete. *Construction and building materials*, 2003(6-7), 471-489.

Li, P., Wu, Y. F., Zhou, Y., and Xing, F. (2019). Stress-strain model for FRP-confined concrete subject to arbitrary load path. *Composites Part B: Engineering*, 163, 9–25.

Li, Y. F., Lin, C. T., & Sung, Y. Y. (2003). A constitutive model for concrete confined with carbon fiber reinforced plastics. Mechanics of Materials, 35(3-6), 603-619.

Liang, M., Wu, Z. M., Ueda, T., Zheng, J. J., and Akogbe, R. (2012). Experiment and modeling on axial behavior of carbon fiber reinforced polymer confined concrete cylinders with different sizes. *Journal of Reinforced Plastics and Composites*, 31(6), 389–403.

Lillistone, D., and Jolly, C. K. (2000). An innovative form of reinforcement for concrete columns using advanced composites. *Structural Engineer*, 78(23/24).

Lim, J. C., and Ozbakkaloglu, T. (2015). Lateral strain-to-axial strain relationship of confined concrete. *Journal of Structural Engineering*, 141(5), 1–18.

Mander, J. B., Priestley, M. J. N., and Park, R. (1988). Theoretical Stress-Strain Model for Confined Concrete. *Journal of Structural Engineering*, 114(8), 1804–1826.

Miyauchi, K., Inoue, S., Kuroda, T., and Kobayashi, A. (1999). Strengthening effects with carbon fiber sheet for concrete column. *Proc Jpn Concr Inst*, 21(3), 1453–1458.

Miyauchi, K., Nishibayashi, S., and Inoue, S. (1997). Estimation of Strengthening Effects with Carbon Fiber Sheet for Concrete Column. *Proceedings of the Third International Symposium on Non-Metallic FRP for Concrete Structures*, 224.

Mohammadi, M., and Wu, Y. F. (2019). Modified plastic-damage model for passively confined concrete based on triaxial tests. *Composites Part B: Engineering*, 159, 211–223.

Mohammadi, M., Dai, J. G., Wu, Y. F., and Bai, Y. L. (2019). Development of extended Drucker–Prager model for non-uniform FRP-confined concrete based on triaxial tests. *Construction and Building Materials*, 224, 1–18.

Moran, D. A., and Pantelides, C. P. (2002). Stress-Strain Model for Fiber-Reinforced Polymer-Confined Concrete. *Journal of Composites for Construction*, 6(4), 233–240.

Moran, D. A., and Pantelides, C. P. (2012). Elliptical and circular FRP-confined concrete sections: A Mohr-Coulomb analytical model. *International Journal of Solids and Structures*, 49(6), 881–898.

Naderpour, H., and Mirrashid, M. (2020). Confinement Coefficient Predictive Modeling of FRP-Confined RC Columns. *Advances in Civil Engineering Materials*, 9(1), 1–21.

Ozbakkaloglu, T., and Vincent, T. (2014). Axial compressive behavior of circular high-strength concrete-filled FRP tubes. *Journal of composites for construction*, 18(2) , 04013037.

Ozbakkaloglu, T., Gholampour, A., and Lim, J. C. (2016). Damage-Plasticity Model for FRP-Confined Normal-Strength and High-Strength Concrete. *Journal of Composites for Construction*, 20(6), 1–13.

Pan, Y., Guo, R., Li, H., Tang, H., and Huang, J. (2017). Analysis-oriented stress–strain model for FRP-confined concrete with preload. *Composite Structures*, 166, 57–67.

Pham, T. M., and Hadi, M. N. S. (2013). Strain estimation of CFRP-confined concrete columns using energy approach. *Journal of Composites for Construction*, 17(6), 1–11.

Piscesa, B., Attard, M. M., and Samani, A. K. (2018). 3D Finite element modeling of circular reinforced concrete columns confined with FRP using a plasticity based formulation. *Composite Structures*, 194, 478–493.

Popovics, S. (1973). A Numerical Approach to the Complete Stress-Strain Curve of Concrete. *Cements and Concrete Research*, 3(5), 583-599.

Richard, R. M., and Abbot, B. J. (1975). Versatile elastic-plastic stress-strain formula. *Journal of the Engineering Mechanics Division*, 101(4), 511–515.

Richart, F. E., Brandtzaeg, A., and Brown, R. L. (1928). A study of the failure of concrete under combined compressive stresses. *In: Bulletin no. 185*, Univ. of Illinois, Eng. Experimental Station: Champaign, Ill.

Rousakis, T., and Tepfers, R. (2001). Experimental investigation of concrete cylinders confined by carbon FRP sheets, under monotonic and cyclic axial compressive load. *Research Rep*, 44, 1–87.

Saadatmanesh, H., Ehsani, M. R., and Li, M. W. (1994). Strength and ductility of concrete columns externally reinforced with fiber composite straps. *Structural Journal*, 91(4), 434–447.

Saafi, M., Toutanji, H. A., and Li, Z. (1999). Behavior of concrete columns confined with fiber reinforced polymer tubes. *ACI Materials Journal*, 96(4), 500–509.

Saberi, H., Bui, T. Q., Furukawa, A., Rahai, A., and Hirose, S. (2020). FRP-confined concrete model based on damage-plasticity and phase-field approaches. *Composite Structures*, 244, 112263.

Sadeghian, P., and Fam, A. (2014). A rational approach toward strain efficiency factor of fiber-reinforced polymer-wrapped concrete columns. *ACI Structural Journal*, 111(1), 135–144.

Sadeghian, P., and Fam, A. (2015). Improved design-oriented confinement models for FRP-wrapped concrete cylinders based on statistical analyses. *Engineering Structures*, 162–182.

Sadeghian, P., and Fillmore, B. (2018). Strain distribution of basalt FRP-wrapped concrete cylinders. *Case Studies in Construction Materials*, 9, e00171.

Sadeghian, P., Seracino, R., Das, B., and Lucier, G. (2018). Influence of geometry and fiber properties on rupture strain of cylindrical FRP jackets under internal ICE pressure. *Composite Structures*, 192, 173–183.

Saiid Saiidi, M., Sureshkumar, K., and Pulido, C. (2005). Simple Carbon-Fiber-Reinforced-Plastic-Confined Concrete Model for Moment-Curvature Analysis. *Journal of Composites for Construction*, 9(1), 101–104.

Samaan, M., Mirmiran, A., and Shahawy, M. (1998). "Model of concrete confined by fiber composites." *Journal of Structural Engineering*, 124(9), 1025–1031.

Sargin, M. (1971). Stress-Strain relationships for concrete and analysis of structural concrete sections. *Study No. 4, Solid Mechanics Division, University of Waterloo, Waterloo, Ontario, Canada.*

Shaat, A., and Fam, A. Z. (2009). Slender Steel Columns Strengthened Using High-Modulus CFRP Plates for Buckling Control. *Journal of Composites for Construction*, 13(1), 2-12.

Shahawy, M., Mirmiran, A., and Beitelman, T. (2000). Tests and modeling of carbon-wrapped concrete columns. *Composites Part B: Engineering*, 31(6), 471-480.

Silva Lobo, P., Faustino, P., Jesus, M., and Marreiros, R. (2018). Design model of concrete for circular columns confined with AFRP. *Composite Structures*, 200, 69–78.

Smith, S. T., Kim, S. J., and Zhang, H. (2010). Behavior and Effectiveness of FRP Wrap in the Confinement of Large Concrete Cylinders. *Journal of Composites for Construction*, 14(5), 573-582.

Song, X., Gu, X., Li, Y., Chen, T., and Zhang, W. (2013). Mechanical behavior of FRP-strengthened concrete columns subjected to concentric and eccentric compression loading. *Journal of Composites for Construction*, 17(3), 336–346.

Spoelstra, M. R., and Monti, G. (1999). FRP-Confined Concrete Model. *Journal of Composites for Construction*, 3(3), 143-150.

Teng, J. G., Jiang, T., Lam, L., and Luo, Y. Z. (2009). Refinement of a Design-Oriented Stress–Strain Model for FRP-Confined Concrete. *Journal of Composites for Construction*, 13(4), 269–278.

Toutanji, H. A. (1999). Stress-strain characteristics of concrete columns externally confined with advanced fiber composite sheets. *ACI materials journal*, 397-404.

Vincent, T., and Ozbakkaloglu, T. (2013). Influence of concrete strength and confinement method on axial compressive behavior of FRP confined high-and ultra high-strength concrete. *Composites Part B: Engineering*, 50, 413–428.

Willam, J. K., and Warnke, E. P. (1975). Constitutive model for the triaxial behaviour of concrete. Proc. Intl. Assoc. *Bridge Structl. Engrs*, 19, 1–30.

Wu, H. L., and Wang, Y. F. (2010). Experimental study on reinforced high-strength concrete short columns confined with AFRP sheets. *Steel and Composite Structures*, 10(6), 501–516.

Wu, H.-L., Wang, Y.-F., Yu, L., and Li, X.-R. (2009). Experimental and Computational Studies on High-Strength Concrete Circular Columns Confined by Aramid Fiber-Reinforced Polymer Sheets. *Journal of Composites for Construction*, 13(2), 125–134.

Wu, Y. F., and Cao, Y. (2017). Energy balance method for modeling ultimate strain of confined concrete. *ACI Materials Journal*, 114(2), 373–381.

Wu, Y. F., and Jiang, J. F. (2013). Effective strain of FRP for confined circular concrete columns. *Composite Structures*, 95, 479–491.

Wu, Y.-F., and Zhou, Y.-W. (2010). Unified Strength Model Based on Hoek-Brown Failure Criterion for Circular and Square Concrete Columns Confined by FRP. *Journal of Composites for Construction*, 14(2), 175–184.

Xiao, Q. G., Teng, J. G., and Yu, T. (2010). Behavior and Modeling of Confined High-Strength Concrete. *Journal of Composites for Construction*, 14(3), 249–259.

Xiao, Y., and Wu, H. (2000). Compressive Behavior of Concrete Confined by Carbon Fiber Composite Jackets. *Journal of materials in civil engineering*, 12(2), 139-146.

Xiao, Y., and Wu, H. (2003). Compressive Behavior of Concrete Confined by Various Types of FRP Composite Jackets. *Journal of Reinforced Plastics and Composites*, 22(13), 1187–1201.

Yan, Z., Pantelides, C. P., and Reaveley, L. D. (2006). Fiber-reinforced polymer jacketed and shape-modified compression members: I - Experimental behavior. *ACI Structural Journal*, 103(6), 885–893.

Yang, J., Wang, J., and Wang, Z. (2020). Axial compressive behavior of partially CFRP confined seawater sea-sand concrete in circular columns – Part II: A new analysis-oriented model. *Composite Structures*, 246, 112368.

Yang, J., Wang, J., and Wang, Z. (2020). Axial compressive behavior of partially CFRP confined seawater sea-sand concrete in circular columns – Part II: A new analysis-oriented model. *Composite Structures*, 246, 112368.

Yu, T., and Teng, J. G. (2011). Design of Concrete-Filled FRP Tubular Columns: Provisions in the Chinese Technical Code for Infrastructure Application of FRP Composites. *Journal of Composites for Construction*, 15(3), 451–461.

Yu, T., Teng, J. G., Wong, Y. L., and Dong, S. L. (2010). Finite element modeling of confined concrete-I: Drucker-Prager type plasticity model. *Engineering Structures*, 32(3), 665–679.

CHAPTER 11 EXPERIMENTAL AND NUMERICAL INVESTIGATION OF SLENDER STEEL REINFORCED CONCRETE COLUMNS STRENGTHENED WITH COMBINED LONGITUDINAL AND TRANSVERSE FRPS

ABSTRACT

In this study, the performance of slender circular concrete columns strengthened with a novel hybrid system of longitudinal bonded fiber-reinforced polymer (FRP) prefabricated laminates and transverse FRP wraps is investigated. The idea is to improve the axial load carrying capacity of slender concrete columns by providing high modulus longitudinal carbon FRP (CFRP) laminates through enhancing the flexural stiffness of the column, and laterally support the longitudinal laminates to allow them function and not to buckle before reaching crushing in compression. To provide lateral support for the longitudinal laminates glass FRP (GFRP) and carbon FRP (CFRP) wraps were used which enhanced the strength of concrete through confinement. A total of 6 large scale circular slender columns were tested under combined axial and flexural loads. Also, the system was investigated using an analytical-numerical model considering the second-order analysis of the slender columns which considered variable confinement effect. The model also considers nonlinearity in material, geometry, and the confinement effects. The model is verified versus experimental test data and showed a good agreement with the test results. A parametric study was conducted to further study the hybrid system. The results showed that for strengthening of the steel reinforced slender concrete columns the hybrid system is a more effective strengthening system than wrapping.

11.1 INTRODUCTION

Carbon fiber-reinforced polymer (CFRP) sheets have been widely produced by multiple manufacturers due to their acceptance in the rehabilitation of existing structures. The physical characteristics of CFRP laminates such as high tensile strength and modulus make them suitable for applications which requires an increase in the strength and stiffness of the existing flexural members by installing these sheets in the tensile side of them. Many researchers have been evaluated the strengthening performance of CFRP laminates on tensile side of concrete beams (Shahawy et al., 1996; Ashour et al., 2004). However, FRPs in compression are not popular to be used in structural members, because the contribution of FRP laminates and bars in load carrying capacity of compressive structural elements have been neglected by the design guidelines (CSA S806, 2012, ACI 440.2R, 2008; ACI 440.1R, 2017). On the other hand, there are researches that showed the capability of FRP laminates (Gajdosova and Bilcik, 2013; Sadeghian and Fam, 2015; Khorramian and Sadeghian, 2017) and FRP bars (Tobbi et al., 2012; Mohamed et al., 2014; Khorramian and Sadeghian, 2017; Fillmore and Sadeghian, 2018) in the enhancement of the strengthened systems or new constructions. Therefore, the study of the behavior of columns strengthened with FRP sheets is a discussing topic which requires more research specially in slender columns.

Also, the wrapping system is not as effective for slender columns as was recognized to be effective for short columns. FRP wrapping has been known very effective especially for concentrically loaded columns (Pessiki et al., 2001; Ozbakkaloglu, 2013; Xiao and Wu, 2000; Cui and Sheikh, 2010; Smith et al., 2010). However, Researchers reported a reduction in the effectiveness of FRP wrapping for circular concrete columns loaded under combined

axial and flexural loading (Parvin and Wang, 2001; Hadi, 2006; Bisby and Ranger, 2010; Al-Nimry and Soman, 2018). Also, ACI-440.2R-17 (2017) limits the effective rupture strain of FRP wraps to 0.004 mm/mm where the load eccentricities are more than 10% of the diameter of the column. Moreover, ACI-440.2R-17 (2017) is silent regarding slender columns.

The idea of a hybrid system using high modulus longitudinal laminates such as CFRP premanufactured laminates is to address the mentioned issue and provide the required additional flexural stiffness to strengthen slender concrete columns where wrapping is not as effective due to the nature of loading and secondary moment effects. Thus, other strengthening options should be considered for strengthening of slender concrete columns. Since more rigidity is required for slender columns, longitudinal FRPs can be considered as a rational solution for strengthening (Sadeghian and Fam, 2015). Despite the potential of extra gain of strength, the guidelines limited the use of FRP laminates in compression due to lack of test data (ACI 440.2R-17, 2017; ACI 440.1R-15, 2015; CSA S806-12, 2012). However, experimental tests showed that FRPs are effective in compression in form of FRPs in form near-surface mounted (NSM) strengthening system (Gajdosova and Bilcik, 2012), and in form of longitudinal and rotated wraps (Fitzwilliam and Bisby 2010, Sadeghian et al. 2010). Due to space limitation between the grooves, the NSM system cannot provide a high reinforcement ratio for longitudinal laminates to increase the rigidity drastically. Also, for applying fabrics and resin system with longitudinal fiber orientation, there is a potential of micro buckling of fibers if any void is available in the resin (ACI 440.2R-17, 2017). On the other hand, the premanufactured unidirectional laminates have been successfully bonded to the tension side of the concrete beams for strengthening

(Triantafillou and Plevris 1992, Sharif et al. 1994, Shahawy et al. 1996). However, the application of the bonded FRP laminates on the concrete columns cannot be directly supported due to lack of lateral support and the occurrence of debonding or buckling of longitudinal FRP laminates as studied in chapter 8 and 9 of this document. The tests of concrete cylinders reinforced with longitudinal FRP laminates and GFRP wraps showed that the debonding and buckling of longitudinal FRP laminates can be prevented if enough confinement is provided. The small scale tests showed that longitudinal FRPs can reach to their crushing capacity by providing lateral support. Therefore, this study was designed to examine the performance of the hybrid strengthening system f premanufactured high modulus longitudinal FRP laminated supported with GFRP or CFRP wrapping for strengthening of slender steel-reinforced concrete columns.

11.2 Experimental Program

For this study, six slender circular reinforced concrete columns (260x3048 mm) were designed per ACI 318-19 (2019) as presented in Figure 11.1. Six 15M steel rebar were used as longitudinal reinforcement and twenty 10M ties were considered as ties. The spacing of ties was 203 mm at the middle of the column and reduced to 102 mm at the distance of 610 mm at the end of the columns. The specimens were cast with normal concrete with a strength of 30 MPa which is close to the concrete strength of aged structures.

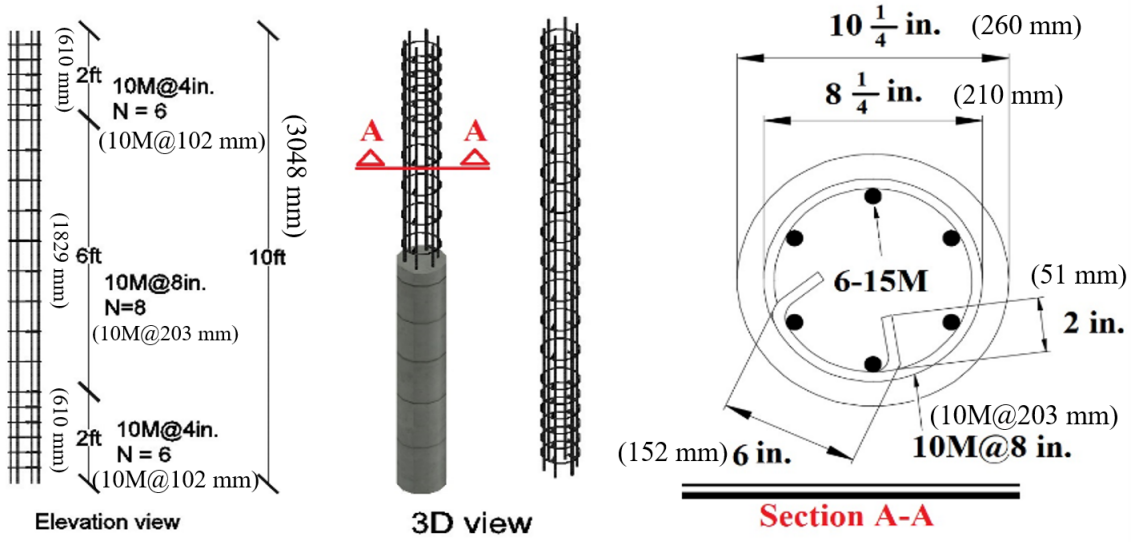

Figure 11. 1 Concrete columns to be strengthened

11.2.1 Test Matrix

The test matrix is presented in Table 11.1. Six specimens were considered: 1) one control specimen was considered without strengthening; 2) two wrapped specimens were considered, one with six layers of GFRP wrapping and one with two layers of CFRP wrapping; 3) three hybrid specimens were considered with sixteen or eight longitudinal CFRP strips (50x1.2 mm) and six layers of GFRP wrapping or two layers of CFRP wrapping.

Table 11. 1 Test Matrix

No.	Specimen ID	D (mm)	L (mm)	λ	e/h	Steel Reinforcement	Transverse Reinforcement	Longitudinal Reinforcement
1	Control	260	3048	47	0.15	6-15M	-	-
2	W-TG6	260	3048	47	0.15	6-15M	6 layer GFRP wraps	-
3	H-TG6-LC8	260	3048	47	0.15	6-15M	6 layer GFRP wraps	8 CFRP strips
4	H-TG6-LC16	260	3048	47	0.15	6-15M	6 layer GFRP wraps	16 CFRP strips
5	W-TC2	260	3048	47	0.15	6-15M	2 layer CFRP wraps	-
6	H-TC2-LC8	260	3048	47	0.15	6-15M	2 layer CFRP wraps	8 CFRP strips

The specimen IDs started with letter “W” or “H”, which stands for wrapped and hybrid system, followed by letter “T” and “L” which stand for transverse and longitudinal reinforcements, respectively. After the letter “T”, the wrapping type (i.e. G for glass and C for carbon), and number of layers were presented, and after the letter “L”, the type and number of longitudinal FRP laminates is given. For example, H-TG6-LC16 is a representative of a hybrid specimen wrapped with 6 layers of GFRP wrapping and longitudinally strengthened with 16 layers of CFRP strips.

The idea of choosing 6 layers of GFRP wrapping (f'_l = 5.35 MPa) for the large-scale specimens was to give a confining pressure close to 4 layers of wrapping (f'_l = 6.19 MPa) presented in chapter 9 to make sure enough lateral support is provided. It should be mentioned that the reinforcement ratio of longitudinal CFRPs was reduced from 2.7% for phase I to 1.8% and 0.9% for large scale tests in comparison to small scale tests presented in chapter 9.

11.2.2 Fabrication

Figure 11.2 shows the fabrication process. Steel cages were built (with the detail presented in Figure 11.1) and were put inside circular cardboard tubes used as mold, as shown in Figure 11.2(a). A ready-mix concrete was poured inside the molds with a slump of 200 mm. After the concrete is poured, the molds were not removed before 28 days to keep the moisture and have better curing. Once the molds were removed, the location of the longitudinal CFRP laminates were marked on the surface of the concrete column. The adhesives were put on the concrete surface as well as the surface of the CFRP laminates, and the CFRP strips were bonded to the concrete. Figure 11.2(b) and 11.2(c) show the specimens with 8 and 16 longitudinal CFRP strips (50 x 1.2 mm), respectively. It should

be noted that the CFRP strips were cut to have a length of 3000 mm and were shorter than the length of columns so that they would not be disturbed at the ends of the specimen where the loading is applied. For specimens with 8 CFRP strips, the space between each two strips was filled with adhesives to make the columns section circular and avoid sharp tips of CFRP strips in order not to disturb the wrapping. After longitudinal CFRPs were installed on the concrete, the specimens were wrapped with GFRP or CFRP wrapping, as shown in Figure 11.2(d). It should be mentioned that 100 mm of overlap for wrapping was considered for all wrapped and hybrid specimens. Also, three layers of additional wrapping with a length of 300 mm was considered for the ends of all specimens to avoid premature failure at the ends of the columns. The final shape of the hybrid specimens before testing are presented in Figure 11.2(e) and 11.2(f) for glass and carbon wrapping, respectively.

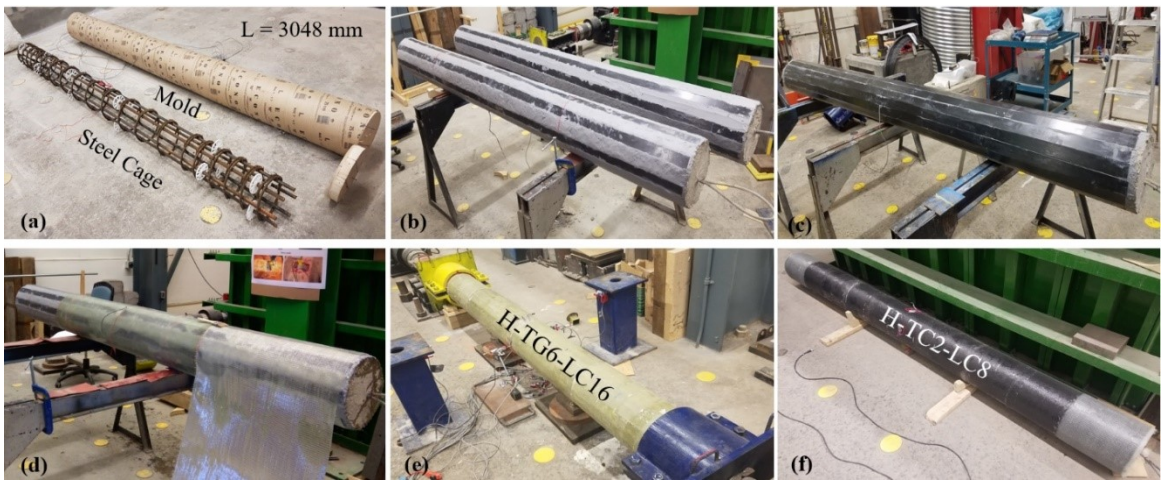

Figure 11. 2 Fabrication: (a) steel cage and Mold; (b) 8 CFRP strips on columns; (c) 16 CFRP strips on column; (d) Wrapping with GFRP fabric and resin; (e) Hybrid specimen with GFRP wrapping; and (f) Hybrid specimen with CFRP wrapping

11.2.3 Material Properties

To mimic aged structures that required retrofitting, a target concrete class of C30 was selected. A ready-mix concrete with concrete strength of 30 MPa at the time of testing was poured for columns. The tensile strength and modulus of elasticity of CFRP and GFRP wraps were determined coupon tests per ASTM D3039M-14 (2014). The tensile and compressive characteristics of CFRP laminates was determined in the study presented in chapter 9, and the rest of the characteristics were reported by the manufacturer as presented in Table 11.2. It should be noted that the ply thicknesses were 1.24, 0.54, and 1.2 mm for CFRP wrap, GFRP wrap, and CFRP premanufactured laminate, respectively.

Table 11. 2 Material Properties

Test	No.	Material Type	f (MPa)	E (GPa)	ε (mm/mm)	F_b (MPa)
Tensile test	1	CFRP laminate	3267	177.8	0.0179	-
	2	Steel bar	443	209	0.0021	-
	3	GFRP wrap	391	25.7	0.0152	-
	4	CFRP wrap	1126	100	0.0113	-
	5	Bonding adhesive*	25	4.5	0.0100	22
	6	Epoxy resin*	69	1.7	0.0406	-
Compressive test	7	CFRP laminate	1089	152.9	0.0071	-
	8	Concrete	30	-	-	-
	9	Bonding adhesive*	59.3	2.7	0.0220	22
	10	Epoxy resin*	101	2.6	0.0388	-

Note: * = the values are reported by the manufacturer. f = ultimate tensile or compressive strength; E = tensile or compressive modulus of elasticity; ε = ultimate tensile or compressive strain; F_b = bond strength.

11.2.4 Test Set-up and Instrumentation

Figure 11.3 presents the test set-up and instrumentation. The test set-up consists of two strong concrete cubes named “End blocks” which were tightened to the strong floor. Between these two end blocks, the load is applied to the system via a 2MN Instron actuator whose force is recorded by the load cell, as shown in Figure 11.3. The columns were loaded using a displacement control approach with a rate of 2 mm/min. The load transfers from the actuator to a shaft, whose direction of movement is controlled by a tunnel, and applied axial load to the concrete column. To provide load eccentricity, two rollers were considered at the ends of the specimen whose distance from the center of the columns gives the desired eccentricity. The rollers are in contact with a v-notched plate which allows the specimen to rotate to provide simply supported boundary conditions. To provide a specimen with easier movement and to cancel the effect of the wight of the column in the horizontal direction, two sets of steel balls were provided for the specimen that allows lateral movement, as shown in Figure 11.3. To record the data, two string pods (SPs) and two linear potentiometers (LPs) were installed at the mid-section of the column to record the lateral displacement. Also, a total of ten strain gauges were installed to record the axial strain in compression and tension sides on steel bars, CFRP strips, and GFRP wrapping, and to record the strain of GFRP wrapping in the hoop direction.

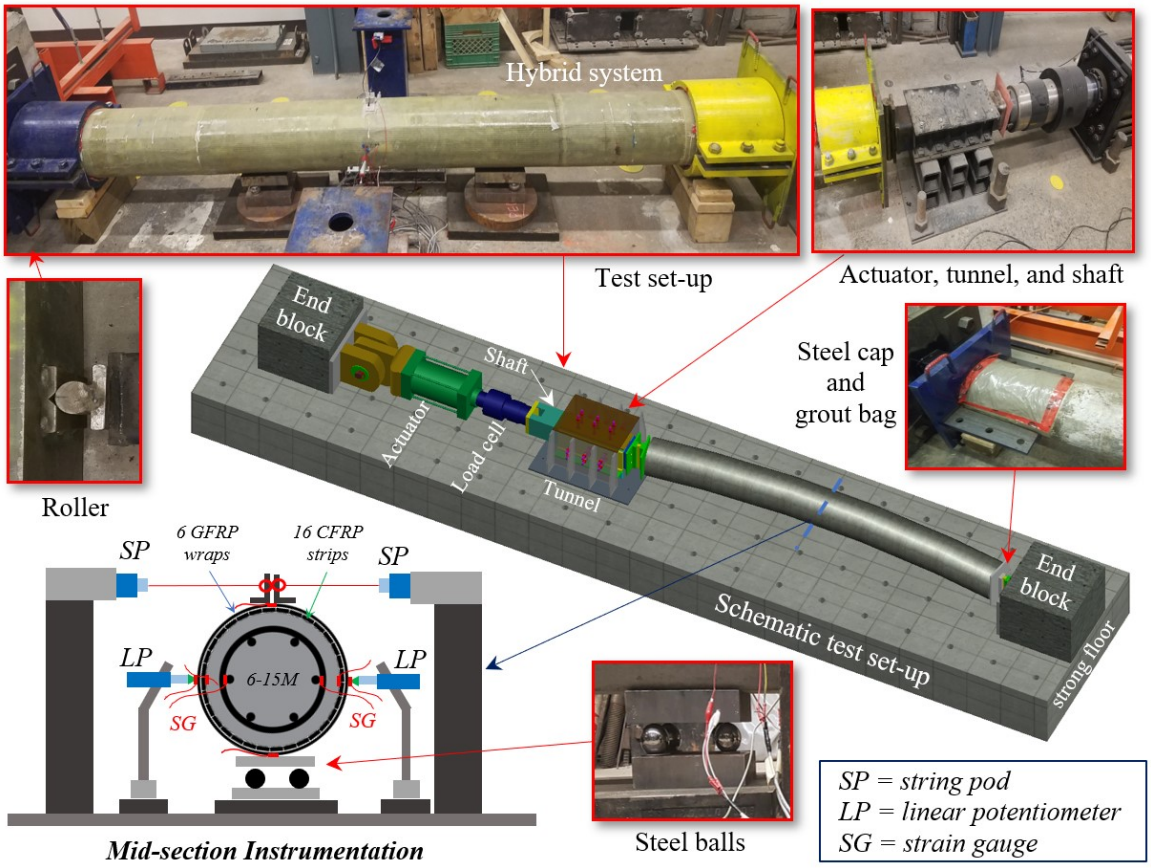

Figure 11. 3 Test set-up and instrumentation

11.3 EXPERIMENTAL RESULTS AND DISCUSSION

11.3.1 Failure Modes

Figure 11.4 shows the failed specimens and the modes of failure. For the control specimen, the loading continued up to the column reached concrete crushing at the middle of the column, as presented in Figure 11.4 (a) and 11.4 (d). After concrete crushed, there was a sudden drop in the axial load as for the control specimen. The specimen wrapped with GFRP did not reach the material failure at its peak load and failed due to the global buckling of the column as presented in Figure 11.4 (b). After buckling, loading continued and the specimen tolerated loads which led to a smooth and long descending branch of the load-

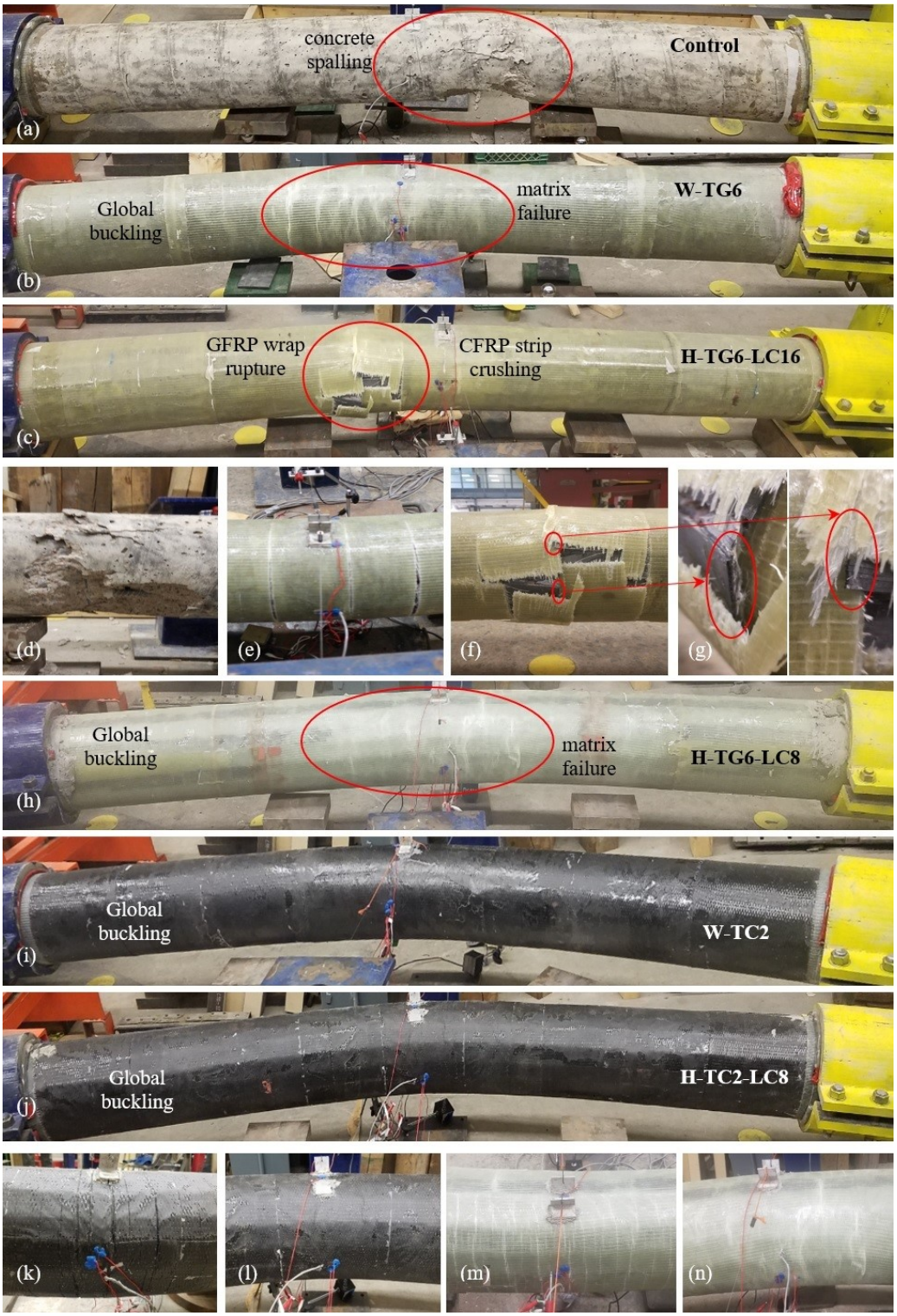

Figure 11. 4 Failure at ultimate state: (a) Control, (b) W-TG6, (c) H-TG6-LC16, (d) concrete spalling control specimen, (e) matrix rupture in W-TG6, (f) rupture of GFRP wrap in H-TG6-LC16, and (g) crushing of CFRP strip, (h) H-TG6-LC8, (i) W-TC2, (j) H-TC2-LC8, (k) matrix rupture in tensile side of H-TC2-LC8, (l) compressive side of H-TC2-LC8, (m) tensile side of H-TG6-LC8, and (n) compressive side of H-TG6-LC8

displacement curve, and the test finally stopped by the operator due to considerable lateral displacement. It should be mentioned that GFRP wrapping did not rupture. Instead, the matrix failure happened which showed matrix crushing in the compression side, as presented in Figure 11.4 (b), and matrix rupture in tension side, as presented in Figure 11.4 (e). The same behavior was observed for CFRP wrapped specimen [Figure 11.4(i)] with the difference that no matrix crushing in compression side was observed [Figure 11.4(l)] while the matrix rupture in tensile side happened [Figure 11.4(k)].

For the hybrid specimen strengthened with 16 CFRP strips and wrapped with 6 layers of GFRP [Figure 11.4(c)], the CFRP strip in the furthest compression side was crushed a considerable noise. However, the loading continued, and the system was able to sustain loads even after the failure of the strips in compression. After peak load, the CFRP at the middle of the column in the compression side was debonded and initiated some small cracks in the GFRP wrapping which was progressed up to reaching the rupture of GFRP wrap, as presented in Figure 11.4(f). Once GFRP ruptured the axial load dropped with a steep slope which leads to total failure of the column, as presented in Figure 11.4(f) and 11.4(g).

For hybrid specimens strengthened with 8 CFRP strips, at the peak load noises started which is attributed to crushing or debonding of CFRP strips in compression side. The final failure position of GFRP and CFRP wrapped hybrid system strengthened with 8 CFRP strips are shown in Figure 11.4 (h) and 11.4(i), respectively. It should be noted for these two specimens, no rupture of GFRP wrapping was observed as loading continued after the peak load, and similar behavior to the wrapped specimens was observed after the peak load. In other words, by decreasing the reinforcement ratio of the CFRP strips, the hybrid system gains more ductility and avoided the rupture of FRP wrapping. Instead, the matrix failure

in tension and compression side were observed, as shown in Figure 11.4(k) to 11.4(n). However, it should be mentioned that for CFRP wrapped column strengthened with 8 CFRPs in compression no sign f the failure was observed in the compression side in the wrapping, as shown in Figure 11.4(l). Also, for that hybrid specimens with strengthened with 8 CFRP strips, the crushing or debonding of the furthest compressive CFRP strips happened at the middle of the column at peak load and continued to expand to the sections further than the middle as the loading continued after the peak load. However, the progressive failure did not cause the total failure of the columns. Instead, after the peak load and by progression the failure of CFFRP strips from the hybrid system strengthened with 8 CFRP strips, its behavior became similar to only wrapped system. Therefore, for the hybrid system, by decreasing the reinforcement ratio, although the capacity decreases, the ductility increases.

11.3.2 Comparison of Hybrid and Wrapping Systems

A summary of the test results of the experimental tests is presented in Table 11.3. Table 11.3 shows the values of axial displacement, lateral displacement, axial load, and bending moment at the peak load, and after 15% drop after the peak load, and at the end of the testing. It should be noted that for all specimens the test was stopped by the user due to safety reasons that might have been caused because of excessive deformation in the columns although the test would have continued further. However, the tests were terminated for the control specimen after the concrete spalling occurred and for the hybrid specimen with 16 CFRP strips after the GFRP wrapping ruptured.

Table 11. 3 Summary of Test Results

No.	Specimen ID	Load stage	Axial Displacement (mm)	Lateral Displacement (mm)	Axial Load (kN)	Bending Moment (kN-m)	PGA (%)	PGM (%)
1	Control	P_u	16.5	20.5	1152	69.76	-	-
		$0.85P_u$	-	-	-	-		
		P_{ult}	-	-	-	-		
2	W-TG6	P_u	18.3	23.2	1335	84.30	15.8	20.8
		$0.85P_u$	20.1	48.7	1134	100.58		
		P_{ult}	33.7	186.6	344	77.93		
3	H-TG6-LC8	P_u	26.1	49.3	1586	141.66	37.6	103.0
		$0.85P_u$	29.6	76.7	1348	157.29		
		P_{ult}	44.7	150.2	1059	201.55		
4	H-TG6-LC16	P_u	35.6	38.9	1921	151.51	66.7	117.2
		$0.85P_u$	44.4	82.3	1632	199.70		
		P_{ult}	47.2	105.5	779	113.34		
5	W-TC2	P_u	19.0	28.1	1335	90.96	15.8	30.4
		$0.85P_u$	21.4	59.6	1135	113.04		
		P_{ult}	56.4	285.9	248	80.97		
6	H-TC2-LC8	P_u	23.7	35.6	1789	135.27	55.3	93.9
		$0.85P_u$	26.5	63.9	1521	157.99		
		P_{ult}	50.4	215.5	541	138.13		

Note: P_u = peak load; P_{ult} = load level corresponding to ultimate displacement; PGA = Percentage gain in axial load with respect to the control specimen at the peak load; PGM = percentage gain in bending moment with respect to the control specimen at the peak load.

Table 11.3 also presents the value for the percentage gain in axial load capacity (PGA) with respect to the control specimen for both wrapped and hybrid specimens as well as the percentage gain of bending moment capacity (PGM). The results showed a considerable gain in the axial and flexural capacity of the hybrid strengthening system in comparison to the wrapping system. For GFRP wrapped specimens, for specimens strengthened with 8 and 16 longitudinal CFRP strips, 82.2% and 96.4% extra gain in flexural capacity, and 21.8% and 50.9% extra gain in the axial capacity of the hybrid strengthening system in comparison to GFRP wrapped system was observed. For CFRP wrapped specimens, 63% and 39.5% extra gain in flexural and axial capacity of the hybrid system strengthened with

8 longitudinal CFRP strips in comparison to the CFRP wrapped system was observed. The results are also presented in Figure 11.5.

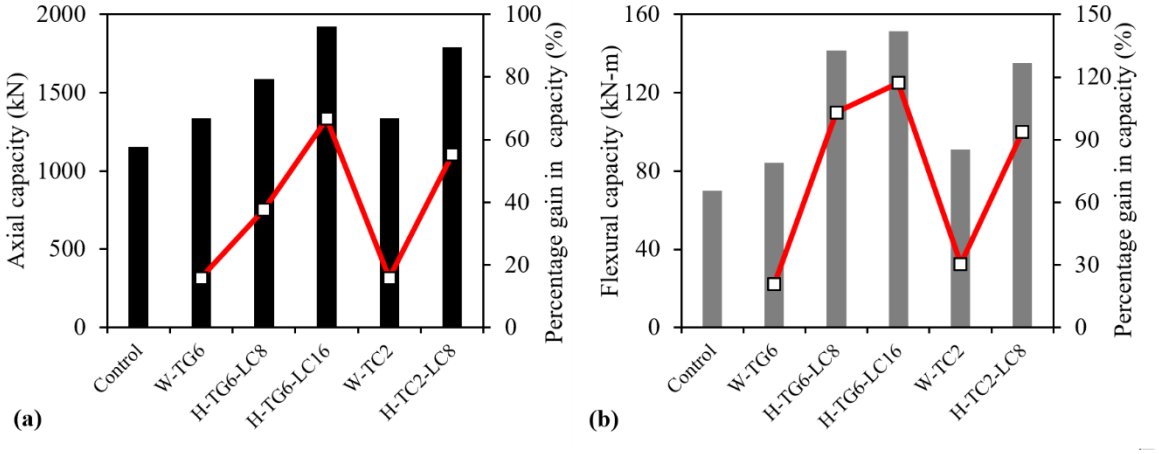

Figure 11. 5 Axial and flexural strength of the tested specimens

Table 11.4 summarized a recording of strains at peak load for the tested specimens. It was observed that the axial strain in the compressive side of the columns increased for the hybrid system in comparison to the wrapped system. The latter shows the additional stiffness of the columns due to the existence of the longitudinal CFRP strips. Also, the confining strain was higher for the hybrid system at the peak load in comparison to the wrapping system.

Table 11. 4 Hoop and axial strains at the peak load

No.	Specimen ID	Axial strain on FRP		Axial strain on steel		Hoop strain on FRP	
		SG_{a_c}	SG_{a_t}	SG_{a_c}	SG_{a_t}	SG_{h_c}	SG_{h_m}
1	Control*	-	-	-0.0015	0.0005	-	-
2	W-TG6	-0.0024	0.0008	-0.0023	0.0008	0.0009	0.0005
3	H-TG6-LC8	-0.0077	0.0041	-	-	0.0026	-
4	H-TG6-LC16	-0.0050	0.0024	-	0.0016	0.0021	0.0016
5	W-TC2	-0.0033	0.0013	-	0.0007	0.0005	-
6	H-TC2-LC8	-0.0062	0.0033	-	-	0.0012	-

Note: * the curvature and stiffness at peak load were calculated based on strain on steel; SG_{a_c} = axial strain in compression side; SG_{a_t} = axial strain in tension side; SG_{h_c} = hoop strain in compression side; SG_{h_m} = hoop strain in in the middle section.

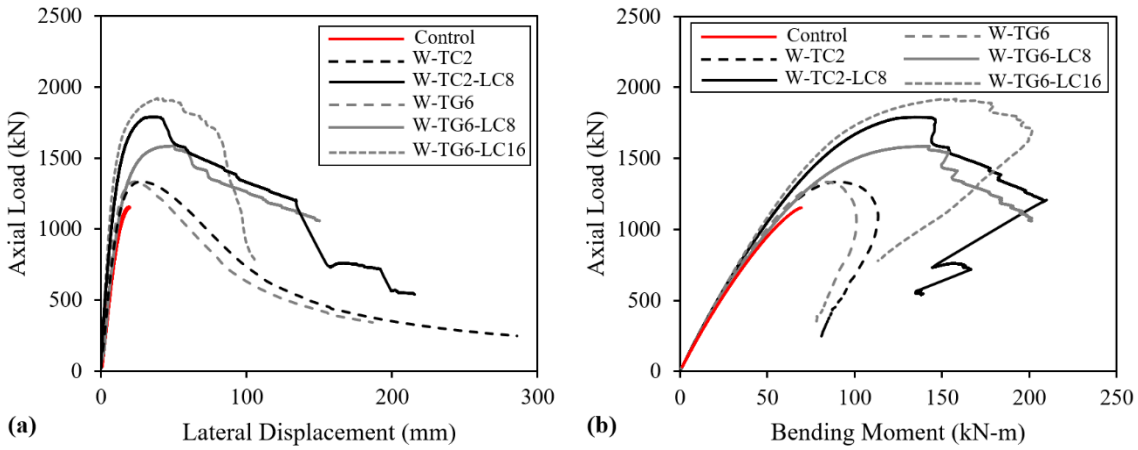

Figure 11. 6 Test results: (a) axial load-lateral displacement curves; and (b) axial load-bending moment curves

Figure 11.6 presents the load-displacement and loading path of the tested specimens. It was observed that the behavior of the wrapped specimen with different confinement levels were the same and similar load-displacement curves were observed for them. However, by adding 8 CFRP strips to the wrapped system, the load-displacement behavior of the specimens was different. Therefore, it can be concluded, that the difference between GFRP and CFRP wrapping for the hybrid system is mostly in providing the lateral support for the CFRP laminates instead of the confinement effect. Since CFRP wrapping provides more lateral support than GFRP, the laminates can continue to sustain the loads more, and the axial capacity of the CFRP wrapped is higher than GFRP wrapped hybrid specimen. Also, it was observed that for CFRP wrapped hybrid specimen, providing more lateral support caused additional stiffness which led to lower displacement at the peak load and an increase in the slope of load-displacement curve. Also, from Figure 11.6, it was observed that by changing the reinforcement ratio of longitudinal CFRPs, the slope of the load-displacement curve increases and the axial capacity of the column. However, the after peak behavior showed less ductile behavior, since the rupture of GFRP wrap for the hybrid system

strengthened with 16 CFRPs caused a sudden drop in the axial load while for hybrid specimens strengthened with 8 CFRP strips, the after peak behavior is similar to the wrapped specimens and tends to continue even after the progressive failure of CFRP strips.

11.4 NUMERICAL STUDIES

This section presents an analytical-numerical model to predict the behavior of slender columns strengthened using the hybrid system described in the previous sections. It should be mentioned that one-dimensional finite difference was involved in solving the differential equation of the column numerically. After verifying the model against experimental test results, a parametric study is presented to evaluate the effect of influential parameters on behavior of slender columns.

11.4.1 Model Description

The analytical-numerical model is an iterative second-order analysis developed in MATLAB using the integration of cross-sectional moment-curvature over the length of a slender column under eccentric loading to compute the deformed shape of the column. The procedure is iterative as the lateral deformation of the slender columns changes the load eccentricity at any given cross-section. As s results, the column was divided in multiple segments and an iterative procedure was considered to calculate the lateral deformation of each node between the segments at any given load until the procedure converged.

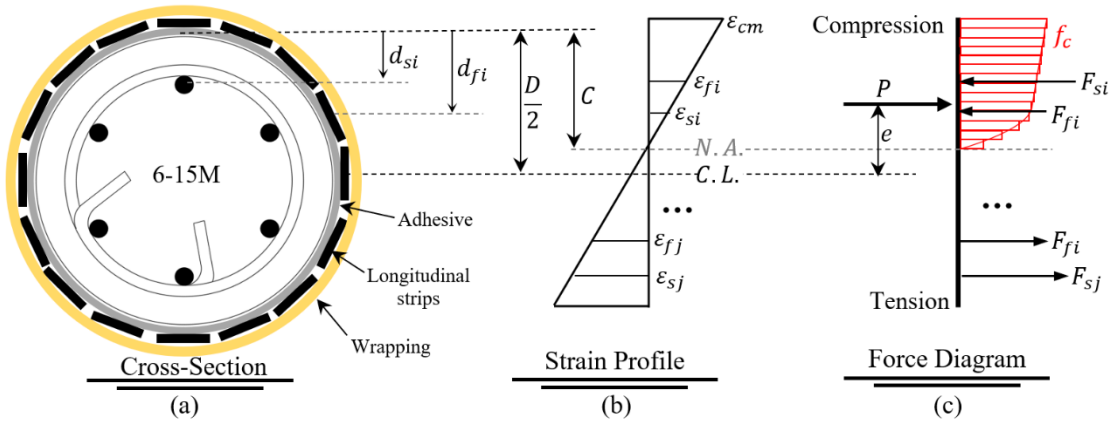

Figure 11. 7 Model description: (a) cross-section; (b) strain profile; and (c) Force diagram

Figure 11.7(a) shows the cross-section of a slender concrete column with internal steel reinforcement strengthened with the hybrid system of longitudinal CFRP strips and transverse GFRP wrapping. As shown in Figure 11.7(b), the strain profile is assumed linear to obtain the strain of each component (i.e. steel, CFRP, and concrete). Based on the stress-strain behavior of each component, the corresponding stress and, in turn, corresponding force can be computed, as shown in Figure 11.6(c). The model assumes a perfect bond between the components up to crushing of the longitudinal CFRP strips, which was observed to be a valid assumption for columns which have enough layers of GFRP and CFRP wrapping.

11.4.1.1 Cross-Sectional Analysis

A cross-sectional analysis is required to find the moment-curvature diagram under a certain load level and eccentricity as well as determining the axial load-bending moment interaction diagram. For a certain load, the axial load can be positioned in different eccentricities from zero to an arbitrary high eccentricity. Afterwards, the equilibrium of moments and forces must be satisfied. The process leads to determination of a unique strain

profile and gives the depth of neutral axis and in turn the curvature for a certain load and different eccentricities which is moment curvature diagram at a certain load. For interaction diagram, the same procedure can be followed with a difference that the ultimate compressive fiber in concrete is set to ε_{cm} which was defined in Figure 11.7b, and the load and strain profile must be determined using equilibrium of forces and moments for different eccentricities. To build the interaction diagram for a steel reinforced concrete column strengthened with longitudinal CFRP and wrapped with lateral GFRP, both unconfined and confined interaction diagrams are required. To find the unconfined interaction diagram, the ultimate compression fiber in the section must be equal to the ultimate axial strain of unconfined concrete, and a sectional analysis must be performed by changing the depth of neutral axis (Figure 11.7) to satisfy the equilibrium as well as finding the corresponding axial load and bending moments. The same procedure applies to the confined concrete, by using the confined concrete stress-strain relationship and setting the maximum compressive fiber to the ultimate axial compressive strain of confined concrete.

For modeling, the stress-strain behavior of the confined concrete is required. Chapter 10 introduces a model for stress-strain behaviour of the confined concrete which is adopted in this chapter for the modeling. However, for the sake of comparison, two different updated models developed recently for the variable confinement is added which is discussed in the verification section.

11.4.1.2 Iterative Procedure

To compute the ultimate capacity of the hybrid system, interaction diagram is not enough since the load eccentricity can be increased due to the secondary moments effects,

especially for slender columns. Therefore, determination of the loading path for the columns is necessary to study their behavior by considering P-delta effects which is illustrated in Figure 11.8. The curvature φ can be defined numerically by using the forward and backward differences about i^{th} node as follows:

$$\varphi = -\frac{d^2y}{dx^2} = -\lim_{\Delta x \to 0} \frac{\frac{y(x+\Delta x)-y(x)}{\Delta x} - \frac{y(x)-y(x-\Delta x)}{\Delta x}}{\Delta x} \tag{11.1}$$

$$\delta_{i+1} = 2\delta_i - \delta_{i-1} - \varphi_i \Delta x^2 \tag{11.2}$$

where y is the deflection of the column, x is the position of a node along column, Δx is the distance between two nodes, and δ_i is the displacement of the i^{th} node. As illustrated in Figure 11.8, and by Equation 11.2, the column can be divided to n nodes and an iterative process can be used to satisfy the boundary conditions and gives the displacement profile of the whole column at a certain load step.

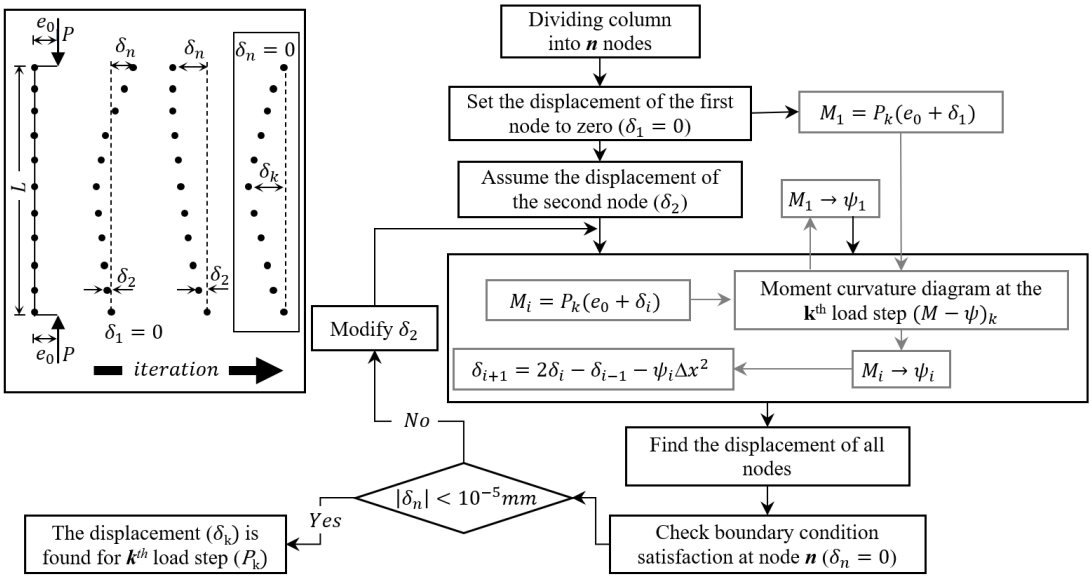

Figure 11. 8 Iterative Procedure for a single load step

The displacement at node 1 and node n are zero (i.e. $\delta_1 = 0$ and $\delta_n = 0$) because the boundary condition of the column is simply supported. The displacement of the second node (δ_2) can be assumed as zero to find the displacement at node 3 (δ_3). Afterwards, all the displacement can be found using Equation 11.2 and displacement of the two previous nodes and the curvature of the previous node. The curvature at each node can be found by using the moment curvature diagram built for that certain load step. It should be noted that the moment (M_i) at each node can be calculated via multiplying the axial load at the k^{th} load step (P_k) by the sum of initial eccentricity (e_0) and the displacement at ith node (δ_i) as shown in Figure 11.8. An iterative process is required to ensure that the displacement at node n (δ_n) is less than 10^{-5} mm to satisfy the boundary condition. The iterative procedure can be repeated for different levels of load to give the loading path or load-displacement curve.

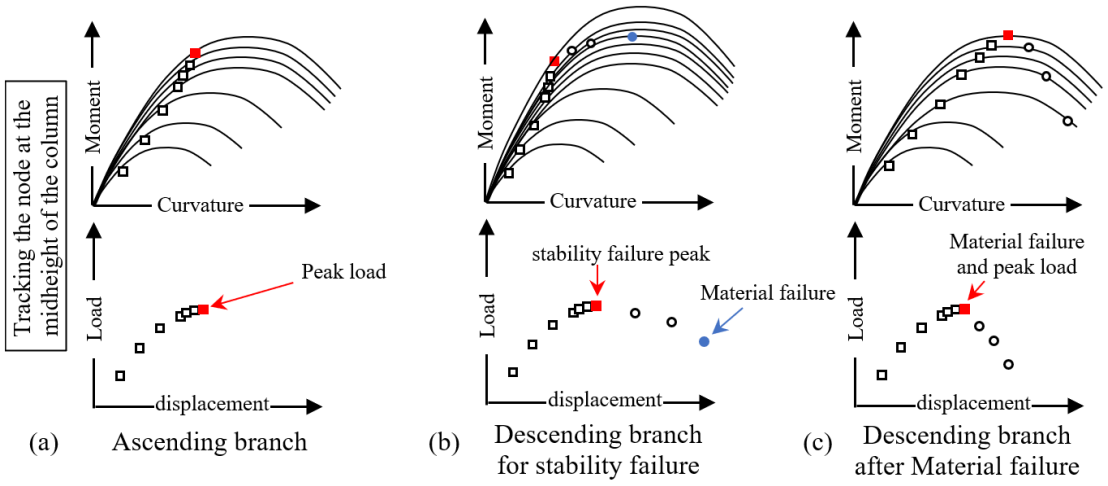

Figure 11. 9 Schematic ascending and descending branches of loading path

In general, the loading path of a slender column can include both ascending and descending branches as shown in Figure 11.9. In the ascending branch, the load can be increased up to the point that a slight additional load demands moment that are higher than the ultimate capacity of the moment-curvature diagram for those loads. In the other words, the iterative process cannot converge, and the load displacement slope tends to zero. This point is the peak load which can be achieved by repeating the iterative process and using smaller load steps close to peak load as shown in Figure 11.9(a) and discussed in more detail in the literature (Jiang and Teng, 2012). It should be noted that Jiang and Teng (2012) proposed a displacement control approach for the descending branch, however, in this paper, a load control approach is introduced for the descending branch. For the case of stability failure before crushing of concrete, as shown in Figure 11.9(b), decreasing load steps can be used after the peak load. The iterative process which used for the ascending branch can be used with the difference that the displacement and the curvature of each point must be increased as the load decreases. Since the displacements are high in the case of stability failure, although the load is decreasing, the moment in each point of the column is increasing as shown in Figure 11.9(b). The process can be followed up to reaching the peak load in the moment-curvature diagram. After this point, by decreasing the load, a very large displacement leads to a higher moment demand than the capacity of the moment-curvature diagram and the iterative process will not converge. It should be noted for columns with low slenderness, the corresponding moment to the peak load reaches the peak point of the moment-curvature diagram in the ascending branch of the loading path as shown in Figure 11.9(c) which is almost close to the crushing of the concrete or interaction diagram. The descending branch after concrete crushing can be determined by reducing the load level

and tracking the curvature and displacement of all nodes to be higher than the previous load step. In this case, as the load decreases, its corresponding moment decreases since the deflections are not as high as the case of stability failure. Therefore, the points on the descending part of the moment-curvature diagram would be corresponding to the descending branch of the loading path that can be captured only by tracking the curvature during the whole load history for every node, as shown in Figure 11.9(c). It should be highlighted that capturing the descending branch of the loading path using the load control approach drastically decrease the cost of calculations in comparison to the displacement control approach.

11.4.2 Model Verification

11.4.2.1 FRP-wrapped specimens

Figure 11.10 shows the verification of the developed model for wrapped concrete columns and the experimental results. It should be mentioned that the core of the models is the same and the only difference between the models is the choice of stress-strain curve for confined concrete. The verification line showed for “Model” was the confined stress-strain curve as defined in chapter 10 (i.e. Equation 10.30). The model predicts the overall behavior of the confined concrete very well, except the peak axial load which is underpredicted.

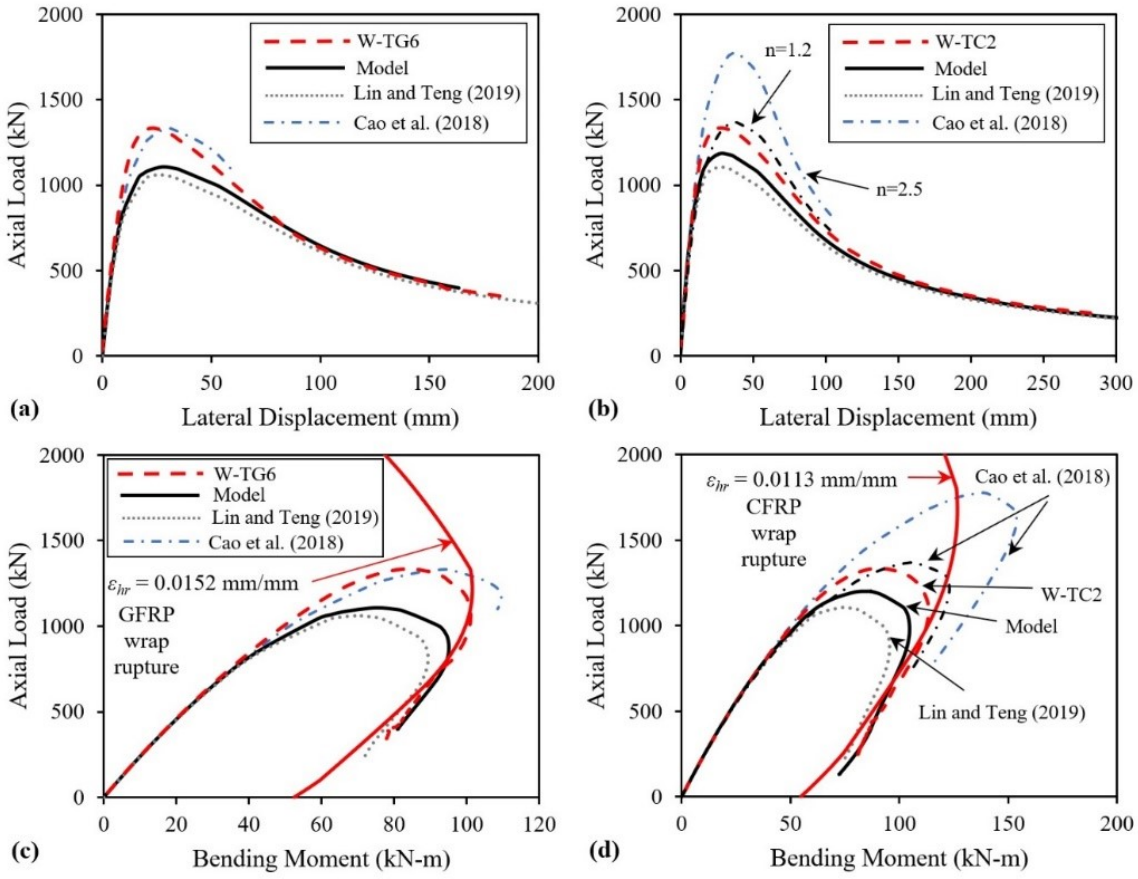

Figure 11. 10 Model verification for wrapped specimens: (a) axial load-lateral displacement curves for W-TG6; (b) axial load-lateral displacement curves for W-TC2; (c) axial load-bending moment curves for W-TG6; and (d) axial load-bending moment curves for W-TC2

To further investigate, different stress-strain models for the confined concrete was selected and compared. Recently, a model was developed by Lin and Teng (2019) which accounts for the effect of eccentricity by changing the secondary slope and the ultimate strain of the confined concrete as the depth of neutral axis changes during the analysis (gray dotted line). The results showed an underprediction of the axial load for this model. The other model compared to experimental results was developed by Cao et al. (2018). This time the secondary slope (E_2), the intercept of secondary part of the stress-strain curve and the stress axis (f_o) were modified and defined as a function of axial load, and eccentricity. The

modification factors were adopted from Cao et al. (2018) and the concentric stress-strain relationship was selected as the one selected in chapter 10 (i.e. Equation10.26 to 10.29) which showed a very good agreement with the experimental tests results (dashed dotted line). It should be mentioned that the curve parameter *n*, which is a polynomial constant that smoothen the transition part in the concentric stress-strain curves, is found to be 2.5 based on minimising the RMSE error of the concentric stress-strain curves in chapter 10. The verification files showed that the value of 2.5 predicts the behavior of the GFRP wrapped column very well, while for CFRP wrapped columns, it over predicts the axial capacity. However, by changing the value of curve parameter n to 1.2, the prediction of the axial load was very well in agreement with the experimental results as shown in Figure 11.10. To further verify the value of n as 1.2, an independent study on CFRP confined concrete columns using different number of layers, different slenderness ratios, and different eccentricity ratios performed by Xing et al. (2020) was selected for verification. Eight confined specimens with column diameter of 300 mm, length to diameter ratios of 3, 6, 9, 11, and eccentricities of 25 mm, 50 mm, 100 mm and 150 mm were verified against the model, as presented in Figure 11.11. The material and section properties can be found in the study by Xing et al. (2020). Figure 11.11 showed a very good agreement between the model with the curve parameter of 1.2 and modification factors introduced by Cao et al. (2018), which is used for further studies and verification of the hybrid system.

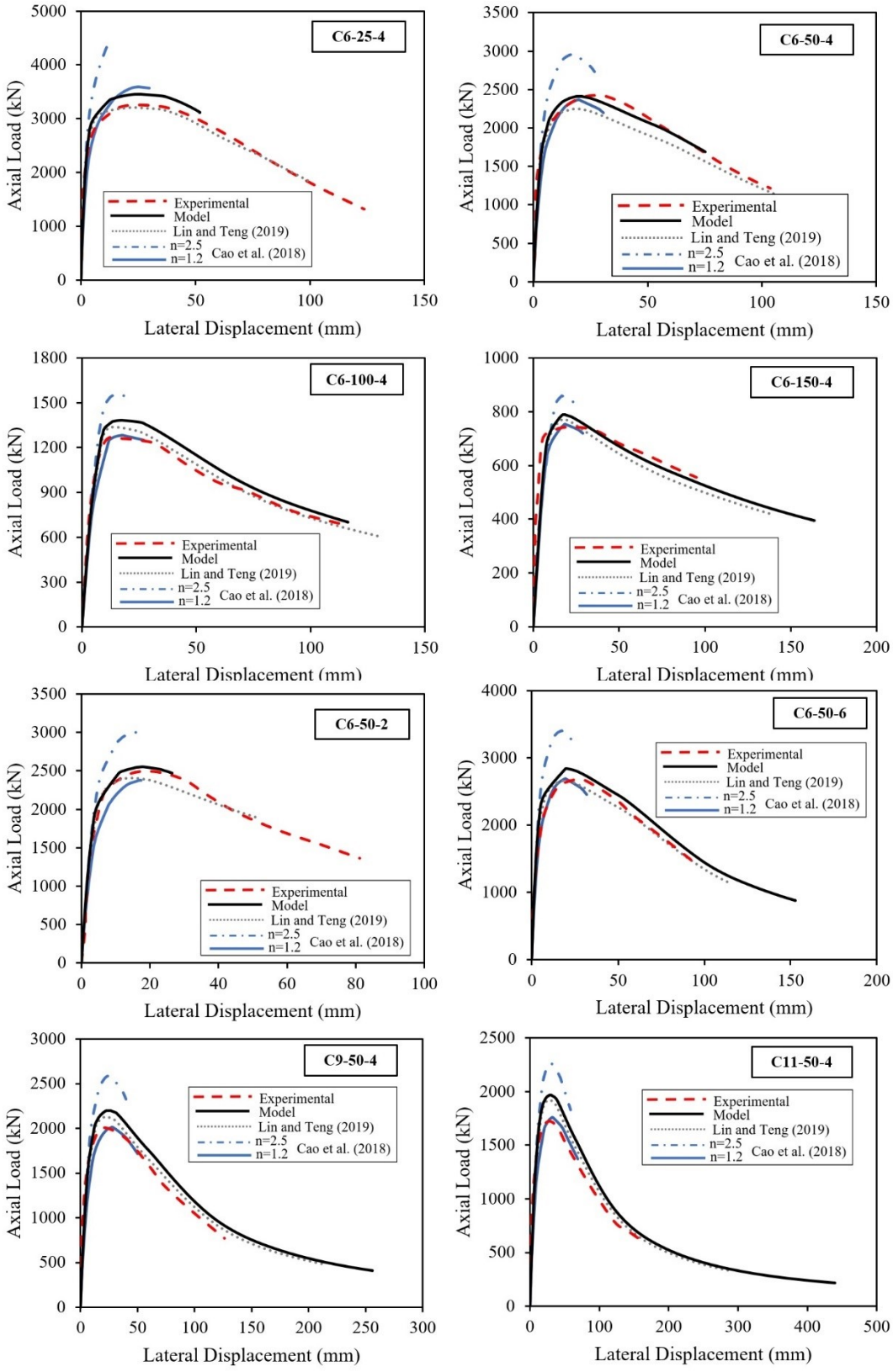

Figure 11. 11 Model verification for study performed by Xing et al. (2020)

Table 11.5 presents the sum of squared error for axial load at the peak load and its corresponding bending moment and lateral displacement, between different variable confinement models and the experimental study conducted by Xing et al. (2020). The results showed that the model which adopted the modifications from Cao et al. (2018), with a curve parameter of *n* equal 1.2 gives the minimum error. The latter is compatible with the results of the verification for the specimen wrapped with CFRP in the current study.

Table 11. 5 Error of the axial load, displacement, and bending moment at peak load for experimental study of Xing et al. (2020) versus second order analysis results with different variable confinement models

Item	SSE			
	Lin and Teng (2019)	Model	Cao et al. (2018) n=2.5	Cao et al. (2018) n=1.2
Axial Load	0.032	0.049	0.639	0.01368
Displacement	0.281	0.182	0.622	0.26106
Bending Moment	0.070	0.062	0.333	0.03588

Note: For ratio of model to experimental, average of each column is considered, and for sum of square error, sum of each column is considered.

11.4.2.2 Hybrid specimens

Figure 11.12 shows the verification of the model versus hybrid specimens. It should be mentioned that the curve parameter *n* was kept the same as what selected for varication of wrapped specimens (i.e. n=1.2 for CFRP wrapping and n=2.5 for GFRP wrapping). Figure 11.12(a) presents the hybrid system wrapped with GFRP and Figure 11.12(b) shows the specimen wrapped with CFRP. In addition to the model which assumes no crushing of CFRP strips (gray line), two curves was developed with considered the failure of the first layer of longitudinal CFRP strips (blue line) and the two first layers of CFRP strips (black line).

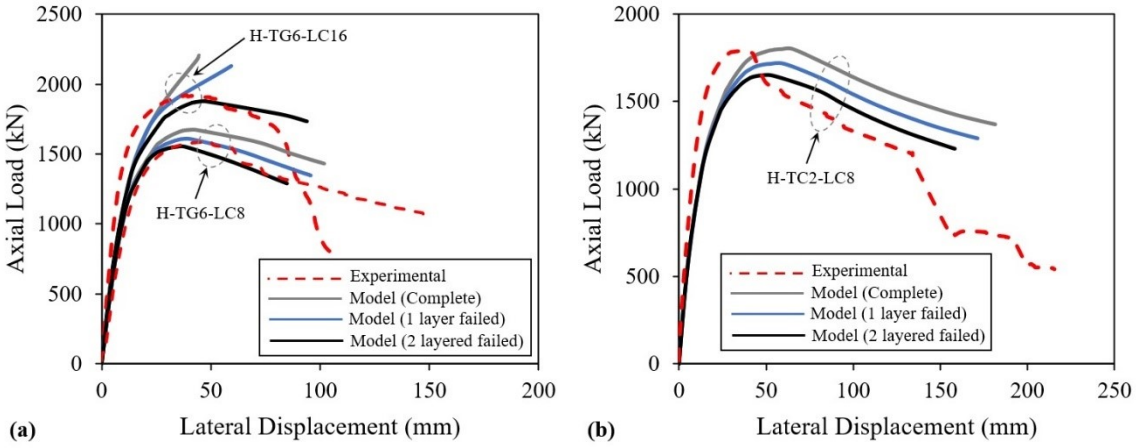

Figure 11. 12 Model verification for hybrid specimens: (a) wrapped with GFRP; and (b) wrapped with CFRP

For hybrid all hybrid specimens, the curve with two layers of failed CFRP strips matches the descending branch of the experimental curve as shown in Figure 11.12. For prediction of the peak load, for CFRP wrapped specimen, the peak load predicted by model without failure of removing any layer of longitudinal CFRP strips. However, for GFRP wrapped hybrid specimens with 8 and 16 longitudinal CFRP strips, the model with two layers and one layer of failed CFRP strips predicts the peak load, respectively. The latter shows that as the reinforcement ratio of longitudinal CFRPs increases, the chance of debonding increases and more layers of longitudinal CFRPs are expected to be removed at the peak load. Also, the analysis showed that as the confining pressure increases, by changing the wrapping from 6 layers of GFRP to 2 layers of CFRP, the lateral support increases and the failed layers longitudinal layers of CFRP decreases. In other words, by providing more lateral support, the system reaches the peak load without experiencing any failure in the longitudinal CFRP strips. Also, the study of the descending branch showed that after the peak load, longitudinal CFRPs may be failed, but the system would not fail, and the load bearing capacity will continue.

11.4.3 Parametric Studies

In this section, the analytical-numerical model was used to compare the effect of the hybrid strengthening system versus the solely wrapping strengthening system of slender concrete columns. For the parametric study, a concrete column with the material properties explained in the experimental part was selected. The column was reinforced with six 15M steel rebar with the cross-sectional area of 200 mm^2. For the longitudinal CFRP reinforcement of the hybrid system, 8 CFRP strips (25×1.2 mm), and for wrapping six layers of GFRP wrapping was considered. The slenderness ratio and eccentricity were the same as experimental study for the base specimen, and one parameter changed at a time while other parameters are constant. It should be mentioned that for calculation of the hybrid system capacity, the first two layers of CFRP strips from compression side of the hybrid specimens did not considered in the calculation to be conservative.

11.4.3.1 Effect of Slenderness Ratio

Figure 11.13 shows the effect of slenderness ratio (λ) on the performance of the hybrid strengthening system in comparison with the wrapping system and control RC columns. Three different slenderness ratios of 22, 40, and 60 were examined at the constant eccentricity of 40 mm. The loading paths corresponding to each slenderness ratio were computes using the analytical-numerical model and presented along the interaction diagram of each cross-section. The results showed a considerable gain in the hybrid specimens in comparison to the wrapped specimens as presented in Figure 11.13. It was observed that as the slenderness ratio increases, the effectiveness of the hybrid system increases. Also, as observed in chapter 9, for short columns, adding longitudinal CFRP strips does not add

considerable gain of strength to the wrapping system, as can be seen in the specimen with slenderness ratio of 22 in Figure 11.13. If the gain in the capacity is considered as the point at which the loading path and interaction diagram intercepts, it was observed that an increase in the slenderness ratio, increase the extra gain in the capacity. However, if the peak loads are used for the comparison, it was seen that the hybrid system with slenderness ratio of 40 showed higher gain in capacity than the hybrid system with slenderness ratio of 60. Since the study is conducted on the hybrid system with 2 first layer of CFRP failed, the intercept of the interaction diagram is chosen as it is more conservative for analysis.

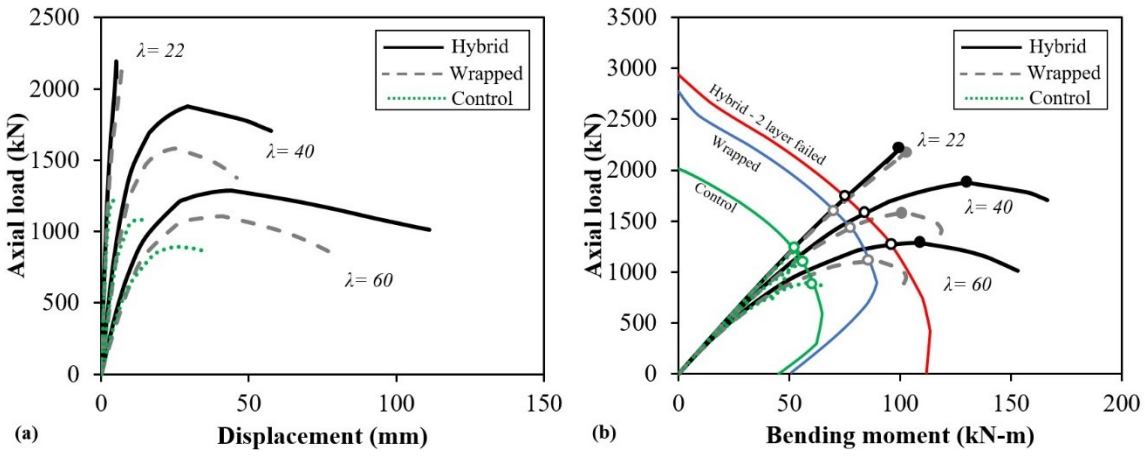

Figure 11. 13 Effect of slenderness ratio: (a) load-displacement curves; and (b) axial load-bending moment curves

11.4.3.2 Effect of Eccentricity

Figure 11.14 shows the effect of load eccentricity on the performance of the hybrid system. Three different e/D ratios of 0.1, 0.2, and 0.5 were examined at constant slenderness ratio of 47. The results showed a considerable gain in the hybrid specimens in comparison to the wrapped specimens as presented in Figure 11.15. It was observed that as the eccentricity increases, the effectiveness of the hybrid system increases by comparing the capacities

found by the intercept of the loading path and interaction diagram. From the interaction diagrams, it was seen that for higher eccentricities, the wrapped specimen tends to act similar to the control specimen while the hybrid specimens increase the capacities considerably.

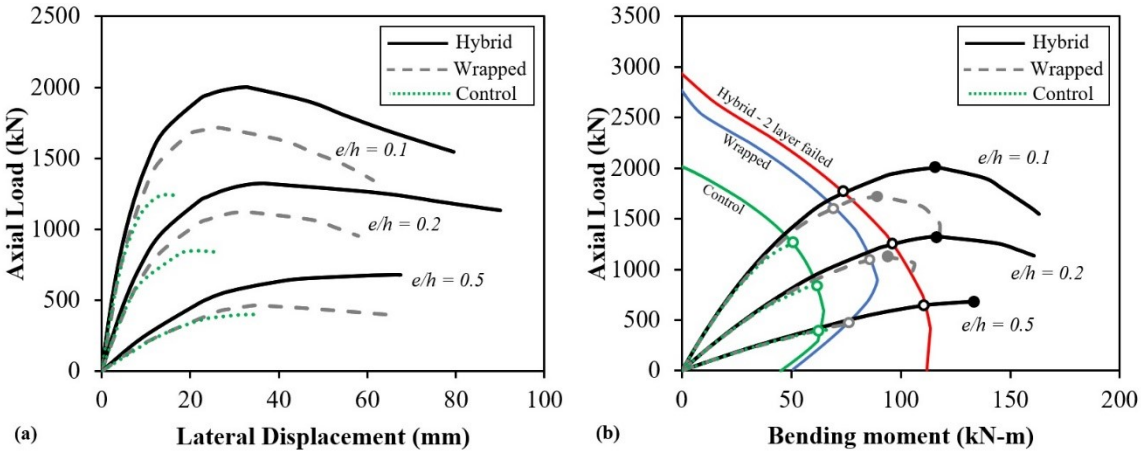

Figure 11. 14 Effect of eccentricity: (a) load-displacement curves; and (b) axial load-bending moment curves

11.5 FUTURE RESEARCH

The number of tests on the subject is limited and more experimental is required to characterize the behavior of the hybrid system for strengthening of slender columns. Therefore, more large-scale experimental tests on the behavior of slender concrete columns strengthened with the proposed hybrid system is crucial to continue the current study. The equivalent stiffness of the hybrid system and proposing simplified design equations using moment magnification method can be considered as the next step once more experimental evidence are available. Also, a reliability analysis will be required to assess the safety of the proposed hybrid system for design applications.

11.6 CONCLUSION

In this study, six large-scale slender circular steel reinforced concrete columns were prepared and tested under combined axial and flexural loading. One specimen was considered as the control specimen without strengthening, two specimens were wrapped with GFRP or CFRP wraps, and three specimens were strengthened with longitudinal CFRP strips and transverse wrapping, known as the hybrid system in this study. Also, an analytical-numerical model was developed which accounts for the nonlinearity in material and geometry, as well as accounting for the effect of eccentricity on the confinement. The following conclusions can be drawn:

- It was observed that the hybrid strengthening system is efficient in enhancing the wrapping strengthening system via improving the flexural stiffness, axial capacity, and flexural capacity of the eccentrically loaded columns drastically.
- For GFRP wrapped specimens, for specimens strengthened with 8 and 16 longitudinal CFRP strips, 82.2% and 96.4% extra gain in flexural capacity, and 21.8% and 50.9% extra gain in the axial capacity of the hybrid strengthening system in comparison to GFRP wrapped system was observed.
- For CFRP wrapped specimens, 63% and 39.5% extra gain in flexural and axial capacity of the hybrid system strengthened with 8 longitudinal CFRP strips in comparison to the CFRP wrapped system was observed.
- The test results showed the spalling of concrete in compression as the mode of failure of the control specimen, matrix rupture as the mode of failure of the wrapped specimens, and the CFRP crushing or debonding in compression as the mode of failure of the hybrid system at the peak load. An additional safety margin was

recognized for the hybrid system after the crushing or debonding of CFRP laminates in compression since the specimen continued to sustain axial load.

- The test results showed that as the reinforcement ratio of longitudinal CFRP strips increases, the axial load capacity increases, while the ductility of the system decreases. Also, the ductility decreases because for higher reinforcement ratios of longitudinal CFRPs, the failure of strips initiated small cracks in GFRP wrap which progressed and ended in the form of rupture of GFRP wrap while it did not happen for lower reinforcement ratio.
- The tests results showed that as the stiffness of the wrapping increases, the lateral support of the longitudinal CFRP strips in the hybrid system increases, stiffness of the load-displacement curve increases, and the load capacity increases while the mode of failure does not change.
- For hybrid specimens strengthened with 8 CFRP strips, as the loading continued after the peak load, the failure of CFRP strips progressed from middle of the column to the sides, and as the failure progress, the behavior of the hybrid system and the wrapped system became similar.
- An analytical-numerical model was developed and verified against the experimental tests which showed a good agreement with the test results. The model accounts for material and geometry nonlinearity as well as considering the effect of eccentric loading on the confinement of the concrete.
- The results of the parametric study showed that the hybrid system is more effective for higher eccentricities and columns with higher slenderness ratios. Also, for short

columns, the performance of the hybrid system does not add considerable gain to the wrapping system of strengthening.

Acknowledgments

Authors would like to thank Blair Nickerson, Brian Kennedy, Jesse Keane, and Brian Liekens and for their assistance in the lab. Also, the author would thank Raghad Kassab and Aidan McCracken for performing material coupon tests for CFRP and GFRP wrapping. The authors would also like to acknowledge and thank NSERC and Dalhousie University for their financial support.

References

ACI 318-14. (2014). Building Code Requirements for Structural Concrete. *American Concrete Institute.* Farmington Hills, MI.

ACI 318-19. (2019). Building Code Requirements for Structural Concrete. *American Concrete Institute.* Farmington Hills, MI.

ACI 440.1R. (2015). Guide for the Design and Construction of Structural Concrete Reinforced Fiber-Reinforced Polymer (FRP) Bars. *American Concrete Institute.* Farmington Hills, MI.

ACI 440.2R. (2017). Guide for the Design and Construction of Externally Bonded FRP Systems for Strengthening Concrete Structures. *American Concrete Institute.* Farmington Hills, MI.

Al-Nimry, H., and Soman, A. (2018). On the slenderness and FRP confinement of eccentrically-loaded circular RC columns. *Engineering Structures*, 164, 92-108.

Ashour, A., El-Refaie, S., and Garrity, S. (2004). Flexural strengthening of RC continuous beams using CFRP laminates. *Cement and concrete composites*, 26(7), 765-775.

Bisby, L., and Ranger, M. (2010). Axial–flexural interaction in circular FRP-confined reinforced concrete columns. *Construction and Building Materials*, 24(9), 1672-1681.

Cao, Y., Wu, Y. F., & Jiang, C. (2018). Stress-strain relationship of FRP confined concrete columns under combined axial load and bending moment. Composites Part B: Engineering, 134, 207-217.

CSA S806-12. (2012). Design and construction of building structures with fiber-reinforced polymers. *Canadian Standards Association.*

Cui, C., and Sheikh, S. A. (2010). Cui, C., and S. A. Sheikh. Experimental study of normal- and high-strength concrete confined with fiber-reinforced polymers. *Journal of Composites for Construction*, 14(5), 553-561.

Fillmore, B., and Sadeghian, P. (2018). Contribution of longitudinal glass fiber-reinforced polymer bars in concrete cylinders under axial compression. *Canadian Journal of Civil Engineers*, 45, 458-468.

Gajdosova, K., and Bilcik, J. (2013). Full-scale testing of CFRP-strengthened slender reinforced concrete columns. *Journal of composites for construction*, 17, 239-248.

Hadi, M. (2006). Behaviour of FRP wrapped normal strength concrete columns under eccentric loading. *Composite Structures*, 72(4), 503-511.

Jiang, T., and Teng, J. (2012). Theoretical model for slender FRP-confined circular RC columns. *Construction and Building Materials*, 32, 66-76.

Lam, L., and Teng, J. (2003). Design-oriented stress–strain model for FRP-confined concrete. *Construction and building materials*, 2003(6-7), 471-489.

Lin, G., Zeng, J. J., Teng, J. G., and Li, L. J. (2020). Behavior of large-scale FRP-confined rectangular RC columns under eccentric compression. Engineering Structures, 216, 110759.

Mohamed, H. M., Afifi, M. Z., and Benmokrane, B. (2014). Performance Evaluation of Concrete Columns Reinforced Longitudinally with FRP Bars and Confined with FRP Hoops and Spirals under Axial Load. *Journal of Bridge Engineering*, 19(7), 04014020.

Nanni, A., and Bradford, N. (1995). FRP jacketed concrete under uniaxial compression. *Construction and Building Materials*, 9(2), 115-124.

Ozbakkaloglu, T. (2013). Compressive behavior of concrete-filled FRP tube columns: Assessment of critical column parameters. *Engineering Structures*, 51, 188-199.

Parvin, A., and Wang, W. (2001). Behaviour of FRP jacketed concrete columns under eccentric loading. *Journal of Composites for Construction*, 5(3), 146-152.

Pessiki, S., Harries, K. A., Kestner, J. T., Sause, R., and Ricles, J. M. (2001). Axial Behavior of Reinforced Concrete Columns Confined with FRP Jackets. *Journal of Composites for Construction*, 5(4), 237-245.

Popovics, S. (1973). A Numerical Approach to the Complete Stress-Strain Curve of Concrete. *Cements and Concrete Research*, 3(5), 583-599.

Sadeghian, P., and Fam, A. (2015). Strengthening slender reinforced concrete columns using high-modulus bonded longitudinal reinforcement for buckling control. *Journal of structural Engineering*, 141, 04014127.

Sadeghian, P., Rahai, A. R., and Ehsani, M. R. (2010). Experimental study of rectangular RC columns strengthened with CFRP composites under eccentric loading. *Journal of Composites for Construction*, 443-450.

Shahawy, M., Arockiasamy, M., Beitelman, T., and Sowrirajan, R. (1996). Reinforced concrete rectangular beams strengthened with CFRP laminates. *Composites Part B: Engineering*, 27(3-4), 225-233.

Sharif, A., Al-Sulaimani, G. J., Basunbul, I. A., Baluch, M. H., and Ghaleb, B. N. (1994). Strengthening of Initially Loaded Reinforced Concrete Beams Using FRP Plates. *ACI structural Journal*, 91(2), 160-168.

Smith, S. T., Kim, S. J., and Zhang, H. (2010). Behavior and Effectiveness of FRP Wrap in the Confinement of Large Concrete Cylinders. *Journal of Composites for Construction*, 14(5), 573-582.

Tao, Z., Teng, J. G. , Han, L.H. and Lam., L., (2004). Experimental behaviour of FRP-confined slender RC columns under eccentric loading. *Advanced Polymer Composites for Structural Applications in Construction. Guildford, UK: 203-212.*

Teng, J. G., Jiang, T., Lam, L., and Luo, Y. Z. (2009). Refinement of a Design-Oriented Stress–Strain Model for FRP-Confined Concrete. *Journal of Composites for Construction*, 13(4), 269–278.

Tobbi, H., Farghaly, A. S., and Benmokrane, B. (2012). Concrete Columns Reinforced Longitudinally and Transversally with Glass Fiber-Reinforced Polymer Bars. *ACI Structural Journal*, 109(4), 551-558.

Triantafillou, T. C., and Plevris, N. (1992). Strengthening of RC beams with epoxy-bonded fibre-composite materials. *Materials and Structures*, 25, 201-211.

Xiao, Y., and Wu, H. (2000). Compressive Behavior of Concrete Confined by Carbon Fiber Composite Jackets. *Journal of materials in civil engineering*, 12(2), 139-146.

Xing, L., Lin, G., and Chen, J. F. (2020). Behavior of FRP-Confined Circular RC Columns under Eccentric Compression. Journal of Composites for Construction, 24(4), 04020030.

Yu, Q., Tao, Z., Gao, X., Yang, YF., Han, LH., and Zhuang, JP., (2004). *Research on seismic performance of FRP-confined RC columns with high axial load ratios,. China: Fuzhou University.*

Zhou, Y. W., and Wu, Y. F. (2012). General model for constitutive relationships of concrete and its composite structures. Composite Structures, 94(2), 580-592.

CHAPTER 12 CONCLUSION AND RECOMMENDATIONS

This study is divided into two main parts including the use of FRP bars as internal reinforcement for new constructions and the used of external FRPs as strengthening device for the existing concrete columns.

The first part of the thesis investigates the behavior of the GFRP reinforced concrete columns to be used in the new constructions as a replacement of the steel reinforced concrete columns. Two major issues which were investigated in this document were the effectiveness of the GFRP bars in compression and the behavior of the slender concrete columns. The investigation for the first part concluded with a study on the slenderness effect for the GFRP bars in concrete columns using a reliability-based approach. Chapters 3 to 6 of this document address the mentioned issues discussed under the branch of "new construction" in this thesis by explaining four first studies.

The second part of the thesis investigates the behavior of CFRP laminates to be used longitudinally on the surface of steel reinforced concrete columns for strengthening purposes. Two possible scenarios of bonded laminates and near-surface mounted laminates were considered for compressive members subjected to combined axial and flexural loading. The modes of failure were recognized and to reach the desire mode of failure which optimizes the use of material and avoid the premature failure, a wrapping system was added to the longitudinal elements to form the hybrid system. The hybrid system was studied through small scale and large-scale experimental tests and numerical investigations. Chapters 7 to 11 of this document address the mentioned issues discussed under the branch

of “strengthening” in this thesis by explaining five studies following the first part of the study. In the following the main conclusions and recommendations are presented.

12.1 CONCLUSION

12.1.1 New Construction (Chapter 3 to 6)

In the 1st study (chapter 3) the performance of short concrete columns reinforced with GFRP bars were investigated experimentally and analytically. A total of fourteen column specimens including nine reinforced and five plain specimens were tested under four load eccentricity to width ratios of 0, 0.1, 0.2, and 0.3. Moreover, an analytical model was developed and verified with test results, and a parametric study was performed using the model. No buckling or crushing of GFRP bars in compression were observed during the test before the failure of specimens. The study revealed that the GFRP bars in compression way below reaching the expected crushing strain of GFRP bars in compression found from compression coupon test. The proposed analytical model showed very good agreement with the experimental results. The model predicted the peak load of the test specimens with an average error of less than 7%. The parametric study revealed that the capacity of column by considering GFRP bars in compression or neglecting them is similar up to the design strain level defined by guidelines, however there is a gain in capacity at the peak load which requires higher strains than the design strain. Overall, for the selected set of tests and parametric study which has performed in this study, the contribution of GFRP bars in compression can be considered in the design of GFRP reinforced short concrete columns and its ignorance in design guidelines is conservatively recommended. It should be mentioned that the 1st study was required to study the behavior of the bars inside the

concrete column with medium scale tests as a preparation phase for the study of the large-scale specimens presented in 3rd study. As a result of the 1st study, the characterization of the GFRP bars in compression was required for further analysis which led to performing the 2nd study.

The 2nd study (chapter 4) was dedicated to determination of the compressive strength, the modulus of elasticity, the crushing strain, and the compressive stress-strain curve of GFRP bars by proposing a new test method. A total of 35 GFRP bar compressive coupons were built and tested using the proposed test method which covered three different bar diameters, provided by three different manufacturers. The proposed test method was successfully implemented to obtain the compressive modulus of elasticity, compressive strength, ultimate crushing strain, and the compressive stress-strain curve of the GFRP bars. It was observed that considering a linear behavior for the compressive stress-strain curves of GFRP bars is a good assumption. In average, the compressive to tensile strength and the modulus of elasticity ratios for all specimens were 1.04 and 0.81, respectively, which shows that the modulus of elasticity in compression and tension could be considered the same for GFRP bars. Thus, for the 3rd study, the compression and tensile modulus of elasticity were considered the same, and the stress-strain behavior of bars in compression were assumed linear. Also, the results of the 2nd study showed no buckling of GFRP bars as a mode of failure. It was found that the crushing strain of GFRP bars cannot be evaluated indirectly from the tensile tests of the GFRP bars due to the wide range of ratio of compressive to tensile modulus of elasticity and strength for different GFRP bars. Therefore, the test method was used for finding the compressive characteristics of the bars in the 3rd study.

In the 3rd study (chapter 5), the behavior of the slender GFRP-RC columns was investigated experimentally. Ten large-scale specimens with two different eccentricity-to-column width ratios of 0.21 and 0.23, two different GFRP reinforcement ratios of 4.8% and 2.78%, and four different slenderness ratios of 16.6, 21.5, 39.7, and 59.5 were tested up to their ultimate failure. A total of three modes of failure were observed including concrete spalling/crushing (CC), global buckling (GB), and crushing of GFRP bars (GC). For short specimens, the specimens did not experience GB, (i.e. specimens with a slenderness ratio of less than or equal 22). For slender specimens, first, the global buckling happened which followed by the spalling/ crushing of concrete. No GFRP crushing occurred prior to the spalling/crushing of concrete columns. No rupture of GFRP bars in tension observed in the tests. The loading continued after concrete failure. It was found that the GFRP-RC columns were able to sustain almost a constant load after spalling/crushing of concrete up to the crushing of the GFRP bars in compression. The specimens were able to tolerate lateral displacement at a certain load level which led to an increase in the moment capacity of the crushed specimens. This moment capacity is attributed to the compressive GFRP bars which were contributed to the axial and bending capacity especially after concrete spalling/crushing. Linear stress-strain behavior of GFRP bars and constant increase in curvature, and in turn strains, make the contribution of GFRP bars in compression more effective. The average compressive strain of GFRP bars in compression at the ultimate loading stage corresponding to GFRP crushing in compression was 73% of the average crushing strain found by material compressive testing. The buckling of GFRP bars after spalling/crushing of concrete was the reason for not reaching the ultimate crushing strain for GFRP bars in compression. Crushing of GFRP bars in compression was corresponding

to a total drop in the load capacity for the tested specimens which led to stop the tests. The unloading stage after failure showed that the bent specimens became straight and their load -axial displacement curve approaches the origin. Also, the flexural stiffness of the specimens calculated from the experimental study and the ones calculated from the available formulas of the literature were compared. Many of the formulas were overestimating or underestimating the flexural stiffness. Overall, the contribution of GFRP bars after failure is considerable. Moreover, GFRP bars in compression were as effective as steel bars in providing the axial force and moment resistance at peak load. Also, by considering them in the calculations of flexural stiffness, more accurate results can be obtained. Therefore, it is suggested not to neglect the effect of GFRP bars in compression. Also, an analytical numerical model was developed to perform second order analysis by considering nonlinearity in material and geometry. The model was verified against the experimental test results. A parametric study performed on the behavior of the columns reinforced with FRP bars using the verified analytical numerical model. Concrete strength, eccentricity, slenderness ratio, reinforcement ratio, and the modulus of elasticity of bars were considered. It was observed that as the eccentricity and slenderness ratio increase, the axial and flexural capacity decreases, and as the modulus of elasticity of FRP bars, concrete strength, and reinforcement ratios increases, the axial and flexural strengths increase. The results of parametric study showed that an increase in the reinforcement ratio is a good solution for enhancing the capacity of slender columns while for short columns, the reinforcement ratio does not significantly affect the capacity. The developed model was used in the 4th study to perform a reliability-based analysis on the slenderness effect for FRP reinforced concrete columns.

In the 4th study (chapter 6), the effect of different effective parameters on the difference between the first-order and second-order analysis was studied using 18432 different cases. It was observed that the major mode of failure f the columns reinforced with FRP bars is crushing of concrete in compression. The worst-case scenario in terms of the difference between the first order and second order analysis was selected from the studied for the reliability-based analysis. The reliability index associated with the critical slenderness ratios of 14, 17, 19, and 22 for GFRP reinforced concrete columns was studied for the first time. For each case 200,000 trials were considered which sums to a total of 800,000 different cases. The study for each selected slenderness ratio was performed by engaging the Monte Carlo simulation to find the probability of the failure of a column if the column is designed based on the first order analysis and then its failure is assessed based on the results of second-order analysis. The results showed that as the critical slenderness ratio decreases from 22 to 17, the reliability index increases from 3.59 to 3.95. However, it should be mentioned that more comprehensive studies are required in the future.

12.1.2 Strengthening (Chapter 7 to 11)

In the 5th study (chapter 7), the behavior of the short concrete columns reinforced with longitudinal NSM CFRP laminates were investigated using experimental and analytical methods. A total of fourteen reinforced concrete specimens were prepared and tested under four different load eccentricities of 0, 10%, 20%, and 30% of the width of the specimen. Furthermore, an analytical model was developed and verified against the available experimental test data which led to a parametric study. The results of the material coupon tests on the CFRP laminates used in this study showed that both compressive and tensile stress-strain curves are linear for this material up to crushing in compression or rupture in

tension. The compressive to tensile strength, modulus of elasticity, and ultimate strain ratios for the tested coupons were 34%, 86%, and 40%, respectively. Four modes of failure were observed in reinforced specimens consisting of concrete spalling (CS), concrete crushing (CC), compressive FRP crushing (CFC), tensile FRP rupture (TFR), however, no buckling or debonding of NSM FRP strips observed during the tests. It should be noted that no crushing or rupture of CFRP strips were observed until long after the peak load. The average compressive strain of CFRP strips for all concrete specimens under eccentric loading was only 41% and 84% of their crushing strain at peak load and after 15% drop from the peak load, respectively. This indicates that crushing of the CFRP strips is not a concern for the specimens considered in this study. Also, it was observed by the parametric study that as the concrete strength increases, the CFRP compressive strain at the peak load increases, but does not reach crushing strain of the laminates found by the coupon tests. The study showed that for short concrete columns strengthen with NSM CFRP laminates, crushing, buckling, or debonding failures of CFRP laminates in compression did not affect the load capacity of the columns and crushing of CFRP strips happened long after peak loads. The results showed that the strengthening of concrete columns using longitudinal NSM FRPs is a viable approach. Moreover, for experimental test data with CFRP reinforcement ratio of 0.21%, the load capacities of the strengthened specimens were improved by 7.7% and 10.9% of the capacity of the plain concrete tested under pure compression and under eccentricity-to-width ratio of 10%, respectively. Since the reinforcement ratio cannot be increased considerably due to space limitations between the grooves, the 6th study was performed on the behaviour of columns strengthened with FRP laminates bonded to the concrete columns.

In the 6th study (chapter 8), the behavior of short concrete columns strengthened with longitudinal CFRP strips and transversely with BFRP wraps were examined experimentally. A total of eighteen simply supported column specimens consisting of five plain concrete, nine longitudinally CFRP bonded, and four longitudinally bonded and transversely wrapped specimens were tested under four load eccentricity to width ratios of 0, 0.1, 0.2, and 0.3. Five modes of failure including concrete crushing, concrete spalling, concrete destruction, debonding of CFRP stirps in compression side, and buckling of CFRP strips in compression were observed. However, no crushing of CFRP strips in compression were observed. The ultimate capacity of each specimen occurred at the peak load for all specimens strengthened with CFRP strips which started by debonding and followed by buckling of CFRP strip in compression. Test results showed that the performance of the longitudinally bonded specimens was improve by adding wrapping system. However, the debonding and buckling of compressive CFRP strips was not avoided even by wrapping even nearly the whole length of the specimens. The experimental results showed that by using narrow transverse straps, the unbraced length of longitudinal strips is certain while for wide wraps, the unbraced length could vary even in two specimens tested under the same condition and is not certain. The study showed that buckling and debonding of CFRP strips was not controlled, but the capacity improved by increasing the length of wrapped area. Thus, in the 7th study the bonded specimens were fully wrapped with different layers of wrapping.

In the 7th study (chapter 9), a total of eighteen short concrete columns were tested under pure axial loading up to failure to validate the effectiveness and performance of a hybrid strengthening system of longitudinal premanufactured bonded CFRP laminates laterally

supported with GFRP wrapping. For strengthened concrete columns, two major modes of failure for the hybrid system were observed: i) debonding of CFRP laminates following by rupture of GFRP wraps, and ii) crushing of CFRP laminates followed by rupture of GFRP wraps. The mode of failure changed as the number of GFRP wrapping increased and caused the mode of failure change from buckling/ debonding of CFRP strips to crushing of CFRPs in compression followed by the rupture of GFRP wrapping. The mechanism of the hybrid system was determined for the short concrete columns. For two layers of GFRP wrapping, the total load capacity of the hybrid system can be calculated by adding the load capacity of unconfined concrete core and the load capacity of CFRP strips at a strain corresponding to the peak load of unconfined concrete (wrapping is not activated). For four layers of GFRP wrapping, the total load capacity of the hybrid system can be calculated by adding the load capacity of the confined concrete core at a strain corresponding to the crushing strain of CFRP strips and the full load capacity of CFRP strips (wrapping is activated). The system followed the same path on the load-strain curves and fails based on the level of the lateral support. For the hybrid system with two layers of GFRP wrapping, the debonding of longitudinal CFRPs happened at the peak load of unconfined concrete. For the hybrid system with four layers of wrapping, the crushing of CFRP laminates controlled the system failure. The experimental results validated the effectiveness of the hybrid strengthening system of longitudinal CFRP laminates and transverse GFRP wraps if enough lateral support is provided. Also, the results showed that the hybrid system is not efficient in axially loaded concrete columns since the capacity is controlled by the crushing of CFRP laminates and does not allow the system to reach the full capacity of the GFRP wrapping for hybrid specimens. Thus, the hybrid system does not have an advantage over the

wrapping system for concentrically loaded short columns. However, it is expected to be effective for strengthening of slender columns. Thus, in 9th study, the effect of the hybrid strengthening system was examined on the behavior of the slender columns. Also, for modeling of the behavior of the columns, a precise eccentric stress-strain curve and ultimate condition of the confining device is required. As more precise concentric stress-strain curves for the confined concrete columns help the modeling of the confined concrete loaded under eccentric loading, in the 8th study, a new stress-strain curve and ultimate condition of the FRP-confined concrete columns was derived based on available experimental tests.

In the 8th study (chapter 10), a design-oriented model for the stress-strain curve of FRP-wrapped concrete columns was calibrated using 200 full stress-strain curves from sixteen different sets of experimental tests which extracted an overall 3272 different points form the literature by adopting a general expression of Richard and Abbot. The initial slope, secondary slope, and intercept stress for all the curves were found and reported in the paper. Also, a database including 788 FRP-wrapped concrete specimens collected by the research group was utilized to find the ultimate strength of the confined concrete. The proposed ultimate confined strain was found as the strain corresponding to the confined concrete strength on the confined stress-stress curve which did not involve direct regression of the ultimate confined strain from the database. The stress-strain model parameters were related only to the FRP wrap stiffness and the unconfined concrete strength instead of the ultimate condition or the confining pressure. It was concluded that excluding the ultimate condition from the adjustment of stress-strain curves of confined concrete leads to more accurate predictions, as it eliminates the effect of rupture strain which impose a large variability in the predictions. The proposed design-oriented stress-strain curve for the FRP-confined

concrete columns was in a very good agreement with the experimental test results and the prediction improved the available predictions in the literature by showing the least error in comparison to fourteen different studies. Also, a five parameter Willam-Warnke failure criterion was used to develop an equation for ultimate confined strength using 788 datapoints. The model improved the available plasticity-based models and showed a very good agreement with the experimental tests. Moreover, the ultimate confined strain was derived using the stress-strain curve and the ultimate confined strength which kept the correlation of the ultimate confined strength, ultimate confined strain. Since the model shown to be in a good agreement with the experimental test results and the proposed stress-strain curve improved the available models, in the 9th study, this model was selected as the stress-strain curve of the confined concrete with some modifications to account for the eccentric loading effect.

In the 9th study (chapter 11), six large-scale slender circular steel reinforced concrete columns were prepared and tested under combined axial and flexural loading. One specimen was considered as the control specimen without strengthening, two specimens were wrapped with GFRP or CFRP wraps, and three specimens were strengthened with longitudinal CFRP strips and transverse wrapping, known as the hybrid system in this study. Also, an analytical-numerical model was developed which accounts for the nonlinearity in material and geometry, as well as accounting for the effect of eccentricity on the confinement. It was observed that the hybrid strengthening system is efficient in enhancing the wrapping strengthening system via improving the flexural stiffness, axial capacity, and flexural capacity of the eccentrically loaded columns drastically. For GFRP wrapped specimens, for specimens strengthened with 8 and 16 longitudinal CFRP strips,

82.2% and 96.4% extra gain in flexural capacity, and 21.8% and 50.9% extra gain in the axial capacity of the hybrid strengthening system in comparison to GFRP wrapped system was observed. For CFRP wrapped specimens, 63% and 39.5% extra gain in flexural and axial capacity of the hybrid system strengthened with 8 longitudinal CFRP strips in comparison to the CFRP wrapped system was observed. The test results showed the spalling of concrete in compression as the mode of failure of the control specimen, matrix rupture as the mode of failure of the wrapped specimens, and the CFRP crushing or debonding in compression as the mode of failure of the hybrid system at the peak load. An additional safety margin was recognized for the hybrid system after the crushing or debonding of CFRP laminates in compression since the specimen continued to sustain axial load. Also, it was observed that as the reinforcement ratio of longitudinal CFRP strips increases, the axial load capacity increases, while the ductility of the system decreases. Also, the ductility decreases because for higher reinforcement ratios of longitudinal CFRPs, the failure of strips initiated small cracks in GFRP wrap which progressed and ended in the form of rupture of GFRP wrap while it did not happen for lower reinforcement ratio. The tests results showed that as the stiffness of the wrapping increases, the lateral support of the longitudinal CFRP strips in the hybrid system increases, stiffness of the load-displacement curve increases, and the load capacity increases while the mode of failure does not change. For hybrid specimens strengthened with 8 CFRP strips, as the loading continued after the peak load, the failure of CFRP strips progressed from middle of the column to the sides, and as the failure progress, the behavior of the hybrid system and the wrapped system became similar. For further studies, an analytical-numerical model was developed and verified against the experimental tests which showed a good agreement with the test results. The model accounts for material and geometry nonlinearity as well as considering the effect of eccentric loading on the confinement of the concrete. Also a parametric study was performed using the verified model whose results showed that the hybrid system is more effective for higher eccentricities and columns with higher

slenderness ratios. Also, for short columns, the performance of the hybrid system does not add considerable gain to the wrapping system of strengthening.

12.2 RECOMMENDATIONS

12.2.1 New Construction

The behavior of GFRP-RC columns after concrete spalling requires more investigations to define a proper ductility or deformability index. The tests showed that the behavior of the columns with slenderness ratios of 17 and 22 was not different and there were very slight secondary moment effects. Therefore, more studies are required to give a more realistic critical slenderness ratio, since the critical slenderness ratio defines the borders between short and slender columns. More investigations are required for proposing a flexural stiffness which predicts the experimental results more accurately. Moreover, a reliability-based analysis is needed to find a proper stiffness reduction factor.

From the study of the interaction diagram for the GFRP-RC columns, it was observed that as the reinforcement ratio increases, the flexural capacity of the beam with no axial load would be higher than the flexural capacity of a beam with very small level of axial load, if the reinforcement ratio increases. The latter may cause unconservative designs for GFRP-RC beams, as they may experience slight axial loads while their effect was not considered in the design. Thus, it is recommended to perform experimental studies on the behavior of the GFRP-RC beam with low levels of axial loading to further investigate this subject which lead to design recommendations.

In terms of the critical slenderness ratio, the current study was only showed a preliminary study, and a more comprehensive study must be performed to cover a wider spectrum of

realistic cases. The concrete strength of 41.4 MPa was the limit for this study, however, the results showed that as concrete strength increases, the difference between first order and second-order analysis increases as well as the percentage drop in the capacity. Thus, higher concrete strength should be considered. In addition, a minimum modular ratio of 2 was considered in this study. However, lower modular ratios can be representative of GFRPs, especially as the concrete strength and modulus of elasticity increases. The strength of FRP bars in compression considered to be less than 50% of its tensile strength which should be modified to be compatible with the most recent findings. Also, only the crushing of concrete was considered. Cases that represent the rupture or crushing of FRP bars should be also considered. Different eccentricities for both ends can be considered, and their randomness can be considered in the analysis which leads to single and double curvature bending. Furthermore, a database of existing experimental studies can be used to find the bias of the second-order model and involve the database inside the simulation. Moreover, circular concrete columns, different dead to live load ratios, and different reinforcement layouts should be studied, which will be considered in future studies to give more accurate reliability indices.

12.2.2 Strengthening

It should be noted that for the study of the hybrid system on short columns, only two different levels of confinement (i.e. 2 and 4 layers of GFRP wrapping) were considered. However, a confinement limit is required to determine if the hybrid mechanism should be considered with or without an activated wrapping effect. Moreover, this limit would be very economically effective, since extra layers of wrapping would not lead to considerable change in the capacity of the system, because the system is controlled by CFRP crushing if

lateral support is enough. Therefore, more tests of hybrid system with different wrapping layers are required to build a database and fid the activation limit for the hybrid system.

For the proposed hybrid strengthening system of longitudinal CFRP laminates and transverse wrapping for slender columns, this study is only the experimental and numerical validation of the performance of the system and more evidence is required to evaluate the hybrid system. Therefore, more large-scale experimental tests on the behavior of slender concrete columns strengthened with the proposed hybrid system is crucial to continue the study on the hybrid system. The equivalent stiffness of the hybrid system and simplified design equations can be further studied as the next step, once more experimental evidence is available. Also, a reliability analysis will be required to assess the safety of the design equations that would be proposed for the hybrid. Also, to give a perspective of the cost of the introduced hybrid strengthening system of longitudinal and transverse FRPs, different strengthening systems can be considered in a separate study for a life cycle analysis.

REFERENCES

Abbasnia, R., and Ziaadiny, H. (2015). Experimental Investigation and Strength Modeling of CFRP-Confined Concrete Rectangular Prisms under Axial Monotonic Compression. *Materials and Structures*, 48(1-2), 485-500.

Abdallah, M. H., Mohamed, H. M., and Masmoudi, R. (2018). Experimental Assessment and Theoretical Evaluation of Axial Behavior of Short and Slender CFFT Columns Reinforced with Steel and CFRP Bars. *Construction and Building Materials*, 181, 535–550.

Abdelazim, W., Mohamed, H. M., Afifi, M. Z., and Benmokrane, B. (2020). Proposed Slenderness Limit for Glass Fiber-Reinforced Polymer-Reinforced Concrete Columns Based on Experiments and Buckling Analysis. *ACI Structural Journal*, 117(1), 241–254.

ACI 318-14. (2014). Building Code Requirements for Structural Concrete. *American Concrete Institute.* Farmington Hills, MI.

ACI 318-19. (2019). Building Code Requirements for Structural Concrete. *American Concrete Institute.* Farmington Hills, MI.

ACI 440.1R. (2015). Guide for the Design and Construction of Structural Concrete Reinforced Fiber-Reinforced Polymer (FRP) Bars. *American Concrete Institute.* Farmington Hills, MI.

ACI 440.2R. (2008). Guide for the Design and Construction of Externally Bonded FRP Systems for Strengthening Concrete Structures. *American Concrete Institute.* Farmington Hills, MI.

ACI 440.2R. (2017). Guide for the Design and Construction of Externally Bonded FRP Systems for Strengthening Concrete Structures. *American Concrete Institute.* Farmington Hills, MI.

Afifi, M. Z., Mohamed, H. M., and Benmokrane, B. (2013). Strength and Axial Behavior of Circular Concrete Columns Reinforced with CFRP Bars and Spirals. *Journal of Composites for Construction*, 18(2), 04013035.

Afifi, M. Z., Mohamed, H. M., and Benmokrane, B. (2014a). Axial Capacity of Circular Concrete Columns Reinforced with GFRP Bars and Spirals. *Journal of Composites for Construction*, ASCE, 18(1), 04013017.

Afifi, M. Z., Mohamed, H. M., and Benmokrane, B. (2014b). Strength and Axial Behavior of Circular Concrete Columns Reinforced with CFRP Bars and Spirals. *Journal of Composites for Construction*, 18(2), 04013035.

Afifi, M. Z., Mohamed, H. M., and Benmokrane, B. (2015). Theoretical Stress-Strain Model for Circular Concrete Columns Confined by GFRP Spirals and Hoops. *Engineering Structures*, 102, 202–213.

Ahmad, S. H., and Shah, S. P. (1982). Complete Triaxial Stress-Strain Curves for Concrete. *ASCE Journal of Structural Division*, 108(ST4), 728-742.

Ahmad, S. H., Khaloo, A. R., and Irshaid, A. (1991). Behaviour of Concrete Spirally Confined by Fibreglass Filaments. *Magazine of Concrete Research*, 43(156), 143–148.

AlAjarmeh, O. S., Manalo, A. C., Benmokrane, B., Karunasena, W., and Mendis, P. (2019a). Axial Performance of Hollow Concrete Columns Reinforced with GFRP Composite Bars with Different Reinforcement Ratios. *Composite Structures*, 213, 153-164.

AlAjarmeh, O. S., Manalo, A. C., Benmokrane, B., Karunasena, W., Mendis, P., and Nguyen, K. T. (2019b). Compressive Behavior of Axially Loaded Circular Hollow Concrete Columns Reinforced with GFRP Bars and Spirals. *Construction and Building Materials*, 194, 12-23.

AlAjarmeh, O. S., Manalo, A. C., Benmokrane, B., Vijay, P. V., Ferdous, W., and Mendis, P. (2019c). Novel Testing and Characterization of GFRP Bars in Compression. *Construction and Building Materials*, 225, 1112-1126.

Albitar, M., Ozbakkaloglu, T., and Fanggi, B. L. (2015). Behavior of FRP-HSC-Steel Double-Skin Tubular Columns under Cyclic Axial Compression. *Journal of Composites for Construction*, 19(2), 04014041.

Alkhrdaji, T., Nanni, A., Chen, G., and Barker, M. (1999). Upgrading the Transportation Infrastructure: Solid RC Decks Strengthened with FRP. *Concrete International: Design and Construction*, 21(10), 37-41.

Al-Nimry, H., and Soman, A. (2018). On the Slenderness and FRP Confinement of Eccentrically-Loaded Circular RC Columns. *Engineering Structures*, 164, 92-108.

Al-Salloum, Y. A., Al-Amri, G. S., Siddiqui, N. A., Almusallam, T. H., and Abbas, H. (2018). Effectiveness of CFRP Strengthening in Improving Cyclic Compression Response of Slender RC Columns. *Journal of Composites for Construction*, 22(3), 04018009.

Alsayed, S. H. (1998). Flexural Behaviour of Concrete Beams Reinforced with GFRP Bars. *Cement and Concrete Composites*, 20(1), 1-11.

Ashour, A. F. (2006). Flexural and Shear Capacities of Concrete Beams Reinforced with GFRP Bars. *Construction and Building Materials*, 20(10), 1005-1015.

Ashour, A., El-Refaie, S., and Garrity, S. (2004). Flexural Strengthening of RC Continuous Beams using CFRP Laminates. *Cement and concrete composites*, 26(7), 765-775.

ASTM A370/A370M-18 (2018). "Standard Test Methods and Definitions for Mechanical Testing of Steel Products. *American Society for Testing and Materials.* West Conshohocken, PA.

ASTM C39/C39M − 18. (2018). Standard Test Method for Compressive Strength of Cylindrical Concrete Specimens. *American Society for Testing and Materials.* West Conshohocken, PA.

ASTM D3039/D3039M-14. (2014). Standard Test Method for Tensile Properties of Polymer Matrix Composite Materials. *American Society for Testing and Materials.* West Conshohocken, PA.

ASTM D6641/D6641M-16. (2016). Standard Test Method for Compressive Properties of Polymer Matrix Composite Materials Using a Combined Loading Compression (CLC) Test Fixture. *American Society for Testing and Materials.* West Conshohocken, PA.

ASTM D695-10. (2010). Standard Test Method for Compressive Properties of Rigid Plastics. *American Society for Testing and Materials.* West Conshohocken, PA.

ASTM D7205 / D7205M - 06. (2016). Standard Test Method for Tensile Properties of Fiber Reinforced Polymer Matrix Composite Bars. *American Society for Testing and Materials.* West Conshohocken, PA.

Atadero, R., Lee, L., and Karbhari, V. M. (2005). Consideration of Material Variability in Reliability Analysis of FRP Strengthened Bridge Decks. *Composite Structures*, 70(4), 430-443.

Badawi, M., and Khaled, S. (2009). Flexural Strengthening of RC Beams with Prestressed NSM CFRP Rods – Experimental and Analytical Investigation. *Construction and Building Materials*, 23(10), 3292-3300.

Bai, Y. L., Dai, J. G., Mohammadi, M., Lin, G., and Mei, S. J. (2019). Stiffness-Based Design-Oriented Compressive Stress-Strain Model for Large-Rupture-Strain (LRS) FRP-Confined Concrete. *Composite Structures*, 223, 110953.

Barros, J. A., Varma, R. K., Sena-Cruz, J. M., and Azevedo, A. F. (2008). Near Surface Mounted CFRP Strips for The Flexural Strengthening of RC Columns: Experimental and Numerical Research. *Engineering Structures*, 30(12), 3412-3425.

Benmokrane, B., and Masmoudi, R. (1996). Flexural Response of Concrete Beams Reinforced with FRP Reinforcing Bars. *ACI Structural Journal*, 93(1), 46-55.

Benmokrane, B., El-Salakawy, E., El-Ragaby, A., and Lackey, T. (2006). Designing and Testing of Concrete Bridge Decks Reinforced with Glass FRP Bars. *Journal of Bridge Engineering*, 11(2), 217-229.

Berg, A. C., Bank, L. C., Olivia, M. G., and Russell, J. S. (2006). Construction and Cost Analysis of an FRP Reinforced Concrete Bridge Deck. *Construction and Building Materials*, 20(8), 515-526.

Berthet, J. F., Ferrier, E., and Hamelin, P. (2006). Compressive behavior of Concrete Externally Confined by Composite Jackets: Part B: Modeling. *Construction and Building Materials*, 20(5), 338–347.

Bing, L., Park, R., and Tanaka, H. (2001). Stress-Strain Behavior of High-Strength Concrete Confined by Ultra-High- and Normal-Strength Transverse Reinforcements. *ACI Structural Journal*, 98(3), 395–406.

Binici, B. (2005). An Analytical Model for Stress-Strain Behavior of Confined Concrete. *Engineering Structures*, 27(7), 1040–1051.

Binici, B. (2008). Design of FRPs in Circular Bridge Column Retrofits for Ductility Enhancement. *Engineering Structures*, 30(3), 766-776.

Bisby, L. A., Dent, A. J. S., and Green, M. F. (2005). Comparison of Confinement Models for Fiber-Reinforced Polymer-Wrapped Concrete. *ACI Structural Journal*, 102(1), 62–72.

Bisby, L., and Ranger, M. (2010). Axial–flexural Interaction in Circular FRP-Confined Reinforced Concrete Columns. *Construction and Building Materials*, 24(9), 1672-1681.

Bournas, D. A., and Triantafillou, T. C. (2009). Flexural Strengthening of Reinforced Concrete Columns with Near-Surface-Mounted FRP or Stainless Steel. *ACI Structural Journal*, 106(4), 495-505.

Broms, B., and Viest, I. M. (1961). Long Reinforced Concrete Columns: A symposium. *Transactions, ASCE,* 126(2), 308-400.

Buyukozturk, O., and Hearing, B. (1998). Failure Behavior of Precracked Concrete Beams Retrofitted with FRP. *Journal of composites for construction*, 138-144.

Cao, Y., Wu, Y. F., & Jiang, C. (2018). Stress-strain Relationship of FRP Confined Concrete Columns under Combined Axial Load and Bending Moment. *Composites Part B: Engineering*, 134, 207-217.

Ceccato, C., Teng, J. G., and Cusatis, G. (2020). Numerical Prediction of the Ultimate Condition of Circular Concrete Columns Confined with a Fiber Reinforced Polymer Jacket. *Composite Structures*, 24, 112103.

Ceroni, F. (2010). Experimental Performances of RC Beams Strengthened with FRP Materials. *Construction and Building Materials*, 24(9), 1547-1559.

Chaallal, O., and Shahawy, M. (2000). Performance of Fiber-Reinforced Polymer-Wrapped Reinforced Concrete Column under Combined Axial-Flexural Loading. *ACI Structural Journal*, 97(4), 659-668.

Chellapandian, M., Suriya Prakash, S., and Raj, A. (2018). Analytical and Finite Element Studies on Hybrid FRP Strengthened RC Column Elements under Axial and Eccentric Compression. *Composite Structures*, 184, 234-248.

Chen, J. F., Li, S. Q., and Bisby, L. A. (2013). Factors Affecting the Ultimate Condition of FRP-Wrapped Concrete Columns. *Journal of Composites for Construction*, 17(1), 67–78.

Chen, W.-F. (1982). Plasticity in Reinforced Concrete. *McGraw-Hill*.

Choo, C. C., Harik, I. E., and Gesund, H. (2006). Strength of Rectangular Concrete Columns Reinforced with Fiber-Reinforced Polymer Bars. *ACI Structural Journal*, 103(3), 452-459.

Claeson, C., and Gylltoft, K. (1998). Slender High-Strength Concrete Columns Subjected to Eccentric Loading. *Journal of Structural Engineering*, 124(3), 233-240.

CSA A23.3-14. (2014). Design of Concrete Structures. *Canadian standard association.*

CSA S6-14. (2014). Canadian Highway Bridge Design Code. *Canadian Standards Association.*

CSA S806-12. (2012). Design and Construction of Building Structures with Fiber-Reinforced Polymers. *Canadian Standards Association.*

Cui, C., and Sheikh, S. A. (2010). Cui, C., and S. A. Sheikh. Experimental Study of Normal- and High-Strength Concrete Confined with Fiber-Reinforced Polymers. *Journal of Composites for Construction*, 14(5), 553-561.

De Luca, A., Matta, F., and Nanni, A. (2010). Behavior of Full-Scale Glass Fiber-Reinforced Polymer Reinforced Concrete Columns under Axial Load. *ACI Structural Journal*, 107(5), 589-596.

Deitz, D. H., Harik, I. E., and Gesund, H. (2003). Physical Properties of Glass Fiber Reinforced Polymer Rebars in Compression. *Journal of Composites for Construction*, 7(4), 363-366.

Deitz, D., Harik, I. E., and Gesund, H. (1999). One-Way Slabs Reinforced with Glass Fiber Reinforced Polymer Reinforcing Bars. *ACI Special Publication*, 188, 279-286.

Demers, M., and Neale K. W. (1994). Strengthening of Concrete Columns with Unidirectional Composite Sheets. *Developments in short and medium span bridge engineering*, 895–905.

Deng, Z. C., and Qu, J. L. (2015). The Experimental Studies on Behavior of Ultrahigh-Performance Concrete Confined by Hybrid Fiber-Reinforced Polymer Tubes. *Advances in Materials Science and Engineering*, Vol 2015, 1–18.

Djafar-Henni, I., and Kassoul, A. (2018). Stress–Strain Model of Confined Concrete with Aramid FRP Wraps. *Construction and Building Materials*, 186, 1016–1030.

Elchalakani, M., and Ma., G. (2017). Tests of Glass Fibre Reinforced Polymer Rectangular Concrete Columns Subjected to Concentric and Eccentric Axial Loading. *Engineering Structures*, 151, 93-104.

Elchalakani, M., Karrech, A., Dong, M., Alib, M., and Yang, B. (2018). Experiments and Finite Element Analysis of GFRP Reinforced Geopolymer Concrete Rectangular Columns Subjected to Concentric and Eccentric Axial Loading. *Structures*, 14, 273-289.

El-Hacha, R., and Abdelrahman, K. (2013). Slenderness Effect of Circular Concrete Specimens Confined with SFRP Sheets. *Composites Part B: Engineering*, 44(1), 152–166.

Elmessalami, N., El Refai, A., and Abed, F. (2019). Fiber-reinforced polymers bars for compression reinforcement: a promising alternative to steel bars. *Construction and Building Materials*, 209, 725-737.

El-sayed, A., El-Salakawy, E., and Benmokrane, B. (2005). Shear Strength of One-Way Concrete Slabs Reinforced with Fiber-Reinforced Polymer Composite Bars. *Journal of Composites for Construction*, 9(2), 147-157.

Fahmy, M. F. M., and Wu, Z. (2010). Evaluating and Proposing Models of Circular Concrete Columns Confined with Different FRP Composites. *Composites Part B: Engineering*, 41(3), 199–213.

Fallah Pour, A., Ozbakkaloglu, T., and Vincent, T. (2018). Simplified Design-Oriented Axial Stress-Strain Model for FRP-Confined Normal- and High-Strength Concrete. *Engineering Structures*, 175, 501–516.

Fam, A. Z., and Rizkalla, S. H. (2001). Confinement Model for Axially Loaded Concrete Confined by Circular Fiber-Reinforced Polymer Tubes. *ACI Structural Journal*, 98(4), 451–461.

Fardis, M. N., and Khalili, H. H. (1982). FRP-Encased Concrete as a Structural Material. *Magazine of Concrete Research*, 34(121), 191–202.

Ferrotto, M. F., Fischer, O., and Cavaleri, L. (2018a). A Strategy for the Finite Element Modeling of FRP-Confined Concrete Columns Subjected to Preload. *Engineering Structures*, 173, 1054–1067.

Ferrotto, M. F., Fischer, O., and Cavaleri, L. (2018b). Analysis-Oriented Stress–Strain Model of CRFP-Confined Circular Concrete Columns with Applied Preload. *Materials and Structures/Materiaux et Constructions*, 51(2), 1–16.

Fib Bulletin 14. (2001). Externally Bonded FRP Reinforcement for RC Structures. *The International Federation for Structural Concrete*, Stuttgart.

Fib Bulletin 40. (2007). FRP Reinforcement in RC Structures. *The International Federation for Structural Concrete*, *Stuttgart.*

Fillmore, B., and Sadeghian, P. (2017). Compressive Behavior of Concrete Cylinders Reinforced with Glass Fiber Reinforced Polymer Bars. *CSCE - Leadership in Sustainable Infrastructures. Vancouver, Canada.*

Fillmore, B., and Sadeghian, P. (2018). Contribution of Longitudinal Glass Fiber-Reinforced Polymer Bars in Concrete Cylinders under Axial Compression. *Canadian Journal of Civil Engineers*, 45, 458-468.

Foret, G., and Limam, O. (2008). Experimental and Numerical Analysis of RC Two-Way Slabs Strengthened with NSM CFRP Rods. *Construction and Building Materials*, 22(10), 2025-2030.

Gajdosova, K., and Bilcik, J. (2013). Full-Scale Testing of CFRP-Strengthened Slender Reinforced Concrete Columns. *Journal of composites for construction*, 17, 239-248.

Galati, N., Tumialan, G., and Nanni, A. (2006). Strengthening with FRP Bars of URM Walls Subject to Out-of-Plane Loads. *Construction and Building Materials*, 20(1), 101-110.

Griffiths, D. V., and Fenton, G. A. (2008). Risk Assessment in Geotechnical Engineering. *John Wiley and Sons Inc*, 381-400.

Guérin, M., Mohamed, H. M., Benmokrane, B., Nanni, A., and Shield, C. K. (2018a). Eccentric Behavior of Full-Scale Reinforced Concrete Columns with Glass Fiber-Reinforced Polymer Bars and Ties. *ACI Structural Journal*, 115(2), 489-499.

Guérin, M., Mohamed, H. M., Benmokrane, B., Shield, C. K., and Nanni, A. (2018b). Effect of Glass Fiber-Reinforced Polymer Reinforcement Ratio on Axial-Flexural Strength of Reinforced Concrete Columns. *ACI Structural Journa*l, 155(4), 1049-3.

Gulbrandsen, P. W. (2005). Reliability Analysis of the Flexural Capacity of Fibre Reinforced Polymer Bars in Concrete Beams, *Doctoral dissertation*, University of Minnesota.

Hadhood, A., Mohamed, H. M., and Benmokrane, B. (2016). Experimental Study of Circular High-Strength Concrete Columns Reinforced with GFRP Bars and Spirals under Concentric and Eccentric Loading. *Journal of Composites for Construction*, 21(2), 04016078.

Hadhood, A., Mohamed, H. M., and Benmokrane, B. (2017). Experimental study of Circular High-Strength Concrete Columns Reinforced with GFRP bars and Spirals Under Concentric and Eccentric Loading. *Journal of Composites for Construction*, 21(2), 04016078.

Hadhood, A., Mohamed, H. M., Benmokrane, B., Nanni, A., and Shield, C. K. (2019). "Assessment of Design Guidelines of Concrete Columns Reinforced with Glass Fiber-Reinforced Polymer Bars." *ACI Structural Journal*, 116(4), 193-207.

Hadhood, A., Mohamed, H. M., Ghrib, F., and Benmokrane, B. (2017). Efficiency of Glass-Fiber Reinforced-Polymer (GFRP) Discrete Hoops and Bars in Concrete Columns under Combined Axial and Flexural Loads. *Composites Part B*, 114, 223-236.

Hadi, M. (2006). Behaviour of FRP Wrapped Normal Strength Concrete Columns under Eccentric Loading. *Composite Structures*, 72(4), 503-511.

Hadi, M. N. (2007). Behaviour of FRP Strengthened Concrete Columns under Eccentric Compression Loading. *Composite Structures*, 77(1), 92-96.

Hadi, M. N., and Youssef, J. (2016). Experimental Investigation of GFRP-Reinforced and GFRP-Encased Square Concrete Specimens under Axial and Eccentric Load, and Four-Point Bending Test. *Journal of Composites for Construction*, 20(5), 04016020.

Hadi, M. N., Karim, H., and Sheikh, M. N. (2016). Experimental Investigations on Circular Concrete Columns Reinforced with GFRP Bars and Helices under Different Loading Conditions. *Journal of Composites for Construction*, 20(4), 04016009.

Hales, T. A., Pantelides, C. P., and Reaveley, L. D. (2016). Experimental Evaluation of Slender High-Strength Concrete Columns with GFRP and Hybrid Reinforcement. *Journal of Composites for Construction*, 20(6), 04016050.

Hales, T. A., Pantelides, C. P., Sankholkar, P., and Reaveley, L. D. (2017). Analysis-Oriented Stress-Strain Model for Concrete Confined with Fiber-Reinforced Polymer Spirals. *ACI Structural Journal*, 114(5), 1263–1272.

Hamilton Iii, H., and Dolan, C. (2001). Flexural Capacity of Glass FRP Strengthened Concrete Masonry Walls. *Journal of Composites for Construction*, 5(3), 170-178.

Hany, N. F., Hantouche, E. G., and Harajli, M. H., (2015). Axial Stress-Strain Model of CFRP-Confined Concrete under Monotonic and Cyclic Loading. *Journal of Composites for Construction*, 19(6), 04015004.

Hasan, H. A., Karim, H., Sheikh, M. N., and Hadi, M. N. (2019). Moment-Curvature Behavior of Glass Fiber-Reinforced Polymer Bar-Reinforced Normal-Strength Concrete and High-Strength Concrete Columns. *ACI Structural Journal*, 116(4), 65-76.

Hoek, E., and Brown, E. T., (1980). Empirical Strength Criterion for Rock Masses. *Journal of Geotechnical and Geoenvironmental Engineering*, 106, 1013-1035.

Hognestad, E. (1951). A Study of Combined Bending and Axial Load in Reinforced Concrete Members, *Bulletin Series No. 399*. Urbana: University of Illinois.

Hussein, M. E., Al-Salloum, Y. A., Alsayed, S. H., and Iqbal, R. A. (2012). Experimental and Numerical Investigation of Size Effects in FRP-wrapped Concrete Columns. *Construction and Building Materials*, 29, 56-72.

Jawdhari, A., Adheem, A. H., and Kadhim, M. M. A. (2020). Parametric 3D Finite Element Analysis of FRCM-Confined RC Columns Under Eccentric Loading. *Engineering Structures*, 212, 110504.

Jesus, M., Silva Lobo, P., and Faustino, P. (2018). Design Models for Circular and Square RC Columns Confined with GFRP Sheets under Axial Compression. *Composites Part B: Engineering*, 141, 60–69.

Jiang, J. F., and Wu, Y. F. (2014). Characterization of Yield Surfaces for FRP-Confined Concrete. *Journal of Engineering Mechanics*, 140(12).

Jiang, J. F., and Wu, Y. F. (2016). Plasticity-Based Criterion for Confinement Design of FRP Jacketed Concrete Columns. *Materials and Structures/Materiaux et Constructions*, 49(6), 2035–2051.

Jiang, K., Han, Q., Bai, Y., and Du, X. (2020). Data-Driven Ultimate Conditions Prediction and Stress-Strain Model for FRP-Confined Concrete. *Composite Structures*, 242, 112094.

Jiang, T., and Teng, J. (2012). Theoretical Model for Slender FRP-Confined Circular RC Columns. *Construction and Building Materials*, 32, 66-76.

Jiang, T., and Teng, J. G. (2007). Analysis-Oriented Stress-Strain Models for FRP-Confined Concrete. *Engineering Structures*, 29(11), 2968–2986.

Karbhari, V. M., and Gao, Y. (1997). Composite Jacketed Concrete under Uniaxial Compression—Verification of Simple Design Equations. *Journal of Materials in Civil Engineering*, 9(4), 185–193.

Khan, Q. S., Sheikh, M., and Hadi, M. N. (2015). Tension and Compression Testing of Fibre Reinforced Polymer (FRP) Bars. *Joint Conference of the 12th International Symposium on Fiber Reinforced Polymers for Reinforced Concrete Structures (FRPRCS-12) and the 5th Asia-Pacific Conference on Fiber Reinforced Polymers in Structures (APFIS-2015). Wollongong, New South Wales, Australia.*

Khorramian, K., and Sadeghian, P. (2017a). Experimental and Analytical Behavior of Short Concrete Columns Reinforced with GFRP Bars under Eccentric Loading. *Engineering Structures*, 761–773.

Khorramian, K., and Sadeghian, P. (2017b). Short Concrete Columns Reinforced with GFRP Rebars Under Eccentric Loading. *CSCE Annual Conference. Vancouver, BC, Canada: Canadian Society of Civil Engineering.*

Khorramian, K., and Sadeghian, P. (2017c). Strengthening Concrete Columns Using Near Surface Mounted (NSM) Carbon Fiber Reinforced Polymer (CFRP) Laminates. *Sixth Asia-Pacific Conference on FRP in Structures. Singapore, Singapore.*

Khorramian, K., and Sadeghian, P. (2018a). New Testing Method of GFRP Bars in Compression. *CSCE Annual Conference. Fredericton, NB, Canada: Canadian Society of Civil Engineering.*

Khorramian, K., and Sadeghian, P. (2018b). Strengthening of Slender Circular Concrete Columns with Longitudinal CFRP Laminates and Transverse GFRP wraps. *CSCE Annual Conference. Fredericton, NB, Canada: Canadian Society of Civil Engineering.*

Khorramian, K., and Sadeghian, P. (2018c). Strengthening Short Concrete Columns Using Longitudinally Bonded CFRP Laminates. *ACI Special Publication*, 327, 24-1:10.

Khorramian, K., and Sadeghian, P. (2019a). Behavior of Slender GFRP Reinforced Concrete Columns. *ASCE-SEI Structures Congress, American Society of Civil Engineers. St. Louis, Missouri, USA*.

Khorramian, K., and Sadeghian, P. (2019b). Material Characterization of GFRP Bars in Compression using a New Test Method. *Journal of Testing and Evaluation (ASTM)*, 49, 2.

Khorramian, K., and Sadeghian, P. (2019c). Performance of High-Modulus Near-Surface-Mounted FRP Laminates for strengthening of Concrete Columns. *Composites Part B*, 164, 90-102.

Khorramian, K., and Sadeghian, P. (2020). Experimental Investigation of Short and Slender Rectangular Concrete Columns Reinforced with GFRP Bars under Eccentric Axial Loads. *Journal of Composites for Construction, under review.*

Kim, Y. J., Longworth, J. M., and Wight, G. R. (2008). Flexure of Two-Way Slabs Strengthened with Prestressed or Non Prestressed CFRP Sheets. *Journal of Composites for Construction*, 12(4), 366-374.

Kobayashi, K., and Fujisaki, T. (1995). Compressive Behaviour of FRP Reinforcement in Non Prestressed Concrete Members. *Non metallic (FRP) reinforcement for concrete structures, Proceedings of the second international RILEM Symposium (FRPRCS-2). London, UK*.

Lam, L., and Teng, J. (2003). Design-Oriented Stress–Strain Model for FRP-Confined Concrete. *Construction and building materials*, 2003(6-7), 471-489.

Li, P., Wu, Y. F., Zhou, Y., and Xing, F. (2019). Stress-Strain Model for FRP-Confined Concrete Subject to Arbitrary Load Path. *Composites Part B: Engineering*, 163, 9–25.

Li, Y. F., Lin, C. T., & Sung, Y. Y. (2003). A Constitutive Model for Concrete Confined with Carbon Fiber Reinforced Plastics. Mechanics of Materials, 35(3-6), 603-619.

Liang, M., Wu, Z. M., Ueda, T., Zheng, J. J., and Akogbe, R. (2012). Experiment and Modeling on Axial Behavior of Carbon Fiber Reinforced Polymer Confined Concrete Cylinders with Different Sizes. *Journal of Reinforced Plastics and Composites*, 31(6), 389–403.

Lillistone, D., and Jolly, C. K. (2000). An Innovative Form of Reinforcement for Concrete Columns Using Advanced Composites. *Structural Engineer*, 78(23/24).

Lim, J. C., and Ozbakkaloglu, T. (2015). Lateral Strain-to-Axial Strain Relationship of Confined Concrete. *Journal of Structural Engineering*, 141(5), 1–18.

Lin, G., and Teng, J. G. (2019). Stress-strain Model for FRP-Confined Concrete in Eccentrically Loaded Circular Columns. *Journal of Composites for Construction*, 23(3), 04019017.

Lin, G., Zeng, J. J., Teng, J. G., and Li, L. J. (2020). Behavior of Large-Scale FRP-Confined Rectangular RC Columns under Eccentric Compression. Engineering Structures, 216, 110759.

Lloyd, A. N., and Rangan, V. B. (1996). Studies on High-Strength Concrete Columns under Eccentric Compression. *ACI Structural Journal*, 93(6), 631-638.

MacGregor, J. G., and Breen, J. E. (1970). Design of Slender Concrete Columns. *In Journal Proceedings* 67(1), 6-28.

Malek, A. M., Saadatmanesh, H., and Ehsani, M. R. (1998). Prediction of Failure Load of R/C Beams Strengthened with FRP Plate Due to Stress Concentration at the Plate End. *ACI structural Journal*, 95, 142-152.

Mallick, P. K. (2008). Fiber Reinforced Composites Materials, Manufacturing, and Design. Boca Raton, Florida: *CRC Press*.

Mander, J. B., Priestley, M. J. N., and Park, R. (1988). Theoretical Stress-Strain Model for Confined Concrete. *Journal of Structural Engineering*, 114(8), 1804–1826.

Maranan, G. B., Manalo, A. C., Benmokrane, B., Karunasena, W., and Mendis, P. (2016). Behavior of Concentrically Loaded Geopolymer-Concrete Circular Columns Reinforced Longitudinally and Transversely with GFRP Bars. *Engineering Structures*, 117, 422-436.

Michaluk, C. R., Rizkalla, S. H., Tadros, G., and Benmokrane, B. (1998). Flexural Behavior of One-Way Concrete Slabs Reinforced by Fiber Reinforced Plastic Reinforcements. *ACI Structural Journal*, 95(3), 353-365.

Mirmiran, A., Shahawy, M., Samaan, M., El Echary, H., Mastrapa, J. C., and Pico, O. (1998). Effect of Column Parameters on FRP-Confined Concrete. *Journal of Composites for Construction*, 2(4), 175-185.

Mirmiran, A., Yuan, W., and Chen, X. (2001). Design for slenderness in Concrete Columns Internally Reinforced with Fiber-Reinforced Polymer bars. *Structural Journal*, 98(1), 116-125.

Mirza, S. A. (1990). Flexural Stiffness of Rectangular Reinforced Concrete Columns. *ACI Structural Journal*, 87(4), 425-435.

Miyauchi, K., Inoue, S., Kuroda, T., and Kobayashi, A. (1999). Strengthening Effects with Carbon Fiber Sheet for Concrete Column. *Proc Jpn Concr Inst*, 21(3), 1453–1458.

Miyauchi, K., Nishibayashi, S., and Inoue, S. (1997). Estimation of Strengthening Effects with Carbon Fiber Sheet for Concrete Column. *Proceedings of the Third International Symposium on Non-Metallic FRP for Concrete Structures*, 224.

Mohamed, H. M., Afifi, M. Z., and Benmokrane, B. (2014). Performance Evaluation of Concrete Columns Reinforced Longitudinally with FRP Bars and Confined with FRP Hoops and Spirals under Axial Load. *Journal of Bridge Engineering*, 19(7), 04014020.

Mohammadi, M., and Wu, Y. F. (2019). Modified Plastic-Damage Model for Passively Confined Concrete Based on Triaxial Tests. *Composites Part B: Engineering*, 159, 211–223.

Mohammadi, M., Dai, J. G., Wu, Y. F., and Bai, Y. L. (2019). Development of Extended Drucker–Prager Model for Non-Uniform FRP-Confined Concrete based on Triaxial Tests. *Construction and Building Materials*, 224, 1–18.

Moran, D. A., and Pantelides, C. P. (2002). Stress-Strain Model for Fiber-Reinforced Polymer-Confined Concrete. *Journal of Composites for Construction*, 6(4), 233–240.

Moran, D. A., and Pantelides, C. P. (2012). Elliptical and Circular FRP-Confined Concrete Sections: A Mohr-Coulomb Analytical Model. *International Journal of Solids and Structures*, 49(6), 881–898.

Mosallam, A. S., and Mosalam, K. M. (2003). Strengthening of Two-Way Concrete Slabs with FRP Composite Laminates. *Construction and Building Materials*, 17(1), 43-54.

Mufti, A. A., Jaeger, L. G., Bakht, B., and Wegner, L. D. (1993). Experimental Investigation of Fibre-Reinforced Concrete Deck Slabs without Internal Steel Reinforcement. *Canadian Journal of Civil Engineering*, 20(3), 398-406.

Naderpour, H., and Mirrashid, M. (2020). Confinement Coefficient Predictive Modeling of FRP-Confined RC Columns. *Advances in Civil Engineering Materials*, 9(1), 1–21.

Nanni, A., and Bradford, N. (1995). FRP Jacketed Concrete under Uniaxial Compression. *Construction and Building Materials*, 9(2), 115-124.

Nanni, A., De Luca, A., and Zadeh, H. J. (2014). Reinforced Concrete with FRP Bars: Mechanics and Design. *CRC Press*.

Newhook, J., Ghali, A., and Tadros, G. (2002). Concrete Flexural Members Reinforced with Fiber Reinforced Polymer: Design for Cracking and Deformability. *Canadian Journal of Civil Engineering*, 29(1), 125-134.

Nordin, H., and Täljsten, B. (2006). Concrete Beams Strengthened with Prestressed Near Surface Mounted CFRP. *Journal of Composites for Construction*, 10(1), 60-68.

Nowak, A. S., and Szerszen, M. M. (2003). Calibration of Design Code for Buildings (ACI 318): Part 1-Statistical Models for Resistance. *ACI Structural Journal*, 100(3), 377-382.

Oudah, F., El Naggar, M. H., and Norlander, G. (2019). Unified System Reliability Approach for Single and Group Pile Foundations–Theory and Resistance Factor Calibration. *Computers and Geotechnics*, 108, 173-182.

Ozbakkaloglu, T. (2013). Compressive Behavior of Concrete-Filled FRP Tube Columns: Assessment of Critical Column Parameters. *Engineering Structures*, 51, 188-199.

Ozbakkaloglu, T., and Vincent, T. (2014). Axial Compressive Behavior of Circular High-Strength Concrete-Filled FRP Tubes. *Journal of composites for construction*, 18(2), 04013037.

Ozbakkaloglu, T., Gholampour, A., and Lim, J. C. (2016). Damage-Plasticity Model for FRP-Confined Normal-Strength and High-Strength Concrete. *Journal of Composites for Construction*, 20(6), 1–13.

Pan, Y., Guo, R., Li, H., Tang, H., and Huang, J. (2017). Analysis-Oriented Stress–Strain Model for FRP-Confined Concrete with Preload. *Composite Structures*, 166, 57–67.

Pantelides, C. P., Gibbons, M. E., and Reaveley, L. D. (2013). Axial Load Behavior of Concrete Columns Confined with GFRP Spirals. *Journal of Composites for Construction*, 17(3), 305-313.

Parvin, A., and Brighton, D. (2014). FRP Composites Strengthening of Concrete Columns under Various Loading Condition. *Polymers*, 6, 1040-1056.

Parvin, A., and Wang, W. (2001). Behaviour of FRP jacketed Concrete Columns under Eccentric Loading. *Journal of Composites for Construction*, 5(3), 146-152.

Paultre, P., and Légeron, F. (2008). Confinement Reinforcement Design for Reinforced Concrete Columns. *Journal of structural engineering*, 134(5), 738-749.

Pessiki, S., Harries, K. A., Kestner, J. T., Sause, R., and Ricles, J. M. (2001). Axial Behavior of Reinforced Concrete Columns Confined with FRP Jackets. *Journal of Composites for Construction*, 5(4), 237-245.

Pham, T. M., and Hadi, M. N. S. (2013). Strain Estimation of CFRP-Confined Concrete Columns using Energy Approach. *Journal of Composites for Construction*, 17(6), 1–11.

Piscesa, B., Attard, M. M., and Samani, A. K. (2018). 3D Finite element modeling of Circular Reinforced Concrete Columns Confined with FRP using a Plasticity Based Formulation. *Composite Structures*, 194, 478–493.

Popovics, S. (1973). A Numerical Approach to the Complete Stress-Strain Curve of Concrete. *Cements and Concrete Research*, 3(5), 583-599.

Rahimi, H., and Hutchinson, A. (2001). Concrete Beams Strengthened with Externally Bonded FRP Plates. *Journal of Composites for Construction*, 5(1), 44-56.

Richard, R. M., and Abbot, B. J. (1975). Versatile Elastic-Plastic Stress-Strain Formula. *Journal of the Engineering Mechanics Division*, 101(4), 511–515.

Richart, F. E., Brandtzaeg, A., and Brown, R. L. (1928). A Study of the Failure of Concrete under Combined Compressive Stresses. *In: Bulletin no. 185*, Univ. *of Illinois, Eng. Experimental Station: Champaign, Ill.*

Rousakis, T., and Tepfers, R. (2001). Experimental Investigation of Concrete Cylinders Confined by Carbon FRP Sheets, under Monotonic and Cyclic Axial Compressive Load. *Research Rep*, 44, 1–87.

Saadatmanesh, H., Ehsani, M. R., and Li, M. W. (1994). Strength and ductility of Concrete Columns Externally Reinforced with Fiber Composite Straps. *Structural Journal*, 91(4), 434–447.

Saafi, M., Toutanji, H. A., and Li, Z. (1999). Behavior of Concrete Columns Confined with Fiber Reinforced Polymer Tubes. *ACI Materials Journal*, 96(4), 500–509.

Saberi, H., Bui, T. Q., Furukawa, A., Rahai, A., and Hirose, S. (2020). FRP-Confined Concrete Model Based on Damage-Plasticity and Phase-Field Approaches. *Composite Structures*, 244, 112263.

Sadeghian, P., and Fam, A. (2014). A Rational Approach Toward Strain Efficiency Factor of Fiber-Reinforced Polymer-Wrapped Concrete Columns. *ACI Structural Journal*, 111(1), 135–144.

Sadeghian, P., and Fam, A. (2015). Improved Design-Oriented Confinement Models for FRP-Wrapped Concrete Cylinders Based on Statistical Analyses. *Engineering Structures*, 162–182.

Sadeghian, P., and Fam, A. (2015). Strengthening Slender Reinforced Concrete Columns using High-Modulus Bonded Longitudinal Reinforcement for Buckling Control. *Journal of structural Engineering*, 141, 04014127.

Sadeghian, P., and Fillmore, B. (2018). Strain Distribution of basalt FRP-Wrapped Concrete Cylinders. *Case Studies in Construction Materials*, 9, e00171.

Sadeghian, P., Rahai, A. R., and Ehsani, M. R. (2010). Experimental Study of Rectangular RC Columns Strengthened with CFRP Composites under Eccentric Loading. *Journal of Composites for Construction*, 443-450.

Sadeghian, P., Seracino, R., Das, B., and Lucier, G. (2018). Influence of Geometry and Fiber Properties on Rupture Strain of Cylindrical FRP Jackets under Internal ICE Pressure. *Composite Structures*, 192, 173–183.

Saiid Saiidi, M., Sureshkumar, K., and Pulido, C. (2005). Simple Carbon-Fiber-Reinforced-Plastic-Confined Concrete Model for Moment-Curvature Analysis. *Journal of Composites for Construction*, 9(1), 101–104.

Salah-Eldin, A., Mohamed, H. M., and Benmokrane, B. (2019). Structural performance of High-Strength-Concrete Columns Reinforced with GFRP Bars and Ties Subjected to Eccentric Loads. *Engineering Structures*, 185, 286-300.

Samaan, M., Mirmiran, A., and Shahawy, M. (1998). "Model of Concrete Confined by Fiber Composites." *Journal of Structural Engineering*, 124(9), 1025–1031.

Sargin, M. (1971). Stress-Strain Relationships for Concrete and Analysis of Structural Concrete Sections. *Study No. 4, Solid Mechanics Division, University of Waterloo, Waterloo, Ontario, Canada.*

Shaat, A., and Fam, A. Z. (2009). Slender Steel Columns Strengthened Using High-Modulus CFRP Plates for Buckling Control. *Journal of Composites for Construction*, 13(1), 2-12.

Shahawy, M., Arockiasamy, M., Beitelman, T., and Sowrirajan, R. (1996). Reinforced Concrete Rectangular Beams Strengthened with CFRP Laminates. *Composites Part B: Engineering*, 27(3-4), 225-233.

Shahawy, M., Mirmiran, A., and Beitelman, T. (2000). Tests and Modeling of Carbon-Wrapped Concrete Columns. *Composites Part B: Engineering*, 31(6), 471-480.

Sharif, A., Al-Sulaimani, G. J., Basunbul, I. A., Baluch, M. H., and Ghaleb, B. N. (1994). Strengthening of Initially Loaded Reinforced Concrete Beams Using FRP Plates. *ACI structural Journal*, 91(2), 160-168.

Sheikh, S. A., and Kharal, Z. (2018). GFRP-Reinforced Concrete Columns Subjected to Seismic Loads. *ACI Special Publication*, 326, 56-1:10.

Siddiqui, N. A., Alsayed, S. H., Al-Salloum, Y. A., Iqbal, R. A., and Abbas, H. (2014). Experimental Investigation of Slender Circular RC Columns Strengthened with FRP Composites. *Construction and Building Materials*, 69, 323–334.

Silva Lobo, P., Faustino, P., Jesus, M., and Marreiros, R. (2018). Design Model of Concrete for Circular Columns Confined with AFRP. *Composite Structures*, 200, 69–78.

Smith, S. T., Kim, S. J., and Zhang, H. (2010). Behavior and Effectiveness of FRP Wrap in the Confinement of Large Concrete Cylinders. *Journal of Composites for Construction*, 14(5), 573-582.

Song, X., Gu, X., Li, Y., Chen, T., and Zhang, W. (2013). Mechanical Behavior of FRP-Strengthened Concrete Columns Subjected to Concentric and Eccentric Compression Loading. *Journal of Composites for Construction*, 17(3), 336–346.

Spoelstra, M. R., and Monti, G. (1999). FRP-Confined Concrete Model. *Journal of Composites for Construction*, 3(3), 143-150.

Sun, L., Wei, M., and Zhang, N. (2017). Experimental Study on the Behavior of GFRP Reinforced Concrete Columns under Eccentric Axial Load. *Construction and Building Materials*, 152, 214-225.

Tarek, H., and Rizkalla, S. (2002). Flexural Strengthening of Prestressed Bridge Slabs with FRP systems. *PCI Journal*, 47(1), 76-93.

Tavassoli, A., Liu, J., and Sheikh, S. (2015). Glass Fiber-Reinforced Polymer-Reinforced Circular Columns under Simulated Seismic Loads. *ACI Structural Journal*, 103-114.

Teng, J. G., Jiang, T., Lam, L., and Luo, Y. Z. (2009). Refinement of a Design-Oriented Stress–Strain Model for FRP-Confined Concrete. *Journal of Composites for Construction*, 13(4), 269–278.

Teng, J., Lorenzis, L., Wang, B., Li, R., Wong, T., and Lam, L. (2006). Debonding Failures of RC Beams Strengthened with Near Surface Mounted CFRP Strips. *Journal of composites for construction*, 92(105), 92-105.

Thériault, M., and Benmokrane, B. (1998). Effects of FRP Reinforcement Ratio and Concrete Strength on Flexural Behavior of Concrete Beams. *Journal of Composites for Construction*, 2(1), 7-16.

Tikka, T., Francis, M., and Teng, B. (2010). "Strength of Concrete Beam-Columns Reinforced with GFRP Bars." *2nd International structures specialty conference*, Winnipeg, Manitoba, 46.1-46.10.

Tobbi, H., Farghaly, A. S., and Benmokrane, B. (2012). Concrete Columns Reinforced Longitudinally and Transversally with Glass Fiber-Reinforced Polymer Bars. *ACI Structural Journal*, 109(4), 551-558.

Tobbi, H., Farghaly, A. S., and Benmokrane, B. (2014). Behavior of Concentrically Loaded Fiber-Reinforced Polymer Reinforced Concrete Columns with Varying Reinforcement Types and Ratios. *ACI Structural Journal*, 111(2), 375-385.

Todeschini, C. E., Bianchini, A. C., and Kesler, C. E. (1964). Behavior of Concrete Columns Reinforced with High Strength Steels. *ACI Journal*, 61(6), 701-716.

Toutanji, H. A. (1999). Stress-Strain Characteristics of Concrete Columns Externally Confined with Advanced Fiber Composite Sheets. *ACI materials journal*, 397-404.

Toutanji, H. A., and Saafi, M. (2000). Flexural Behavior of Concrete Beams Reinforced with Glass Fiber-Reinforced Polymer (GFRP) Bars. *ACI Structural Journal*, 97(5), 712-719.

Triantafillou, T. C., and Plevris, N. (1992). Strengthening of RC beams with Epoxy-Bonded Fibre-Composite Materials. *Materials and Structures*, 25, 201-211.

Vincent, T., and Ozbakkaloglu, T. (2013). Influence of concrete strength and Confinement Method on Axial Compressive Behavior of FRP Confined High- and Ultra High-Strength Concrete. *Composites Part B: Engineering*, 50, 413–428.

Wight, J. K., and MacGregor, J. G. (2012). Reinforced Concrete Mechanics and Design. *Upper Saddle River*, *NJ: Pearson Education Inc*.

Willam, J. K., and Warnke, E. P. (1975). Constitutive Model for the Triaxial Behaviour of Concrete. *Proc. Intl. Assoc. Bridge Structural Engineers*, 19, 1–30.

Wu, H. L., and Wang, Y. F. (2010). Experimental Study on Reinforced High-Strength Concrete Short Columns Confined with AFRP Sheets. *Steel and Composite Structures*, 10(6), 501–516.

Wu, H.-L., Wang, Y.-F., Yu, L., and Li, X.-R. (2009). Experimental and Computational Studies on High-Strength Concrete Circular Columns Confined by Aramid Fiber-Reinforced Polymer Sheets. *Journal of Composites for Construction*, 13(2), 125–134.

Wu, Y. F., and Cao, Y. (2017). Energy Balance Method for Modeling Ultimate Strain of Confined Concrete. *ACI Materials Journal*, 114(2), 373–381.

Wu, Y. F., and Jiang, J. F. (2013). Effective Strain of FRP for Confined Circular Concrete Columns. *Composite Structures*, 95, 479–491.

Wu, Y.-F., and Zhou, Y.-W. (2010). Unified Strength Model Based on Hoek-Brown Failure Criterion for Circular and Square Concrete Columns Confined by FRP. *Journal of Composites for Construction*, 14(2), 175–184.

Xiao, Q. G., Teng, J. G., and Yu, T. (2010). Behavior and Modeling of Confined High-Strength Concrete. *Journal of Composites for Construction*, 14(3), 249–259.

Xiao, Y., and Wu, H. (2000). Compressive Behavior of Concrete Confined by Carbon Fiber Composite Jackets. *Journal of materials in civil engineering*, 12(2), 139-146.

Xiao, Y., and Wu, H. (2003). Compressive Behavior of Concrete Confined by Various Types of FRP Composite Jackets. *Journal of Reinforced Plastics and Composites*, 22(13), 1187–1201.

Xie, T., and Ozbakkaloglu, T. (2015). Behavior of Steel Fiber-Reinforced High-Strength Concrete-Filled FRP Tube Columns under Axial Compression. *Engineering Structures*, 90, 158–171.

Xing, L., Lin, G., and Chen, J. F. (2020). Behavior of FRP-Confined Circular RC Columns under Eccentric Compression. *Journal of Composites for Construction*, 24(4), 04020030.

Xue, W., Peng, F., and Fang, Z. (2018). Behavior and Design of Slender Rectangular Concrete Columns Longitudinally Reinforced with Fiber-Reinforced Polymer Bars. *ACI Structural Journal*, 115(2), 311-322.

Yan, Z., Pantelides, C. P., and Reaveley, L. D. (2006). Fiber-Reinforced Polymer Jacketed and Shape-Modified Compression Members: I - Experimental Behavior. *ACI Structural Journal*, 103(6), 885–893.

Yang, J., Wang, J., and Wang, Z. (2020). Axial Compressive Behavior of Partially CFRP Confined Seawater Sea-Sand Concrete in Circular Columns – Part II: A New Analysis-Oriented Model. *Composite Structures*, 246, 112368.

Yu, F., Xu, G., Niu, D., Cheng, A., Wua, P., and Kong, Z. (2018). Experimental Study on PVC-CFRP Confined Concrete Columns under Low Cyclic Loading. *Construction and Building Materials*, 177, 287–302.

Yu, T., and Teng, J. G. (2011). Design of Concrete-Filled FRP Tubular Columns: Provisions in the Chinese Technical Code for Infrastructure Application of FRP Composites. *Journal of Composites for Construction*, 15(3), 451–461.

Yu, T., Teng, J. G., Wong, Y. L., and Dong, S. L. (2010). Finite Element Modeling of Confined Concrete-I: Drucker-Prager Type Plasticity Model. *Engineering Structures*, 32(3), 665–679.

Zadeh, H. J., and Nanni, A. (2013). Design of RC Columns Using Glass FRP Reinforcement. *Journal of Composites*, 17(3), 294–304.

Zadeh, H. J., and Nanni, A. (2017). Flexural Stiffness and Second-Order Effects in Fiber-Reinforced Polymer-Reinforced Concrete Frames. *ACI Structural Journal*, 114(2), 533–544.

Zhou, Y. W., and Wu, Y. F. (2012). General Model for Constitutive Relationships Of Concrete and Its Composite Structures. *Composite Structures*, 94(2), 580-592.